DYNAMIC ANALYSES OF PILE DRIVING

BY

SA'AD A-W AHMED
B.Sc. ; M.Sc. (CIVIL ENGG.)

A THESIS SUBMITTED FOR THE DEGREE OF DOCTOR OF PHILOSOPHY

DEPARTMENT OF CIVIL ENGINEERING
UNIVERSITY OF GLASGOW

SEPTEMBER - 1989

To my Wife Asjad and
Sons Wakas and Wasak

ABSTRACT

Several approaches to the dynamic analyses of pile driving are explored in this Thesis. These include pile driving formulae, single degree of freedom (SDOF) models, the wave equation approach and a finite element model.

In the elementary models, the pile is modelled as a rigid mass while the soil is represented by various simple rheological mechanisms (spring–slider–dashpot models). Analytical and numerical formulations are developed and the parametric results of the analyses are presented in non–dimensional form.

A study of the wave equation method of the analysis culminates in the development of some simple analytical expressions (analogous to the pile driving formulae) which may prove useful in practice. Some comparisons between the elementary SDOF models, the pile driving formulae and the wave equation have been undertaken in order to assess their strengths and highlight their various shortcomings.

The development of a finite element model for pile driving is discussed in detail with particular emphasis on spatial discretisation (especially the viscous boundaries) and the time integration schemes. A limited parametric study has been conducted in order to gain some insight into the behaviour of piles during driving and to follow the evolution of failure in soils around and beneath the piles. Further work in this area is indicated although computational costs seems to be too high to justify routine use of the finite element method.

ACKNOWLEDGEMENTS

The work described in this Thesis was carried out at the Department of Civil Engineering at Glasgow University under the direction of Dr. T. G. Davies. I am greatly indebted to him for his invaluable advice and encouragement throughout the work and for many suggestions for improvements to this Thesis.

My thanks are due to Dr. D. R. Green, the Head of the Department, for allowing me the use of the facilities of the Department. I also wish to thank Professor D. Muir Wood for his interest in this research study.

I am deeply grateful to Miss. J. Sutherland, for her invaluable help in the enhancement of the Computer Program MIXDYN.

My thanks are also due to my wife for her support and encouragement throughout my work.

I would also like to acknowledge the support of my fellow research students, who were always willing to discuss aspects of my work with me.

Finally, my thanks are due to the Iraqi Embassy for their financial support, without which the work could not have been completed.

S. A–W AHMED

CONTENTS

		Page No.
ABSTRACT		i
ACKNOWLEDGEMENT		ii
CONTENTS		iii
NOTATION		vi
CHAPTER 1	INTRODUCTION	1–14
1.1	INTRODUCTION	1
1.2	LITERATURE REVIEW	2
1.2.1	Pile Driving Formulae	2
1.2.2	Wave Equation Method	4
1.2.3	Finite Element Method	7
1.3	CLOSURE	8
CHAPTER 2	ELEMENTARY MODELS	15 –70
2.1	INTRODUCTION	15
2.2	PILE DRIVING FORMULAE	15
2.2.1	Introduction	15
2.2.2	Formulation	16
2.2.3	Discussion	19
2.3	SINGLE DEGREE OF FREEDOM MODELS	19
2.3.1	Introduction	19
2.3.2	Pile subjected to Initial Velocity	20
2.3.3	Results	26
2.3.4	Pile subjected to Cushioned Impact	28
2.3.5	Results	30
2.3.6	Discussion	31
2.4	CONCLUSION	32
CHAPTER 3	THE WAVE EQUATION MODEL	71 –159
3.1	INTRODUCTION	71
3.2	FORMULATION	72
3.2.1	Discrete Equations	72
3.2.2	Critical Time Step	74
3.3	NUMERICAL IMPLEMENTATION	75

			Page No.
	3.4	RESULTS	76
	3.4.1	Wave Equation	76
	3.4.2	Comparison with Elementary Models	79
	3.4.2.1	Wave Equation versus SDOF Model	79
	3.4.2.2	Wave Equation versus Pile Driving Formulae	81
	3.5	DISCUSSION	85
	3.6	CONCLUSION	85
CHAPTER 4		THE FINITE ELEMENT MODEL	160 –218
	4.1	INTRODUCTION	160
	4.2	THEORETICAL FORMULATION	160
	4.2.1	Introduction	160
	4.2.2	Governing Equations	161
	4.3	CONSTITUTIVE LAWS	169
	4.3.1	Introduction	169
	4.3.2	Yield Criteria	170
	4.3.3	The Critical State Model	173
	4.3.4	Conclusion	177
	4.4	SPATIAL DISCRETISATION	177
	4.4.1	Introduction	177
	4.4.2	Geometric Modelling	178
	4.4.3	Transmitting Boundaries	179
	4.4.4	Interface Elements	186
	4.5	TIME INTEGRATION SCHEMES	187
	4.5.1	Introduction	187
	4.5.2	Explicit Integration Schemes	188
	4.5.3	Implicit Integration Schemes	191
	4.5.4	Implicit–Explicit Integration Schemes	193
	4.5.5	Conclusion	194
	4.6	CONCLUSION	194
CHAPTER 5		FINITE ELEMENT ANALYSIS OF PILE DRIVING	219 –259
	5.1	INTRODUCTION	219
	5.2	CONVERGENCE STUDIES	220
	5.3	PARAMETRIC STUDIES	221
	5.4	DISCUSSION	224

			Page No.
	5.5	CONCLUSION	224
CHAPTER	6	CONCLUSIONS AND RECOMMENDATIONS FOR FUTURE STUDIES	260 –261
	6.1	CONCLUSIONS	260
	6.2	RECOMMENDATIONS FOR FUTURE STUDIES	261
REFERENCES			262
APPENDIX A		COMPUTER PROGRAM	275
APPENDIX B		SUBROUTINE SDAMP	284
APPENDIX C		PROGRAM WAVE	286

NOTATION

Symbols which are not given below are defined in the text.

Elementary Models and Wave Equation:

A	cross sectional area of the pile
C	ratio between the actual pile head displacement and that given by Hooke's law
E	Young's modulus of elasticity
E_p	Young's modulus of elasticity of the pile
E_1	energy reaching the pile
E_2	energy left after impact
e_f	efficiency factor for the hammer
e_g	efficiency factor for impact
g	gravitational acceleration
H	drop height of the hammer
J	viscous damping coefficient of soil
K_p	internal spring (pile) stiffness
K_s	external spring (soil) stiffness
L	pile length
m	mass
m_p	pile mass
m_r	ram mass
n	coefficient of restitution
n	soil to pile stiffness ratio (K_s/K_p)
Q	quake value
R	ultimate soil resistance
S	permanent pile penetration per blow (set)
ΔS_{pp}	plastic deformation of pile
ΔS_{ep}	elastic deformation of pile
ΔS_{es}	elastic deformation of soil
t	time
Δt	time interval
T	period ($2\Pi/\omega$)
u	hammer velocity after impact

u_p	pile velocity after impact
v	hammer velocity before impact
v_p	pile velocity before impact
V	velocity of discrete pile mass
V_0	initial velocity
$\overline{V}$	dimensionless velocity (V.J)
ω	circular frequency $\sqrt{(K/m)}$
$\omega_n t$	dimensionless time
W	weight of the hammer
β	numerical coefficient

Soil and Foundation Parameters/Finite Element Model:

E	Young's modulus of elasticity
G	shear modulus of elasticity
ν	Poisson's ratio
ρ	mass density
c_u	undrained cohesive strength of soil
α	adhesion coefficient at pile–soil interface
r_0	radius of the pile
J_s, J_p	damping coefficients for pile shaft, pile tip, respectively
V_s, V_p	shear and compression wave velocities, respectively

Stress and Strain Parameters:

σ, τ	normal and shear stresses, respectively
ϵ	normal strain
I	stress invariant
J	deviator stress invariant
F	yield function

Matrices and Vectors:

C	damping matrix
F	force matrix
M	mass matrix
K	stiffness matrix
c	diagonal damping matrix
f	diagonal force matrix
m	diagonal mass matrix
k	diagonal stiffness matrix

Dynamic Analysis Parameters:

x, $\dot{x}$, $\ddot{x}$	displacement, velocity and acceleration, respectively
Δt	time step
t	time
c	velocity of the stress wave
α, β	Newmark collocation parameters

Symbols for Transmitting Boundaries:

	fixed boundary
	roller boundary
	viscous boundary

CHAPTER 1

INTRODUCTION

1.1 INTRODUCTION

1.2 LITERATURE REVIEW

1.2.1 Pile Driving Formulae

1.2.2 Wave Equation Method

1.2.3 Finite Element Method

1.3 CLOSURE

CHAPTER 1

INTRODUCTION

1.1 INTRODUCTION

Load tests provide the most reliable means of determining the bearing capacities of piles but such tests are expensive and laborious to perform. Consequently, the performance of piles during driving is usually used as an indicator of their subsequent load capacities. This process of interpretation may be effected by such means as the pile driving formulae (e.g. the Hiley Formula) or, latterly, the wave equation method (incorporated into field equipment such as the Pile Driving Analyser). Even more sophisticated are the Finite Element analyses, but these remain as yet within the domain of research although some applications to critical offshore installations have been reported in the literature. The major thrust of this Thesis is a critical examination of these various approaches to the analysis of pile driving and to extend the current knowledge of the mechanics of the driving process.

Chapter Two begins with a brief review of pile driving formulae, their reliability and accuracy. Some simple single degree of freedom (mass–spring–dashpot) models of pile driving are then considered and the results of a parametric study of the problem are discussed.

Chapter Three deals with the wave equation method of analysis (in which the pile is idealised as a compressible body) and the results are then compared with those predicted by the elementary models described in Chapter Two. These comparisons culminate in a new "pile driving formula".

In Chapter Four, the finite element method and its applications to non–linear dynamic analyses is discussed. The modelling of infinite boundaries, the pile–soil interface (slip) conditions, yield criteria for soils and spatial and temporal discretisations are discussed in detail.

Chapter Five documents the results of a limited parametric study of the pile driving problem using the finite element model. Parameters examined in this study include the soil strength, stiffness, pile–soil adhesion and the pile–head loading conditions, and the evolution of failure in the soil around and underneath the pile during driving is examined. Finally, in Chapter Six, the relevance of each of these methods to engineering practice is discussed and some recommendations for further research effort are proposed.

1.2 LITERATURE REVIEW

The literature on pile driving analyses is extensive and the subject commands the attention of a long running series of international conferences. In this section, a representative set of some of the more important publications is briefly reviewed. Some publications which deal with narrow specialist topics, particularly in the finite element domain, are reviewed in the relevant Chapters.

1.2.1 Pile Driving Formulae

The most frequently used method of estimating the load carrying capacity of driven piles is to use pile driving formulae, Taylor (1948). The basic principle of these formulae is that the energy input from the hammer is dissipated in the pile and surrounding soil. However, there are major differences between different pile driving formulae in the way in which they account for the various energy losses. All these formulae relate the ultimate load capacity to the pile set and, in practice, it is often assumed that the driving resistance is equal to the load carrying capacity of the pile. Pile driving formulae can not predict the effect of soil consolidation etc. subsequent to driving on pile bearing capacities.

Agerschou (1962) analysed statistically the Engineering News Record (ENR) formula based on data from 171 load tests to failure of piles embedded in sands and gravel. The piles were driven by drop hammers and single/double acting

steam hammers. He concluded that the ENR formula was unreliable because 96% of the allowable loads determined from this formula would have safety factors varying from 1.1 to 30. He also suggested that there was no way of knowing a priori what the safety factor was. However, he found that the Hiley formula and Janbu formula were much more accurate.

Flaate (1964) discussed the derivation of the general pile driving formula and the limitations and use of three pile driving formulae, namely, the Hiley formula, the Engineering News Record formula and the Janbu formula. Results from a great number of loading tests on piles were analysed statistically. All the piles were driven in a mainly cohesionless material or through a cohesive material into a dense cohesionless layer; the bearing capacity of piles thus being obtained in a cohesionless material. He found that the mean nominal safety factors of these formulae (Hiley, ENR and Janbu) were 2.7, 6.0 and 3.0, respectively. However, the wide range of safety factors given by the ENR formula were so great that Flaate advocated abandoning the formula. Both the Hiley formula and the Janbu formula gave relatively good results, but of these two the Janbu was judged to be preferable.

Housel (1966) analysed data drawn from research conducted by the Michigan State Highway Department into the performance characteristics of pile driving hammers and piles. Eighty–eight instrumented piles were driven at three sites using several different pile driving hammers and load tests were conducted on nineteen of these piles to determine their static bearing capacities. The pile lengths tested varied from 13 m to 54 m and their bearing capacities were estimated using pile driving formulae. Housel concluded that the ENR formula yielded safety factors ranging from about one to a maximum of three or four, compared with its implicit safety factor of six.

Poulos and Davis (1980) discussed pile driving formulae in detail. They concluded from their literature survey that the Janbu formula, Danish formula and Hiley Formula were the most reliable while Engineering News Record (ENR) formula was the least reliable.

1.2.2 Wave Equation Method

The gradual realisation that pile driving cannot be accurately analysed by rigid body mechanics (pile driving formulae) led to the development of an analysis utilizing wave theory. This method of analysis takes into account the fact that hammer blows produce stress waves that propagate along pile shafts. A wave equation approach was first considered by Isaacs (1931) and Fox (1932) but Smith (1955,1960) was the first to carry out numerical calculations by this method.

The wave equation method is based on consideration of the one–dimensional dynamic equilibrium of a prismatic bar subjected to impact at one end. It can be shown that the differential equation of motion is:

$$\frac{\partial^2 u}{\partial t^2} = c^2 \frac{\partial^2 u}{\partial x^2} \qquad (1.1)$$

where, the wave velocity c is defined as follows:

$$c = \sqrt{\left(\frac{E}{\rho}\right)} \qquad (1.2)$$

where,

E is the Young's modulus of elasticity of the bar,

ρ is the mass density,

u is the displacement on the bar from its original position, and,

t is the time.

In pile driving analyses, the resistance of the surrounding soil must also be considered. Equation 1.1 then becomes:

$$\frac{\partial^2 u}{\partial t^2} = c^2 \frac{\partial^2 u}{\partial x^2} + R \qquad (1.3)$$

where R is the soil resistance.

Unfortunately, an analytic solution to this equation is not possible. Hence, recourse is made to numerical solutions such as that developed by Smith (1955) and (1960). In Smith's (1955) paper he solved the wave equation by means of a simple numerical technique (essentially a multidegree of freedom analysis) in preference to a direct finite difference approach. In this numerical solution, the pile shaft was subdivided into so–called "unit lengths" (finite segments) connected by springs. He showed however that the solution was not unconditionally stable and, in particular, the time integration scheme failed if time intervals greater than some critical value were employed. In his later paper (Smith,1960), the soil resistance along the shaft and below the pile tip was idealised by slider–spring and dashpot mechanisms. The springs (soil) deform linearly elastically a certain distance (termed the quake, Q) then fail plastically at the ultimate resistance R. The dashpots were characterised by their coefficients of viscous damping, J.

Hirsch et. al, (1970) studied the effect of various parameters (including type and size of hammer and pile and soil conditions) on the bearing capacities predicted by the wave equation method. They found that the driving accessories significantly affected the pile driving performance and that stiffer piles could overcome greater soil resistance to penetration. They recommended use of cushions of low stiffness in order to facilitate energy transfer and to limit driving stresses.

Poulos and Davis (1980) discussed Smith's (1960) empirical soil parameters; quake, Q, and coefficient of viscous damping, J. They thought that it might be possible to derive values of Q theoretically from pile–settlement theory and, hence, quake values would vary along the pile shaft with the values near the pile tip being greater than those along the shaft. They gave empirical correlations between the coefficient of viscous damping for the pile tip J_p and pile shaft J_s and soil type. Further, they suggested that the available data confirmed that pile tip viscosity was several times greater than shaft viscosity, typically $J_p = 3J_s$. They presented some results which showed that pile length above the ground and embedded pile length had little effect on pile driving performance. They showed that pile bearing capacities increased only slowly with increased hammer energy and suggested that there would be an optimum cushion stiffness that could provide protection for both the hammer and the pile while not seriously affecting the driving capability of the system. They also showed that pile impedance had a

significant influence on peak driving stresses. Higher impedance piles (heavier and/or stiffer sections) induced higher peak stresses than the lighter sections.

Authier and Fellenius (1980) presented the results of a comprehensive study of quake values determined from dynamic measurements. In their analysis, they use the Case Pile Driving Analysis Program (CAPWAP). Good results were obtained for piles driven into a very dense sandy silty glacial till using tip quake value of 20 mm rather than the usual value of 2.5 mm. However, for piles driven through thick clay deposits into underlying dense clayey silty glacial tills, good results were obtained with 8 mm quake values. The authors believed that the large quakes observed might be related to pore pressure build–up in the soil. The occurrence of large quakes has practical importance since they inhibit driving.

Ebecken et. al, (1984) described a numerical solution based on the discretisation of piles into one–dimensional finite elements. The soil was represented by non–linear springs and dashpots attached to the finite elements at their nodes. Their soil model allowed soil degradation during load cycles and they applied the model to calcareous soils in Brazil.

Corte and Lepert (1986) proposed a new soil model to describe the soil shaft resistance. In this model, the soil was separately idealised into two zones (Fig. 1.1*a*); the first zone of the model simulates the soil reaction to large strains while in the second (outer) zone the soil response is elastic. They showed that this soil model could allow larger velocities in the pile than in the soil during penetration and believed that this would give better estimates of energy radiated by elastic waves than Smith's (1960) model.

Wu et. al, (1986) described a soil model (shown in Fig. 1.2*b*) consisting of a slip mechanism and an elastic shear wave energy absorbing boundary. The accuracy of the model was verified by comparing its predictions with those obtained from a finite element analysis (Fig. 1.2*a*).

Yip and Poskitt (1986) used the wave equation method to interpret the data obtained from an instrumented pile during driving. Their main finding was that shaft and tip quake damping values were equal, notwithstanding some earlier findings to the contrary.

Randolph and Simons (1986) presented an improved soil model based on the results of analyses of pile foundation vibration. In their new soil model, dynamic soil stiffness and viscous and radiation damping are modelled by a series of springs and dashpots but these are now expressed in terms of fundamental soil properties (Fig. 1.3*b*) while Fig. 1.3*a* shows the original model developed by Smith (1960). They obtained good results with their new soil model but recommended further comparisons with field data in order to fully validate their analysis.

Lee et. al, (1988) developed a variational formulation of the wave equation (Fig. 1.4) based on visco–elasto dynamic theory. In this model, the loss of energy to the soil through radiation damping and hysteresis due to the plasticity were accounted for. Unlike Smith's (1960) rheological soil model, the parameters for this soil model can be determined experimentally or correlated to conventional soil properties.

1.2.3 Finite Element Method

The finite element method is, as is well known, a rigorous and general solution technique. However, computational costs for pile driving analyses are typically two or three orders of magnitude greater than the costs of wave equation analyses. On the other hand, finite element models can reproduce the essential features of dynamic soil–structure interaction based on the classical governing equations of dynamics and expressed in terms of real soil properties. A brief review of the most important research studies on pile driving using this method follows.

Smith (1976,1982) used the finite element model to analyse pile driveability and pile bearing capacity. In his analyses, the piles were idealised by a chain of one–dimensional finite elements while the soil resistance was modelled by a series of soil 'springs' attached to the nodes of the pile elements, Fig. 1.5.

Chow (1981) used axisymmetric finite elements and the Wilson–θ implicit time marching scheme to analyse the pile driving problem. He used a viscous

time marching scheme to analyse the pile driving problem. He used a viscous boundary to avoid the spurious stress wave reflections which occur at simply truncated boundaries and six noded elements were used to model the pile–soil interface. He thought that the significant differences between the results of the wave equation model and the finite element model were probably due to the more complex nature of damping in the latter model. Using the Von Mises soil model, he found that the dynamic tip resistance factor, N_D (analagous to N_c for static loading), during driving ranged from 7 to 35, with the higher values obtained for softer clays.

To (1985) extended the work of Chow (1981) on pile driving. He used the same discretisation scheme as Chow (1981) and "predicted" Rigden et al's (1979) full–scale field data on closed and open–ended piles. He refined his discretisation scheme but obtained essentially the same results although the refined mesh exhibited less spurious oscillations. This result suggests that the discretisation scheme adopted by Chow (1981), should be adequate for predictions of pile driveability.

Simons (1985) used a one–dimensional finite element analysis to study pile driveability. This model involved an elasto–dynamic theory to prescribe the form of the dynamic pile soil interaction. He concluded that this method might offer a very effective approach to the analysis of pile driving. In the finite element analysis, he used explicit temporal integration rather than implicit integration in order to reduce computational costs. However, he believed that the most effective scheme would be to integrate the structural elements implicitly and the soil elements explicitly since this would exclude the stiffer elements from critical time step considerations and, also, the numerical damping characteristics of the implicit scheme would mitigate somewhat the problem of spurious high frequency resonance.

1.3 CLOSURE

Pile driving analyses have attained considerable maturity in recent years although only recently have these advances filtered down into engineering practice. In this respect, we cite the Pile Driving Analyzer which appeared on the market in early years of this decade although the basic ideas on which it is based (the

wave equation method) were well known over twenty years earlier. The major thrust of this Thesis is to develop computer programs for the analysis of pile driving using a variety of algorithms and to assess their relative merits for further study in this area.

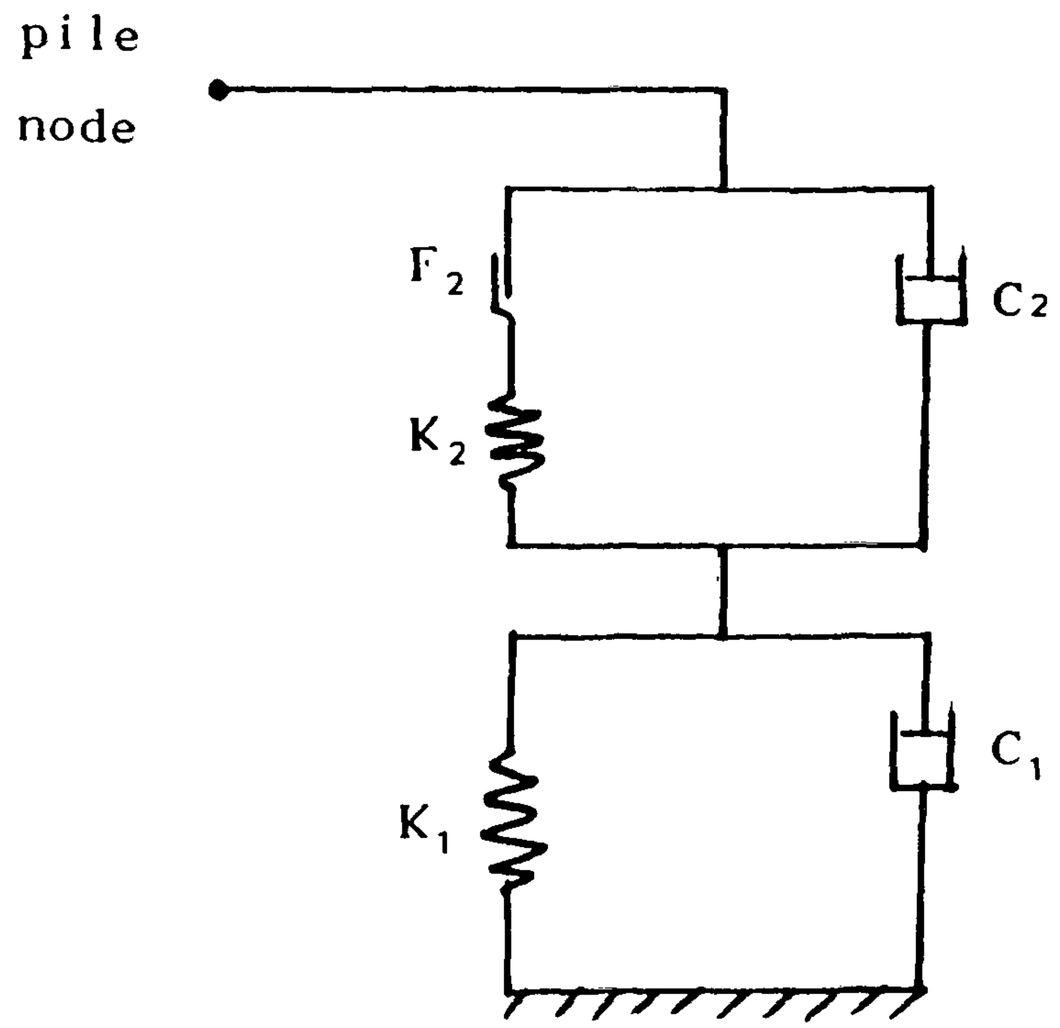

(a) Discretized Model with Two Stages

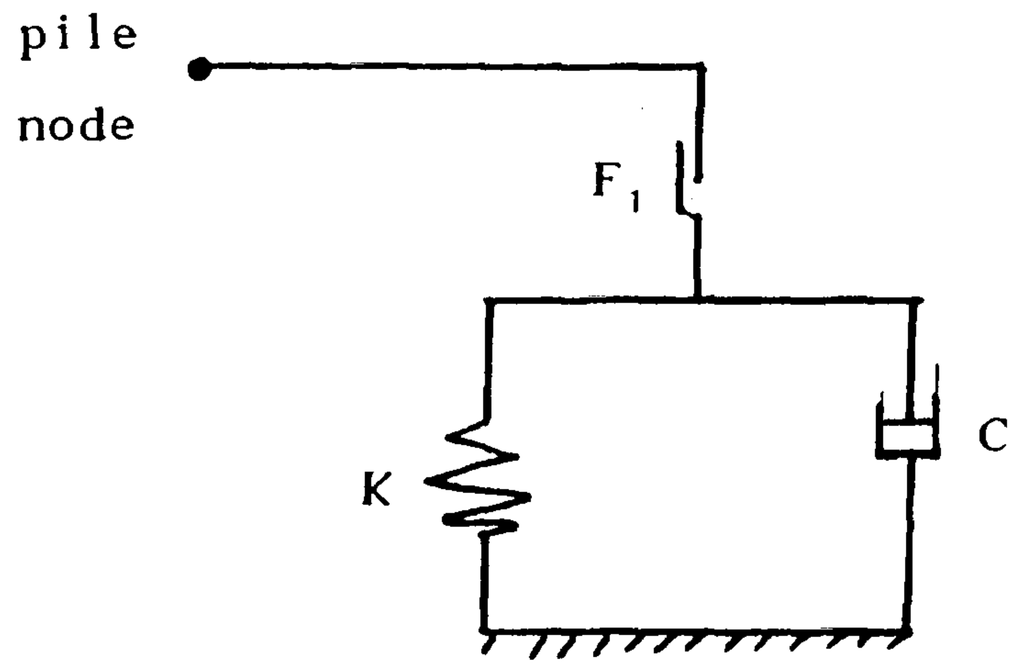

(b) Proposed Simplified Model

FIGURE (1.1) NEW SOIL MODEL FOR ONE DIMENSIONAL WAVE EQUATION MODEL (AFTER CORTÉ & LEPERT, 1986)

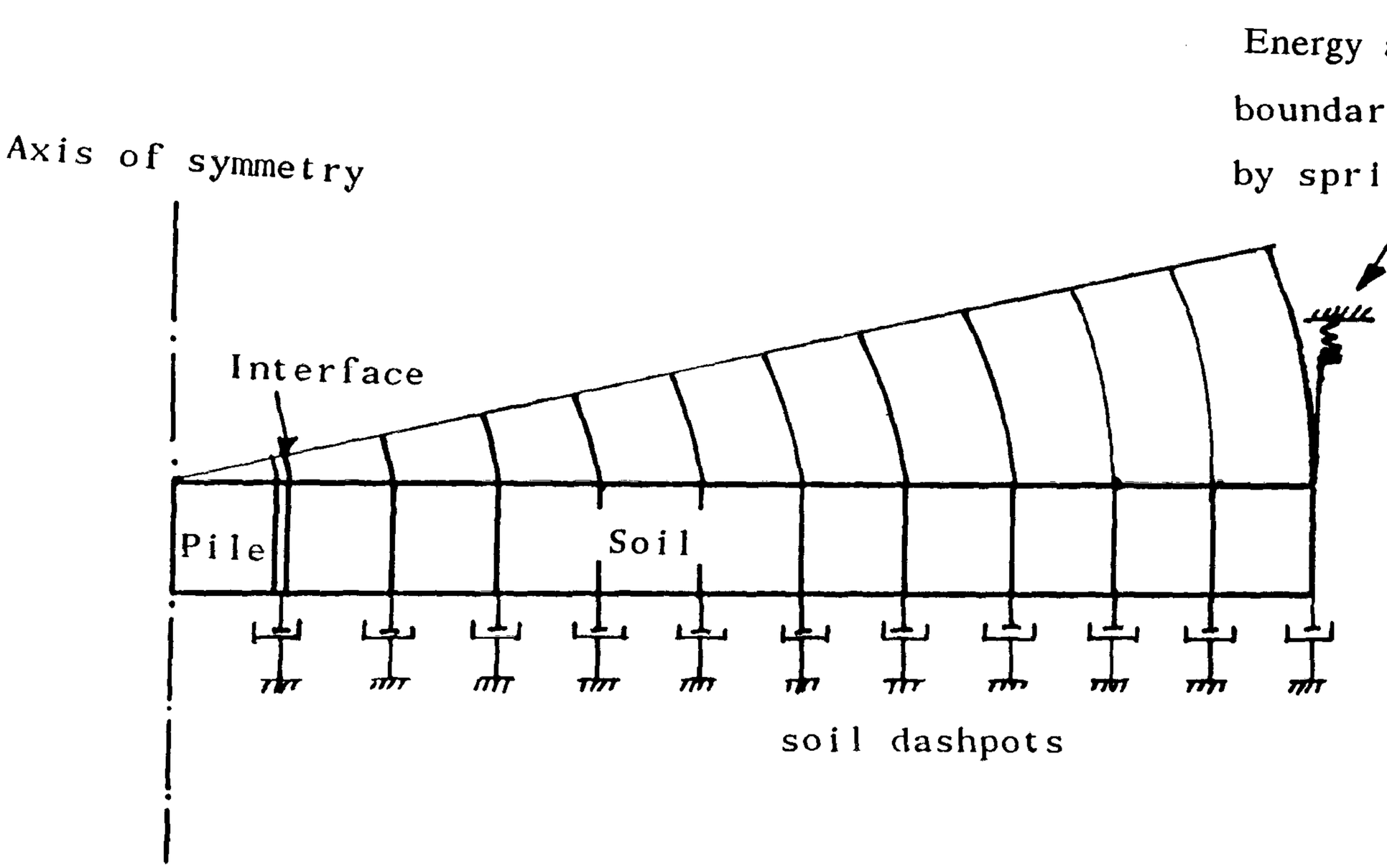

(a) Finite Element Model

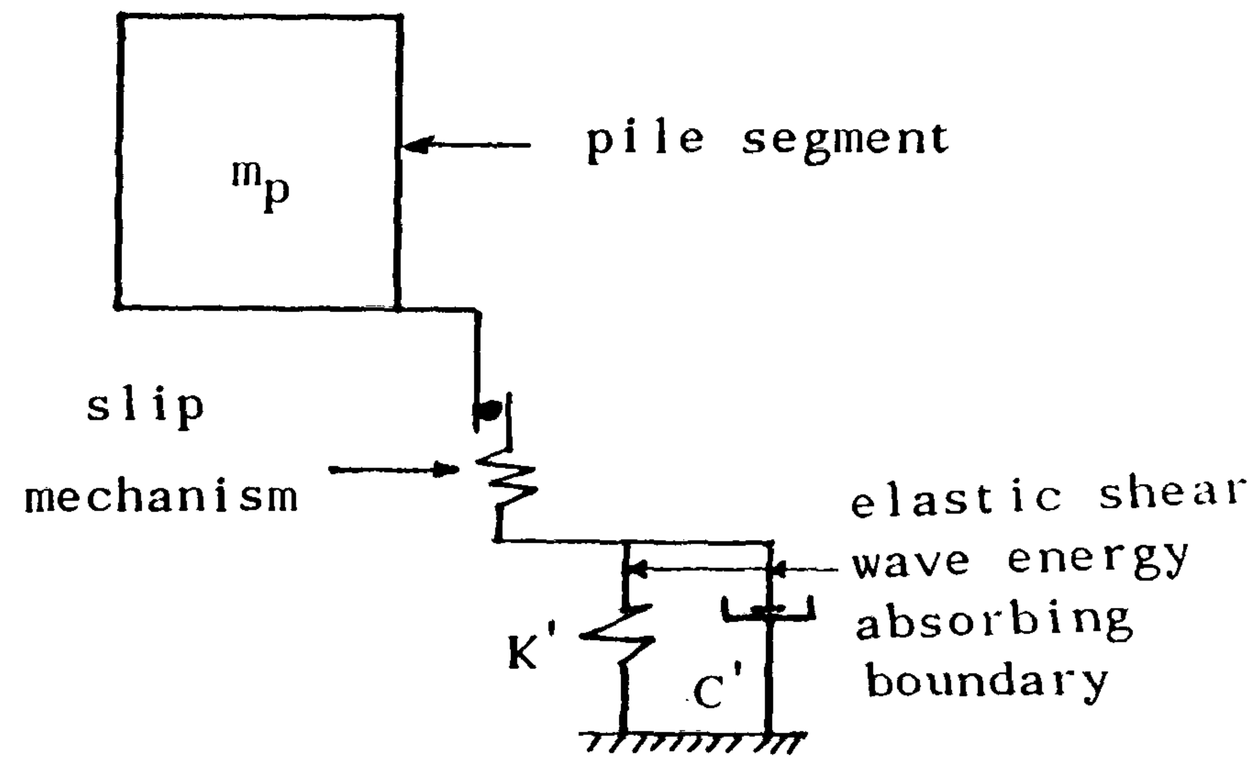

(b) The New Pile–Soil Model

FIGURE (1.2) PILE DRIVING ANALYSIS MODELS
(AFTER WU ET. AL, 1986)

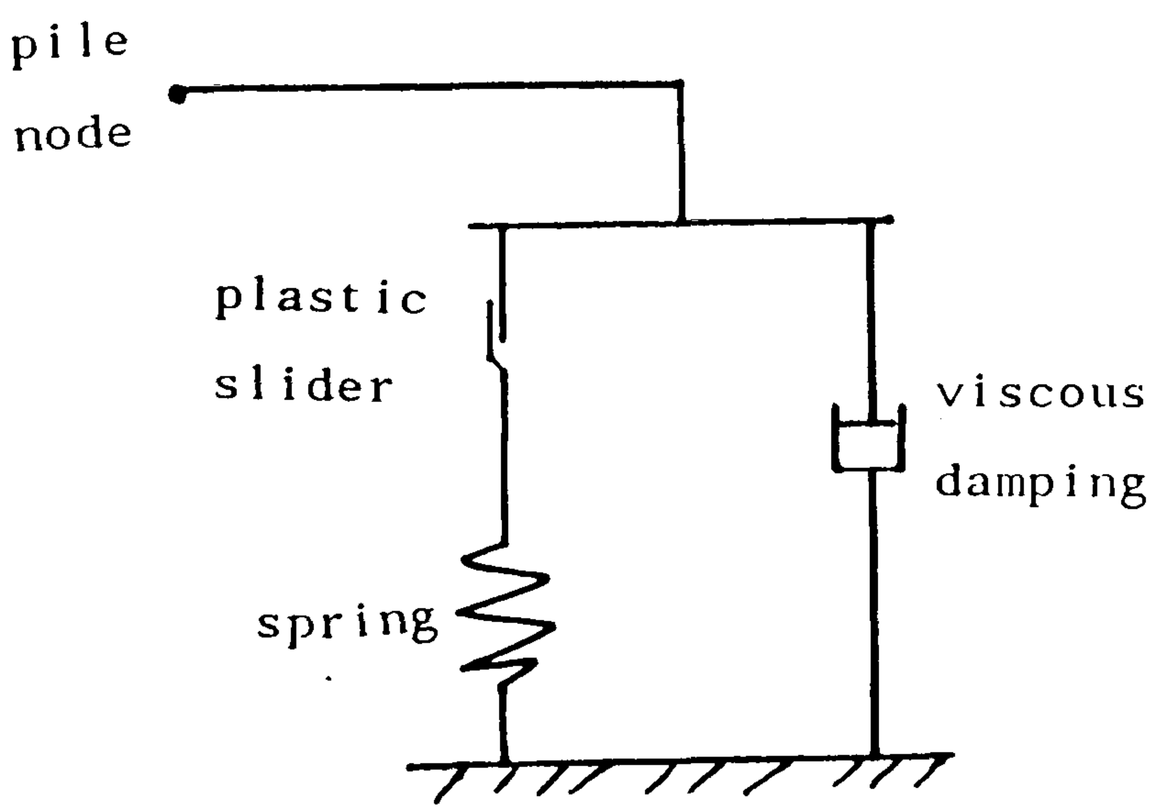

(a) Conventional Soil Model
(after E.A.L.Smith,1960)

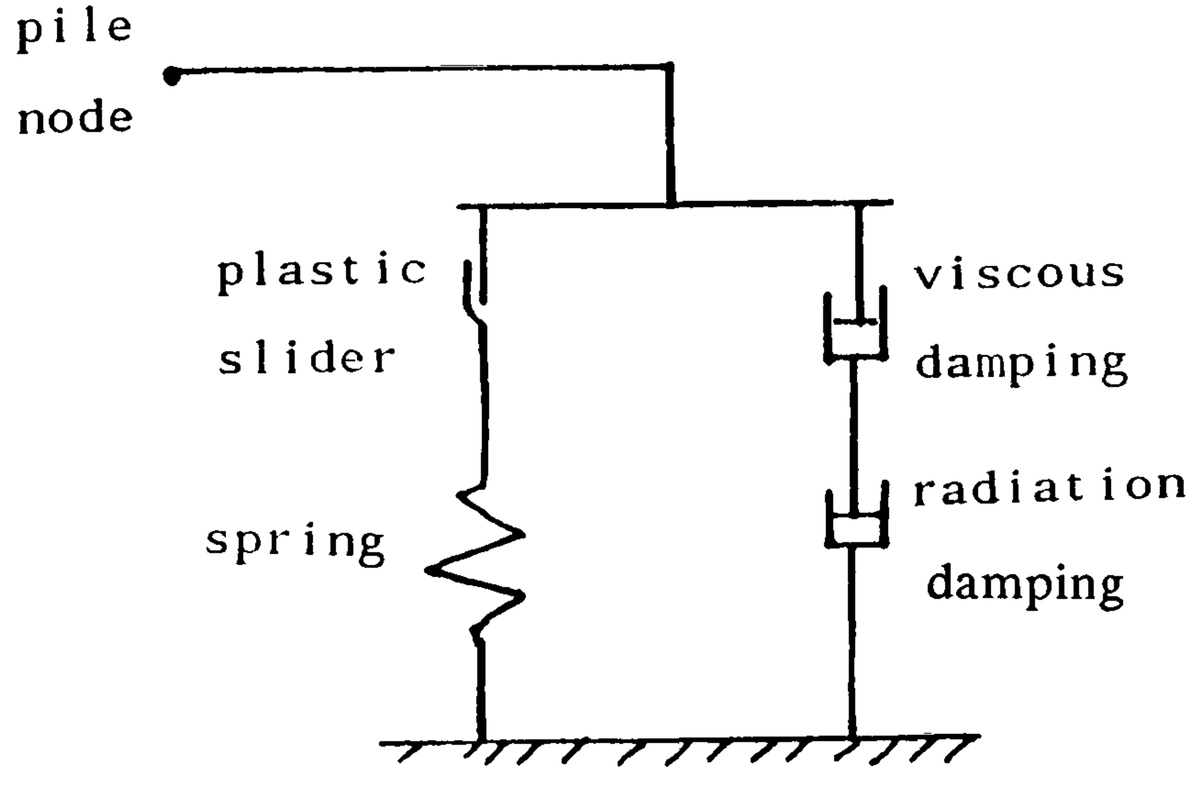

(b) Alternative Soil Model
(after Randolph&Simons,1986)

FIGURE (1.3) SOIL MODELS FOR PILE DRIVING ANALYSIS

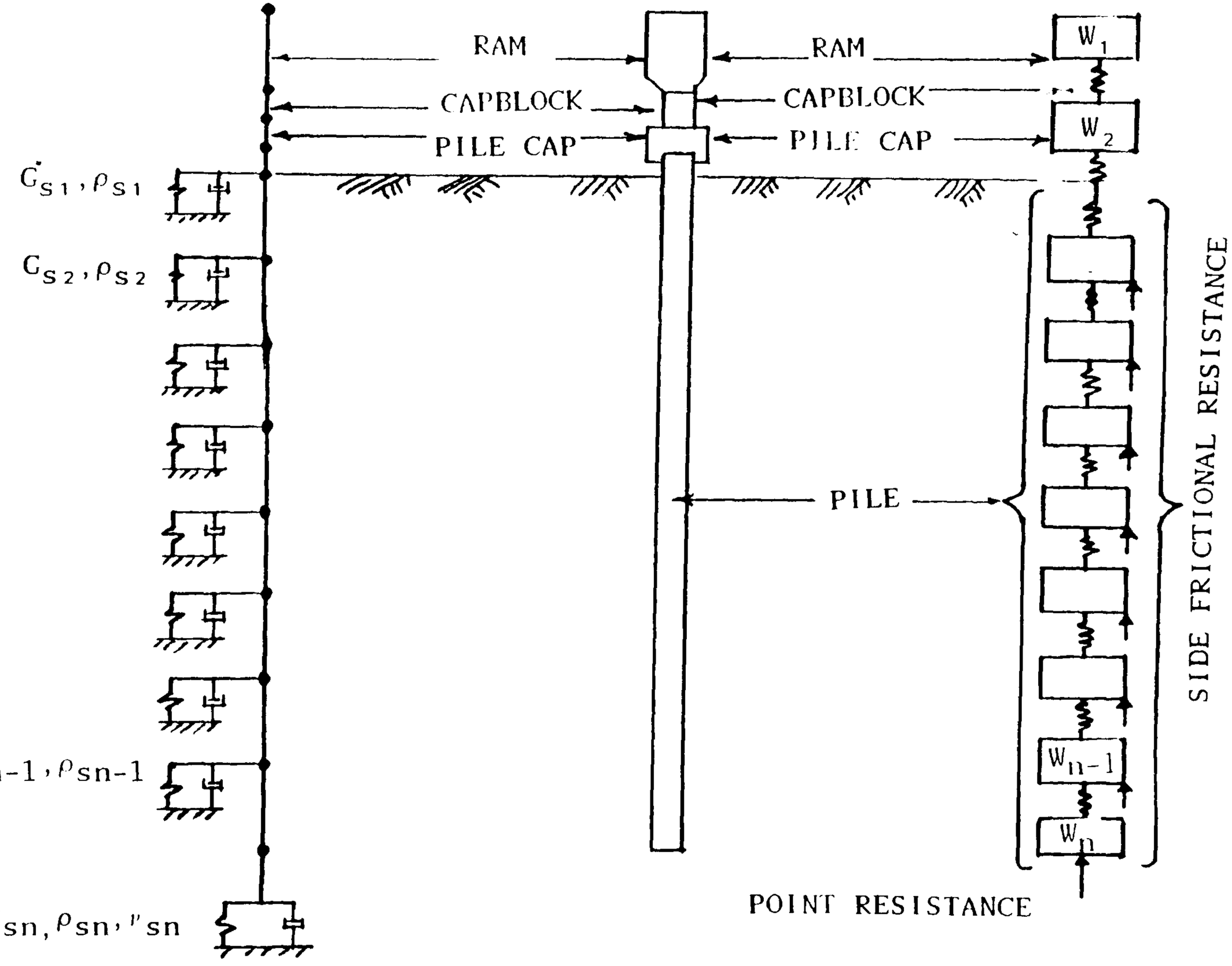

(a) Finite Element Model
(after Lee et. al,1988)

(b) Wave Equation Model
(after E.A.L.Smith,1960)

FIGURE (1.4) ONE DIMENSIONAL MODELS

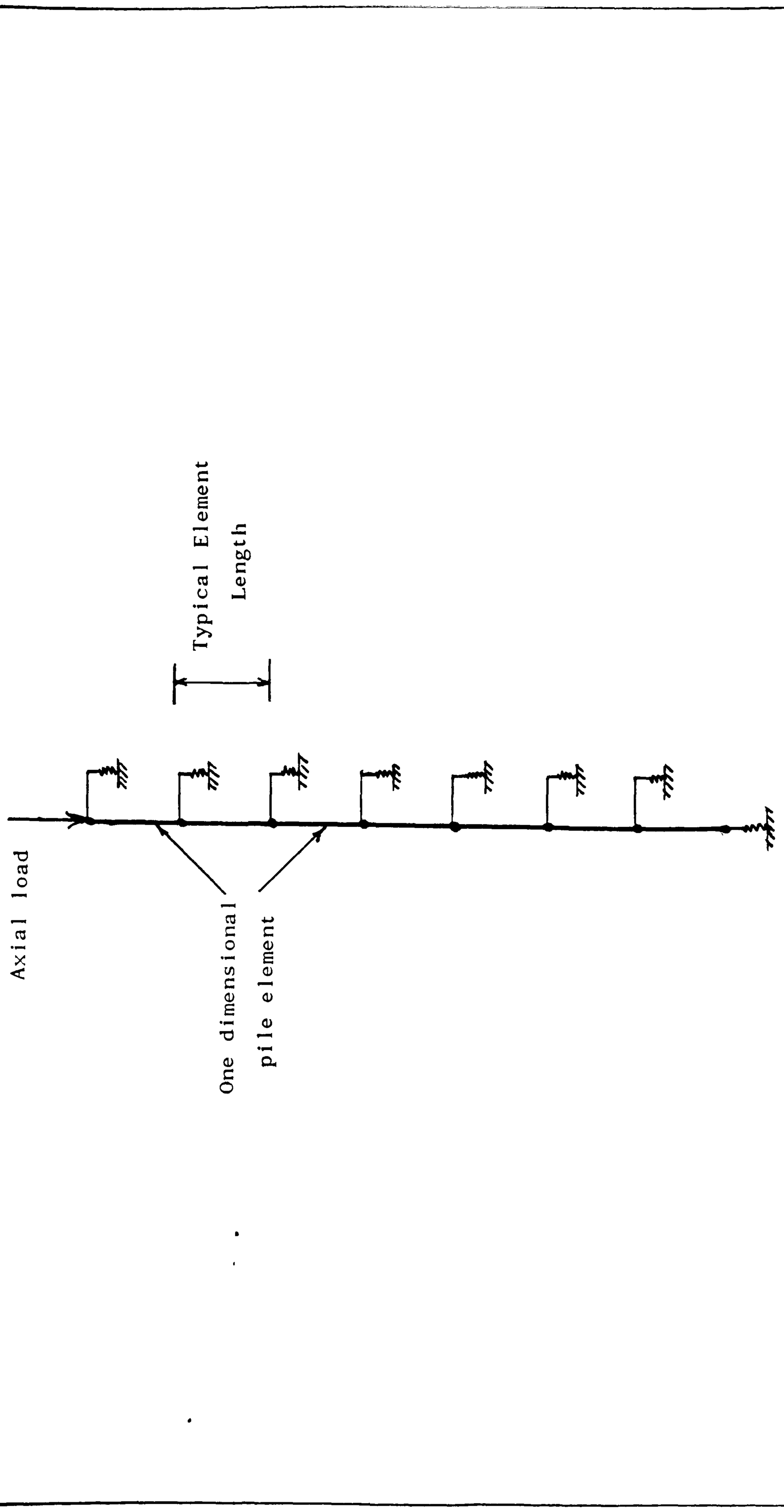

FIGURE (1.5) REPRESENTATION OF PILE AND SOIL BY ONE DIMENSIONAL FINITE ELEMENT MODEL (AFTER I.M. SMITH, 1976)

CHAPTER 2

ELEMENTARY MODELS

2.1 INTRODUCTION

2.2 PILE DRIVING FORMULAE

2.2.1 Introduction

2.2.2 Formulation

2.2.3 Discussion

2.3 SINGLE DEGREE OF FREEDOM MODELS

2.3.1 Introduction

2.3.2 Piles subjected to Initial Velocity

2.3.3 Results

2.3.4 Piles subjected to Cushioned Impact

2.3.5 Results

2.3.6 Discussion

2.4 CONCLUSION

CHAPTER 2

ELEMENTARY MODELS

2.1 INTRODUCTION

Pile driving formulae, based on energy principles, are still widely used in engineering practice to predict the bearing capacity of driven piles although numerous studies (e.g. summarised by Poulos and Davis, 1980) have shown that these formulae are unreliable. For completeness, these formulae and their deficiencies are briefly explored in the first part of this Chapter.

More realistic, but still simplistic, single degree of freedom models are considered in the latter part of this Chapter. In these models, the pile is assumed to be a rigid body and the soil resistance is described by simple visco–elasto–plastic models. These models approach the problem from the viewpoint of force, time and displacement and give greater insight into the mechanics of the impact process. Development of these latter models to include pile compressibility leads to the wave equation model, described in the next Chapter.

2.2 PILE DRIVING FORMULAE

2.2.1 Introduction

Pile driving formulae relate the ultimate capacity of driven piles to their permanent sets during driving. They are based on consideration of the energy of the hammer blow and its transformation during the driving process into useful work (of pile penetration) and its dissipation as a consequence of pile and cushion deformation. Of course, such formulae cannot predict the increase in the bearing capacity which often occurs subsequent to driving. For completeness a

general derivation of these dynamic formulae and a discussion on their reliability and accuracy will be presented in the next section.

2.2.2 Formulation

The assumed relationship between pile resistance and downward movement is shown in Fig. 2.1, and the process of energy transfer and pile penetration during one blow of the hammer is shown in Fig. 2.2.

Following Flaate (1964), the hammer energy at impact is:

$$E_1 = e_f \; W \; H \qquad (2.1)$$

where,
e_f is the efficiency of the drop,
W is the weight of the hammer, and,
H is the height of the drop.

During impact, useful mechanical energy is lost in numerous ways – hammer rebound, plastic deformation of the capping material, wave propagation through the soil etc. These losses may be lumped together in terms of a notional coefficient of elastic restitution n (with reference to Newtonian theory) which yields an impact energy efficiency factor:

$$e_g = \frac{W + n^2 \; W_p}{W + W_p} \qquad (2.2)$$

where W_p is the weight of the pile.

Because the pile is not a free–body, there is no direct relation between the intrinsic coefficient of restitution and the notional coefficient. Thus, the parameter e_g could equally well be assigned some empirical value instead of being computed

from equation 2.2.

The kinetic energy of the pile immediately after impact is:

$$E = e_f \, e_g \, E_1 \qquad (2.3)$$

It may be assumed that this kinetic energy is partly dissipated by plastic work during driving and partly converted into recoverable strain energy. Energy is also dissipated by propagation of stresses waves through the soil but this (major) energy loss is invariably neglected in this type of analysis. Assuming, that the soil responds elasto–plastically to loading (Fig. 2.1) it may be assumed that:

$$E = R \left(S + \Delta S_{pp} + \frac{1}{2} \Delta S_{ep} \right) \qquad (2.4)$$

where,

R is the bearing capacity of the soil,

S is the permanent set (irrecoverable downward displacement of the pile through the soil),

ΔS_{pp} is the plastic deformation of the pile head, and,

ΔSep is the elastic deformation of the pile.

It is by no means clear that the work done during plastic deformation of the pile head is equal to $R.\Delta S_{pp}$ since the impact force will probably be many times greater than the soil resistance (dynamic equilibrium being maintained by the inertia of the pile and surrounding soil). Further, this term may be accommodated within the impact efficiency factor (e_g) briefly discussed earlier.

The third term, representing the stored strain energy imparted to the pile, which in practice will be manifest by longitudinal vibrations in the pile after impact, can be recast in the form:

$$\Delta S_{ep} = C \, \frac{R \; L}{A \; E_p} \qquad (2.5)$$

where,

C is an empirical constant (defined as the ratio between the actual elastic displacement and that given by Hooke's law),

L is pile length,

A is the pile cross–sectional area, and,

E_p is the Young's modulus of elasticity of the pile.

Equation 2.5 is simply an empirical equation based on Hooke's law. Combining equations 2.4 and 2.5 we obtain:

$$E = R \left(S + \frac{C}{2} \frac{R\ L}{A\ E_p} \right) \qquad (2.6)$$

Introducing the constant:

$$a = \frac{C\ L}{2\ A\ E_p} \qquad (2.7)$$

we obtain the solution:

$$R = \frac{1}{2\ a} \left(- S + \sqrt{S^2 + 4\ a\ E} \right) \qquad (2.8)$$

or, if elastic strain energy is neglected (a = 0):

$$R = \frac{E}{S} \qquad (2.9)$$

These equations and variants thereof are recognizable in the list of conventional pile driving formulae recorded in Table 2.1. Their diversity is a testament to their inaccuracy. Further, although some of these formulae are said to give better results for particular soil types, it is not apparent why this should be so.

2.2.3 Discussion

Clearly the pile driving formulae cannot provide a rational basis for analysis of the driving process. Several investigations have been carried out to determine the reliability of various pile driving formulae by comparing the predicted load capacities with the measured capacities from pile load tests. For example, Agerschou (1962) showed that Engineering News Record formula, despite its popularity, was unreliable since it yielded safety factor ranging from 1.1 to 30. Flaate (1964) investigated the accuracy of the Janbu formula, Hiley formula and Engineering News Record formula for piles in sand. He confirmed Agerschou (1962) findings regarding the Engineering News Record formula but obtained better results with the Janbu formula and Hiley formula. However, pile driving formulae may be helpful in some cases where local knowledge exists and also as a means of comparison between piles on a given site.

2.3 SINGLE DEGREE OF FREEDOM MODELS

2.3.1 Introduction

In this section, the pile is assumed to be a rigid mass. The surrounding soil is represented by a slider–spring mechanism and a parallel dashpot connected to the rigid mass (Fig. 2.3). The spring deforms elastically up to a limiting displacement, termed the quake,Q. Thereafter, the slider limits the spring reaction force. In addition, the increased soil resistance observed under dynamic loading conditions is represented by dashpot; defined by a viscous dashpot coefficient, c. This parameter introduces damping into this simple system.

The response of this SDOF system subjected to initial velocity and, also, cushioned impact is explored in this section. The results of a parametric study of typical hammer, pile and soil systems are then described.

2.3.2 Piles subjected to Initial Velocity

The response of the spring–slider mechanism to static loading is depicted in Fig. 2.4*a*. When the pile penetrates the soil, it compresses it elastically to a limiting distance termed the quake Q, and plastic failure occurs when the ultimate soil resistance R is attained. Under dynamic loading conditions the response is more complex as shown in Fig. 2.4*b*. This is, of course, the response characteristic of the Kelvin rheological model, depicted in Fig. 2.5.

The initial motion of a rigid pile subjected to an initial velocity V_0 under these conditions be determined from the well–known theory of linear elasto–dynamics. The governing equation is:

$$m \ddot{x} + c \dot{x} + k x = 0 \qquad (2.10)$$

where,

c is the damping coefficient,

k is the soil stiffness, and,

x, $\dot{x}$ and $\ddot{x}$ are the displacement, velocity and acceleration, respectively.

Equation 2.10 has the general solution:

$$x = e^{\beta t} \qquad (2.11)$$

which yields the following roots:

$$\beta_{1,2} = \frac{1}{2\ m} \left(-c \mp \sqrt{\Delta}\ \right) \qquad (2.12)$$

where, the discriminant Δ is given by the equation:

$$\Delta = c^2 - 4\ k\ m \qquad (2.13)$$

Depending on the magnitude and the sign of the discriminant, three distinct mathematical cases can be identified corresponding to the physical states of overdamping, critical damping and underdamping.

Data from Novak (1977) for harmonic loading of axially loaded single piles (and utilised by Randolph and Simons (1986) to develop an improved wave equation model) suggests that critical damping is a reasonable approximation here. This conclusion may be verified by calculation based on the following values for the constants:

$$m = \pi\ r^2\ L\ \rho_p$$

$$k = 2.9\ G\ L$$

$$c = 2\pi\ r\ L\ (\rho\ G)^{1/2}$$

where,

r is the pile radius,

L is the pile length,

G is the soil shear modulus,

ρ is the soil mass density, and,

ρ_p is the pile mass density.

This result is in accord with the physical intuition that a pile subjected to an initial velocity will rapidly come to rest. For critical damping, the displacement–time relation is:

$$x = (C_1 + C_2\ t)\ e^{-(\frac{ct}{2m})} \qquad (2.14)$$

Substitution of the initial conditions:

$$x(0) = 0$$

$$\dot{x}(0) = V_0 \qquad (2.15)$$

yields

$$C_1 = 0$$

$$C_2 = V_0$$

Thus, in general:

$$x = V_0 \; t \; e^{-(\frac{ct}{2m})} \qquad (2.16)$$

resulting in the type of motion depicted qualitatively in Fig. 2.6. However, in practice permanent deformations will occur when the pile displacement exceeds the elastic limit. At this juncture, equation 2.16 no longer applies. During plastic pile penetration, the spring–slider model furnishes a constant resistance, namely R. Furthermore, the viscous resistance reduces substantially since if slip takes place along the pile shaft, radiation damping into the surrounding soil would be sharply curtailed. Hence, the magnitude of the viscous coefficient (c) during plastic pile penetration is likely to be substantially smaller than the values used in equation 2.16. Consequently, during plastic pile penetration, the response is governed approximately by the equation:

$$m \ddot{x} + R = 0 \qquad (2.17)$$

Choosing a new origin in time/displacement space at the onset of soil failure; integrating of equation 2.17 yields:

$$x = V_1 \; t - \frac{R}{m} \; t^2 \qquad (2.18)$$

where,

V_1 is the velocity of the pile at the onset of soil failure,

t is the time from this point, and,

x is the permanent displacement.

Consequently, the permanent set (maximum plastic deformation) is:

$$S = \frac{m \; V_1^{\,2}}{4 \; R} \qquad (2.19)$$

Clearly, for practical purposes, equation 2.19 is insufficient since the velocity V_1 is not known at the outset. Further, equation 2.16 is not amenable to direct analytical solution. Recourse has therefore been made to a numerical solution, the results which are depicted in Fig. 2.7. This shows that the velocity ratio (V_1/V_0) is approximately linearly related to the product $\alpha\beta$, where:

$$\alpha = \frac{Q}{V_0}$$

$$\beta = \frac{c}{2\ m} \qquad (2.20)$$

Assuming, the empirical relationship:

$$\frac{V_1}{V_0} = 1 - 2\ \alpha\beta \qquad (2.21)$$

we obtain;

$$S = \frac{m}{4\ R}\left(V_0 - \frac{Q\ c}{m} \right)^2 \qquad (2.22)$$

This result shows that there is some threshold initial velocity below which pile driving becomes ineffective, typically one or two meters per second. At high initial velocities, equation 2.22 simplifies after re–arrangement to;

$$R = \frac{m\ V_0^{\,2}}{4\ S} \qquad (2.23)$$

Assuming no energy loss at ram impact, this equation can be rewritten, in Janbu (formula) equation form, as:

$$R = \frac{1}{k}\ \frac{W\ H}{S} \qquad (2.24)$$

where W is the weight of the ram and

$$k = \frac{(1 + b)^2}{2b} \tag{2.25}$$

and the pile/ram mass ratio b is defined as follows:

$$b = \frac{W_p}{W} \tag{2.26}$$

Typical values of the pile/ram mass ratio are approximately 0.5 leading to k values of 1.1 which are similar to those obtained using the Janbu formula. Further development of this approach would be possible but has not been pursued here since the basic premises of the SDOF model are too simplistic to warrant exhaustive analysis. In the reminder of this Chapter, the major thrust is the exploration of a rather more complex model by numerical means as a prelude to the study of the wave equation method of analysis. This model is superficially similar to the nonlinear Kelvin model described above, i.e. it consists of a slider–spring and a dashpot, but there is one important difference; the dashpot is not independent of the slider–spring mechanism. Under elastic conditions, the governing differential equation is:

$$m \ddot{x} + J k x \dot{x} + k x = 0 \tag{2.27}$$

where J is the viscosity parameter.

Under plastic conditions, the corresponding equation is:

$$m \ddot{x} + J R \dot{x} + R = 0 \tag{2.28}$$

where

$$R = k\ Q \tag{2.29}$$

This rather unusual formulation originates from Smith's (1960) work on the wave equation and may alternatively be described in terms of a "dynamic" soil resistance (under elastic conditions);

$$F = k\ x\ (\ 1 + J\ V\ ) \tag{2.30}$$

Equations 2.27 and 2.28 are too complex to admit analytical solutions, and, consequently, an incremental numerical solution based on rigid body mechanics was developed as follows. Assuming the pile displacement at time t is x_t, the displacement after time increment Δt is (approximately);

$$x_{t+\Delta t} = x_t + V_t\ \Delta t \tag{2.31}$$

where V_t is the velocity of the pile at time t.

This displacement compresses the soil spring resulting in a resisting force R;

$$R = -\ k\ x_{t+\Delta t}\ (\ 1 + J\ V\ ) \tag{2.32}$$

The resulting velocity is given by the equation;

$$V_{t+\Delta t} = V_t + \frac{R}{m}\ \Delta t \tag{2.33}$$

Equations 2.31–2.33 form the basis for a simple incremental (in time) solution strategy. Provided that sufficiently small time steps are employed, the process is convergent. In addition, in view of the single degree of freedom,

computational costs are very modest. The computer program which was used to generate the results presented in the following section is listed in Appendix C.

2.3.3 Results

For convenience, the model parameters used in the study have been expressed in dimensionless form as follows. The natural circular frequency of vibration of the undamped system is:

$$\omega = \sqrt{(\frac{k}{m})} \qquad (2.34)$$

Hence, dimensionless time (T) is defined by the product;

$$T = \omega\ t \qquad (2.35)$$

Velocities are normalised with respect to the damping coefficient, thus;

$$\overline{V} = J\ V \qquad (2.36)$$

Displacements are normalised with respect to quake, i.e.

$$\overline{X} = \frac{x}{Q} \qquad (2.37)$$

And, finally, the natural circular frequency of vibration is rendered dimensionless as follows:

$$\omega = \omega \; Q \; J \qquad (2.38)$$

Fig. 2.8 shows the algorithm's convergence characteristics with respect to the displacement–time relationship for a typical pile. The results show that convergence is rapid and suggests that useful results can be obtained with as large as a dimensionless time interval (ω t) 0.1. In each case, the following parameters were assumed, Q= 2.5mm, J= 0.5s/m, m= 2000kg.

Fig. 2.9 shows the algorithm's convergence characteristics with respect to maximum displacement for three soils (ω = 0.05, 0.2 and 0.5). Again, the results converged in each case provided that a sufficiently small time interval (ω t< 0.1) was adopted.

Fig. 2.10 shows a similar plot for the same pile but in this case, the initial (dimensionless) velocity of the pile is much higher, i.e. increased from unity (in Fig. 2.9) to four. Convergence is affected by this change in velocity. However, the results of the three different soils all now converge to the "analytical" solution– a solution obtained by assuming that the elastic response of the soil may be neglected. As expected the "analytical" solution provides excellent results for piles subjected to high initial velocities since these undergo much higher (plastic) displacements. however for low initial velocities, pile response is dominated by the soils elastic behaviour.

Fig. 2.11 shows the pile maximum displacement–initial velocity relationship. It is clear that greater initial velocities results in greater displacement. Typically, a fourfold increase in initial velocity causes a ninefold increase in pile displacement. Under constant force restraint, a sixteenfold increase in maximum displacement would be expected but viscosity rapidly slows the pile down in the early stages of pile penetration.

Fig. 2.12 shows the maximum pile displacement–soil stiffness relationship and, in particular, that these displacement may be very large in soft soils.

Fig. 2.13 shows the time taken for piles to reach their maximum displacements for various soil conditions and a range of initial velocities. Clearly, high soil stiffness is associated with fast peak response times as are high initial velocities.

In order to assess the physical validity of this model we consider the following typical case:

Steel pipe pile; L = 30 m
A = 0.01 m^2
m = 2400 kg
ω = 288 rad/s
Soil; (soft normally consolidated clay)
Q = 2.5 mm
J = 0.5 s/m
K_s= $2x10^8$ N/m

The pile is subjected to an initial velocity V_0 of 4 m/s. The corresponding dimensionless parameters are:
$V = J\ V = 2$; $\bar{\omega} = \omega\ Q\ J = 0.36$,

and therefore the corresponding maximum displacement from Fig. 2.12 is X/Q = 20, i.e. a displacement of 50 mm. This is a rather high penetration and suggests that real piles would not gain this magnitude of linear momentum.

2.3.4 Piles subjected to Cushioned Impact

Cushioned impact can be treated in the same manner as before except that an additional mass is used to model the ram and, also, the cushion is modelled by a spring capable of transferring compression but not tension, Fig. 2.14.

An approximate solution for the forcing function, F(t) supplied by the ram can be found by considering the mass–spring system depicted in Fig. 2.15. The governing equation is;

$$m_r \ddot{x} + k_r x = 0 \qquad (2.39)$$

where,

m_r is the ram mass, and,

k_r is the cushion stiffness.

Solving, we obtain;

$$x = \frac{V_0}{\omega} \sin(\omega t) \qquad (2.40)$$

where V_0 is the impact velocity of the ram, and,

$$\omega = \sqrt{\left(\frac{k_r}{m_r}\right)} \qquad (2.41)$$

Thus, from Newton's second law;

$$F(t) = V_0\ \omega\ m_r \sin(\omega t) \qquad (2.42)$$

and, since the spring cannot sustain tension, the forcing function represents a half–sine function. In practice, the peak force will be rather less than $V_0\ \omega\ m_r$ since the support (pile) will displace downwards during impact.

Optimum Time Interval

In this numerical model, the optimum time interval (the largest time interval which produces an accurate solution) is found to be a function of several variables. Clearly, both the impact and the pile displacement have to be properly modelled. Assuming a dimensionless time interval of 0.01 (by reference to the convergence rate for piles subjected to initial velocities), the optimum time interval will be the lesser of the following:

$$\dot{t} = \frac{0.01}{\omega}$$

$$\dot{t} = \frac{0.01}{\omega_r} \qquad (2.43)$$

where ω and ω_r are the natural frequencies of vibration of the pile/soil system and the ram/cushion system, respectively.

2.3.5 Results

The parameters which form the basis of the parametric study are as follows:

Hammer; m_r= 1600 kg

V_r= 6 m/s (impact velocity)

Cushion; k_r=6x10^8 N/m

Soil; Q = 2.5 mm

J = 0.5 s/m

k_s= 8x10^9 N/m

Steel pipe pile; L = 20 m

A = 0.01 m^2

m_p=1600 kg

The corresponding non–dimensional parameters are;
$m_r/m_p = 1$, J V= 3, $k_r/k_p = 6$, L/Q= 8000 and $k_s/k_p = 8$.

The effect of increasing the ram mass/pile mass ratio from unity to three ($m_r/m_p = 1$ to $m_r/m_p = 3$) on the peak ram force is shown in Figs. 2.16 and 2.18, respectively. This large increase of the ram mass causes typically, only a thirty percent increase in the peak ram force. But this causes a corresponding threefold increase in the pile maximum displacement (or set) as depicted in Figs. 2.17 and 2.19.

Figs. 2.20 and 2.22 show the effect of increasing the ram velocity from 2 m/s to 8 m/s (JV= 1 to JV= 4), on the peak ram force. This causes a typical increase in the peak ram force of ninety five percent, which results in a very

significant sixfold increase in the pile displacement, shown in Figs. 2.21 and 2.23.

The effect of increasing the cushion stiffness from $k_r/k_p = 3$ to $k_r/k_p = 10$, on the peak ram force, is shown in Figs. 2.24 and 2.26. The stiff cushion causes a typical increase in the peak ram force of fifty percent. However, this only results in a minor increase (6%) in the peak displacement of the pile, Figs. 2.25 and 2.27.

Figs. 2.28 and 2.30 show the effect of driving the same pile in soft and stiff soils ($k_s/k_p = 5$ to $k_s/k_p = 10$, respectively). The increased soil stiffness does not increase the peak ram force markedly. However, in the stiff soil the pile displacement is decreased by about fifty percent, as depicted in Figs. 2.29 and 2.31.

The effect of increasing the pile length from 10 m to 60 m ($L/Q = 4000$ to $L/Q = 12000$, respectively) on the peak ram force is rather small as shown in Figs. 2.32 and 2.34, respectively. This increase in pile length (keeping the other nondimensional parameters unchanged) implies an increase in ram mass in proportion to pile length and hence a high displacement is obtained as expected, Figs. 2.33 and 2.35.

2.3.6 Discussion

These simple models are inadequate from the practical point of view since they seem to yield unrealistic values of permanent set (based on values of the corresponding wave equation parameters) and fail to capture the complex detail of pile motion after impact. The results indicate that heavier ram masses and high ram velocities produce higher pile sets but cushion stiffnesses have only a minor effect on pile driveability.

2.4 CONCLUSION

Pile driving formulae and single degree of freedom models can only provide very approximate solutions to the pile driving problem because they ignore the complex interactions that take place between piles and the surrounding soil. Further, they are based on highly idealised representations of soil behaviour and neglect wave propagation along the pile and energy radiation into the soil. The wave equation approach, which is discussed in the following Chapter, rectifies some of these omisions by taking into account the axial compressibility of piles.

Formula	Equation for R_u	Remarks
Sanders	$\frac{WH}{S}$	
Engineering News	$\frac{WH}{S+C}$	C = 1.0 in. for drop hammer 0.1 in. for steam hammer 0.1 W_p/W in. for steam hammer on very heavy piles
Eytelwein (Dutch)	$\frac{WH}{S} \cdot \frac{W}{W+W_p}$	
Weisbach	$-\frac{SAE_p}{L} + \sqrt{\left(\frac{2WHAE_p}{L}\right) + \left(\frac{SAE_p}{L}\right)^2}$	
Hiley	$\frac{e_f WH}{S+\frac{1}{2}(C_1+C_2+C_3)} \cdot \frac{W+n^2 W_p}{W+W_p}$	See Tables 2.2, 2.3 and 2.4 for values of e_f, C_1, C_2, C_3, and n.
Janbu	$\left(\frac{1}{k_u}\right)\left(\frac{WH}{S}\right)$	$k_u = C_d(1+\sqrt{1+\gamma e/C_d})$ $C_d = 0.75 + 0.15\ W_p/W$ $\lambda e = WHL/AES^2$
Danish	$\frac{e_f WH}{S+(2e_f WHL/AE_p)^{1/2}}$	See Table 2.2 for e_f values.
Gates	$5.6\sqrt{e_f WH}\log_{10}(10/S)$	Units are inches and tons (short).
	$4.0\sqrt{e_f WH}\log_{10}(25/S)$	Units are metric tons (1000 kg) and centimeters.

TABLE (2.1) SUMMARY OF PILE DRIVING FORMULAE

(After POULOS& DAVIS,1980)

Hammer Type	e_f
Drop hammer released by trigger	1.00
Drop hammer actuated by rope and friction winch	0.75
McKiernan-Terry single-acting hammers	0.85
Warrington-Vulcan single-acting hammers	0.75
Differential-acting hammers	0.75
McKiernan-Terry, Industrial Brownhoist, National & Union double-acting hammers	0.85
Diesel hammers	1.00

TABLE (2.2) VALUES OF THE HAMMER EFFICIENCY, e_f
(After CHELLIS, 1961)

Pile Type	Head Condition	Drop, Single-acting, or Diesel Hammers	Double-acting Hammers
Reinforced concrete	Helmet with composite plastic or greenheart dolly and packing on top of pile	0.4	0.5
	Helmet with timber dolly, and packing on top of pile	0.25	0.4
	Hammer direct on pile with pad only	–	0.5
Steel	Driving cap with standard plastic or greenheart dolly	0.5	0.5
	Driving cap with timber dolly	0.3	0.3
	Hammer direct on pile	–	0.5
Timber	Hammer direct on pile	0.25	0.4

TABLE (2.3) VALUES OF COEFFICIENT OF RESTITUTION, n
(After WHITAKER, 1970)

(a) *Values of* C_1

Temporary Compression Allowance C_1 for Pile Head and Cap

Material to Which Blow Is Applied	Easy Driving: P_1 = 500 psi on Cushion or Pile Butt If No Cushion (in.)	Medium Driving: P_1 = 1000 psi on Head or Cap (in.)	Hard Driving: P_1 = 1500 psi on Head or Cap (in.)	Very Hard Driving P_1 = 2000 psi on Head or Cap (in.)
Head of timber pile	0.05	0.10	0.15	0.20
3–4 in. packing inside cap on head of precast concrete pile	0.05 + 0.07[b]	0.10 + 0.15[b]	0.15 + 0.22[b]	0.20 + 0.30[b]
1/2–1 in. mat pad only on head of precast concrete pile	0.025	0.05	0.075	0.10
Steel-covered cap, containing wood packing, for steel piling or pipe	0.04	0.08	0.12	0.16
3/16–in. red electrical fiber disk between two 3/8–in. steel plates, for use with severe driving on Monotube pile	0.02	0.04	0.06	0.08
Head of steel piling or pipe	0	0	0	0

(b) *Value of* C_2

$C_2 = R_u L/AE_p$
(Include additional value for followers.)

(c) *Values of* C_3

C_3 is temporary compression allowance for quake of ground.
Nominal value = 0.1 inches
Range = 0.2 for resilient soils to 0 for hardpan

[b] The first figure represents the compression of the cap and wood dolly or packing above the cap, whereas the second figure represents the compression of the wood packing between the cap and the pile head.

TABLE (2.4) VALUES OF C_1, C_2, C_3 FOR HILEY FORMULA
(After CHELLIS, 1961)

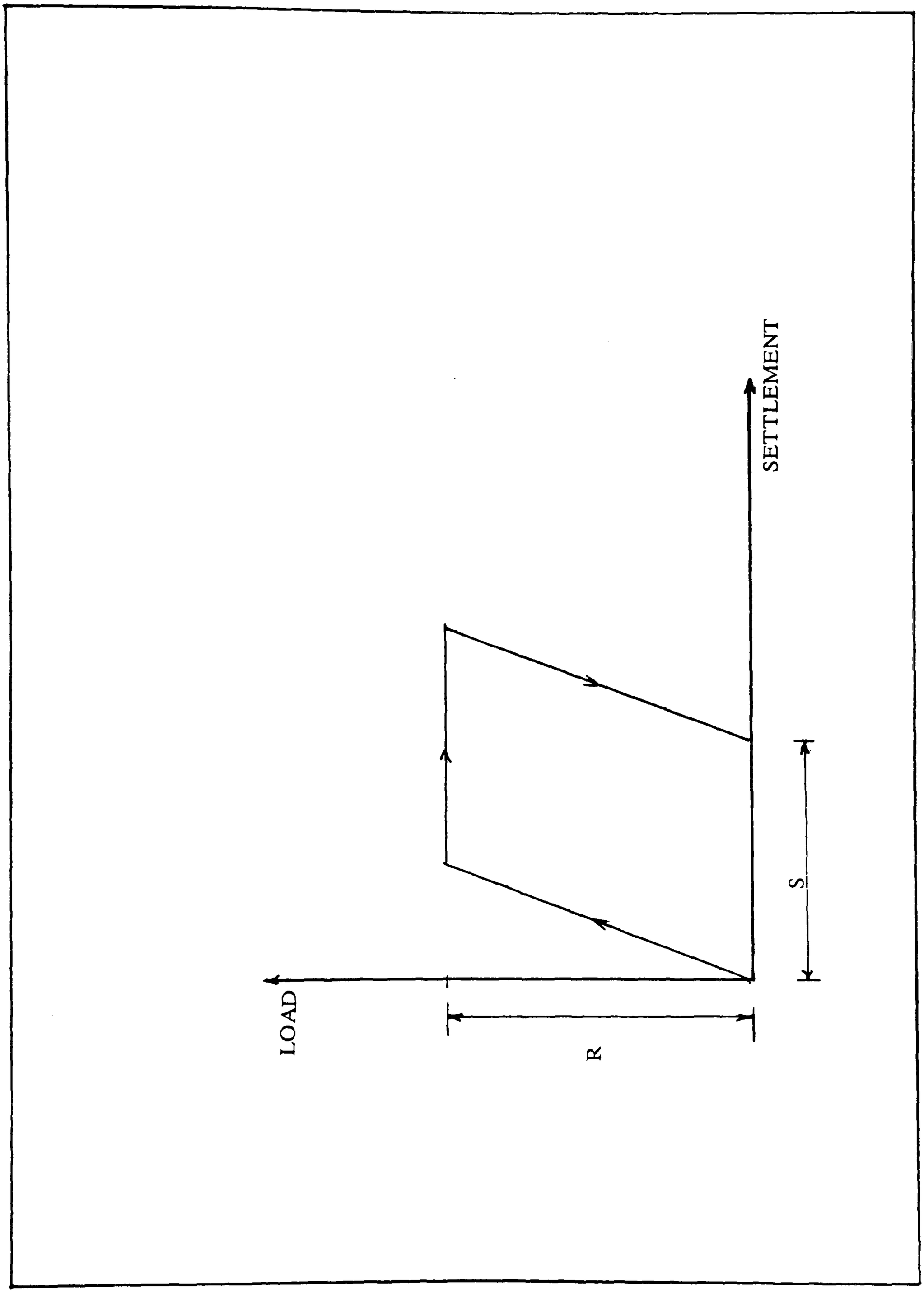

FIGURE (2.1) ASSUMED LOAD_SETTLEMENT CURVE FOR PILE

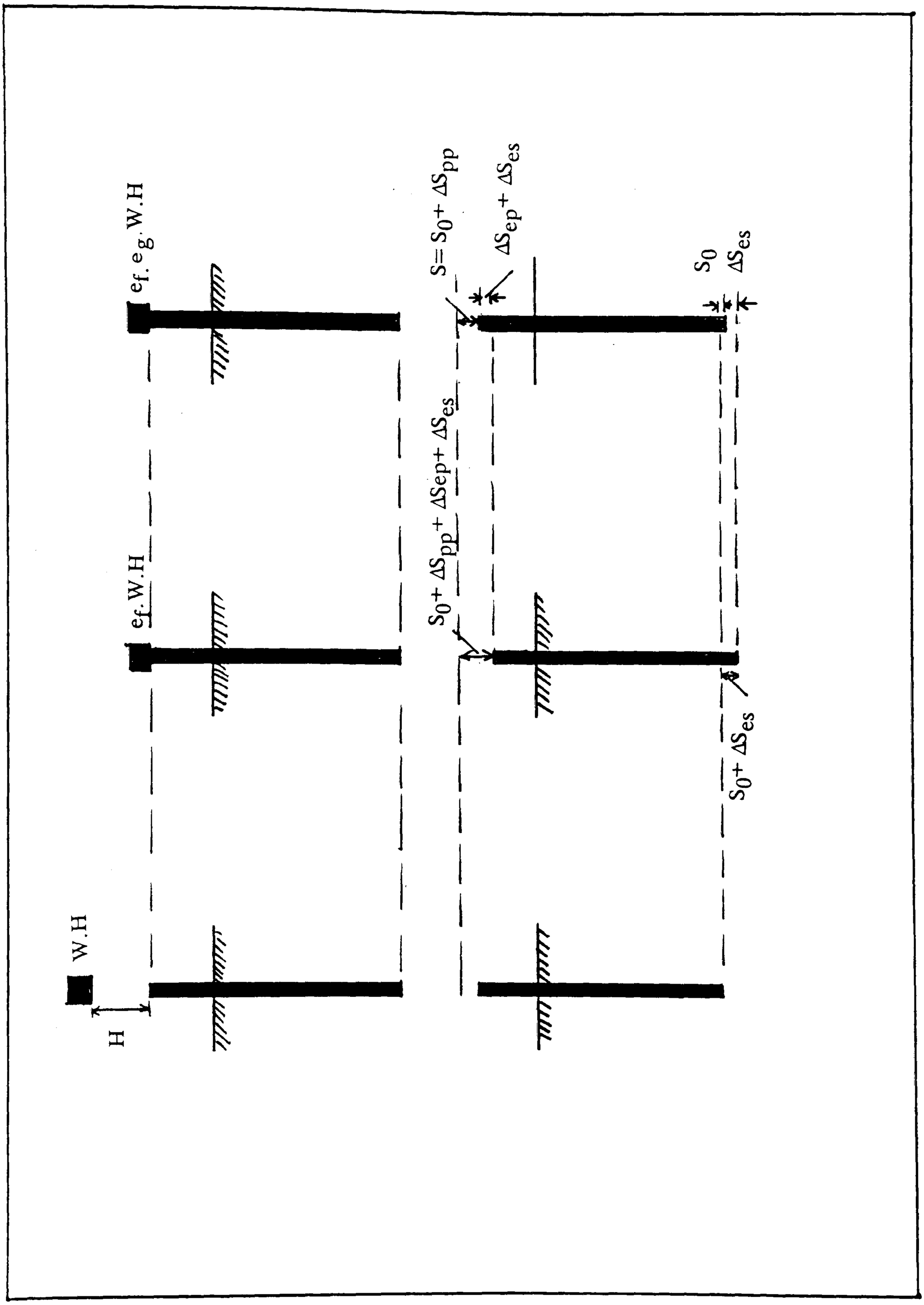

FIGURE (2.2) TRANSFER OF ENERGY AND PENETRATION OF PILE DURING ONE BLOW OF THE PILE DRIVING HAMMER (AFTER FLAATE, 1964)

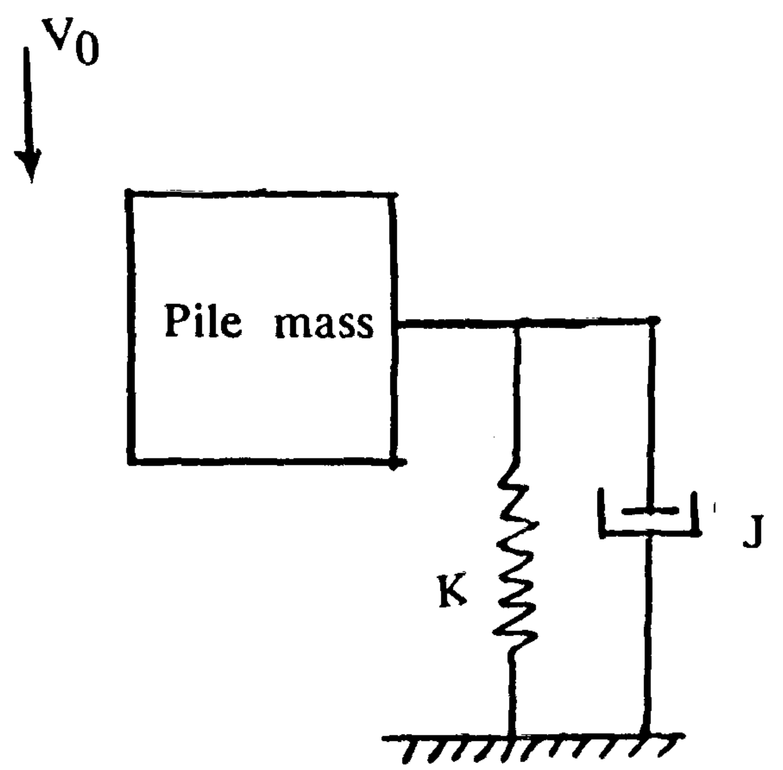

(a)

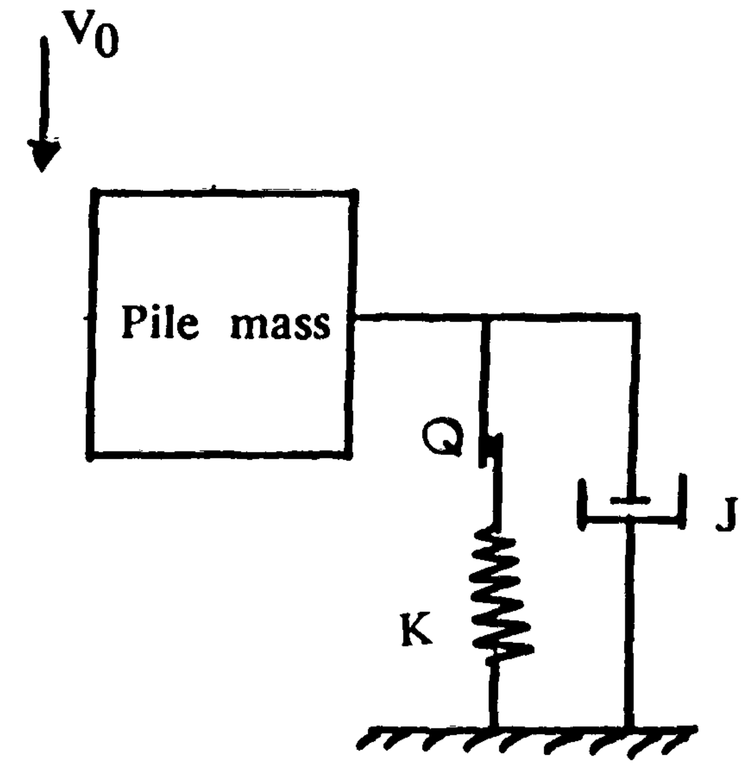

(b)

FIGURE (2.3) SINGLE DEGREE OF FREEDOM MODELS

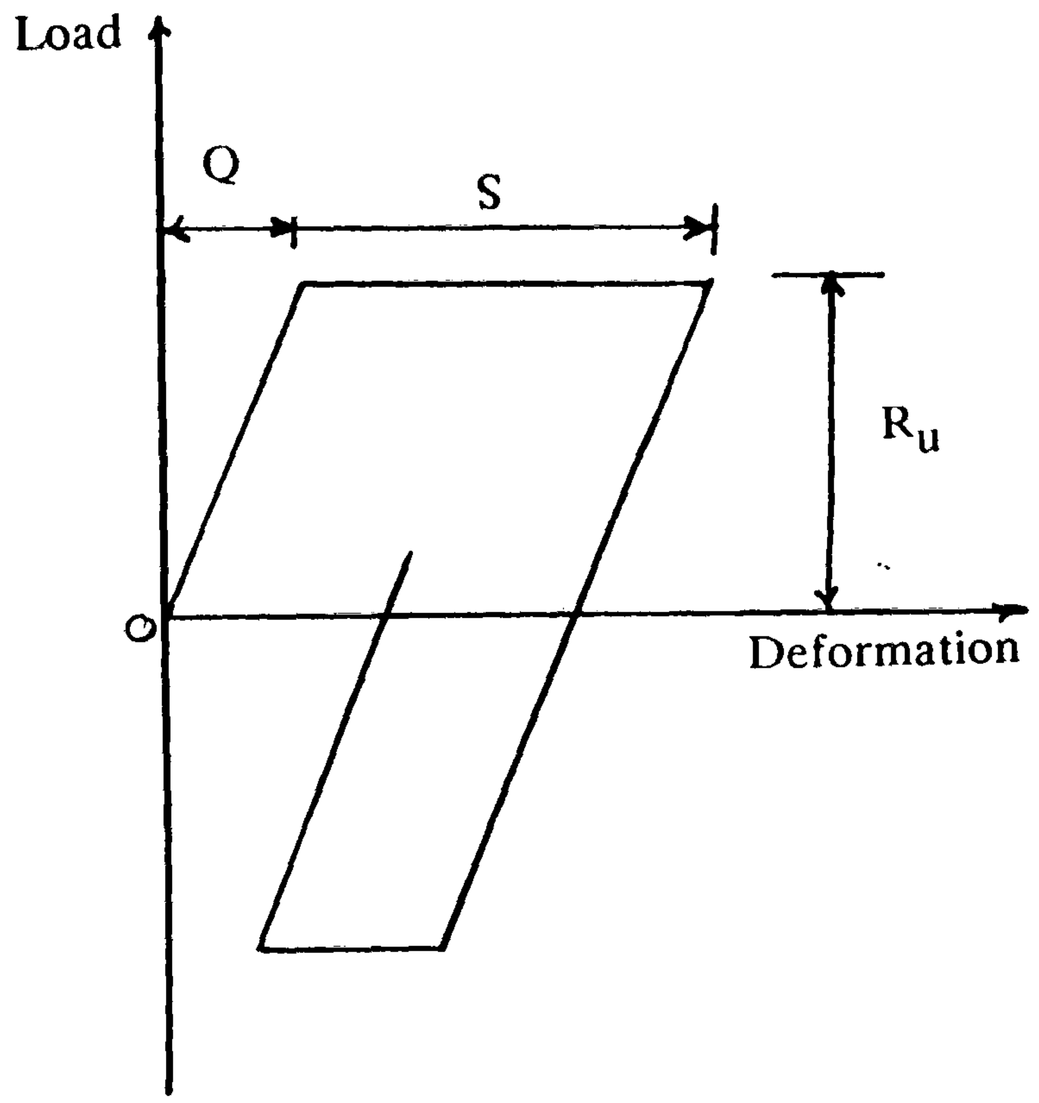

(a) Static Loading

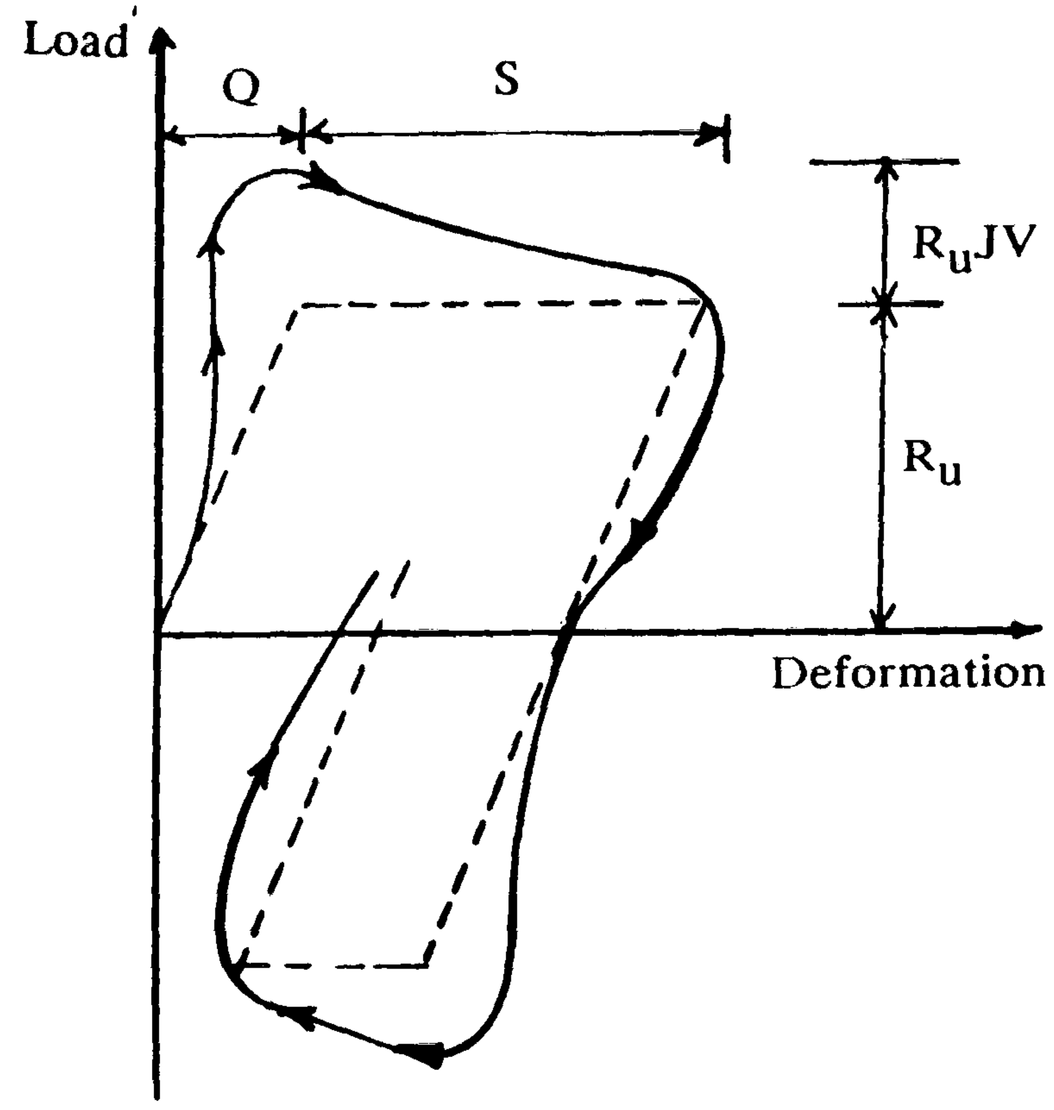

(b) Dynamic Loading

FIGURE (2.4) LOAD_DEFORMATION RELATIONSHIPS FOR SOIL

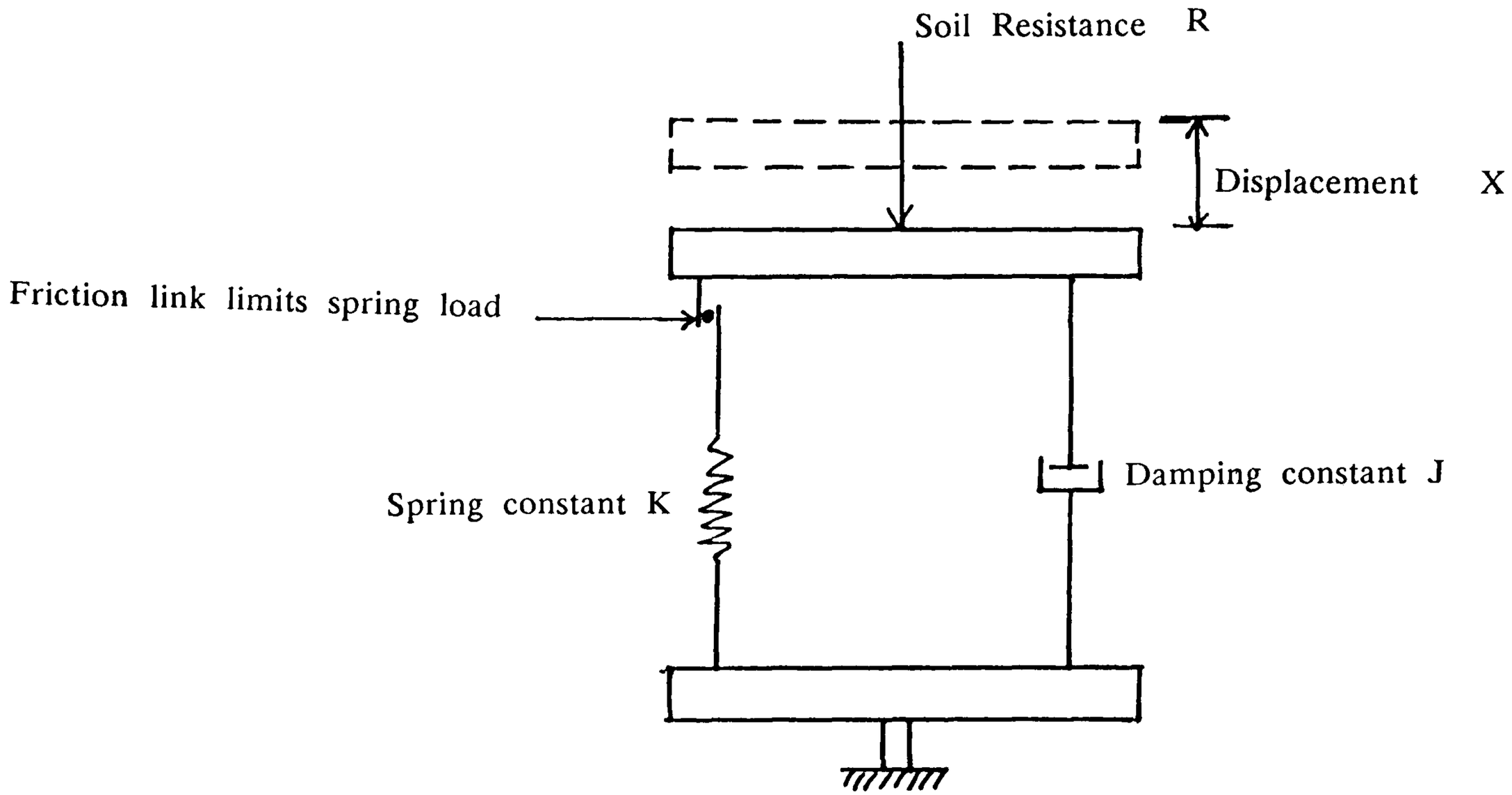

FIGURE (2.5) KELVIN RHEOLOGICAL MODEL OF SOIL

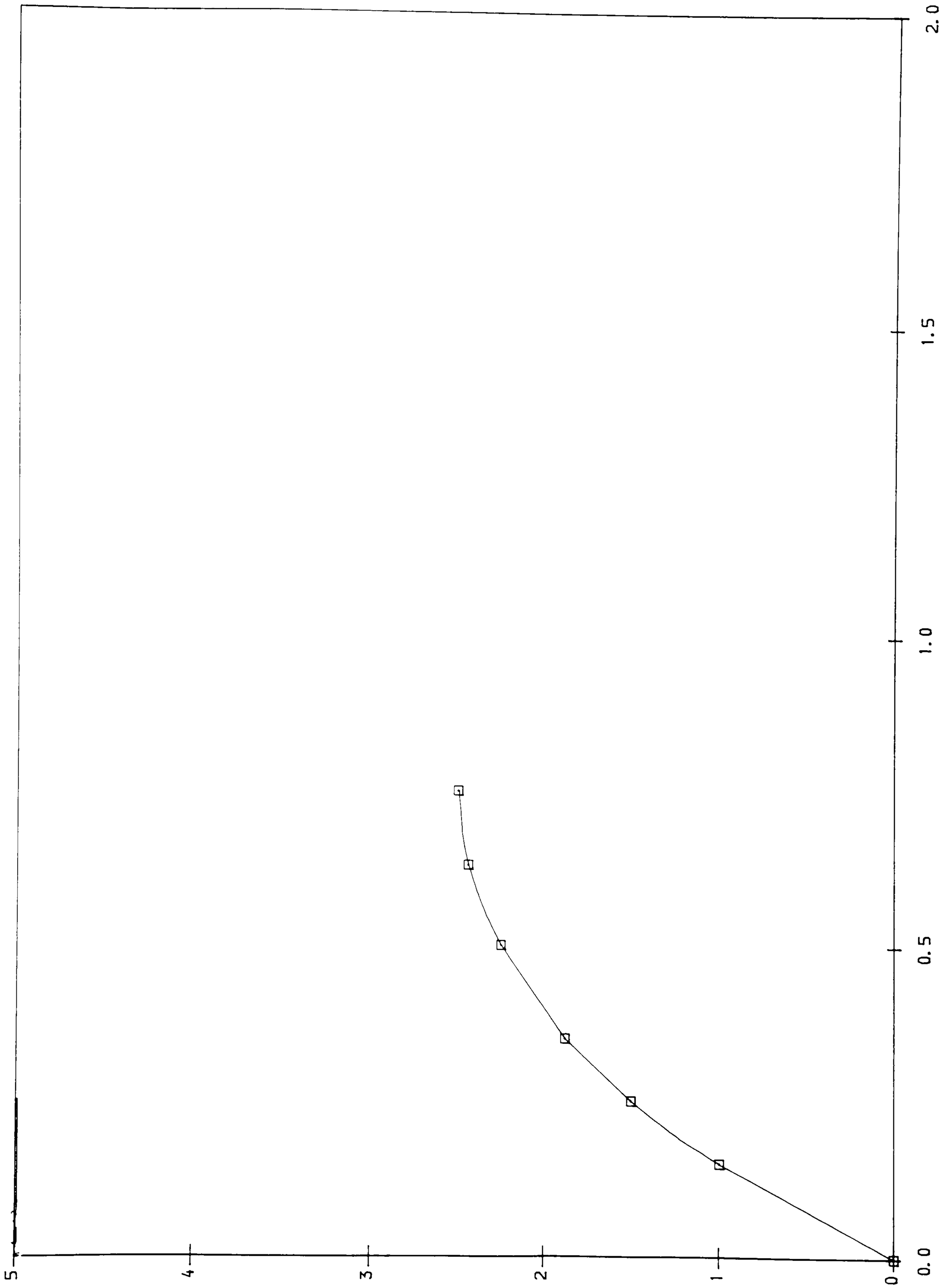

FIGURE (2.6) ELASTIC DISPLACEMENT_TIME RELATIONSHIP

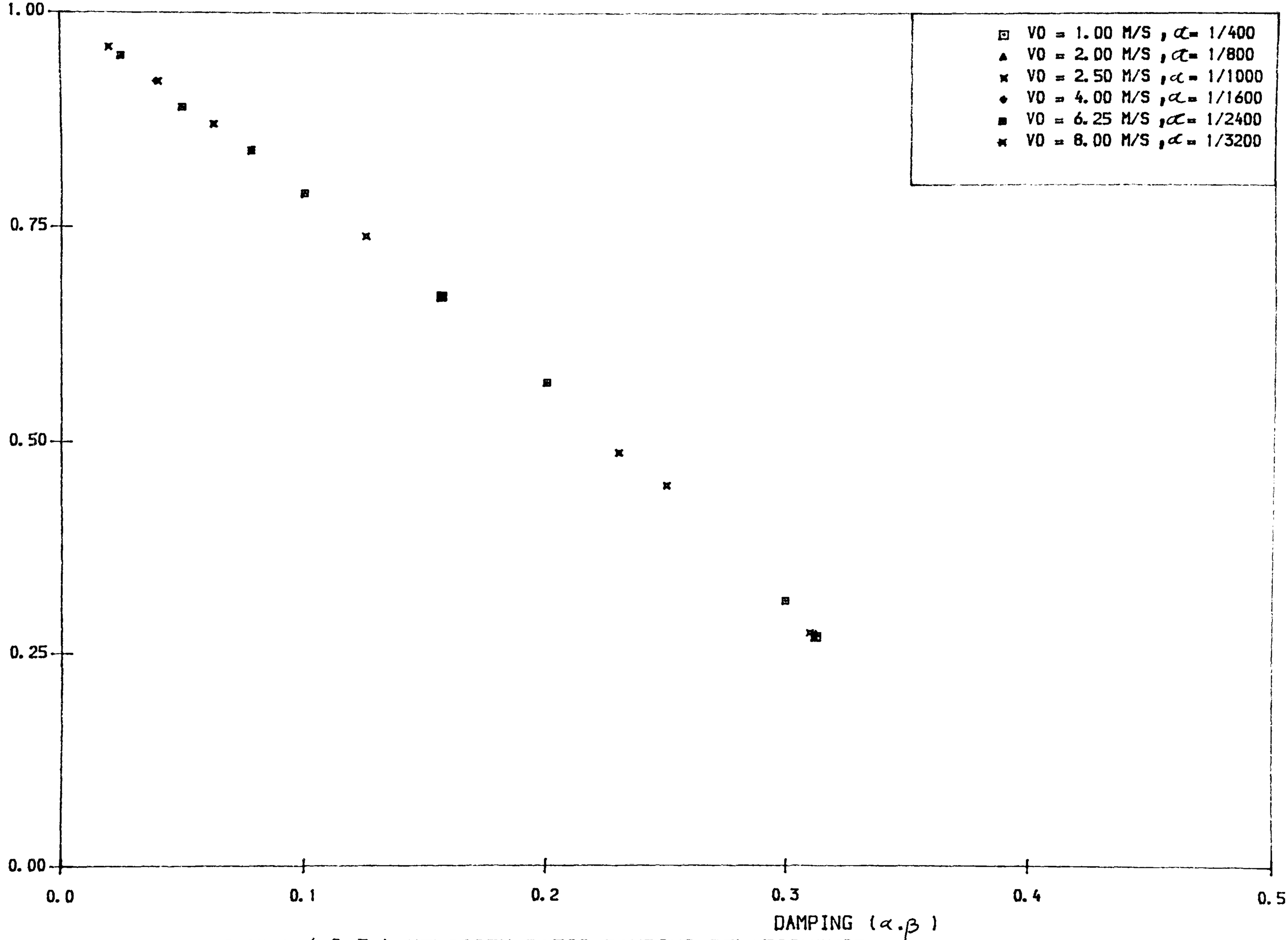

FIGURE (2.7) VELOCITY RATIO_DAMPING RELATIONSHIP

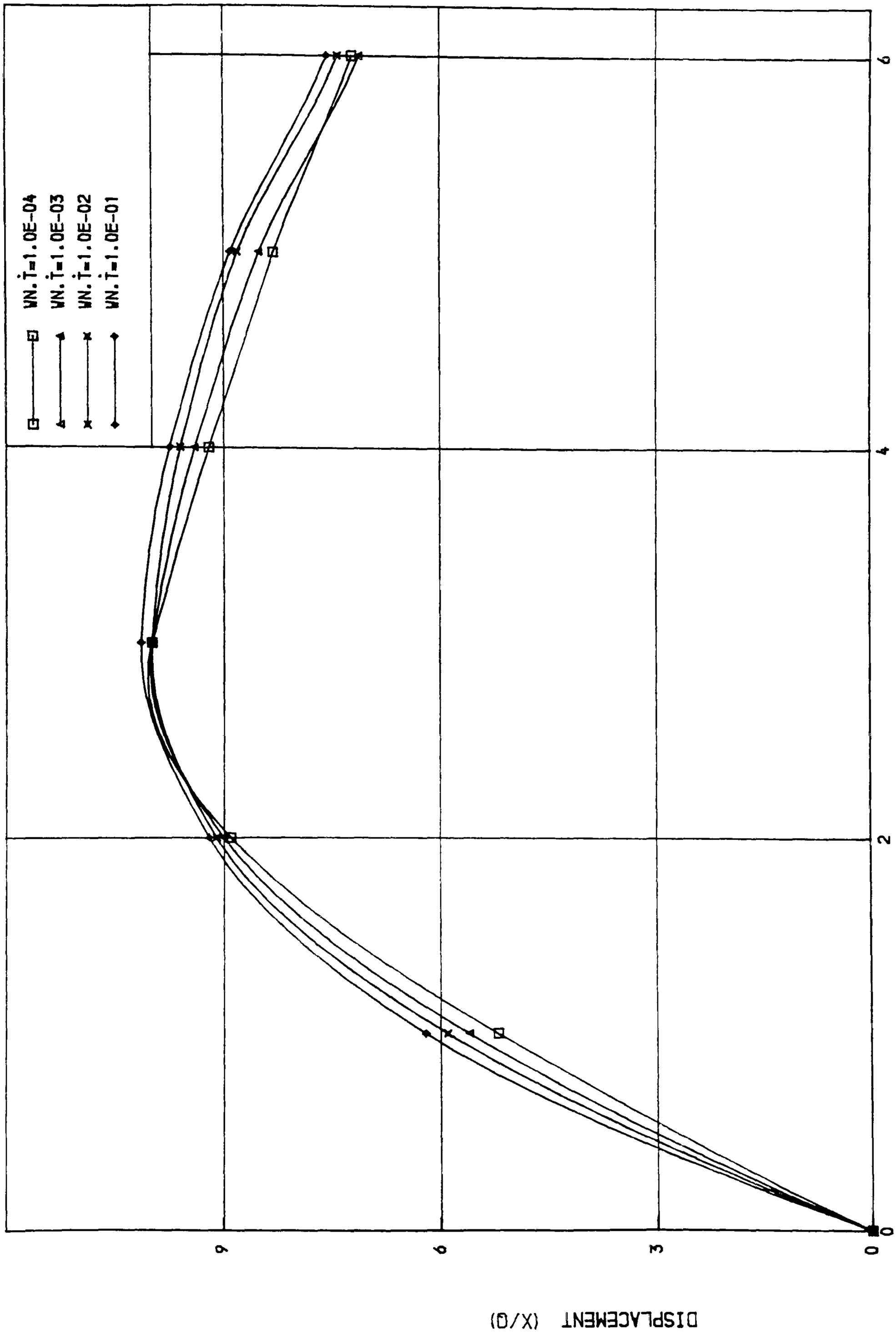

FIGURE (2.8) MAXIMUM PILE DISPLACEMENT_TIME RELATIONSHIP OF A SINGLE MASS PILE SUBJECTED TO AN INITIAL VELOCITY

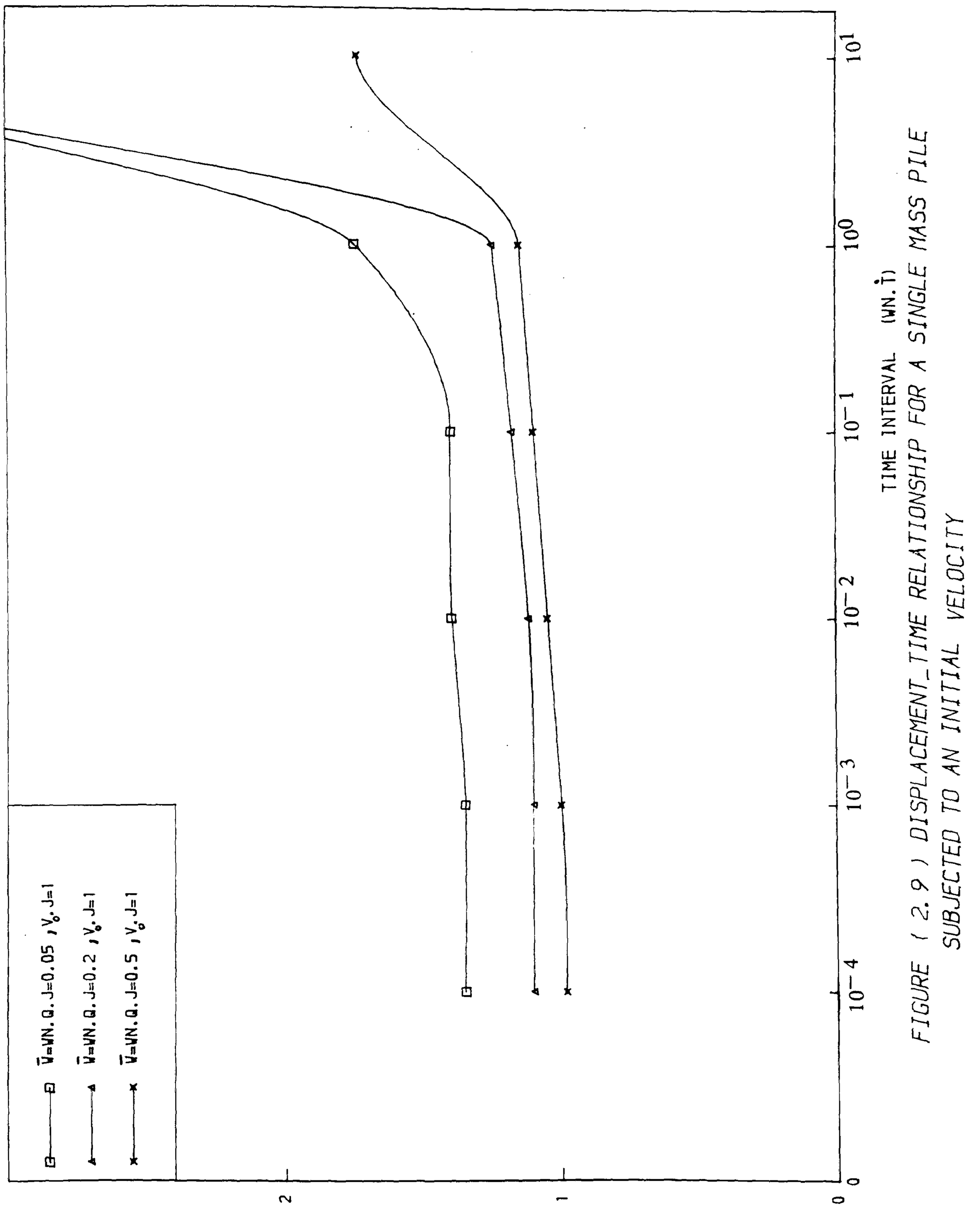

FIGURE (2.9) DISPLACEMENT_TIME RELATIONSHIP FOR A SINGLE MASS PILE SUBJECTED TO AN INITIAL VELOCITY

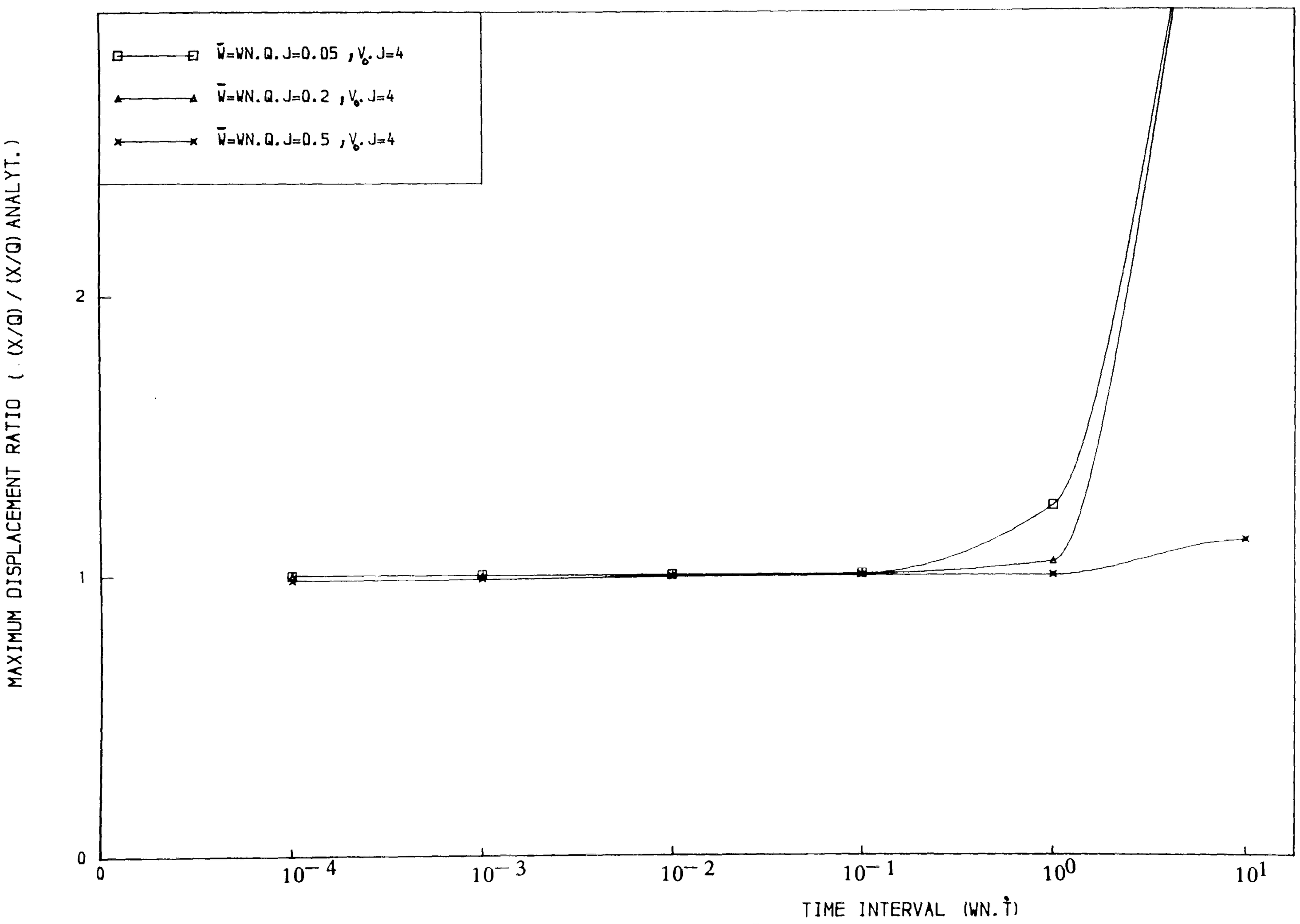

FIGURE (2.10) MAXIMUM PILE DISPLACEMENT_TIME INTERVAL RELATIONSHIP OF A SINGLE MASS PILE SUBJECTED TO AN INITIAL VELOCITY

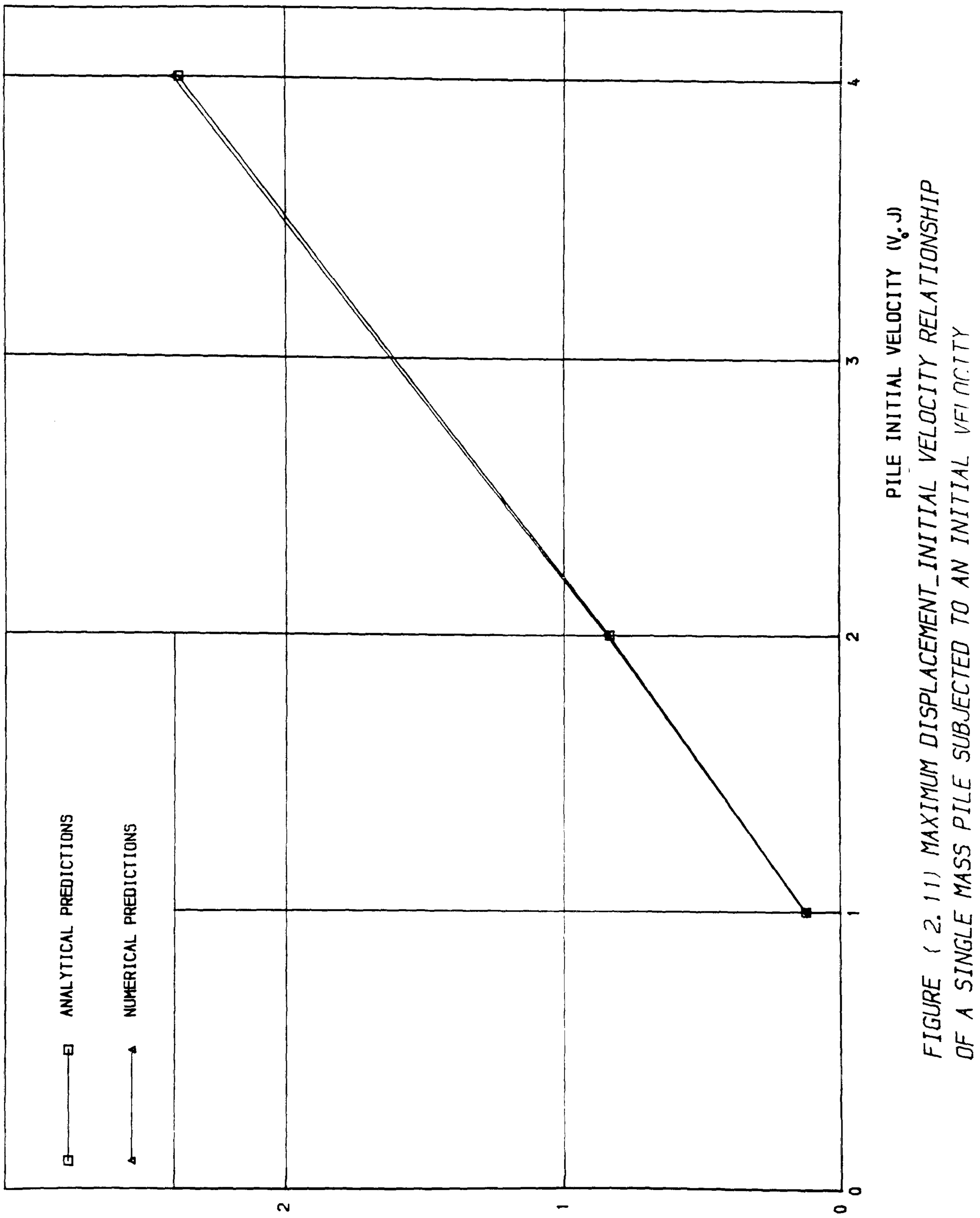

FIGURE (2.11) MAXIMUM DISPLACEMENT_INITIAL VELOCITY RELATIONSHIP OF A SINGLE MASS PILE SUBJECTED TO AN INITIAL VELOCITY

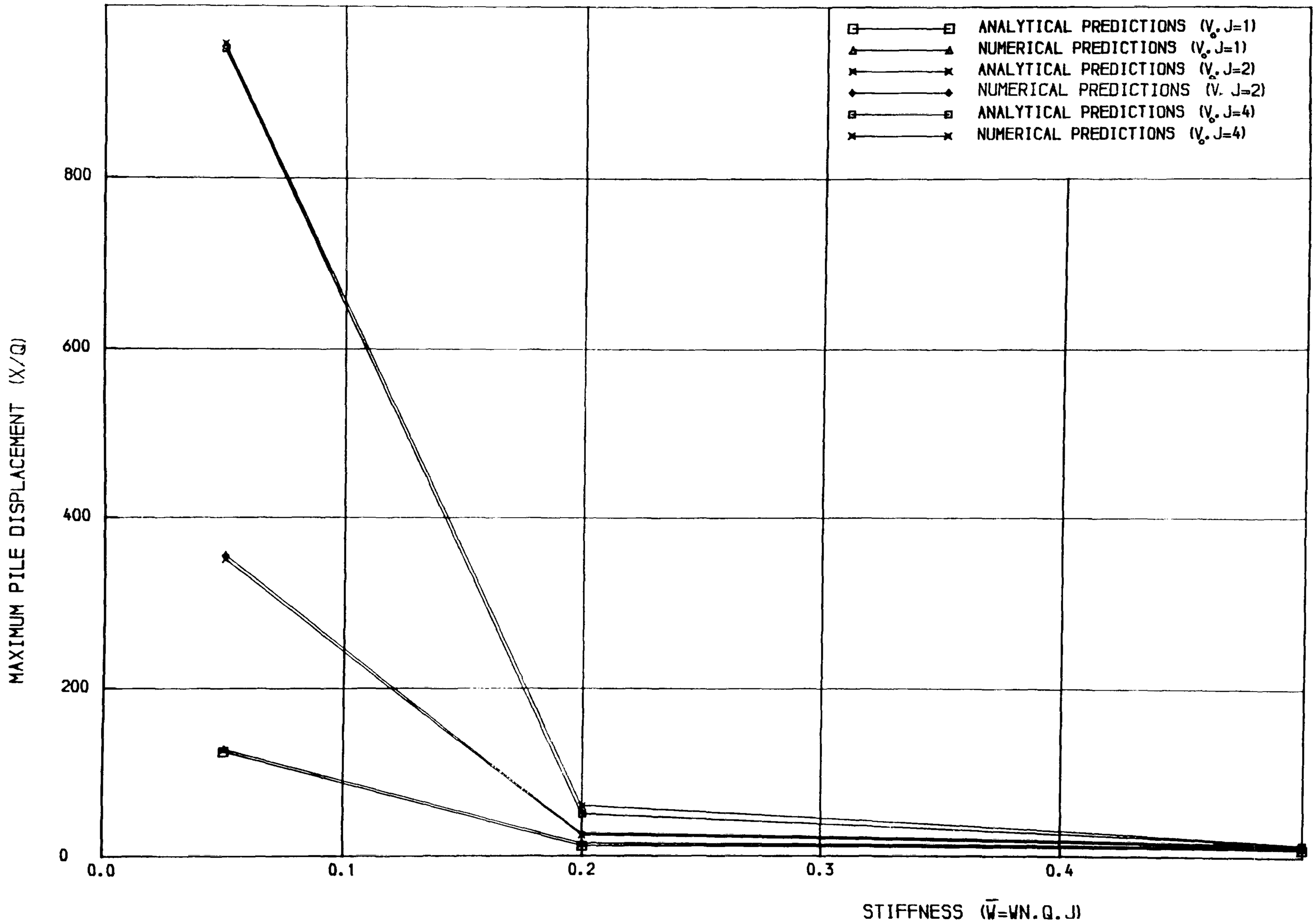

FIGURE (2.12) MAXIMUM PILE DISPLACEMENT_SOIL STIFFNESS RELATIONSHIP OF A SINGLE MASS PILE SUBJECTED TO AN INITIAL VELOCITY

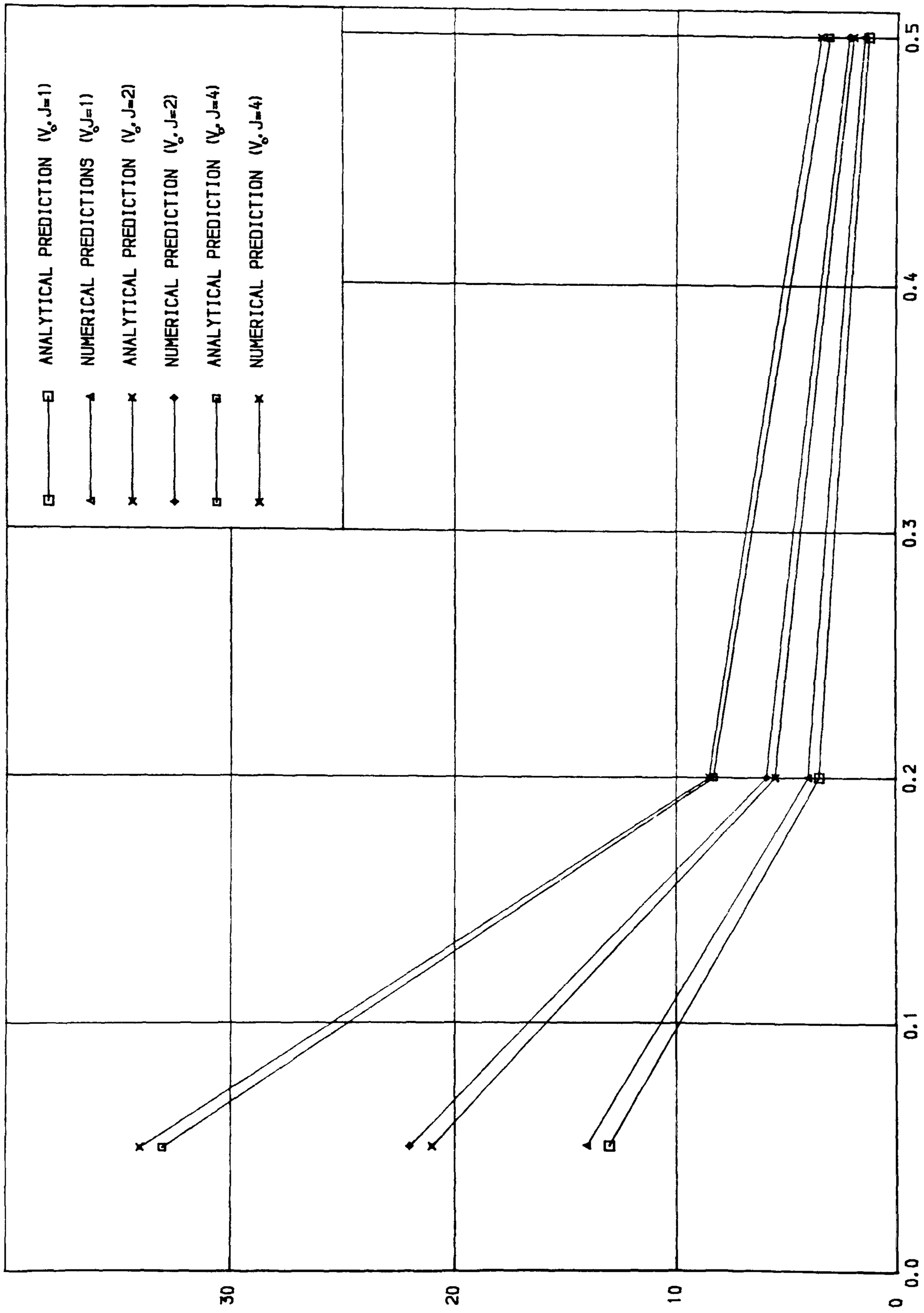

FIGURE (2. 13) TIME AT MAXIMUM PILE DISPLACEMENT_SOIL STIFFNESS RELATIONSHIP OF A SINGLE MASS PILE SUBJECTED TO AN INITIAL VELOCITY

TEXT CUT OFF IN ORIGINAL

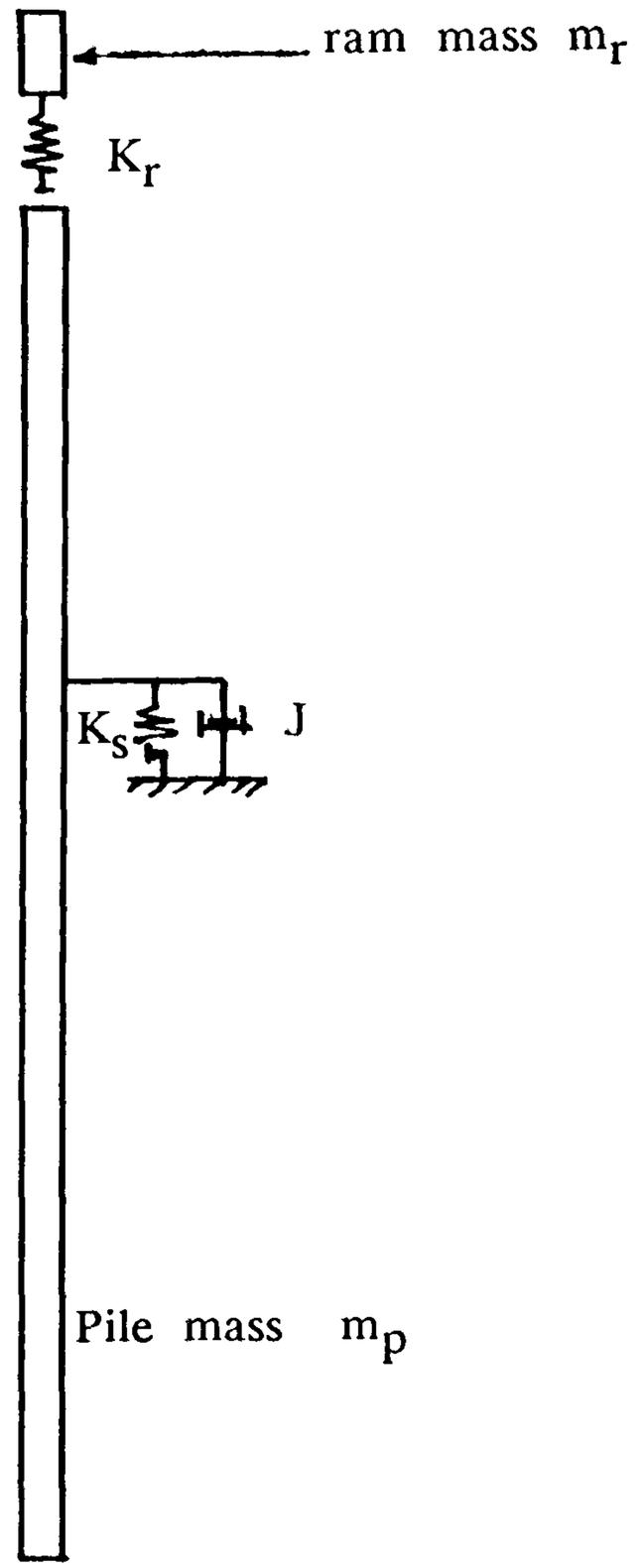

FIGURE (2.14) FREE BODY DIAGRAM OF A SINGLE MASS PILE SUBJECTED TO A CUSHIONED HAMMER IMAGT

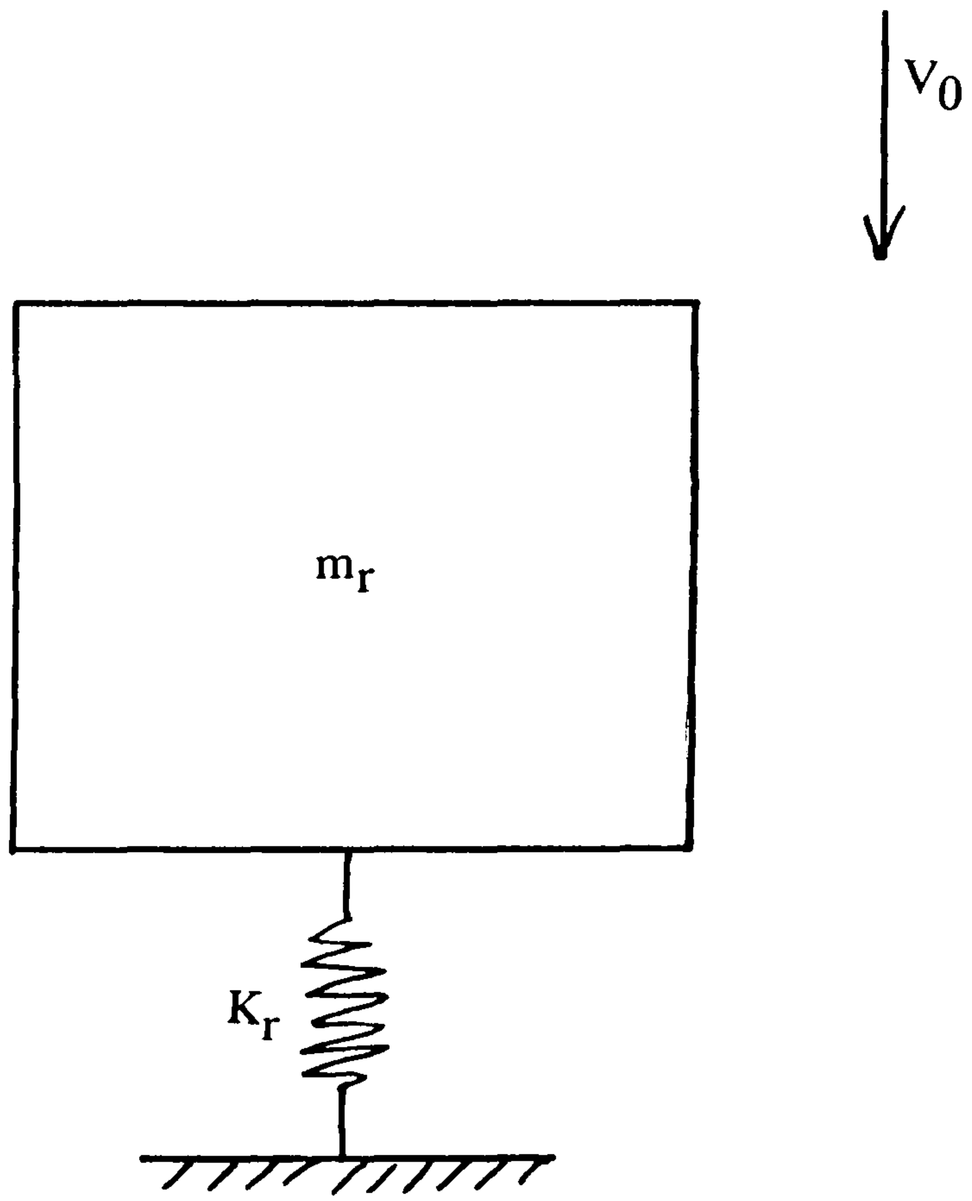

FIGURE (2.15) FREE BODY DIAGRAM OF THE HAMMER STRIKING A RIGID SURFACE

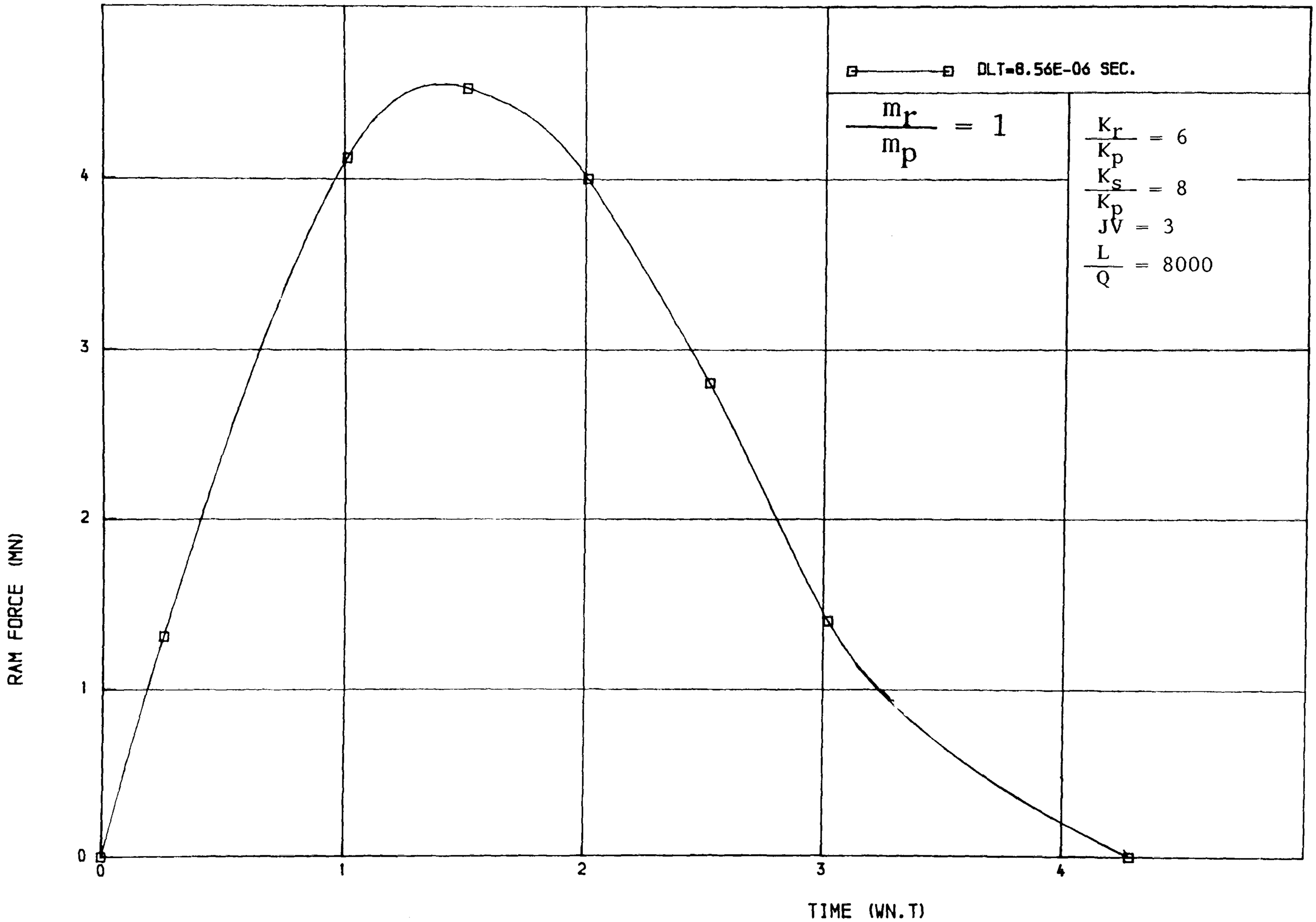

FIGURE (2.16) RAM FORCE TIME RELATIONSHIP

(SINGLE MASS PILE SUBJECTED TO A CUSHIONED HAMMER IMPACT)

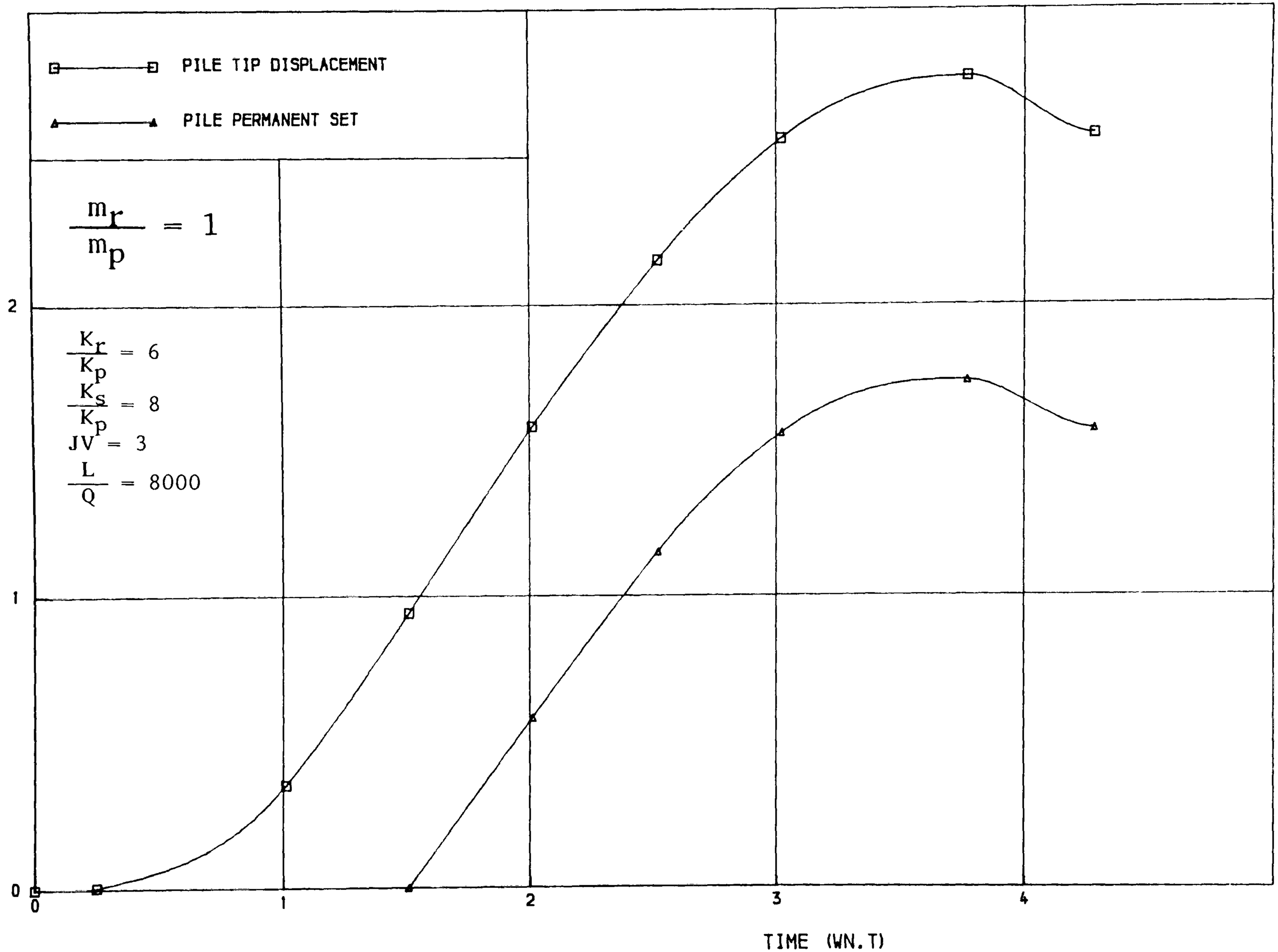

FIGURE (2. 17) DISPLACEMENT TIME RELATIONSHIP

(SINGLE MASS PILE SUBJECTED TO A CUSHIONED HAMMER IMPACT)

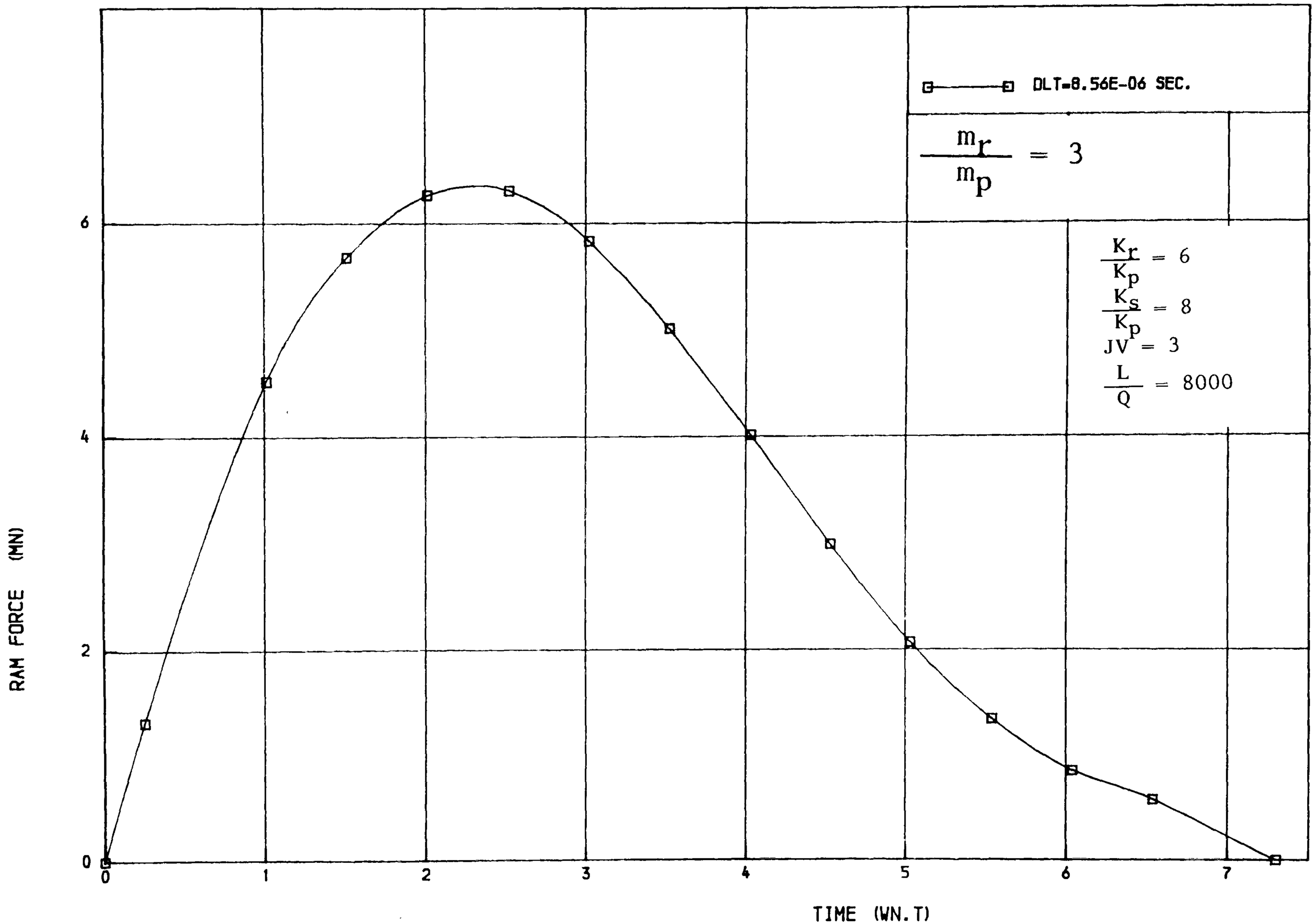

FIGURE (2.18) RAM FORCE TIME RELATIONSHIP

(SINGLE MASS PILE SUBJECTED TO A CUSHIONED HAMMER IMPACT)

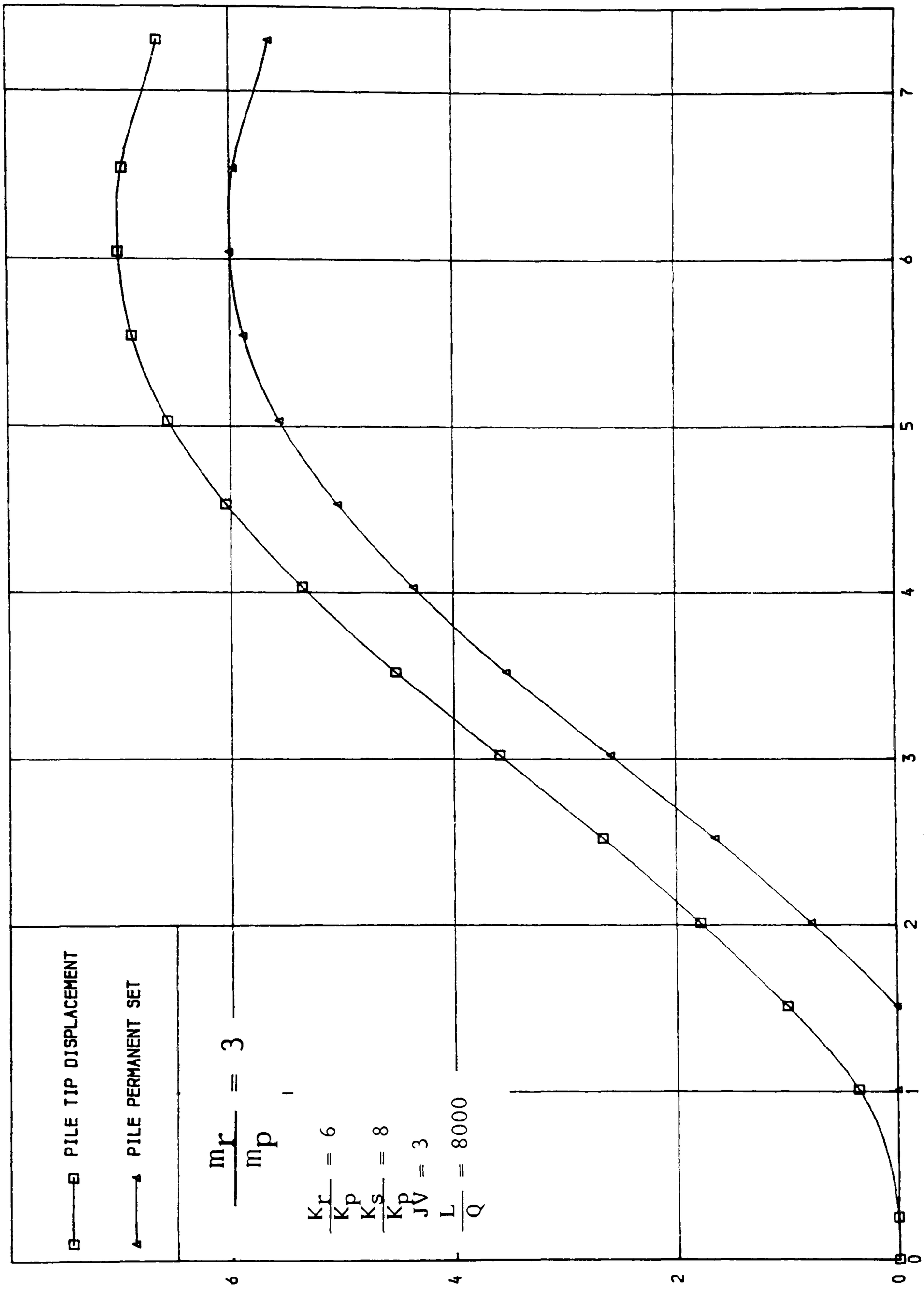

FIGURE (2.19) DISPLACEMENT TIME RELATIONSHIP
(SINGLE MASS PILE SUBJECTED TO A CUSHIONED HAMMER IMPACT)

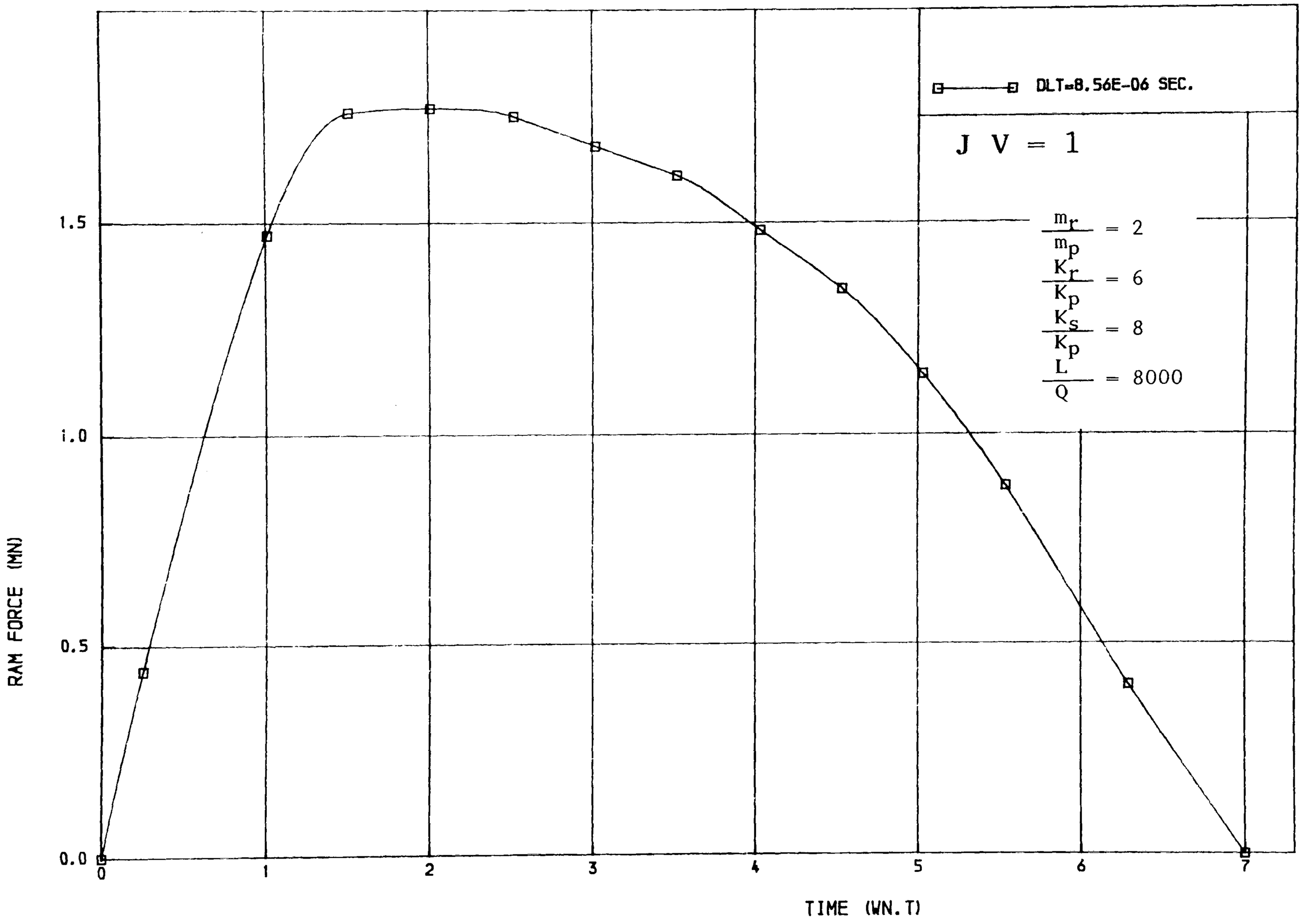

FIGURE (2.20) RAM FORCE TIME RELATIONSHIP

(SINGLE MASS PILE SUBJECTED TO A CUSHIONED HAMMER IMPACT)

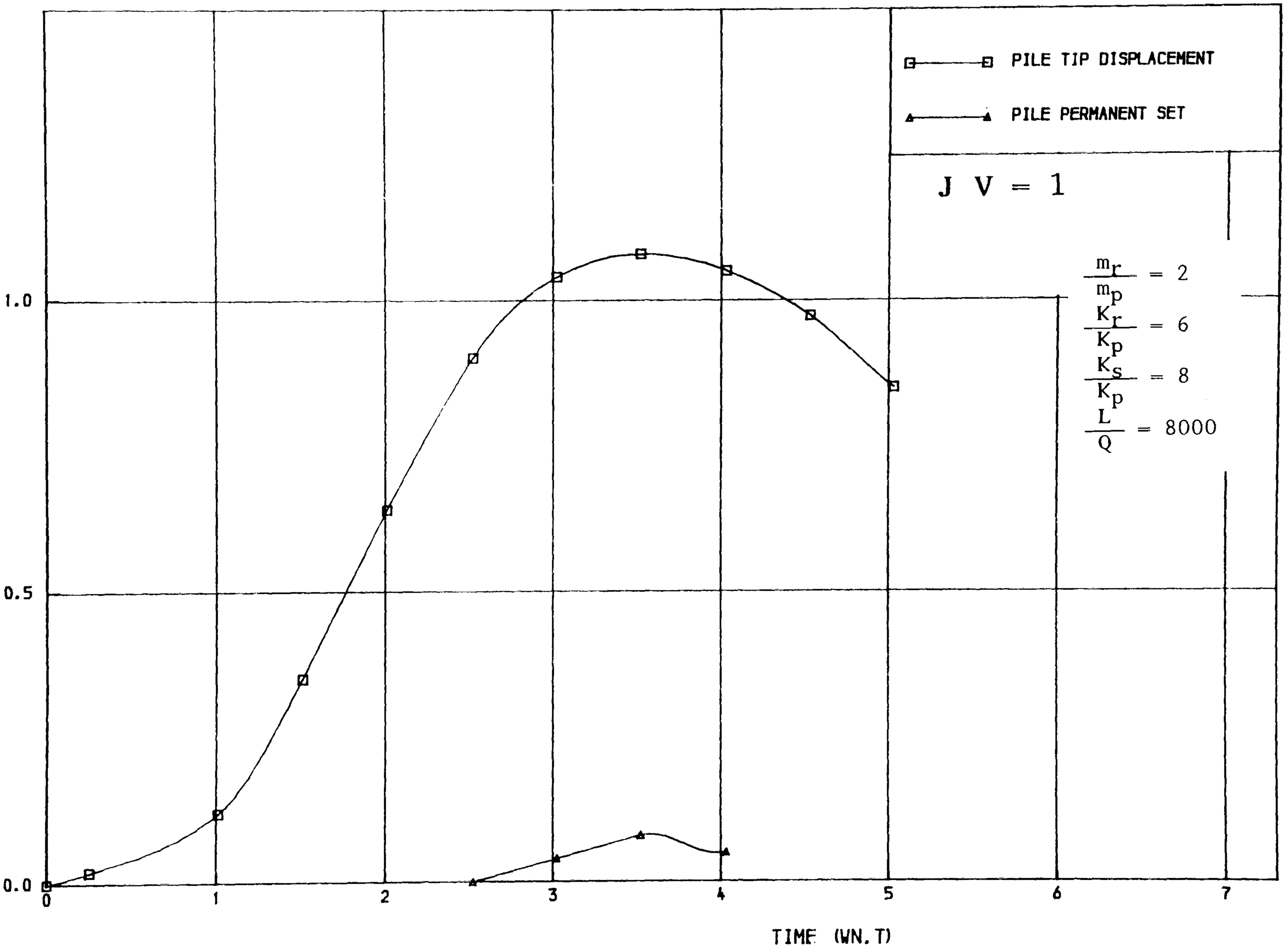

FIGURE (2.21) DISPLACEMENT TIME RELATIONSHIP

(SINGLE MASS PILE SUBJECTED TO A CUSHIONED HAMMER IMPACT)

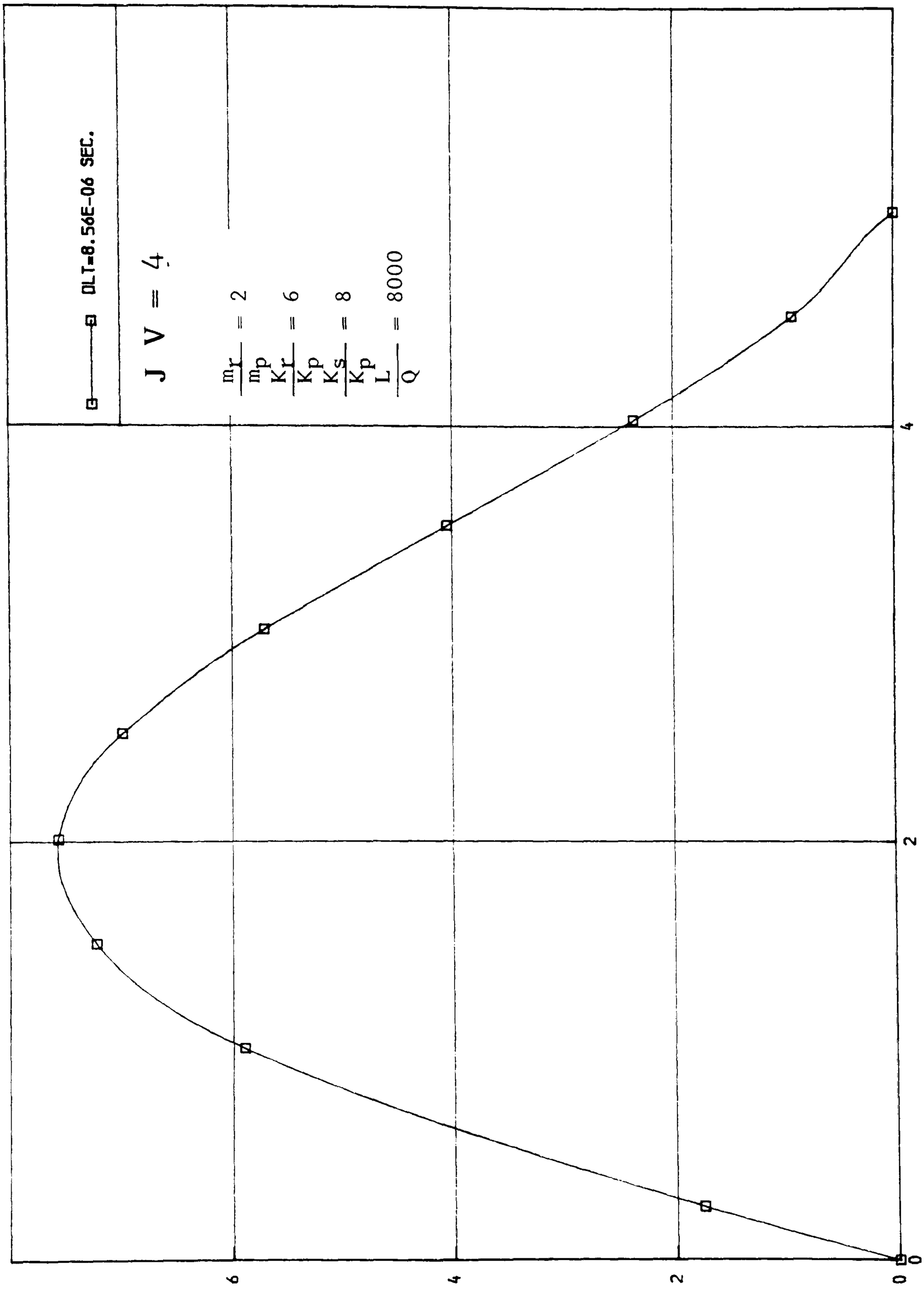

FIGURE (2.22) RAM FORCE TIME RELATIONSHIP
(SINGLE MASS PILE SUBJECTED TO A CUSHIONED HAMMER IMPACT)

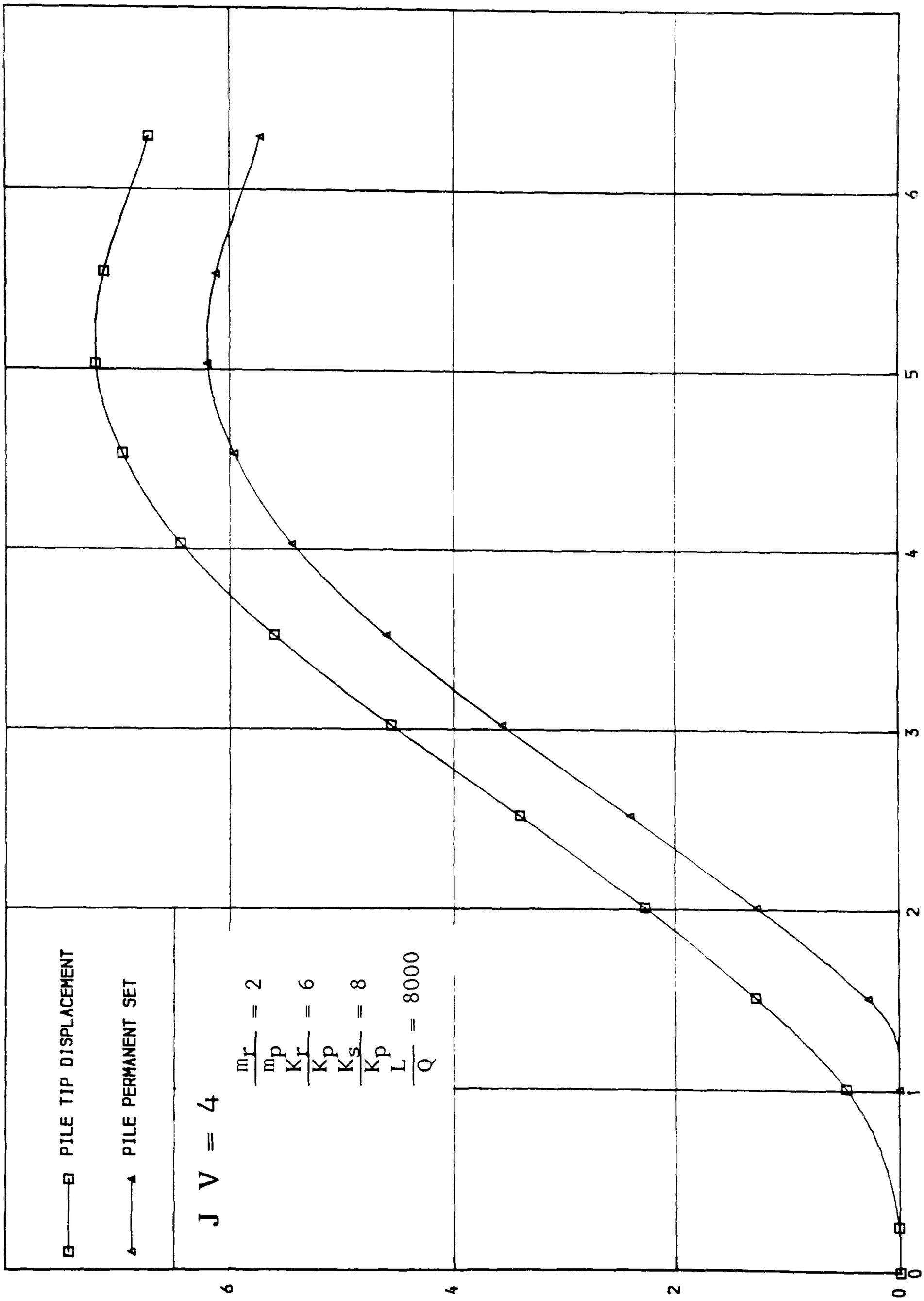

FIGURE (2.23) DISPLACEMENT TIME RELATIONSHIP (SINGLE MASS PILE SUBJECTED TO A CUSHIONED HAMMER IMPACT)

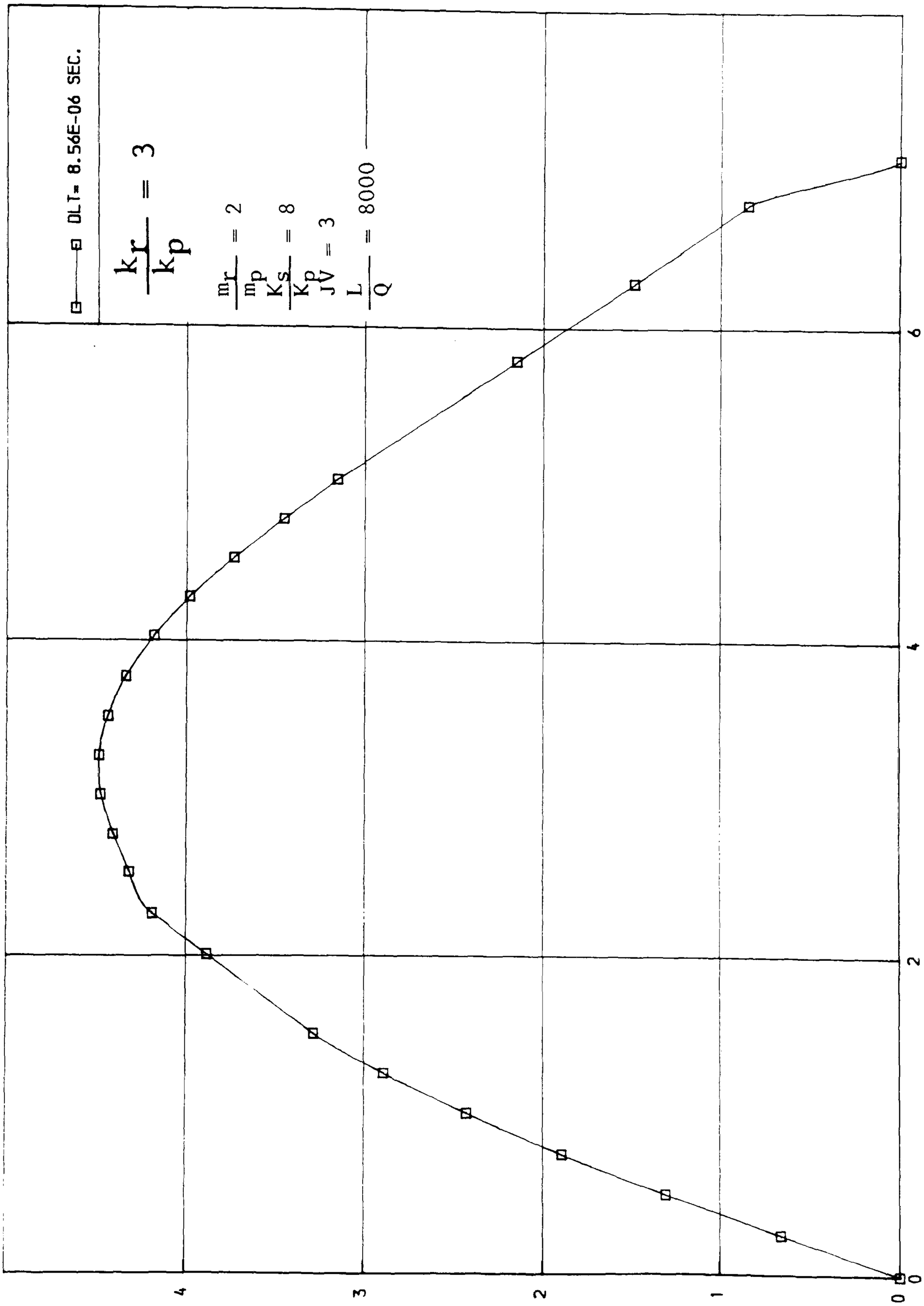

FIGURE (2.24) RAM FORCE TIME RELATIONSHIP
(SINGLE MASS PILE SUBJECTED TO A CUSHIONED HAMMER IMPACT)

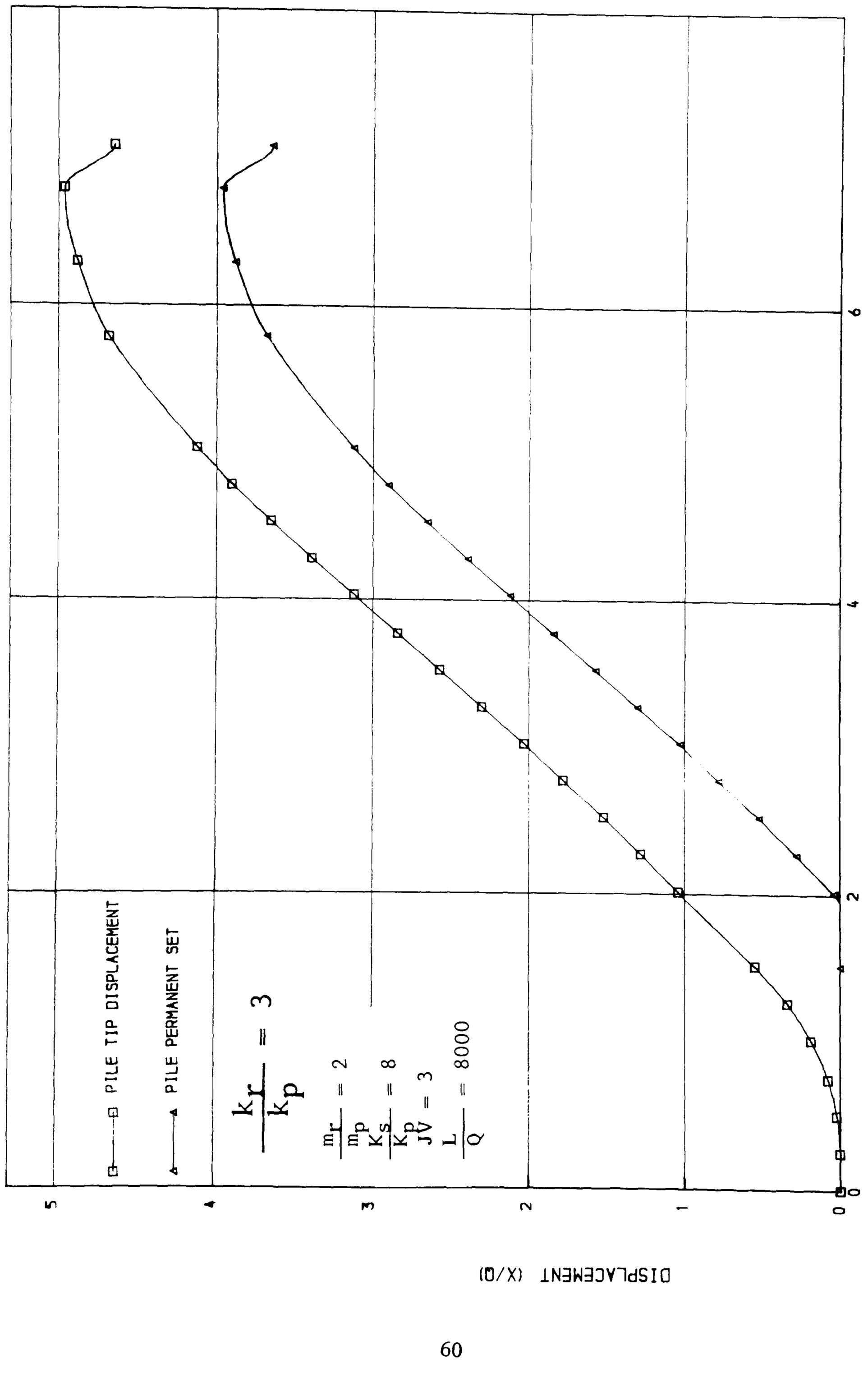

FIGURE (2.25) DISPLACEMENT TIME RELATIONSHIP
(SINGLE MASS PILE SUBJECTED TO A CUSHIONED HAMMER IMPACT)

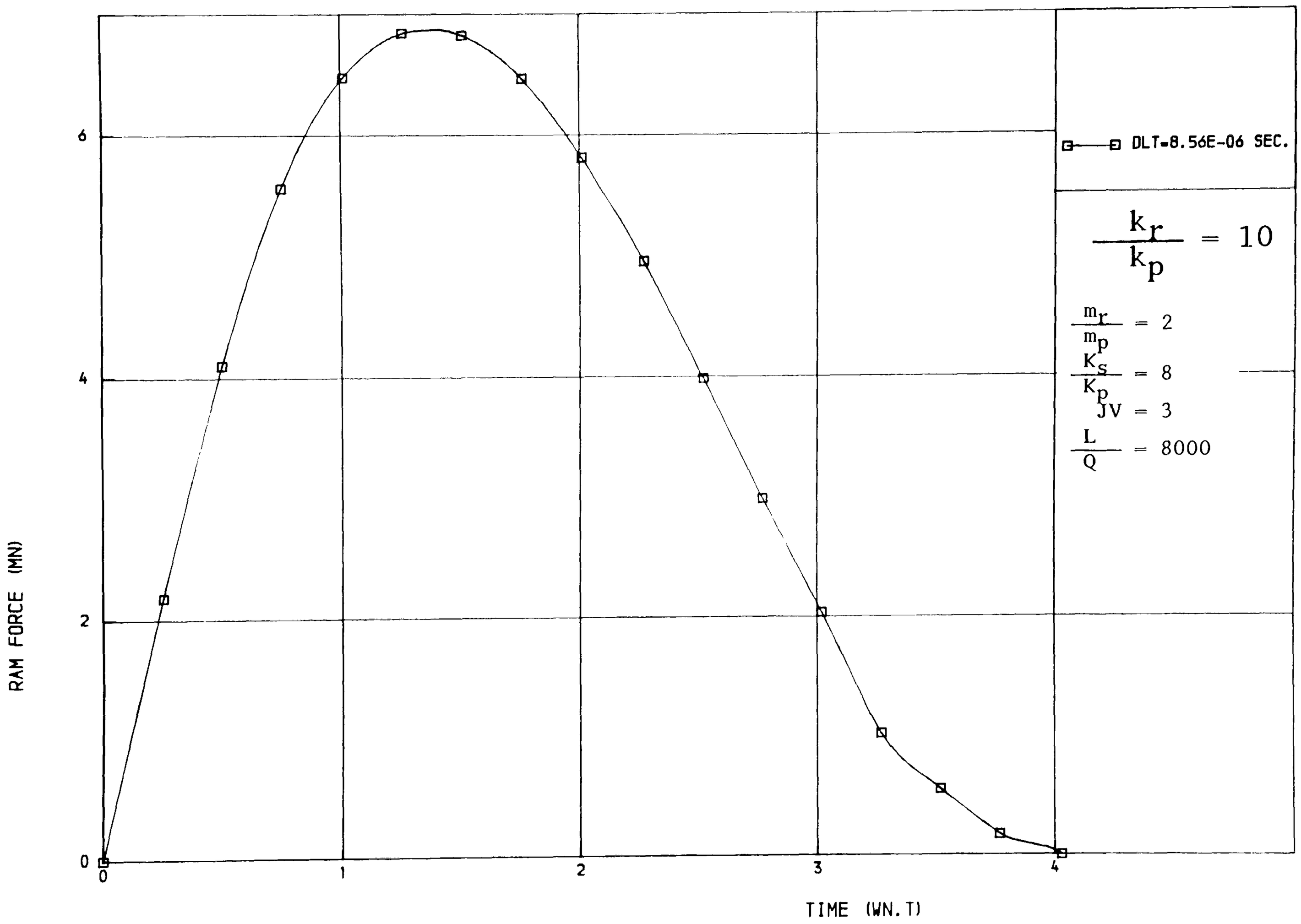

FIGURE (2.26) RAM FORCE TIME RELATIONSHIP

(SINGLE MASS PILE SUBJECTED TO A CUSHIONED HAMMER IMPACT)

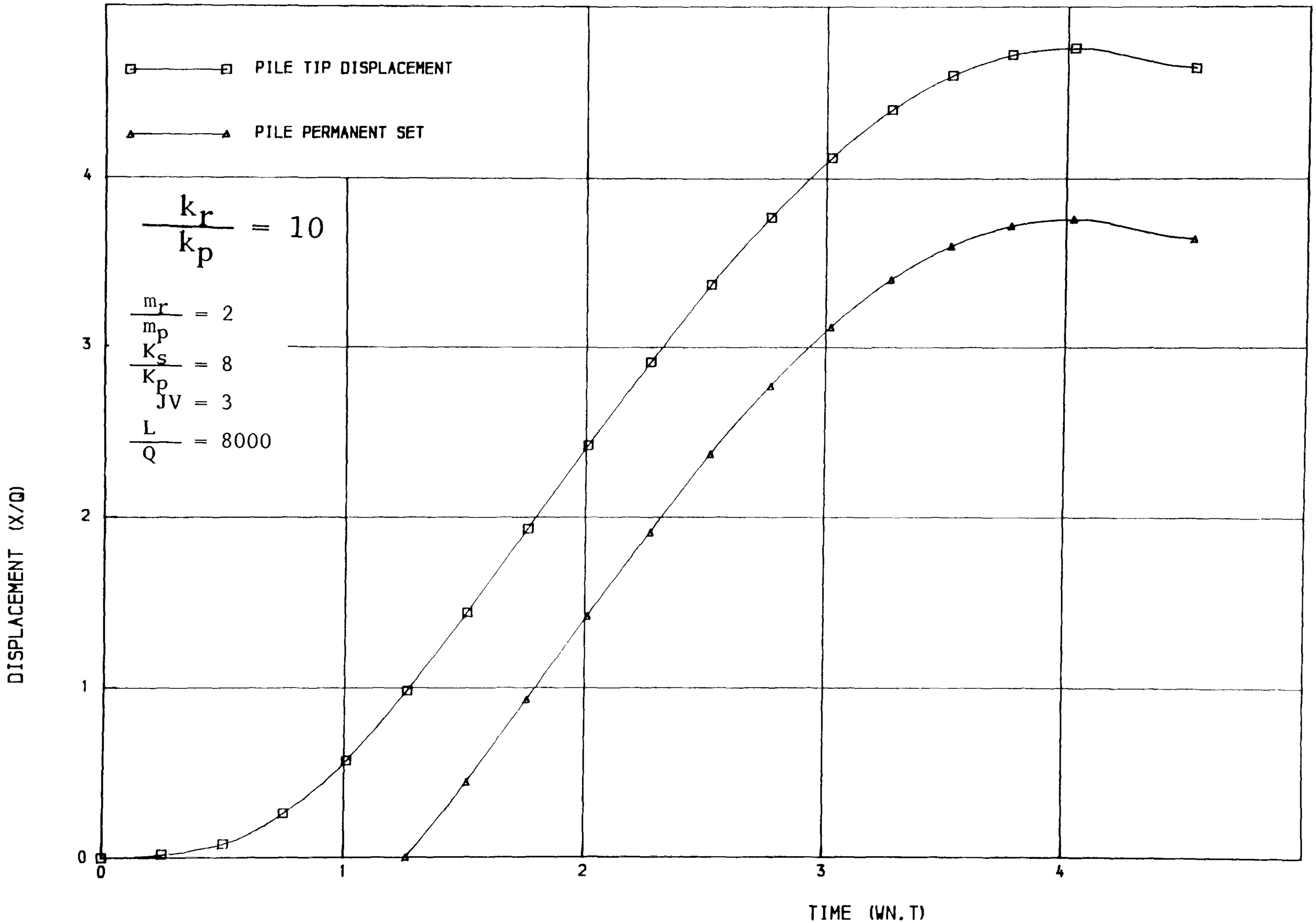

FIGURE (2.27) DISPLACEMENT TIME RELATIONSHIP

(SINGLE MASS PILE SUBJECTED TO A CUSHIONED HAMMER IMPACT)

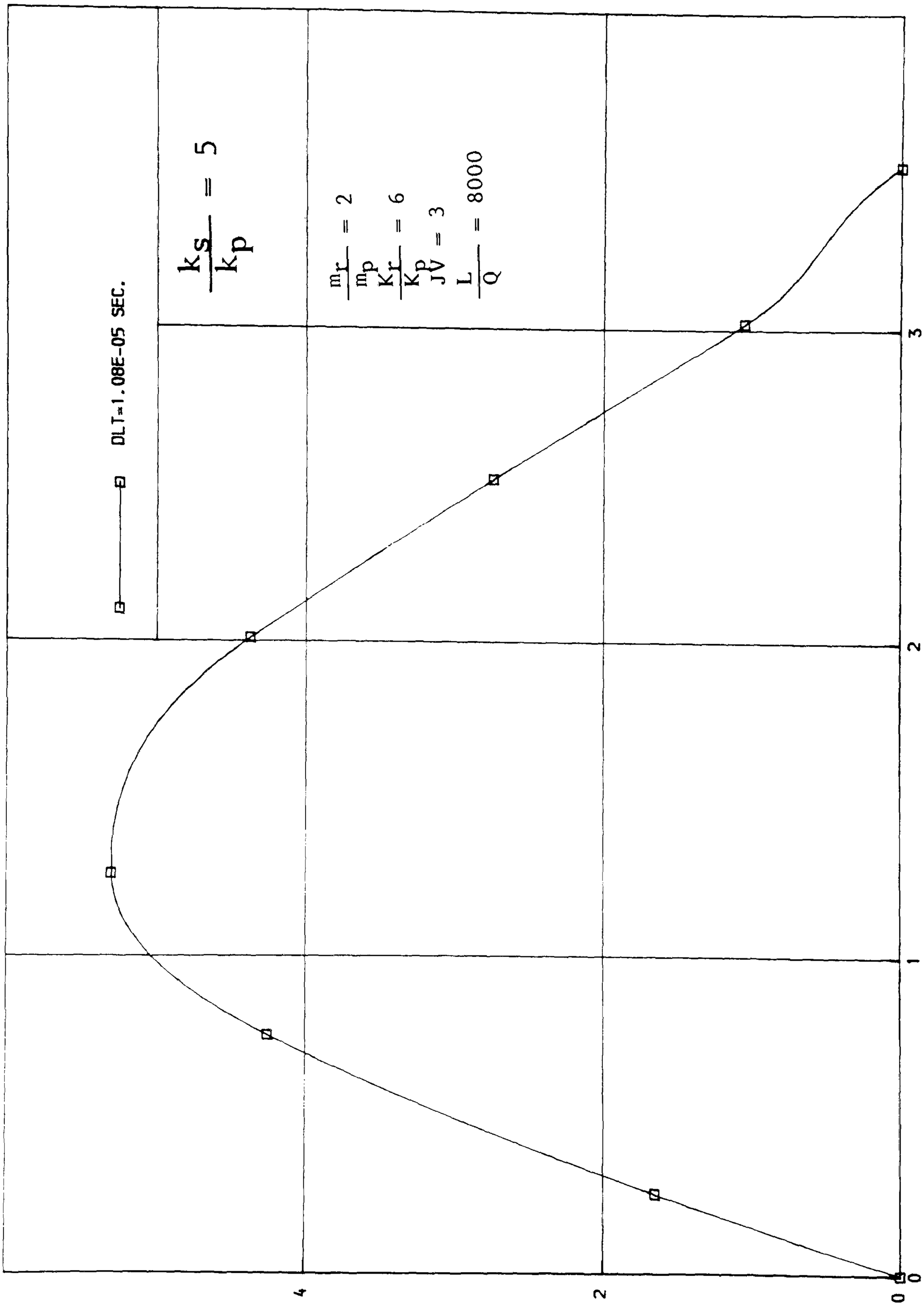

FIGURE (2.28) RAM FORCE TIME RELATIONSHIP
(SINGLE MASS PILE SUBJECTED TO A CUSHIONED HAMMER IMPACT)

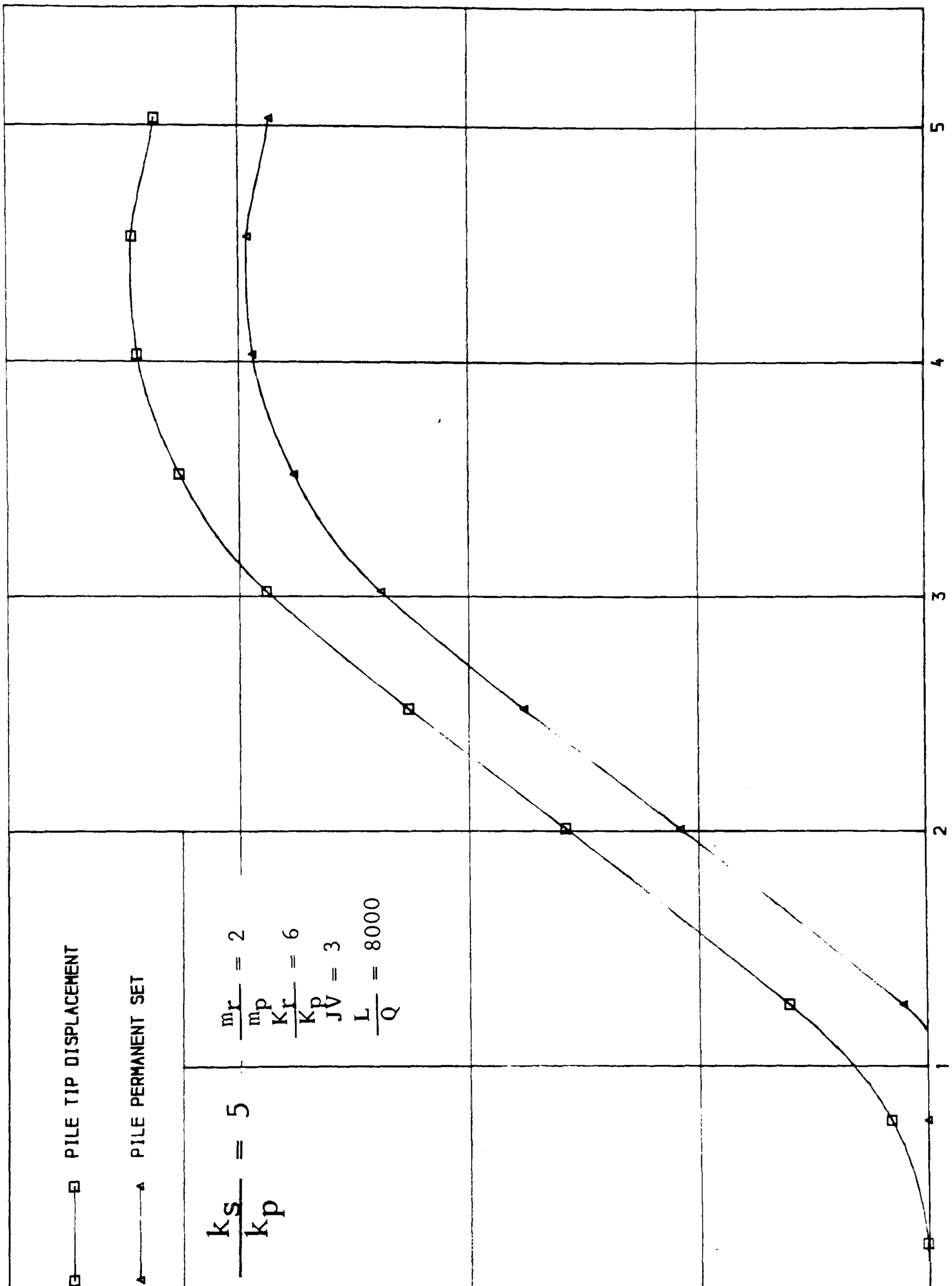

FIGURE (2.29) DISPLACEMENT TIME RELATIONSHIP
(SINGLE MASS PILE SUBJECTED TO A CUSHIONED HAMMER IMPACT)

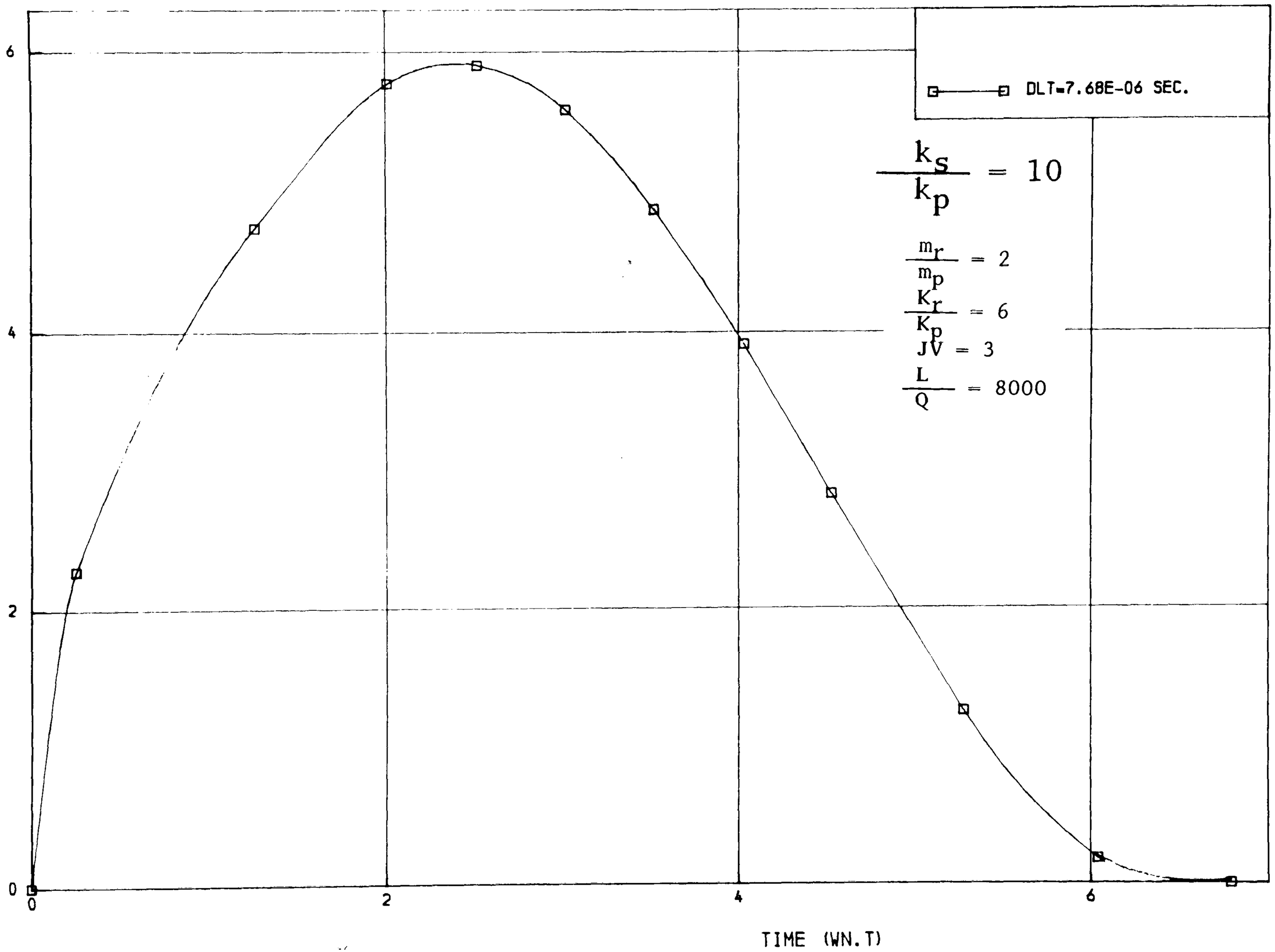

FIGURE (2.30) RAM FORCE TIME RELATIONSHIP

(SINGLE MASS PILE SUBJECTED TO A CUSHIONED HAMMER IMPACT)

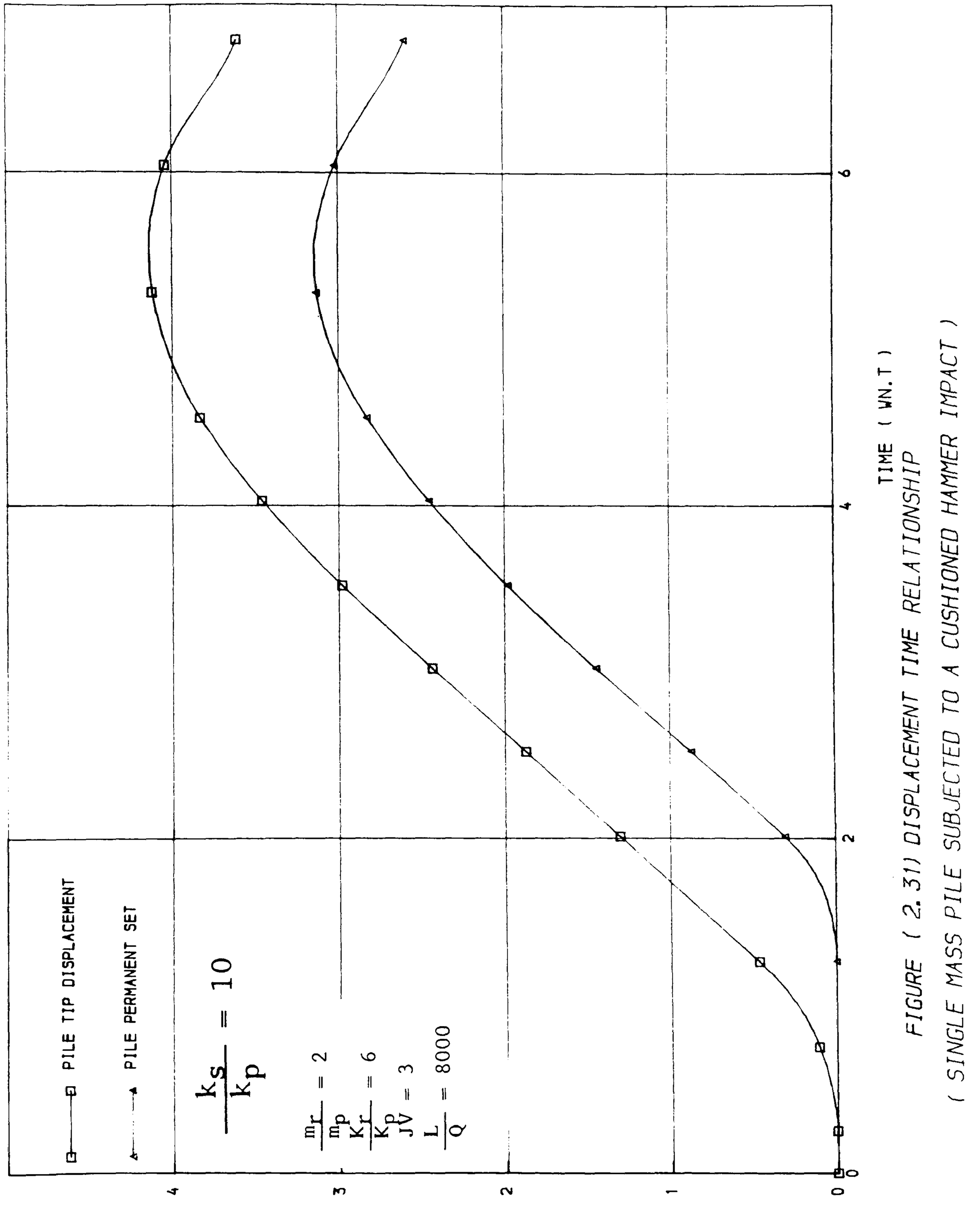

FIGURE (2.31) DISPLACEMENT TIME RELATIONSHIP
(SINGLE MASS PILE SUBJECTED TO A CUSHIONED HAMMER IMPACT)

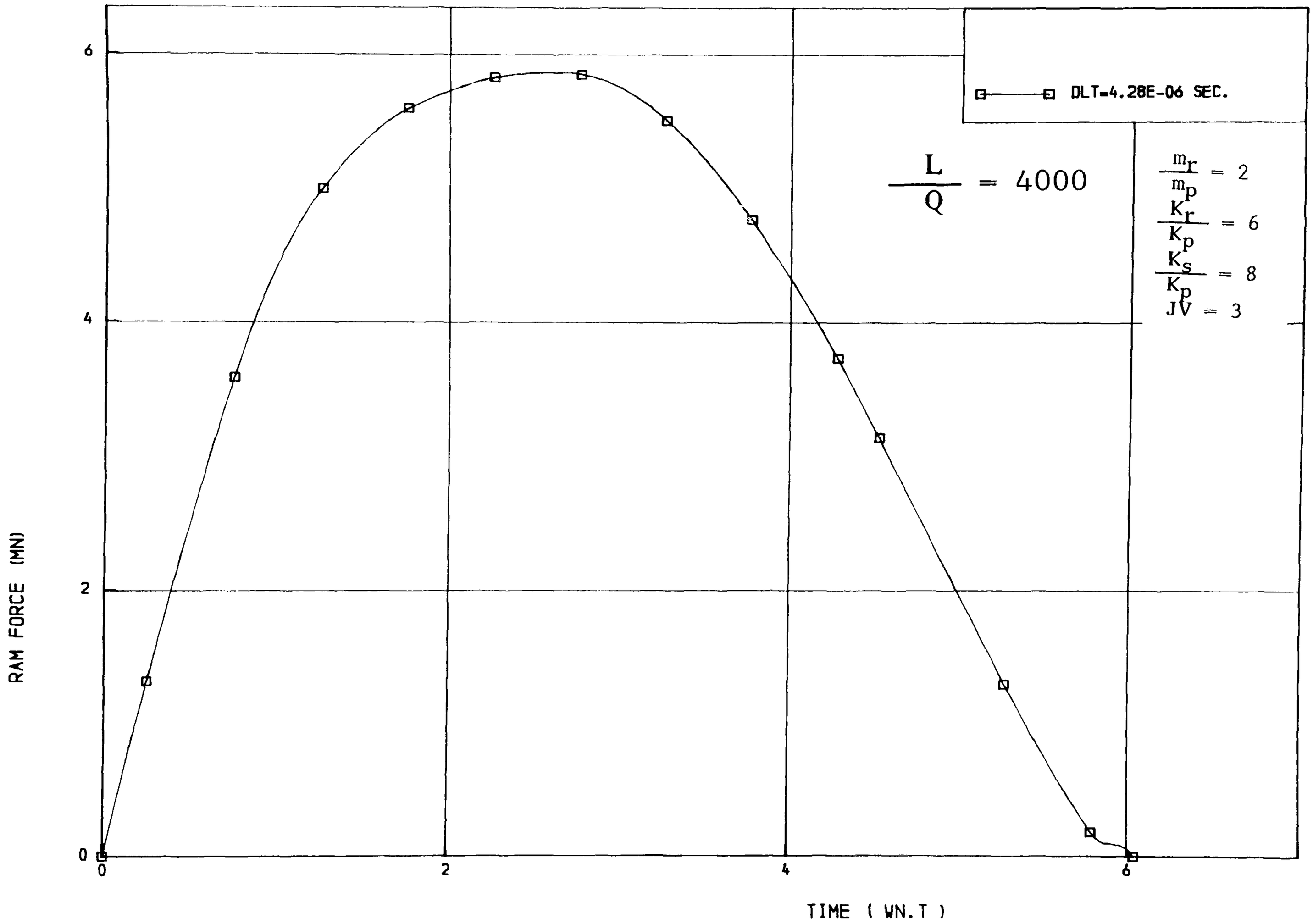

FIGURE (2.32) RAM FORCE TIME RELATIONSHIP

(SINGLE MASS PILE SUBJECTED TO A CUSHIONED HAMMER IMPACT)

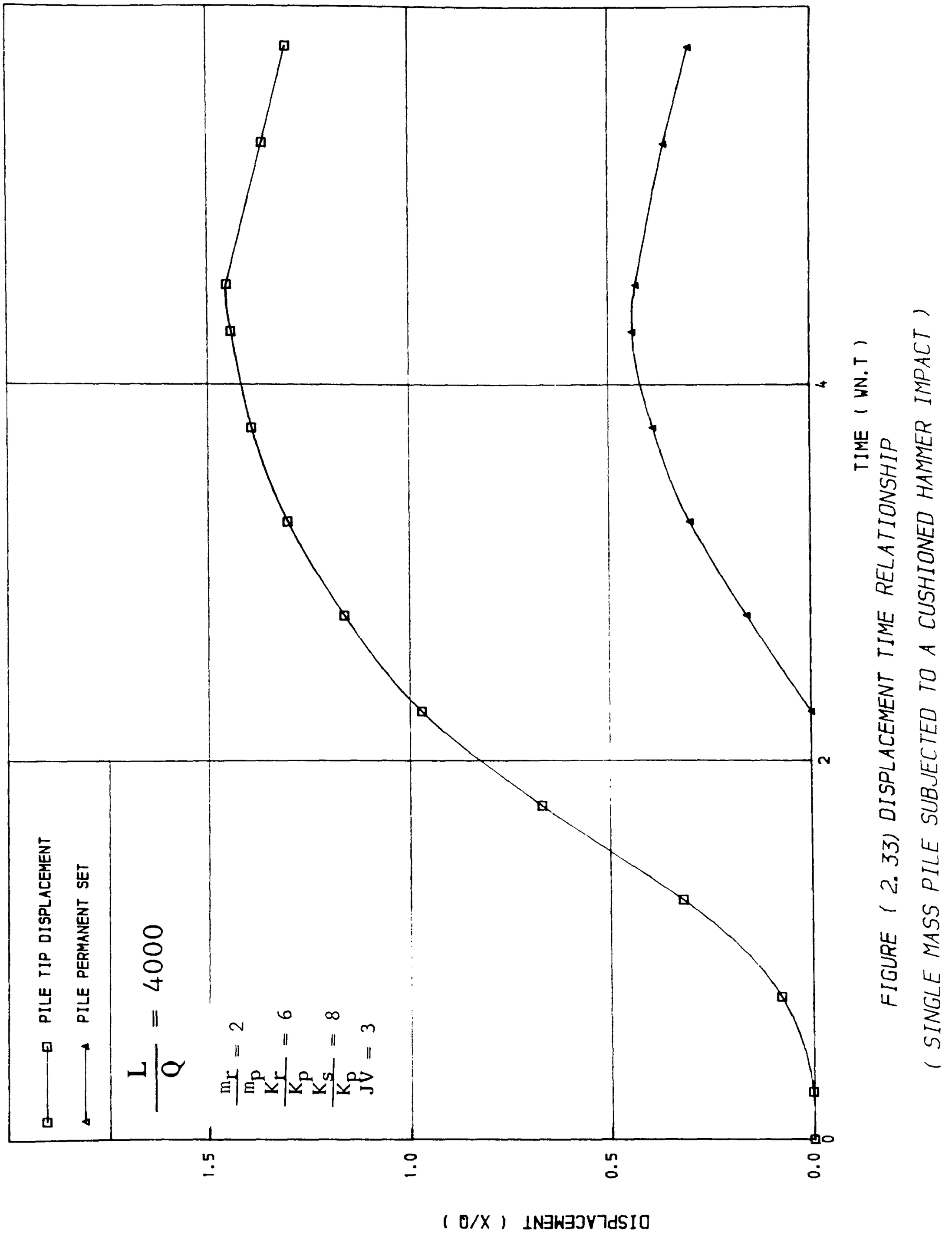

FIGURE (2.33) DISPLACEMENT TIME RELATIONSHIP
(SINGLE MASS PILE SUBJECTED TO A CUSHIONED HAMMER IMPACT)

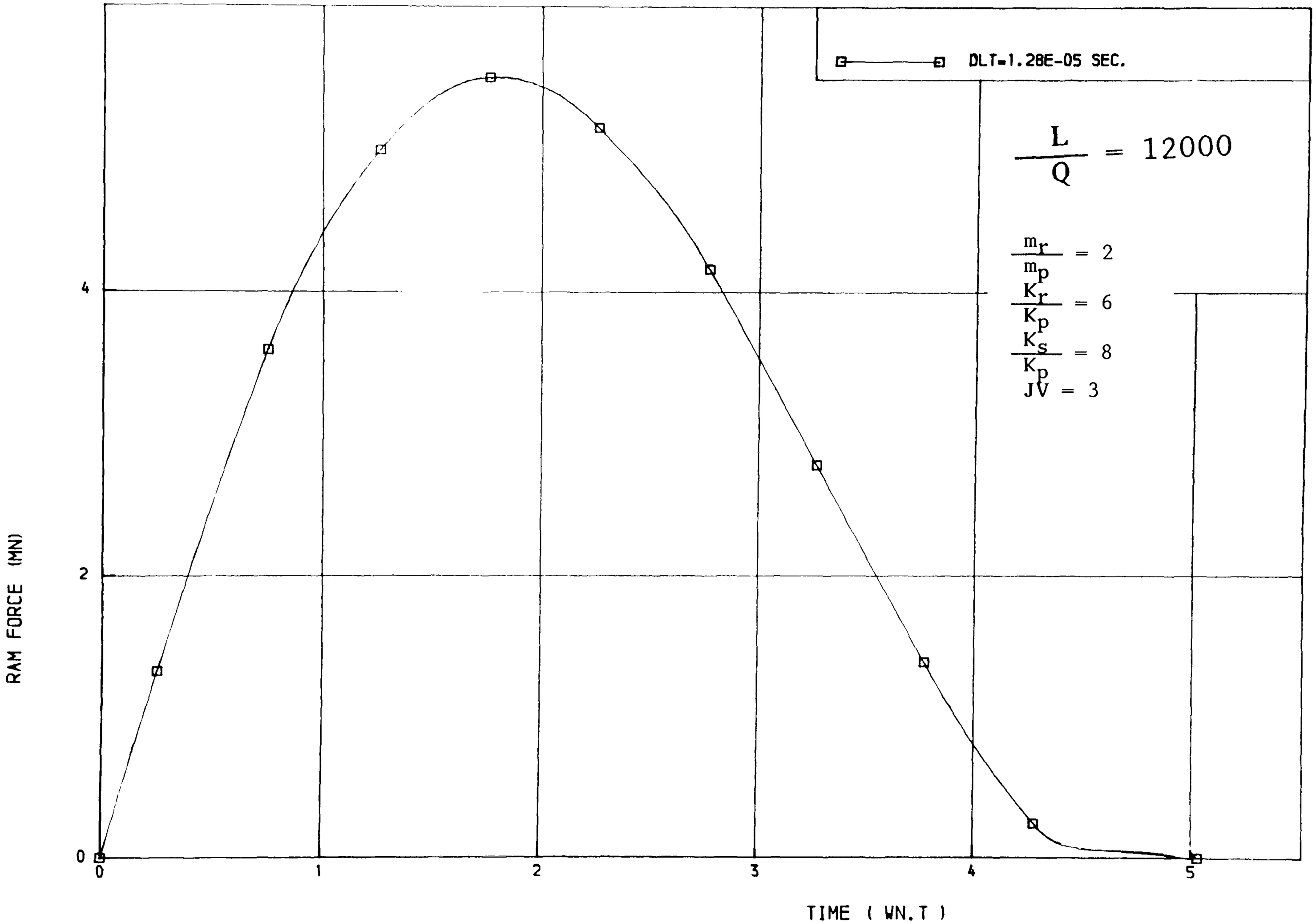

FIGURE (2.34) RAM FORCE TIME RELATIONSHIP

(SINGLE MASS PILE SUBJECTED TO A CUSHIONED HAMMER IMPACT)

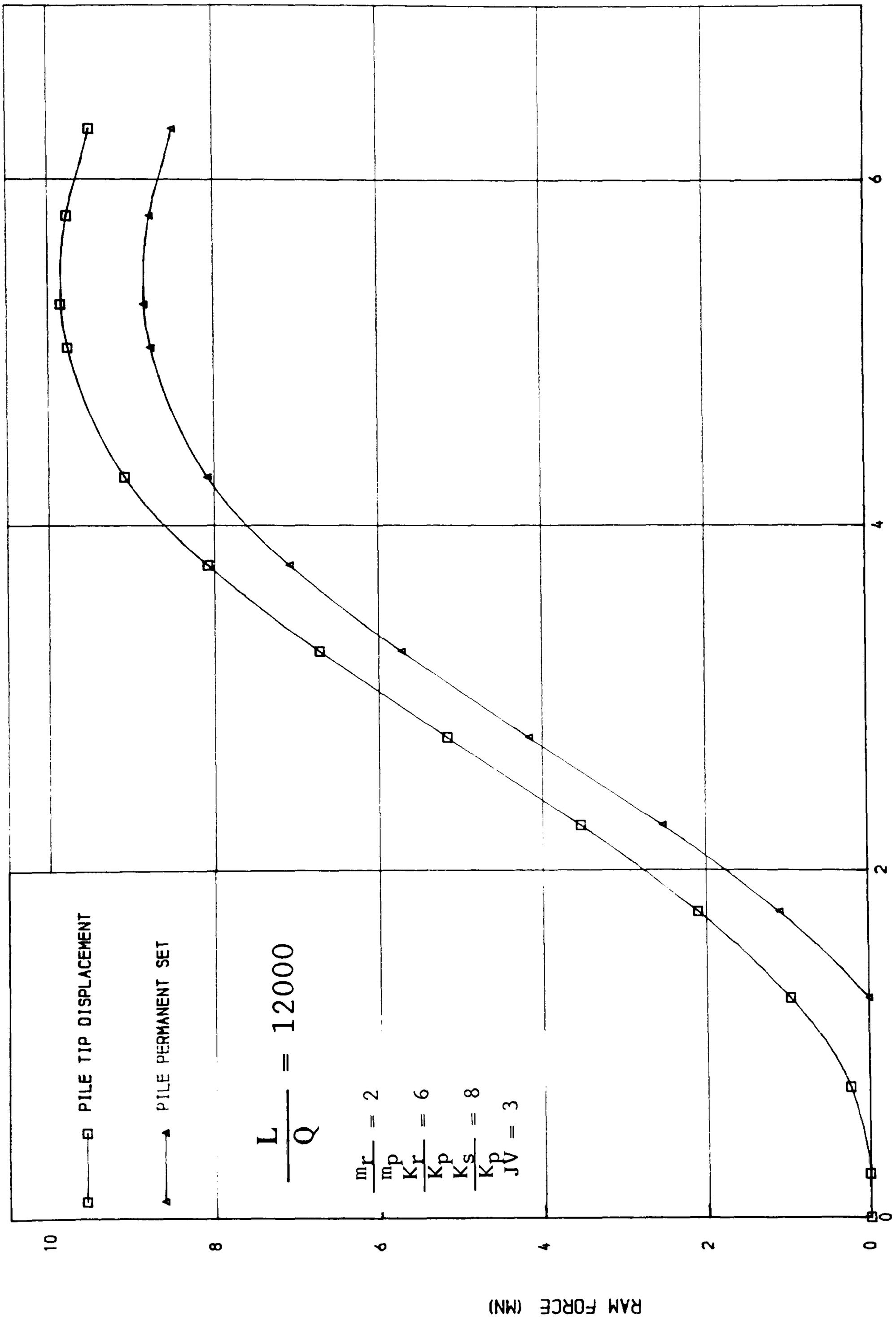

FIGURE (2.35) DISPLACEMENT TIME RELATIONSHIP
(SINGLE MASS PILE SUBJECTED TO A CUSHIONED HAMMER IMPACT)

CHAPTER 3

THE WAVE EQUATION MODEL

3.1 INTRODUCTION

3.2 FORMULATION

3.2.1 Discrete Equations

3.2.2 Critical Time Step

3.3 NUMERICAL IMPLEMENTATION

3.4 RESULTS

3.4.1 Wave Equation

3.4.2 Comparison with Elementary Models

3.4.2.1 Wave Equation versus SDOF models

3.4.2.2 Wave Equation versus Pile Driving Formulae

3.5 DISCUSSION

3.6 CONCLUSION

CHAPTER 3

THE WAVE EQUATION MODEL

3.1 INTRODUCTION

The elementary single (rigid) mass models described in the previous Chapter provide some insights into the behaviour of piles during driving. However, due to pile compressibility, real piles respond in a more complex manner to hammer blows. In particular, there is a time lag between the occurrence of the hammer blow at the pile head and the arrival at the pile toe of the resulting compressive stress wave.

Smith (1960) proposed an idealisation of the hammer, pile and soil system which is capable of representing the passage of the stress wave down the pile, (refer to Figs. 3.1 – 3.3). In this idealisation, the pile is modelled as a series of discrete rigid masses connected by springs (which act in both compression and tension). The surrounding soil is represented by a set of slider–springs connected to the rigid masses. These springs deforms elastically up to a limiting displacement, termed the quake (Q). Thereafter, the slider limits the spring reaction force. In addition the increased soil resistance observed under dynamic loading conditions is represented by a dashpot ; defined by a viscous damping coefficient, J. This parameter introduces damping into the system. The hammer ram can, similarly, be modelled as a discrete mass (or masses) and the cushion by a spring capable of transferring compression but not tension.

A numerical solution of this system, based on the solution developed by Smith (1955,1960) is described in this Chapter. The results of a parametric study of typical hammer, pile and soil systems are then described and these are compared with those predicted by elementary models. Some useful relationships were obtained from this work which form the basis of a new formula (in the form of a "pile driving formula") which may be of some value in practice. Application of this pile driving formula to full–scale pile load test results from the North Sea yielded encouraging results.

3.2 FORMULATION

3.2.1 Discrete Equations:

Smith (1955,1960) showed that the "discrete equation" solution of the wave equation was simpler to implement than the usual (at that time) finite difference strategy and with very little modification this approach is still used to date. For completeness, the main steps are outlined below.

Let the displacement of any discrete mass at time $t+\Delta t$ be denoted by $X_{t+\Delta t}$. Assuming constant velocity V_t during the time interval Δt, then:

$$X_{t+\Delta t} = X_t + V_t \Delta t \qquad (3.1)$$

If the displacement of a second (adjacent) mass is denoted by the superscript prime (') then the compressive force between the masses (f') is,

$$f' = K (X' - X) \qquad (3.2)$$

where,
K is the spring constant, and,
the subscript ($t+\Delta t$) has been dropped for clarity.

The resultant force P due to pile compression acting on any particular mass is the sum of the spring forces acting above and below it, i.e.

$$P = 'f + f'$$

$$= K ('X - 2X + X') \qquad (3.3)$$

where the pre–superscript prime denotes the second adjacent mass.

Clearly, equation 3.3 will require modification at the pile head and at the pile toe (refer to Figs. 3.4 and 3.5). The external resisting force due to the soil is denoted by the symbol R where, by definition, under elastic conditions:

$$R = K_S \; X \; (\; 1 + J \; V \;) \qquad (3.4)$$

where

K_S is the soil stiffness, and,

J is the viscosity coefficient.

During soil failure (X> Q), the soil resistance is limited to,

$$R = K_S \; Q \; (\; 1 + J \; V \;)$$

We note that viscous damping (under elastic conditions) is assumed to increase with increasing soil displacement, a departure from classical rheological models. The resultant force acting on a typical discrete mass is, therefore;

$$F = P + R \qquad (3.5)$$

from which the mass accelerations and velocities can be determined. Thus,

$$V_{t+\Delta t} = V_t + F \; \frac{\Delta t}{m} \qquad (3.6)$$

Equations 3.1 to 3.6 form the basis for a simple incremental (in time) solution strategy. Provided that sufficiently small time steps are employed, the process is convergent. Further, in view of the small number of degrees of freedom, computational costs are very modest and, consequently, great

sophistication in deriving more efficient algorithms is hardly warranted.

Fig. 3.6 shows a typical displacement–time relationship predicted by this method. In the figure, the permanent set of the pile is indicated by subtracting the quake from the pile tip displacement.

3.2.2 Critical Time Step:

Smith (1960) pointed out that the greater the number of discrete masses in the model (i.e. the shorter the "unit length" of pile modelled as a discrete rigid mass) the smaller must be the time interval, Δt to avoid numerical instabilities. Fundamentally, during each cycle of calculation, the stress waves must not travel further than one discrete mass length. On the other hand, reducing the time interval much beyond this limit serves only to increase computational costs but without any increase in accuracy.

The speed of wave propagation in the pile is essentially equal to the uniaxial wave speed (c), i.e.

$$c = \sqrt{\left(\frac{E}{\rho}\right)} \qquad (3.7)$$

where,

E is the Young's modulus of elasticity, and,

ρ is the mass density.

If n discrete masses are used to model a pile of length L, then the critical time step is:

$$\Delta t_{crit} = \frac{L}{n\ c} \qquad (3.8)$$

or, in terms of discrete quantities,

$$\Delta t_{crit} = \sqrt{\left(\frac{m}{K}\right)} \qquad (3.9)$$

where m is the discrete mass:

$$m = \frac{\rho \; L \; A}{n} \qquad (3.10)$$

where

A is the pile cross–sectional area, and,

K is the spring constant:

$$K = \frac{n \; E \; A}{L} \qquad (3.11)$$

Using either equation 3.8 or 3.9, the critical time step can be readily evaluated within the computer program and an appropriate time step can be selected.

3.3 NUMERICAL IMPLEMENTATION

The value of the quake, Q, used in this study is taken to be 2.5 mm, following Smith (1960), Hirsch et. al, (1970), Goble and Rausche (1976), Coyle et. al, (1977), Goble et. al, (1980), although, Authier and Fellenius (1980) have proposed higher values of quake (8 – 20 mm), (see also Hannigan, 1984).

Some workers, for example Litkouhi and Poskitt (1980), have assumed two different values for the viscous damping coefficient J; one for the pile tip and one for the pile shaft. Typically, the former is assumed to be one third (1/3) of the latter. In this study, a single value of viscous damping is used (0.5 s/m) for

simplicity, following the work of Yip and Poskitt (1986).The optimal time interval used in this analysis is found from convergence tests based on the critical time interval defined by equation 3.8.

In what follows, the influence of the major parameters in some typical cases is explored and the results are presented in dimensionless form. In most cases, subdivision of the pile into ten (10) discrete masses was found to yield results of sufficient accuracy.

3.4 RESULTS

3.4.1 Wave Equation

Fig. (3.7) shows the displacement–time relationship of the pile head of a typical pile subdivided successively into 2, 4, 8 and 16 discrete masses. The results show the rapid rate of convergence and suggests that useful results can be obtained with as few as eight elements. The ramforce–time relationship predicted from the numerical calculations is approximately a half–sine curve, similar in shape to that given theoretically by equation 2.42. However, the peak ramforce generated by impact on a compressible pile is well below the corresponding value predicted for impact on a rigid pile (Fig. 3.8), as might be expected.

The typical hammer–cushion–pile and soil system parameters which form the basis of the parametric study are as follows:

Hammer; m_r = 1600 kg.

V_r = 6 m/s (impact velocity)

Cushion; $K_r = 6 \times 10^8$ N/m

Soil; (a very stiff highly over consolidated clay)

Q = 2.5 mm

J = 0.5 s/m

$K_s = 8 \times 10^9$ N/m

Pile; $L = 20$ m

$A = 0.01$ m^2

$E = 2 \times 10^{11}$ N/m^2

$\rho = 8000$ kg/m^3

$m_p = 1600$ kg

The corresponding non–dimensional parameters are:

$m_r/m_p = 1$, V J $= 3$, $K_r/K_p = 6$, L/Q $= 8000$, $K_s/Kp = 8$.

The effect of increasing the ram mass on the peak ramforce is shown in Fig. 3.8 and 3.10. An increase of the ram/pile mass ratio from unity to three, causes, typically, a fifty percent increase in the peak ramforce. Moreover, using the heavier ram, the pile displacement (permanent set) is typically eleven times greater than that produced by the lighter ram. Figs. 3.9 and 3.11 show the pile displacement–time response.

The time taken for the pile to reach its maximum displacement is typically forty percent longer for the heavy ram compared with that for the light ram. This is largely due to the fact that the displacements are much greater in the former case. Clearly, in practice heavy ram masses may be necessary to attain adequate penetration and these longer times (to reach maximum displacement) are inconsequential in comparison with the duration of the loading cycle.

Figs. 3.12 and 3.14 show that an increase in the ram velocity from 2 m/s to 8 m/s results in a seventyfive percent greater impact force and this increase in ram force increases the pile set by , typically, eighteenfold, Figs. 3.13 and 3.15.

Figs. 3.16 and 3.18 show that a stiff cushion ($K_r/K_p = 10$) causes typically a twentyfive per cent increase in the peak ram force, compared to that using a soft cushion ($K_r/K_p = 3$). The effect of this increase on the pile displacement–time relationship is shown in Figs. 3.17 and 3.19. The maximum displacement (and set) using a stiff cushion is typically ten per cent greater than those predicted using a softer cushion.

Figs. 3.20 and 3.22 show that an increase in soil stiffness (from $K_s/K_p = 5$ to $K_s/K_p = 10$) increases the ram force by, typically, one hundred and fifty percent. Further, this increase in the soil stiffness reduces the pile displacement (or set) by typically fivefold, as shown in Figs. 3.21 and 3.23. It may be noted that this change in soil stiffness increases the time taken for the pile to reach its maximum penetration.

Figs. 3.24 and 3.26 show the ramforce–time relationship as a function of the pile length. Here the pile length is increased from 10 m ($L/Q = 4000$) to 30 m ($L/Q = 12000$) which causes a typical decrease of twenty percent in the peak ramforce.

Figs. 3.25 and 3.27 show the displacement– time relationships of short ($L/Q = 4000$) and long piles ($L/Q = 12000$) driven in the same soil. The maximum displacement (and set) of the longer pile is typically thertyfive fold greater than those of the short pile. However, increasing the pile length does not result in any significant change in the time taken for the pile to reach its maximum penetration.

Figs. 3.28 and 3.29 show that if a pile's length is increased, but keeping its mass and stiffness (K_p) unchanged, the maximum ram force and displacement are unaffected.

The effect of an increase in the pile stiffness (K_p) on the ram force–time relationship is shown in Fig. 3.30. For a stiff pile, the peak ram force is typically five percent greater than that for a less stiff pile, driven under the same conditions. Fig. 3.31 shows that the pile moves vertically as a rigid body some time after ram impact. This should be contrasted with the motion with for example Fig. 3.27 where considerable compression of the pile takes place. It may be inferred therfore that very stiff piles undergo rigid body motion.

In all cases, it may be observed that the piles reach their maximum penetration after the ramforce has reached its peak value due to the inertia of the pile–soil system.

3.4.2 Comparison with Elementary Models

3.4.2.1 Wave Equation versus SDOF Model

In this section, results from the single degree of freedom model (SDOF) are compared with those obtained from the wave equation (MDOF) analysis. The same parameters (excluding pile compressibility in the SDOF model, of course) are used in both models.

The effect of increasing the ram/pile mass ratio from unity to three ($m_r/m_p = 1$ to $m_r/m_p = 3$) on the ramforce time relationship is shown in Figs. 3.32 and 3.34, respectively. The peak ramforce obtained by the SDOF model is typically eighty percent greater than that predicted by the MDOF model for light rams. But this increase is typically sixty percent for heavy rams.

The effect of ram/pile mass ratio on the pile displacement–time relationship is shown in Figs. 3.33 and 3.35. The pile set predicted by the SDOF model is typically two hundred percent greater than that predicted by the MDOF model for light rams. However, this increase is typically twenty percent for heavy rams. Further, the pile set predicted by the SDOF model are typically sixty percent greater using the heavy ram while the increase predicted by the MDOF model is ninety percent.

The effect of increasing the ram velocity from unity to four (VJ = 1 to VJ = 4 i.e. the hammer velocity increases from 2 m/s to 8 m/s) on the ramforce–time relationship is shown in Figs. 3.36 and 3.38, respectively. The peak ram–force predicted by the SDOF model is typically fifteen percent higher than that predicted by the MDOF model for the slower ram and the peak ramforce predicted by the SDOF model is typically seventy percent higher than that predicted by the MDOF model for the faster ram. The increase in hammer velocity causes an increase of three fold in the peak ramforce, predicted by both the SDOF and MDOF models.

Figs. 3.37 and 3.39 show the pile displacement–time relationships predicted by the SDOF and the MDOF models. For the slower ram, no permanent pile displacement was predicted by the MDOF model while a relatively small pile set was predicted by the SDOF model. On the other hand, pile set were predicted to increase sixfold by both models when the piles were driven by the faster ram. However, the pile penetration predicted by the SDOF model is typically fifty percent greater than that predicted by the MDOF model in this case.

Figs. 3.40 and 3.42 show the ramforce–time relationships for two cushion increased stiffnesses ($K_r/K_p = 3$ to $K_r/K_p = 10$). In these figures, the peak ramforce predicted by the SDOF model is typically sixty percent higher than that predicted by the MDOF model (for the soft cushion). But, the use of a stiffer cushion causes an increase of sixty percent of the peak ramforce obtained from the SDOF model but no remarkable increase is predicted using the MDOF model.

The influence of increasing the cushion stiffness from $K_r/K_p = 3$ to $K_r/K_p = 10$ on the pile displacement–time relationship is shown in Figs. 3.41 and 3.43, respectively. The pile set predicted by the SDOF model using a soft cushion is twice that predicted by the MDOF model. Using a stiffer cushion has little effect on pile penetration.

Figs. 3.44 and 3.46 show how the ramforce–time relationship is influenced by changing the soil stiffness from $K_s/K_p = 5$ to $K_s/K_p = 10$. The peak ramforce predicted by the SDOF model is typically sixty percent higher than that predicted by the MDOF model in driving into a soft soil. The effect of soil stiffness on pile set predicted by the SDOF and MODF models are shown in Figs. 3.45 and 3.47. Driving piles into soft soils yields virtually the same results by both models. However, pile penetration into the stiffer soil is predicted to be much less by the MDOF model. Clearly, SDOF models are only valid when piles are relatively rigid compared to the surrounding soil.

Figs. 3.48 and 3.50 show the ramforce–time relationships obtained from the SDOF and MODF models as a function of the length (keeping other non–dimensional parameters unchanged); specifically from 10 m piles ($L/Q = 4000$) and 30 m piles ($L/Q = 12000$). The peak ramforce predicted by the SDOF model is typically fifty percent higher than that predicted by the MDOF model for the

short pile. The increase in pile length causes a decrease of thirty percent in the peak ramforce predicted by both models and the peak ramforce predicted by the SDOF model (for this long pile) is sixty percent higher than that predicted by the MDOF pile model.

Figs. 3.49 and 3.51 show the effect of increasing the pile length on the displacement–time relationships. For short piles, some penetration is predicted by the SDOF model but no permanent penetration is predicted by the MDOF model.

A summary of these different effects is shown in Figs. 3.52 to 3.56. In these figures the pile tip displacements as predicted by the MDOF model and the corresponding sets are plotted for comparison with the results predicted by the SDOF model.

3.4.2.2 Wave Equation versus Pile Driving Formulae

The pile set predicted by the wave equation method for a wide range of parameters is depicted in Figs. 3.57 to 3.61, plotted against ram mass, ram velocity, cushion stiffness, soil stiffness and pile length, respectively. Also shown in these figures are the pile driving formula predictions based on equation 2.6 (after some re–arrangement):

$$S = \frac{e_g\, e_f W\, H}{R} - \frac{1}{2}\,\Delta S_{ep} - \Delta S_{pp} \qquad (2.6)bis$$

where,

S is the pile permanent penetration (set),

W is the weight of the hammer,

H is the drop of the hammer,

R is the ultimate load capacity of the pile,

e_g is the efficiency of the drop,

e_f is the efficiency of the hammer blow,

S_{ep} is the elastic compression of the pile, and,

S_{pp} is the plastic compression of the pile.

and,

$$\Delta S_{ep} = C \frac{R\ L}{A\ E_p} \qquad (2.5)bis$$

To permit a proper comparison to be made, no ram losses are allowed and plastic compression of the pile is neglected; hence the only outstanding variable is the pile compression parameter C. A range of values is assumed in these comparisons but it may be seen that the curves predicted by this approach intersect the wave equation results at a sharp angle indicating that the two methods can not be easily reconciled (Figs. 3.57` – 3.61).

Examination of the results obtained from the wave equation model and the pile driving formula suggests that a good match may be obtained if it is assumed that pile compression and set are related by the empirical equation (Fig. 3.62):

$$C = 1 + 0.5 \frac{S}{Q}$$

Denoting the effective work done by the hammer by the symbol E the permanent set can be re–written as:

$$S = \frac{E}{R} - \frac{1}{2} C \frac{R}{K_p} \qquad (3.12)$$

where K_p is the pile stiffness ($A\ E_p/L$).

Noting that:

$$R = Q\ K_s \qquad (3.13)$$

and introducing the soil/pile stiffness ratio (n), where

$$n = \frac{K_s}{K_p} \qquad (3.14)$$

and the parameter γ, where

$$\gamma = 1 + \frac{n}{4} \qquad (3.15)$$

We obtain after some manipulation (and dropping the subscript p from the symbol K_p for clarity), the equation:

$$R = - S K \gamma + \sqrt{(S K \gamma)^2 + 2 E K} \qquad (3.16)$$

This new "pile driving formula" may not be of universal validity since it is likely that the coefficients in equation 3.16 are a function of some parameters which were held constant during this study; notably the viscosity coefficient J.

The principal unknown in this equation is the parameter γ but this may be estimated from the following equation:

$$K_s = \frac{16 \times 10^6}{Q^{3/2}} \qquad (N/m) \qquad (3.17)$$

derived from the data given by Authier and Fellenious (1980).

The new "pile driving formula" can be re–written in dimensionless form as follows:

$$\frac{R}{S\ K} = - \gamma + \sqrt{\gamma^2 + \frac{2\ E}{K\ S^2}} \qquad (3.18)$$

The predictions of this equation are shown in Figs. 3.63 to 3.66 and are compared with the original wave equation results. The effect of increasing the ram mass, ram velocity, soil stiffness and pile length on the pile displacement (set) are shown in Figs. 3.63, 3.64, 3.65 and 3.66 , respectively. As expected, the new "pile driving formula" reproduces these results very well.

Fig. 3.67 shows the pile set as a function of work done by the hammer as predicted by equation 3.16. If the hammer rating is known and the pile set is measured, this figure can be used to determine the soil's ultimate resistance.

The relationship between ultimate resistance and the work done by the hammer is shown in Fig. 3.68. The results are plotted from equation 3.18. Again, given the rating of the hammer and the pile set the ultimate soil resistance can be determined. Fig. 3.68 shows that the greater the relative soil stiffness ($n = K_s/K_p$) the greater is the ultimate soil resistance.

Fig. 3.69 shows the ultimate soil resistance versus the pile penetration (set) (or number of blows per meter penetration)for a typical system, as predicted by equation 3.16. For a given hammer rating, the greater the relative soil stiffness ($n = K_s/K_p$) the lower is the pile penetration.

Fig. 3.70 shows the relationship between the ultimate resistance and the pile penetration (set) (or number of blows /meter penetration). These sets of curves are predicted by equation 3.16. It may be seen that the greater the soil resistance is the higher is the required rating of the hammer to reach a given set. Also, a specified soil resistance may not be reached by hammer of low rating.

Fig. 3.71 shows also the relationship between the ultimate resistance and the work done by the hammer predicted by equation 3.18. It may be seen from this figure that the greater the soil resistance the greater must be the hammer rating to attain the requisite set.

In order to test the applicability of equation 3.16 a comparison between its predictions and the full scale data obtained by Forehand and Reese (1964), shown in Fig. 3.72, has been carried out. This figure depicts ultimate resistance versus set and shows that the predicted ultimate resistances were typically ten percent

greater than those observed by these authors. This comparison illustrates the effectiveness of this formula for determination of pile ultimate capacities.

3.5 DISCUSSION

The wave equation results for a typical hammer, pile and soil system have been presented in the last section. Increases in ram mass and velocity increase the work done by the hammer and hence result in increased pile penetration. However, increases in cushion stiffness have only a minor effect on the pile penetration although particularly soft cushions dissipate energy. However, stiff soils offer much greater resistance to penetration than softer soils.

Comparisons between the results predicted by the wave equation with those predicted by the SDOF model reveal significant differences except where the pile is relatively rigid in relation to the surrounding soil. A comparison between the results predicted by the pile driving formula with those predicted by the wave equation leads to the derivation and development of a new "pile driving formula" which was found to be effective in determining pile driving performance.

3.6 CONCLUSION

The single degree of freedom (SDOF) model is less accurate than the wave equation (MDOF model); however it may give useful results, with very little calculation, for soft soils.

The wave equation and pile driving formula approaches cannot be easily reconciled (Fig. 3.73). However, by comparing the results obtained from the two methods it is possible to develop a new semi–empirical formula in the form of the latter. The predictions of this analytical expression are explored and used to develop guidelines for the selection of the most efficient hammer systems.

However, the major weakness of both the wave equation and this new "pile driving formula" lies in the use of fictitious soil parameters which cannot be determined from conventional soil tests.

A more realistic soil model is therefore needed which incorporates non–linear behaviour of soil in a rational model of dynamic soil structure interaction. The most promising method for accomplishing this task is the finite element method.

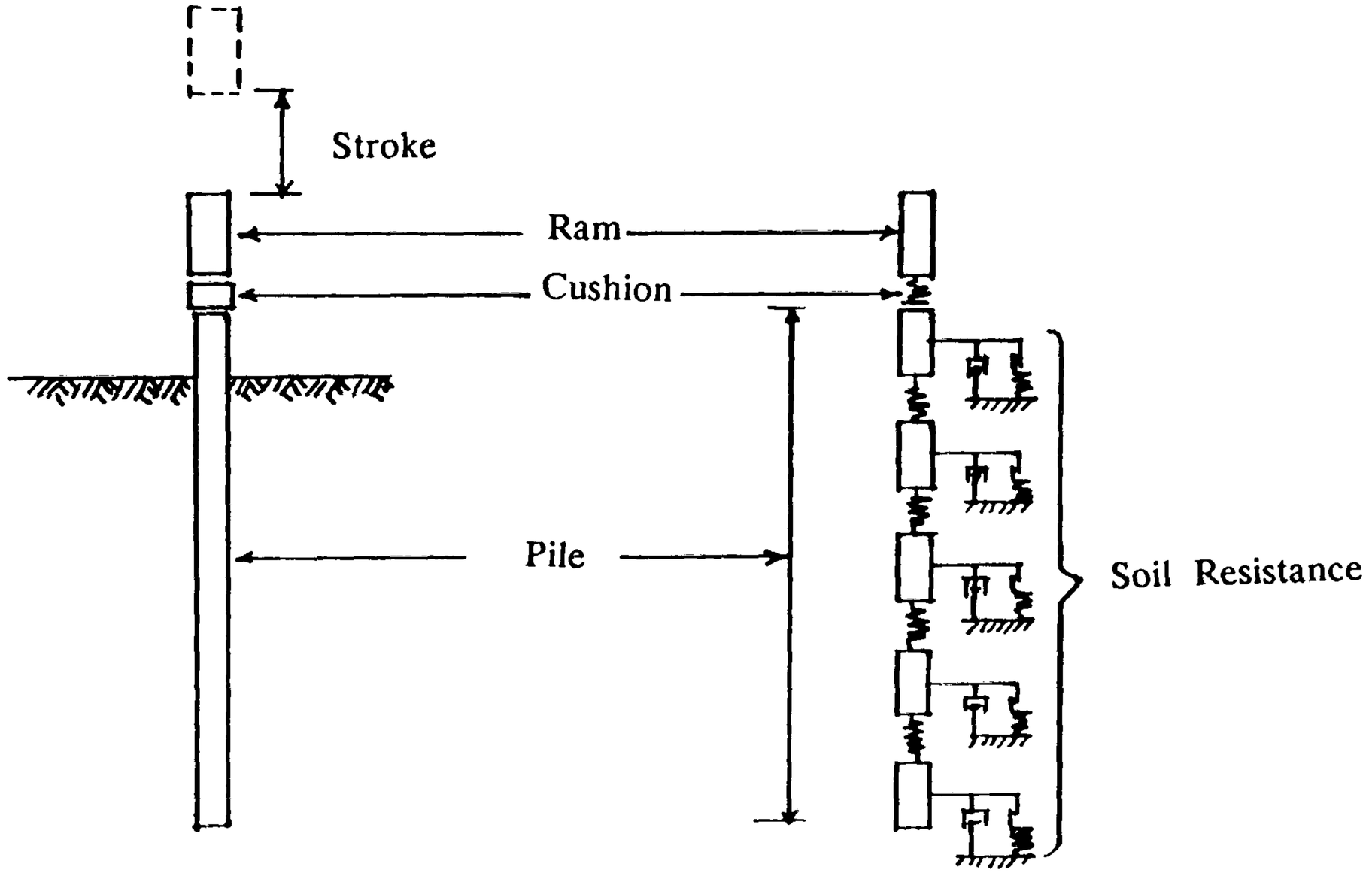

FIGURE (3.1) ACTUAL HAMMER_PILE_SOIL SYSTEM AND ITS WAVE EQUATION IDEALIZATION (AFTER E. A. L. SMITH, 1960)

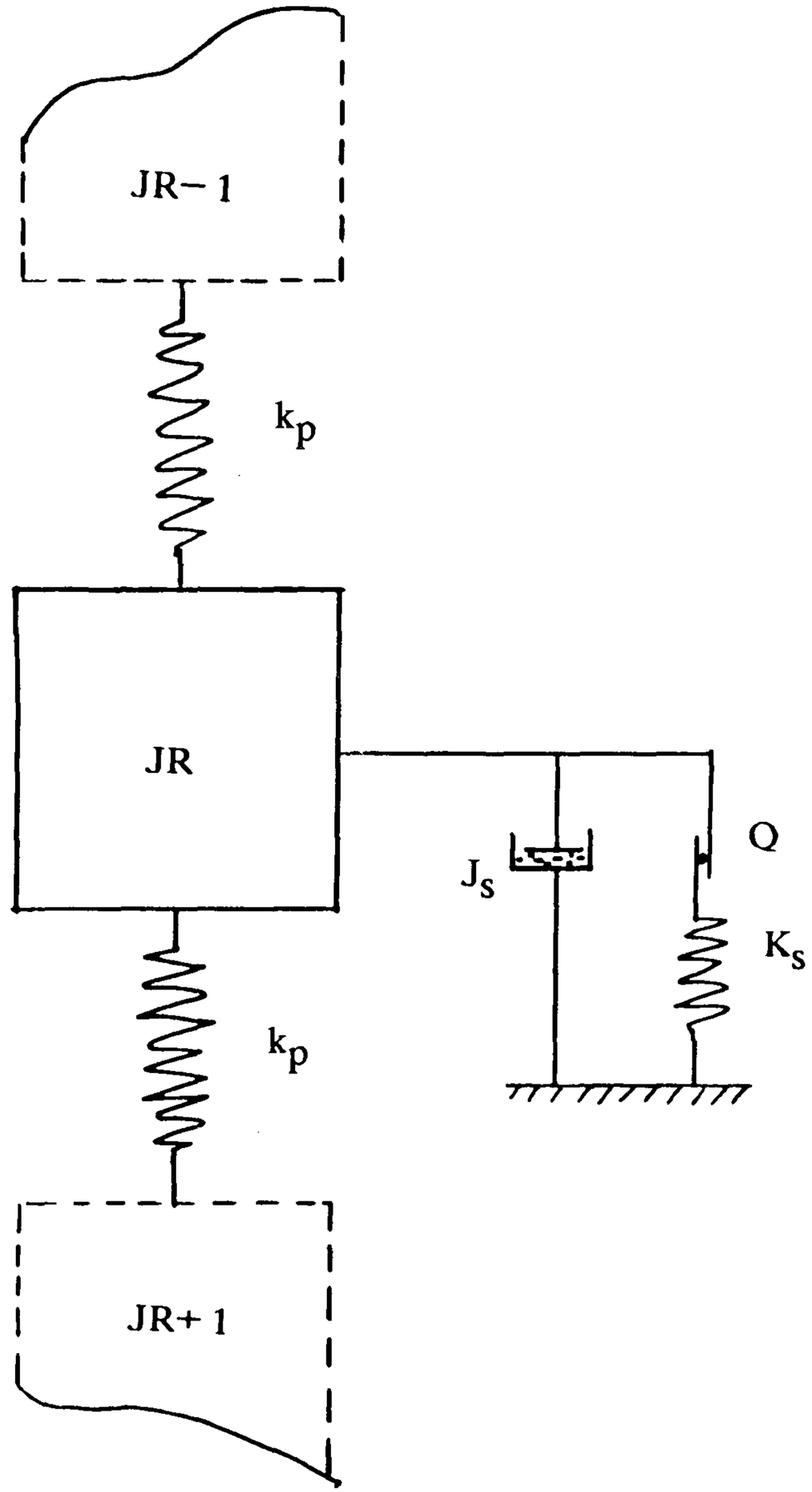

FIGURE (3.2) FREE BODY DIAGRAM OF AN IDEAL PILE ELEMENT ALONG

TEXT CUT OFF IN ORIGINAL

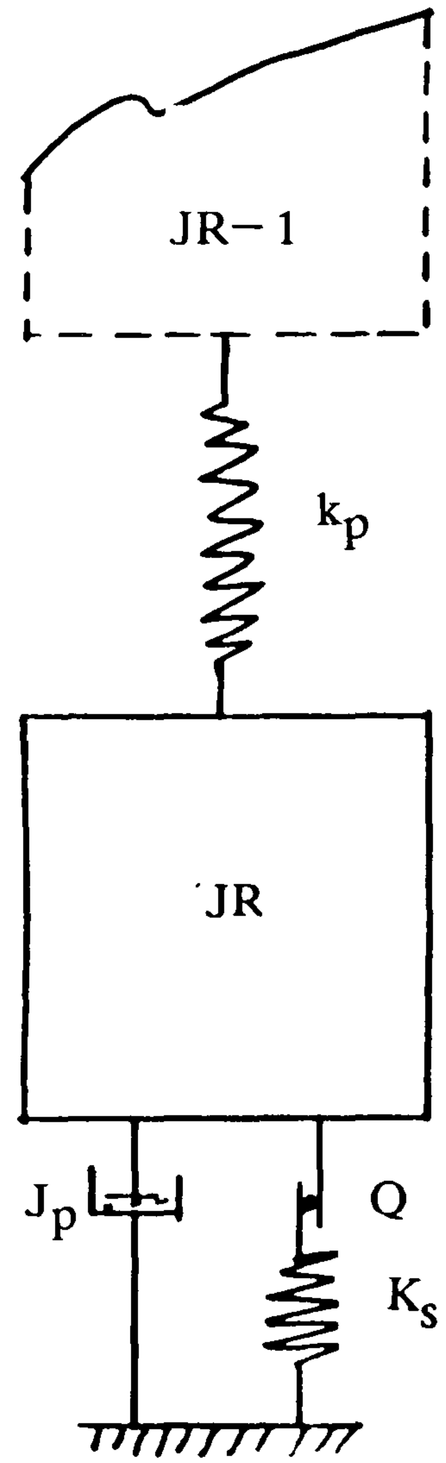

FIGURE (3.3) FREE BODY DIAGRAM OF AN IDEAL PILE ELEMENT ON THE

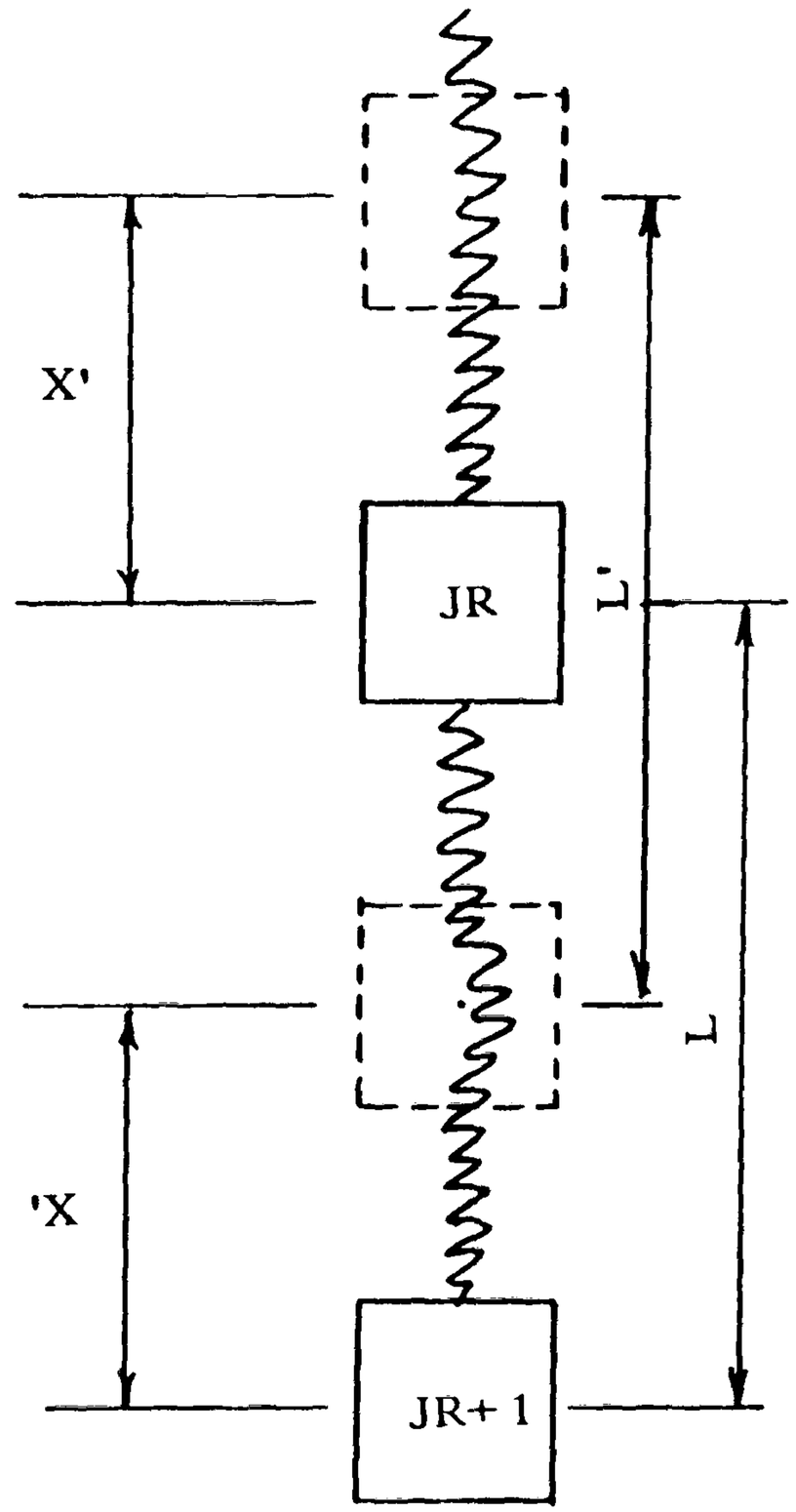

FIGURE (3.4) INTERNAL SPRING COMPRESSION (AFTER E. A. L. SMITH, 1955)

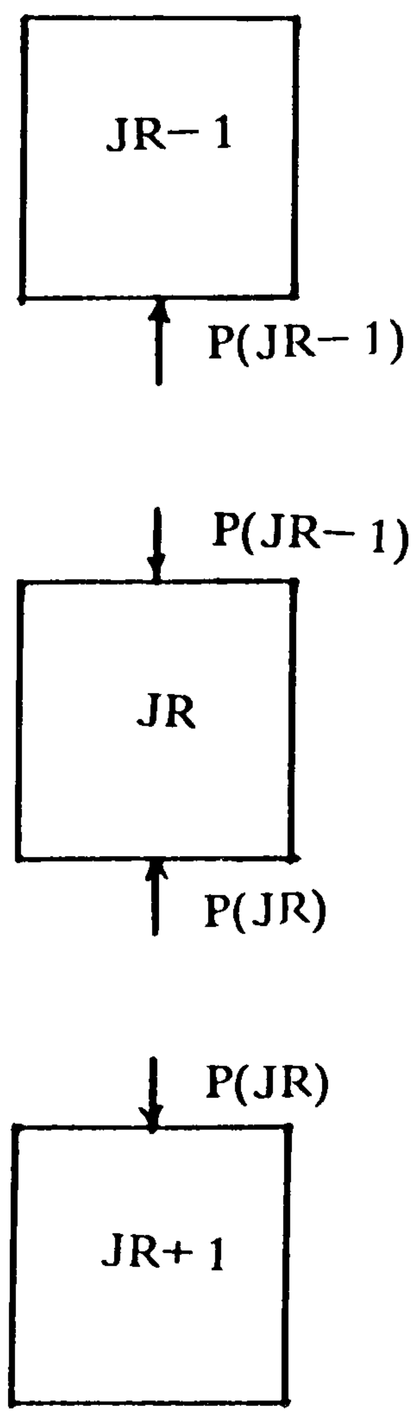

FIGURE (3.5) INTERNAL PILE SPRING FORCES ACTING ON THE DISCRETE MASSES

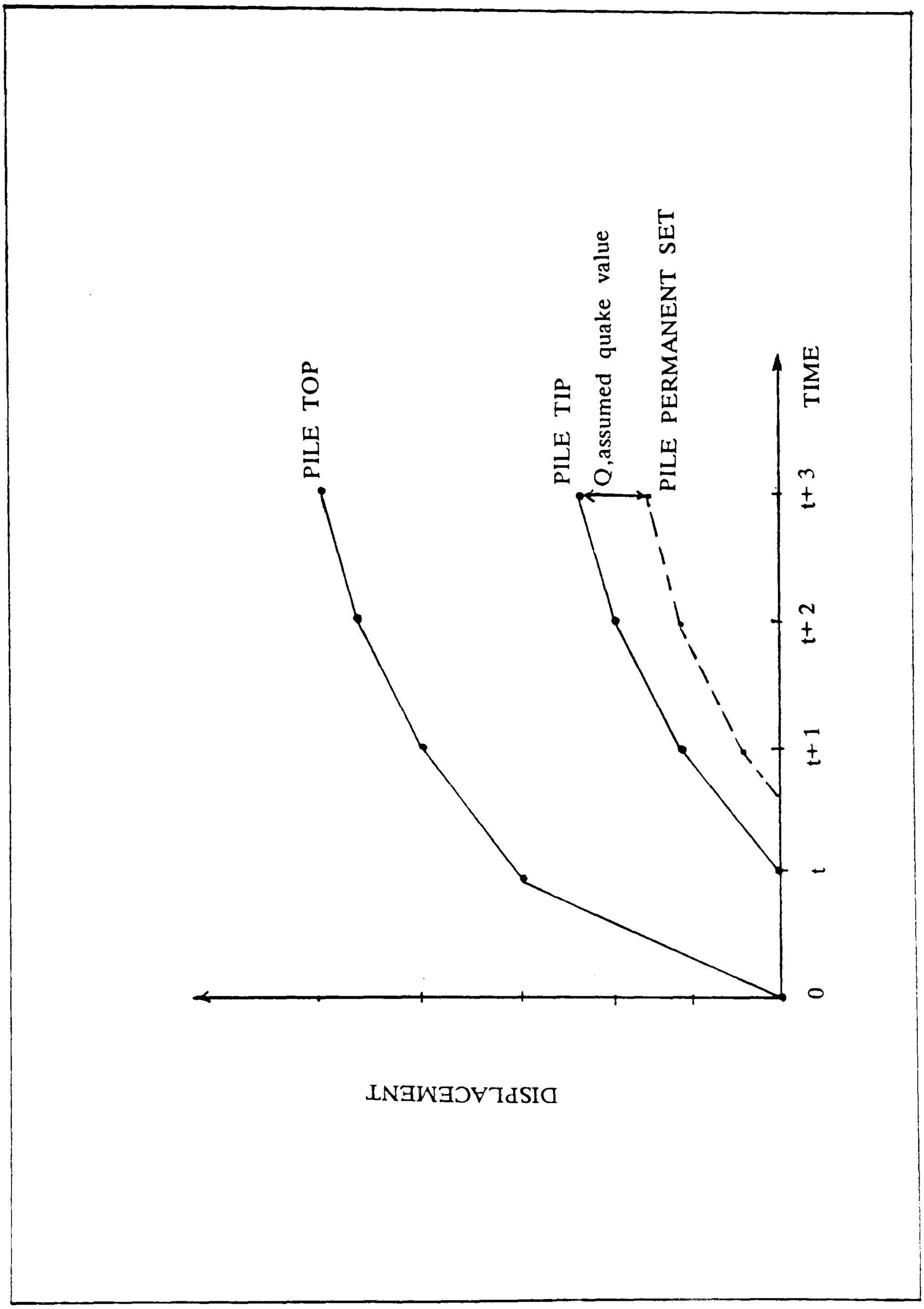

FIGURE (3.6) TYPICAL PILE DISPLACEMENT_TIME RELATIONSHIP PREDICTED
BY THE DISCRETE EQUATION SOLUTION OF THE WAVE EQUTION MODEL

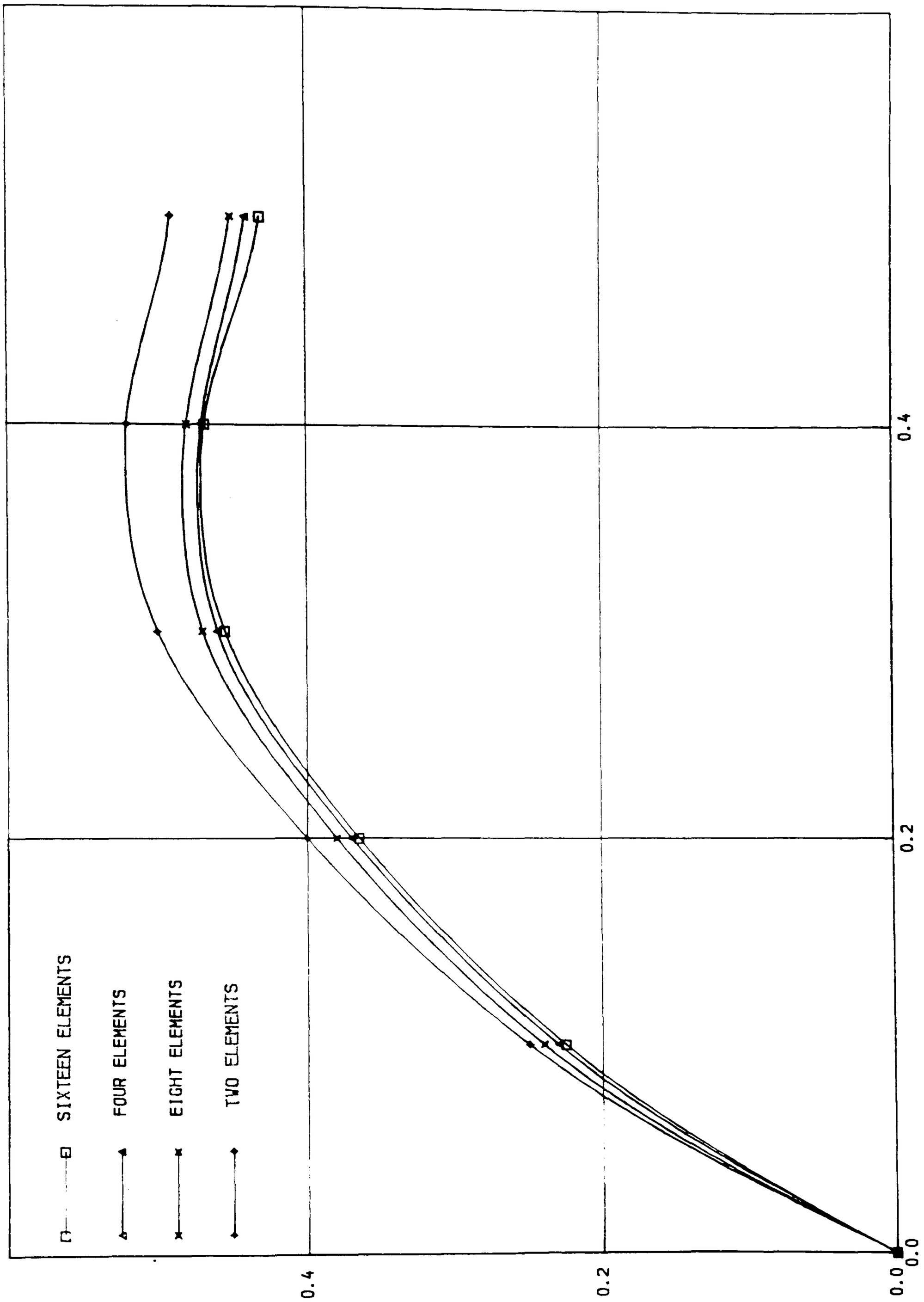

FIGURE (3.7) RAM FORCE-TIME RELATIONSHIP

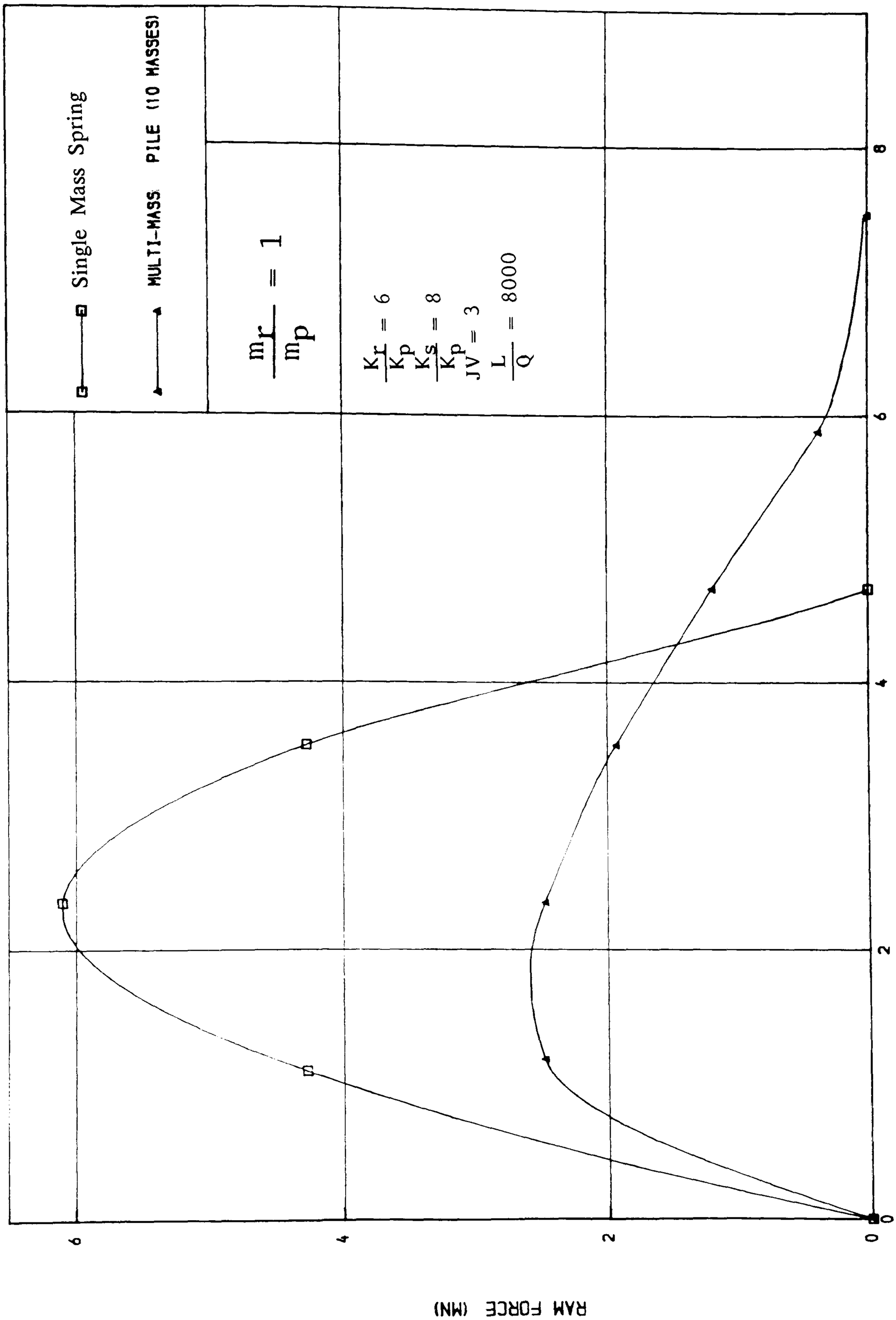

FIGURE (3.8) RAM FORCE_TIME RELATIONSHIP

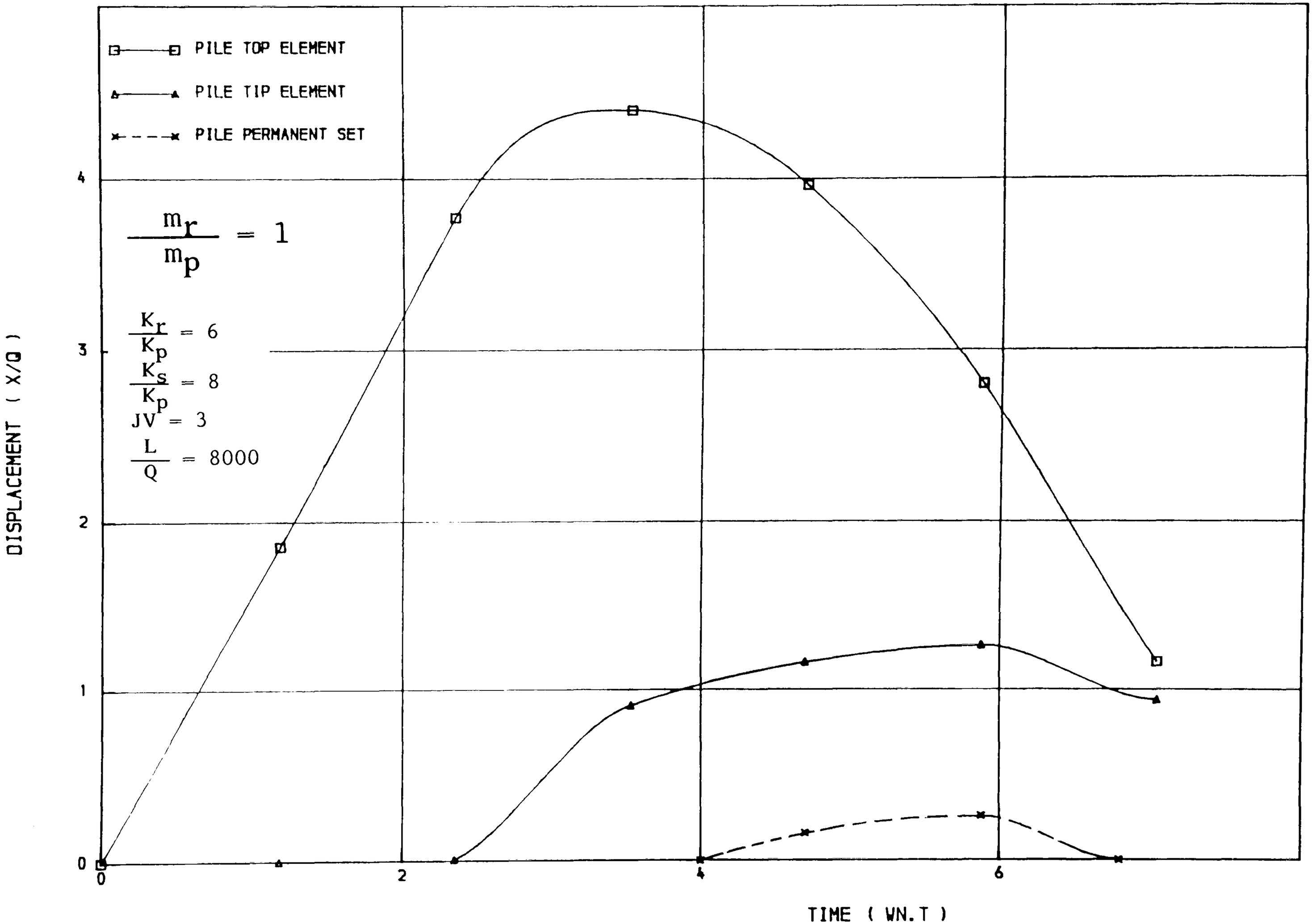

FIGURE (3.9) DISPLACEMENT_TIME RELATIONSHIP

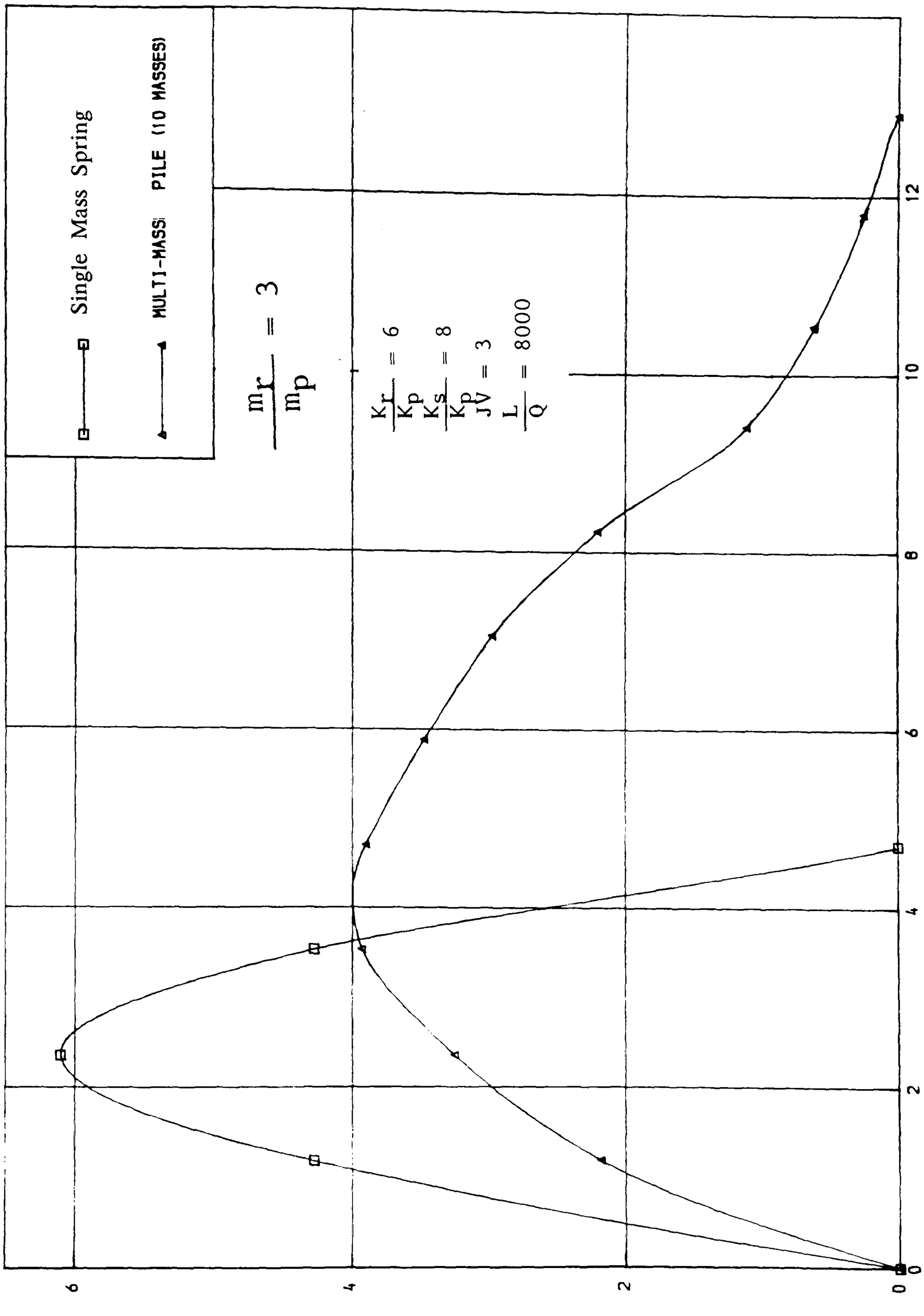

FIGURE (3.10) RAM FORCE-TIME RELATIONSHIP

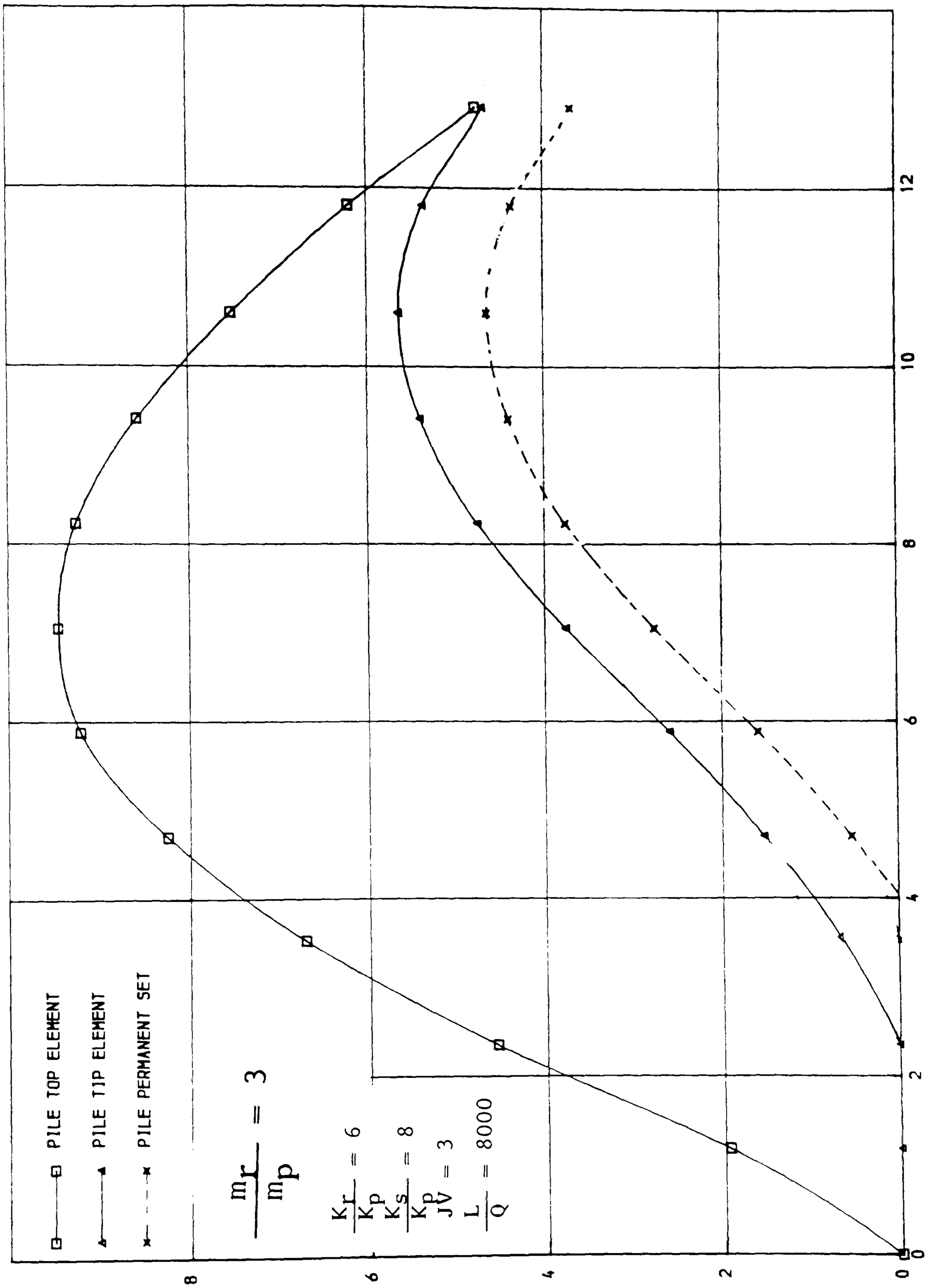

FIGURE (3.11) DISPLACEMENT-TIME RELATIONSHIP

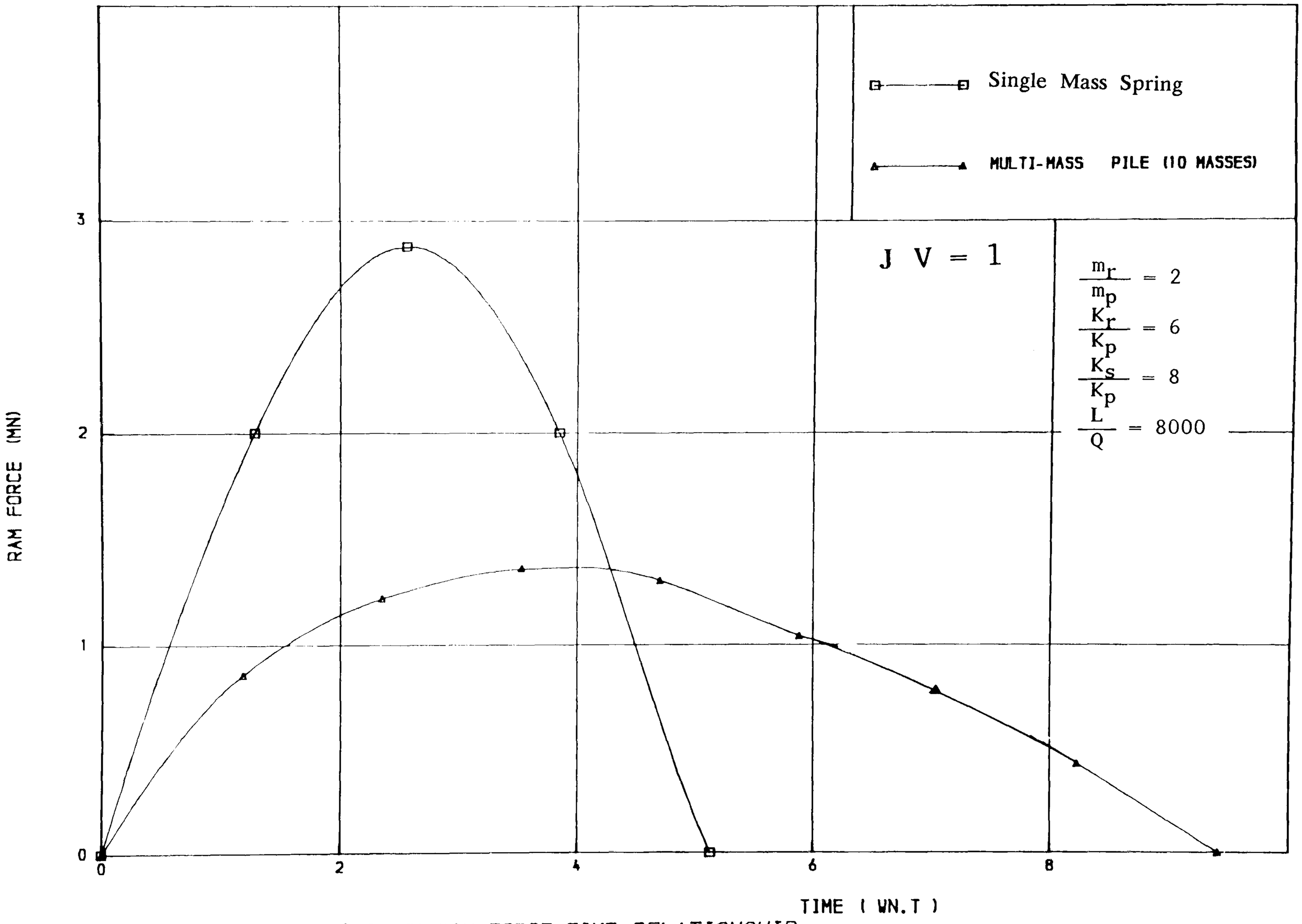

FIGURE (3. 12) RAM FORCE_TIME RELATIONSHIP

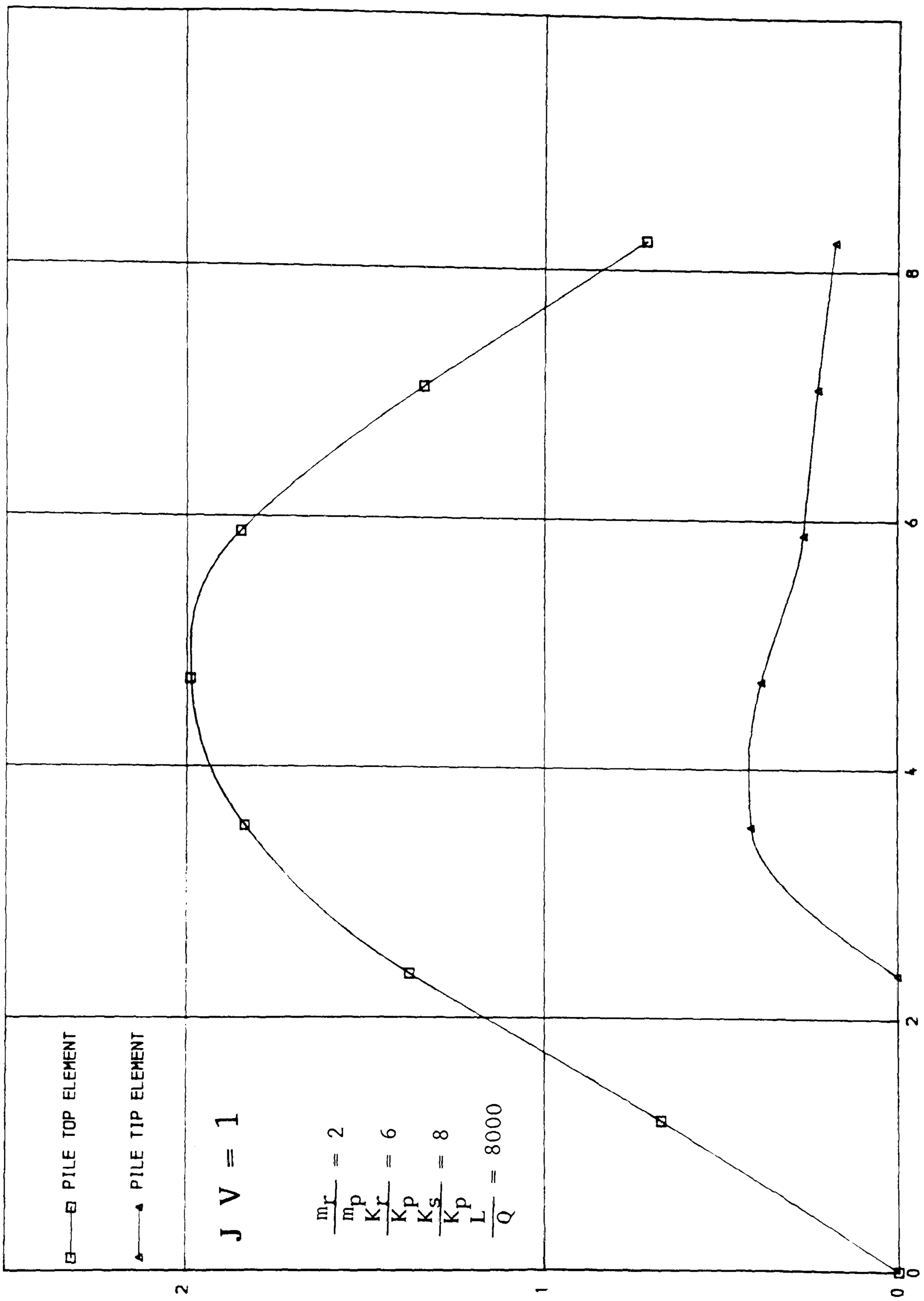

FIGURE (3.13) DISPLACEMENT_TIME RELATIONSHIP

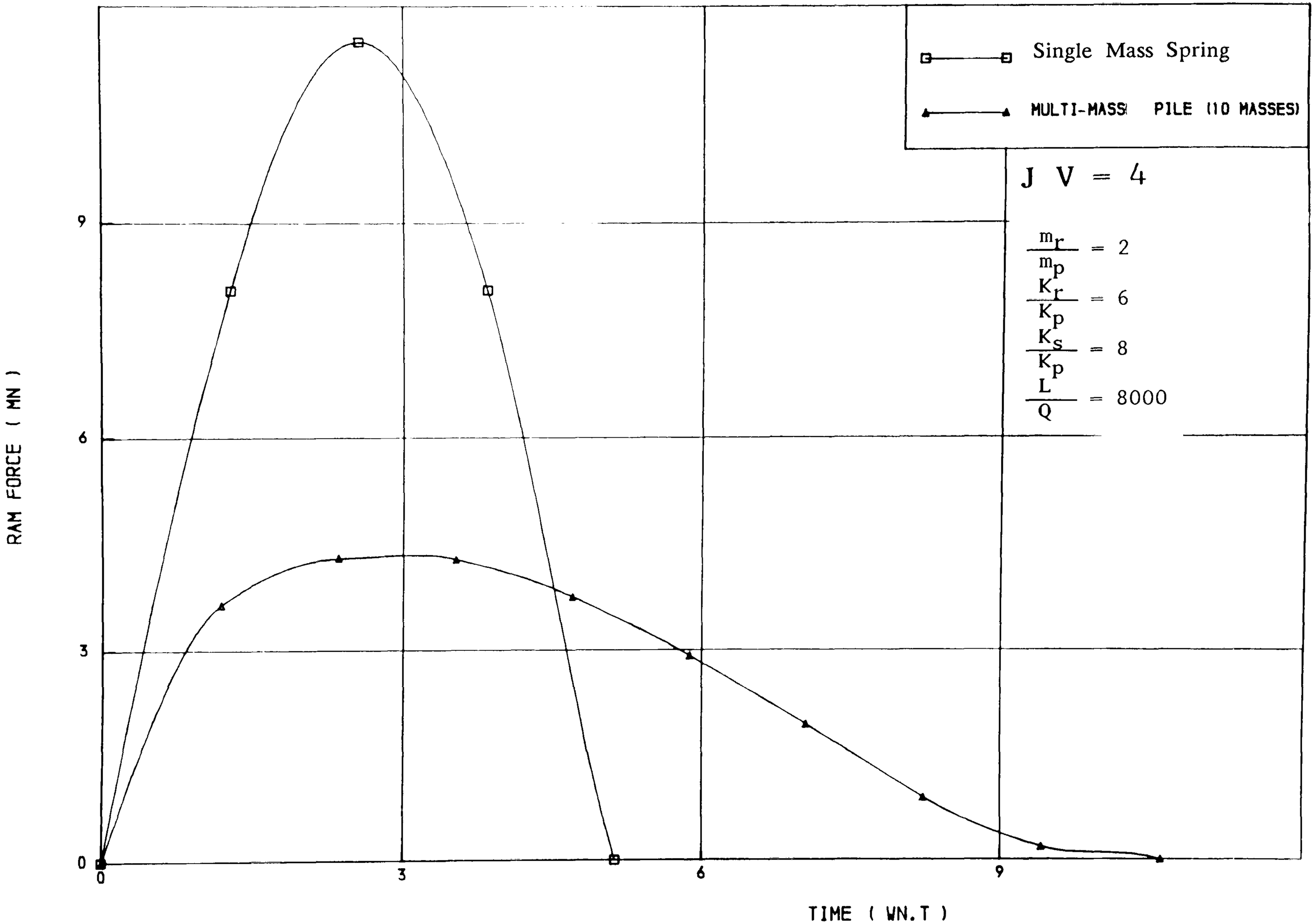

FIGURE (3.14) RAM FORCE_TIME RELATIONSHIP

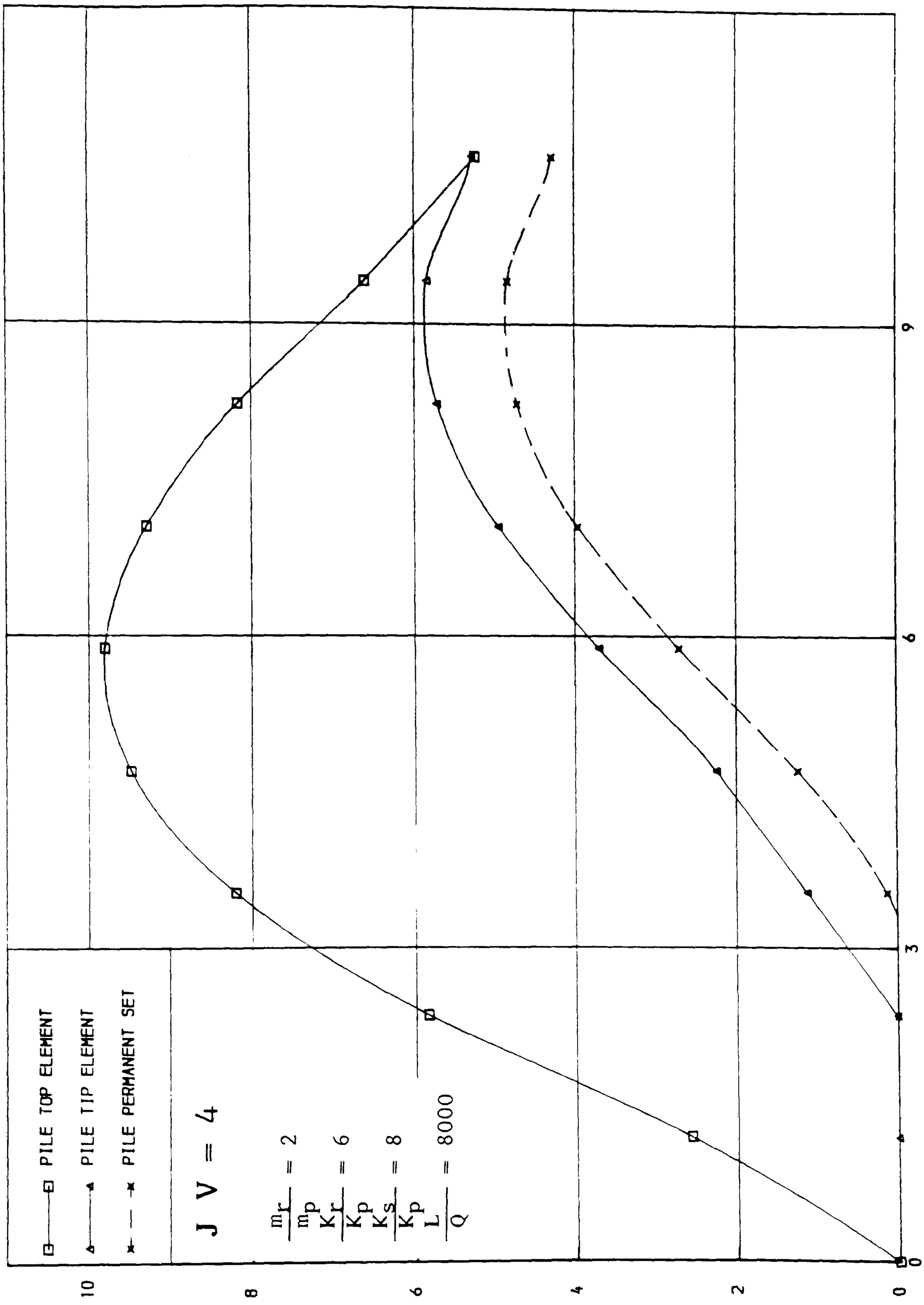

FIGURE (3.15) DISPLACEMENT_TIME RELATIONSHIP

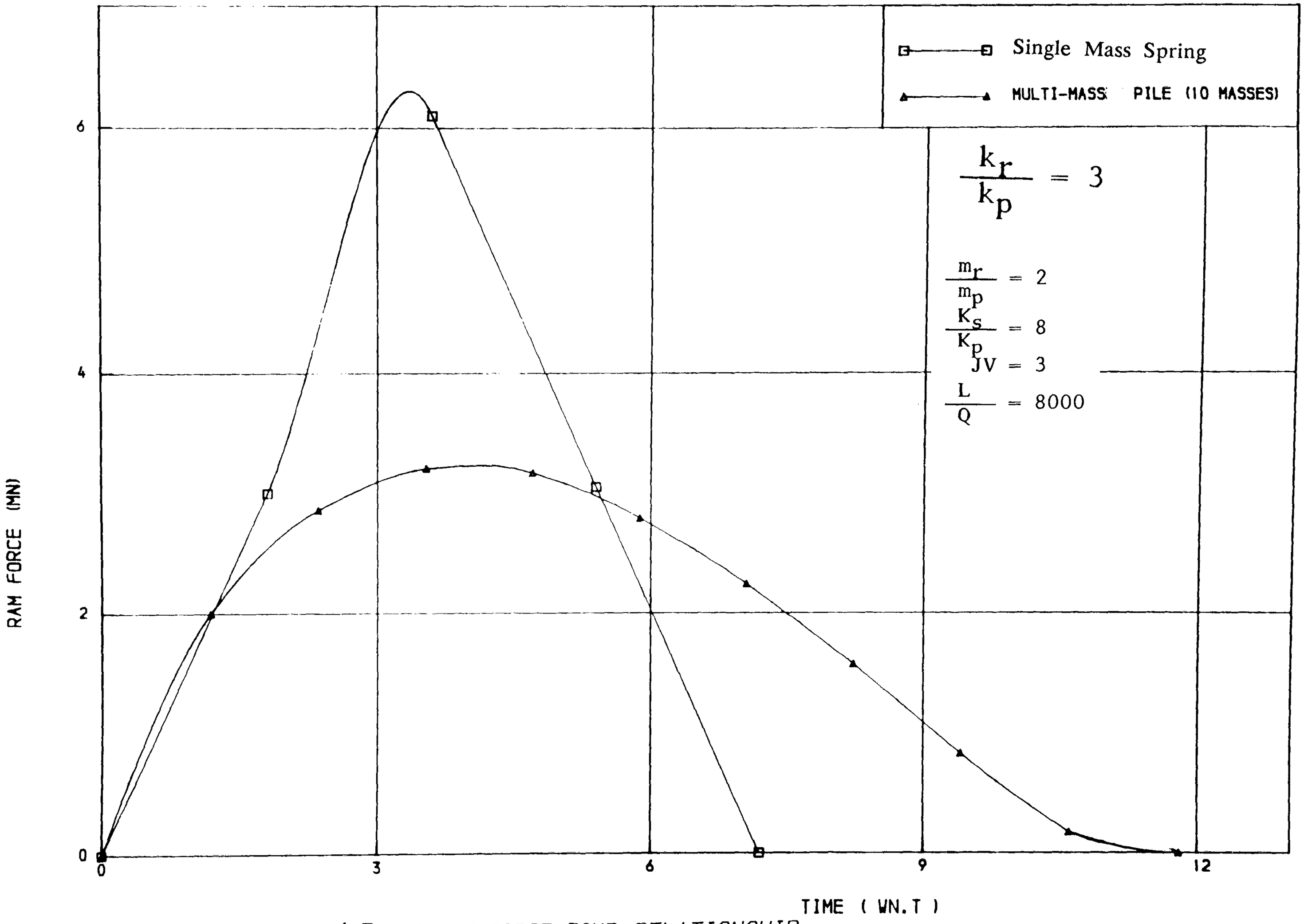

FIGURE (3.16) RAM FORCE-TIME RELATIONSHIP

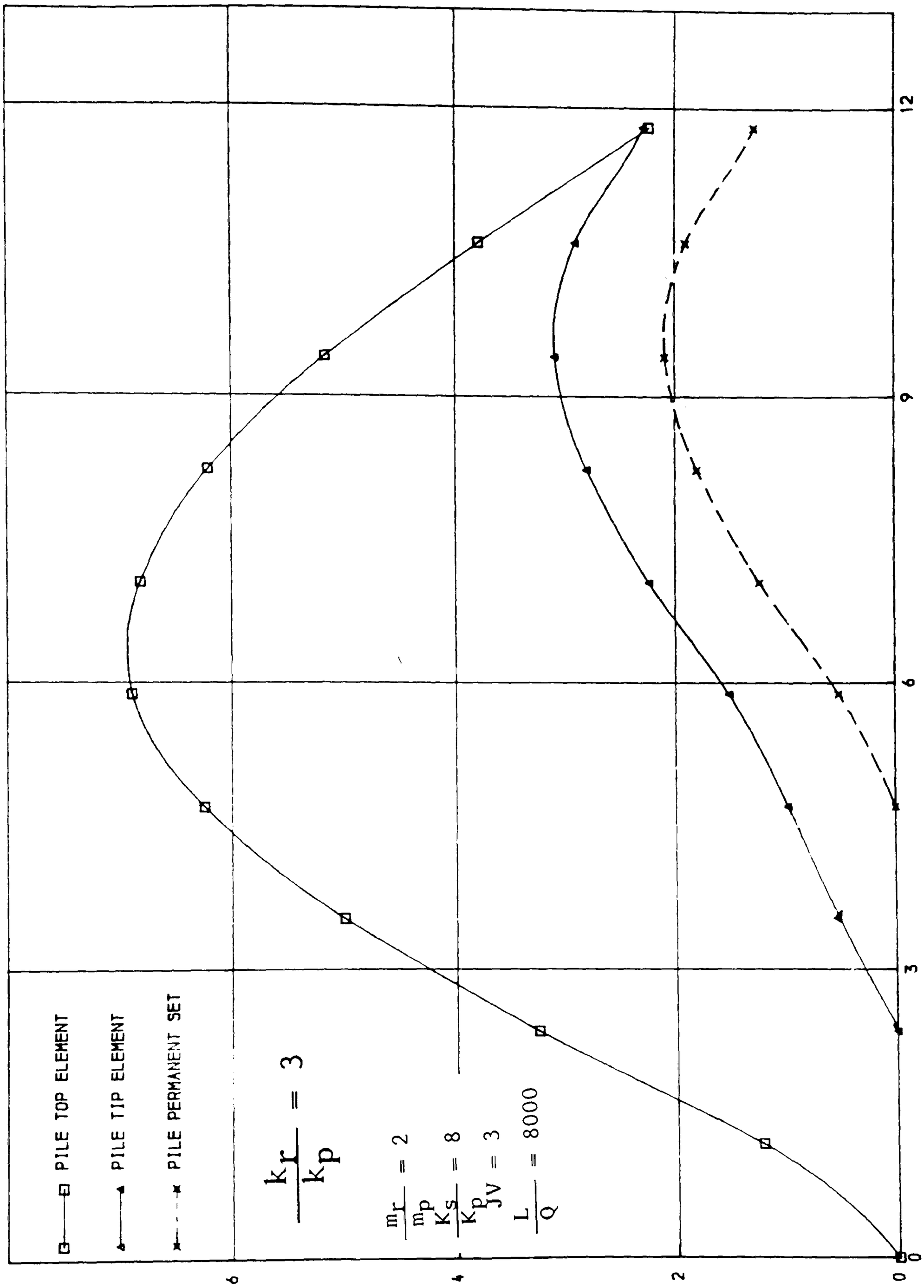

FIGURE (3.17) DISPLACEMENT-TIME RELATIONSHIP

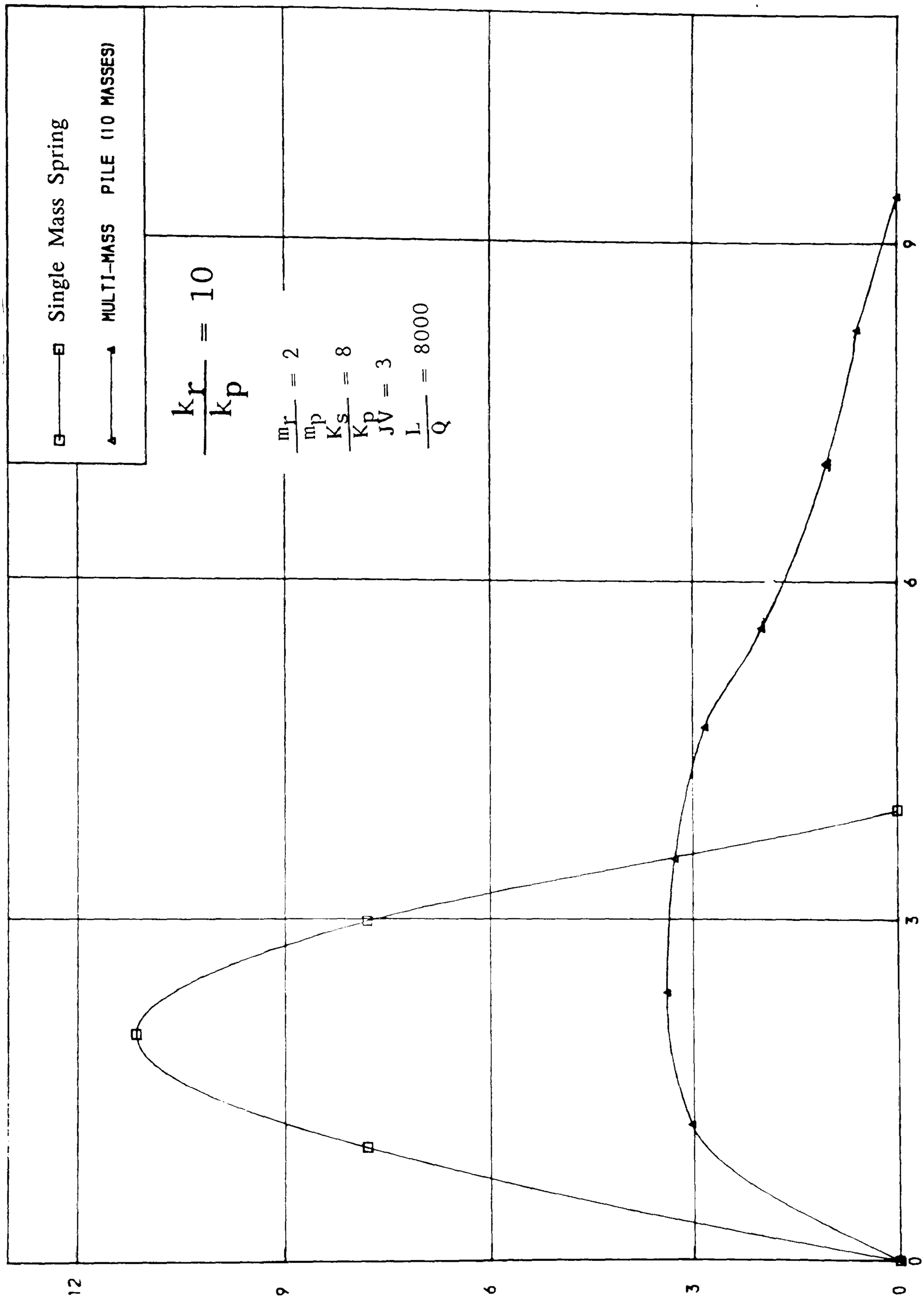

FIGURE (3.18) RAM FORCE_TIME RELATIONSHIP

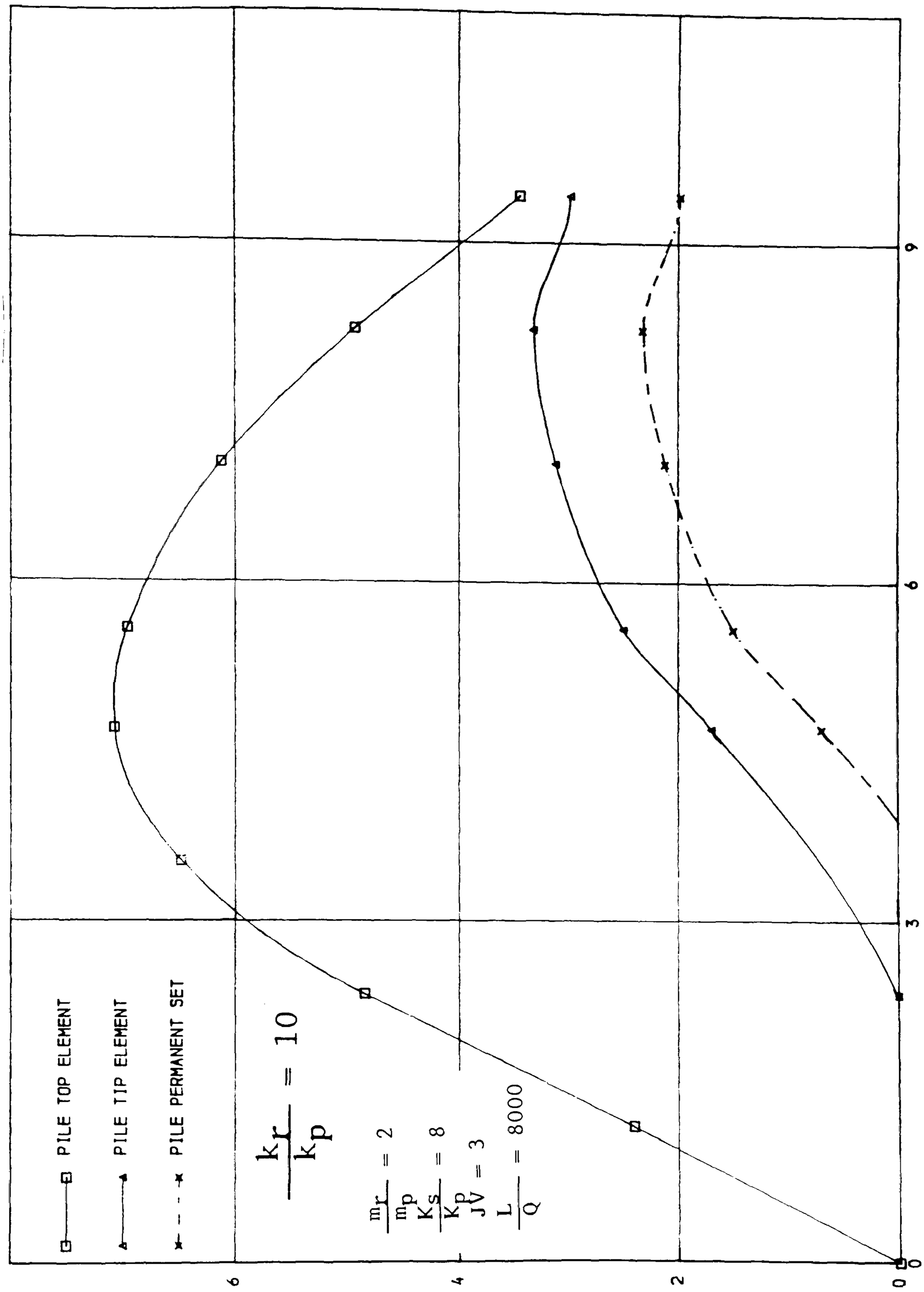

FIGURE (3.19) DISPLACEMENT-TIME

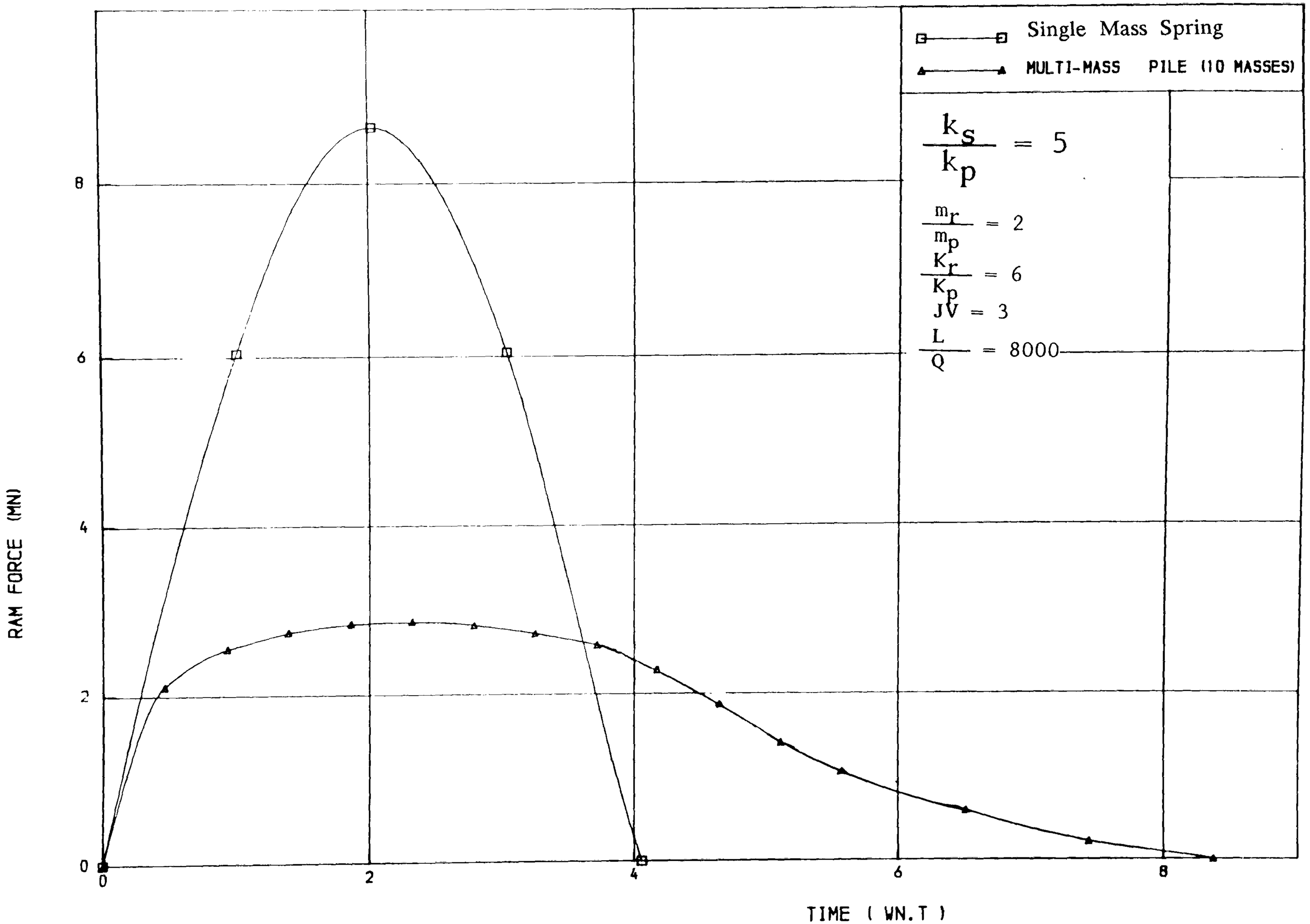

FIGURE (3.20) RAM FORCE-TIME RELATIONSHIP

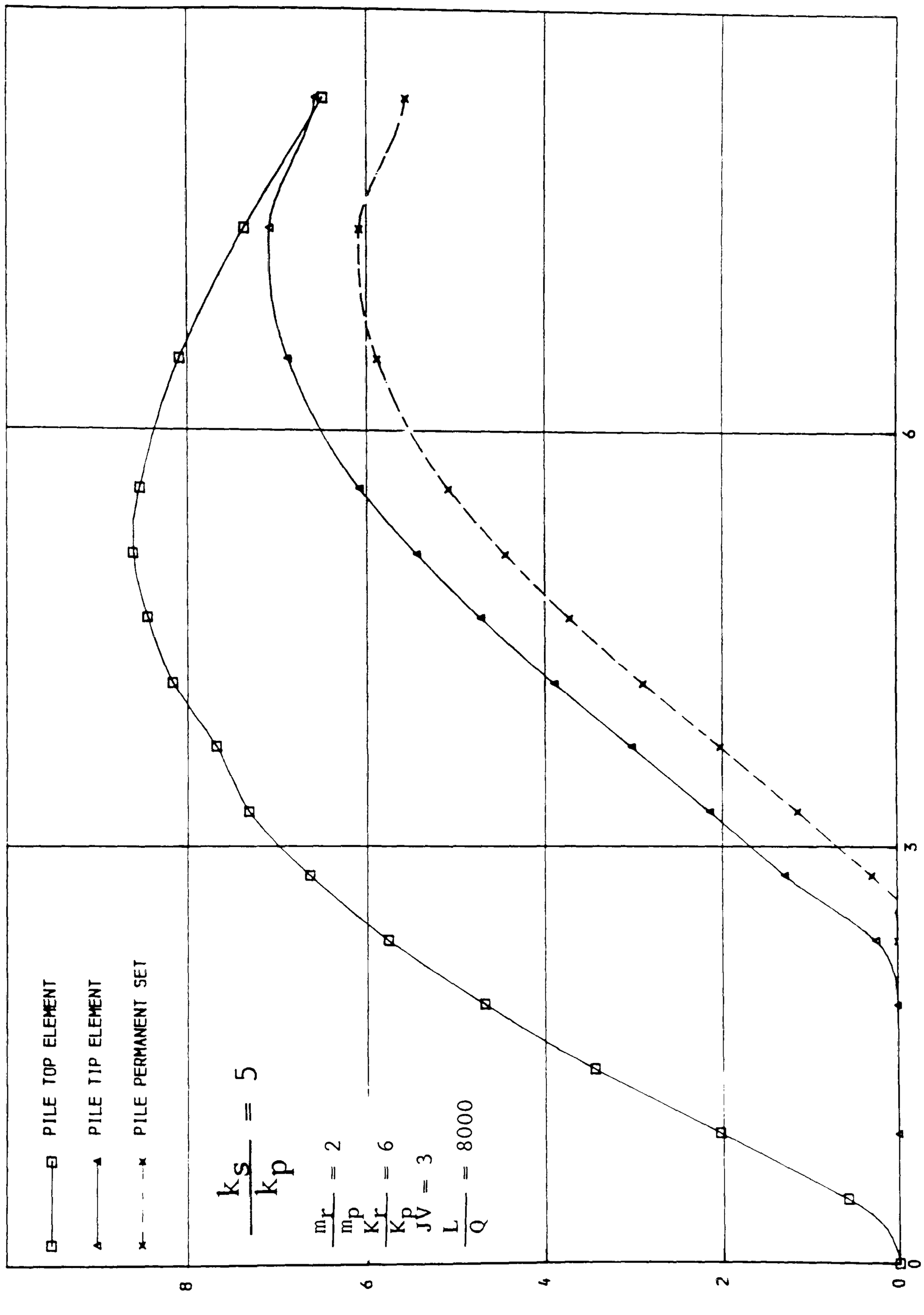

FIGURE (3.21) DISPLACEMENT-TIME RELATIONSHIP.

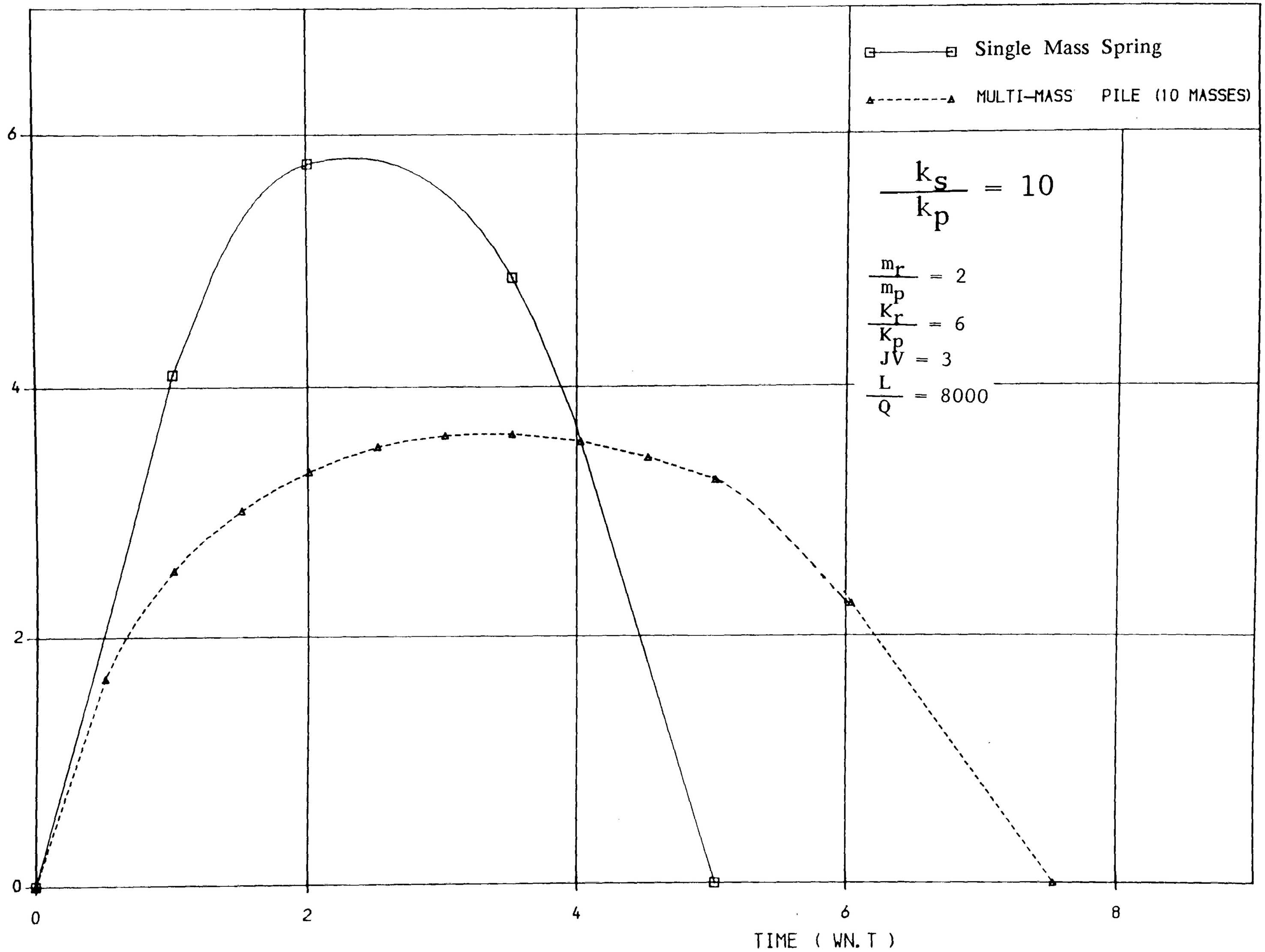

FIGURE 4.3.22 RAMFORCE-TIME RELATIONSHIP

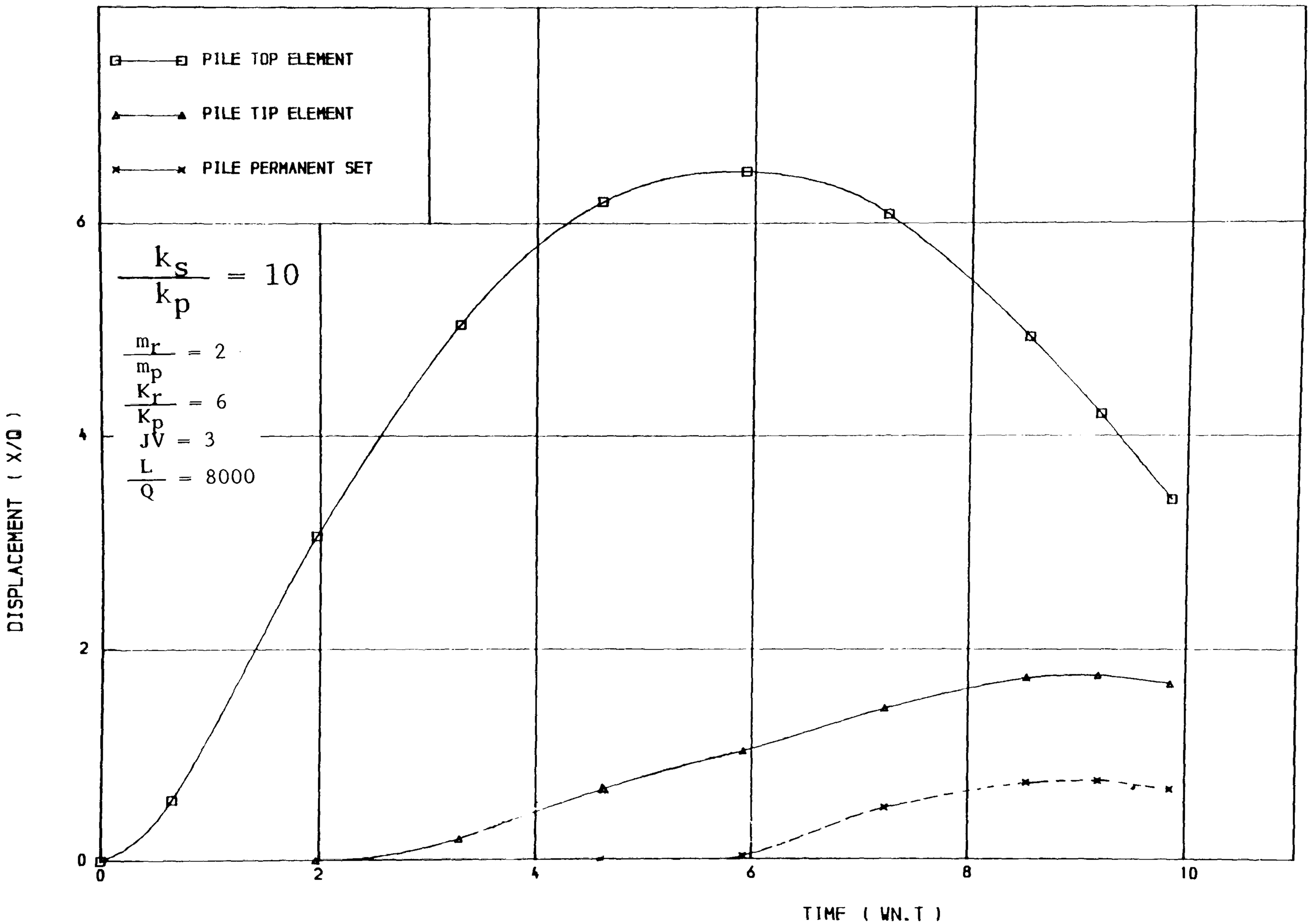

FIGURE (3.23) DISPLACEMENT_TIME RELATIONSHIP

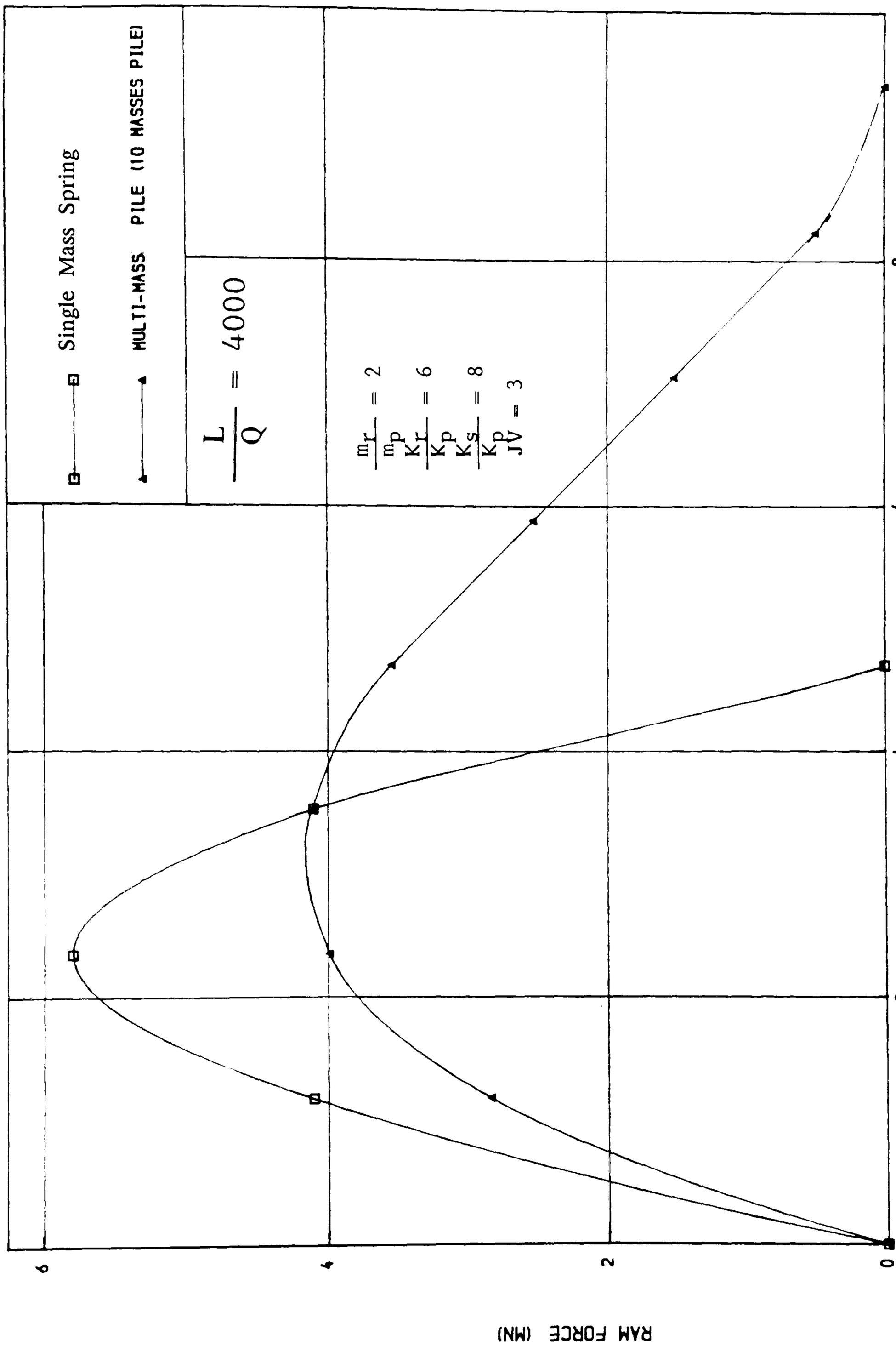

FIGURE (3.24) RAM FORCE_TIME RELATIONSHIP

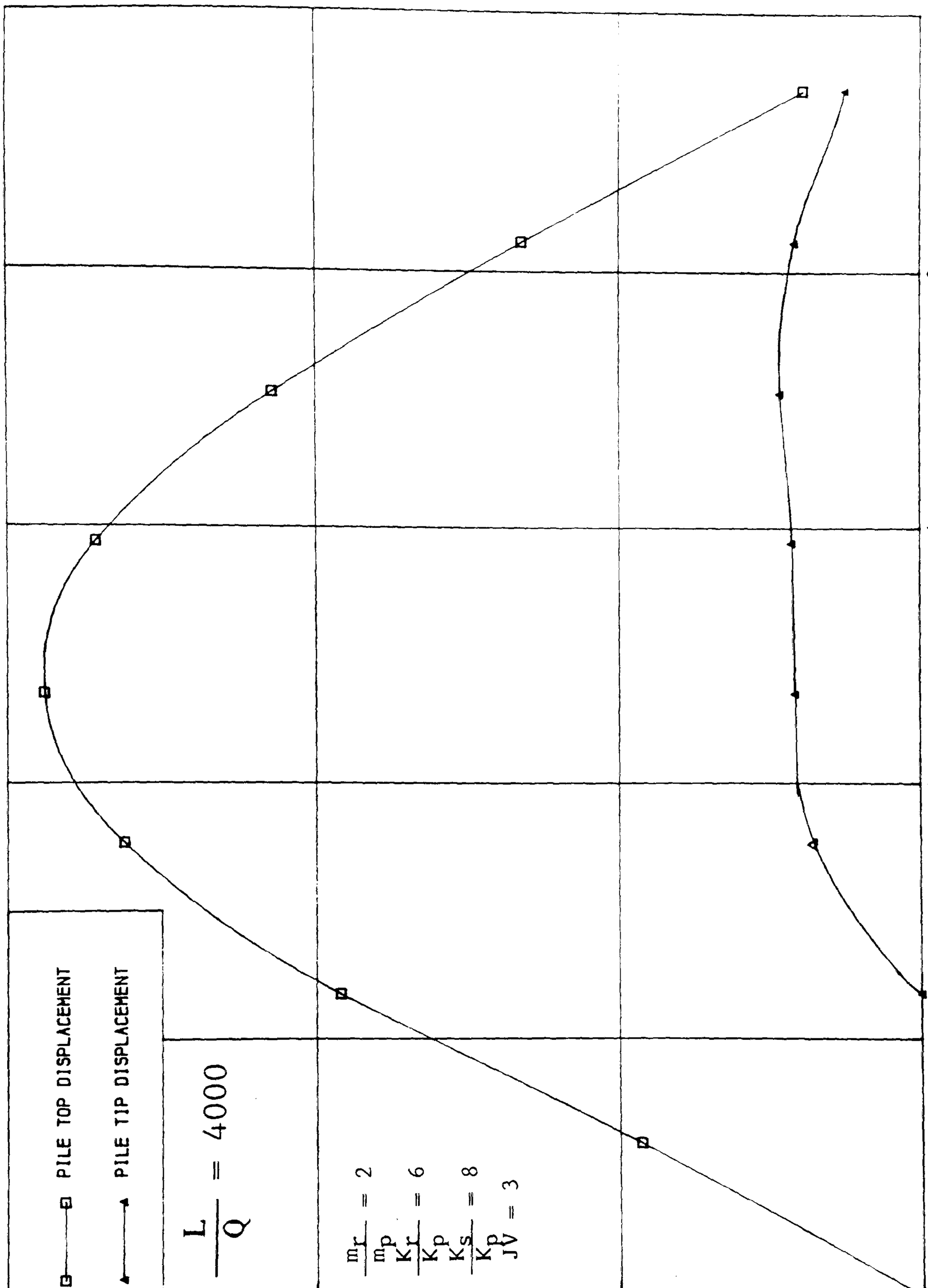

FIGURE (3.25) DISPLACEMENT-TIME RELATIONSHIP

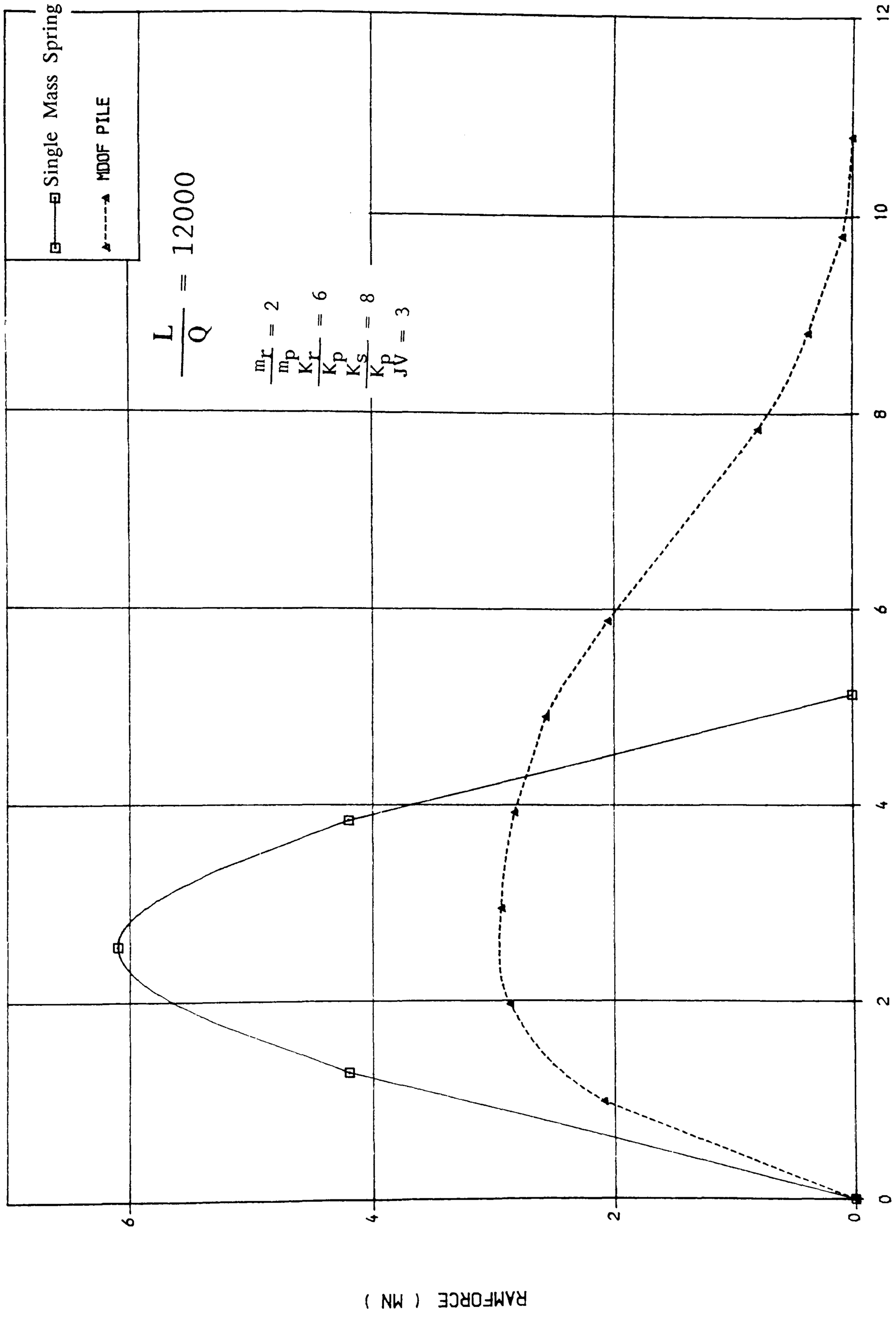

FIGURE (3.26) RAMFORCE_TIME RELATIONSHIP

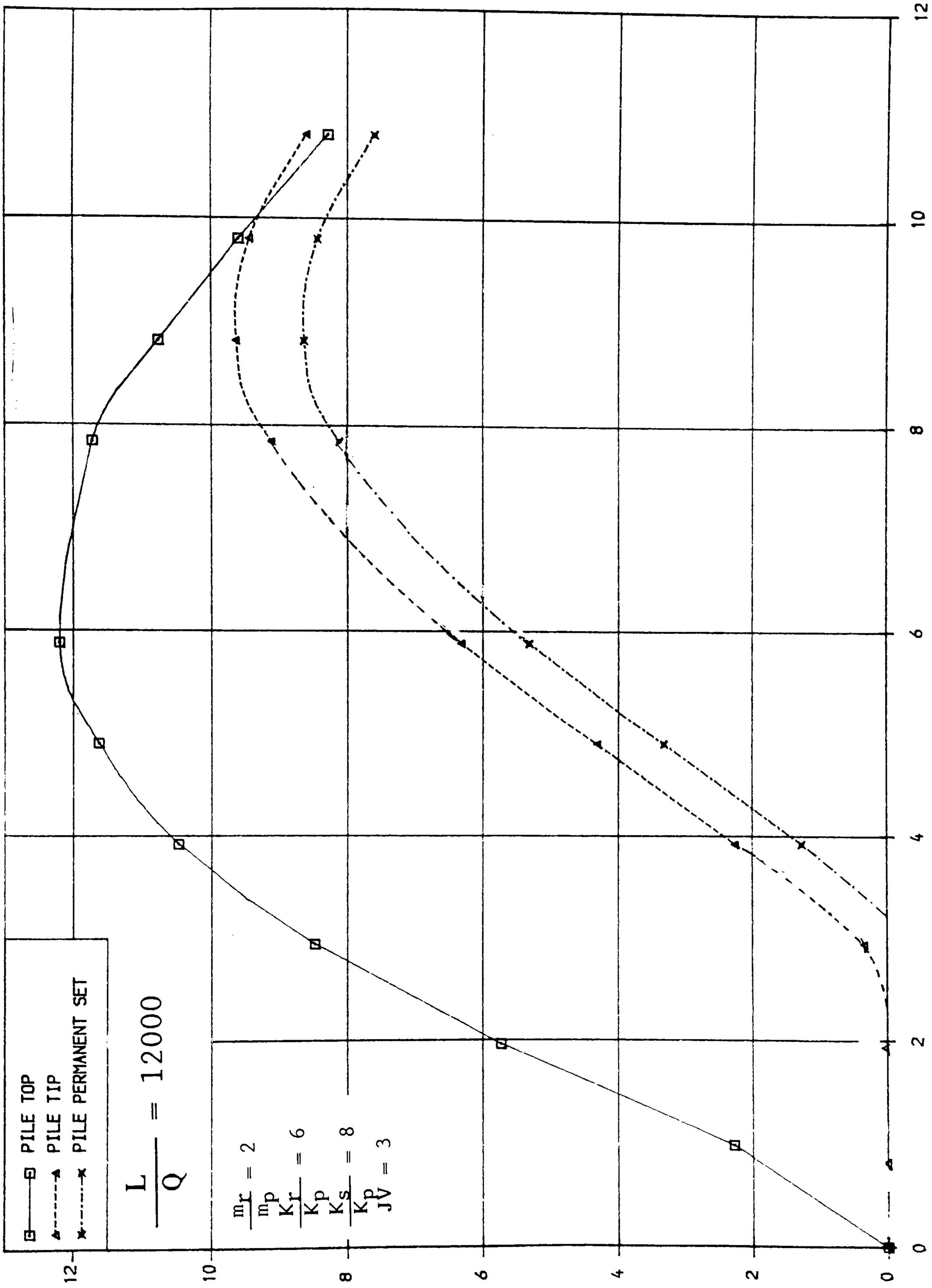

FIGURE (3.27) DISPLACEMENT_TIME RELATIONSHIP

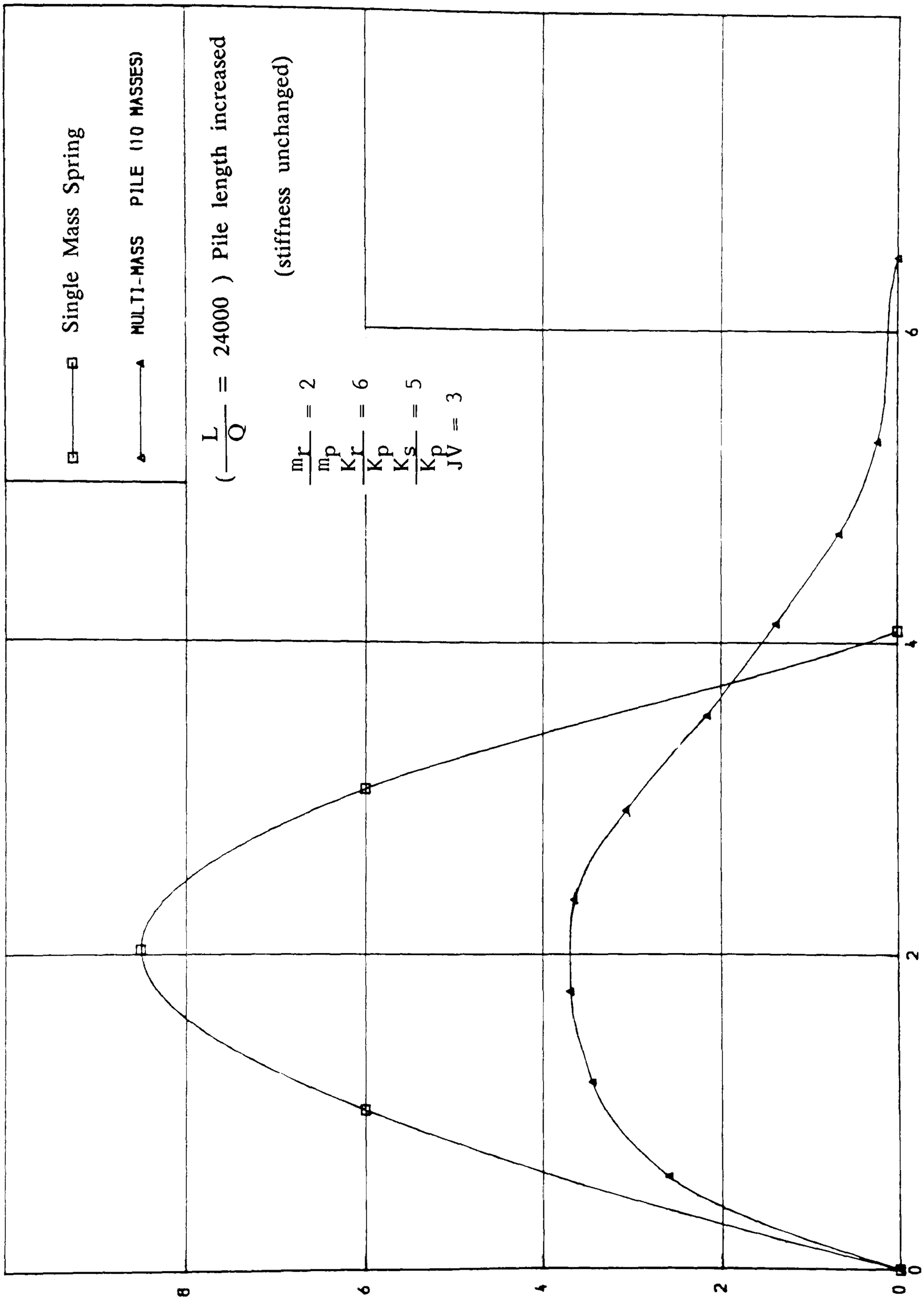

FIGURE (3.28) RAM FORCE-TIME RELATIONSHIP

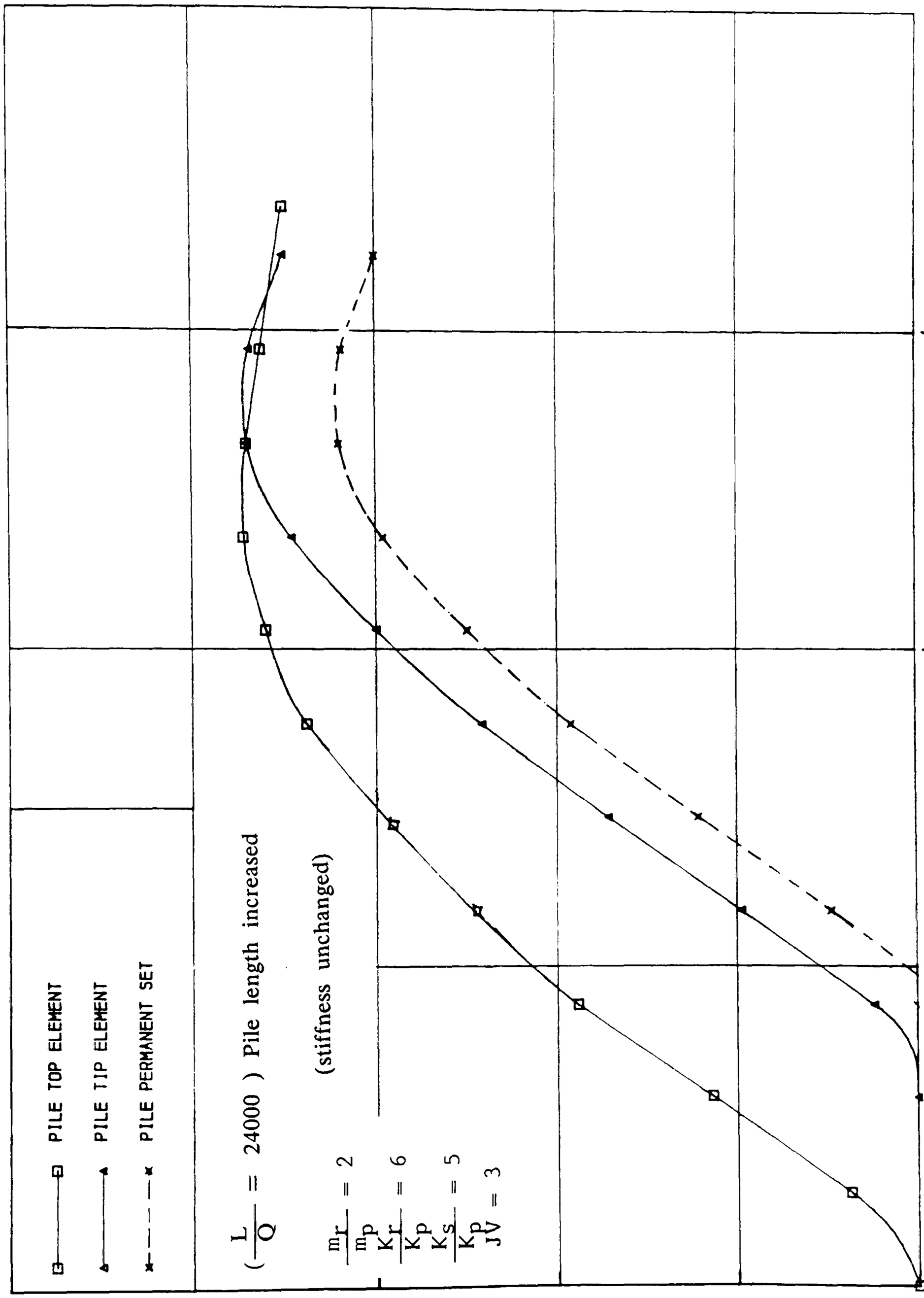

FIGURE (3.29) DISPLACEMENT-TIME RELATIONSHIP

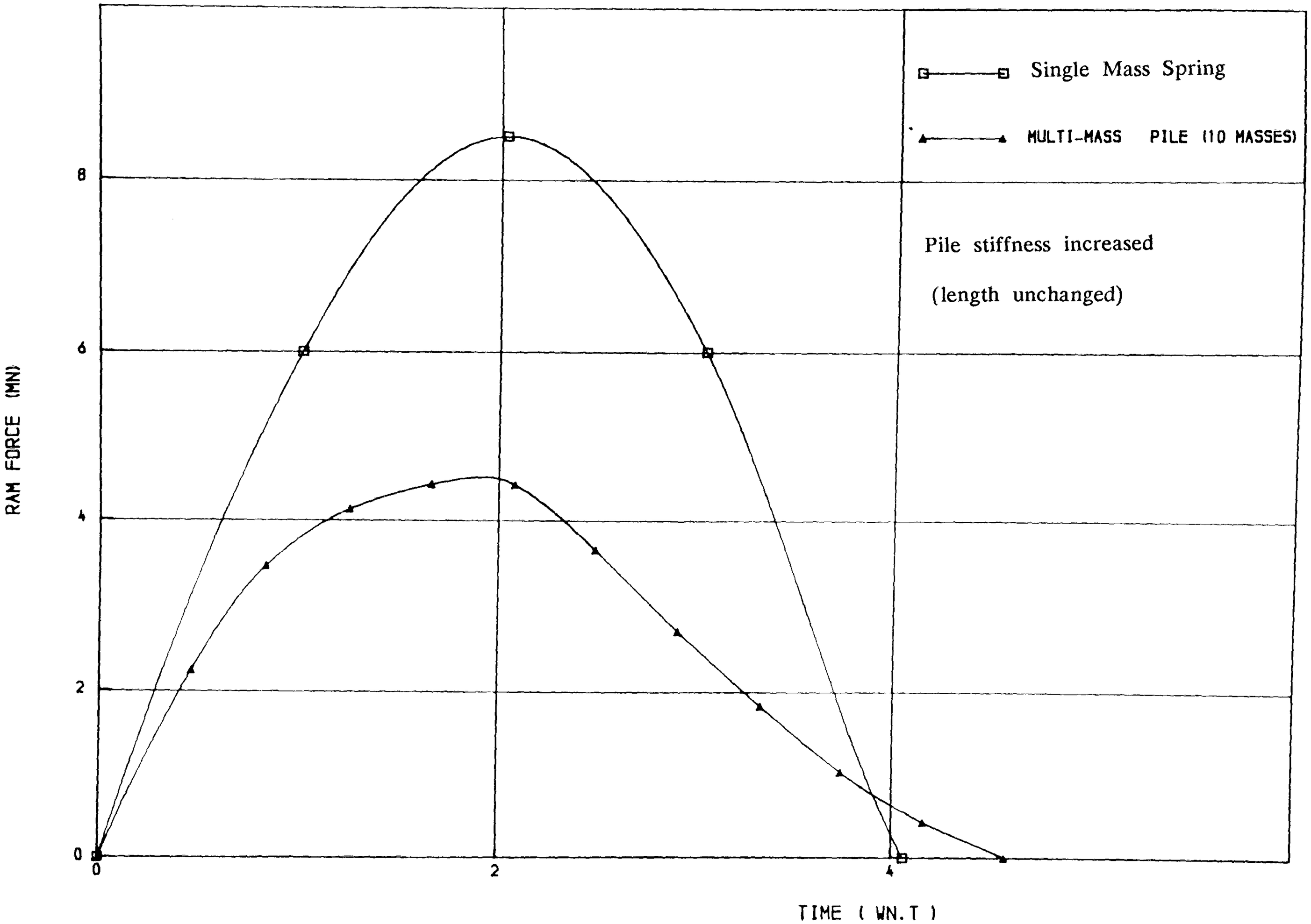

FIGURE (3.30) RAM FORCE_TIME RELATIONSHIP

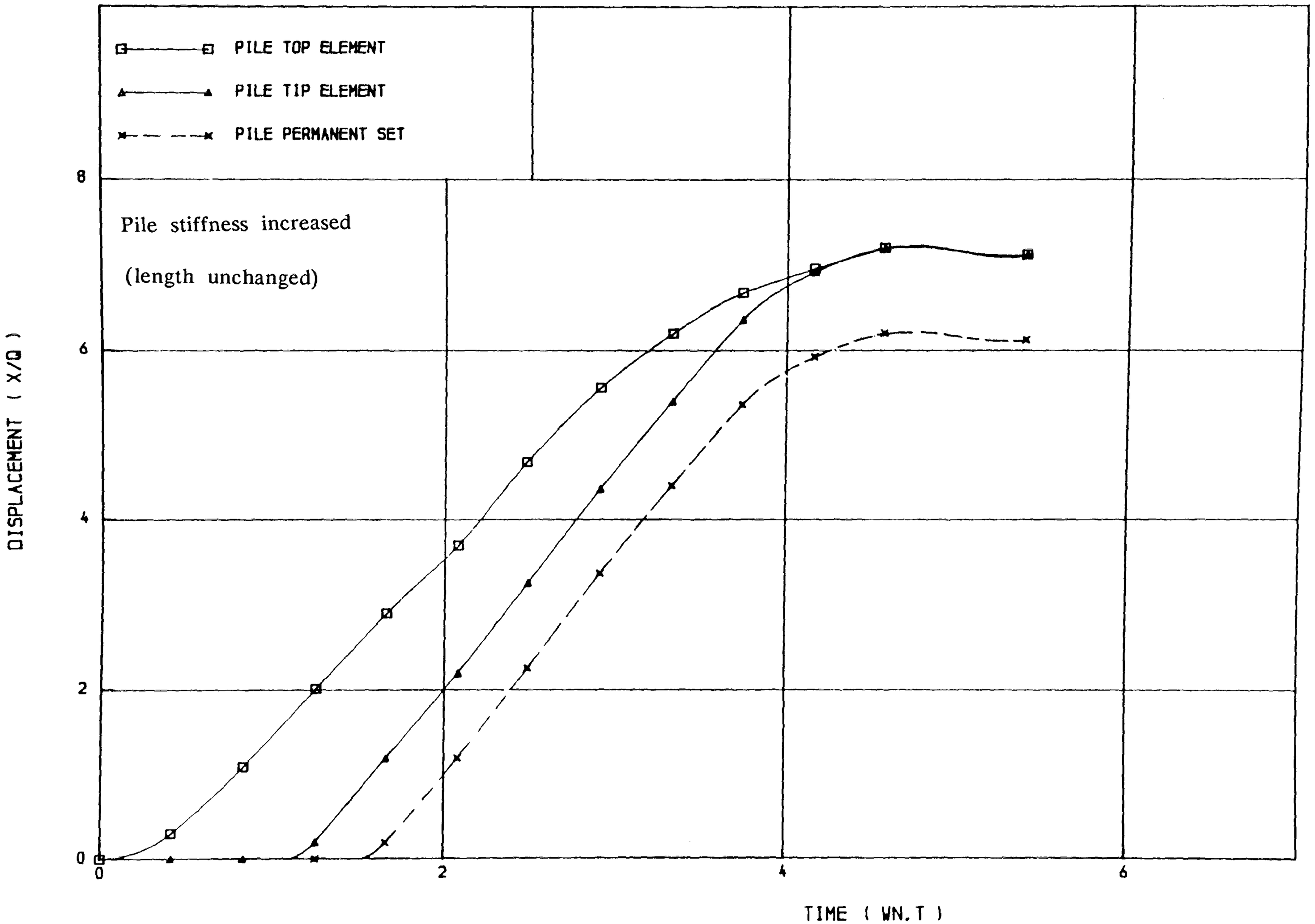

FIGURE (3.31) DISPLACEMENT_TIME RELATIONSHIP

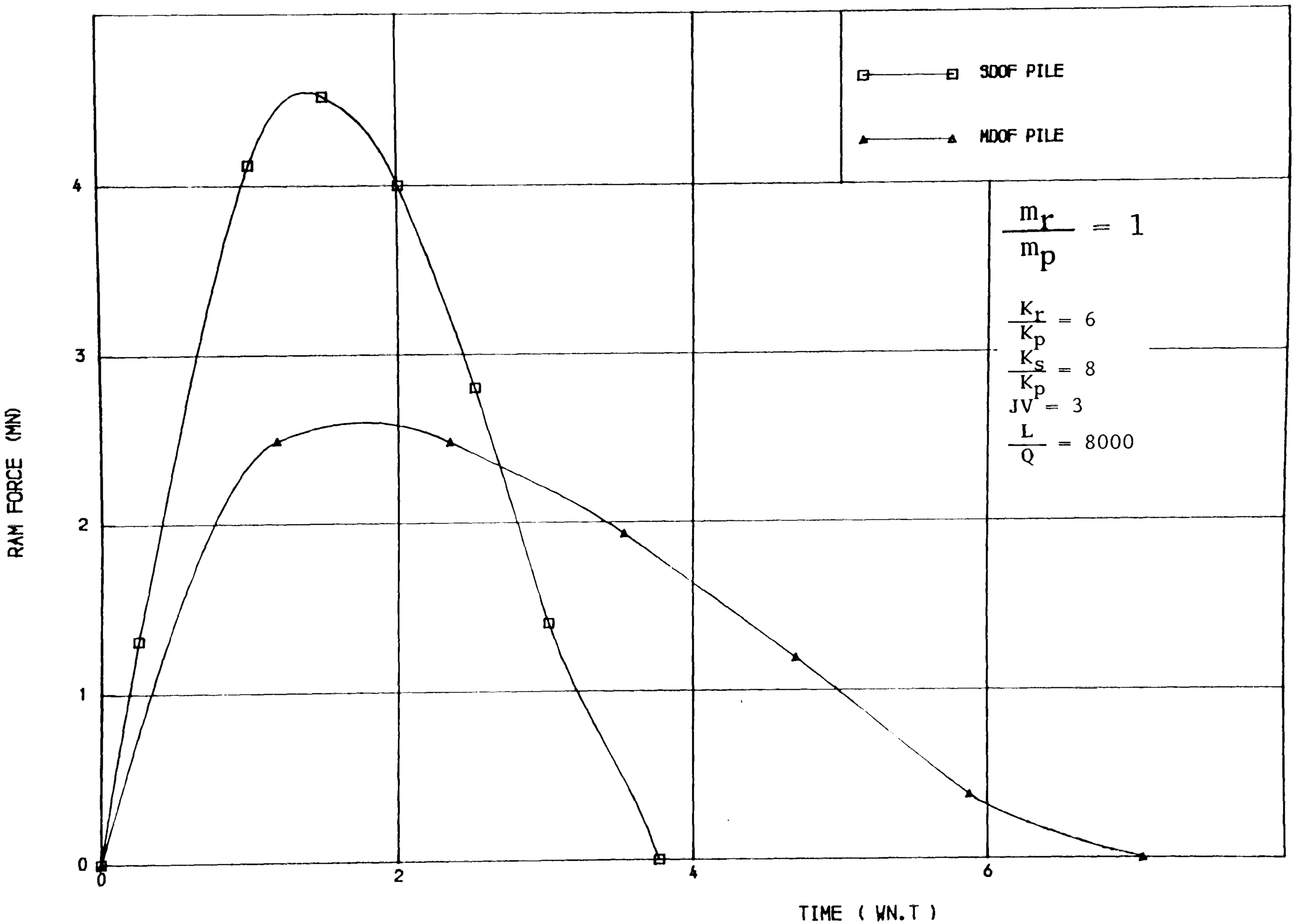

FIGURE (3.32) RAM FORCE_TIME RELATIONSHIP

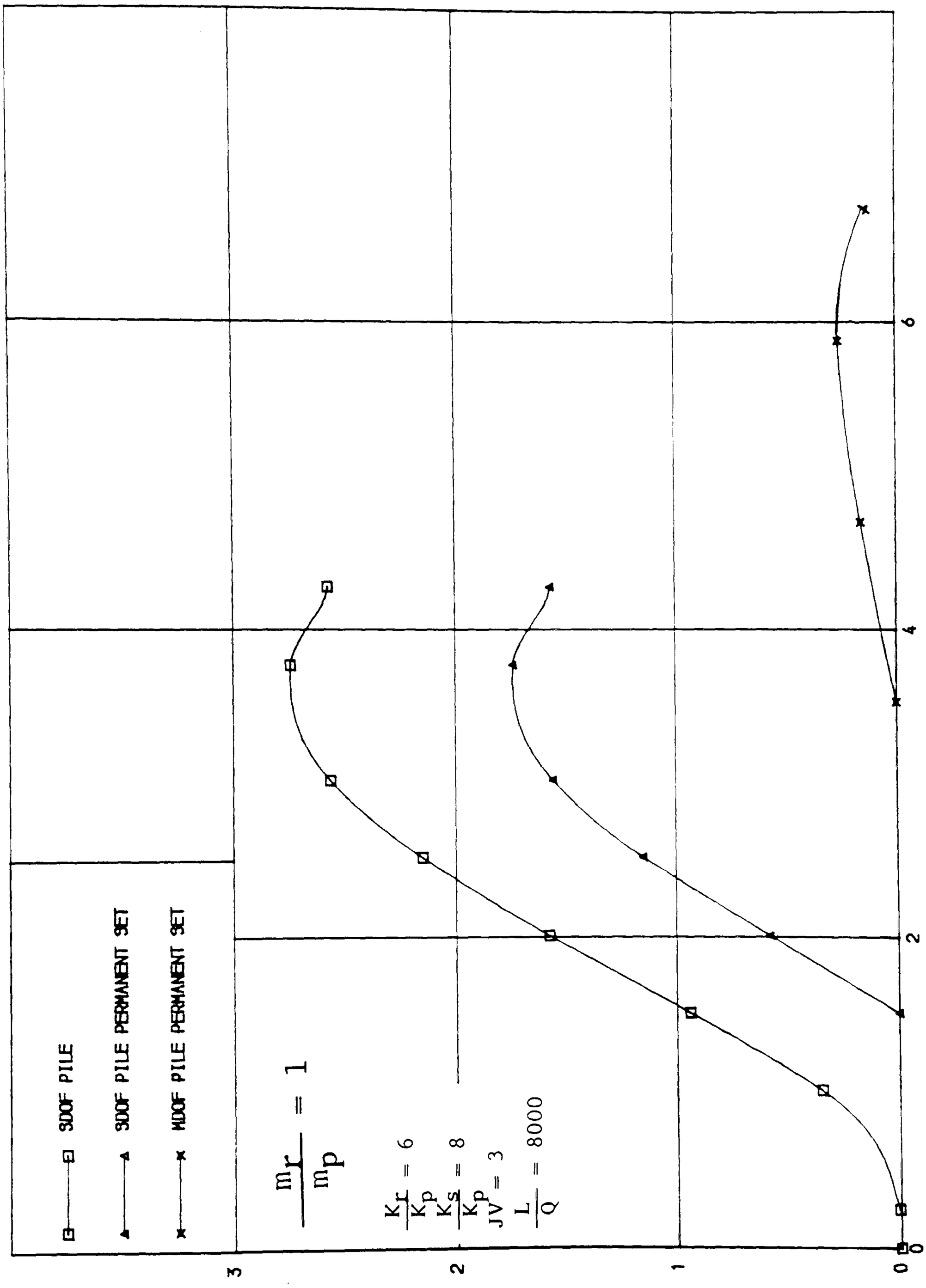

FIGURE (3.33) DISPLACEMENT-TIME RELATIONSHIP

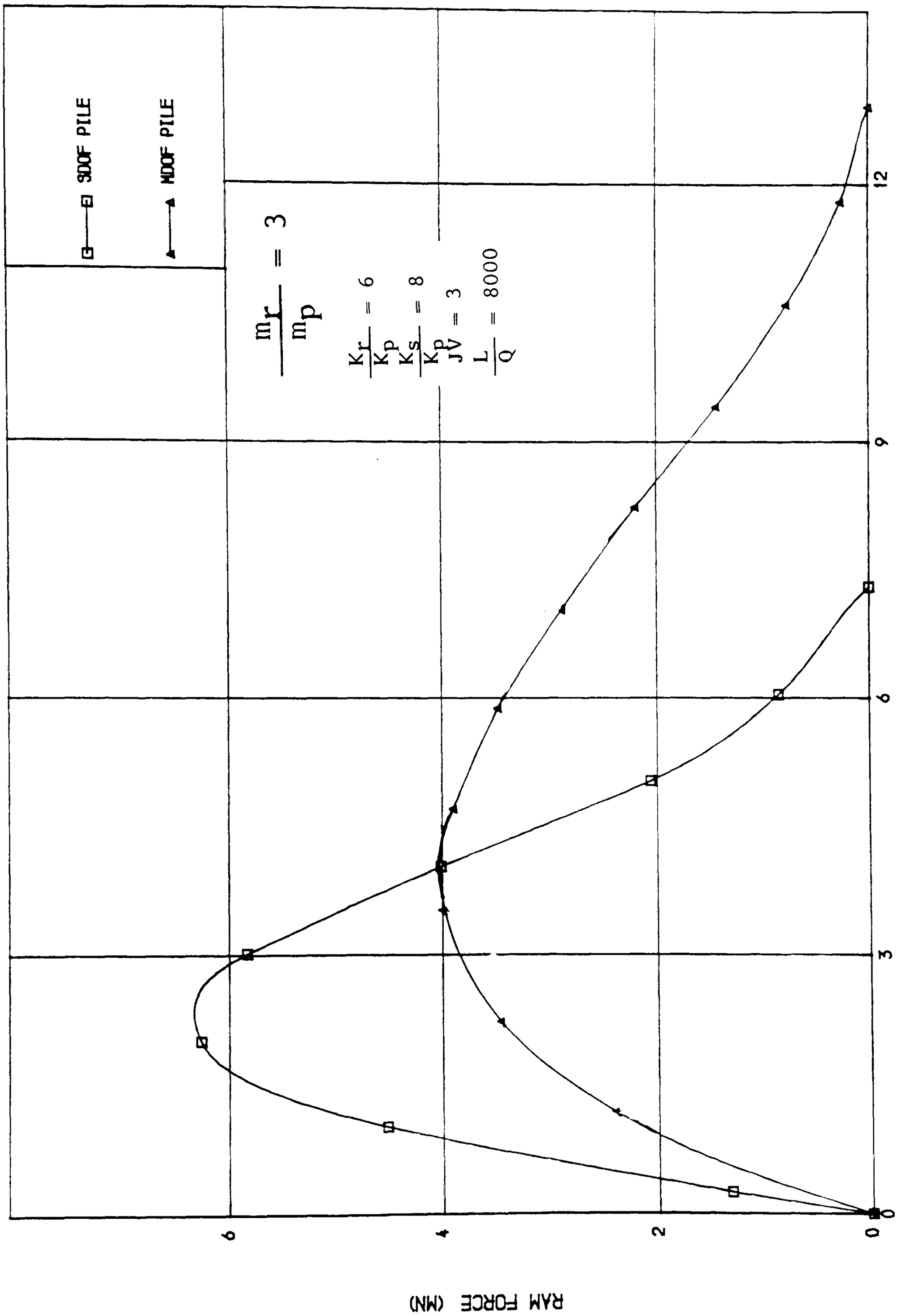

FIGURE (3.34) RAM FORCE-TIME RELATIONSHIP

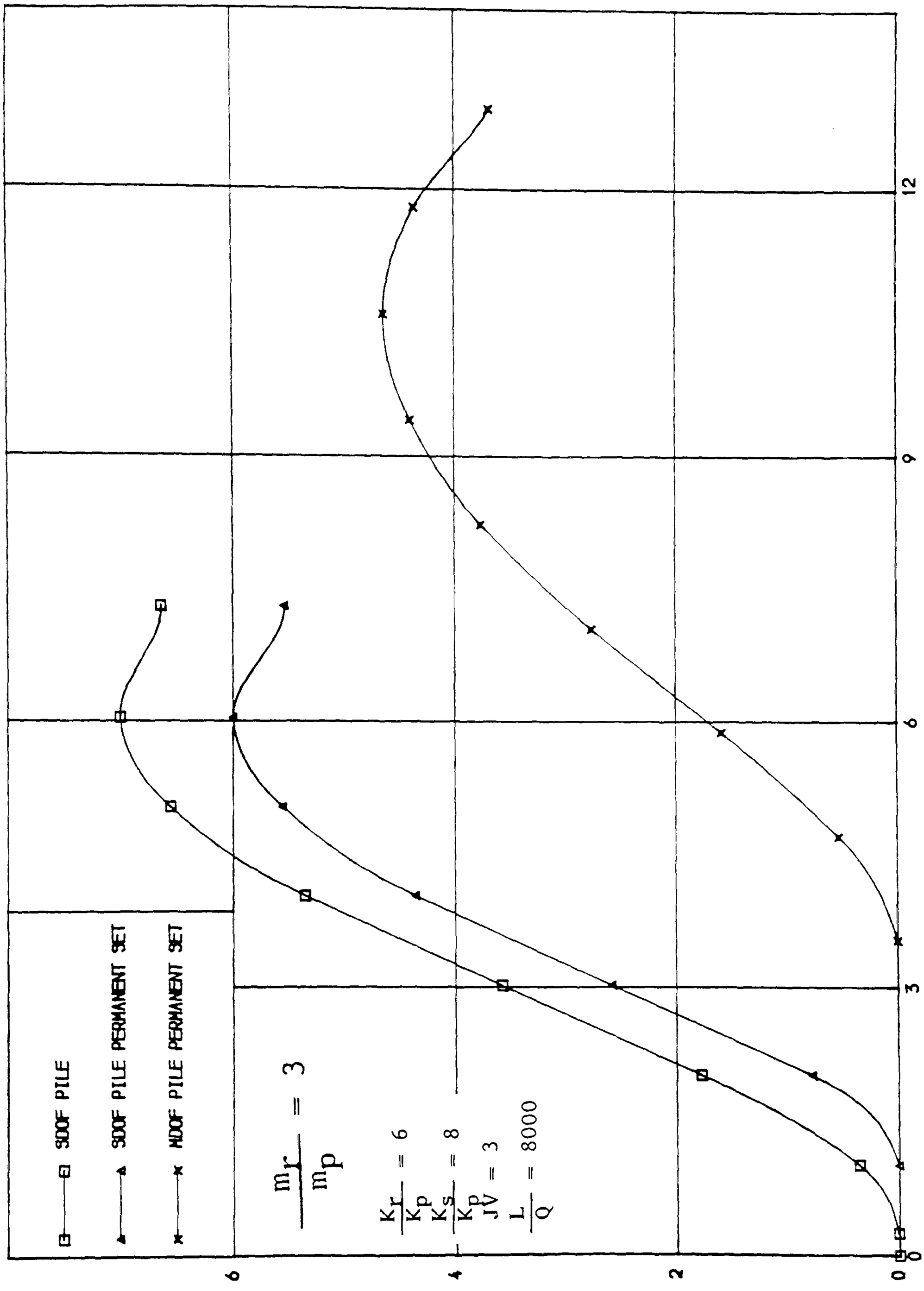
DISPLACEMENT (MN)
0
2
4
6
3
6
9
12
TIME (WN.T)
(3.35) DISPLACEMENT-TIME RELATIONSHIP
FIGURE
$\frac{m_r}{m_p} = 3$
$\frac{K_r}{K_p} = 6$
$\frac{K_s}{K_p} = 8$
$\frac{JV}{} = 3$
$\frac{L}{Q} = 8000$
SDOF PILE
SDOF PILE PERMANENT SET
MDOF PILE PERMANENT SET

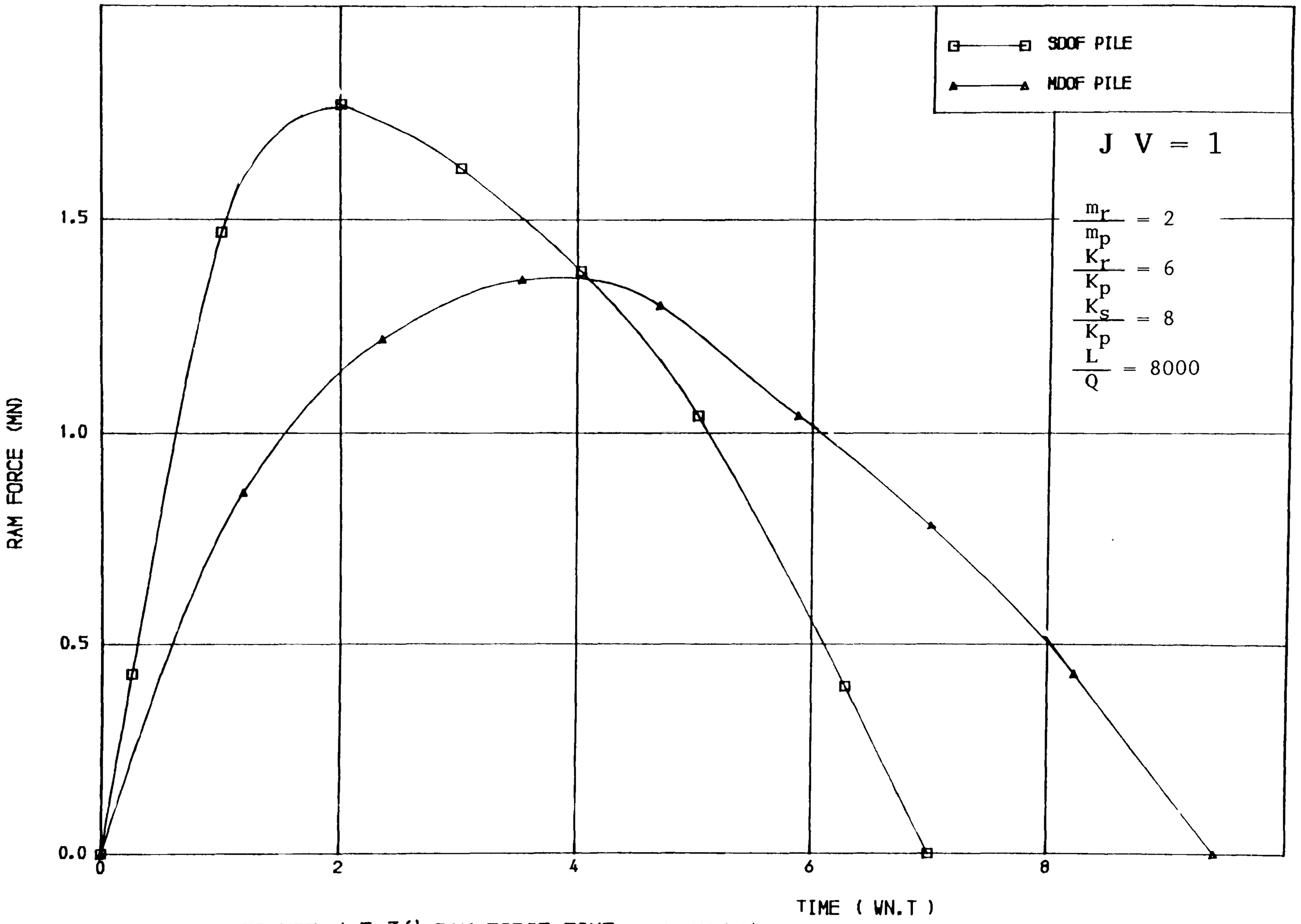

FIGURE (3.36) RAM FORCE_TIME RELATIONSHIP

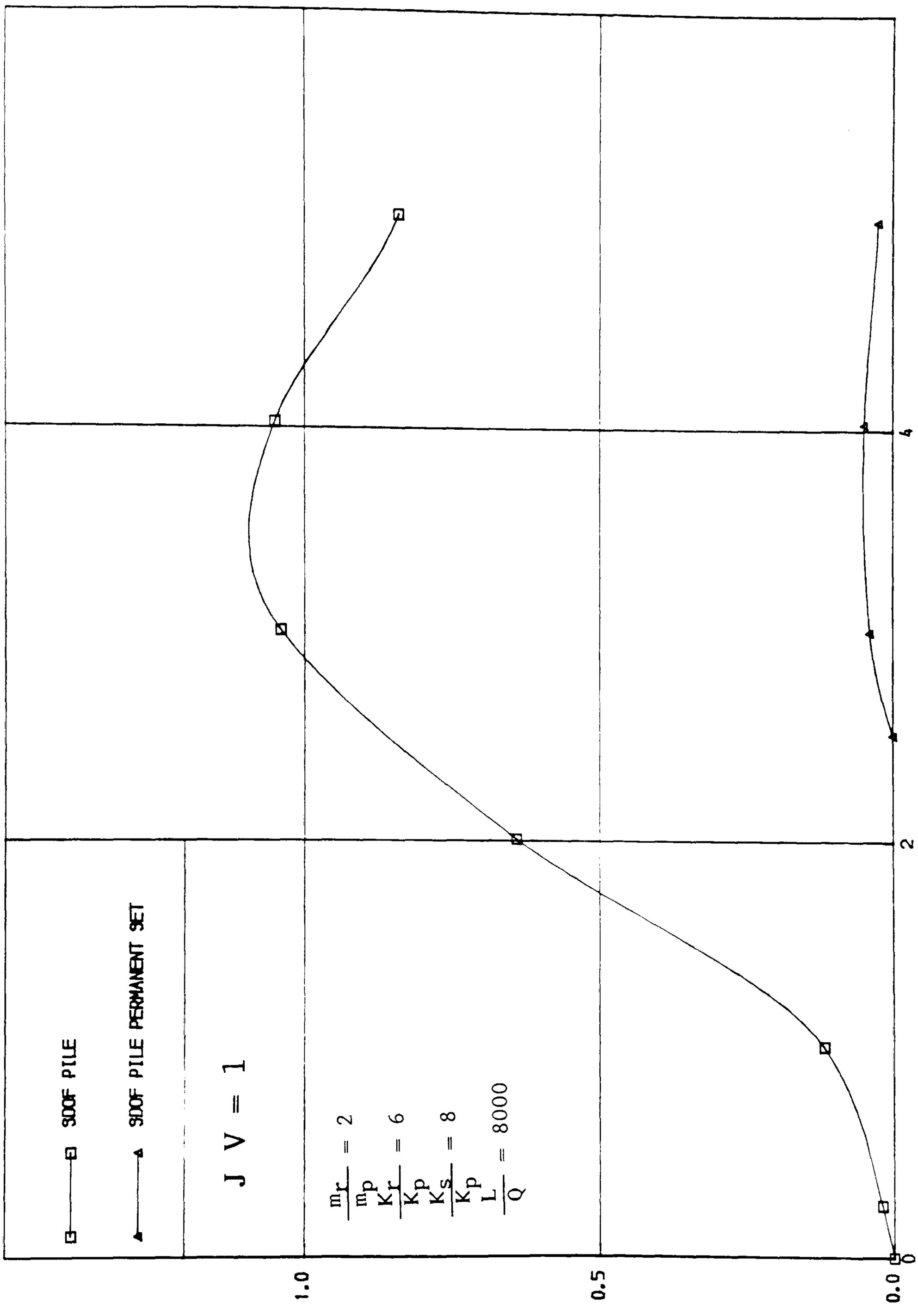

FIGURE (3.37) DISPLACEMENT-TIME RELATIONSHIP

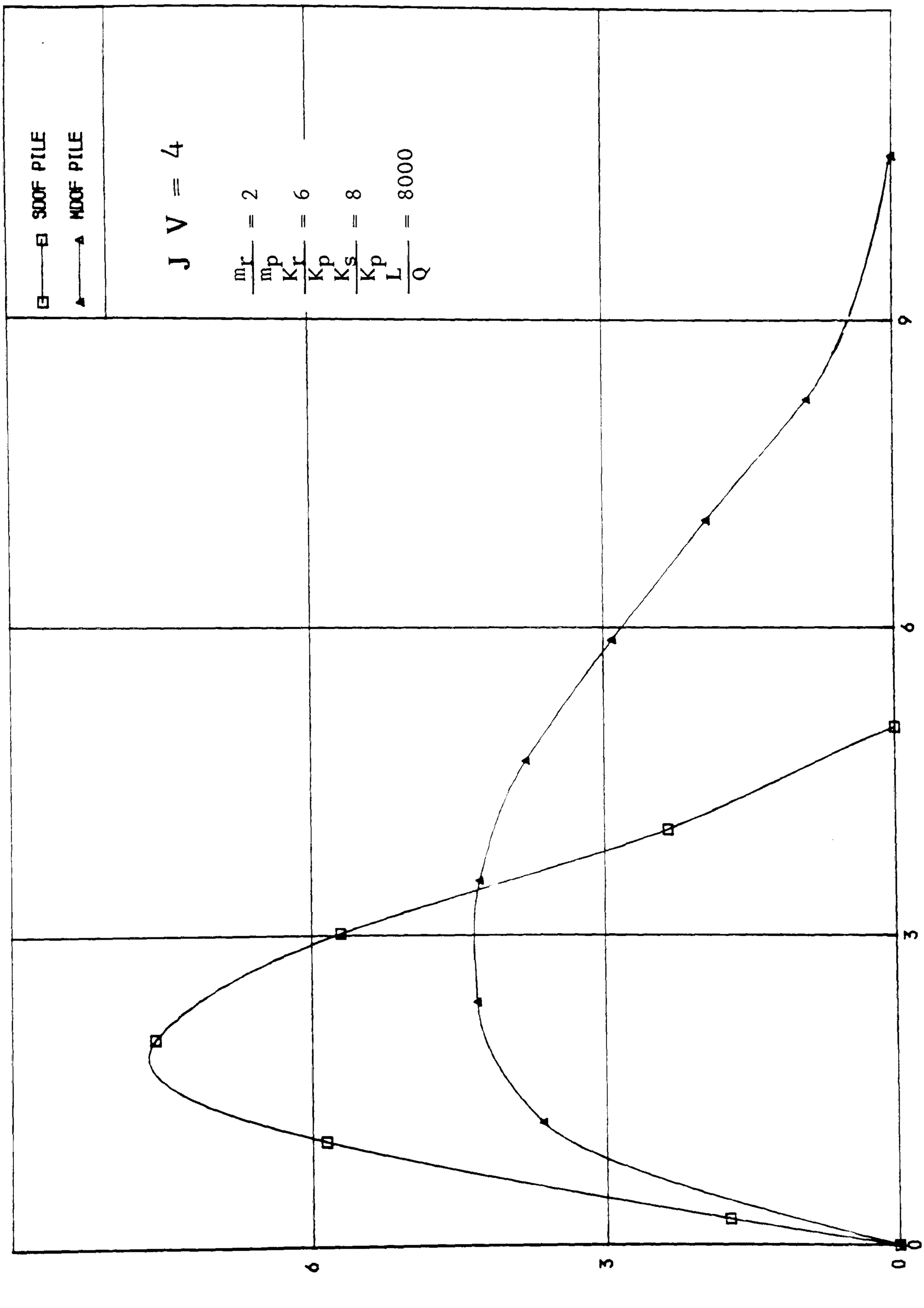

FIGURE (3.38) RAM FORCE-TIME RELATIONSHIP

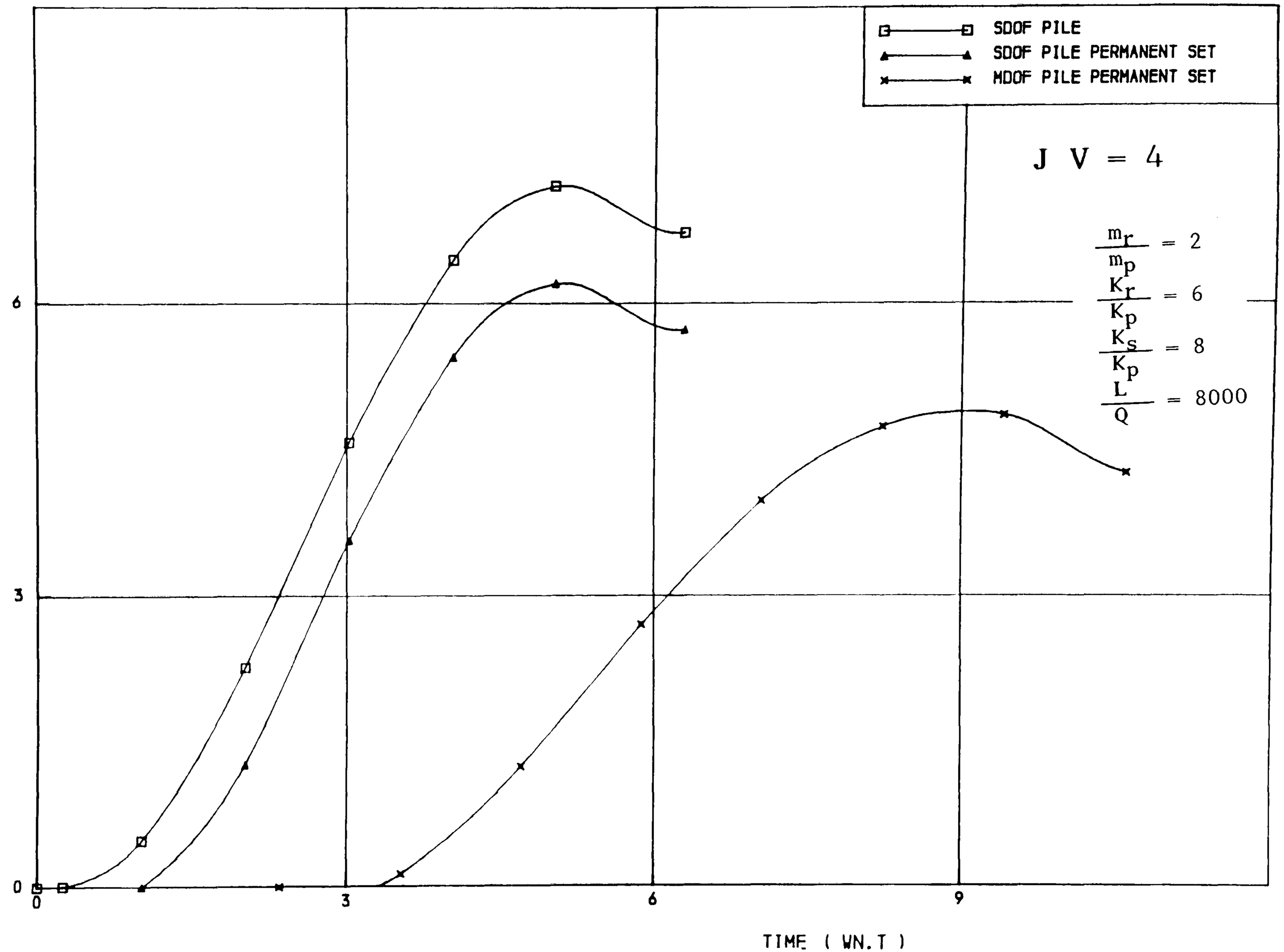

FIGURE (3.39) DISPLACEMENT-TIME RELATIONSHIP

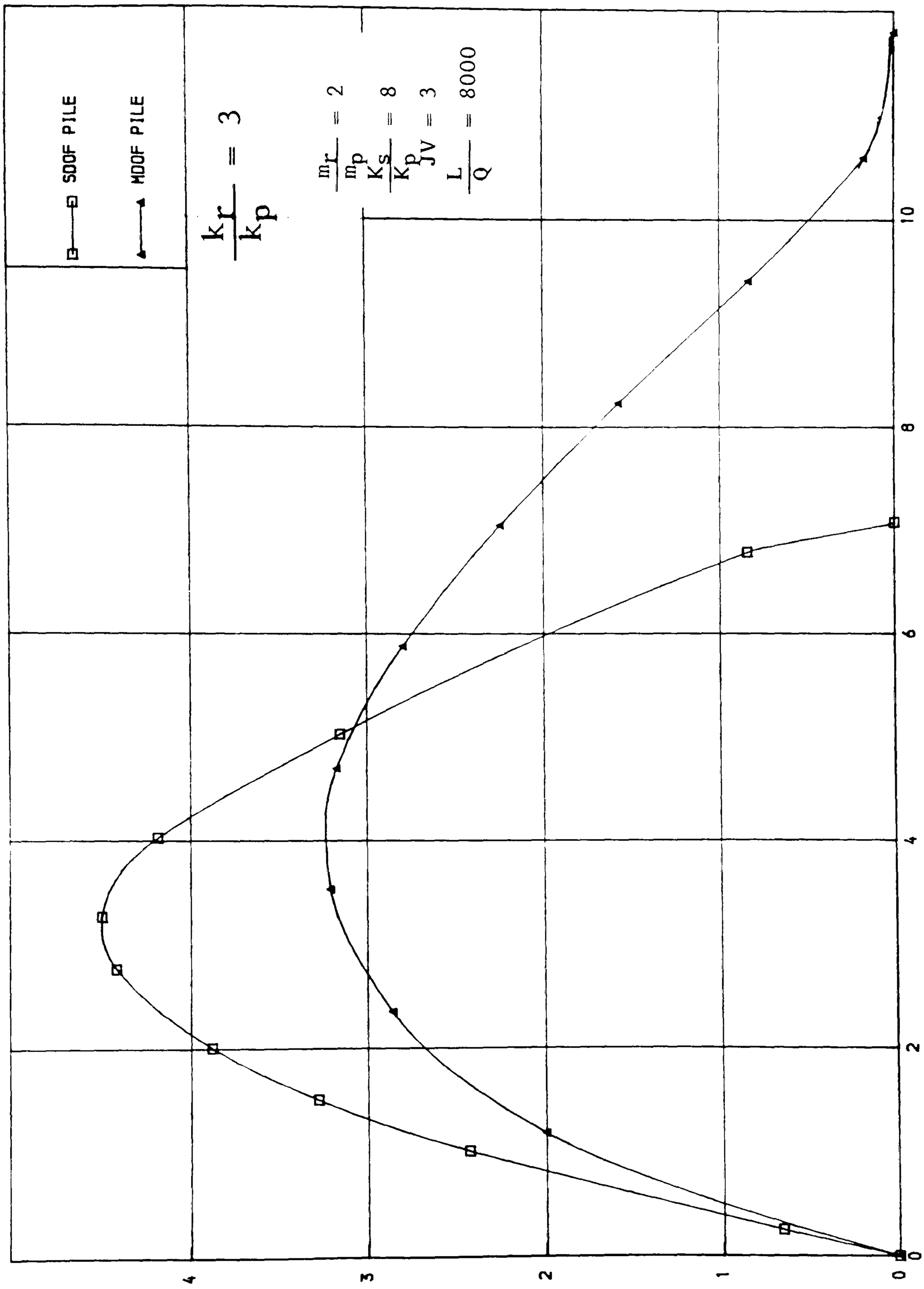

FIGURE (3.40) RAM FORCE-TIME RELATIONSHIP

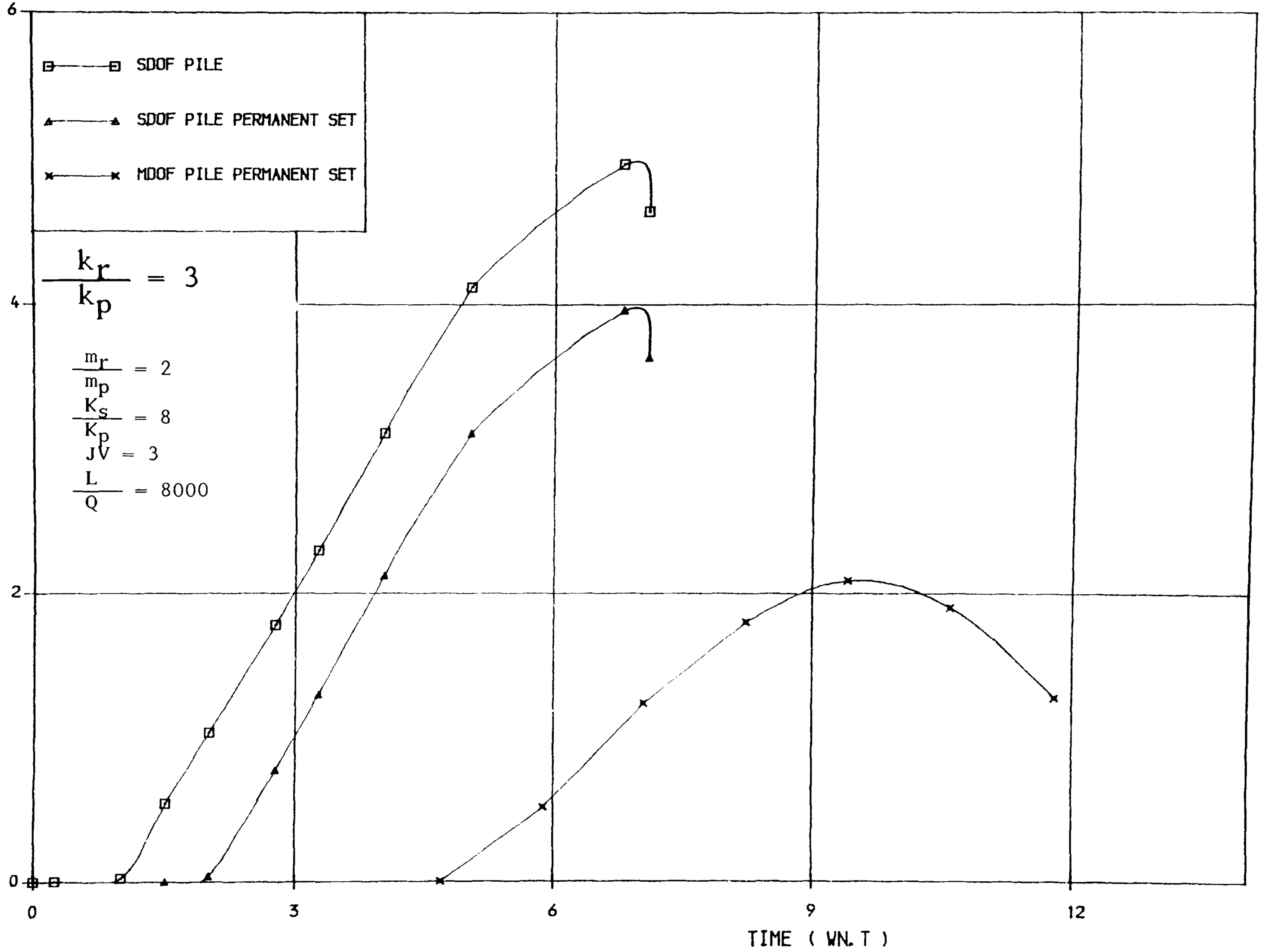

FIGURE (3.41) DISPLACEMENT_TIME RELATIONSHIP

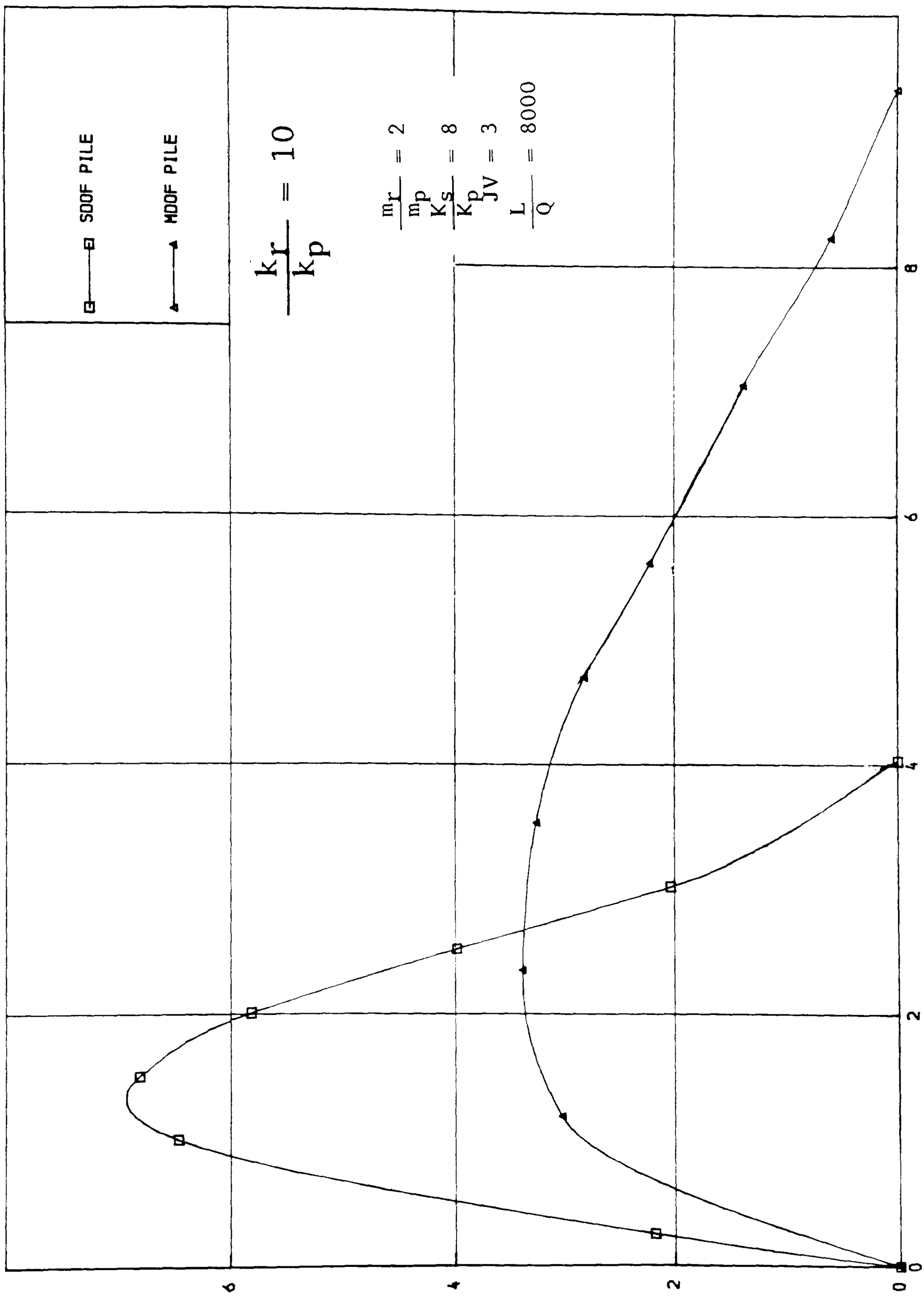

FIGURE (3.42) RAM FORCE-TIME RELATIONSHIP

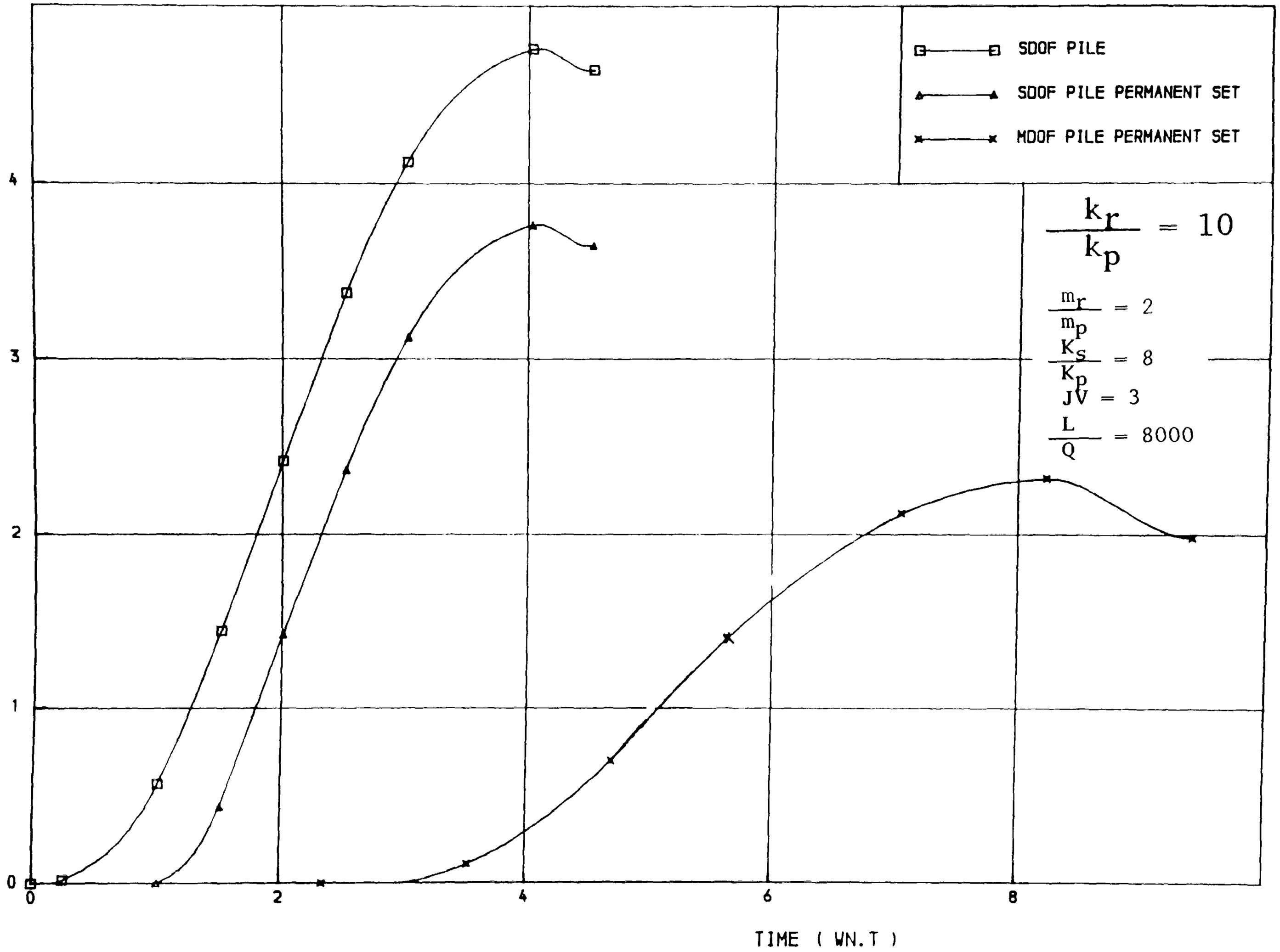

FIGURE (3.43) DISPLACEMENT_TIME RELATIONSHIP

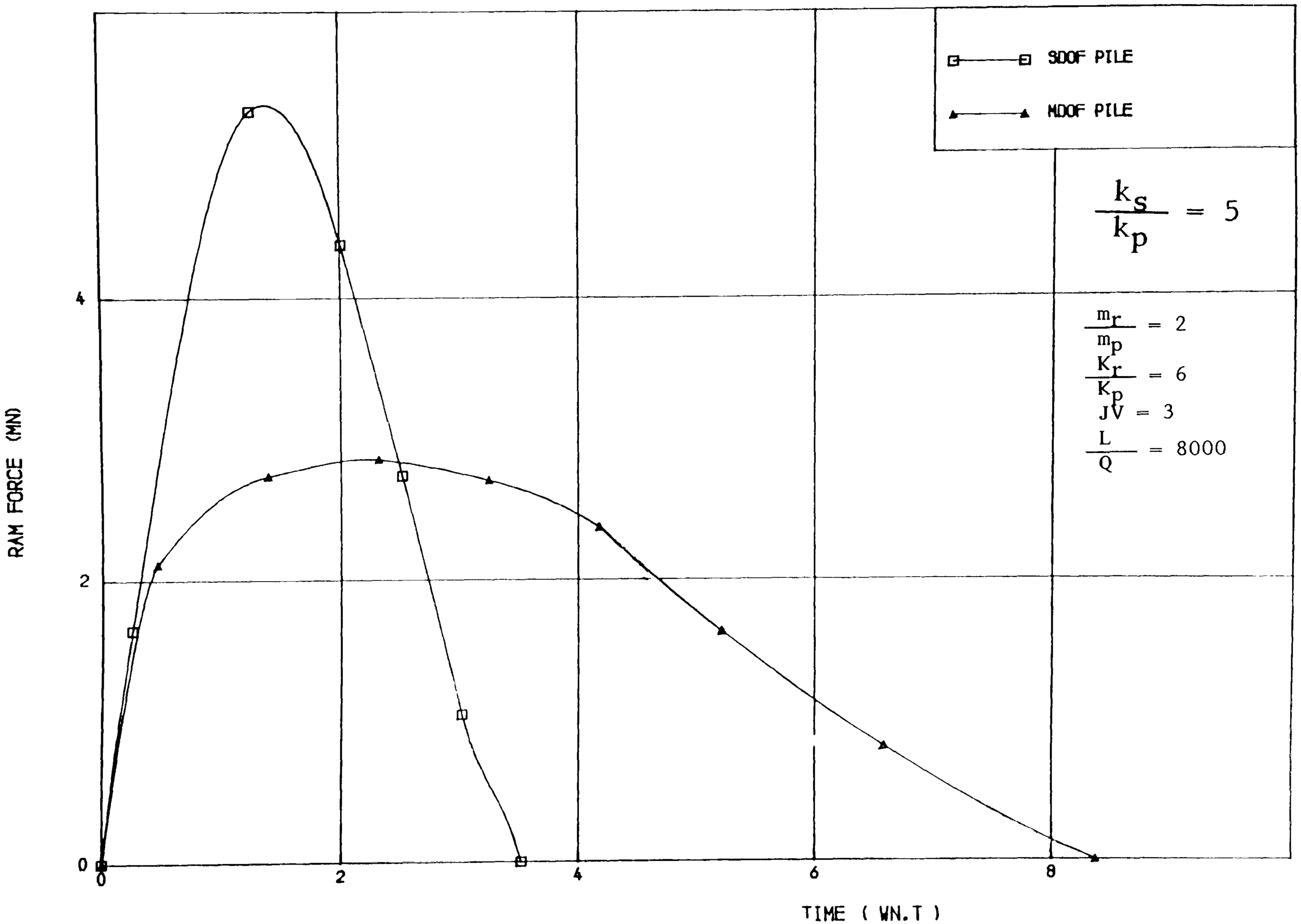

FIGURE (3. 44) RAM FORCE_TIME RELATIONSHIP

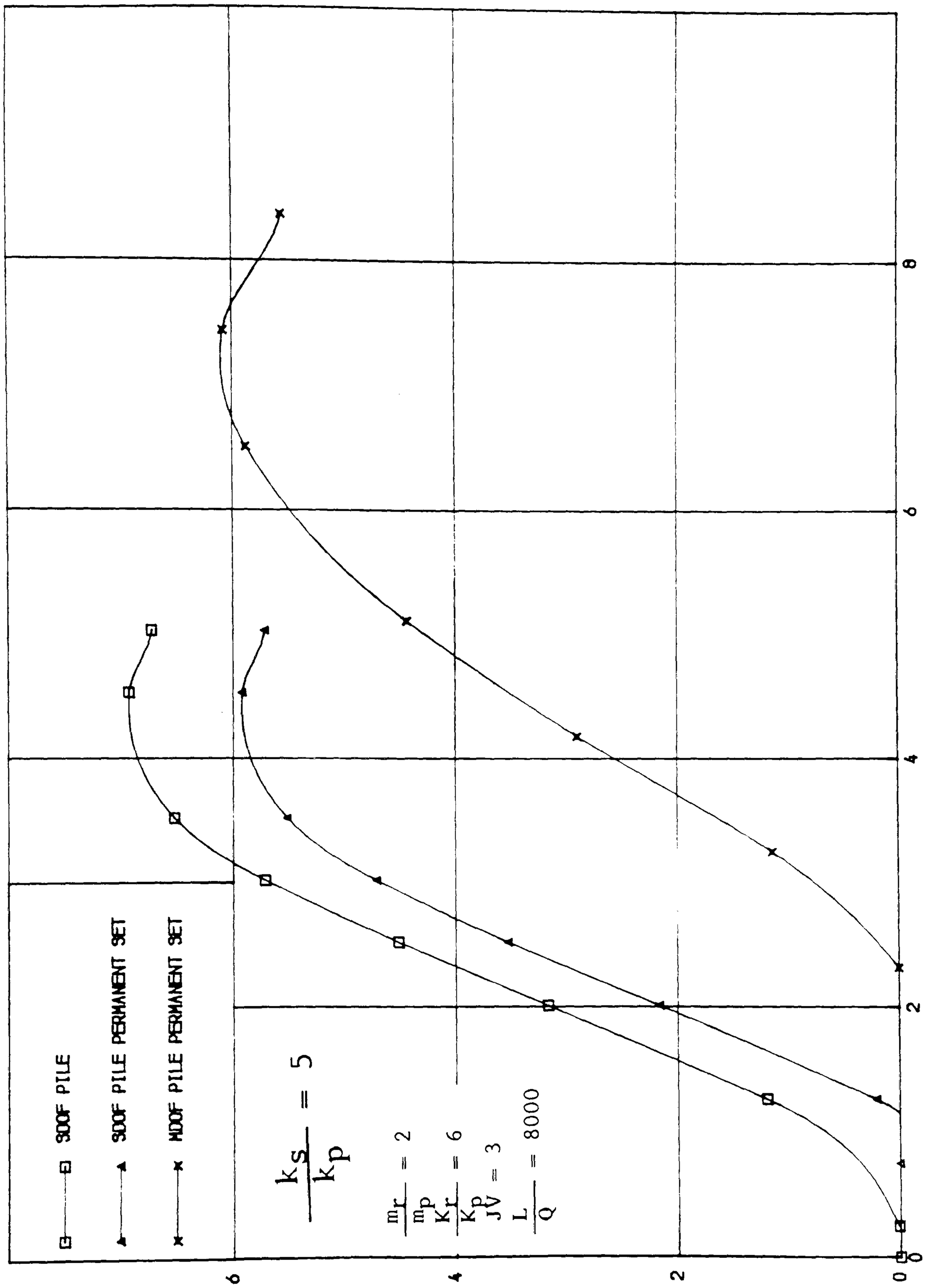

FIGURE (3.45) DISPLACEMENT-TIME RELATIONSHIP

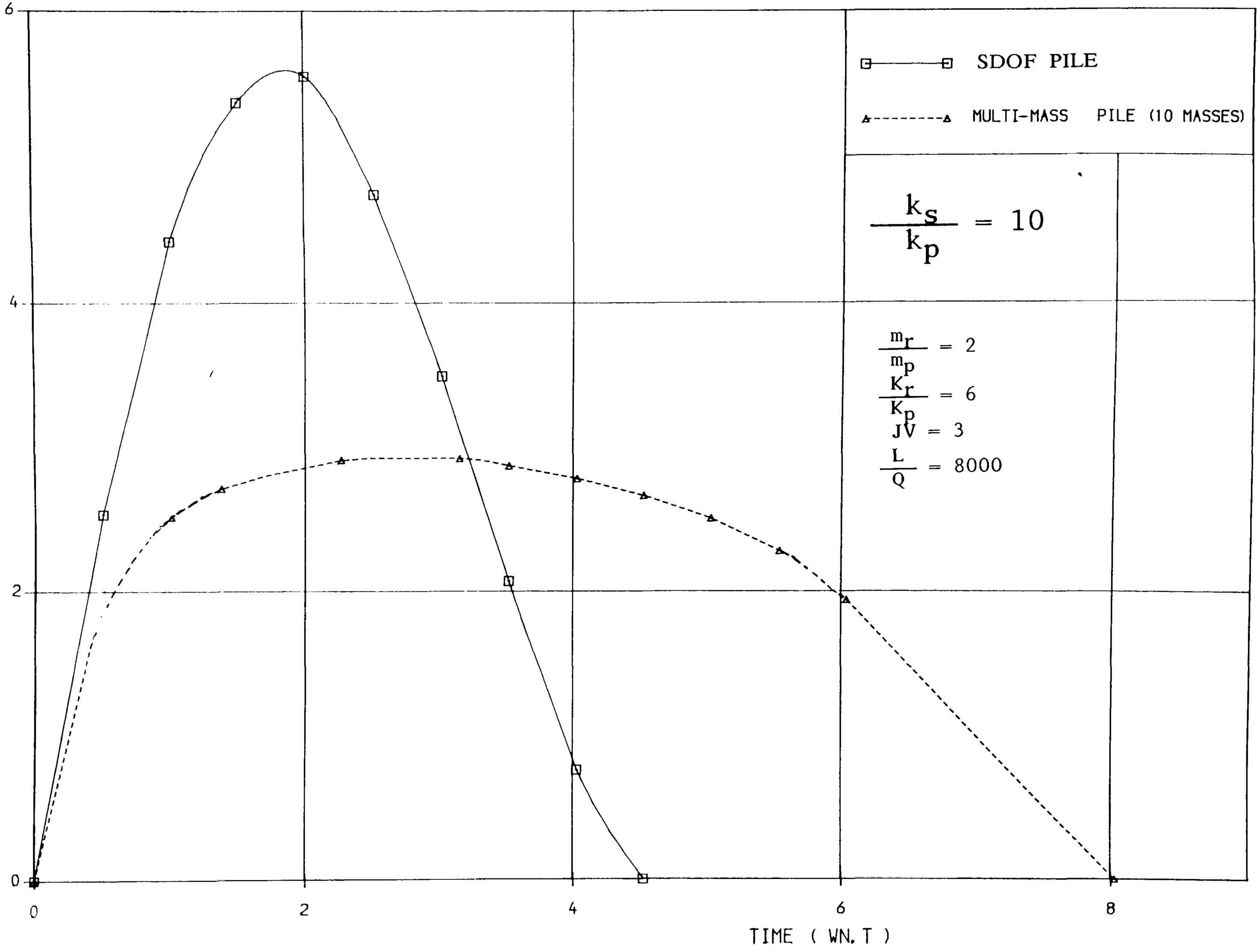

FIGURE (3.46) RAMFORCE_TIME RELATIONSHIP

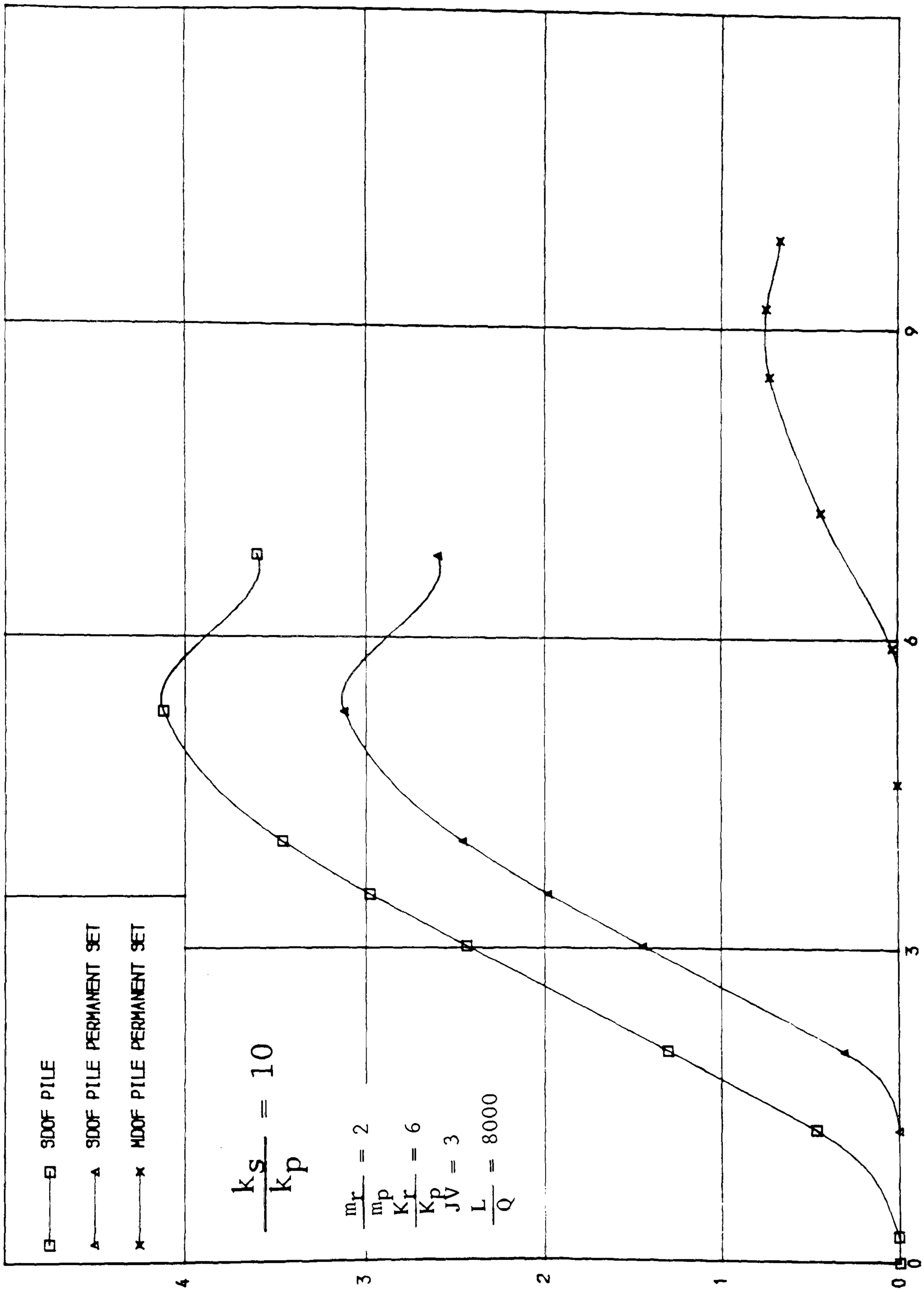

FIGURE (3.47) DISPLACEMENT-TIME RELATIONSHIP

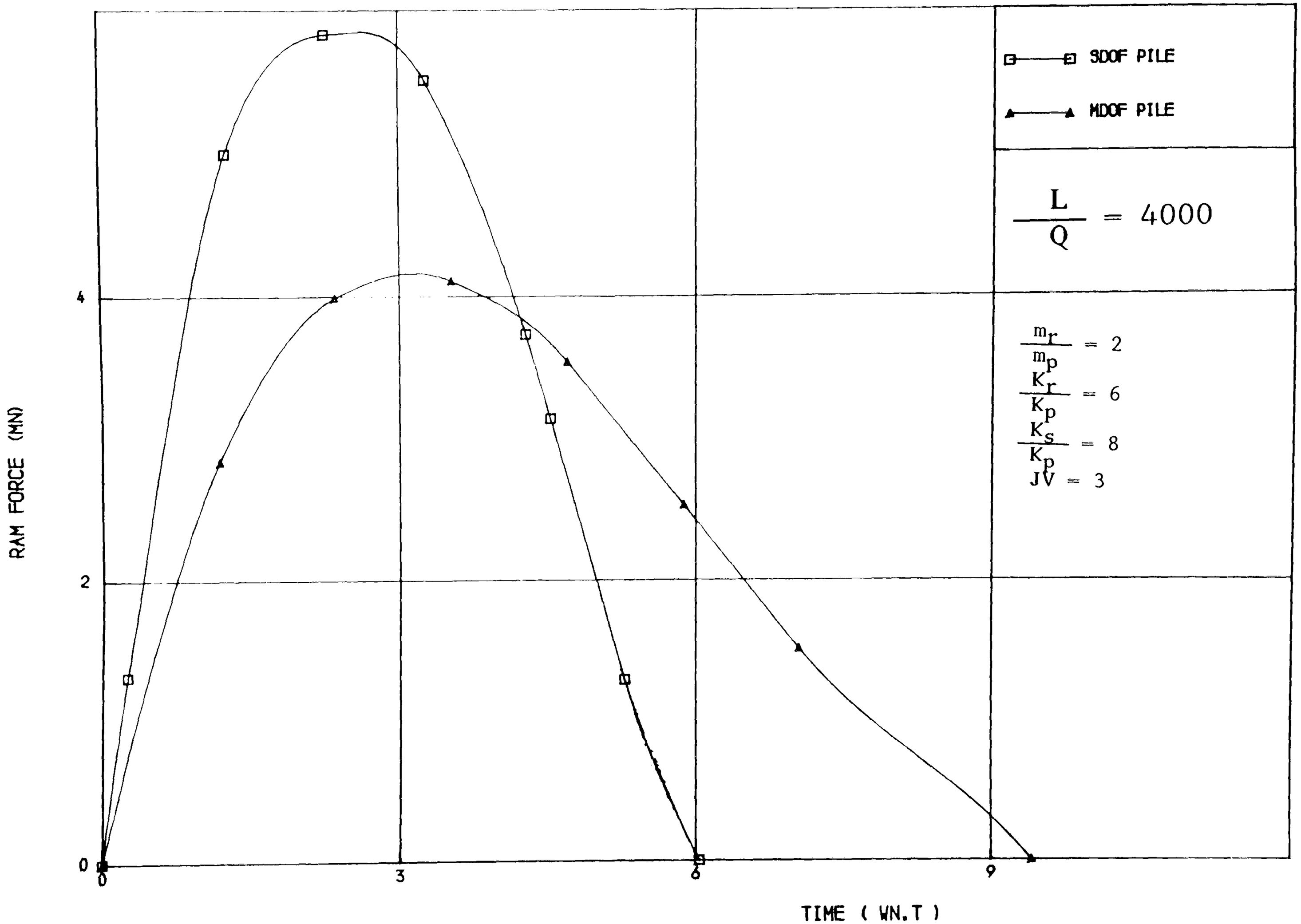

FIGURE (3.48) RAM FORCE_TIME RELATIONSHIP

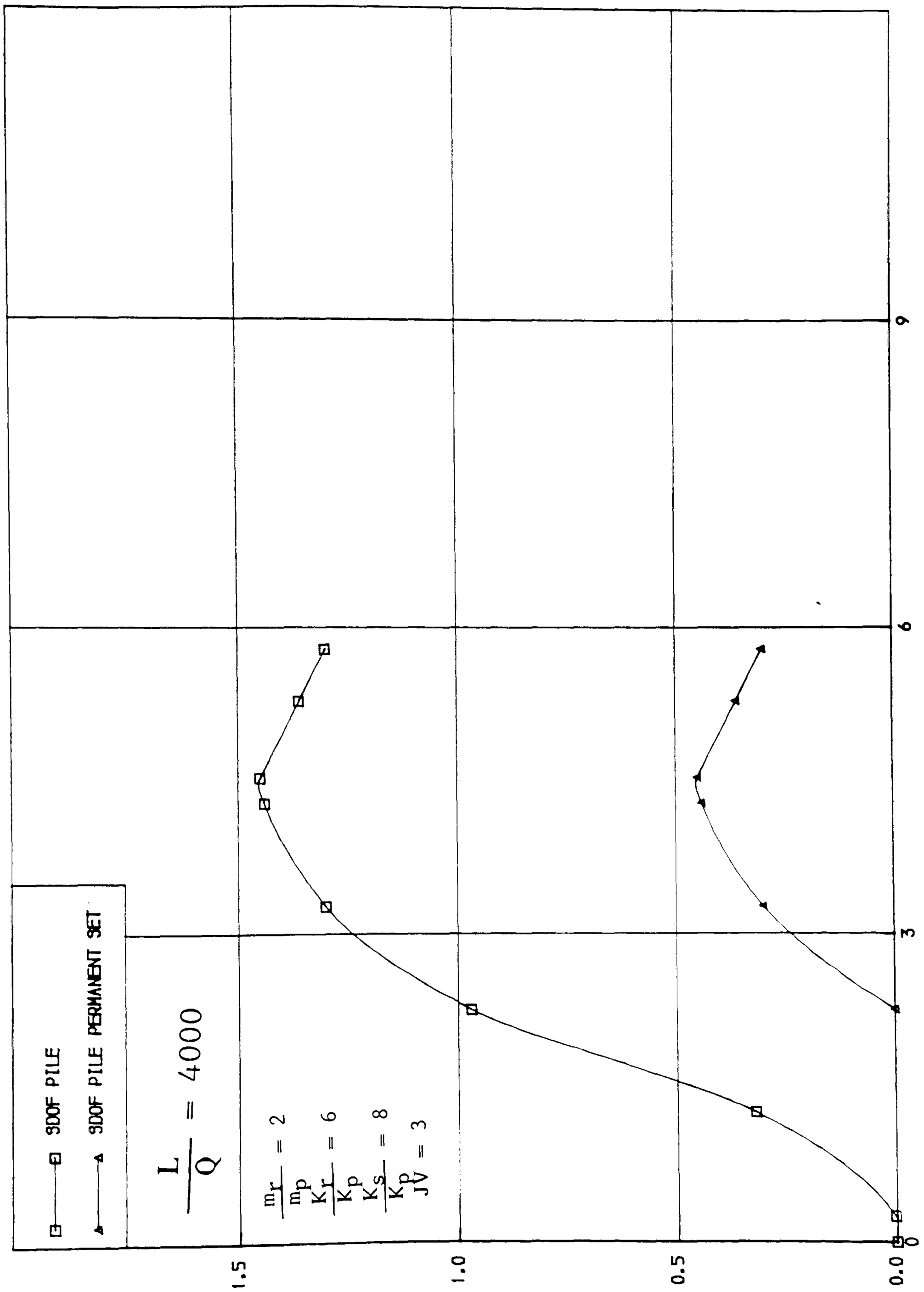

FIGURE (3.49) DISPLACEMENT-TIME RELATIONSHIP

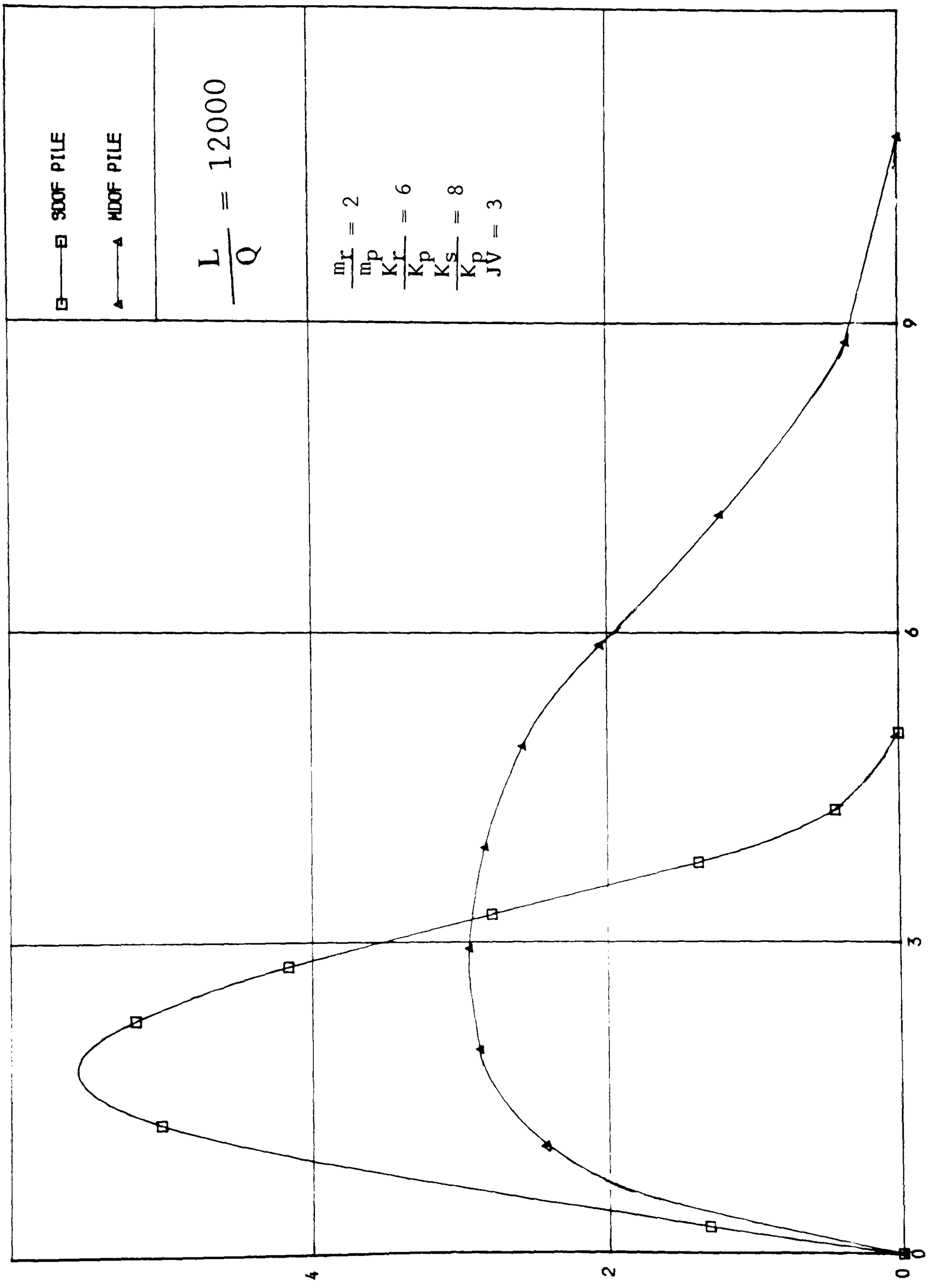

FIGURE (3.50) RAM FORCE_TIME RELATIONSHIP

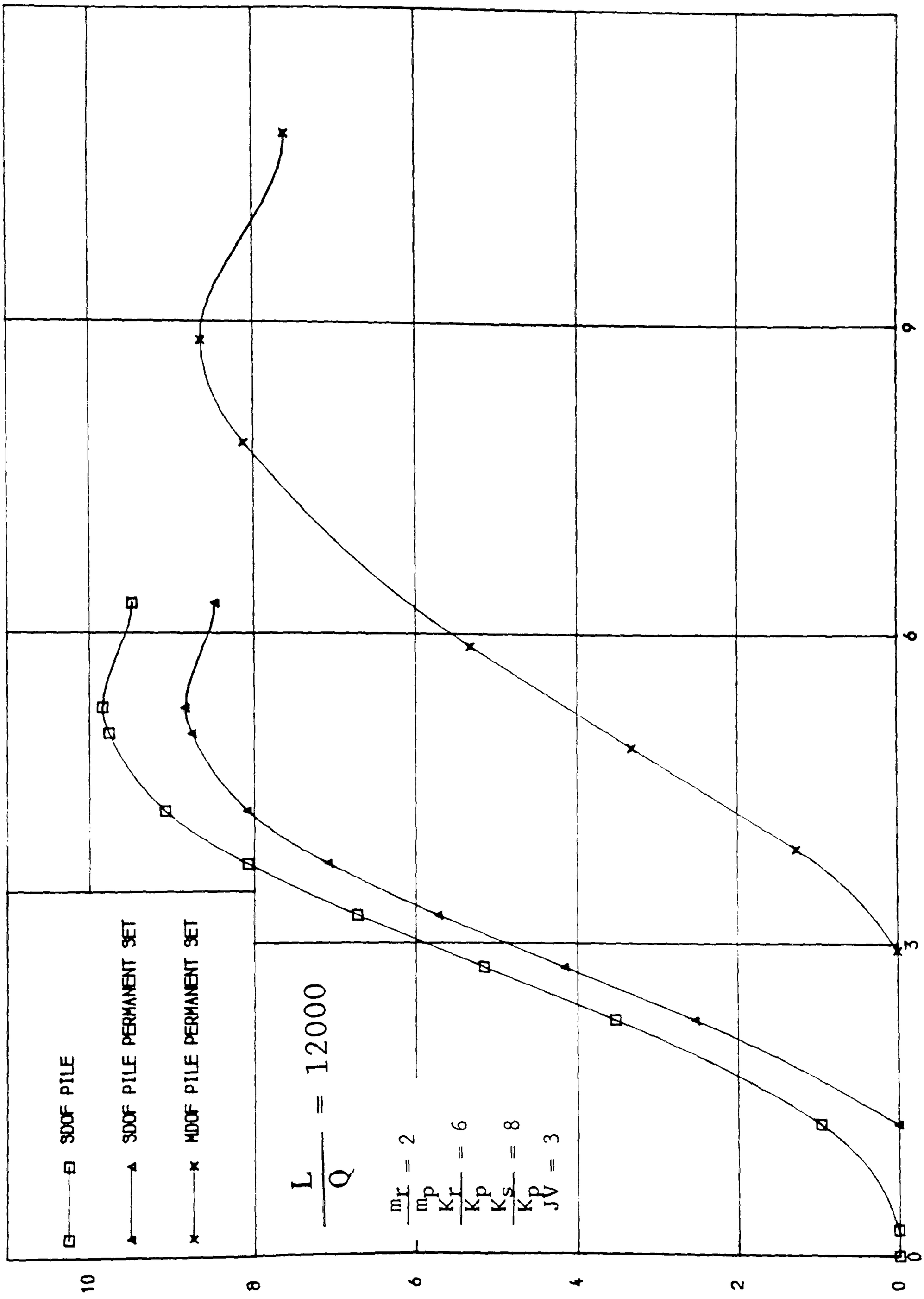

FIGURE (3.51) DISPLACEMENT-TIME RELATIONSHIP

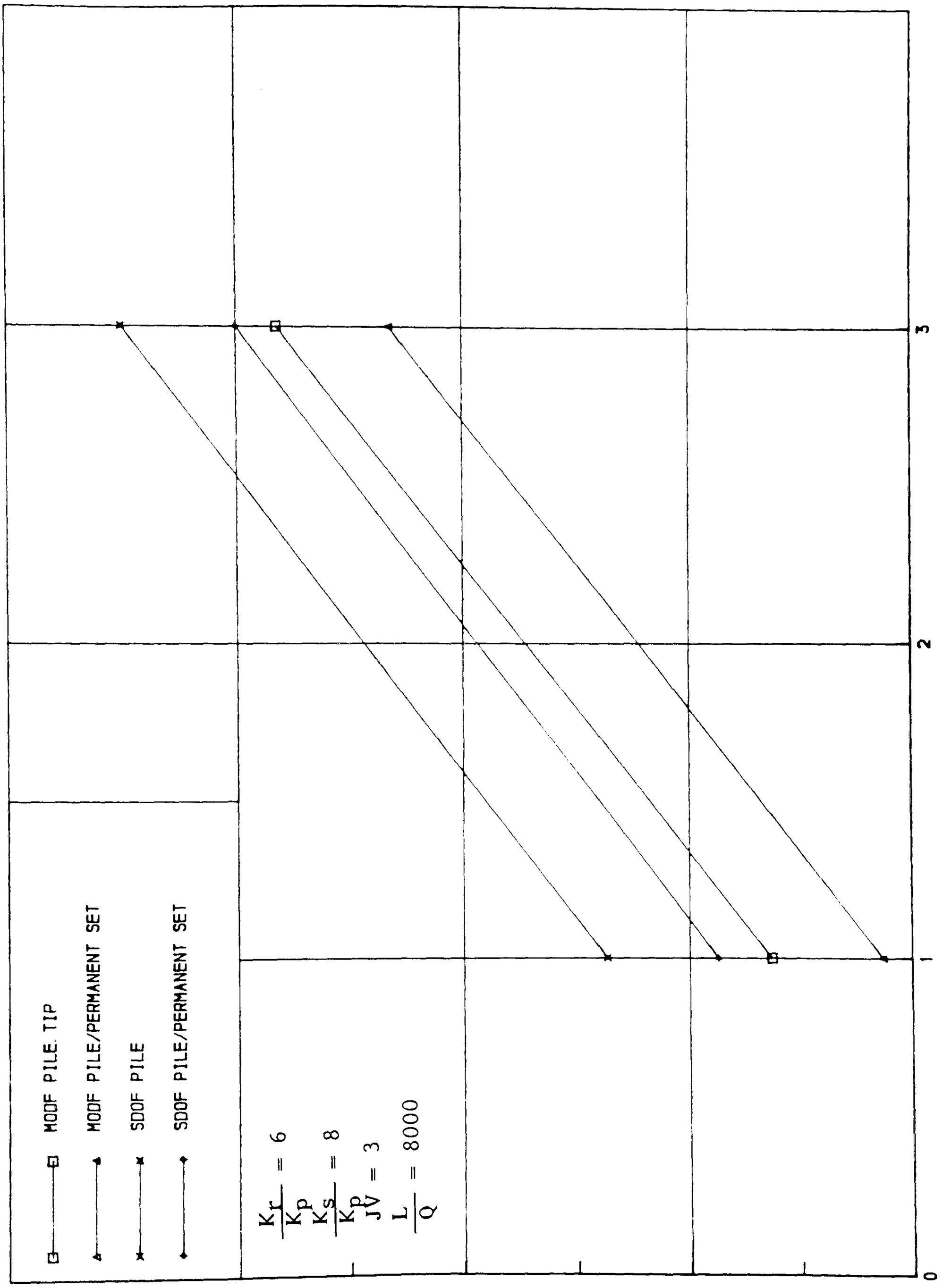

FIGURE (3.52) MAXIMUM DISPLACEMENT-RAM MASS RELATIONSHIP

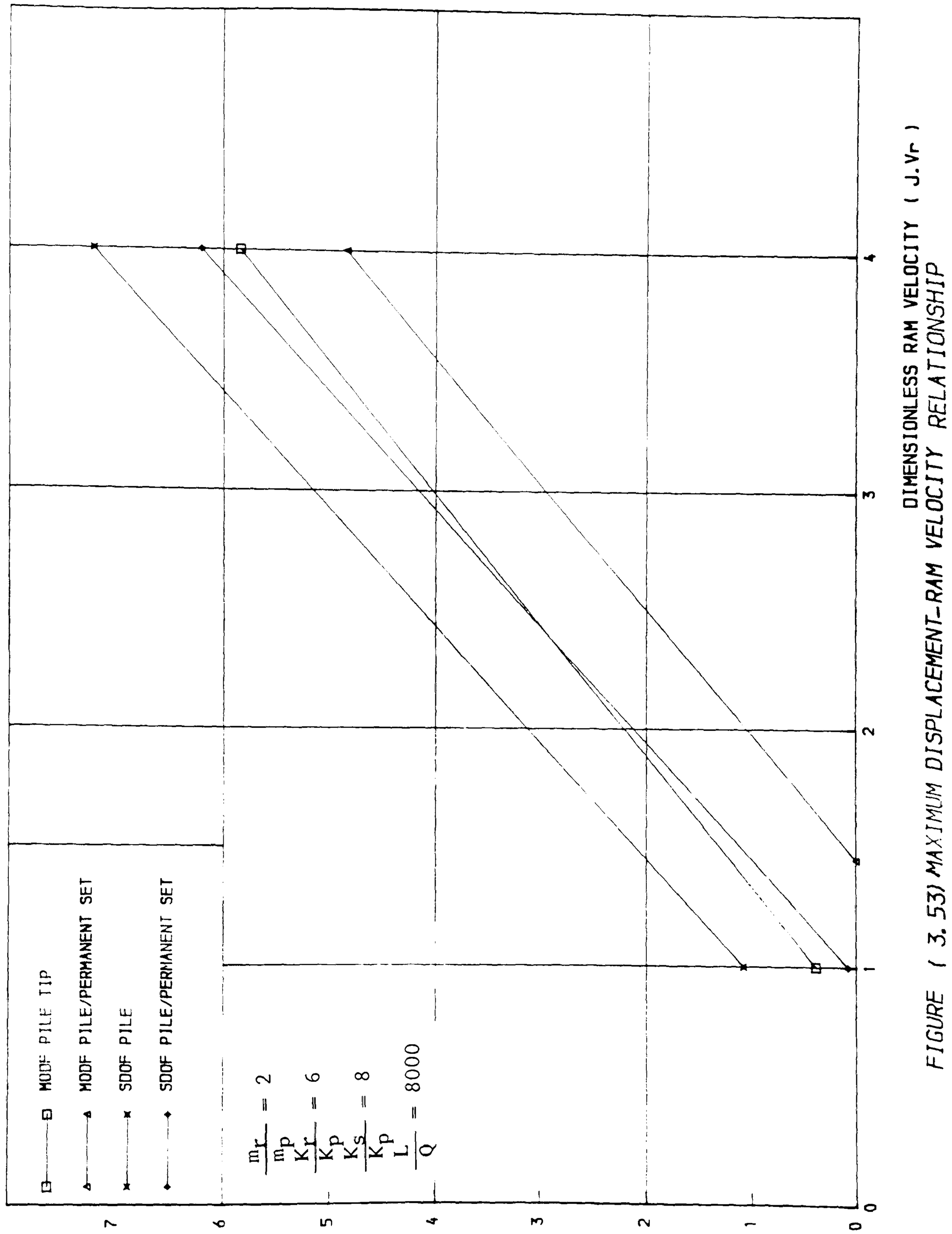

FIGURE (3.53) MAXIMUM DISPLACEMENT-RAM VELOCITY RELATIONSHIP

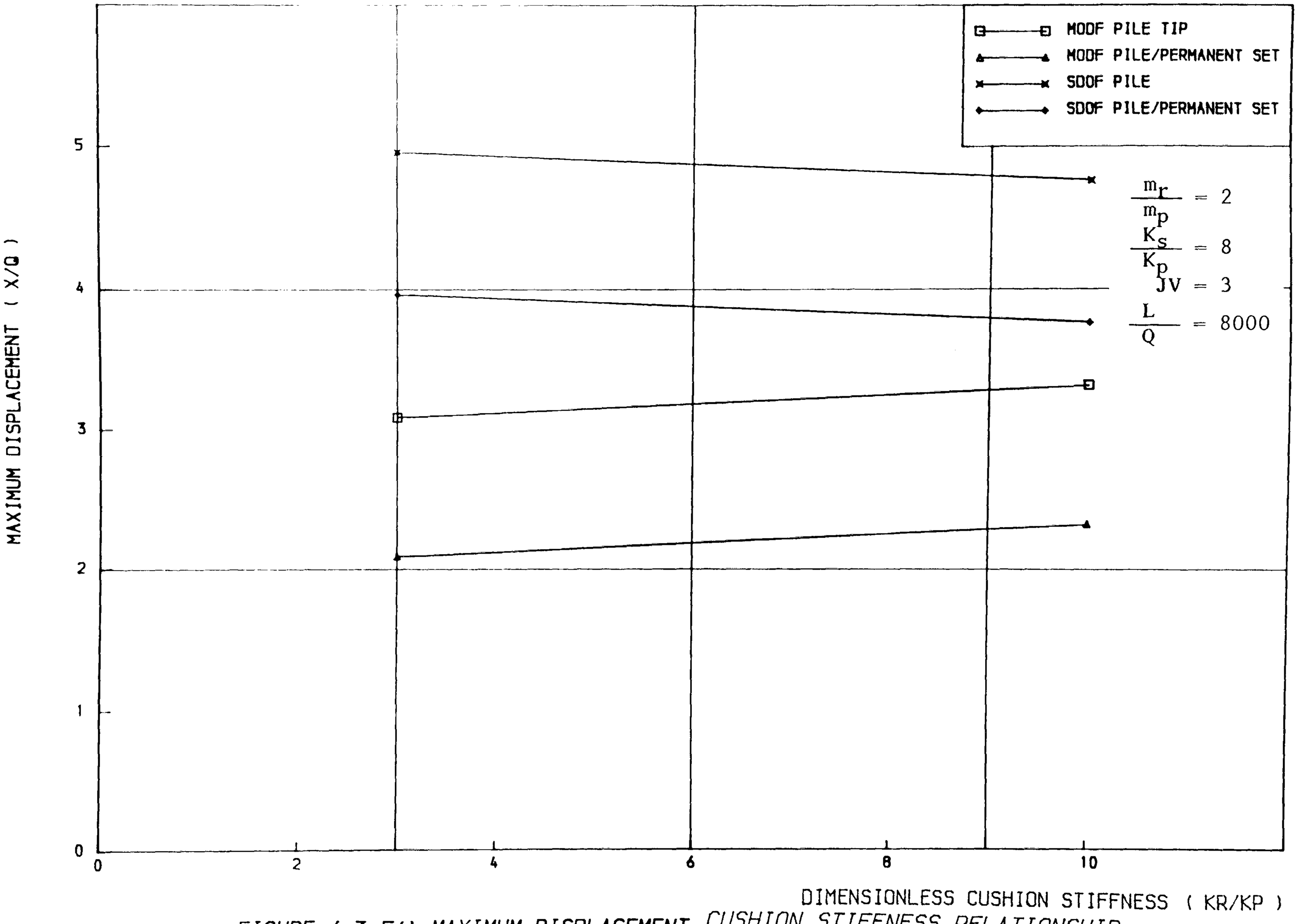

FIGURE (3.54) MAXIMUM DISPLACEMENT-CUSHION STIFFNESS RELATIONSHIP

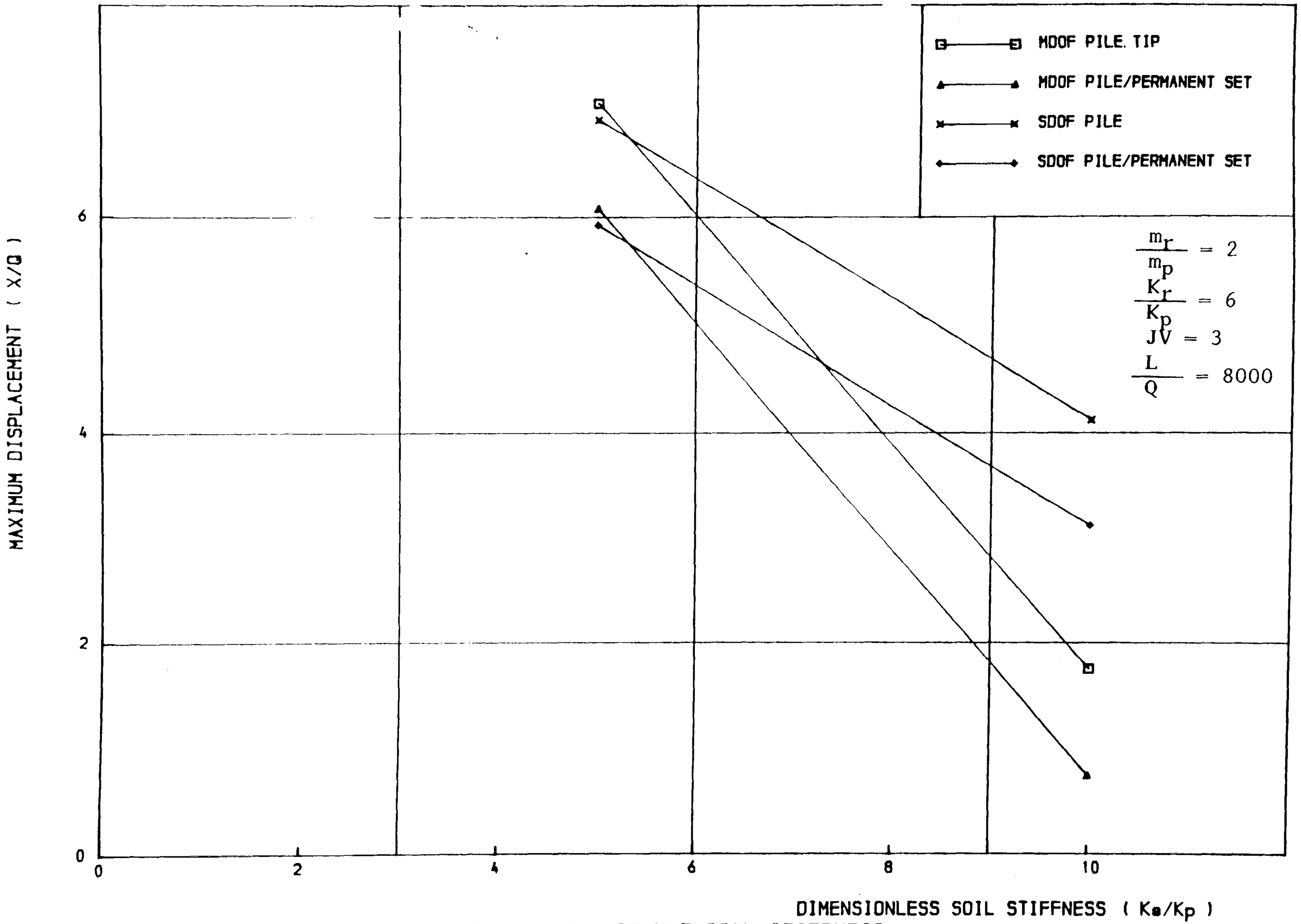

FIGURE (3.55) MAXIMUM DISPLACEMENT-SOIL STIFFNESS RELATIONSHIP

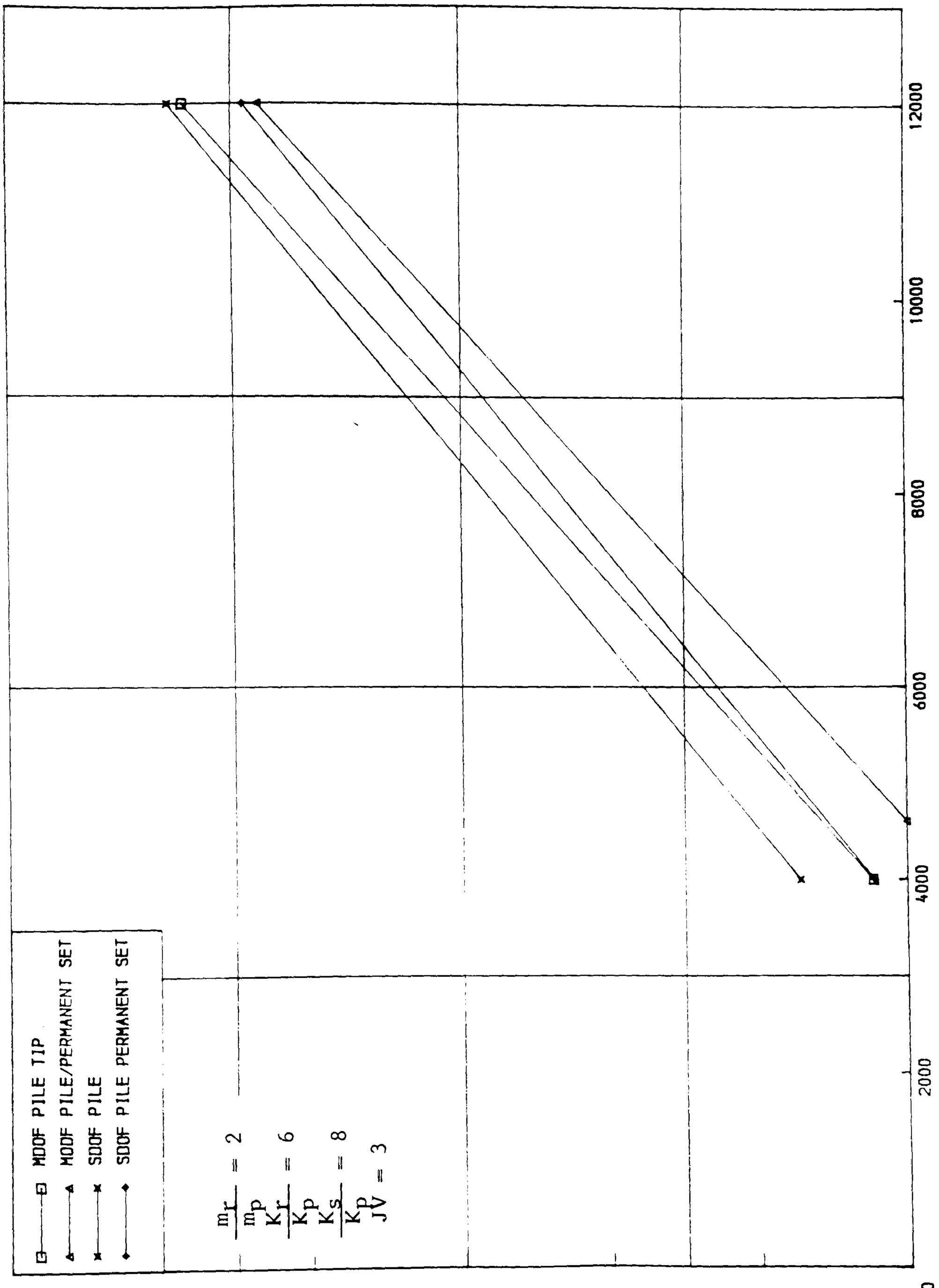

FIGURE (3.56) MAXIMUM DISPLACEMNT-PILE LENGTH RELATIONSHIP

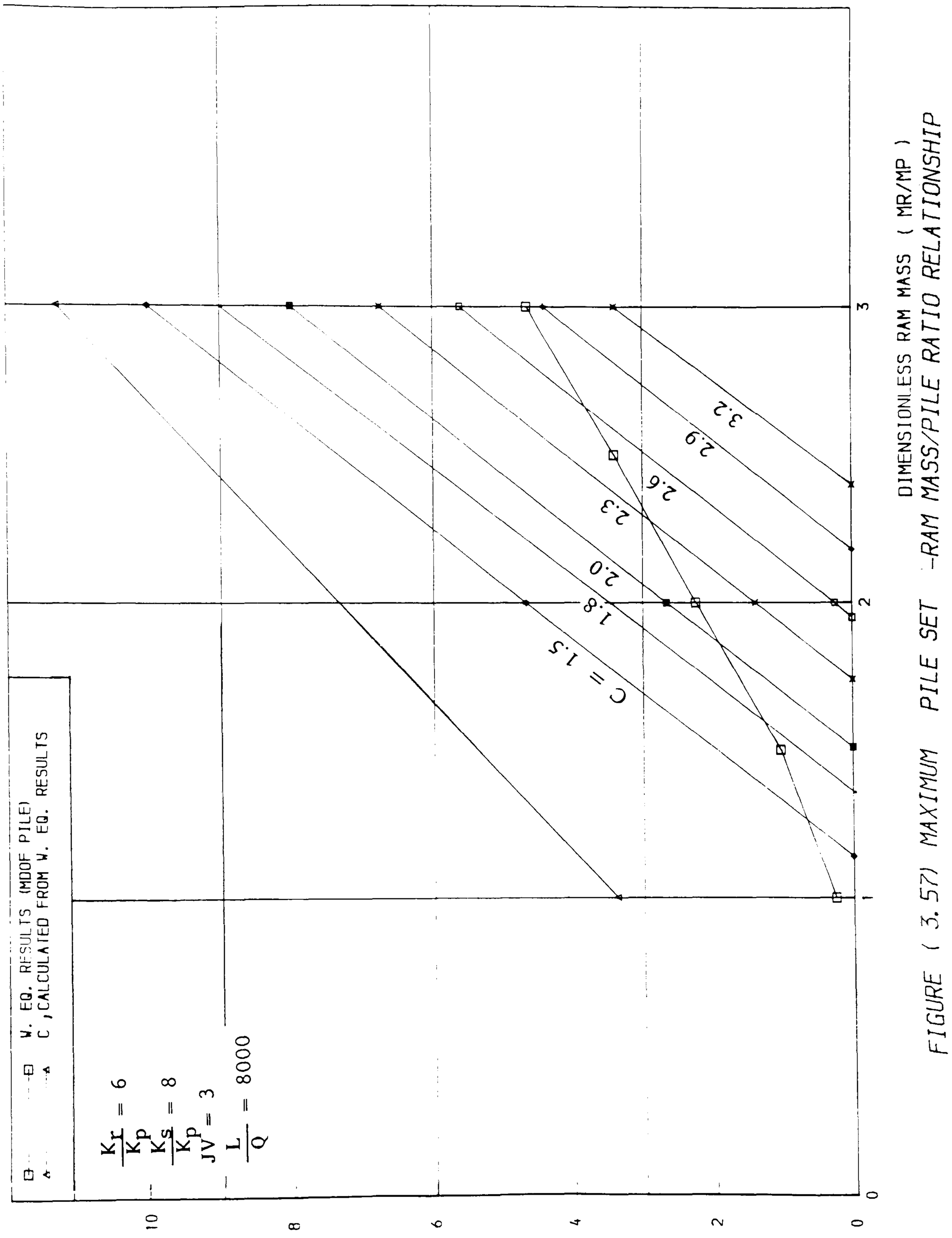
FIGURE (3.57) MAXIMUM PILE SET -RAM MASS/PILE RATIO RELATIONSHIP
DIMENSIONLESS RAM MASS (MR/MP)
MAXIMUM SET (S/Q)
3.2
2.9
2.6
2.3
2.0
1.8
1.5
C =
W. EQ. RESULTS (MDOF PILE)
C , CALCULATED FROM W. EQ. RESULTS
$\frac{Kr}{Kp} = 6$
$\frac{Ks}{Kp} = 8$
$JV = 3$
$\frac{L}{Q} = 8000$

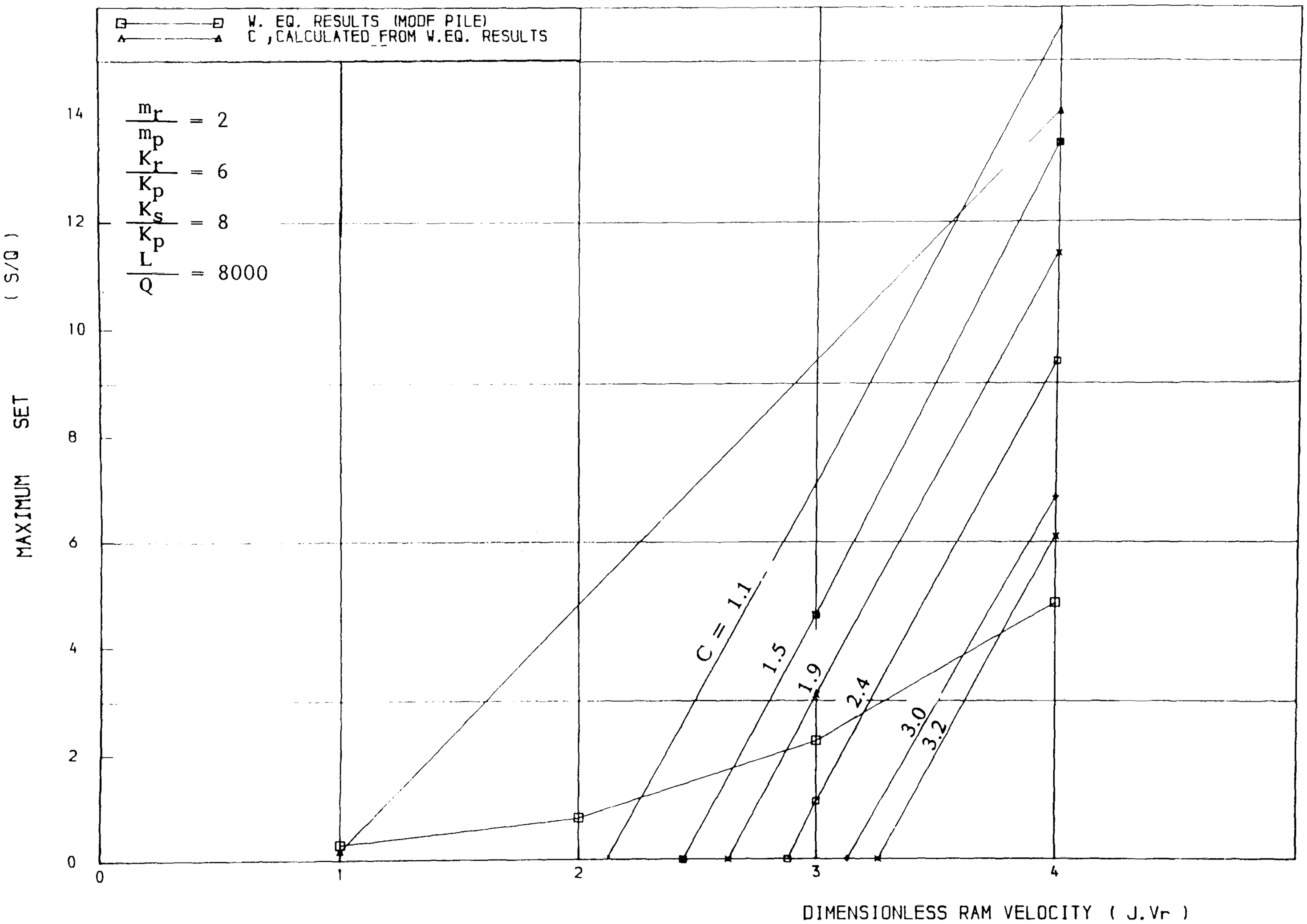

FIGURE (3.58) MAXIMUM PILE SET -RAM VELOCITY RELATIONSHIP

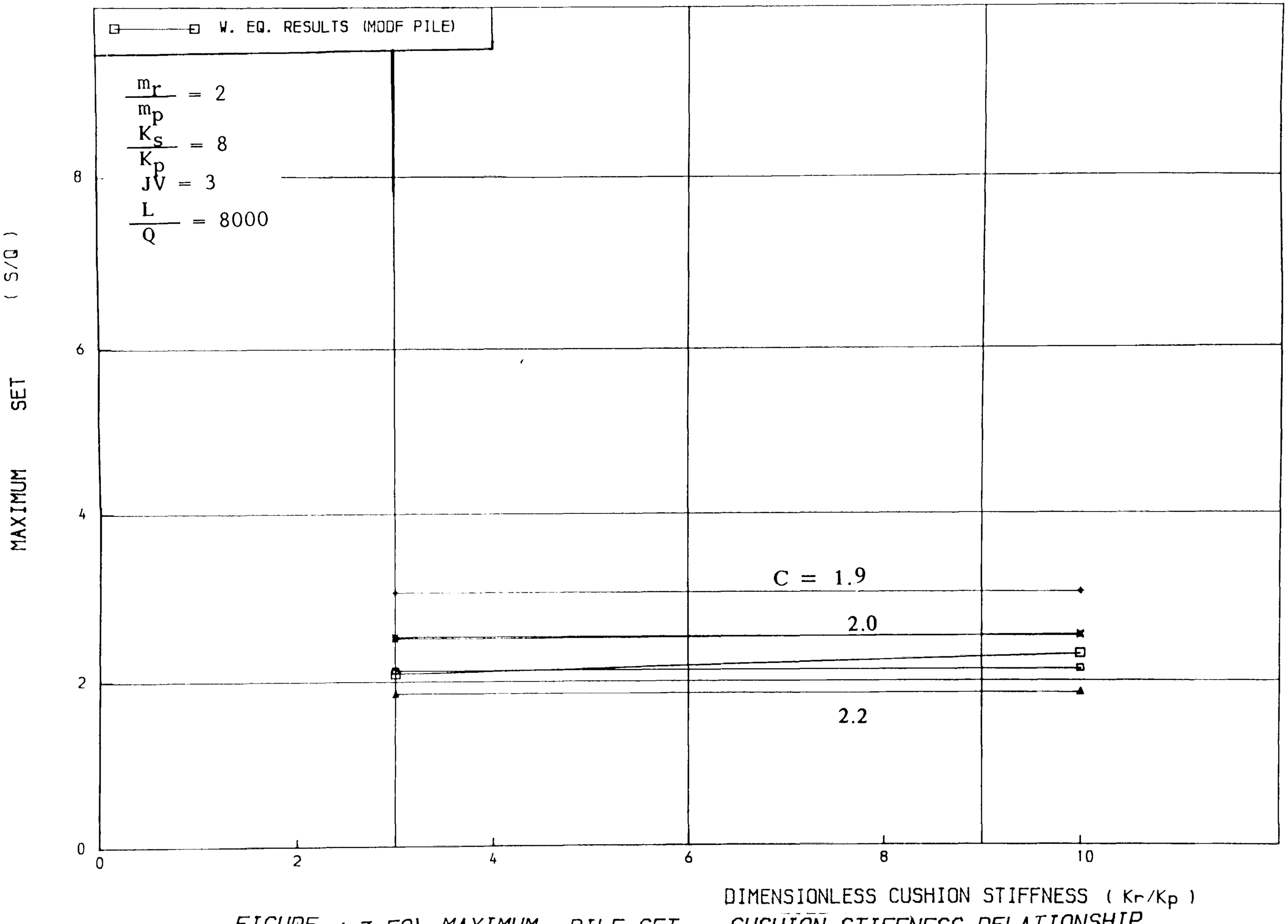

FIGURE (3.59) MAXIMUM PILE SET -CUSHION STIFFNESS RELATIONSHIP

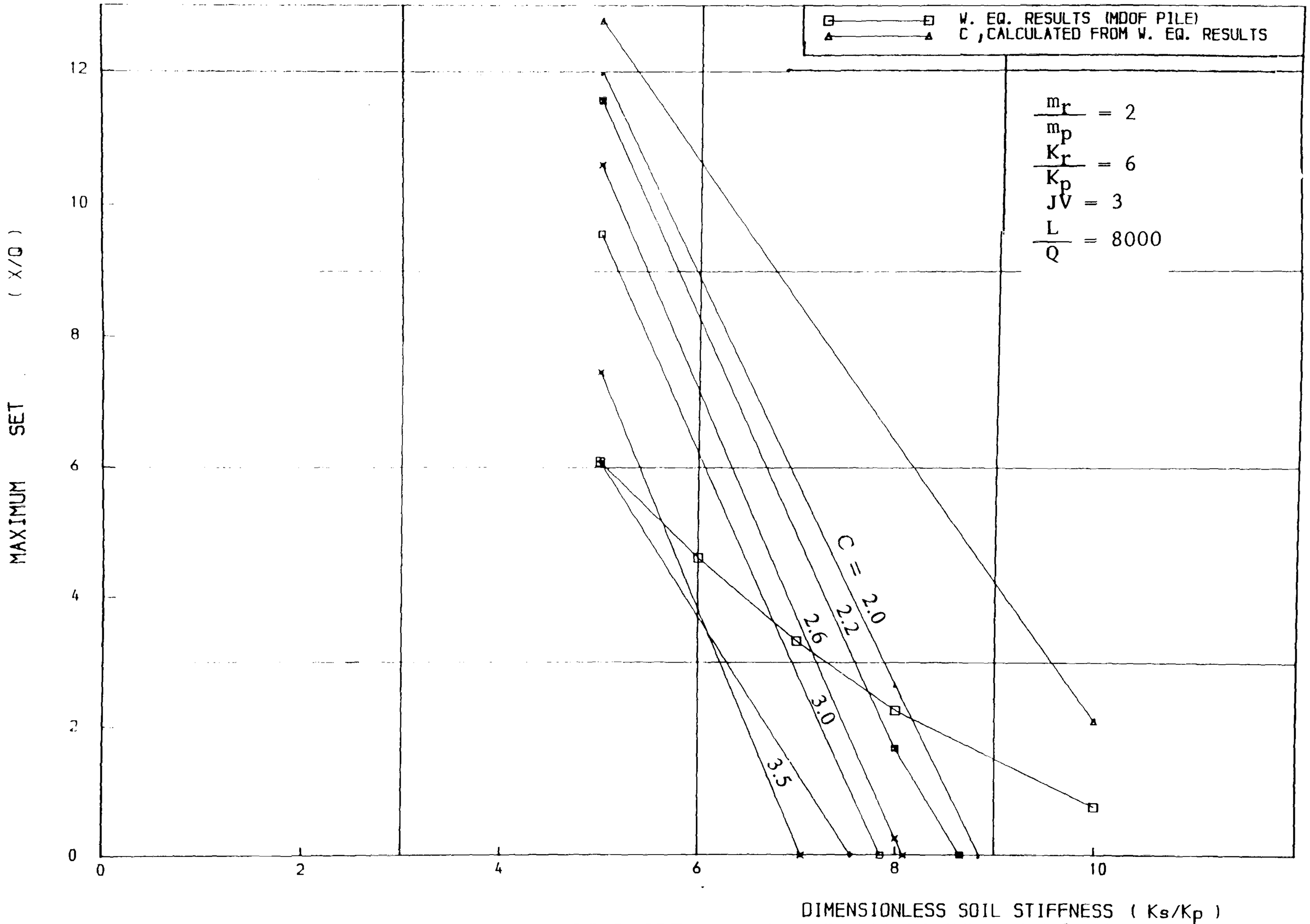

FIGURE (3.60) MAXIMUM PILE SET -SOIL STIFFNESS RELATIONSHIP

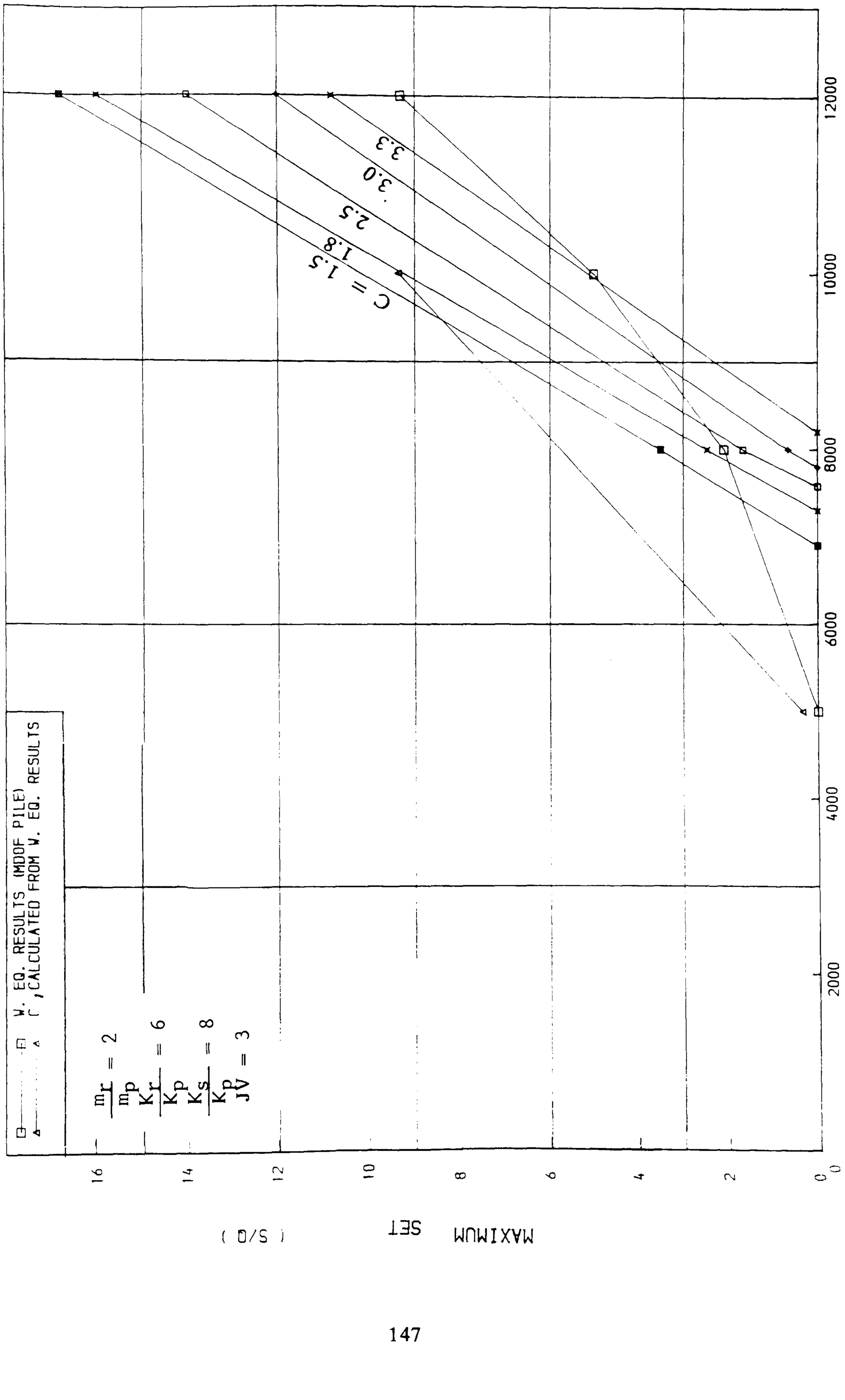

FIGURE (3.61) MAXIMUM PILE SET -PILE LENGTH RELATIONSHIP

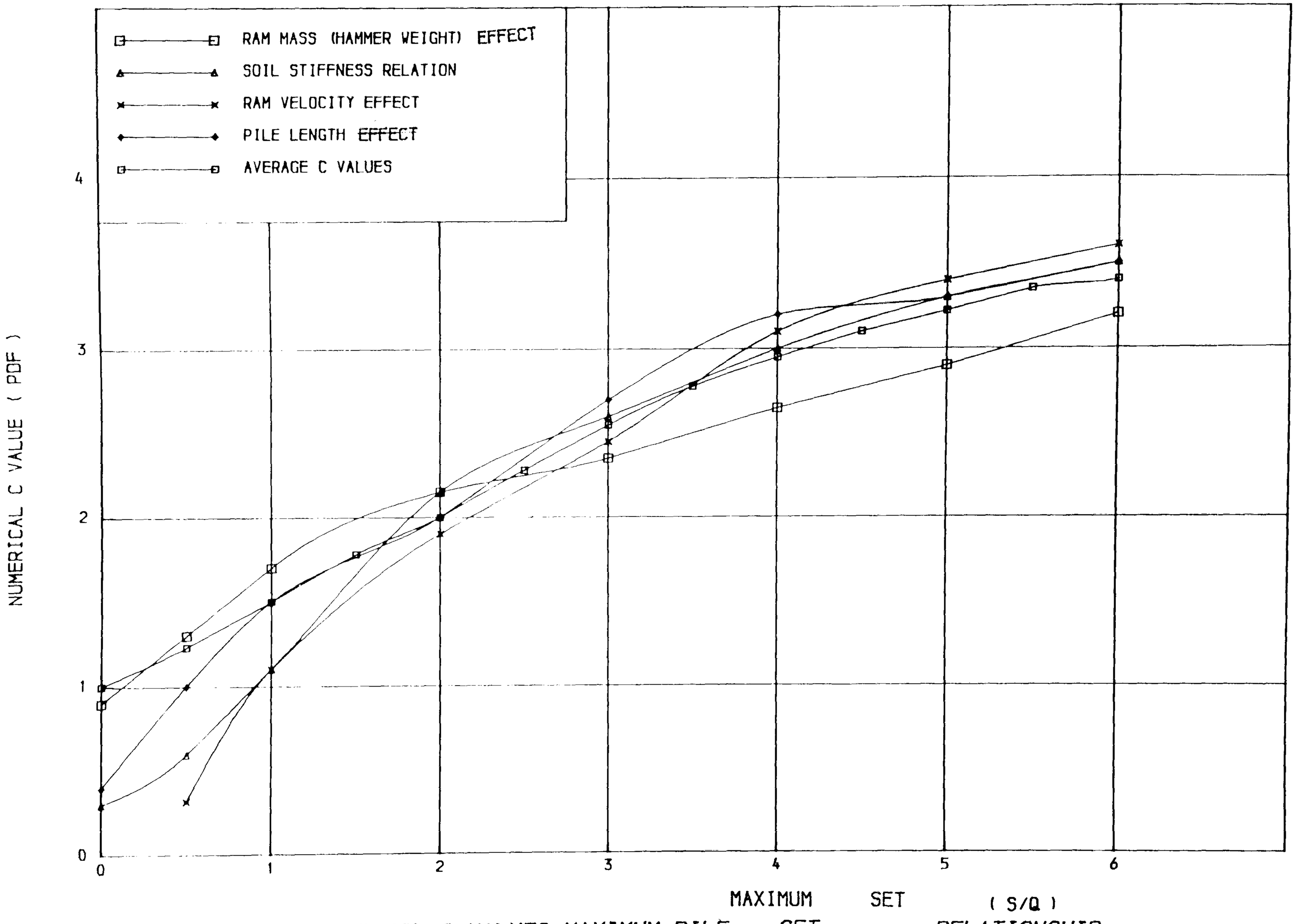

FIGURE (3.62) C VALUES MAXIMUM PILE SET RELATIONSHIP

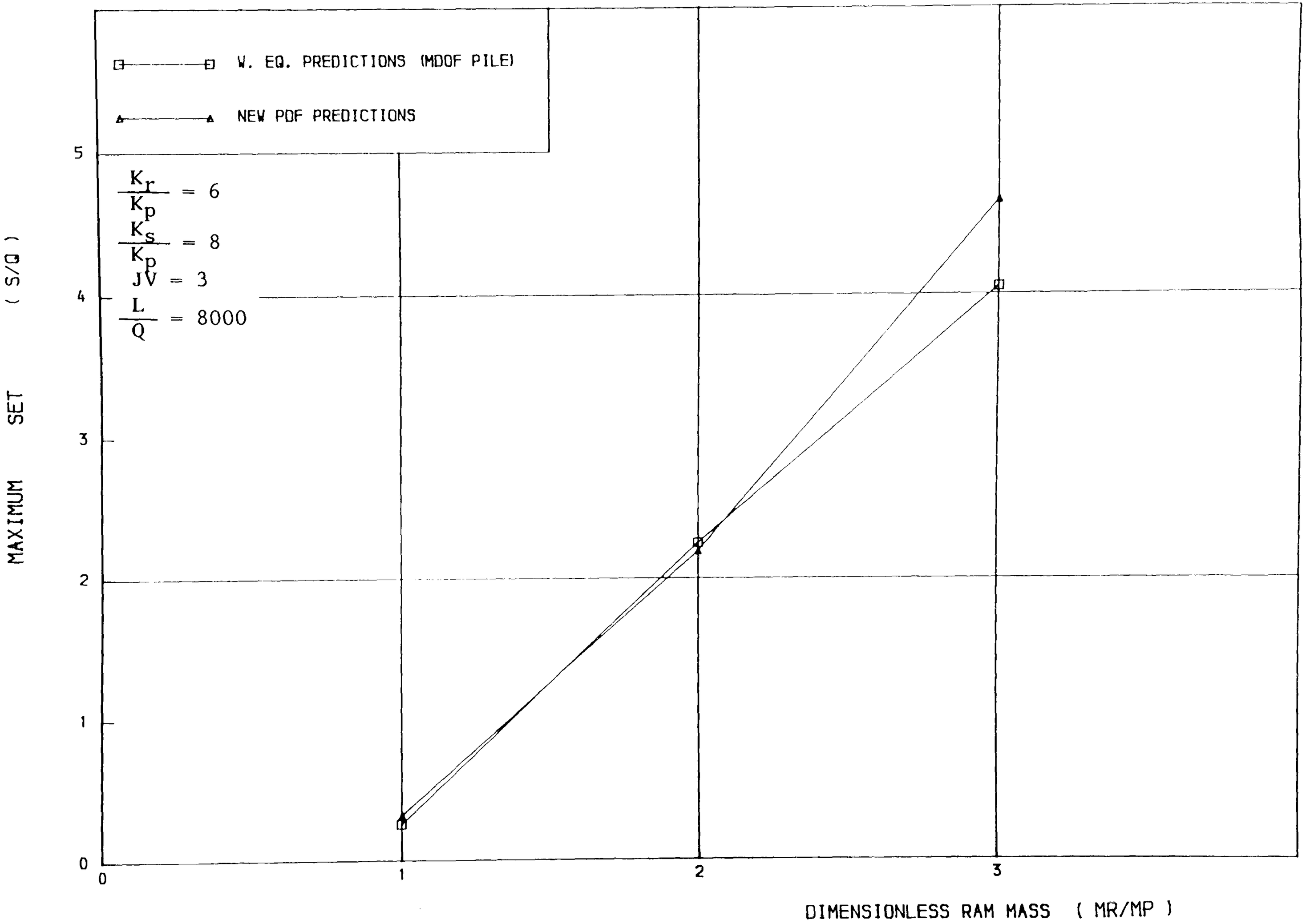

FIGURE (3.63) MAXIMUM PILE SET -RAM MASS/PILE RATIO RELATIONSHIP

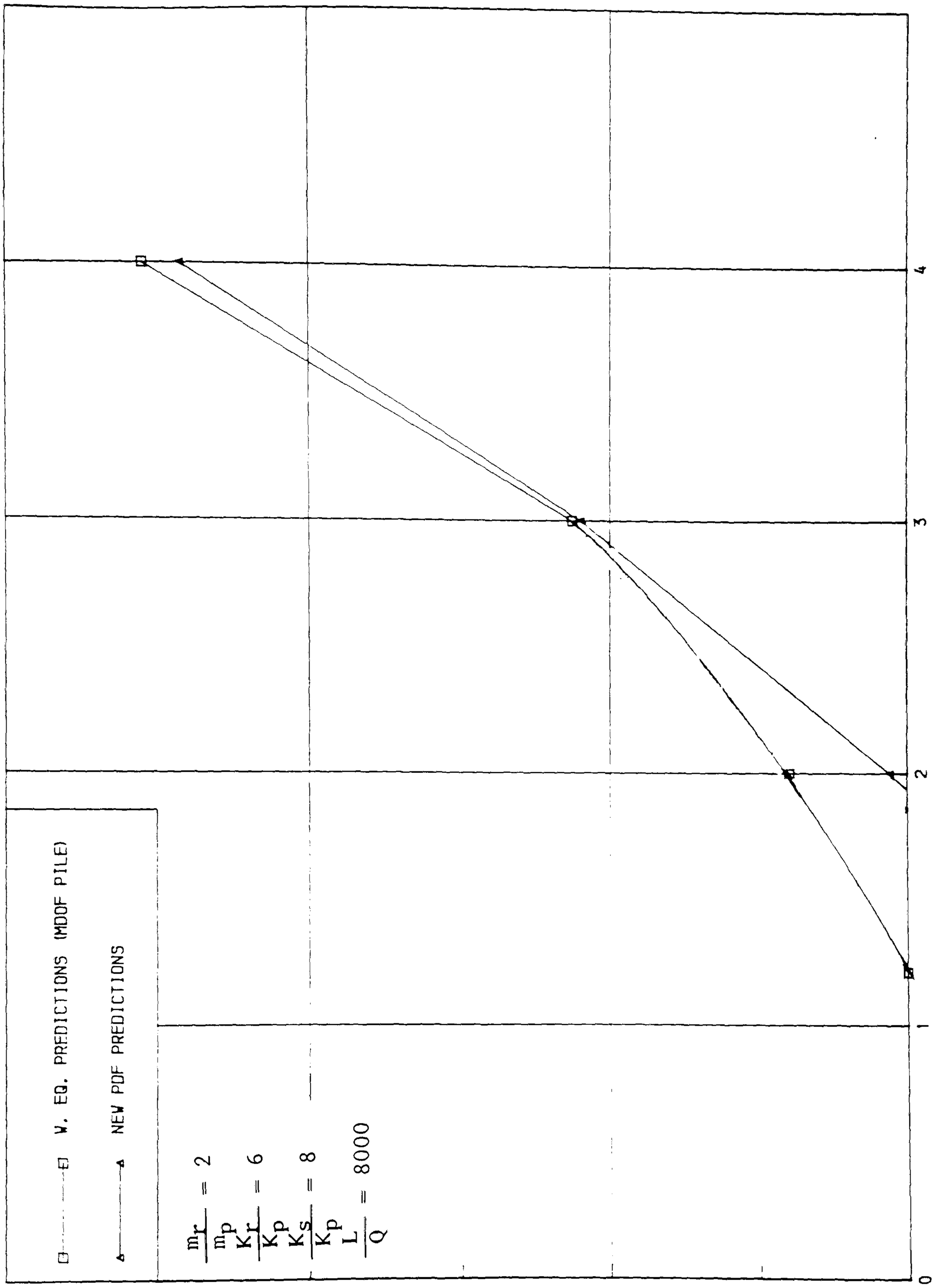

FIGURE (3.64) MAXIMUM PILE SET

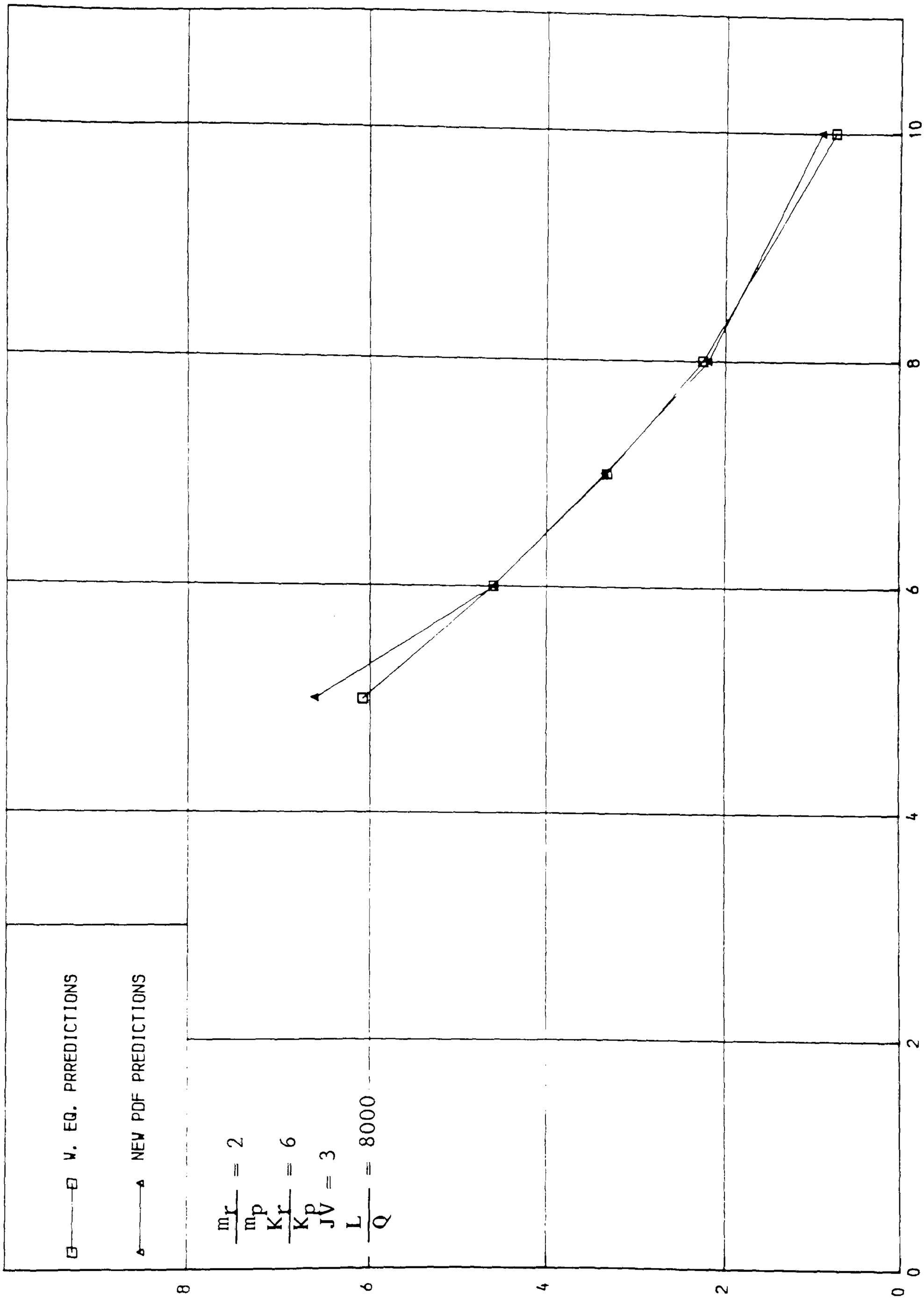

FIGURE (3.65) MAXIMUM PILE SET -SOIL STIFFNESS RELATIONSHIP

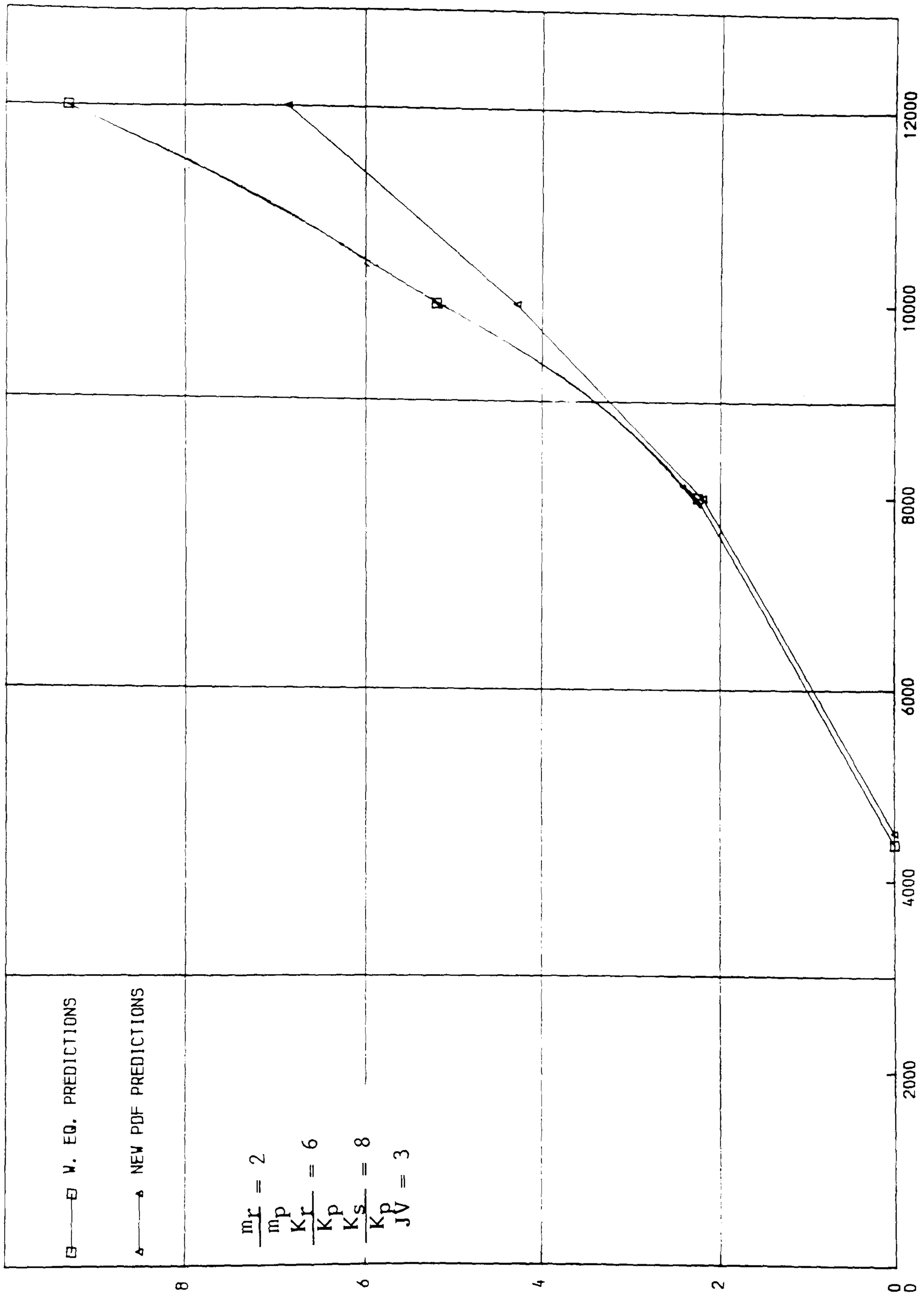

FIGURE (3.66) MAXIMUM PILE SET -PILE LENGTH RELATIONSHIP

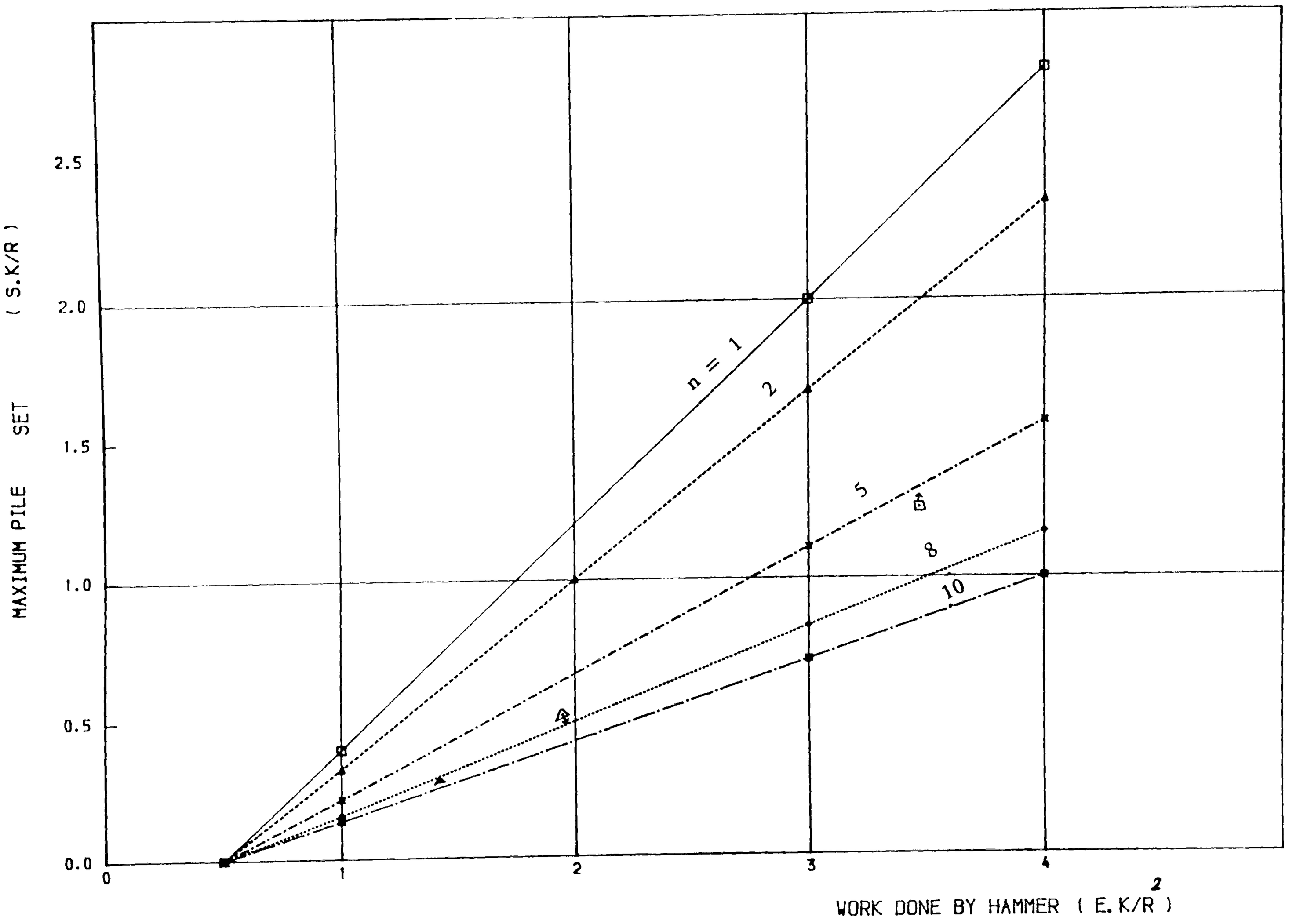

FIGURE (3.67) MAXIMUM PILE SET_HAMMER WORK RELATIONSHIP

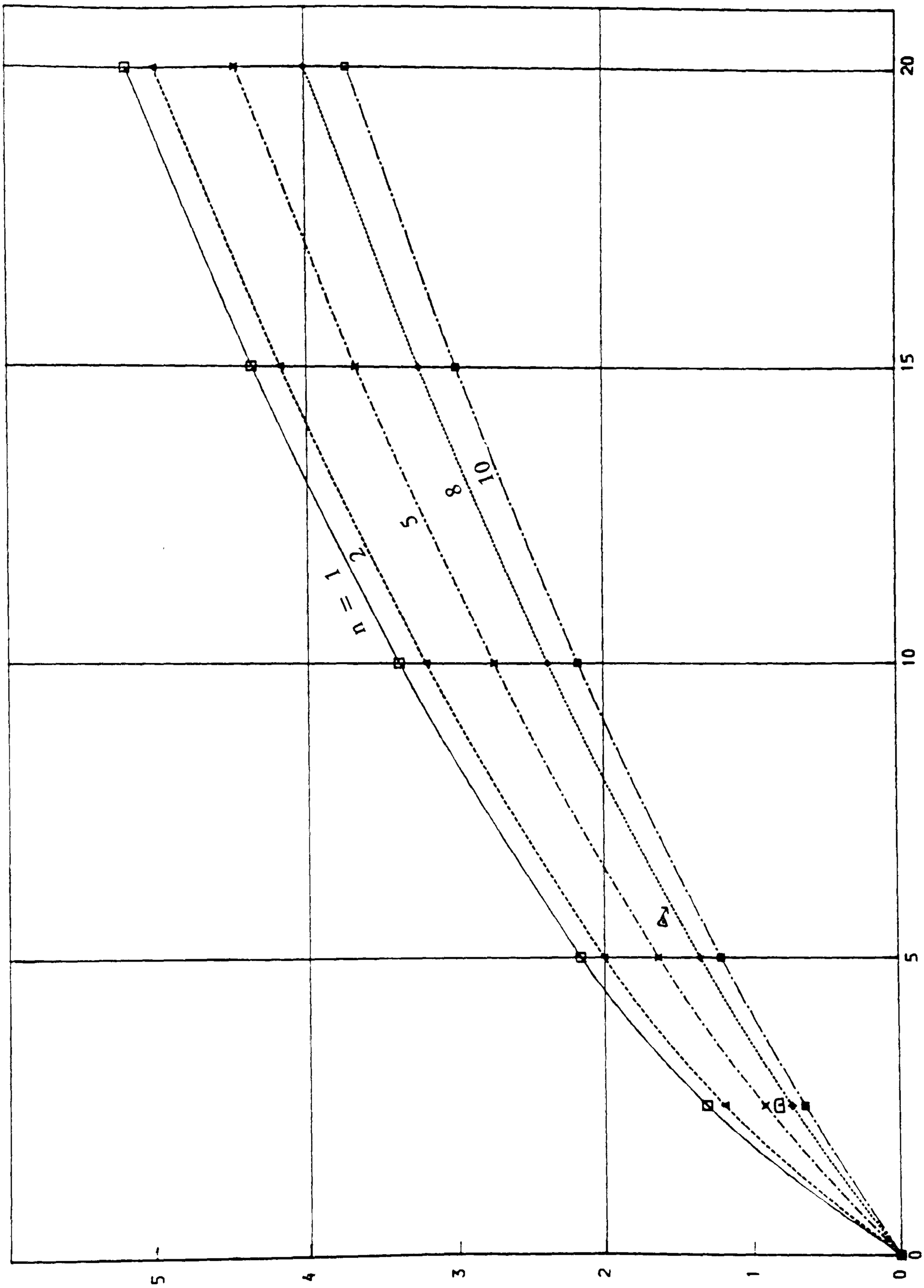

FIGURE (3.68) ULTIMATE SOIL RESISTANCE-HAMMER WORK RELATIONSHIP

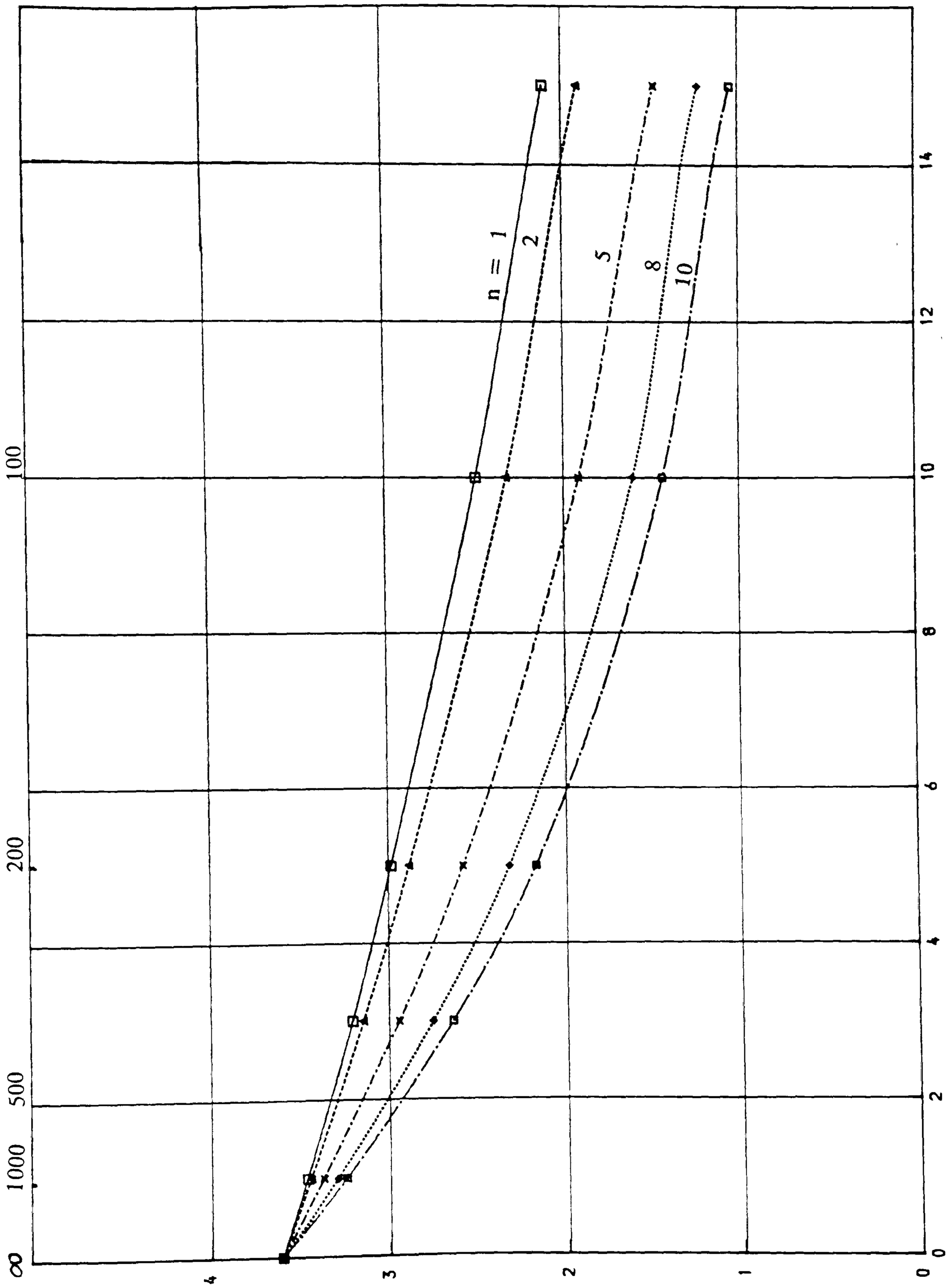

FIGURE (3.69) ULTIMATE SOIL RESISTANCE_MAXIMUM PILE SET RELATIONSHIP
(VARIOUS SOIL RELATIVE STIFFNESSES)

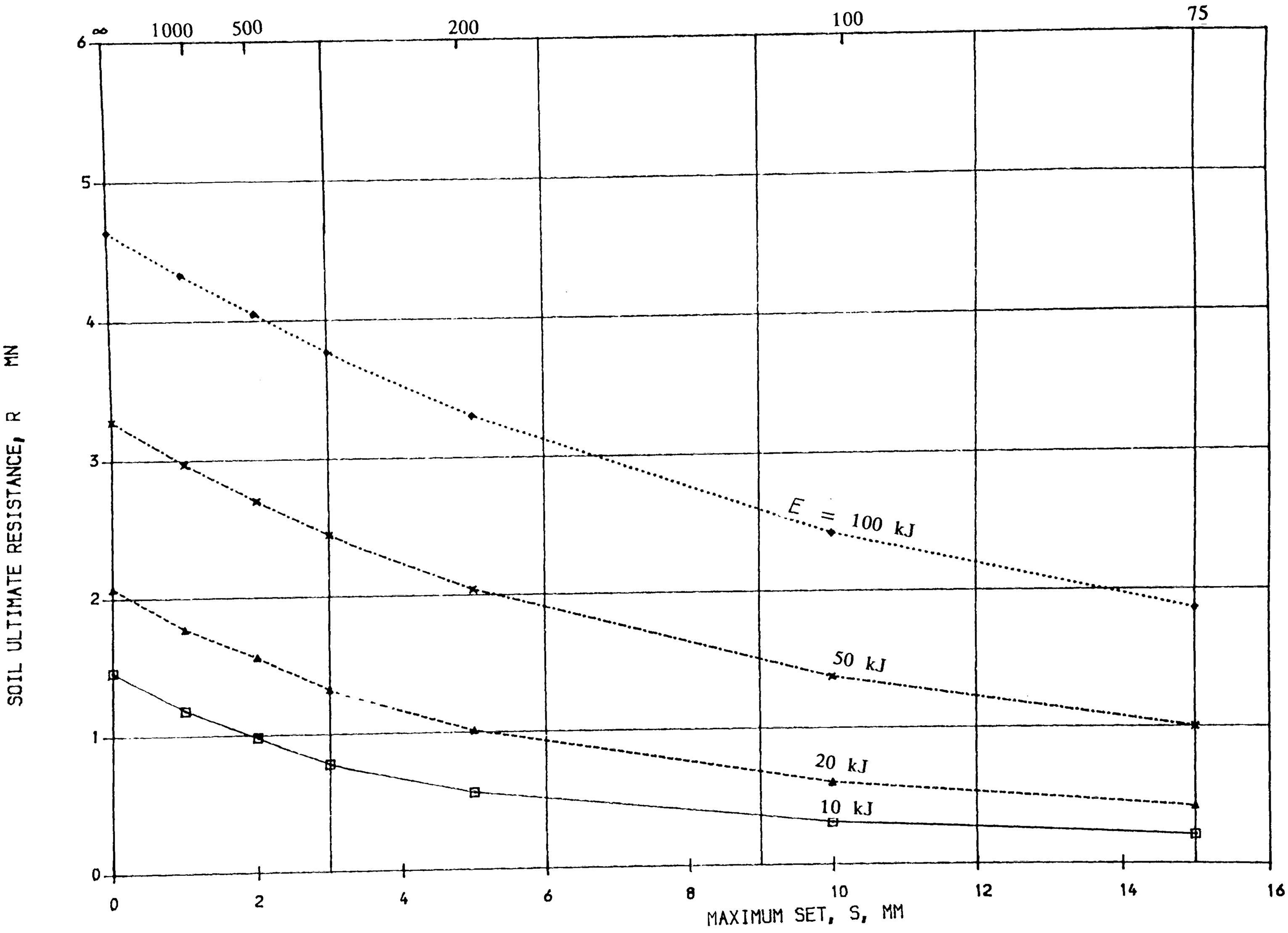

FIGURE (3.70) ULTIMATE SOIL RESISTANCE-MAXIMUM PILE SET RELATIONSHIP (VARIOUS HAMMER ENERGIES)

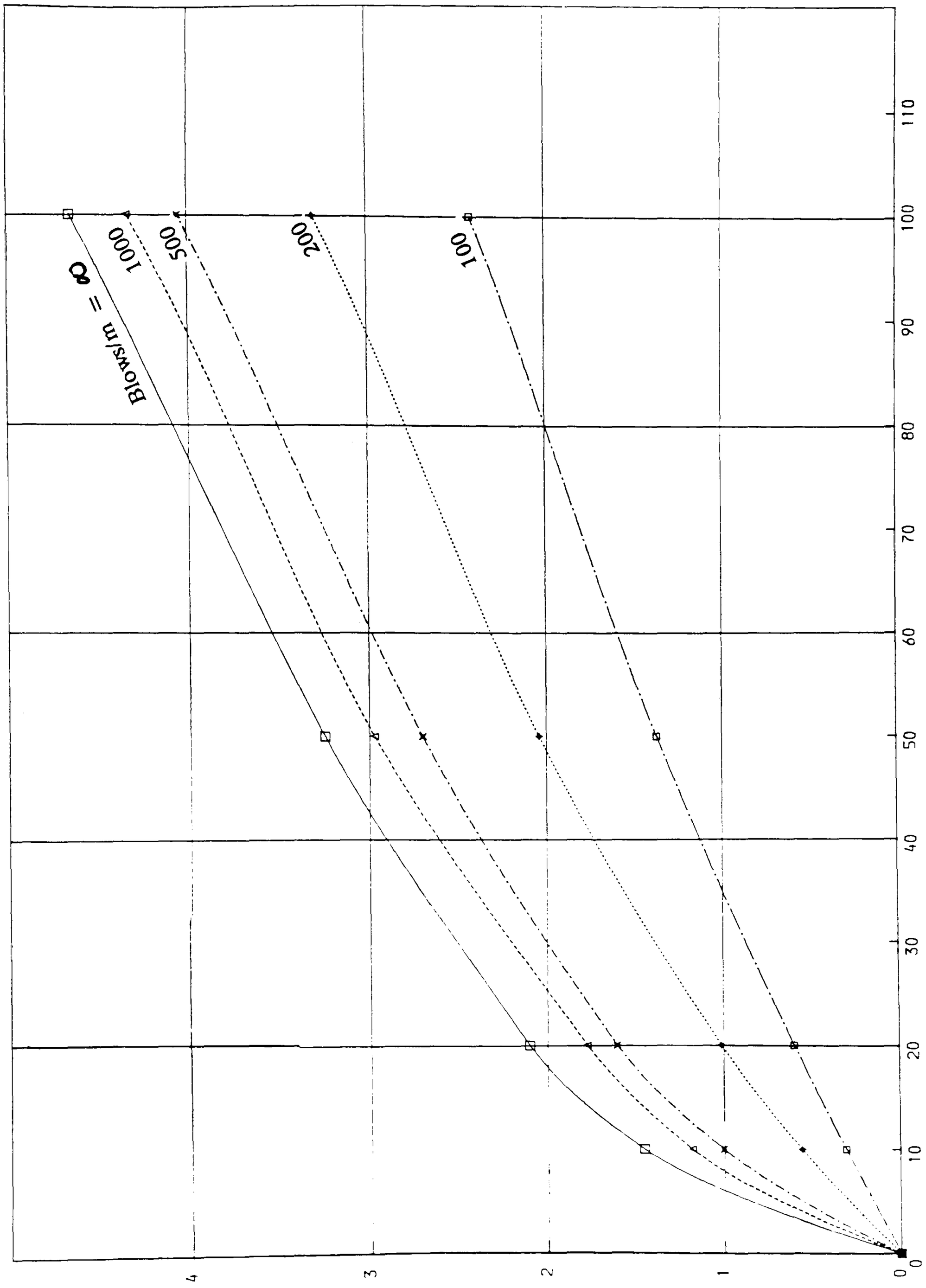

FIGURE (3.71) ULTIMATE SOIL RESISTANCE-MAXIMUM DISPLACEMENT RELATIONSHIP (VARIOUS HAMMER ENERGIES)

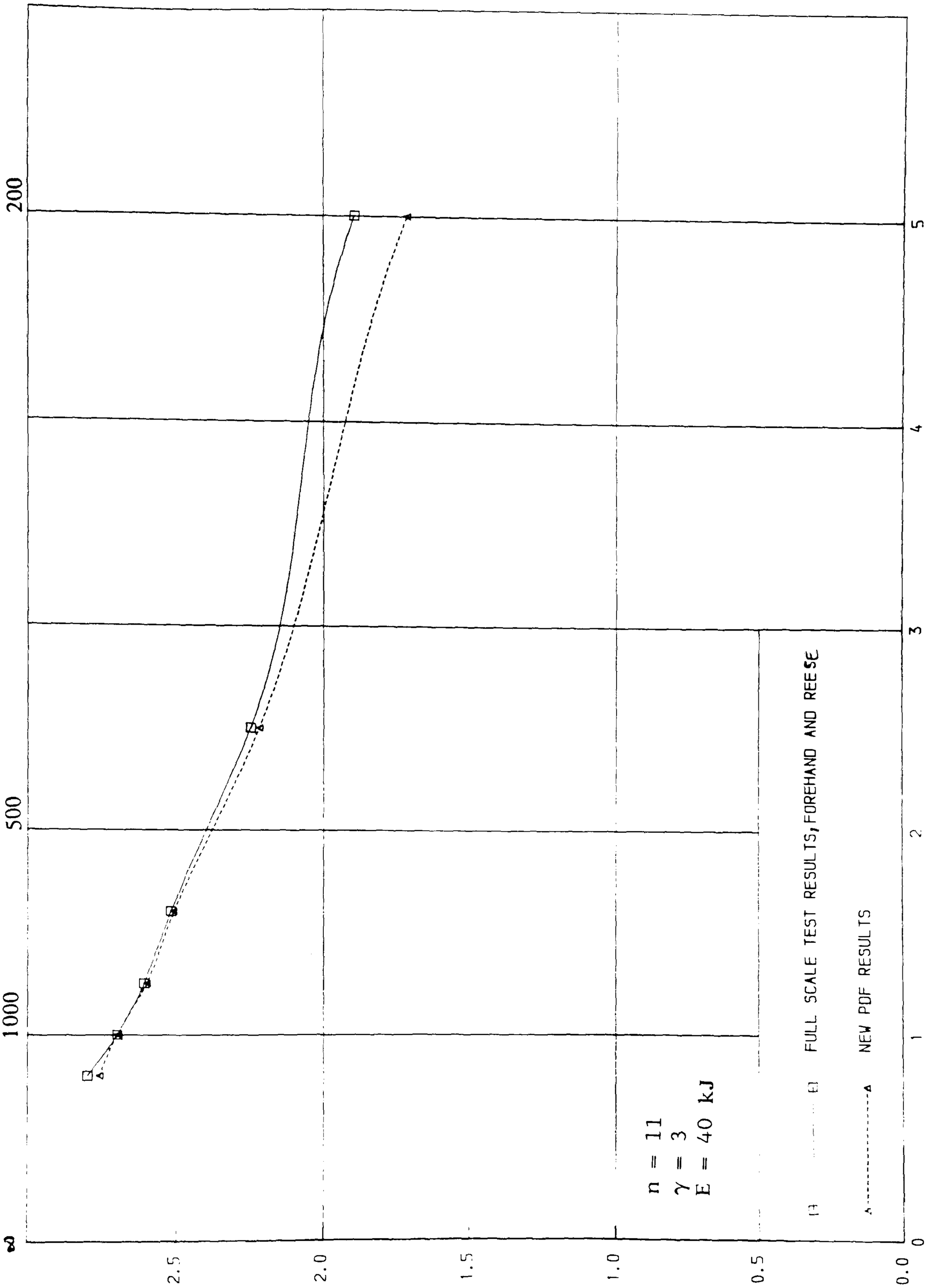

FIGURE (3.72) ULTIMATE SOIL RESISTANCE-MAXIMUM PILE SET RELATIONSHIP

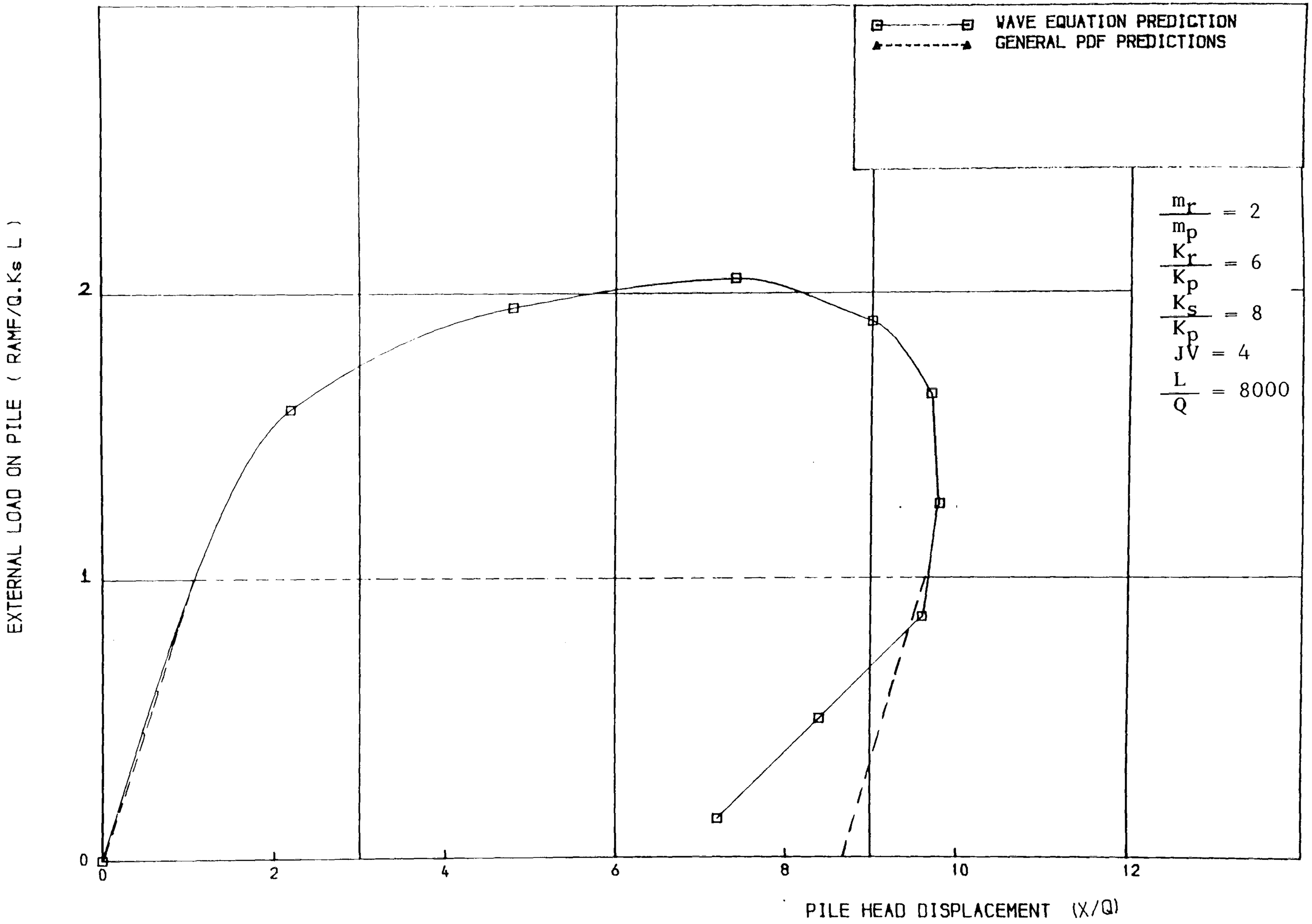

FIGURE (3.73) LOAD-PILE HEAD DISPLACEMENT RELATIONSHIP

CHAPTER 4

THE FINITE ELEMENT MODEL

4.1 INTRODUCTION

4.2 THEORETICAL FORMULATION

4.2.1 Introduction
4.2.2 Governing Equations

4.3 CONSTITUTIVE LAWS

4.3.1 Introduction
4.3.2 Yield Criteria
4.3.3 The Critical State Model
4.3.4 Conclusion

4.4 SPATIAL DISCRETISATION

4.4.1 Introduction
4.4.2 Geometric Modelling
4.4.3 Transmitting Boundaries
4.4.4 Interface Elements

4.5 TIME INTEGRATION SCHEMES

4.5.1 Introduction
4.5.2 Explicit Integration Schemes
4.5.3 Implicit Integration Schemes
4.5.4 Implicit–Explicit Integration Schemes
4.5.5 Conclusion

4.6 CONCLUSION

CHAPTER 4

THE FINITE ELEMENT MODEL

4.1 INTRODUCTION

The finite element method (Zienkiewicz,1971) is too cumbersome to be attractive for routine pile driving analyses since computational costs are typically two or three orders of magnitude greater than for the wave equation analysis. Its main role therefore lies in providing accurate results using real soil properties.

In this Chapter, the essential concepts of the finite element model of analysis for dynamic problems are outlined. Tensor notation is employed for convenience in the development of the numerical algorithm from the governing differential equations of motion.

Clearly, it is important to incorporate realistic soil models in the numerical study and to that end, a number of alternatives, including a critical state model are considered. However, since soil failure during driving takes place very quickly, i.e. under undrained conditions, total stress analysis offers considerable advantages and this approach is favoured in the sequel.

Spatial discretisation, energy absorbing boundaries and interface elements are treated in depth. Further, convolution in the time domain, by various time marching schemes (both explicit and implicit) is examined and the attributes of the alternative formulations are discussed.

4.2 THEORETICAL FORMULATION

4.2.1 Introduction

The finite element method (Zienkiewicz,1977) is, as is well known, a very

powerful and general solution technique. Algorithms for solution of non–linear dynamics problems were published quite early (Seed and Idriss,1970; Lysmer et al, 1975; Angelides and Roesset, 1980) but significant problems remain in regard to practical implementation of the method, viz spurious energy reflections at element interfaces (Holmes and Belytschko,1976) and at curtailed (infinite) boundaries (Lysmer and Kuhlemeyer,1969; Chow and Smith,1981), suppression of higher modes within elements (Celep and Bazant, 1983) and high computational costs. These difficulties are discussed in the sequel but first the derivations of the governing differential equations and the basic formulation of the numerical algorithm are given for completeness.

4.2.2 Governing Equations

In the linear theory of elasticity, the strains can be written in terms of displacements as:

$$\epsilon_{ij} = \frac{1}{2}\,(u_{i,j} + u_{j,i}) \qquad (4.1)$$

where,

u_i is the i–th cartesian component of displacement,

i,j are subscripts ranging from 1 to 3, and,

the comma, denotes differentiation with respect to the space variable, i.e.

$u_{i,j} = \partial u_i / \partial x_j$.

The law of conservation of momentum states that the rate of change of momentum is equal to the net force acting on the body, (Eringen and Suhubi,1974; Graff,1975). For an infinitesimal element, this may be written as:

$$\sigma_{ij,j} + b_i = \rho \ddot{u}_i \qquad (4.2)$$

where,

σ_{ij} is the stress tensor,

b_i is the body force,

ρ is the mass density, and,

$\ddot{u}$ is the acceleration (the super–imposed dots denote the second derivative with respect to time).

On the boundary, the stress tensor must satisfy the equilibrium condition, namely:

$$\sigma_{ij}\, n_j = s_i \tag{4.3}$$

where,

s is the surface traction tensor, and,

n is the unit vector normal to the surface.

The behaviour of a linearly elastic materiai is characterized by a unique relationship between stresses and strains called Hooke's law namely:

$$\sigma_{ij} = D_{ijkl}\ \epsilon_{kl} \tag{4.4}$$

where,

D_{ijkl} is the elastic stiffness tensor.

For an isotropic material, the general form of Hooke's law is:

$$\sigma_{ij} = \lambda\ \delta_{ij}\ \epsilon_{kk} + 2G\ \epsilon_{ij} \tag{4.5}$$

where,

δ_{ij} is the Kronecker delta ($\delta_{ij}=1$ for $i=j$, $\delta_{ij}=0$ for $i\neq j$) and the repeated subscript k implies the summation of the term ϵ_{kk}.

Lame's constants are related to the conventional elastic constants E,G,ν (Young's modulus, shear modulus and Poisson's ratio, respectively) by the relations:

$$\lambda = \frac{E\ \nu}{(1+\nu)(1-2\nu)} \tag{4.6}$$

$$G = \frac{E}{2(1+\nu)} \tag{4.7}$$

Substituting equations 4.1 and 4.5 into equations 4.2 leads to the differential equation of equilibrium:

$$G\ u_{i,jj} + (\lambda+G)\ u_{j,ji} + b_i = \rho\ \ddot{u}_i \tag{4.8}$$

where the double subscript after the comma indicates second order differentiation with respect to the space variables.

Equation 4.8 is the basic governing differential equation of elasto–dynamics. In order to solve it, Hamilton's principle (or the variational principle) is employed; it can be stated (Rao,1982) as follows:

> "of all possible histories of displacement states which satisfy the compatibility equations and the constraints or the kinematic boundary conditions and which also satisfy the conditions at initial and final times (t_1 and t_2), the history corresponding to the actual solutions makes the Lagrangian functional a minimum".

This can be expressed as:

$$\delta \int_{t_1}^{t_2} L\ dt = 0 \tag{4.9}$$

where L is the Lagrangian functional:

$$L = K - U - \Pi \tag{4.10}$$

and,

K is the kinetic energy of the body,

U is its strain energy, and,

Π is the potential energy of the external forces acting on the body.

Now let the volume of the body under consideration be V, and its surface area be S. Applying the principle of virtual work (the principle states that at equilibrium, for any compatible, small virtual displacements imposed on a body, the total internal virtual work is equal to the total external virtual work; Bathe and Wilson, 1976) and using the methods of variational calculus, Hamilton derived a general formulation of the equations of mechanics that describes the motion of the system with finite or infinite degrees of freedom. The mathematical statement of Hamilton's principle (Rao, 1982) is:

$$\delta \int_{t_1}^{t_2} (L + W) \, dt = 0 \tag{4.11}$$

where W is the total external work,except that done by inertial forces, and,

$$\delta W = \int_S S_i \, \delta u_i \, dS + \int_V b_i \, \delta u_i \, dV \tag{4.12}$$

where,

δW is the virtual work done, and,

δu is the virtual displacement.

Equation 4.11 can also be expressed in terms of kinetic energies as follows:

$$\delta \int_{t_1}^{t_2} (K - \Pi + W) \, dt = 0 \tag{4.13}$$

where,

$$\delta \int_{t_1}^{t_2} K \, dt = \int_{t_1}^{t_2} dt \int_{V} \frac{\partial K}{\partial u_i} \, \delta u_i \, dV \qquad (4.14)$$

and,

$$\delta \int_{t_1}^{t_2} \Pi \, dt = \int_{t_1}^{t_2} dt \int_{V} \frac{\partial \Pi}{\partial \epsilon_{ij}} \, \delta \epsilon_{ij} \, dV \qquad (4.15)$$

also we have,

$$\delta \dot{u}_i = \frac{\partial}{\partial t} \, (\delta u_i) \qquad (4.16)$$

and,

$$\delta \epsilon_{ij} = \frac{1}{2} \left[\, (\delta u_i)_{,j} + (\delta u_j)_{,i} \, \right] \qquad (4.17)$$

By applying the divergence theorem;

$$\int_{V} \sigma_{ij} \, \dot{u}_{i,j} \, dV = \int_{S} \sigma_{ij} \, \dot{u}_i \, n_j \, dS \qquad (4.18)$$

and assuming that

$$\sigma_{ij} = \frac{\partial \Pi}{\partial \epsilon_{ij}} \quad ; \quad f_i = \frac{\partial K}{\partial u_i} \quad \text{and,} \quad \sigma_{ij} \, n_j = S_i$$

then, equation 4.13 (after substitution and simplifications) becomes

$$\int_{t_1}^{t_2} dt \left\{ \int_V (\sigma_{ij,j} - \rho \ddot{u}_i + b_i) \delta u_i \, dV \right\} - \left[\int_V f_i \delta u_i \, dV \right]_{t_1}^{t_2} = 0 \quad (4.19)$$

This represents the integral form of the equation of elasto–dynamics. Equation 4.19 can also be written by dropping the tensor notation as:

$$\int_{t_1}^{t_2} dt \left\{ \int_V (\sigma - \rho \ddot{u} + b) \delta u \, dV \right\} - \left[\int_V f \delta u \, dV \right]_{t_1}^{t_2} = 0 \quad (4.20)$$

where,

b is the internal body force vector, which can also be defined in terms of the damping parameter (in the form b= c $\dot{u}$, where c is the damping coefficient) and,

u, $\dot{u}$ and $\ddot{u}$ are the displacement, velocity and acceleration vectors, respectively (

Following the usual finite element procedures, the displacements, velocities and accelerations can be expressed in terms of the associated (element) nodal values as:

$$u = \sum N x \quad (4.21)$$

$$\dot{u} = \sum N \dot{x} \quad (4.22)$$

$$\ddot{u} = \sum N \ddot{x} \quad (4.23)$$

where, the summation is carried over each element node,

$x, \dot{x}$ and $\ddot{x}$ are the vectors of nodal displacements, velocities and accelerations, respectively, and

N is the element shape function.

By applying the principle of virtual work, equation 4.20 can be written for

any time instant,t, irrespective of the material behaviour and, after some re–arrangements we get (Owen and Hinton,1980):

$$\int_V \delta\epsilon_t{}^T \sigma_t \, dV - \int_V \delta u_t{}^T (f_t - \rho \ddot{u}_t + b_t) \, dV = 0 \qquad (4.24)$$

where,

$\delta\epsilon$ is the vector of the virtual strains,

T (superscript) denotes the matrix transpose, and,

t (subscript) indicates the time station,

Invoking Hooke's law (equation 4.4), namely:

$$\sigma = D \epsilon$$

where,the elastic stiffness matrix D for an isotropic axisymmetric element is :

$$D = \frac{E}{(1+\nu)(1-2\nu)} \begin{bmatrix} 1 & \frac{\nu}{(1-\nu)} & \frac{\nu}{(1-\nu)} & 0 \\ & 1 & \frac{\nu}{(1-\nu)} & 0 \\ \text{sym.} & & 1 & 0 \\ & & & \frac{(1-2\nu)}{(1-\nu)} \end{bmatrix} \qquad (4.25)$$

and,

$$\sigma^T = \{ \sigma_z \ , \sigma_r \ , \sigma_\theta \ , \tau_{rz} \} \qquad (4.26)$$

$$\epsilon^T = \{ \epsilon_z \ , \epsilon_r \ , \epsilon_\theta \ , \gamma_{rz} \} \qquad (4.27)$$

The strains can be written in terms of the nodal displacements as:

$$\epsilon = \sum B \ x \qquad (4.28)$$

where B is the strain–displacement matrix. For the isotropic axisymmetric element, it is defined as follows:

$$B = \begin{bmatrix} \frac{\partial N}{\partial r} & 0 \\ 0 & \frac{\partial N}{\partial z} \\ \frac{N}{r} & 0 \\ \frac{\partial N}{\partial r} & \frac{\partial N}{\partial z} \end{bmatrix} \qquad (4.29)$$

By substituting equations 4.20,4.21,4.22 and 4.23 into equation 4.24 we get :

$$\int_V B^T D B \, \delta x \, x \, dV - \int_V N^T f \, \delta x \, dV + \int_V N^T \rho N \, \delta x \, \ddot{x} \, dV +$$

$$\int_V N^T c N \, \delta x \, \dot{x} \, dV = 0 \qquad (4.30)$$

For a single finite element, equation 4.30 can be written in the form:

$$\sum M \ddot{x} + \sum C \dot{x} + \sum K x = \sum f \qquad (4.31)$$

where, the summation is carried out over each element node,
M is called the mass matrix, where,

$$M = \int_V N^T \rho N \, dV \qquad (4.32)$$

C is called the damping matrix, where,

$$C = \int_V N^T \; c \; N \; dV \qquad (4.33)$$

and K is called the element stiffness matrix, where,

$$K = \int_V B^T \; D \; B \; dV \qquad (4.34)$$

Assembly of equations 4.31 for each element of the body and invoking the compatibility and equilibrium conditions of the nodes, yields by superposition the global system equations:

$$M \ddot{x} + C \dot{x} + K x = F \qquad (4.35)$$

where, **M** ,**C** ,**K** and **F** are the global mass, damping and stiffness matrices, respectively, and **F** is the forcing matrix.

The solution of these equations can be achieved by integrating them in the time domain by means of the methods discussed later in this Chapter.

4.3 CONSTITUTIVE LAWS

4.3.1 Introduction

Realistic constitutive laws are essential if reliable results are to be obtained using the finite element method. However, advances in numerical analysis have far exceeded knowledge of soil behaviour, Hill (1950), Desai and Siriwardane (1984). Thus results from sophisticated numerical analyses should be treated with some caution.

The simplest constitutive model assumes isotropic linear elasticity. However, this model is only useful at small strain levels and it is necessary to use elasto–plastic flow theory to describe soil behaviour at strain levels of interest. Due to the fact that pile driving involves impact forces of short duration, undrained behaviour can be assumed to occur. Consequently, total stress analyses and simple elastic–perfectly plastic soil models can be used for convenience. Some of these models are discussed in what follows.

4.3.2 Yield Criteria

It is postulated that flow occurs within a material when the current stress state satisfies certain energy criteria or reaches specific critical values. The one–dimensional concept of a yield stress, from the simple tension test, Fig. 4.1 and Fig. 4.2, leads naturally to the idea of the yield " surface", Fig. 4.3, in (principal) stress space. The yield criterion is then conveniently defined by a yield function F as (Davies,1979 and Desai and Siriwardane,1984):

$$F(\sigma_{ij}) = 0 \tag{4.36}$$

where,

$F = 0$ implies that the material is on the yield surface,i.e. plastic flow takes place,

$F < 0$ implies that the material lies within the elastic domain i.e. the material deforms elastically,

$F > 0$ is inadmissible.

In general, plasticity theory can be developed to allow for expansion (work hardening, strain hardening), contraction (work softening, strain softening) and

translation (kinematic hardening) of the yield surface depending on the type of the flow rules and hardening parameters used.

Since, for isotropic materials, the yield function must be invariant with respect to all reference frames, it must be expressed in terms of the invariants of the stress tensor, i.e.

$$F(I_1, I_2, I_3) = 0 \qquad (4.37)$$

where I_1, I_2, I_3 are the first, second and third invariants of the stress tensor, given by :

$$I_1 = \sigma_{ii}$$

$$I_2 = 1/2\ (\sigma_{ii}\ \sigma_{jj} - \sigma_{ij}\ \sigma_{ij}) \qquad (4.38)$$

$$I_3 = 1/3\ (\sigma_{ij}\ \sigma_{jk}\ \sigma_{ki})$$

In metal plasticity, it is assumed that yielding is unaffected by the hydrostatic stress ($1/3\ \sigma_{ii}$) and, accordingly, the yield function is usually expressed in terms of the invariants of the deviatoric stress tensor (s_{ij}) or :

$$F(J_2, J_3) = 0 \qquad (4.39)$$

where,

$$J_1 = 0$$

$$J_2 = 1/2 \; s_{ij} \; s_{ij} \qquad (4.40)$$

$$J_3 = 1/3 \; s_{ij} \; s_{jk} \; s_{ki}$$

where the deviatoric stress tensor s_{ij} is defined as follows :

$$s_{ij} = \sigma_{ij} - 1/3 \; \delta_{ij} \; \sigma_{kk} \qquad (4.41)$$

Many yield criteria have been proposed, of which the most well known are those due to Tresca, Von Mises, Mohr–Coulomb and Drucker–Prager. Tresca's criterion (the condition of constant maximum tangential stress) defines a hexahedral prism in principal stress space and implies that the maximum shear stress within the body can not not exceed a certain specific value. The attendant mathematical difficulties of formulation in three dimensions (because of the corners) has precluded its general use in theoretical analysis.

Von Mises criterion, which defines the circumscribed cylinder, is much more amenable to theoretical development; it is simply a function of the second deviatoric invariant:

$$F(J_2) = 0 \qquad (4.42)$$

Since J_2 corresponds precisely, up to a scalar factor,with the energy of the elastic change of shape,the Von Mises criterion is some times called a distortional energy criterion. This criterion was first proposed by Von Mises in 1913. According to this theory, plastic yielding starts when the elastic strain energy due to shearing reaches a critical value, when the following equation (in terms of principal stresses) is satisfied:

$$(\sigma_1 - \sigma_2)^2 + (\sigma_2 - \sigma_3)^2 + (\sigma_3 - \sigma_1)^2 = 2\sigma_y^2 \qquad (4.43)$$

where σ_y is the yield stress (in uniaxial loading).

In principal stress space, the Von Mises yield criterion describes a cylindrical surface, Fig. 4.4 , about the hydrostatic axis.

These two criteria were developed specifically for metals from observations of their behaviour. The behaviour of soils differs in many respects; in particular, the yielding of soil is highly dependent on the hydrostatic component of effective stress. Further, a realistic constitutive model for soils should be capable of taking into account features like dilatancy, sensitivity and strain hardening. Much research effort has been developed to improve the predictive capacity of constitutive laws for sands and clays. Important conference proceedings have been edited by Parry (1972), Palmer(1973), Murayamo and Schofield (1977), Yong and Ko (1981), Desai and Saxena (1981) and Desai and Gallagher (1983). The workshop chaired by Yong and Ko (1981) is especially interesting since many of the important existing soil models were compared for their predictive ability. The general conclusion was that a complicated, all–encompassing soil model is un–necessary (and undesirable on the grounds of cost) since simple models can often provide equally useful results. Further, these models are generally, strictly speaking, valid only for simple stress states. Thus, in view of the complicated state of stress adjacent to the pile wall during driving and subsequent consolidation, utilization of sophisticated material models offers little advantage.

4.3.3 The Critical State Model

The critical state model (Schofield and Wroth,1968) is an elasto–plastic constitutive law relating increments of strains to increments of effective stress.

When a loose soil sample is sheared, it passes through progressive states of yielding before reaching a state of collapse. This means that the stress path passes through several yield surfaces which results in (plastic) permanent

deformations. Yielding continues until the material reaches a critical void ratio, after which the void ratio remains constant (i.e. no volume change occurs) during subsequent deformation. This is called the critical void ratio and the failure stress–volume condition of the soil is termed the critical state. However, when a dense soil sample is sheared, the maximum shear resistance is developed during dilation but as the critical void ratio is approached the shear resistance falls to its critical state value.

Critical state models were originally developed by Roscoe's research group at Cambridge University in the 1950's and 60's, (Schofield and Wroth,1968) based on conventional triaxial tests on consolidated reconstituted kaolin slurry. The model is described in terms of the effective stress invariants (p and q) and the specific volume V as defined below (Wood,1984).

Mean normal effective stress (p) :

$$p = \frac{1}{3} [\sigma_1 + \sigma_2 + \sigma_3] \qquad (4.44)$$

Deviatoric stress (q):

$$q = \frac{1}{\sqrt{2}} [(\sigma_1-\sigma_2)^2 + (\sigma_2-\sigma_3)^2 + (\sigma_3-\sigma_1)^2]^{1/2} \qquad (4.45)$$

Specific volume (V) :

$$V = 1 + e \qquad (4.46)$$

where e is the void ratio.

Under conventional triaxial conditions at least two of the principal stresses are equal resulting in some simplification. Further, by the principle of effective stress, total and effective stresses are related via equations of the form

$$\sigma_1 = \sigma_1^t - u \qquad \text{etc.} \tag{4.47}$$

where u is the pore water pressure.

In the critical state theory, the consolidation and swelling lines are assumed to be straight in the (ln p–V) plots,with slopes (λ) and (κ),respectively, (Fig. 4.5) which assume the role of material parameters in the critical state theory. These lines can be described by the equations:

$$V = \Gamma_0 - \lambda \ln p \tag{4.48}$$

where Γ_0 is the specific volume at unit mean effective stress on the consolidation line, and,

$$V = V_m + \kappa \ln \left(\frac{p}{p_m}\right) \tag{4.49}$$

where V_m is the specific volume on the consolidation line at a mean effective stress of p_m.

When the soil sample is sheared, it approaches the critical state line which is assumed to be parallel to the consolidation line in the V–p space :

$$V = \Gamma - \lambda \ln p \tag{4.50}$$

where Γ is the specific volume at unit pressure on the critical state line.

In terms of stress–invariants, the Mohr–Coulomb failure criterion can be expressed in the form

$$q = M p \tag{4.51}$$

where, for example, for triaxial test results the parameter M is given by the equation:

$$M = \frac{6 \sin \Phi}{(3 - \sin \Phi)} \qquad (4.52)$$

where Φ is the angle of internal friction (at the critical state).

The value of M determines the slope of the critical state line in the p–q plot, Fig. 4.6 , while Γ locates this line in the corresponding p–V plot shown in Fig. 4.6. Although this line (curve) describes the failure state of the soil, detailed observations from a comprehensive series of tests are necessary to establish the shape of the yield surface. As noted earlier, this is a function of both the deviatoric stress q and the hydrostatic effective stress p. Schofield and Wroth (1968) first proposed a yield surface described by the equation (in q–p space) :

$$q = M\, p\, \ln \left(\frac{p_m}{p} \right) \qquad (4.53)$$

where p_m is the past maximum mean effective stress which the soil has suffered.

This gives rise to the idea of a state boundary surface in (q–p–V) space given by the equation (Fig. 4.8):

$$q = \frac{M\, p}{(\lambda - \kappa)} \left[\Gamma + \lambda - \kappa - V - \lambda \ln p \right] \qquad (4.54)$$

When the state of stress of the soil lies within this surface, the behaviour is elastic (over–consolidated) while the behaviour on the surface is elasto–plastic; any stress state outside this surface is inadmissible.

It is assumed that the under elastic conditions changes in the deviatoric stress,q, do not cause changes in the void ratio and consequently the elastic

behaviour is constrained to a vertical "elastic wall", whose locus with the state boundary surface defines the current yield criterion. Upon further consolidation, or elasto–plastic loading the stress–state passes through successive adjacent yield surfaces and their associated elastic walls (Fig. 4.9).

This model of soil behaviour which accommodates the phenomena of dilatancy, frictional failure and consolidation behaviour has been modified by several investigators (notably the modified Cam–clay model of Burland ,1965) to overcome (not entirely successfully) shortcomings in the original model. Current opinion is that these models can give excellent quantitative predictions of soil behaviour in many cases but in general real soils behaviour is too complex to admit highly accurate predictions from such simple models, no matter how elegant.

4.3.4 Conclusion

The behaviour of saturated clays subjected to undrained loading during pile driving is clearly very complex. Probably not even the more complex soil models can adequately describe soil behaviour under these conditions and for that reason, simple models are probably equally valid in these circumstances. Further, total stress analyses have the added advantage of cost effectiveness and robustness as exemplified by the work of Chow (1981), To (1985),Willson (1985) and Simons (1985). This approach is followed in this thesis.

4.4 SPATIAL DISCRETISATION

4.4.1 Introduction

The constraints for spatial discretisation of the finite elements in a dynamic analysis are different from those governing a static problem. Due to the low–pass filtering action of the finite elements, the element size in a dynamic analysis must

be limited by certain criteria based on the type of the element, the type of mass formulation and the nature of the applied loads,(Isenberg and Vaughan,1981). Although, it is common practice to grade the elements in a static problem, more severe restrictions are imposed when mesh grading is adopted in a dynamic problem due to the possibility of spurious reflection,(Celep and Bazant,1983).

The main distinction between static and dynamic analysis lies in the inclusion of mass and damping matrices which correspond to the inertial and viscous damping resistances. A study of the effect of the mass formulation (whether it is "lumped" or "consistent" or a combination of these two) is desirable in some wave propagation problems. It should be noted that the damping resistance may arise either physically (due to material viscosity,for example) or geometrically (due to radiation) and both serve to absorb energy from the source. Dynamic analyses are complex, time consuming and susceptible to the accumulation of errors since the response must be calculated at each and every successive time step size throughout the entire period of interest.

4.4.2 Geometric Modelling

One of the advantages of the finite element method is the possibility of introducing mesh refinements locally around the zones of interest in the hope of obtaining a more accurate solution. However, for wave propagation problems variation in the element sizes can cause spurious reflections even in a homogeneous medium,(Isenberg and Vaughan,1981).

The element size is a critical consideration in the finite element analysis since it affects not only the accuracy of the solution but also the cost of the analysis. Therefore, the criteria for selection of the optimum element size and mesh grading for dynamic analysis must be carefully considered.

The principal constraint governing the size of the element to be used in wave propagation problems is that it should be able to transmit the highest dominant frequency wave that may be present. Shipley et al,(1967) have shown that finite elements act as low–pass filters, i.e. high frequency waves cannot

propagate across elements. Therefore, in order to transmit all important high frequency waves, it is necessary that the size of the finite elements must be sufficiently small. A maximum allowable ratio of wave length to element dimension (λ/L), taking into consideration economy and accuracy of approximately four (4) has been proposed (in consistent mass matrix formulations) by Valliappan and Ang (1985), for eight noded quadratic elements.

Celep and Bazant (1983) studied the spurious reflections which occur when element sizes are changed gradually over a transition zone of several elements in a homogeneous medium. They concluded that when the wave length is four times the larger element size (or shorter) spurious reflections are very significant. Increasing the number of transition elements in the transition zone between regions of small and large elements was found to mitigate this phenomenon. This improvement is significant when the difference between the element sizes in the two regions is not very large, but becomes less effective when the difference in size exceeds 50%. However, in consistent mass formulations, spurious reflection is less severe than for lumped mass formulations.

To (1985) discussed the effect of the ratio of the wave length to the element dimension (λ/L) in the direction of the wave. He demonstrated that high frequency waves which remain within the discretised grid causing spurious node–to–node oscillations can be eliminated or minimized by incorporating internal soil damping. Alternatively, specifying very small time steps and postprocessing the results by means of digital filters,(Holmes and Belytschko,1976), can be an effective solution strategy. This latter method may, however, cause further dispersion and is not recommended. To (1985) also recommended a wave length/element dimension ratio of four (4) to ensure transmission of high frequency waves.

4.4.3 Transmitting Boundaries

In finite element analyses of statics, various methods have been used to model the stiffness of the exterior domain beyond the artificially curtailed boundaries. However, in dynamics, analysts are often confronted with the problem of wave propagation into the far field. In order to simulate this energy radiation,

provision must be made to absorb the stress waves arriving at the boundary. Failure to do this will result in wave reflection at the boundary leading to spurious resonances and stress amplifications. In addition, the finite element model must allow for the stiffness of the exterior domain.

A simple solution of this problem is to combine sufficiently high material damping with a finite element model of an abnormally large region of the body to ensure that the reflected waves are damped out before they reach the region of interest. However, the computational costs incurred by this approach may be prohibitively high.

Much effort has consequently been expended in developing special absorbing boundaries for dynamic finite element analysis. Some of these energy absorbing boundaries have properties which are frequency dependent and are therefore only suitable for analyses in the frequency domain. Clearly, analyses performed in the time domain require the use of frequency independent transmitting boundaries.

The commonly available boundaries for the time domain are of three major types; the viscous boundaries which includes the standard viscous boundary and the unified boundary, the consistent boundary and the superposition boundary.

Viscous Boundary

This type of energy absorbing boundary was first proposed for elastic wave problems by Lysmer and Kuhlemeyer (1969). The principle underlying its operation is illustrated by considering the response of a semi–infinite rod to periodic loading (Fig. 4.10). The infinite dimension precludes wave reflection and therefore the displacement (at position x and time t) can be expressed in the form (Simons and Randolph,1986):

$$u = A\, e^{i\omega(t-x/c)} \qquad (4.55)$$

where,

A is the amplitude of the incident wave,

ω is the exciting frequency, and,

c is the velocity of wave propagation.

The tensile stress in the longitudinal direction is:

$$\sigma = E \frac{\partial u}{\partial x} \tag{4.56}$$

$$= - \frac{i A E \omega}{c} e^{i\omega(t-x/c)} \tag{4.57}$$

where E is the elastic modulus of the material.

The stress boundary condition at $x = 0$ yields

$$\sigma = - \sigma_0 e^{i\omega t} = - \frac{i A E \omega}{c} e^{i\omega t} \tag{4.58}$$

giving

$$A = - \frac{i \sigma_0}{\omega \rho c} \tag{4.59}$$

where,

σ_0 is the initial applied stress on the end of the rod (Fig. 4.10), and

ρ is the material mass density.

Then, the end displacement is

$$u = - \frac{i \sigma_0 e^{i\omega t}}{\omega \rho c} \tag{4.60}$$

which represents the steady state solution to the first order differential equation

$$\sigma_0 e^{i\omega t} = \rho c \frac{\partial u}{\partial t} \tag{4.61}$$

Equation 4.61 is the equation of motion of a simple viscous dashpot of coefficient $C = \rho\ c$. Such a dashpot allows the simulation of energy dissipation due to viscous damping.

This principle has been extended by Lysmer and Kuhlemeyer (1969) to two dimensions. This was done by considering an imaginary convex boundary enclosing an excited zone;Fig. 4.11. Propagation of energy is assumed to occur only from the interior to the exterior region. For absorption of the incident energy at the boundary, the following boundary conditions were imposed by analogy with the one–dimensional model (Fig. 4.11 and 4.12) :

$$\sigma = a\ \rho\ c_p\ \dot{u} \tag{4.62}$$

$$\tau = b\ \rho\ c_s\ \dot{v} \tag{4.63}$$

where,

σ and τ are the normal and shear stresses, respectively,

$\dot{u}$ and $\dot{v}$ are the normal and tangential velocities, respectively,

c_p and c_s are the velocities of the compression (P) and the shear (S) waves,respectively, and,

a and b are dimensionless parameters, usually taken as unity.

In effect, the absorbent boundary consists of infinitesimal, small dashpots oriented in both the normal and tangential direction.

Lysmer and Kuhlemeyer (1969) assessed the efficiency of these dashpots in terms of the energy absorption over a unit area of surface and showed it to be 98.5% effective in absorbing P–waves and 95% effective in absorbing S–waves (for a typical case of Poisson's ratio, $\nu = 0.25$). Their formulation of the standard viscous boundary is strictly applicable to plane strain conditions. However, implementation of the standard viscous boundary for axisymmetric finite elements has been described by Chow (1981) and used by To (1985) and Simons (1985).

Unified Boundary

The unified boundary was developed by White et al,(1977). The unified boundary includes optimisation of its parameters according to the angle of incidence of the impinging wave and the Poisson's ratio of the medium. It is based on rather more rigorous grounds than the earlier work of Lysmer and Kuhlemeyer (1969) and is applicable to anisotropic materials.

White et al,(1977) showed that the dimensionless constants a and b are given by the equations :

$$a = \frac{8}{15\ \Pi} (5 + 2S - 2S^2) \qquad (4.64)$$

$$b = \frac{8}{15\ \Pi} (3 + 2S) \qquad (4.65)$$

where,

$$S^2 = \frac{(1 - 2\nu)}{2\ (1 - \nu)} \qquad (4.66)$$

where ν is the Poisson's ratio.

The values of a and b which yield the maximum absorption are therefore (slightly) dependent on Poisson's ratio. For example, the optimum values of a and b for Poisson's ratio of 0.3 are 0.99 and 0.74,respectively. However, for Poisson's ratio of 0.45 the corresponding values are 1.01 and 0.77.

For axisymmetric stress analysis, the stress waves propagate as cylindrical rather than plane waves. White et al (ibid) show that for $r/\lambda > 0.5$ (r is the location of lateral boundary, and, λ is the wave length) the coefficients a and b are practically equal to the values for the plane strain case. This boundary is more efficient than the "standard viscous boundary"; it can be placed closer to the source of excitation without loss of accuracy.

Consistent Boundary

This type of boundary is particularly suitable for the analysis of soil–structure interaction problems where the soil is underlain by a rigid stratum at finite depth, (Fig. 4.13). It can even be used to solve problems where the rigid stratum lies directly next to the structure. Waas (1972) was the first to propose the "consistent boundary" for both plane and axisymmetric problems. Boundary conditions are established by expanding the displacement functions in the infinite region into their constituent modes. If no rigid base layer actually exists then an artificial base layer may be specified at a depth of eight to ten times the radius of the footing,(Waas,1972). The "consistent boundary" has been modified and generalised by Kausel (1974) for axisymmetric problems under general loading conditions using a Fourier expansion of the shape functions.

Superposition Boundary

The analytical formulation of the superposition boundary was first proposed by Smith (1974). The basic principle can be illustrated by considering the one–dimensional wave propagation problem (Fig. 4.14), described by the wave equation :

$$\frac{\partial^2 u}{\partial t^2} = c^2 \frac{\partial^2 u}{\partial x^2} \qquad (4.67)$$

where c is the wave speed.

The solution of equation 4.67 is of the form

$$u = A\, e^{i(kx+\omega t)} + B\, e^{-i(kx-\omega t)} \qquad (4.68)$$

The first term on the right represents an incident wave, while the second

term represents the reflected wave. The two boundary conditions to be considered are the fixed boundary and the free boundary. For the fixed boundary ($u=0$ at $x=0$) $A=-B$. However, for the free boundary ($\partial u/\partial x=0$ at $x=0$) $A=B$, (Chow, 1981). The displacements after reflection for the two boundary conditions are:

$$u_{fixed} = A\ (e^{i(kx+\omega t)} - e^{-i(kx-\omega t)}) \qquad (4.68a)$$

$$u_{free} = A\ (e^{i(kx+\omega t)} + e^{-i(kx-\omega t)}) \qquad (4.68b)$$

The average of their sum is:

$$u = A\ e^{i(kx+\omega t)} \qquad (4.69)$$

This solution for an absorbent boundary involves the incident wave only; i.e. the reflected wave is artificially cancelled.

The superposition boundary originally proposed by Smith (1974) is only applicable to linear problems. A refinement of Smith's original idea was proposed by Cundall et al, (1978). Their solution procedure may be summarized as follows:
(a) In addition to the main element mesh,two overlapping element meshes are required with the following boundary conditions (i)constant stress in x–direction, constant velocity in y–direction,(ii)constant velocity in x–direction,constant stress in y–direction.
(b) Three (3) or four (4) zones are necessary in the overlapping meshes. This is to enable the reflected waves to be established before they are cancelled.
(c) All variables in the overlapping meshes are added after 3 to 4 time steps.

As 3 to 4 zones of overlapping meshes are required for superposition boundary, the cost of an analysis increases rapidly with the size of the problem. Fig. 4.15 shows a typical mesh having the two overlapping element meshes

required with this type of boundary,(Chow,1981; Simons and Randolph,1986).

Several other formulations have also appeared in the literature and these are briefly mentioned here for completeness. For example, Bettess and Zienkiewicz (1977) used Lagrangian periodic infinite elements to solve unbounded problems involving surface water waves where only a single type of wave is present. Chow and Smith (1981) have shown how 'Serendipity' periodic infinite elements' may be used when multiple wave types are present in unbounded solids, Fig. 4.16. Werkle (1986) proposed a transmitting boundary for a three–dimensional soil model; later Werkle (1987) developed a similar boundary for cross–anisotropic soils. Kato et al, (1986) proposed a modified thin layer element (a modification of the consistent boundary) for the far field to account for soil–structure interaction with an axisymmetric structure subjected to incident earthquake motion, Fig. 4.17.

4.4.4 Interface Elements

Interface elements have been developed in the past decade or so to simulate relative movement (slip) at interfaces between two dissimilar materials. Some of these are briefly reviewed here.

Goodman et al,(1968) were the first to suggest using 'joint elements' to analyse the behaviour of rock joints. Their element had 4–nodes and had zero thickness; displacements were assumed to vary linearly between the nodes.

Zienkiewicz et al, (1970) recommended the use of conventional isoparametric elements to model the rock joints. Linear variation of displacements across the joints was assumed but in the tangential direction both linear and quadratic displacement functions were examined. However,they showed that to maintain adequate stiffness, the joint's stiffness (Young's modulus) must be reduced as its thickness decreases.

Ghaboussi et al, (1973) proposed a joint element which uses the relative displacement across the joint as an independent degree of freedom, (Fig. 4.18), since this transformation eliminates the numerical illconditioning of the problem.

Pande and Sharma (1979) used an 8–noded isoparametric element instead of the 6–noded element proposed by Zienkiewicz et al, (1970), again based on the relative displacement formulation. This resulted in an improved representation of the conditions at the interface since although the thickness of the joint element is normally small, sharp variation of strain across the joint is usual and higher order (linear) interpolation of strain is required, Fig. 4.19.

Wilson (1981) introduced a new type of interface element for two and three dimensional interfaces. His study encompassed both fluid elements for fluid–structure interaction and solid elements for earthquake analysis of soil–structure interaction.

Katona (1983) presented a simple interface element aimed principally for modelling the interface between soil and flexible culverts. His element allows for both overlapping and slipping along the interface. However, these type of elements are applicable to static two–dimensional problems only, Fig. 4.20.

Desai et al, (1984) advocated using a 'thin layer element' in soil–structure interaction and rock joints. The element is essentially a conventional element of small but finite thickness. The thickness of the element is crucial and their numerical studies showed that satisfactory results could be obtained provided that the aspect ratios of these elements lie within the range of 10–100.

Griffiths (1985) also used an 8–noded quadratic element to model soil–structure interface behaviour, Fig. 4.21. From his convergence study, he concluded that an aspect ratio of approximately 10 would produce the required sliding response but at higher aspect ratios (100–1000) an overstiff response is predicted. He concluded, in agreement with Desai et al, (1984) that aspect ratios between these two extremes provided the optimum solution with regard to accuracy and numerical stability.

4.5 TIME INTEGRATION SCHEMES

4.5.1 Introduction

To solve problems in dynamics, the governing equations (4.35) must be

integrated in the time domain. However, several factors need to be considered in order to optimise the solution strategy, (Hughes and Liu, 1978a). Basically, these methods can be broadly classified into two main categories, namely , explicit integration methods and implicit integration methods.

Implicit algorithms tend to be unconditionally stable, permitting large time steps but the cost per step is high. Explicit algorithms require less memory for each step than implicit algorithms but very small time steps need to be used to ensure numerical stability. However, for complex problems involving several different element types and local mesh refinements neither method is very efficient, (Hughes and Liu,1978a).

It is useful to be able to assess the stability and accuracy of particular time integration schemes without having to resort to extensive numerical evaluations. However, the choice of a suitable time step size and time integration scheme is affected by several factors such as the frequency content of the travelling waves, the loading conditions, the nonlinearity of the material response etc., Smith(1978). In this section, only single step methods, such as the central difference explicit schemes and the Newmark implicit method will be discussed. Other methods, such as the Wilson–θ method are described in more detail by Chow (1981) and To (1985). Multi step methods requiring the transformation of the second order differential equation into a first order problem have been discussed in detail by Smith (1977).

4.5.2 Explicit Integration Schemes

Large time steps are preferred in numerical analysis for reasons of economy. The conditional stability of the explicit central difference method is dependent on the time step size which is limited by the expression (Owen and Hinton,1980)

$$\Delta t_{cr} \leq \frac{2}{\omega_{max}} \tag{4.70}$$

where ω_{max} is the highest circular frequency of interest.

The mathematical formulation of the explicit scheme is based on the Taylor series expansion of the first order derivative of a function, (Desai and Christian,1976):

$$x_{t+\Delta t} = x_t + \Delta t \frac{\partial x}{\partial t} + \frac{(\Delta t)^2}{2!} \frac{\partial x^2}{\partial t^2} + \ldots\ldots + \ldots\ldots \qquad (4.71)$$

$$x_{t-\Delta t} = x_t - \Delta t \frac{\partial x}{\partial t} + \frac{(\Delta t)^2}{2!} \frac{\partial x^2}{\partial t^2} - \ldots\ldots - \ldots\ldots \qquad (4.72)$$

where x_t is the displacement at the end of the time step t.

By simple manipulation of equations 4.71 and 4.72 we can obtain three different (finite difference) approximations to the time derivative of function x at the end of the time step:

$$\frac{\partial x}{\partial t} = \frac{x_{t+\Delta t} - x_t}{\Delta t} + O[(\Delta t)] \qquad (4.73)$$

$$\frac{\partial x}{\partial t} = \frac{x_t - x_{t-\Delta t}}{\Delta t} + O[(\Delta t)] \qquad (4.74)$$

$$\frac{\partial x}{\partial t} = \frac{x_{t+\Delta t} - x_{t-\Delta t}}{2\ \Delta t} + O[(\Delta t)^2] \qquad (4.75)$$

These are so called the forward, backward and central difference approximations, respectively. The expression $O[(\Delta t)]$ indicates that the error is of the order Δt. In these schemes, the value of x at the time instant $t+\Delta t$ in terms of the known values of x at the current time t is required. It should be noted that the error term for the central difference method is proportional to the square of the time interval and therefore the error reduces rapidly with increasingly small time intervals.

In practice, the most popular method is the central difference algorithm, in

which the equation of motion, equation 4.35, is solved at time stations $t-\Delta t$,t and $t+\Delta t$.

The central difference approximations for acceleration and velocities can be expressed as:

$$x_t = \frac{1}{(\Delta t)^2} (x_{t+\Delta t} - 2\, x_t + x_{t-\Delta t}) \qquad (4.76)$$

$$x_t = \frac{1}{2\ \Delta t} (x_{t+\Delta t} - x_{t-\Delta t}) \qquad (4.77)$$

Combining equations 4.35, 4.76 and 4.77 we obtain after some manipulation the displacement as:

$$x_{t+\Delta t} = (M + \frac{\Delta t}{2} C)^{-1} \{(\Delta t)^2 (F - K\, x_t) + 2M\, x_t - (M - \frac{\Delta t}{2} C) x_{t-\Delta t}\} \qquad (4.78)$$

In other words the displacements at time station $t+\Delta t$ are given explicitly in terms of the displacements at time stations t and $t-\Delta t$, (Owen and Hinton,1980).

This scheme is only conditionally unstable and a time step less than the critical value must be used, e.g. Shantaram et al,(1976) as:

$$\Delta t \leq \frac{\Lambda\ L}{c_p} \qquad (4.79)$$

where,

Λ is a coefficient dependent on the type of element employed.

The following values of Λ are suggested to maintain the stability of the solution:

parabolic elements $\Lambda = 0.45$, $\rangle 0.5$,and,

for linear elements $\Lambda = 0.9 - 1.0$.

L is the smallest length between any two nodes, and,

c_p is the compression wave velocity.

If the mass matrix,**M**, the damping matrix,C, and the stiffness matrix,**K**, are diagonal matrices (lumped) then the solution of equation 4.35 becomes trivial. For plane stress and plane strain applications, equation 4.78 reduces to:

$$x_{t+\Delta t}=(m+\frac{\Delta t}{2}\ c)^{-1}\ \{(\Delta t)^2\ (F-k\ x_t)+2m\ x_t-(m-\frac{\Delta t}{2}\ c)\ x_{t-\Delta t}\} \qquad (4.80)$$

where **m**, **c** and **k** are diagonal matrices. Fig. 4.22 shows a typical profile of a lumped stiffness matrix for three 4–noded elements.

4.5.3 Implicit Integration Schemes

An implicit integration scheme involves the solution of a set of simultaneous equations at the time instant t+ Δt. One approach is due to Newmark (1959) who introduced two parameters γ and β to factorise the acceleration at the end of the time step t+ Δt. Newmark's (1959) equations are:

$$\dot{x}_{t+\Delta t}=\dot{x}_t+[(1-\gamma)\ \ddot{x}_t+\gamma\ \ddot{x}_{t+\Delta t}]\ \Delta t \qquad (4.81)$$

$$x_{t+\Delta t}=x_t+\dot{x}_t\ \Delta t+[(\frac{1}{2}-\beta)\ \ddot{x}_t+\beta\ \ddot{x}_{t+\Delta t}](\Delta t)^2 \qquad (4.82)$$

It have been shown by Newmark (1959) that unless the quantity γ is taken as 1/2, spurious damping is introduced (proportional to the quantity $\gamma-1/2$). Also, if γ is zero, negative damping results which involves a self–excited vibration arising solely from the numerical procedure. If γ is greater than 1/2, positive damping is introduced which reduces the magnitude of the response.

In general, unless β is zero the general procedure recommended by Newmark(1959) is as follows:

(1)Assume values of accelerations of each mass at the end of the time interval t+ Δt.

(2)Compute the velocity and displacement of each mass at the end of the interval from equations 4.81 and 4.82, respectively (unless damping is present, it is not necessary to compute the velocity at the end of the interval until step 5. is computed).

(3)For the computed displacements at the end of the interval, compute the resisting forces,R.

(4)From the equation $(a=(F-R)/m)$ and the applied loads (F) and resisting forces (R) at the end of the interval recompute the accelerations at the end of the interval.

(5)Compare the derived accelerations with the assumed accelerations at the end of the interval. If these are the same the calculation is completed. If these are different, repeat the calculations with different values of assumed accelerations. It is often best to use the derived values of the accelerations for the next guess. The rate of convergence of accelerations is a function of the time interval,Δt, Newmark (1959).

Hilber et al,(1977) proposed a three parameter method based on the original Newmark method. The additional parameter,α, is used in the following manner:

$$M\,\ddot{x}_{t+\Delta t} + C\,\dot{x}_{t+\Delta t} + (1-\alpha)K\,x_{t+\Delta t} - \alpha\,K\,x_t = F_{t+\Delta t} \qquad (4.83)$$

In particular, a one parameter,α, method may be obtained from the three parameter family by writing:

$\gamma=1/2\ (1-2\alpha)$, and, $\beta=1/4\ (1-\alpha)^2$

when $\alpha=0$, the proposed method reduces to the Newmark $\beta=1/4$ method.

The large storage requirement of implicit time integration algorithms is due to the need to use consistent matrices. Fig. 4.23 shows a typical two–

dimensional finite element mesh and the profile structure of one of its consistent matrices.

4.5.4 Implicit–Explicit Integration Schemes

The implicit–explicit method proposed by Hughes and Liu (1978a,1978b), is a combination of the two methods. Their algorithm which is a composite of the Newmark implicit method and the explicit predictor–corrector algorithm is given below:

$$M \ddot{x}_{t+\Delta t} + C^I \dot{x}_{t+\Delta t} + C^E \dot{x}_{t+\Delta t} + K^I x_{t+\Delta t} + K^E x_{t+\Delta t} = F_{t+\Delta t} \quad (4.84)$$

$$\hat{x}_{t+\Delta t} = x_t + \Delta t \, \dot{x}_t + \frac{(\Delta t)^2}{2} (1-2\beta) \ddot{x}_t \quad (4.85)$$

$$\hat{\dot{x}}_{t+\Delta t} = \dot{x}_t + (\Delta t) (1-\gamma) \ddot{x}_t \quad (4.86)$$

$$x_{t+\Delta t} = \hat{x}_{t+\Delta t} + (\Delta t)^2 \beta \ddot{x}_{t+\Delta t} \quad (4.87)$$

$$\dot{x}_{t+\Delta t} = \hat{\dot{x}}_{t+\Delta t} + \Delta t \, \gamma \ddot{x}_{t+\Delta t} \quad (4.88)$$

where,

$$M = M^I + M^E \quad (4.89)$$

$$F = F^I + F^E \quad (4.90)$$

M^I, C^I, K^I and F^I are the global consistent mass,damping, stiffness and force matrices, respectively,

M^E, C^E, K^E and F^E are the global diagonal (lumped) mass, damping, stiffness and force matrices, respectively.

$\hat{\dot{x}}$ and $\hat{x}$ are the predictor values of velocity and displacement, respectively.

$\dot{x}$ and x are the corrector values of velocity and displacement, respectively.

Fig. 4.24 shows a typical two dimensional finite element mesh and the profile structure of a global matrix, which contains groups of both implicit and

explicit elements. It has been shown by Hughes and Liu (1978b) that the implicit –explicit integration schemes retain the stability behaviour of the constituent implicit and explicit algorithms. In particular the critical time step of the explicit elements governs for the system.

4.5.5 Conclusion

Two general classes of algorithms are used for solving dynamics problems; implicit and explicit. Implicit integration schemes are unconditionally stable, permitting large time steps. But, the explicit integration schemes are relatively straight forward, permitting a step–by–step evaluation of unknowns directly,and do not require solution of simultaneous equations. However, due to their conditional stability, very small time step sizes are required. In this study, an implicit integration scheme was used since this was found to be more economical although this conclusion is not universally true, computational costs are also a function of degree of nonlinearity in the load–displacement response.

4.6 CONCLUSION

This Chapter contains a summary of the analytical formulations and numerical algorithms which form the basis of the finite element solution procedure for nonlinear dynamic problems. Clearly, there are major numerical and practical difficulties in applying finite element methods to the pile driving problem beyond those normally encountered in static analyses. Notwithstanding these difficulties, the following Chapter contains a description of the results of a limited series of finite element analyses which have been undertaken to explore the potential of the method.

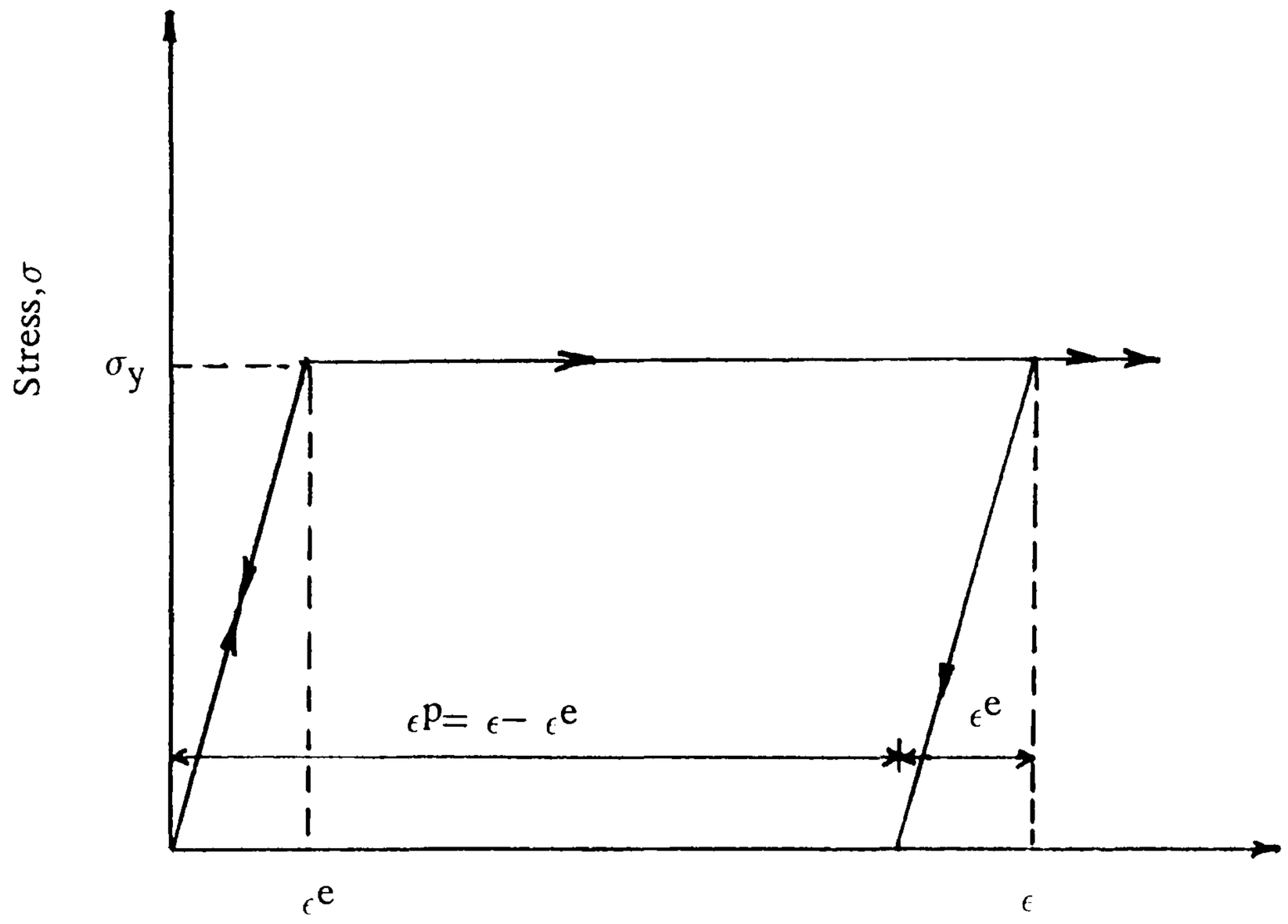

FIGURE (4. 1) UNI-AXIAL STRESS-STRAIN RELATIONSHIP OF AN ELASTIC-PERFECTLY PLASTIC MATERIAL

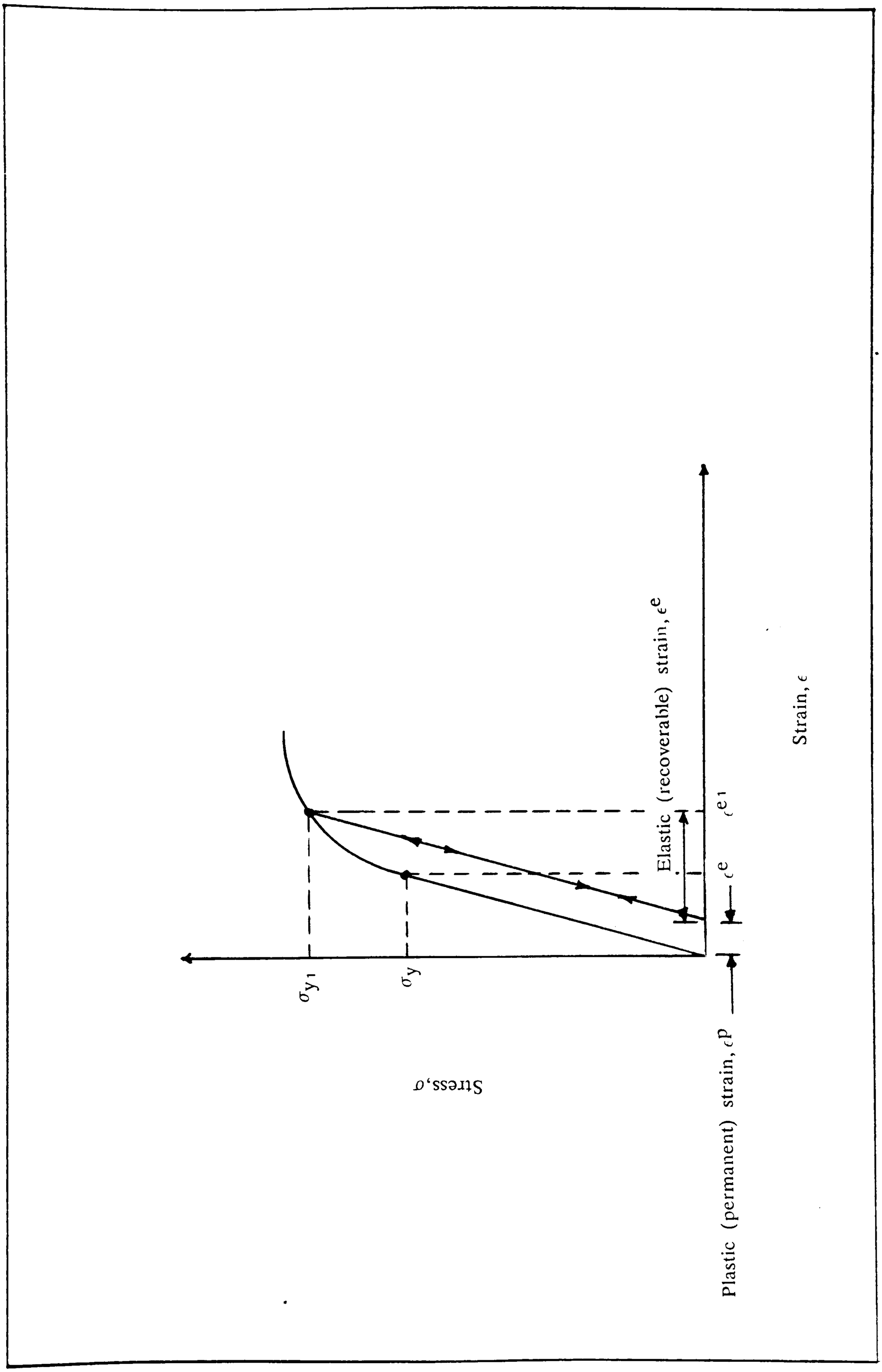

FIGURE (4.2) AN IDEALIZED UNI_AXIAL STRESS-STRAIN RELATIONSHIP

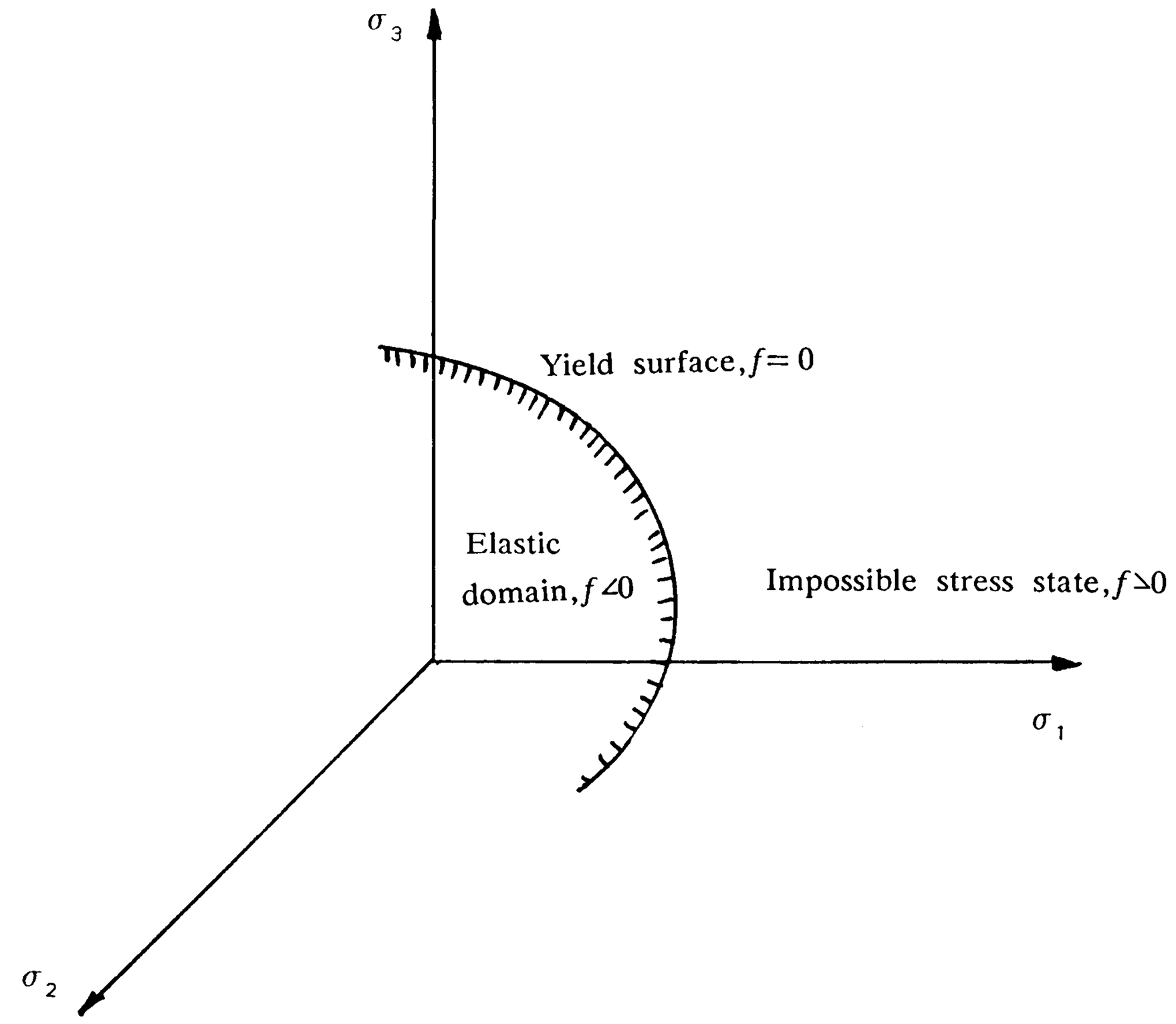

FIGURE (4.3) REPRESENTATION OF YIELD SURFACE IN STRESS SPACE

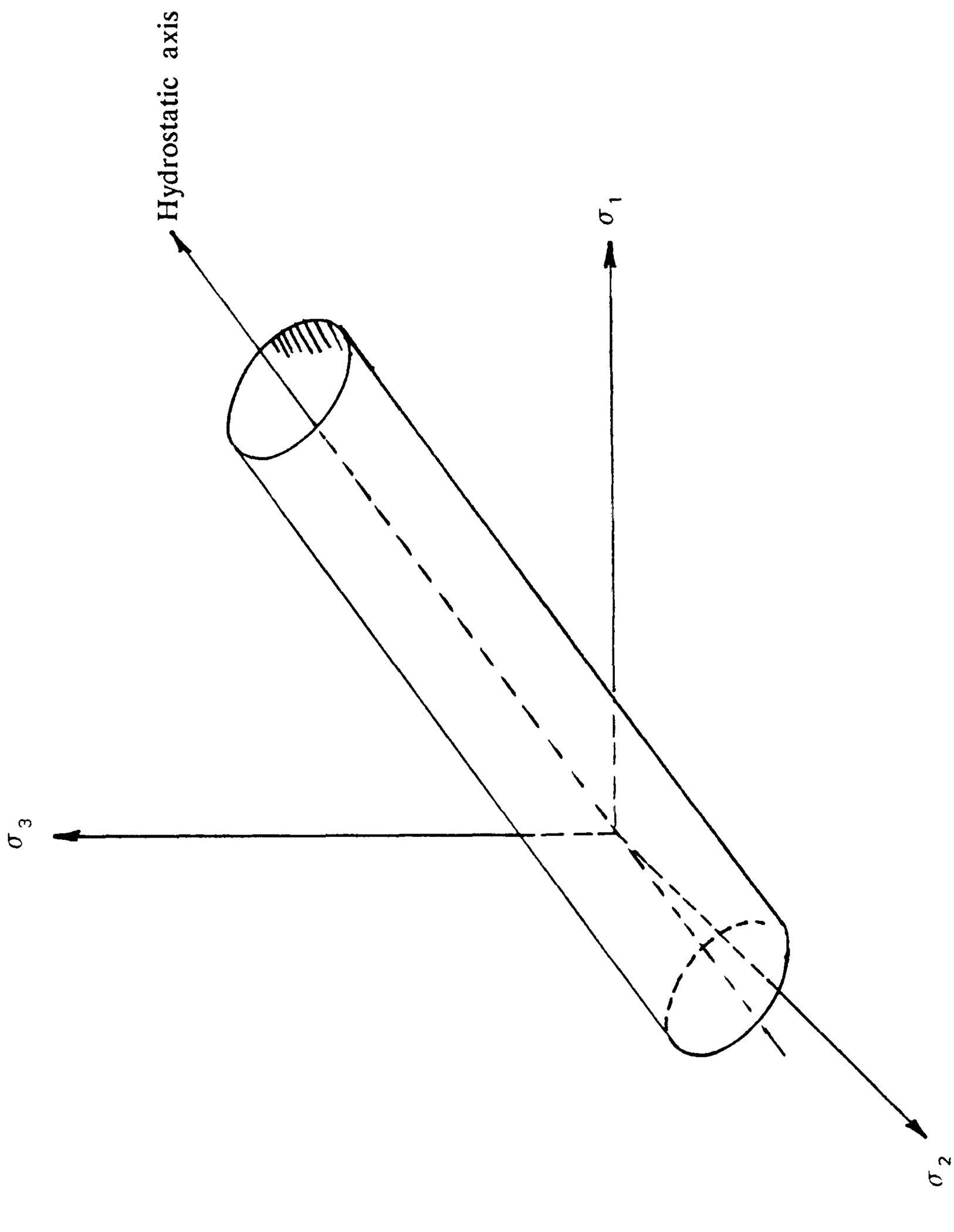

FIGURE (4. 4) THE VON_MISES YIELD SURFACE

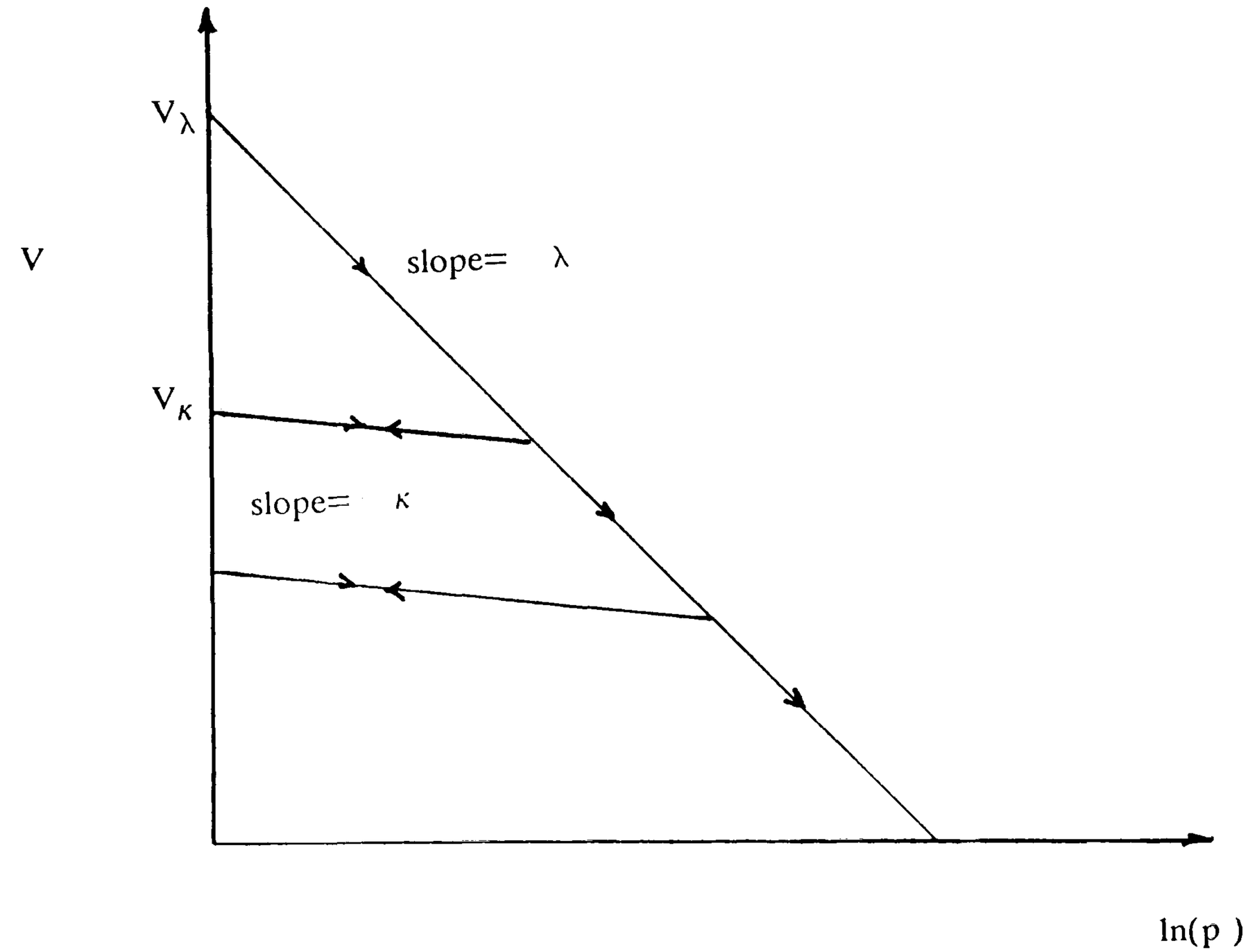

FIGURE (4.5) IDEALIZED (lnp , V) PLOT IN CRITICAL STATE THEORY

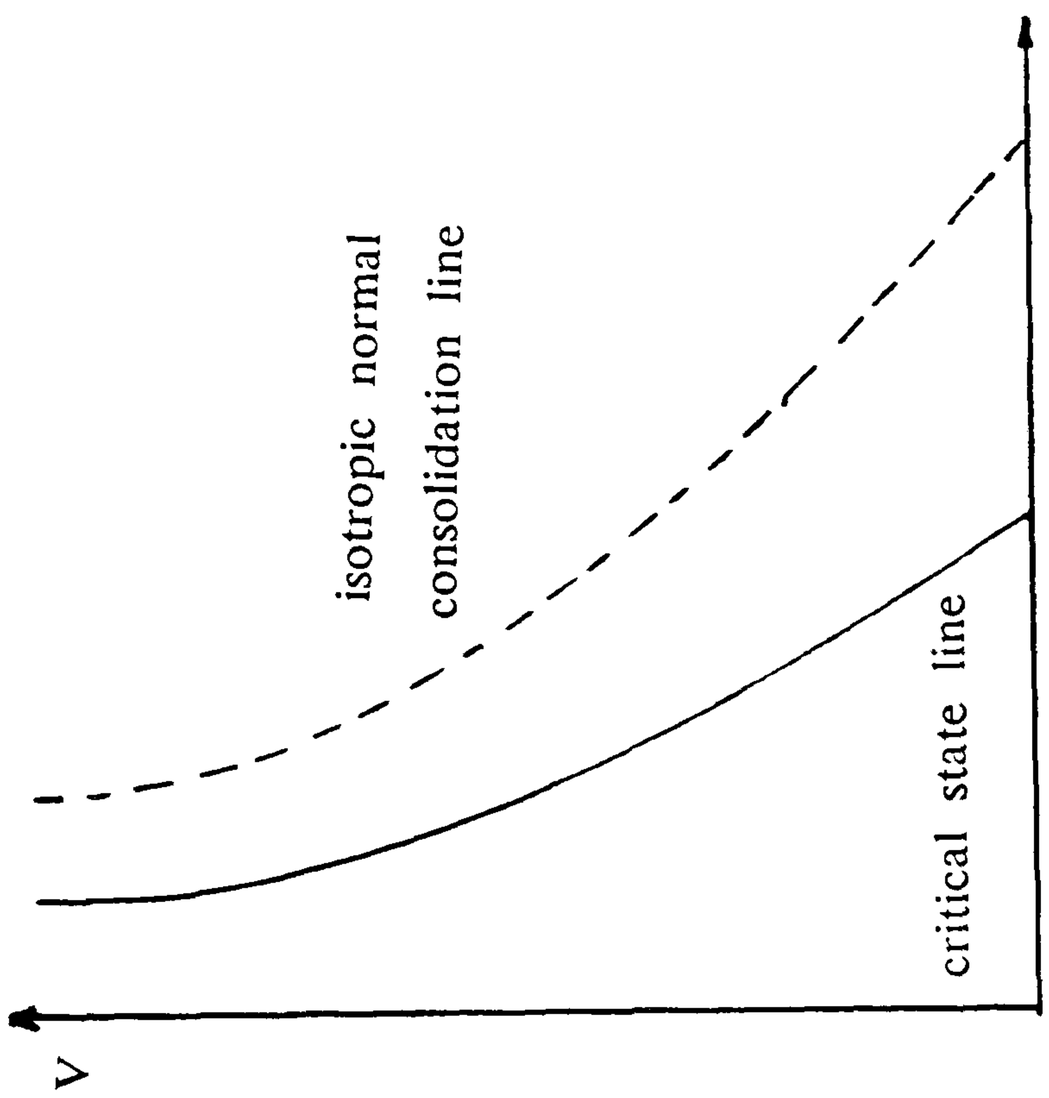

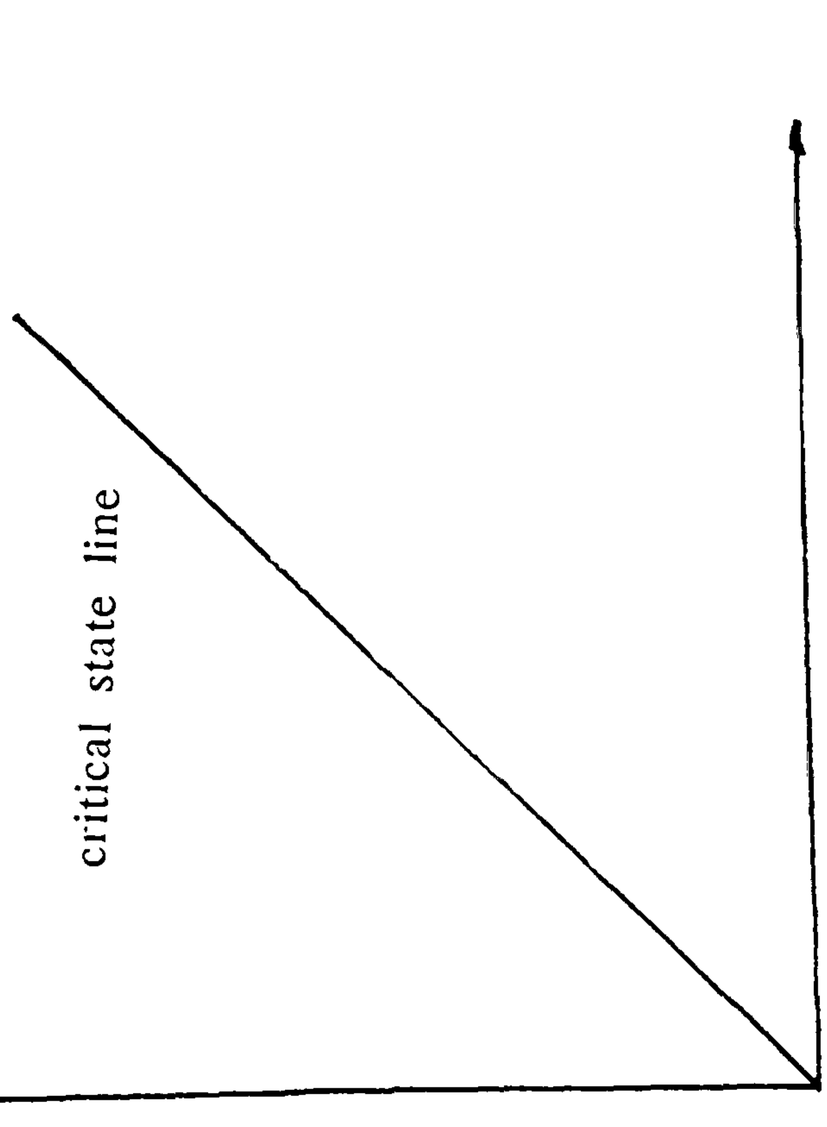

FIGURE (4.6) THE CRITICAL STATE LINE

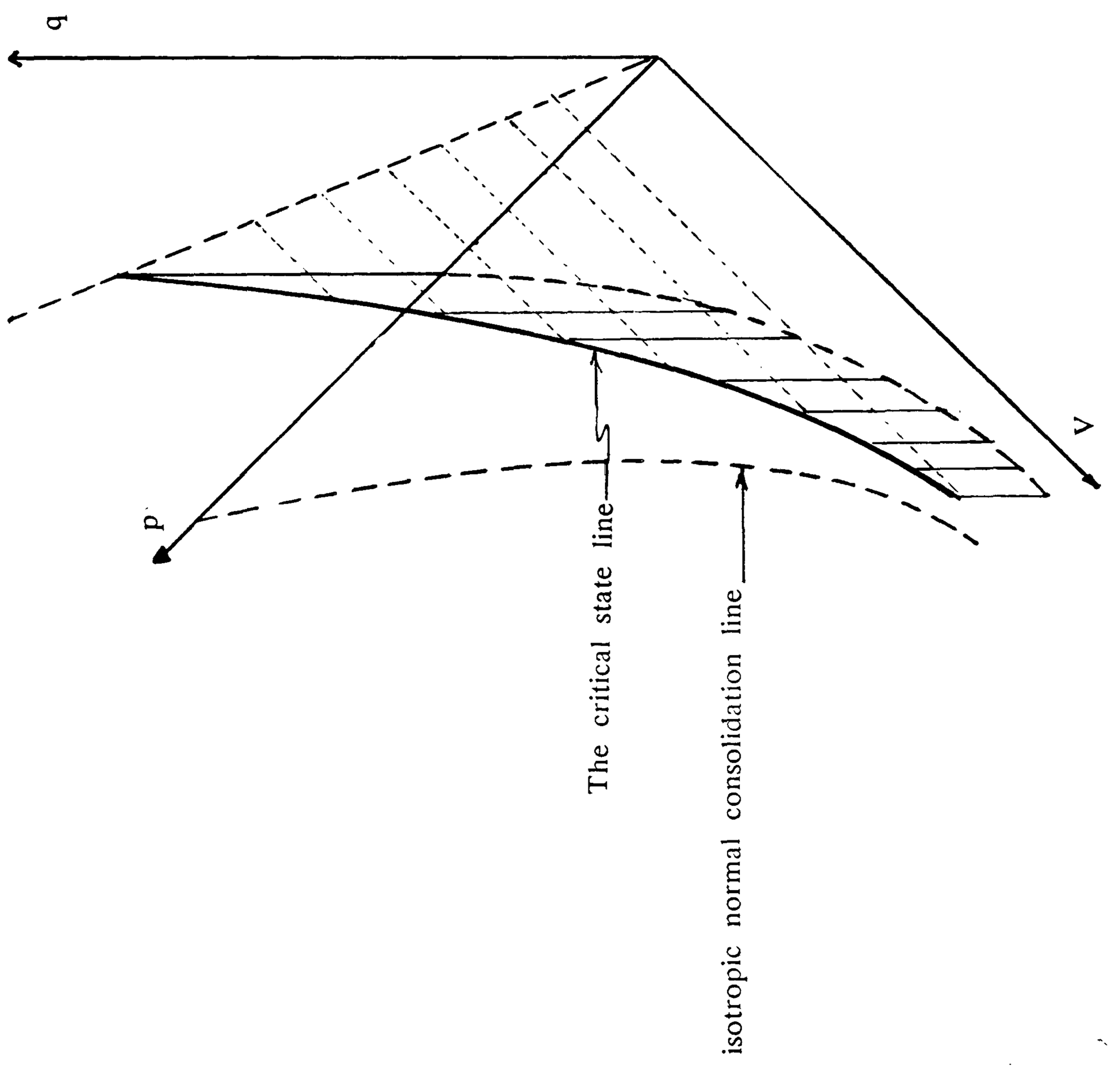

FIGURE (4.7) THE CRITICAL STATE LINE IN (p',v,q) SPACE
(SCHOFIELD AND WROTH, 1968)

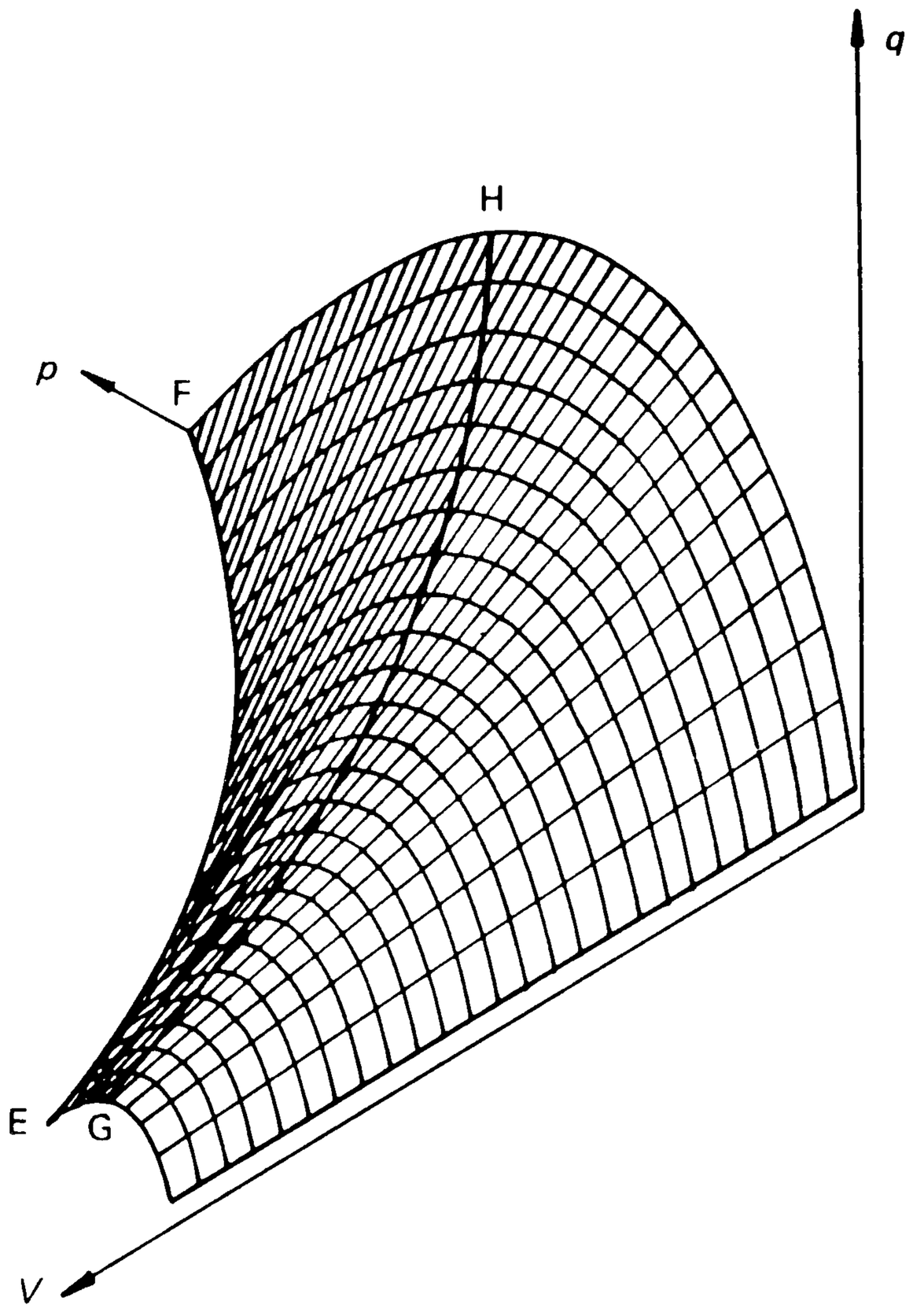

FIGURE (4.8) THE STABLE STATE BOUNDARY SURFACE IN ((p ,V,q) SPACE
(SCHOFIELD AND WROTH, 1968)

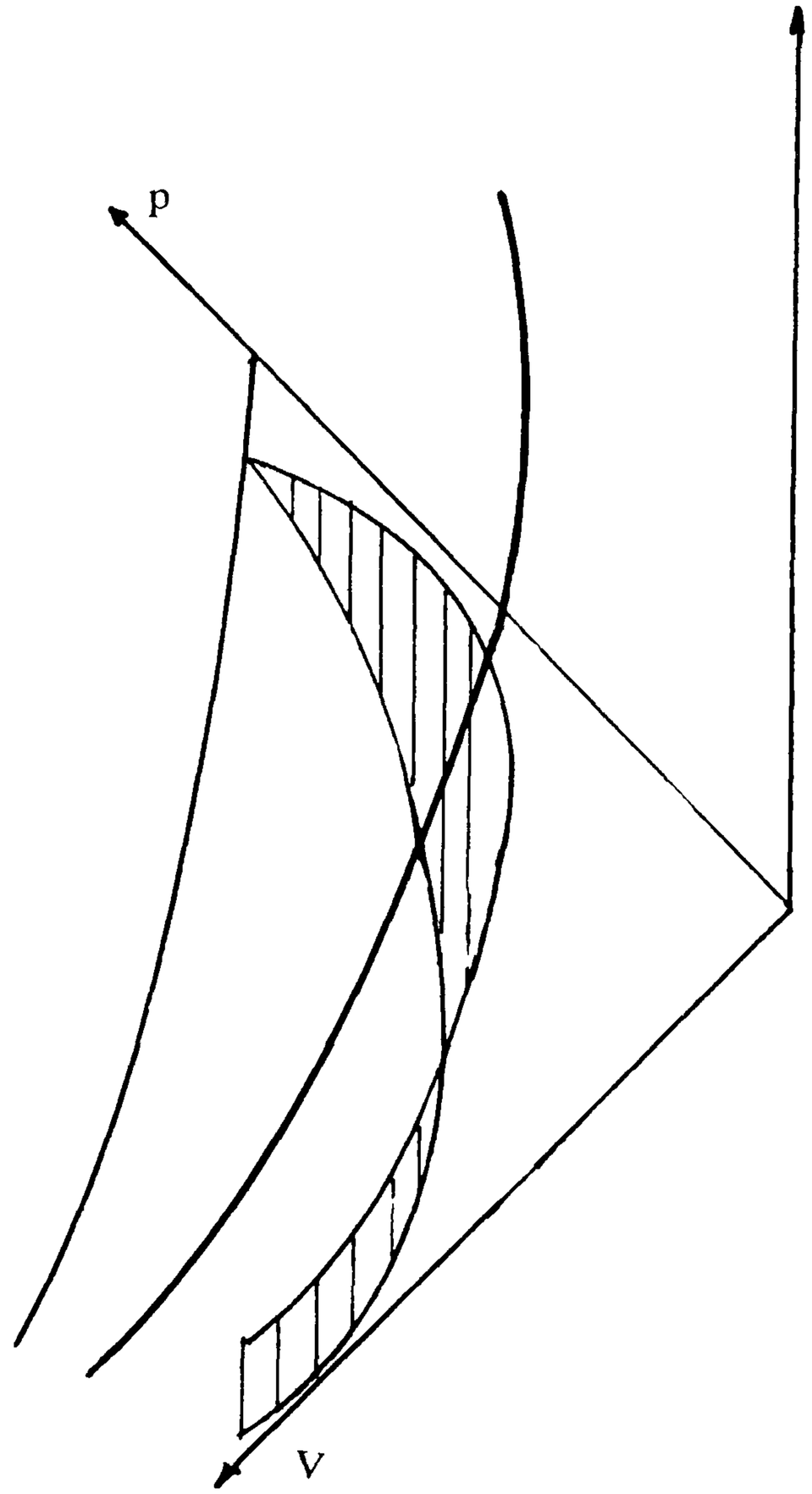

FIGURE (4.9) ELASTIC WALL IN THE (p ,V,q)' SPACE
(SCHOFIELD AND WROTH, 1968)

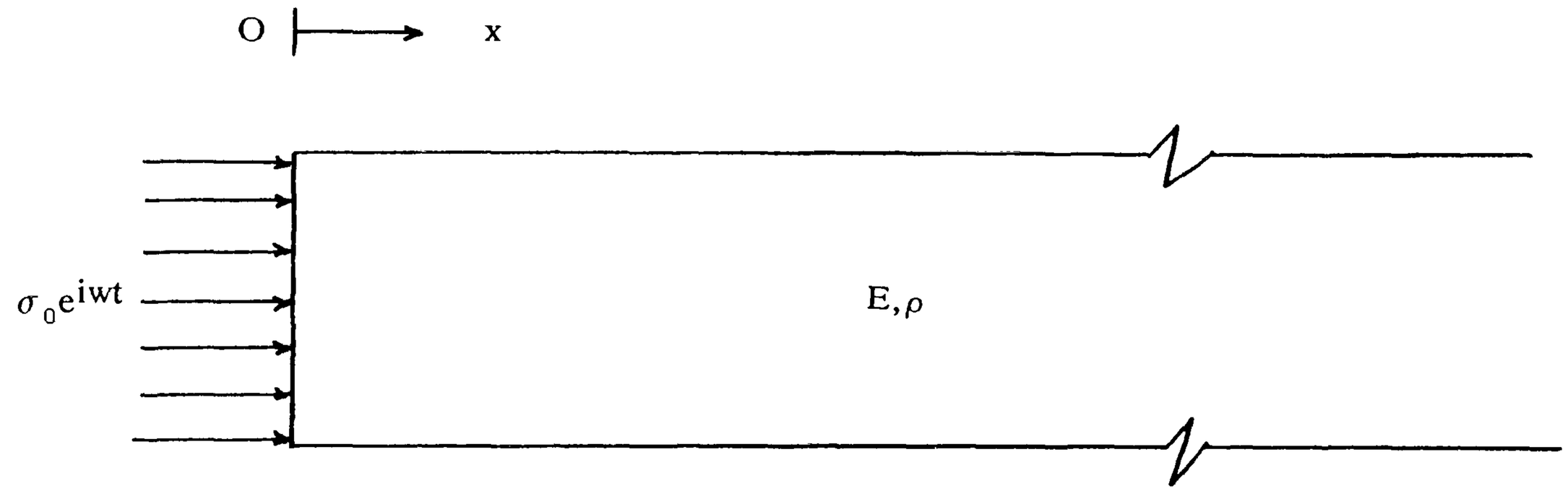

FIGURE (4. 10) PERIODIC LOADING OF SEMI_INFINITE BAR
(AFTER LYSMER & KUHLEMEYER, 1969)

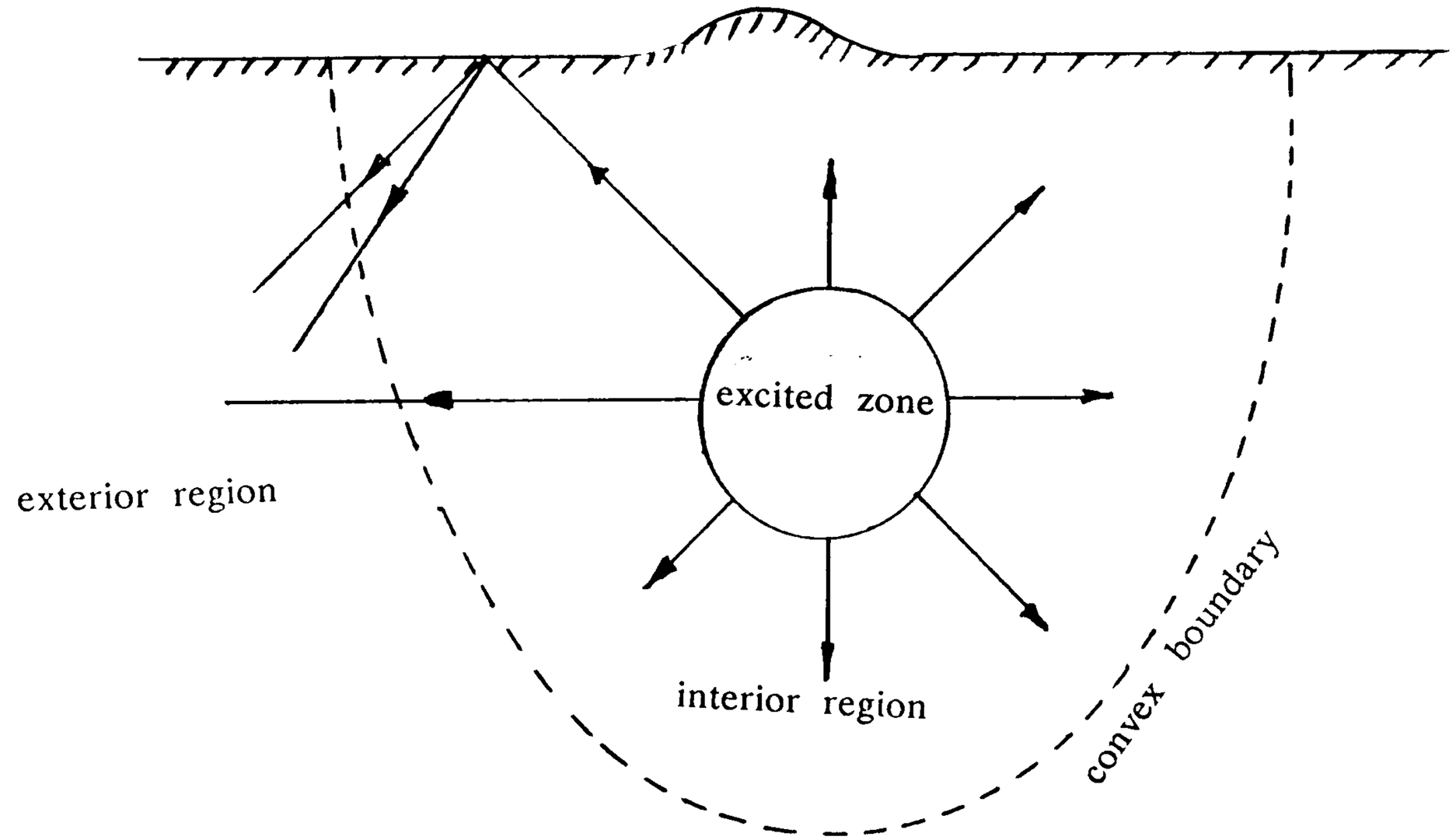

FIGURE (4. 11) TYPICAL INFINITE SYSTEM
(AFTER LYSMER & KUHLEMEYER, 1969)

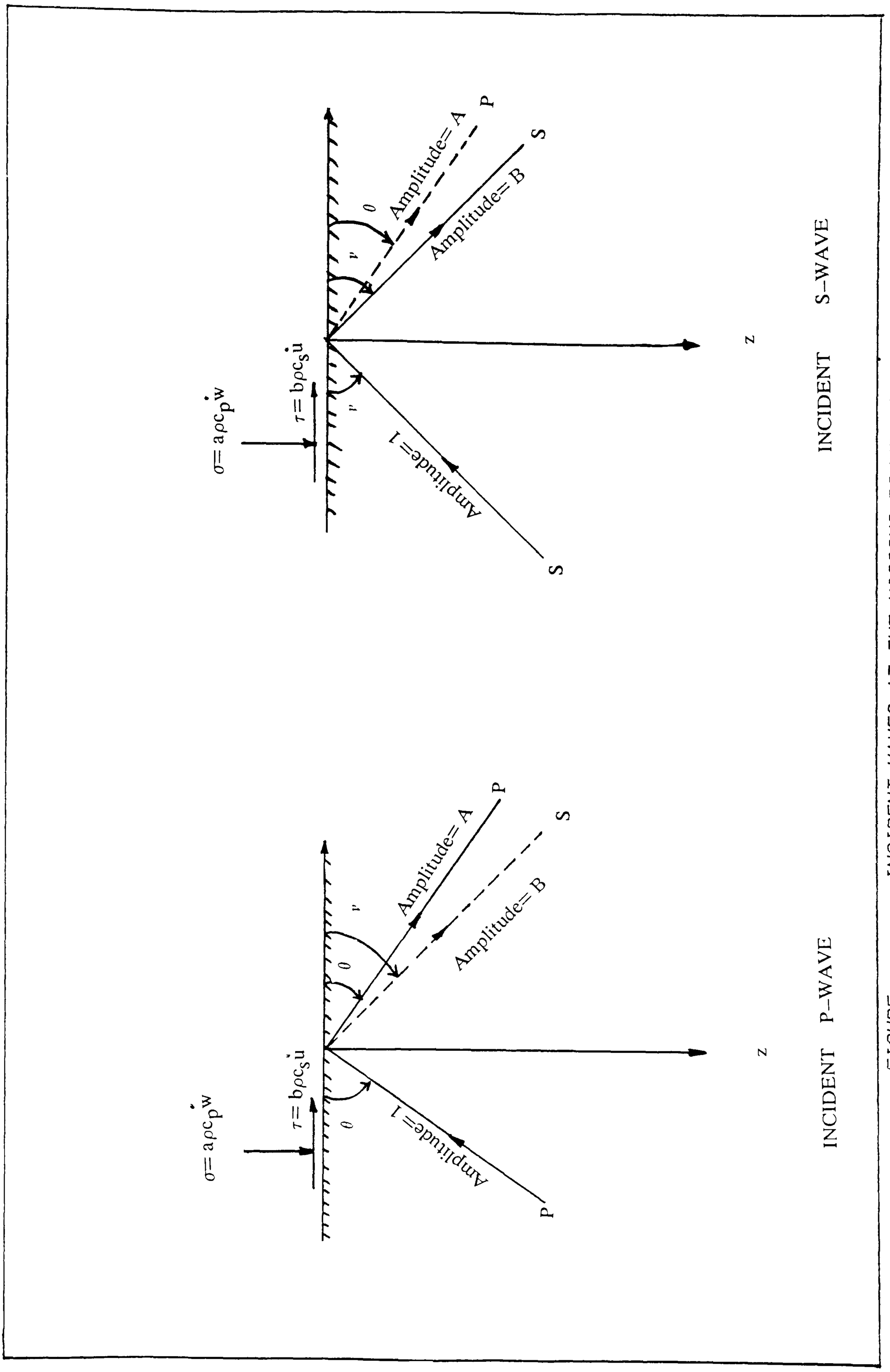

FIGURE (4.12) INCIDENT WAVES AT THE VISCOUS BOUNDARY
(AFTER LYSMER & KUHLEMEYER, 1969)

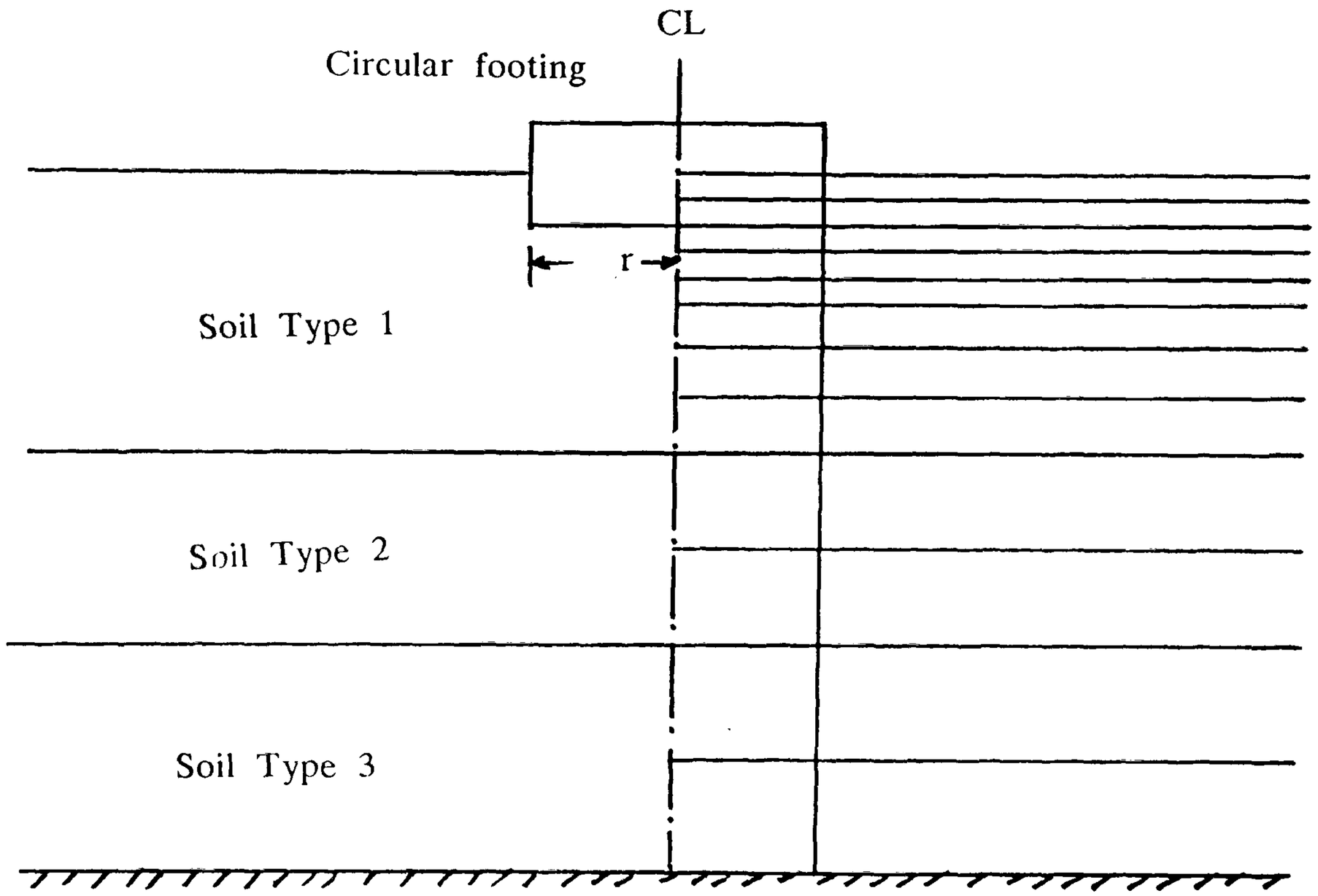

FIGURE (4. 13) THE CONSISTENT BOUNDARY
(AFTER WAAS, 1972)

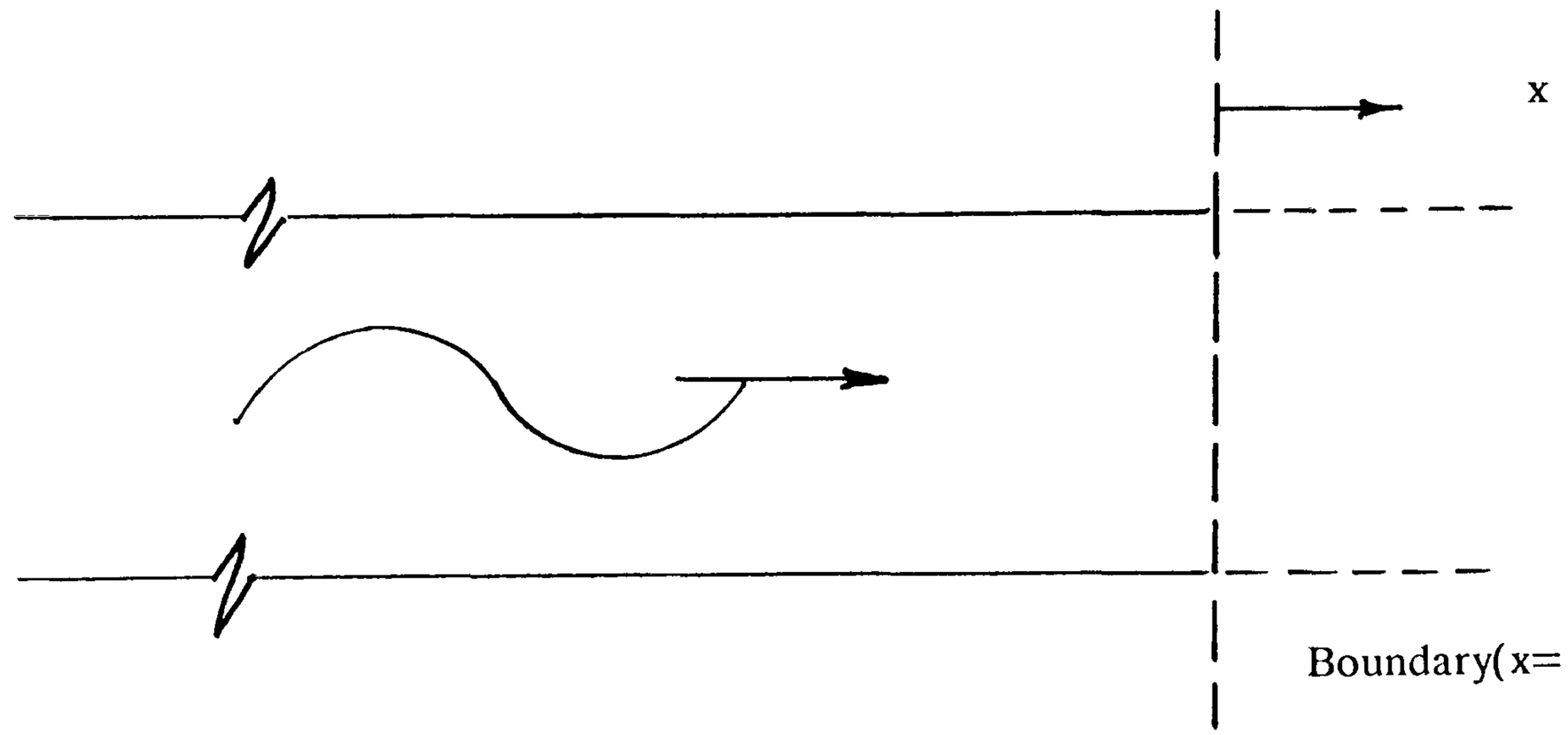

FIGURE (4. 14) ILLUSTRATION OF SUPERPOSITION BOUNDARY PRINCIPLE
(AFTER W. D. SMITH, 1974)

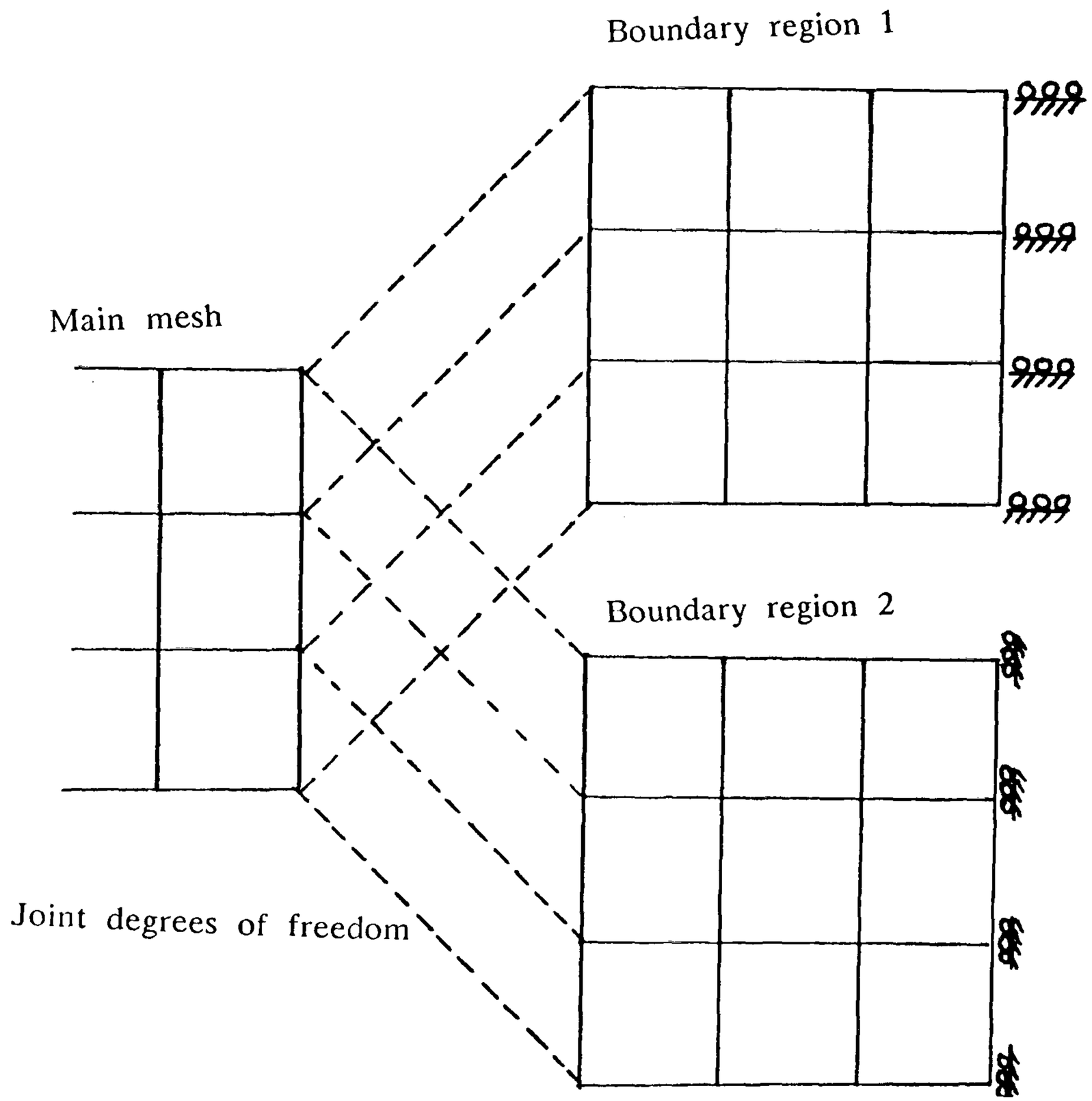

FIGURE (4. 15) IMPLEMENTATION OF SUPERPOSITION BOUNDARY
(AFTER W. D. SMITH, 1974)

$N_j(\xi,\eta) = N_j(\xi,\eta) e^{-ik\xi}\ e^{(\xi_l - \xi)/L}$

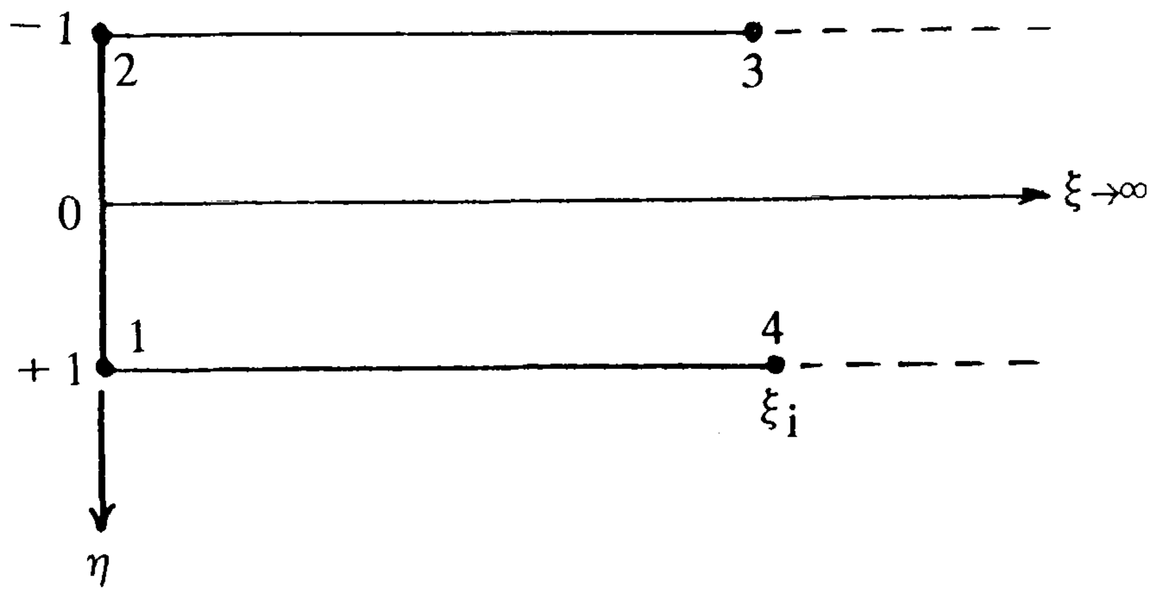

Extending to ∞ in the ξ− direction

$N_j(\xi,\eta) = N_j(\xi,\eta) e^{-ik\eta}\ e^{(\eta_l - \eta)/L}$

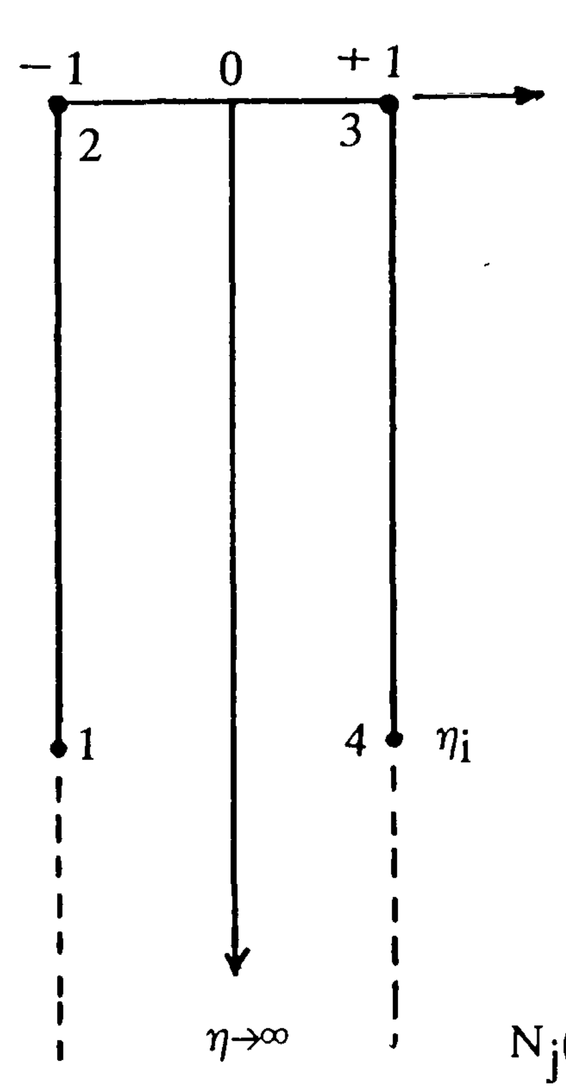

Extending to ∞ in the η–direction

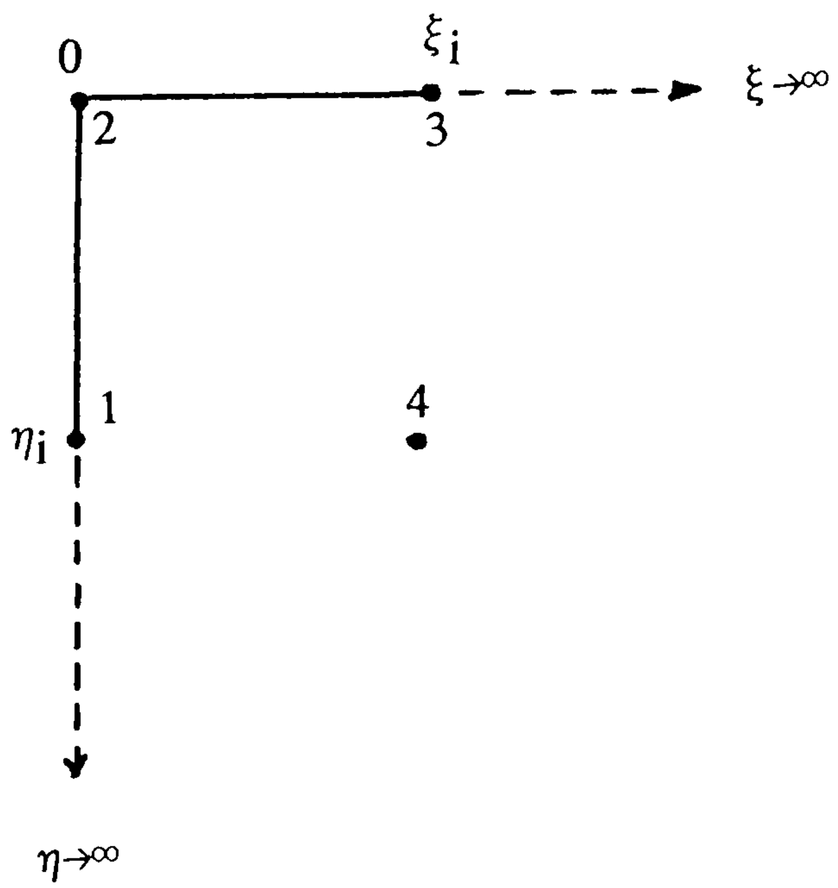

$N_j(\xi,\eta) = N_j(\xi,\eta) e^{-ik_1\xi}\ e^{-ik_2\eta}\ e^{(\xi_l - \xi)/L}\ e^{(\eta_l - \eta)/L}$

Extending to ∞ in the ξ and η directions

(j= 1,2,3,4 and L= arbitrary scaling length)

FIGURE (4. 16) TYPICAL SHAPES OF INFINITE ELEMENTS AND THEIR SHAPE FUNCTIONS FOR PERIODIC ANALYSIS (AFTER CHOW & I. M. SMITH, 1981)

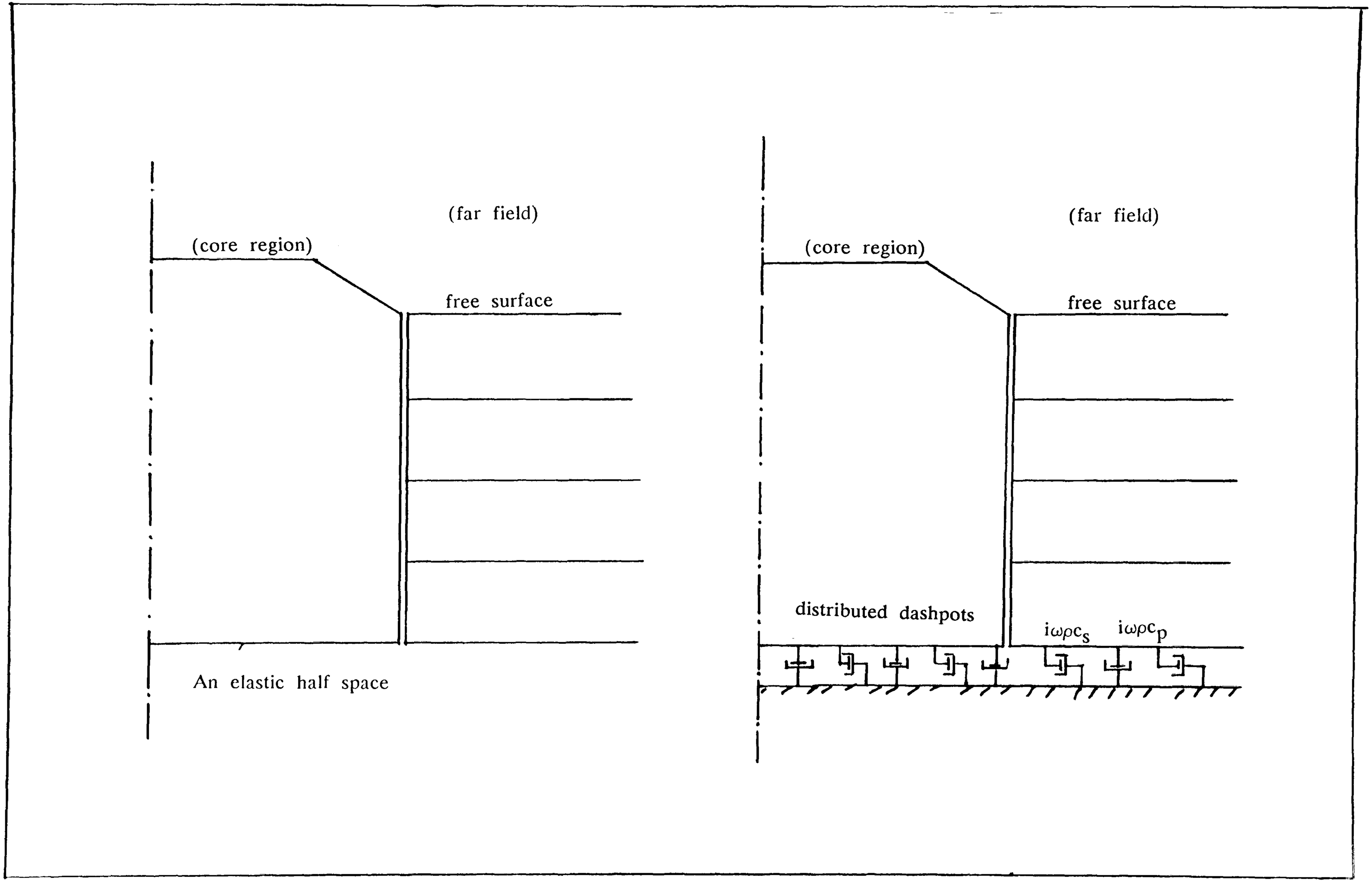

FIGURE (4.17) THE MODIFIED CONSISTENT BOUNDARY MODEL
(AFTER KATO ET. AL, 1986)

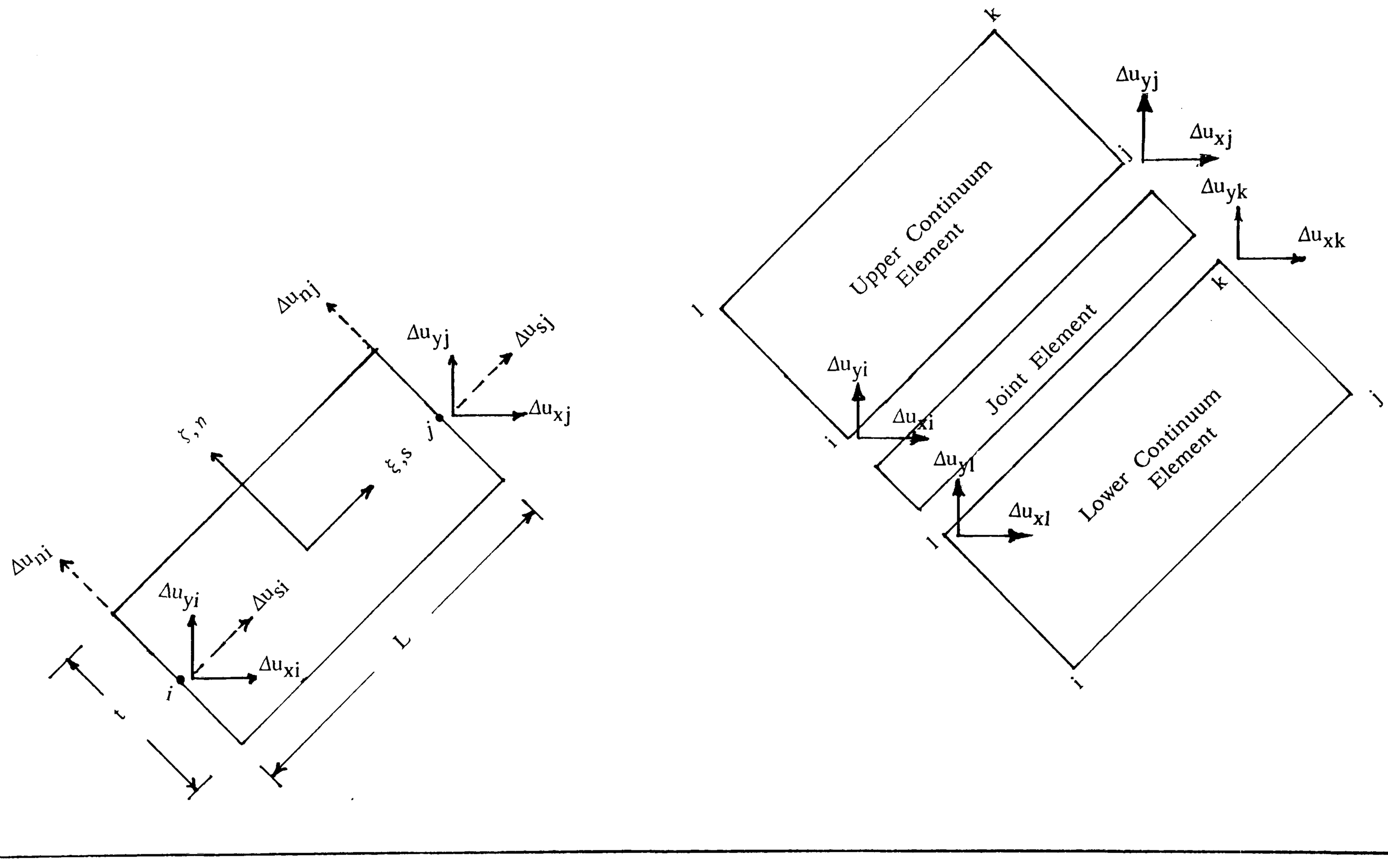

FIGURE (4.18) JOINT ELEMENT (AFTER GHABOUSSI ET. AL., 1973)

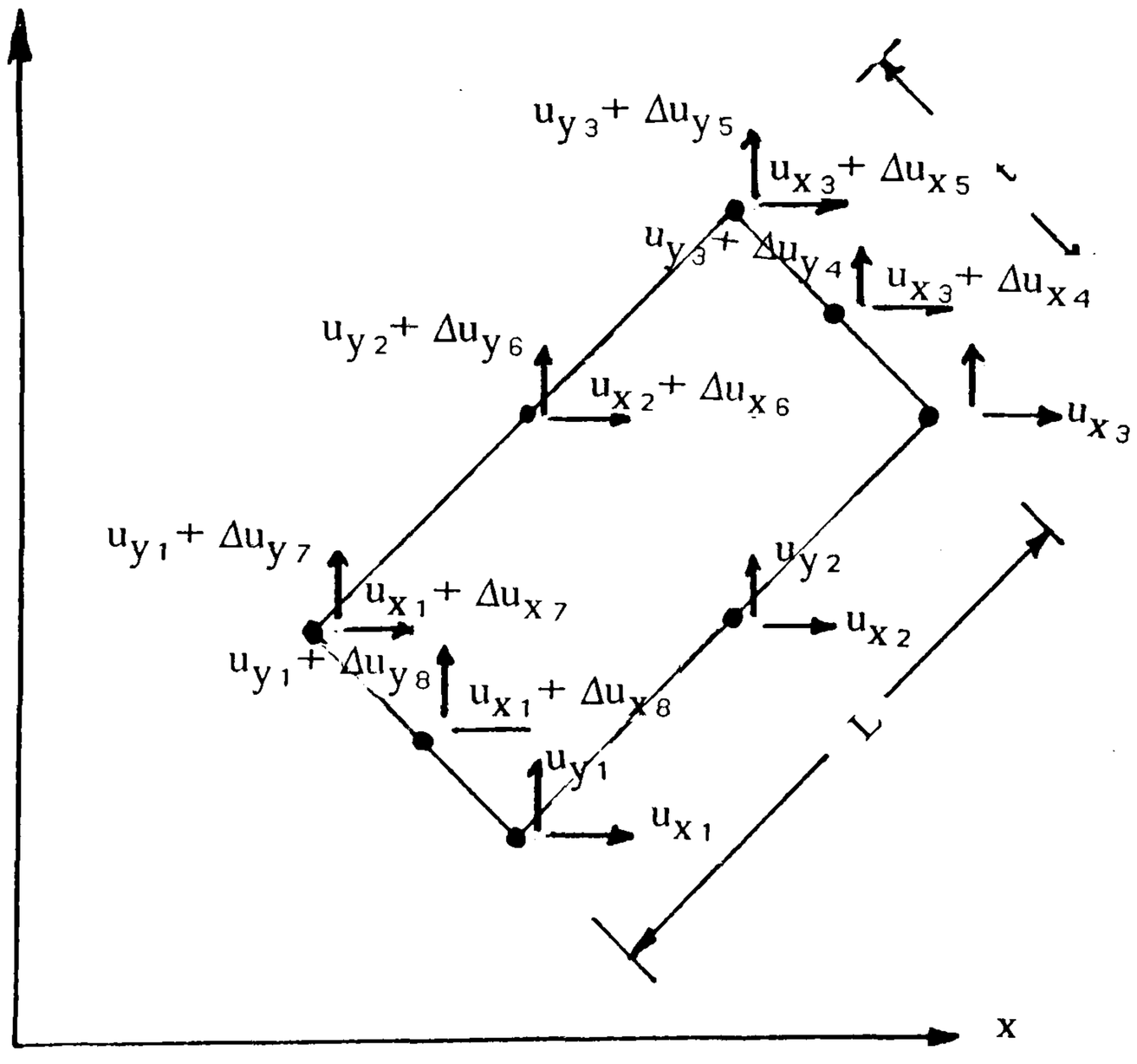

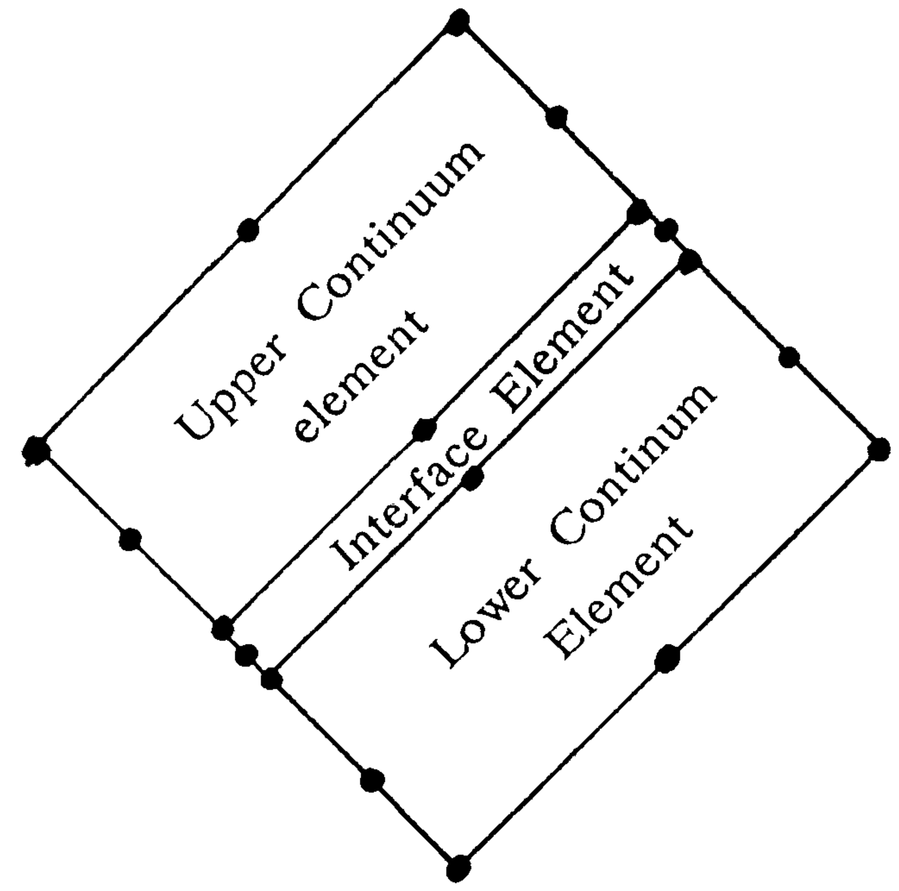

FIGURE (4. 19) INTERFACE ELEMENT (AFTER PANDE AND SHARMA, 1979)

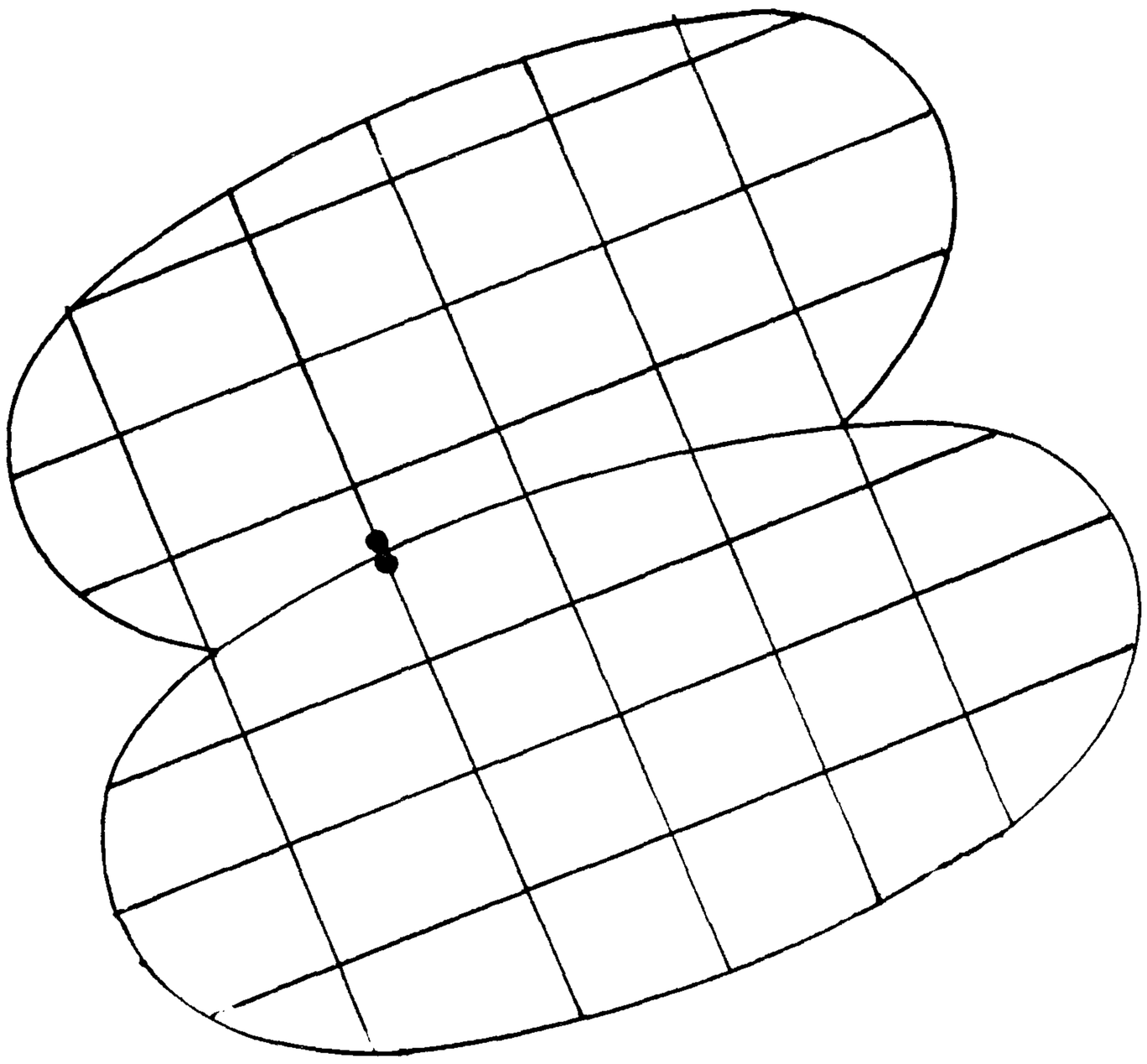

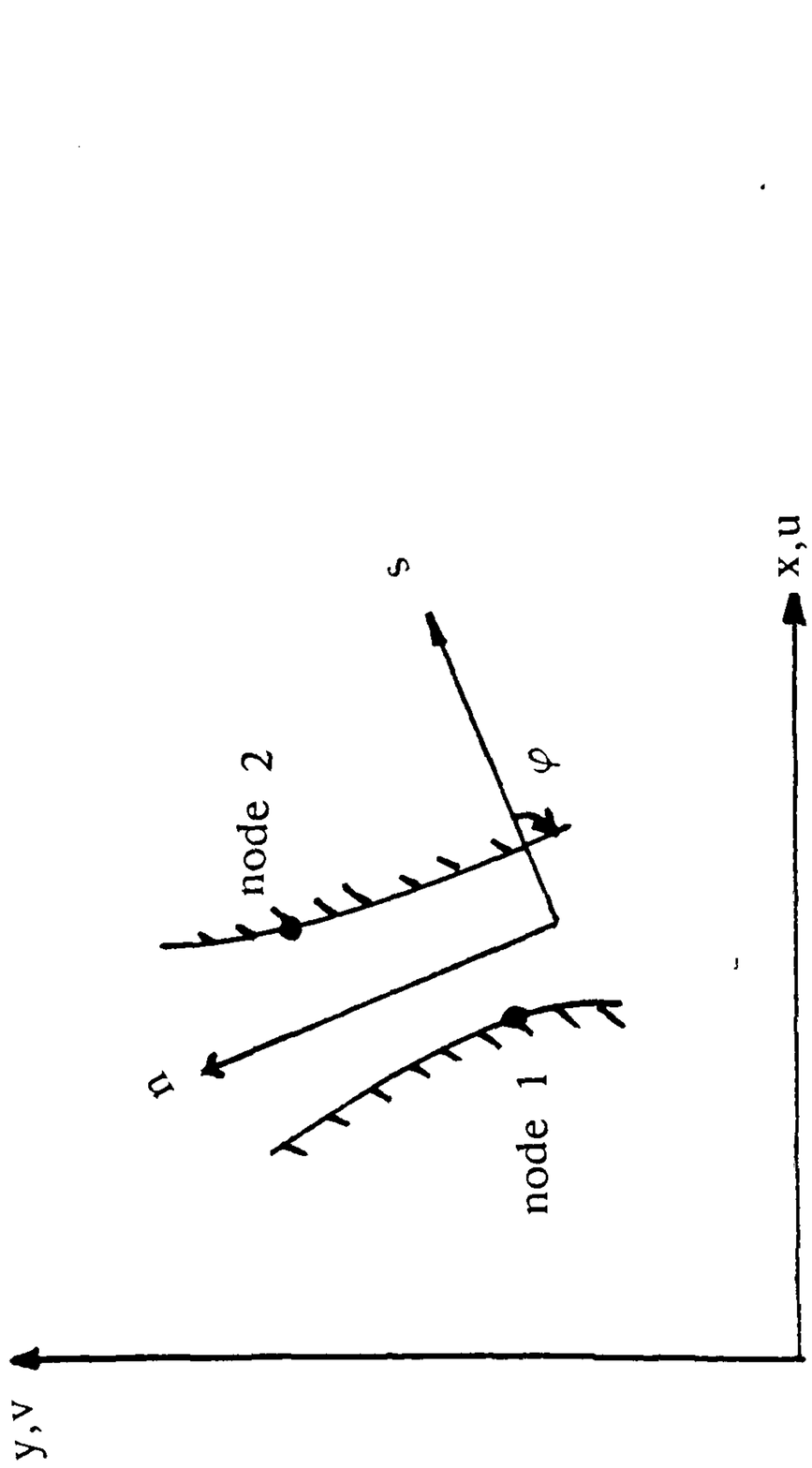

FIGURE (4.20) INTERFACE ELEMENT (AFTER KATONA , 1983)

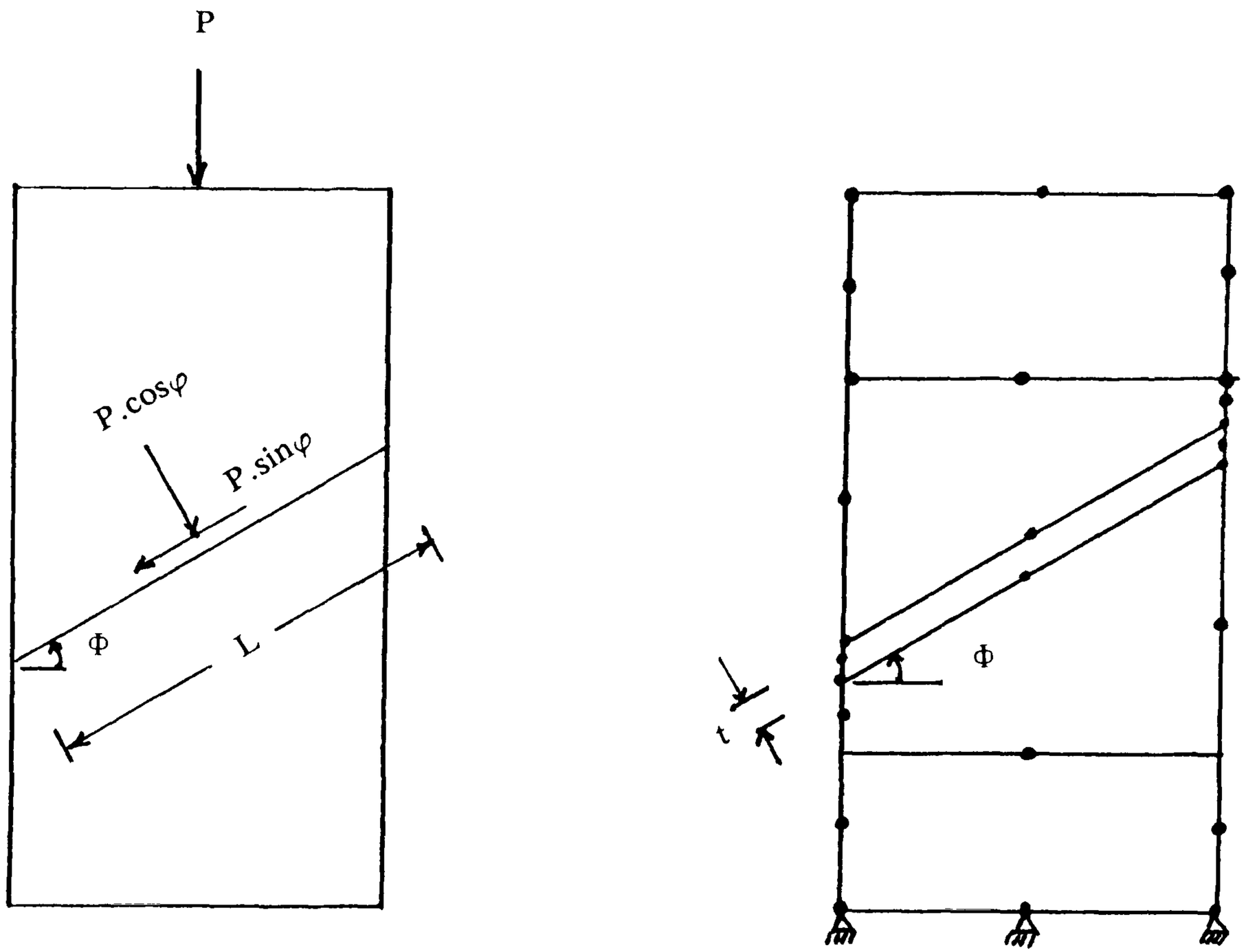

Slipping Assumption

Finite Element Formulation

FIGURE (4.21) INTERFACE ELEMENT (AFTER GRIFFITHS, 1985)

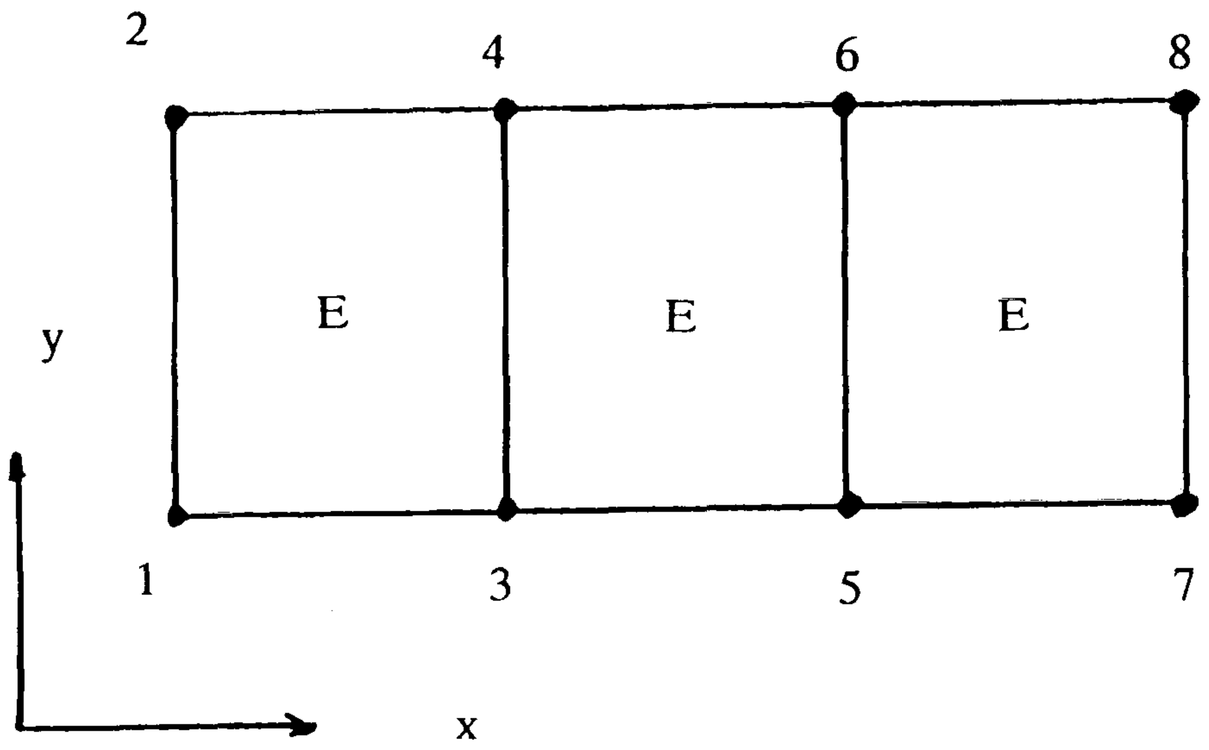

E explicit element

Finite element mesh–2 degrees of freedom per node

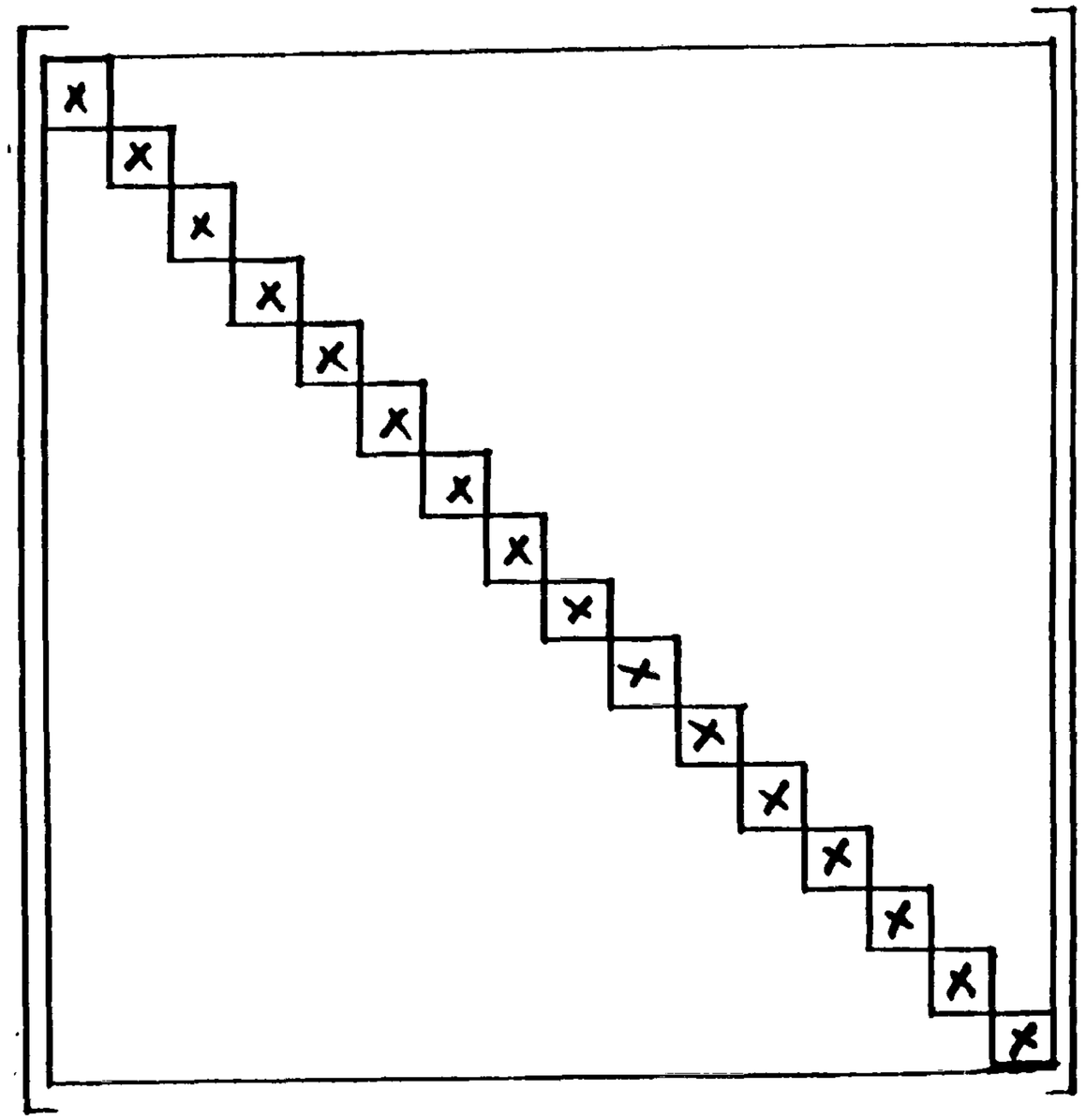

Typical profile of lumped matrix

FIGURE (4.22) TWO_DIMENSIONAL FINITE ELEMENT MESH AND PROFILE STRUCTURE OF ITS GLOBAL LUMPED MATRIX _EXPLICIT ELEMENTS ONLY (OWEN & HINTON, 1980)

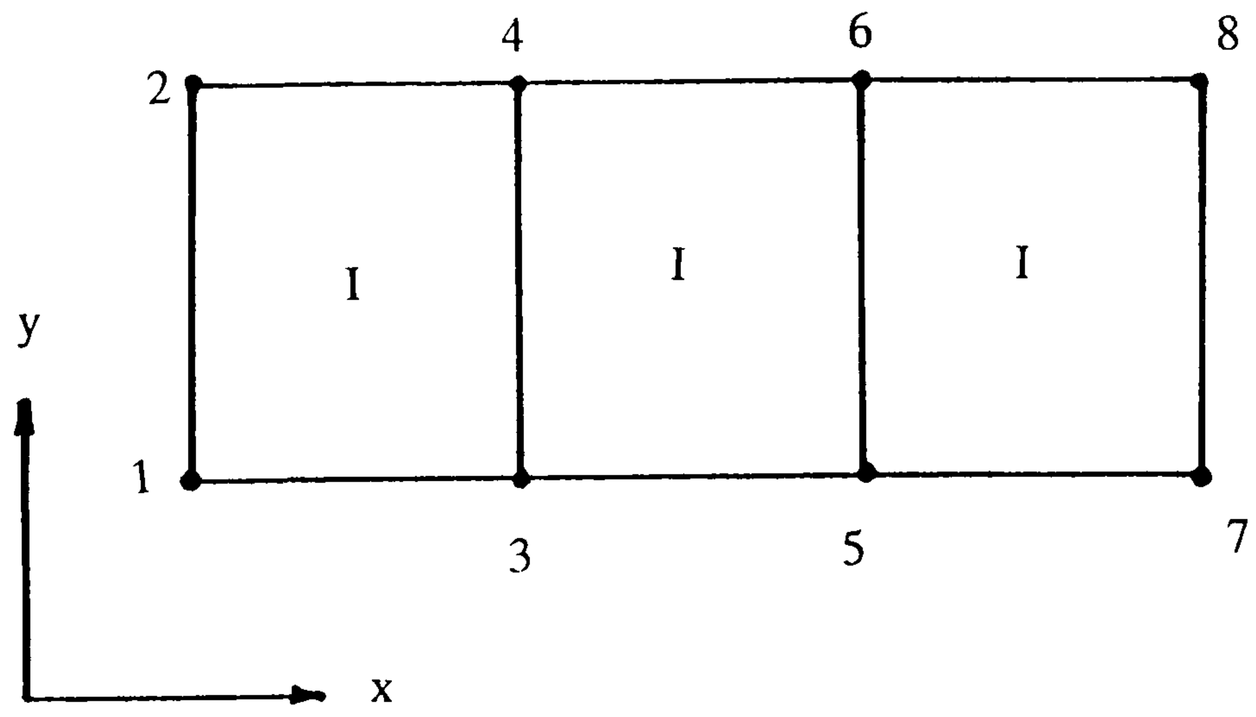

I implicit element

Finite element mesh–2 degrees of freedom per node

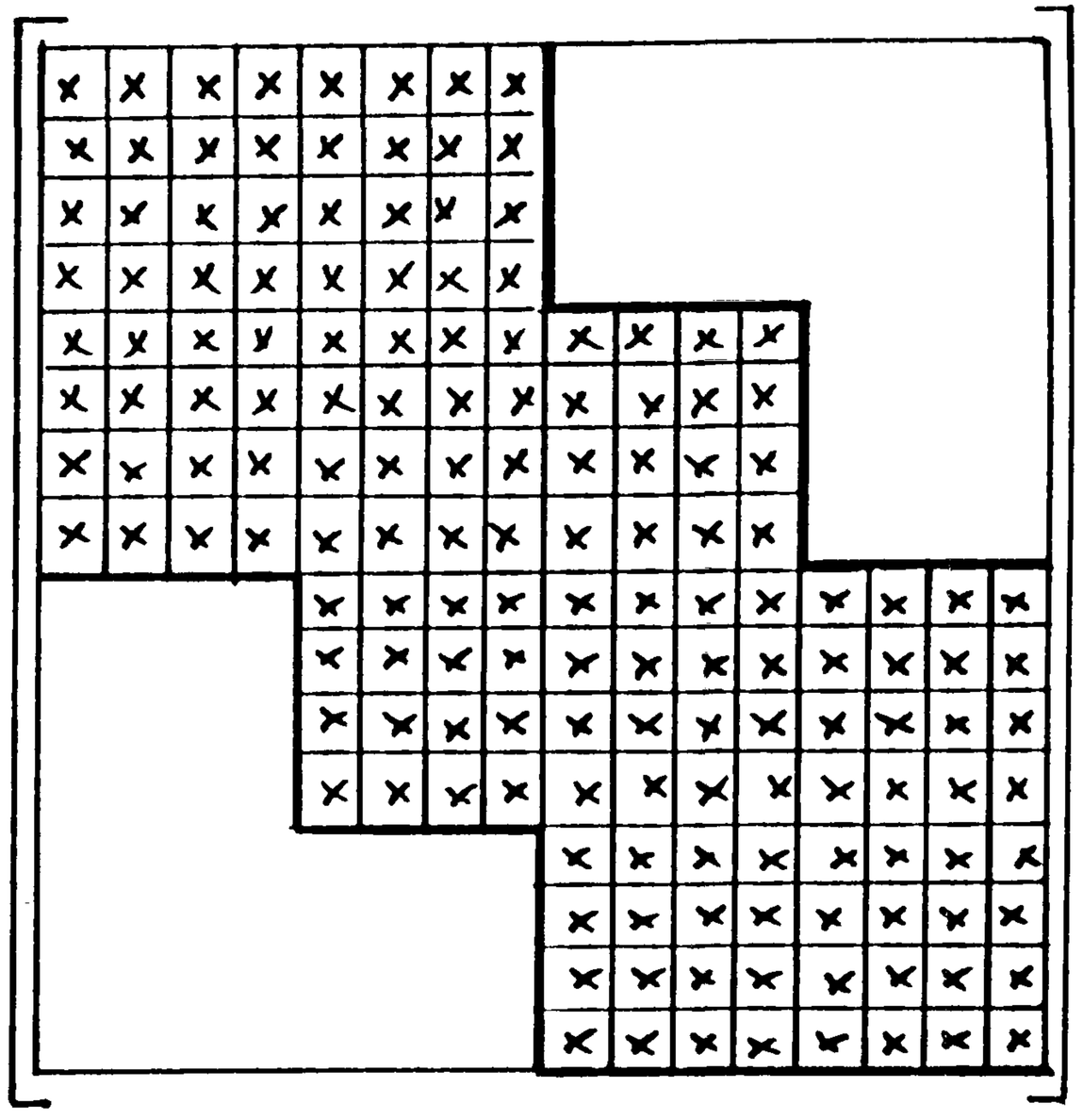

Typical profile of consistent matrix

FIGURE (4.23) TWO_DIMENSIONAL FINITE ELEMENT MESH AND PROFILE STRUCTURE OF ITS GLOBAL CONSISTENT MATRIX_IMPLICIT ELEMENTS (OWEN & HINTON, 1980)

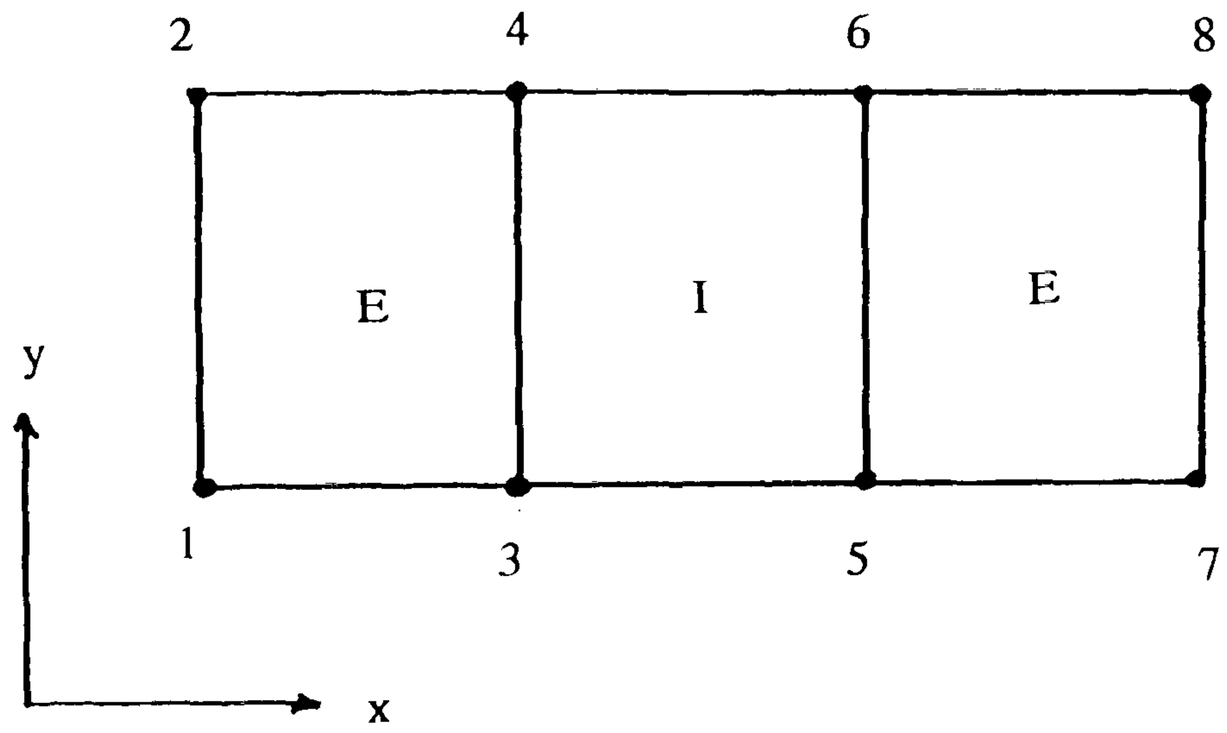

E explicit element

I implicit element

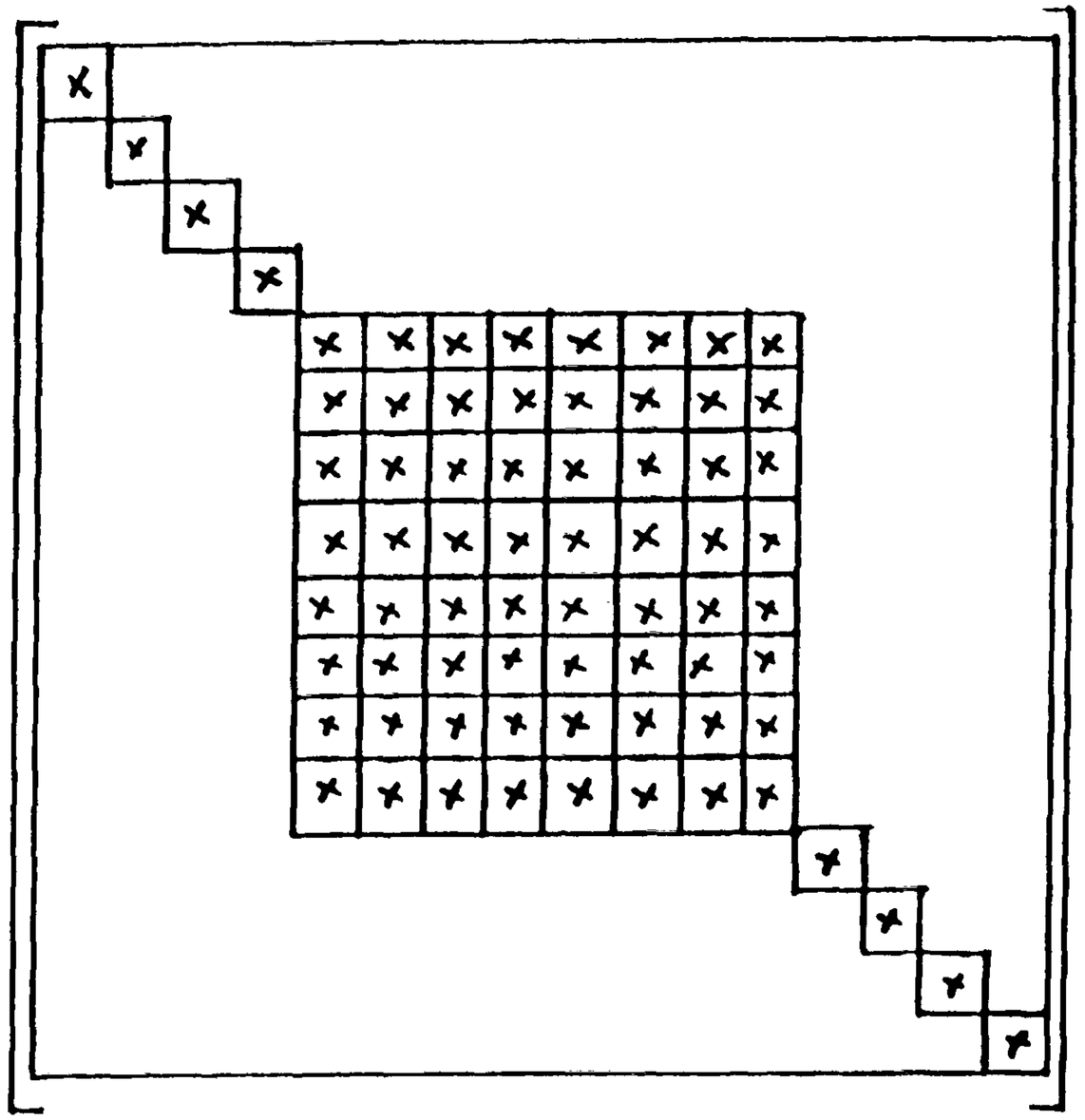

Finite element mesh –2 degrees of freedom per node

Typical profile of an implicit–explicit matrix

FIGURE (4.24) TWO_DIMENSIONAL FINITE ELEMENT MESH AND PROFILE STRUCTURE OF ITS GLOBAL MATRIX FOR IMPLICIT_EXPLICIT ELEMENTS (OWEN&HINTON, 1980)

CHAPTER 5

FINITE ELEMENT ANALYSIS OF PILE DRIVING

5.1 INTRODUCTION

5.2 CONVERGENCE STUDIES

5.3 PARAMETRIC STUDIES

5.4 DISCUSSION

5.5 CONCLUSION

CHAPTER 5

FINITE ELEMENT ANALYSIS OF PILE DRIVING

5.1 INTRODUCTION

Until the finite element work of Chow (1981) and Smith and Chow (1982), the pile driving problem had been analysed almost exclusively by means of one dimensional models. In these simple models, stiffness and damping were simulated by means of springs and dashpots attached at discrete points to the pile shaft and pile base. As discussed earlier, this approach necessitates the use of essentially fictitious parameters. By contrast, the three–dimensional (axisymmetric) finite element models make use of real soil properties (Young's modulus, mass density, etc.) and can therefore furnish a more realistic picture of the driving process. No assumptions have to be made regarding the distribution of soil resistance along the pile and both radiation and viscous damping can be accounted for in a rational manner. The major disadvantage of the method, however, is that computational times are prodigious.

One of the numerical difficulties arising in the application of the finite element method to pile driving analysis occurs as a consequence of the very great difference in stiffnesses between piles and typical soils. High frequency stress waves may build–up in the pile since these can not propagate into the soil elements (wavelengths in soil are much shorter). However, one method of overcoming this difficulty is by introducing a small amount of damping at the pile–soil interface to reduce the high frequency noise to an acceptable level while only marginally affecting the overall pile response, Randolph and Simons (1986).

The only essential additional piece of information necessary to carry out a dynamic finite element analysis (as opposed to a static analysis) is the soil mass density. Special provision must be made however for damping at the boundaries to prevent wave reflection and in order to reduce computational costs. It is only feasible to analyse piles with circular cross sections, reducing the problem to an axisymmetric one.

In this study, the soil has been modelled as non–viscous elastic, perfectly plastic Von Mises material and the transmitting boundary in the far field has been modelled using the viscous boundary devised by Lysmer and Kuhlemeyer (1969) and modified by White et al, (1977). Allowance has been made for slip at the pile soil interface at a specified value of skin friction, using Griffiths (1985) thin eight noded, interface elements. A limited parametric study has been conducted in order to gain some insight into the behaviour of the pile during the driving process and to follow the evolution of failure in the soil around and beneath the pile.

During impact pile driving many modes of vibration will be excited. However, the higher modes in the discretised finite element system are likely to be in error and there is little justification in including their contribution to the response. Consequently, since a time integration scheme which possesses some numerical damping has certain advantages, an unconditionally stable implicit algorithm, namely the predictor–corrector scheme (developed by Hughes and Liu (1978) and implemented by Owen and Hinton (1980) program MIXDYN), is used to integrate the equations of motion in this study.

Initiation of the driving process can be performed by prescribing an initial ram velocity or by specifying an appropriate forcing function based on hammer manufacturer's force–time plots. In this Chapter, the latter method is preferred (see also Borja,1988; Shibata et al,1989).

5.2 CONVERGENCE STUDIES

To verify the simulation of axial wave propagation down the pile (in the absence of soil resistance) a simple test was carried out, as follows. Basically, a uniform rod fixed at one end and free at the other was subjected to a suddenly applied (and thereafter maintained) impact force (i.e. a Heaviside forcing function). Wave propagation along the rod was examined with the use of , successively, 5,10 and 20 axisymmetric elements and by varying the length of the time step. The effect of time step size and the number of elements is shown in Figs. 5.1 to 5.9. Clearly, smaller time steps and more elements provide better

solutions but computational costs may prove to be a constraint in practice.

A numerical simulation of the pile driving tests performed by Rigden et al, (1979) at the Building Research Establishment site at Cowden (known there after as the Rigden pile; To, 1985) was then carried out and the results were compared with those obtained by To (1985). The simulation process was initiated by prescribing an impact force of short duration (corresponding to the type of the hammer used by Rigden) to the pile head. The hammer used for driving the Rigden pile was a BSP (British Steel Piling) hydraulically actuated type having a falling weight of 3.5 tonnes, Rigden et al, (1979). The final depth of penetration of this pile was 9.14 m and the set per blow was 10.2 mm. These results were simulated (for the pile termed A in their study) by Rigden et al, (1979), using the wave equation method using shaft and point viscous damping coefficients of 0.656 s/m and 0.033 s/m, respectively.

The response computed using the mesh shown in Fig. 5.10 gives essentially the same penetration namely 10 mm, Fig. 5.11, compared with the actual set of 10.2 mm obtained by Rigden et al, (1979) and To (1985) from his finite element analysis, Fig. 5.12. A refined mesh was not analysed since To (1985) had found that for this particular problem mesh refinement had very little effect on results. However, various forcing functions (but identical in impulsive strength) have been considered; these were essentially square functions. The results of this study are shown in Fig. 5.13 and reveal that the shape of the loading function, within quite wide limits, has very little effect on the pile response.

The slight differences between these results and those obtained by To (1985) are probably due to (i) differences in the initial condition, namely specification of a forcing function rather than the hammer's initial velocity; (ii) the use of a different integration scheme, and; (iii) the use of eight noded interface (slip) elements instead of the six noded elements used by Chow (1981).

5.3 PARAMETRIC STUDIES

Clearly, there are too many parameters to take a comprehensive parametric study of the pile driving problem; instead the influence of the major parameters

has been explored in typical cases. In this study, maximum pile segment lengths of 1.0 m and a maximum transverse element dimension of 2.0 m; as shown in Fig. 5.14, have been employed based on past experience. Further, in general, time steps of 0.2 ms have been employed throughout.

The response of a concrete pile with an aspect ratio (L/d) of 20, and length 10 m, to impact is the main object of this study. The surrounding soil is assumed to be a uniform saturated clay (variously assumed to have a stiffness (Young's modulus) of 2, 10 and 50 MPa). The soil's undrained strengths are computed from these stiffnesses by selecting a strength ratio β (= E_s/c_u); typical values are 200, 500 and 1000. The strength of the interface material is defined by means of the adhesion factor α (= c_a/c_u); typical values are 0.1, 0.5 and 1.0. The applied impact pressure P is prescribed variously as 12 MPa, 23 MPa and 46 MPa, all acting for 5 ms (i.e. as Heaviside functions).

The primary parameters are thus four (4) in number, viz, the soil stiffness E_s, the strength ratio β, the adhesion factor α and the hammer pressure P. The mean values of each of these (namely, 10 MPa, 500, 0.5, and 23 MPa) constitute the "basic case" and while any three of these are held constant, the fourth may be varied to explore the sensitivity of the pile response to this parameter alone. The plots given here depict the variation of the mean and shear stresses beneath the pile tip as a function of time and the evolution of failure within the soil.

Fig. 5.15 illustrates the influence of changing the adhesion factor α on the maximum shear stress–time relationship. It is clear that the pile shaft adhesion has no important effect on the shear stresses in the soil during driving. Failure in the soil takes place after about 6 ms.

Fig. 5.16 depicts the mean stress–time relationship and reveals the greater influence of the pile adhesion in this case. It also illustrates that this parameter has no important effect on the soil mean stresses. The oscillations in these values indicate that the pile itself vibrates during driving.

Fig. 5.17 shows the maximum shear stress–time relationship in the soil underneath the pile tip as a function of the strength ratio, β. This figure shows that, as expected, soil strength has an important effect on the final state of the soil after driving.

Fig. 5.18 shows the mean stress–time relationship in the same soils. Again, soil strength has an important effect on the residual stress level in the soil after driving.

The severe oscillations in these stress–time plots may be masked unless the output is sampled at sufficiently fine intervals as depicted in Figs. 5.19 – 5.23 where the output is based on values calculated at, variously, 10, 5, 2 and 1 time steps. The principal peaks in these response curves correspond to the return times for the applied stress wave reflected from the pile base.

Fig. 5.24 shows the maximum shear stress–time relationship in the soil underneath the pile tip as a function of soil stiffness. The results show that the change in soil stiffness has negligible effect on the response. This result is confirmed by Fig. 5.25 which shows the mean stress–time relationship in the same soil (element) underneath the pile tip.

The effect of increasing the pile head driving pressure on the maximum shear stress and mean stress time relationships, respectively, is shown in Figs. 5.26 and 5.27. It is clear that the higher the driving pressure the higher will be the residual shear stress after driving in the soil but the final mean stress is largely unaffected by an increase in driving stress.

During pile driving, body waves and Rayleigh waves propagate radially out ward from the pile along hemispherical wave fronts . This is shown in Fig. 5.28 for a circular surface footing on a homogeneous, isotropic elastic half–space (Woods, 1968) subjected to forced excitation. Kezdi (1957,1975) has discussed the effect of wave propagation during driving on a cohesionless soil and Taylor (1948) has discussed the sequences of compression and disturbance occurring in clays during pile driving. Taylor's study concentrated on an analysis of changes in shear strength. His conclusion that driving a pile in a soft impervious saturated clay causes horizontal displacements has been confirmed by numerical results obtained by Chow (1981) and To (1985), in which they concluded that the displacement vectors and yielding are localized underneath the pile.

The evolution of the yielding around and underneath the pile during and directly after driving is shown in Figs. 5.29 to 5.34. The yielding is indicated as a 'dot' in the centroid of each element. It is clear that the yielding zone initiates

at the pile–soil interface and then it propagates away from the pile, as time proceeds. These bands appear to move a considerable distance out from the pile and continue to do so for some time after impact has ceased.

5.4 DISCUSSION

As discussed in earlier Chapters, in a wave equation analysis, the permanent set of the pile is determined by subtracting the quake value from the maximum displacement at the first peak (Smith,1960). However, in the finite element model, the permanent set of the pile is determined from the equilibrium position of the pile tip, i.e. the computation proceeds until there is negligible movement of the pile tip corresponding to a nearly zero velocity.

The impact loading is a large amplitude loading type and this may cause changes in the soil structure strength. Many investigators (Richart et al, 1970) have examined the dynamic stress–strain behaviour of soils using triaxial tests and other means and these results should properly be incorporated into dynamic analyses of pile driving. Casagrande and Shannon (1948) and Seed and Lundgern (1954), found that this type of loading on saturated sand caused a typical increase of strength ranging from 10–20%. Moreover, substantial increases of shear strength of saturated clay were obtained by increasing the loading strain rate.

5.5 CONCLUSION

The Rigden pile (Rigden et al, 1979) previously analysed by To (1985) has been re–analysed using a different interface element and a different time integration scheme. The results obtained here were in very good agreement with those obtained previously.

A parametric study of the behaviour of a driven concrete pile has been carried out using a modified form of the Owen and Hinton (1981) MIXDYN

program. The principal modification, introduced into the program was the inclusion of the Lysmer and Kuhlemeyer (1969) viscous boundary to prevent spurious reflections at artificially curtailed boundaries.

The results indicated that neither pile shaft adhesion nor soil stiffness had much effect on the stresses in the surrounding soil after driving but increases in soil strength and ram force were found to have significant effects on the residual stresses following impact. A study of the evolution of yielding around and underneath the pile shows that the failure zone propagates a considerable distance away from the pile shaft and continues to do so for some time after the ram forces has subsided.

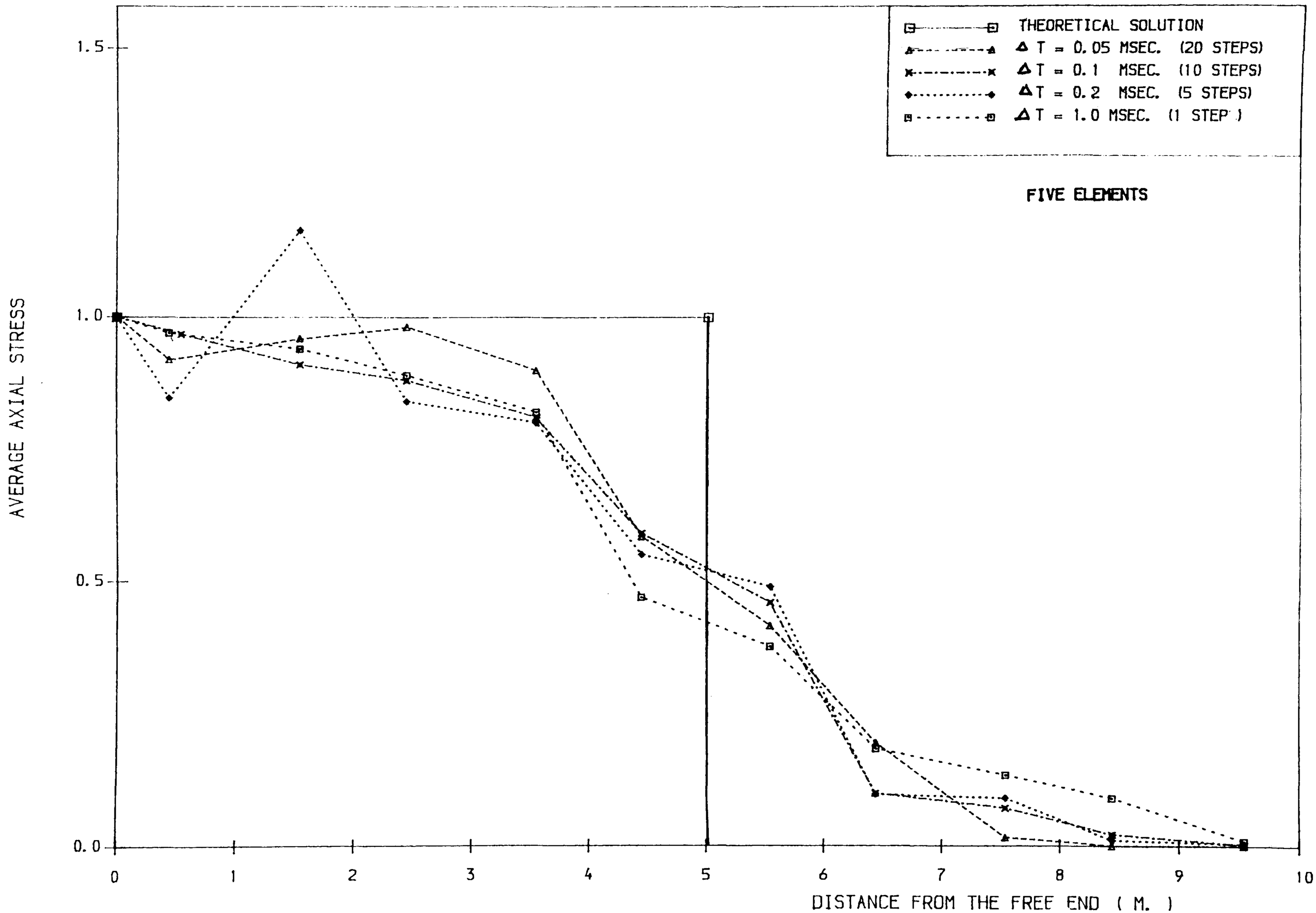

FIGURE (5.1) STRESS PROPAGATION THROUGH THE PILE
(E = 2.0E+11 N/SQ.M, ρ =8.0E+03 KG/CU.M , LP = 10.0 M, P = 1.0E+05 N/SQ.M

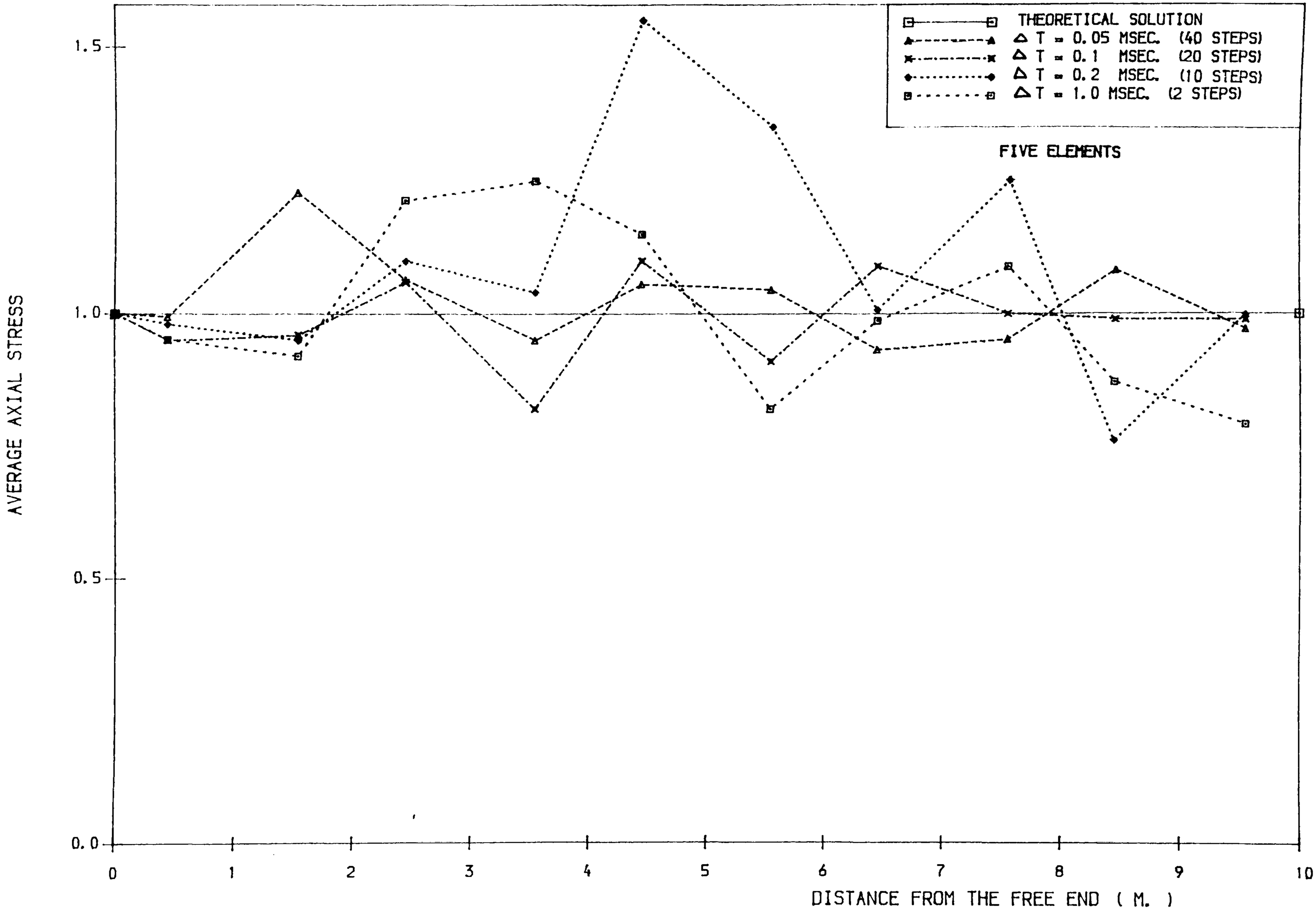

FIGURE (5.2) STRESS PROPAGATION THROUGH THE PILE .
(E = 2.0E+11 N/SQ.M, ρ = 8.0E+03 KG/CU.M, LP = 10.0 M, P = 1.0E+05 N/SQ.M

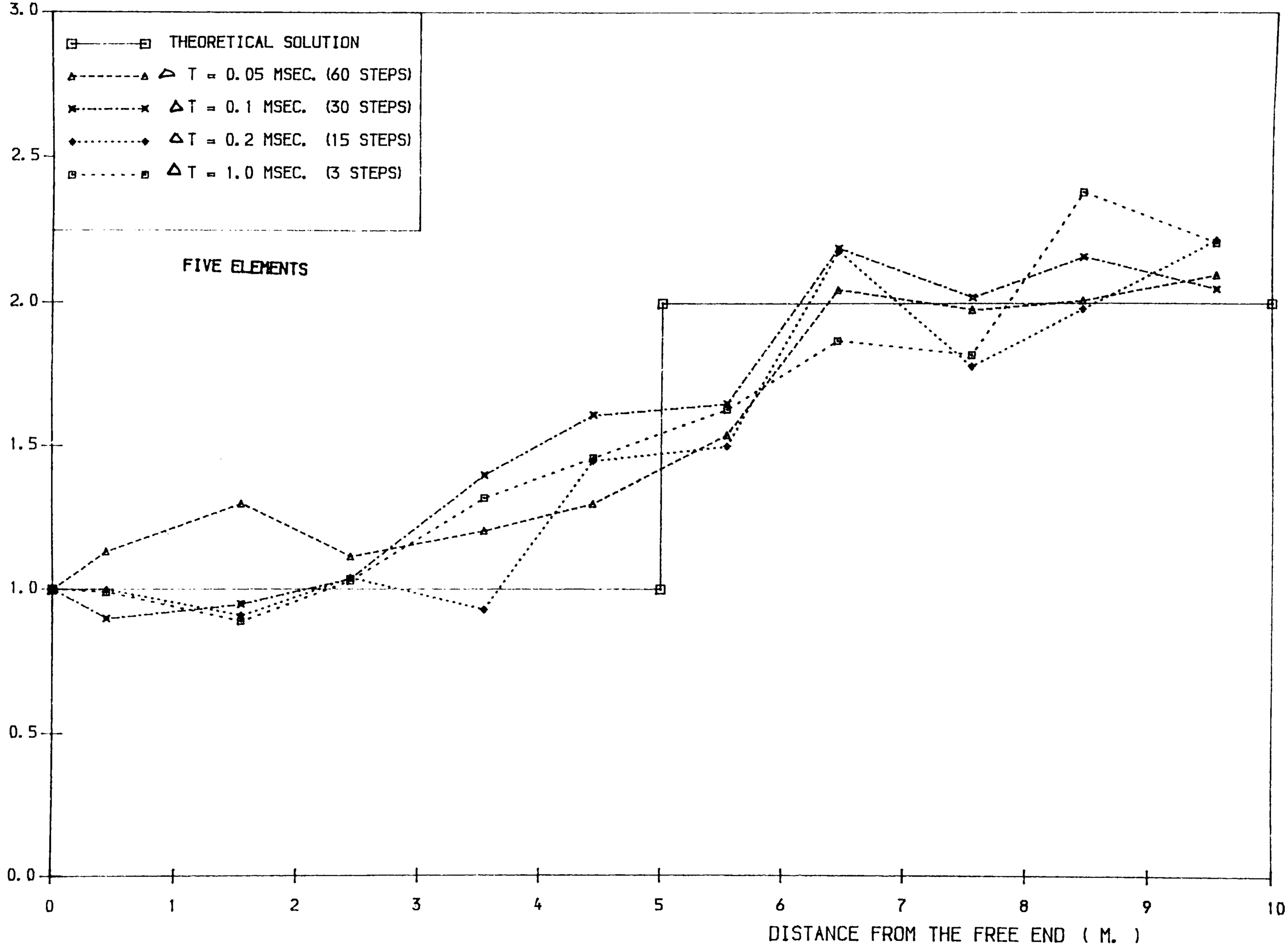

FIGURE (5.3) STRESS PROPAGATION THROUGH THE PILE

(E= 2.0E+11 N/SQ.M, ρ=8.0E+03 KG./CU.M, LP= 10.0 M, P = 1.0E+05 N/SQ.M)

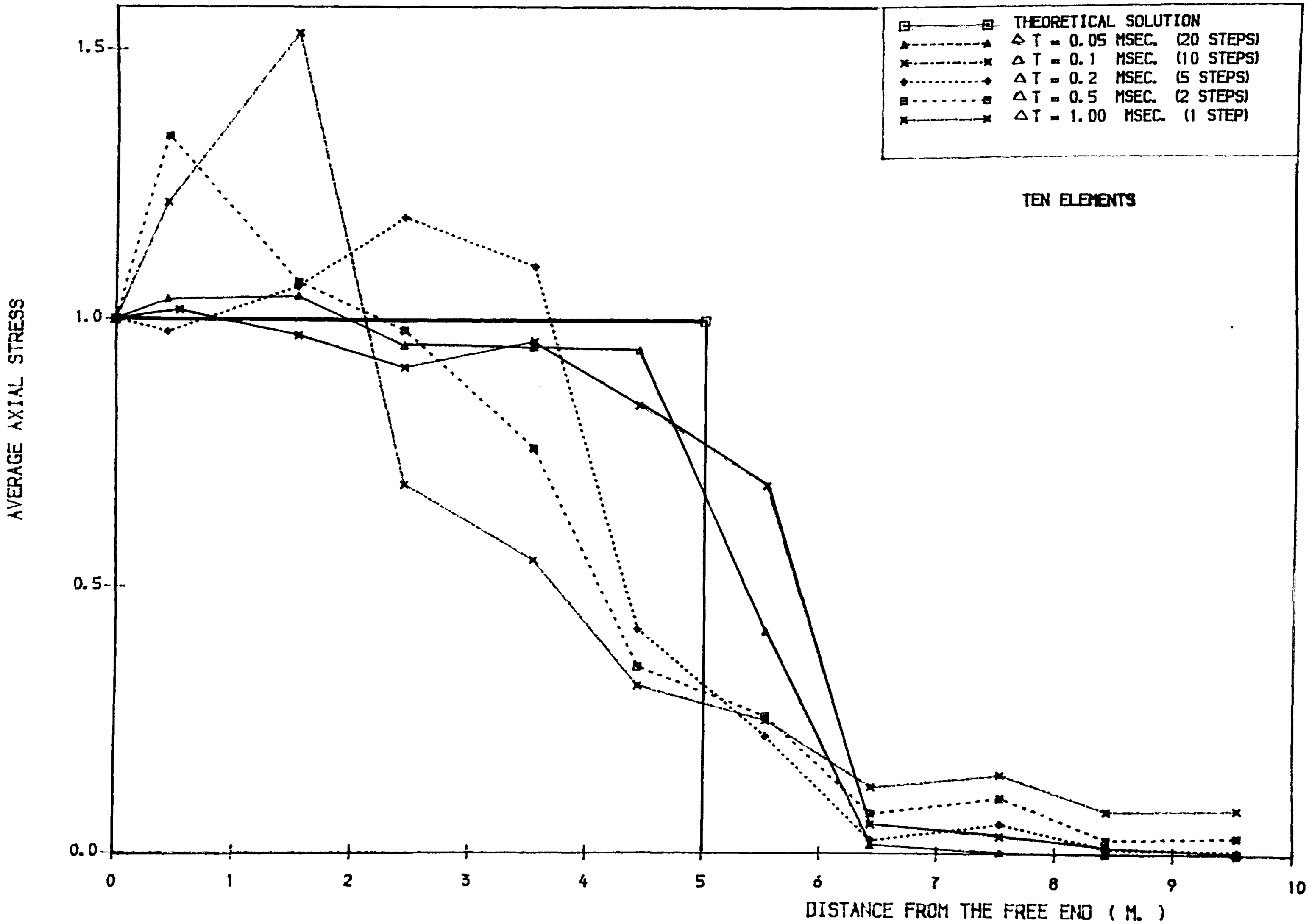

FIGURE (5.4) STRESS PROPAGATION THROUGH THE PILE
(E = 2.0E+11 N/SQ.M, ρ=8.0E+03 KG/CU.M , LP = 10.0 M, P = 1.0E+05 N/SQ.M

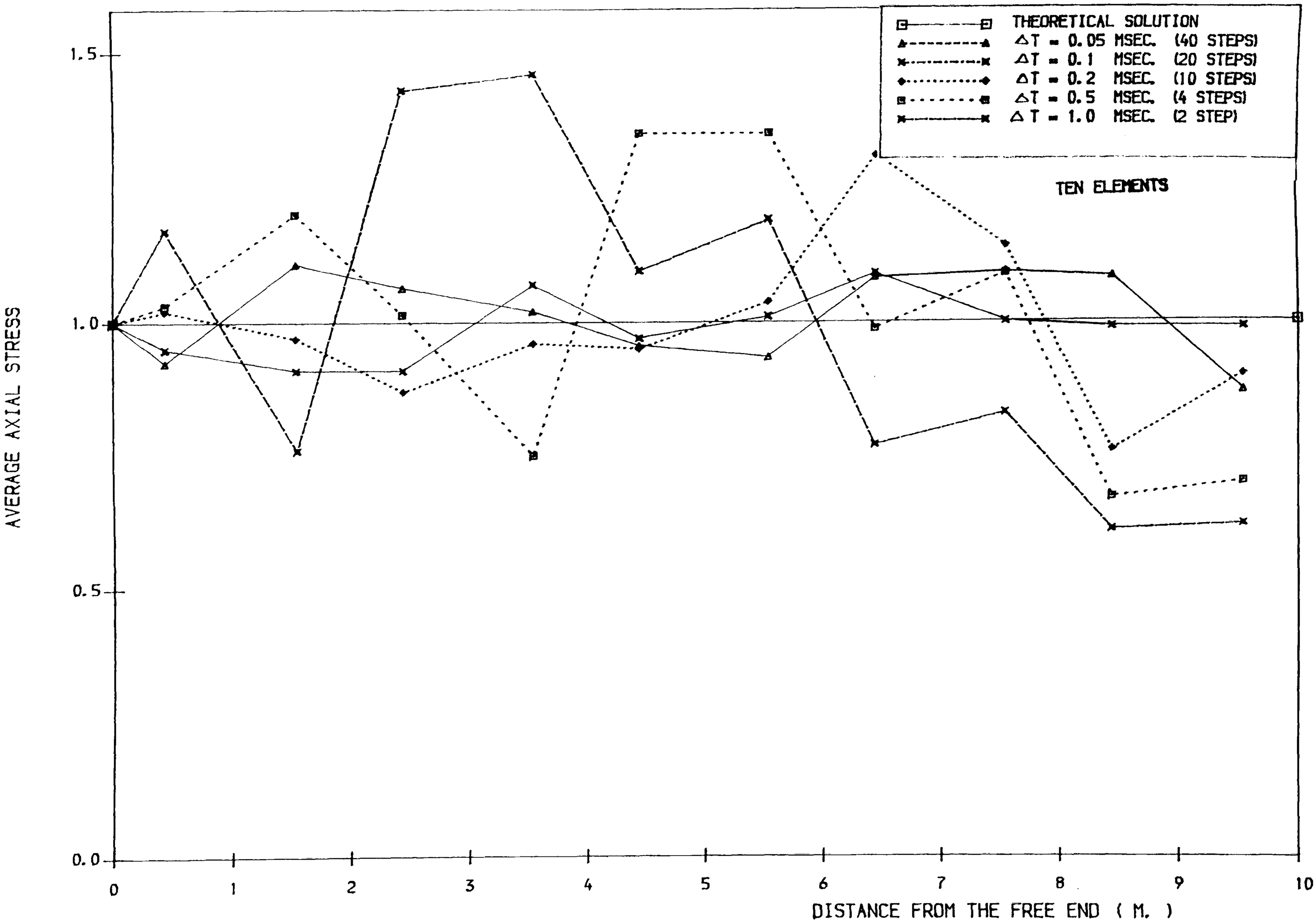

FIGURE (5.5) STRESS PROPAGATION THROUGH THE PILE
(E = 2.0E+11 N/SQ.M, ρ = 8.0E+03 KG/CU.M, LP = 10.0 M, P = 1.0E+05 N/SQ.M)

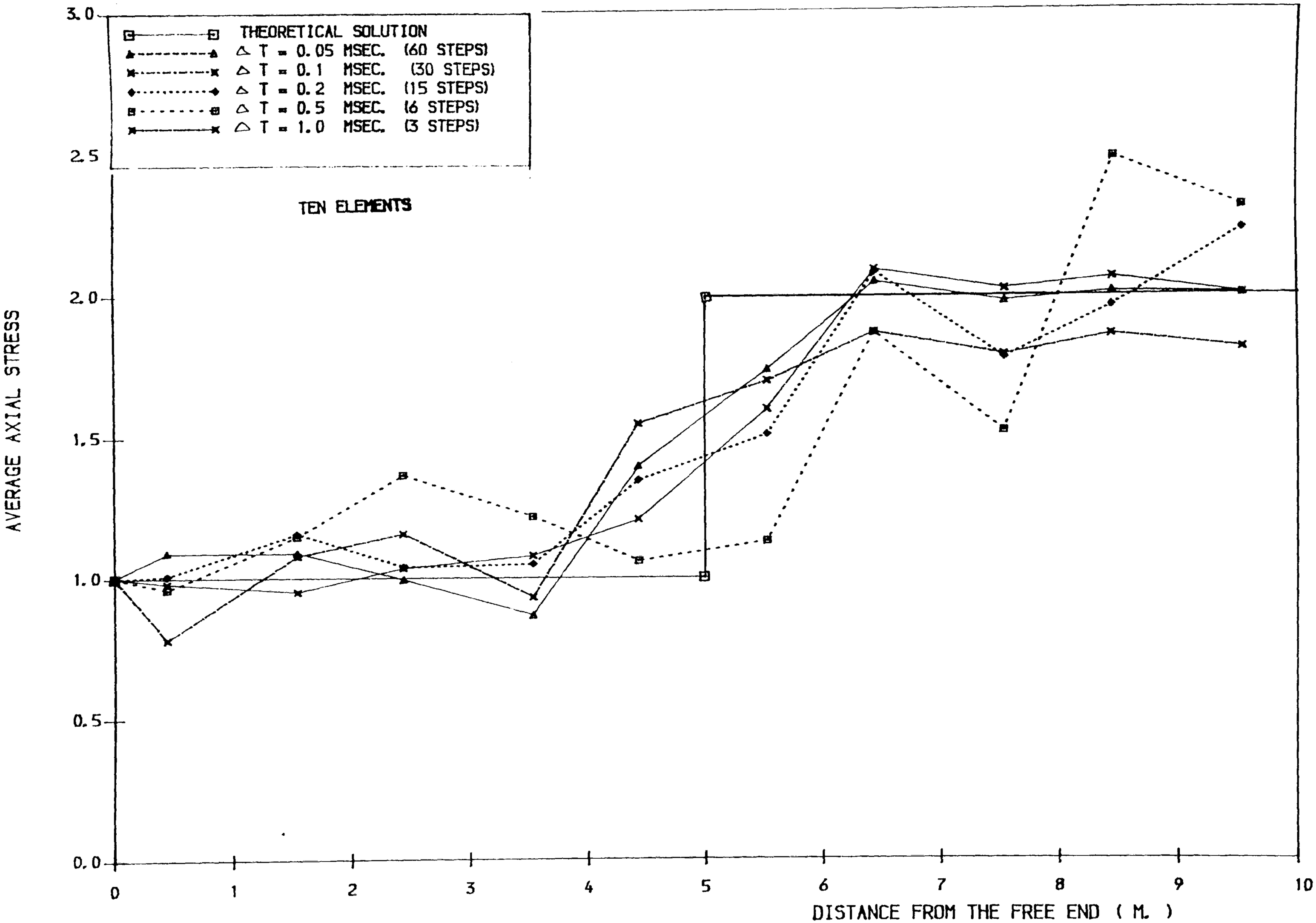

FIGURE (5.6) STRESS PROPAGATION THROUGH THE PILE
(E= 2.0E+11 N/SQ.M, ρ=8.0E+03 KG./CU.M, LP= 10.0 M, P = 1.0E+05 N/SQ.M)

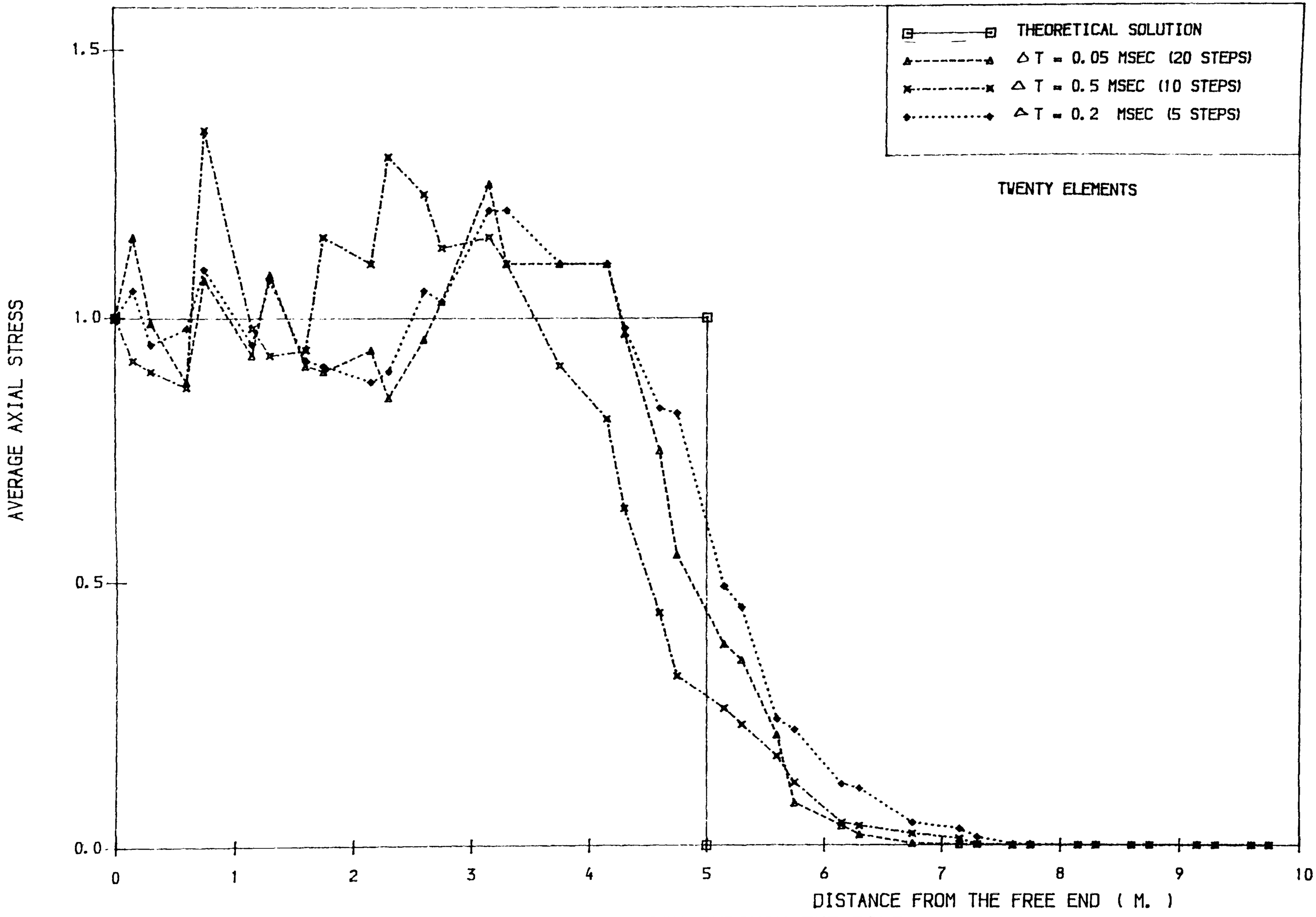

FIGURE (5.7) STRESS PROPAGATION THROUGH THE PILE
(E = 2.0E+11 N/SQ.M, ρ=8.0E+03 KG/CU.M , LP = 10.0 M, P = 1.0E+05 N/SQ.M

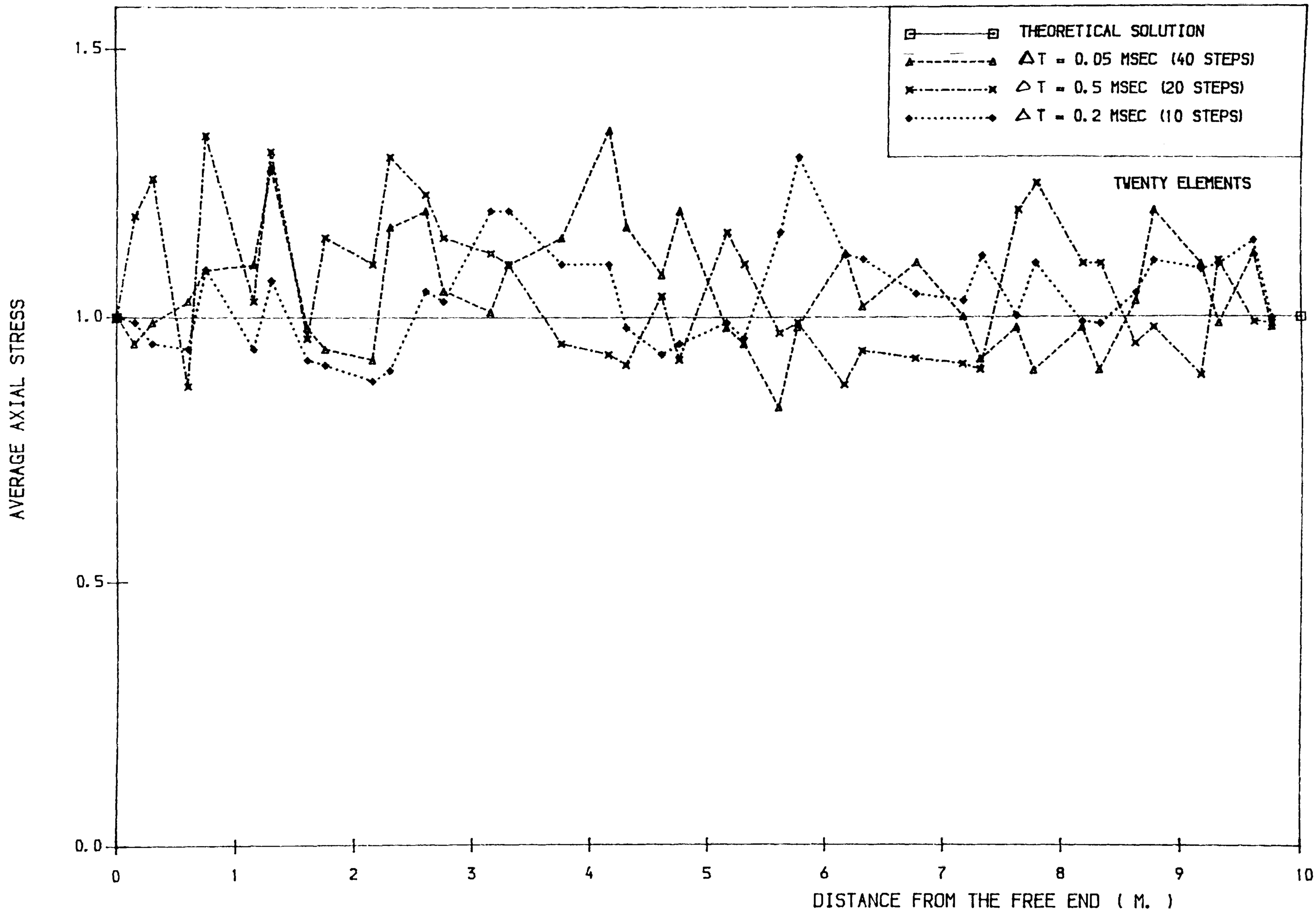

FIGURE (5.8) STRESS PROPAGATION THROUGH THE PILE
(E = 2.0E+11 N/SQ.M, ρ =8.0E+03 KG/CU.M , LP = 10.0 M, P = 1.0E+05 N/SQ.M

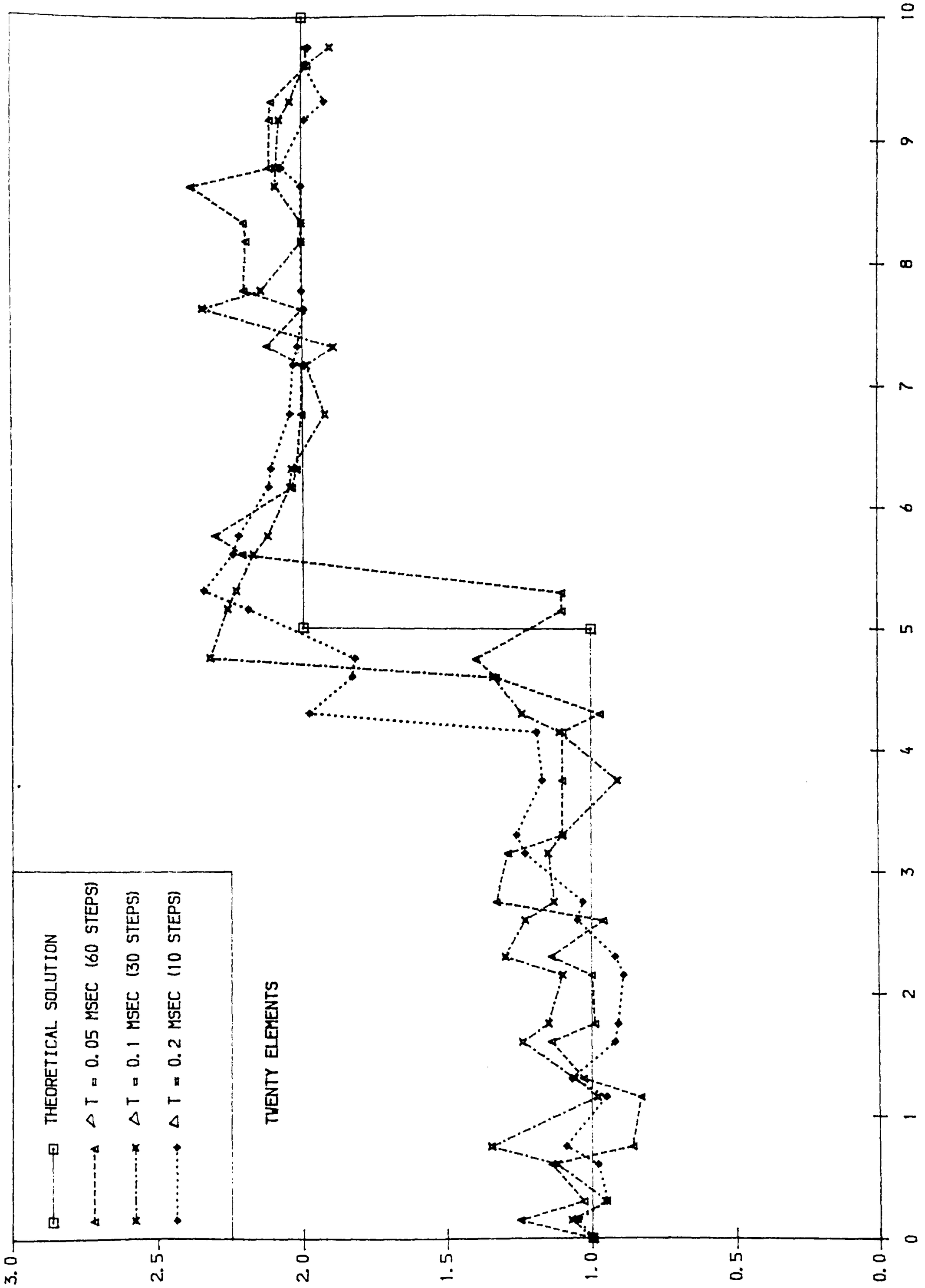

FIGURE (5.9) STRESS PROPAGATION THROUGH THE PILE
(E = 2.0E+11 N/SQ.M , LP = 10.0 M, P = 1.0E+05 N/SQ.M , ρ=8.0E+03 KG/CU.M)

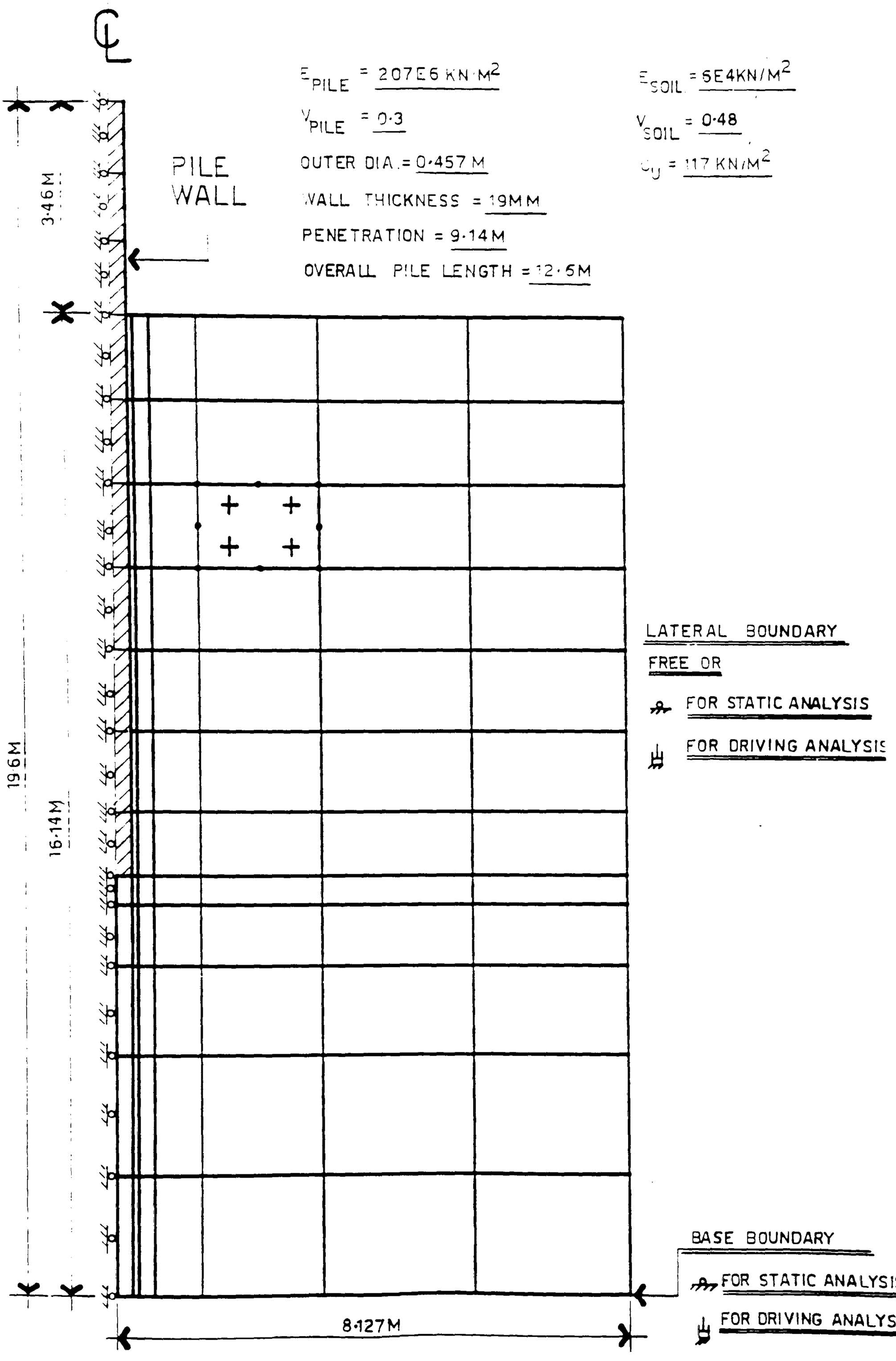

FIGURE (5. 10) FINITE ELEMENT MESH FOR RIGDEN'S (1979) CLOSED ENDED PILE.

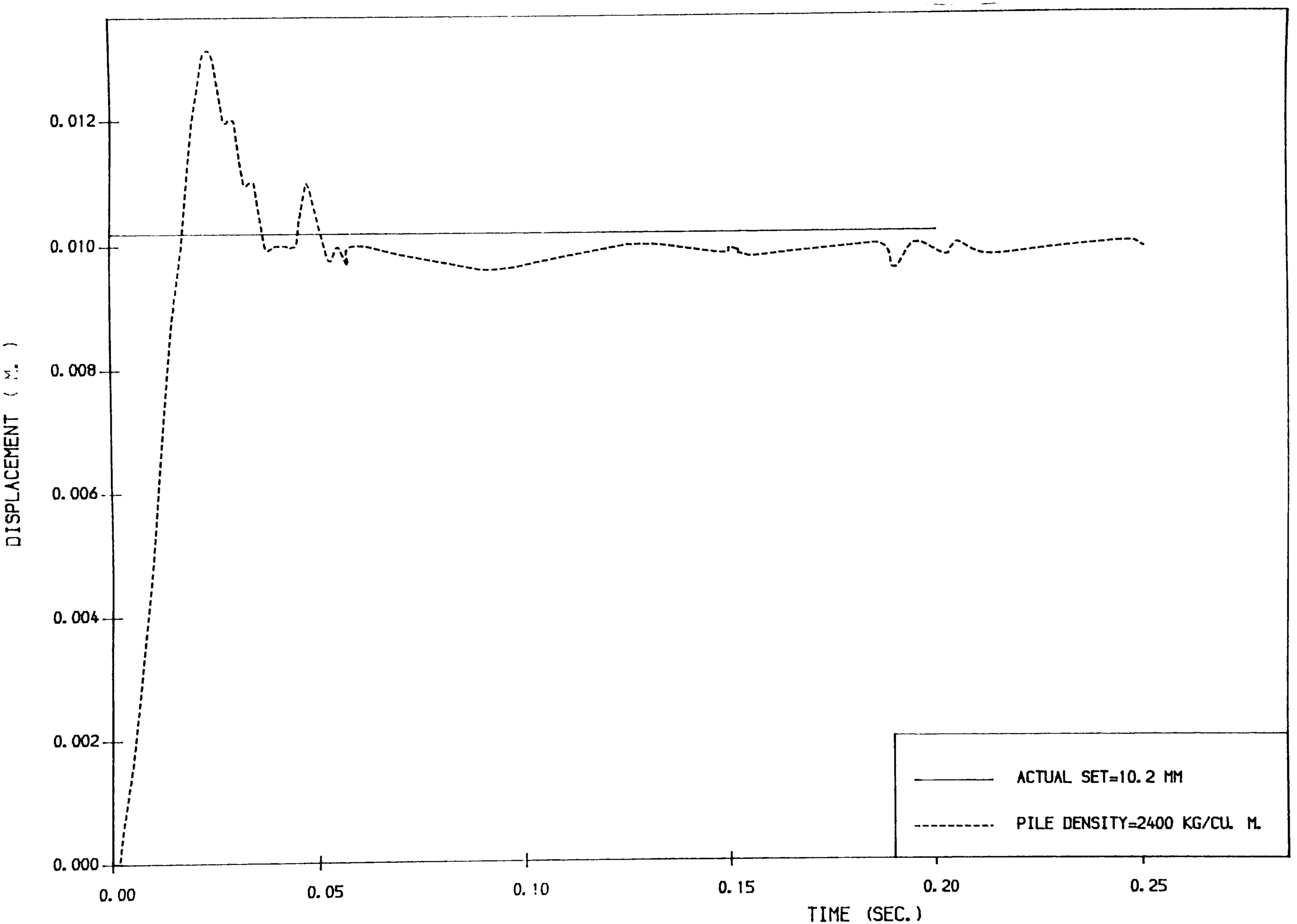

FIGURE (5.11) TIP DISPLACEMENT FOR CLOSED_ENDED PILE (RIGDEN ET AL, 1979). NEWMARK METHOD

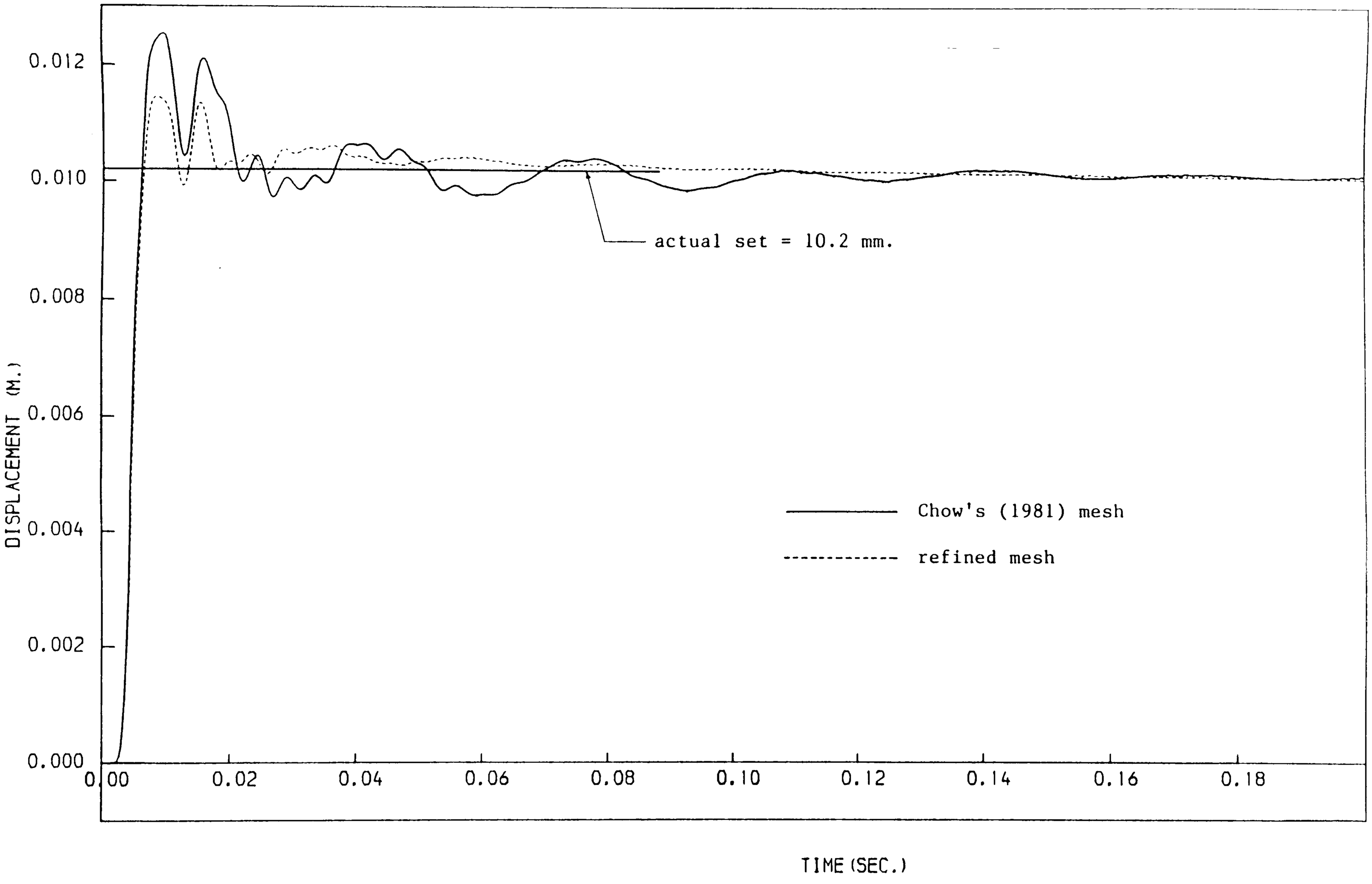

FIG. (5.12) COMPARISON OF DISPLACEMENT RESPONSE

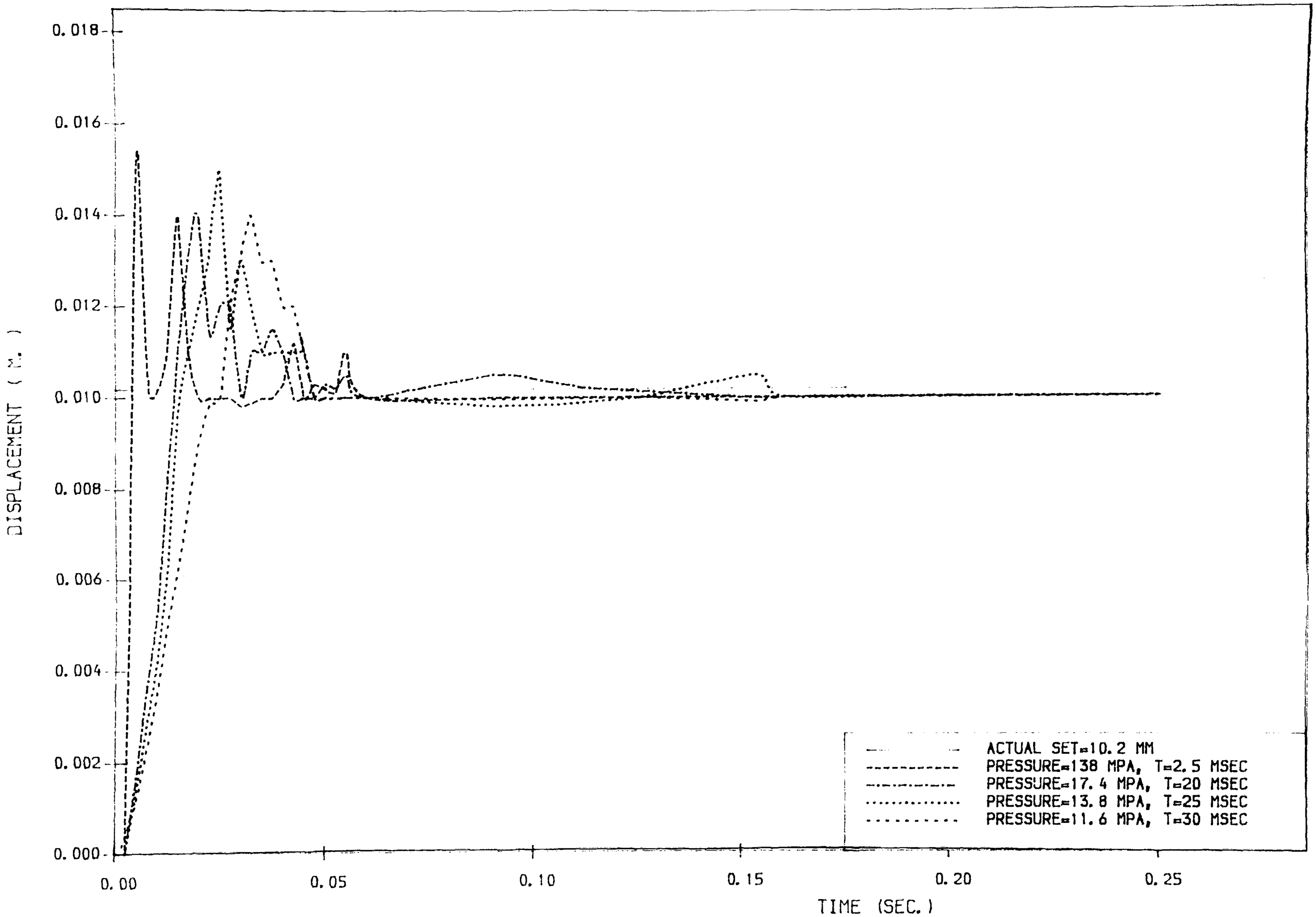

FIGURE (5. 13) TIP DISPLACEMENT FOR CLOSED_ENDED PILE (RIGDEN ET AL., 1979). NEWMARK METHOD

E_{PILE} = 25E3 MPA

V_{PILE} = 0·3

OUTER DIA. = 0·5M

PENETRATION = 10·0M

OVERALL PILE LENGTH = 10·0M

TIME STEP SIZE =

E_{SOIL} = 50MPA , 10MPA , 2MFA

$G_U = E_{SOIL}/200 , E_{SOIL}/500 , E_{SOIL}/1000$.

G_A = 1 , 0·5 , 0·1

PRESSURE = 12MPA , 23MPA , 46MPA FOR 5MSEC.
(INITIAL VELOCITIES 2·5M/S , 4·65M/S , 9·5M/S .)

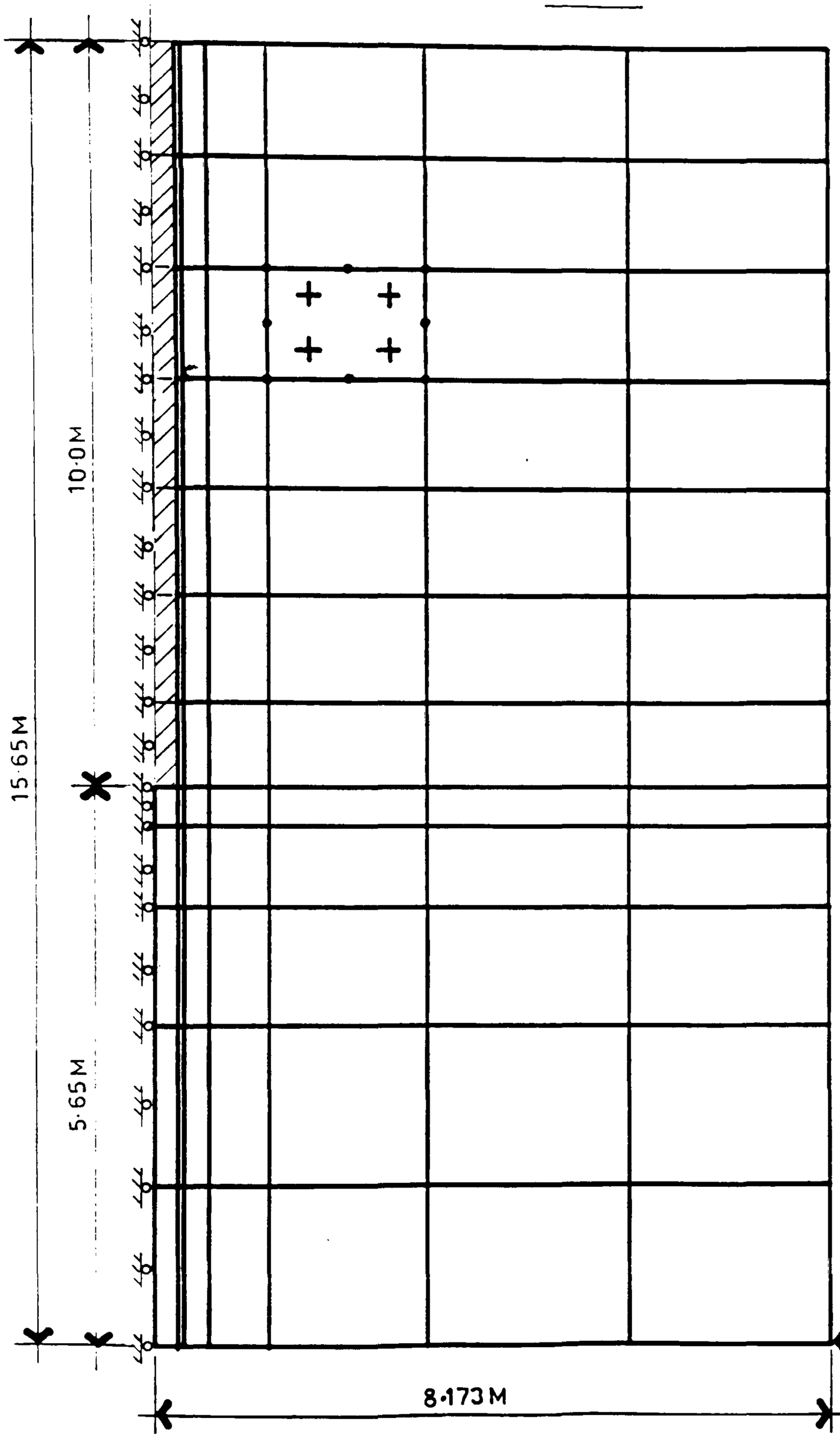

FIG. (5.14) FINITE ELEMENT MESH FOR THE CONCRETE PILE

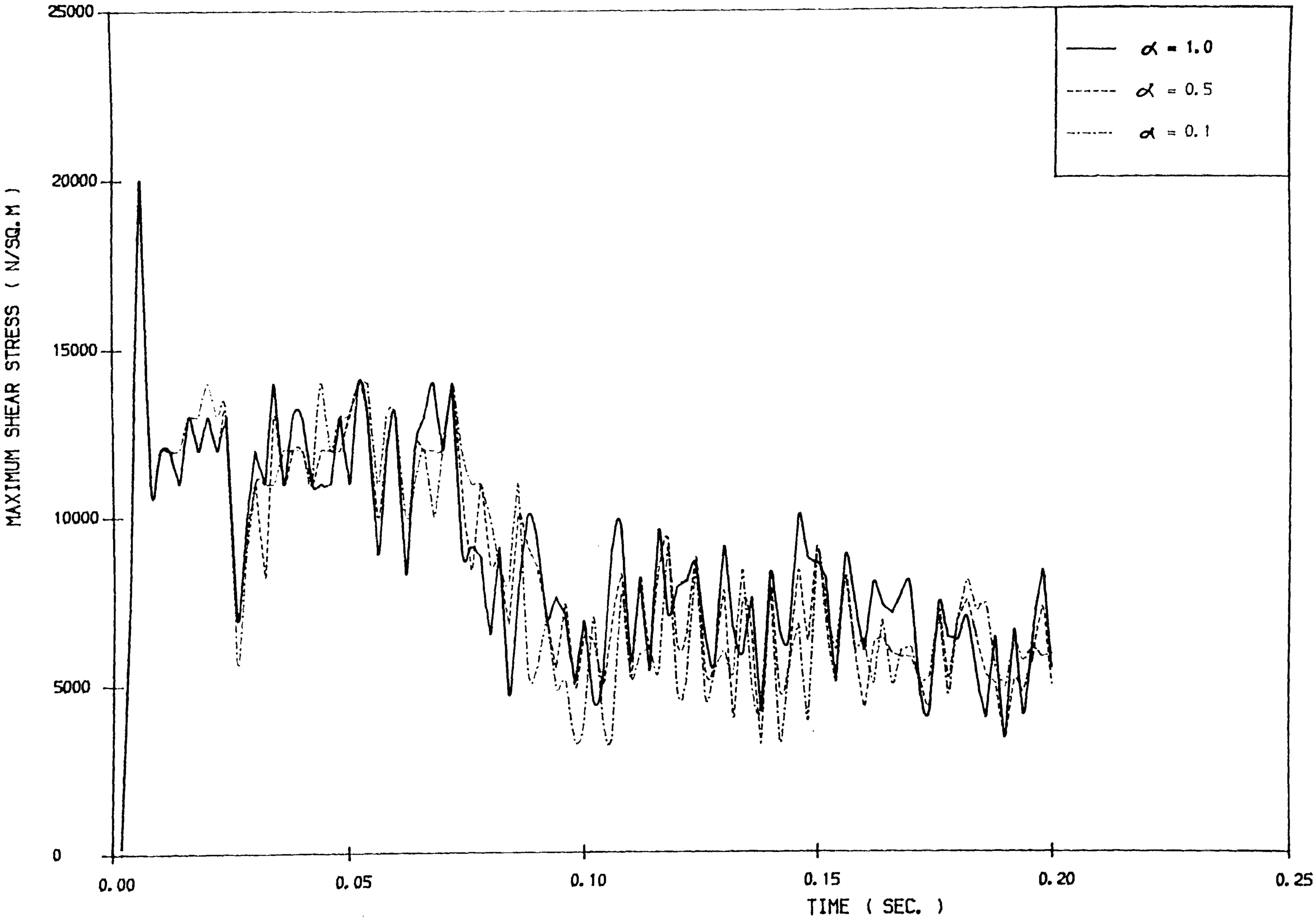

FIG. (5.15) MAXIMUM SHEAR STRESS IN SOIL UNDERNEATH PILE TIP_TIME RELATIONSHIP
(E = 10E6 N/SQ.M , β = 500 , P = 23E6 N/SQ.M)

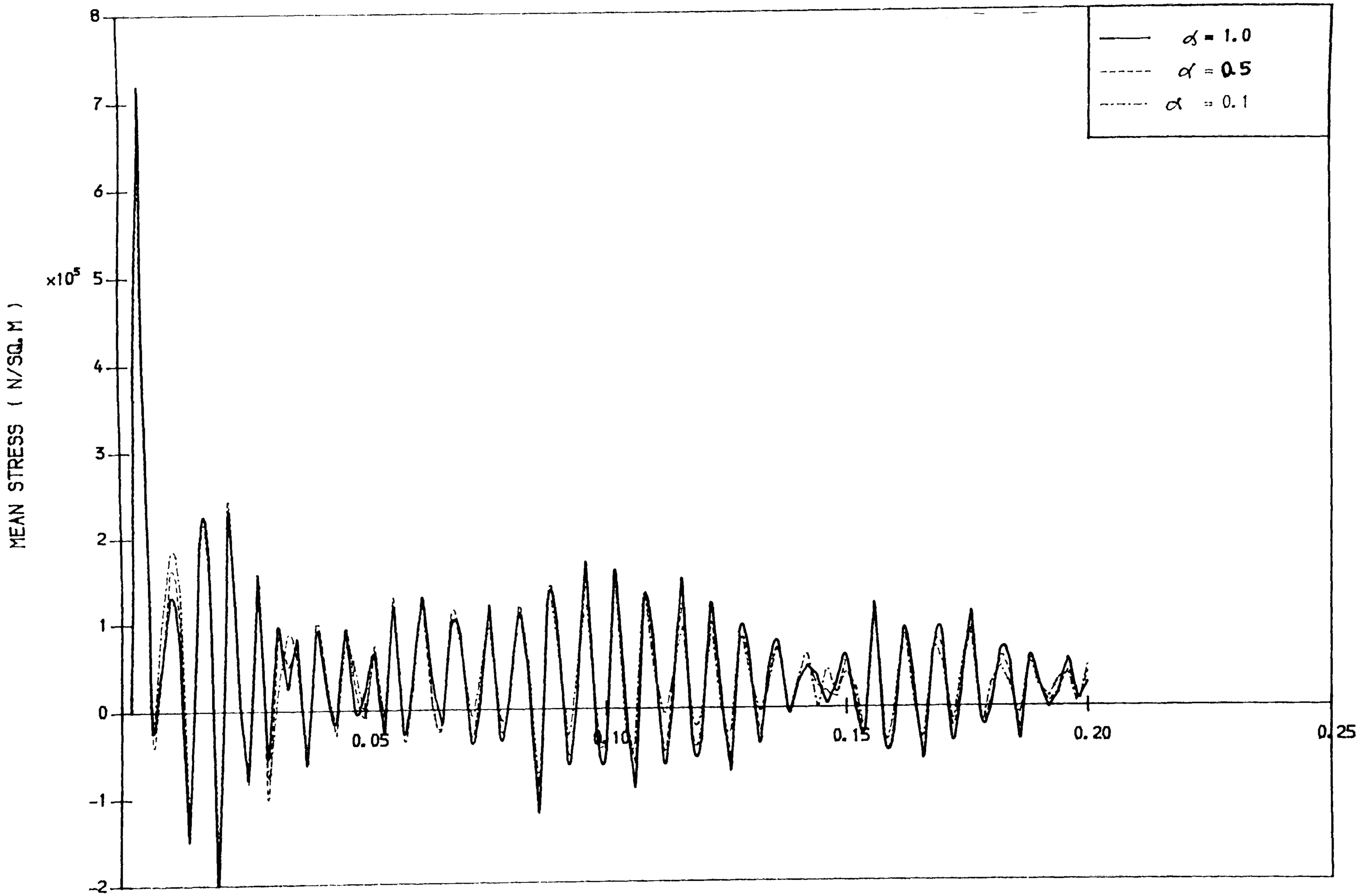

FIG. (5.16) MEAN STRESS IN SOIL UNDERNEATH PILE TIP_TIME RELATIONSHIP
(E = 10E6 N/SQ.M , β = 500 , P = 23E6 N/SQ.M)

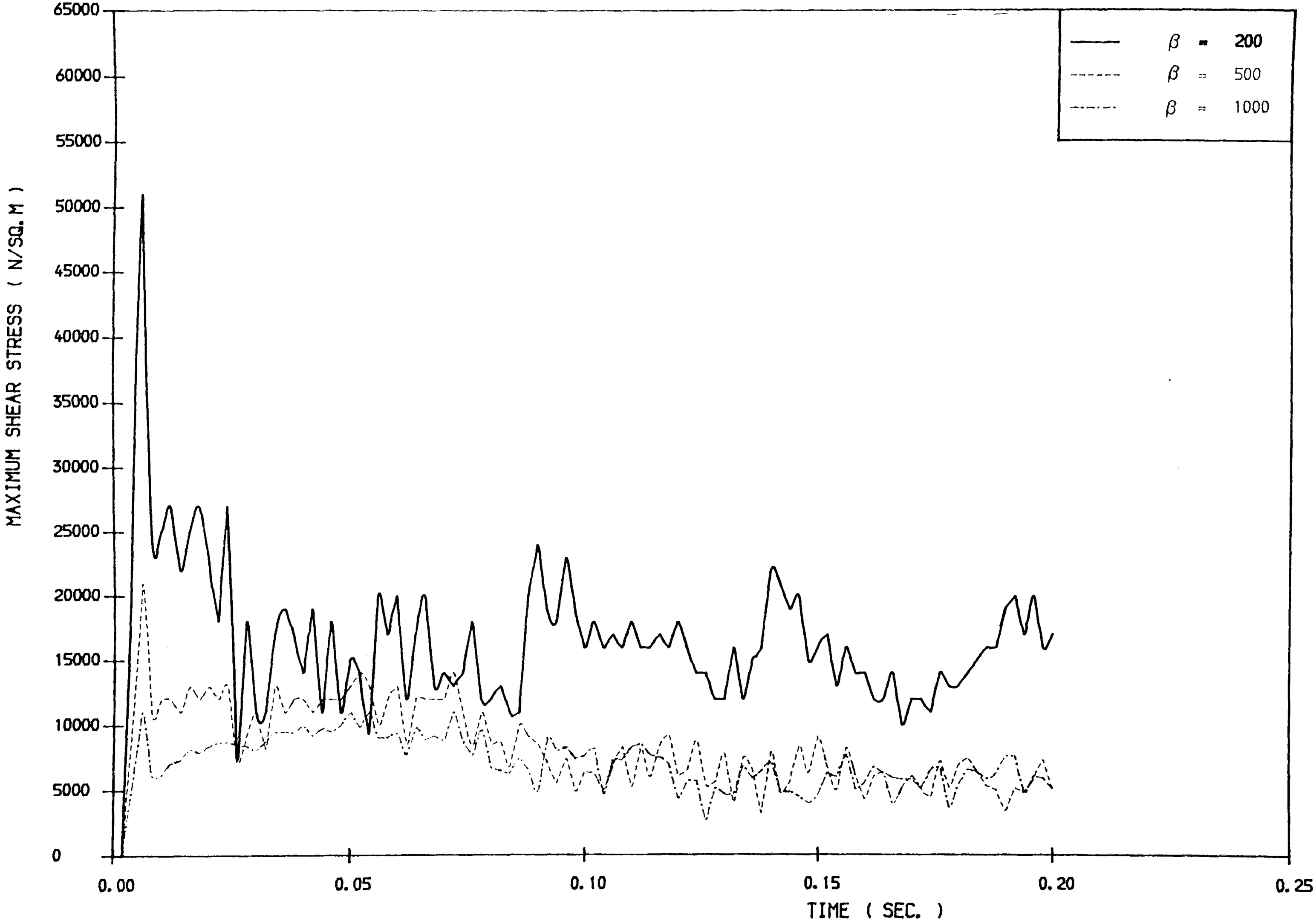

FIG. (5.17) MAXIMUM SHEAR STRESS IN SOIL UNDERNEATH PILE TIP_TIME RELATIONSHIP
(E = 10E6 N/SQ.M , α = 0.5 , P = 23E6 N/SQ.M)

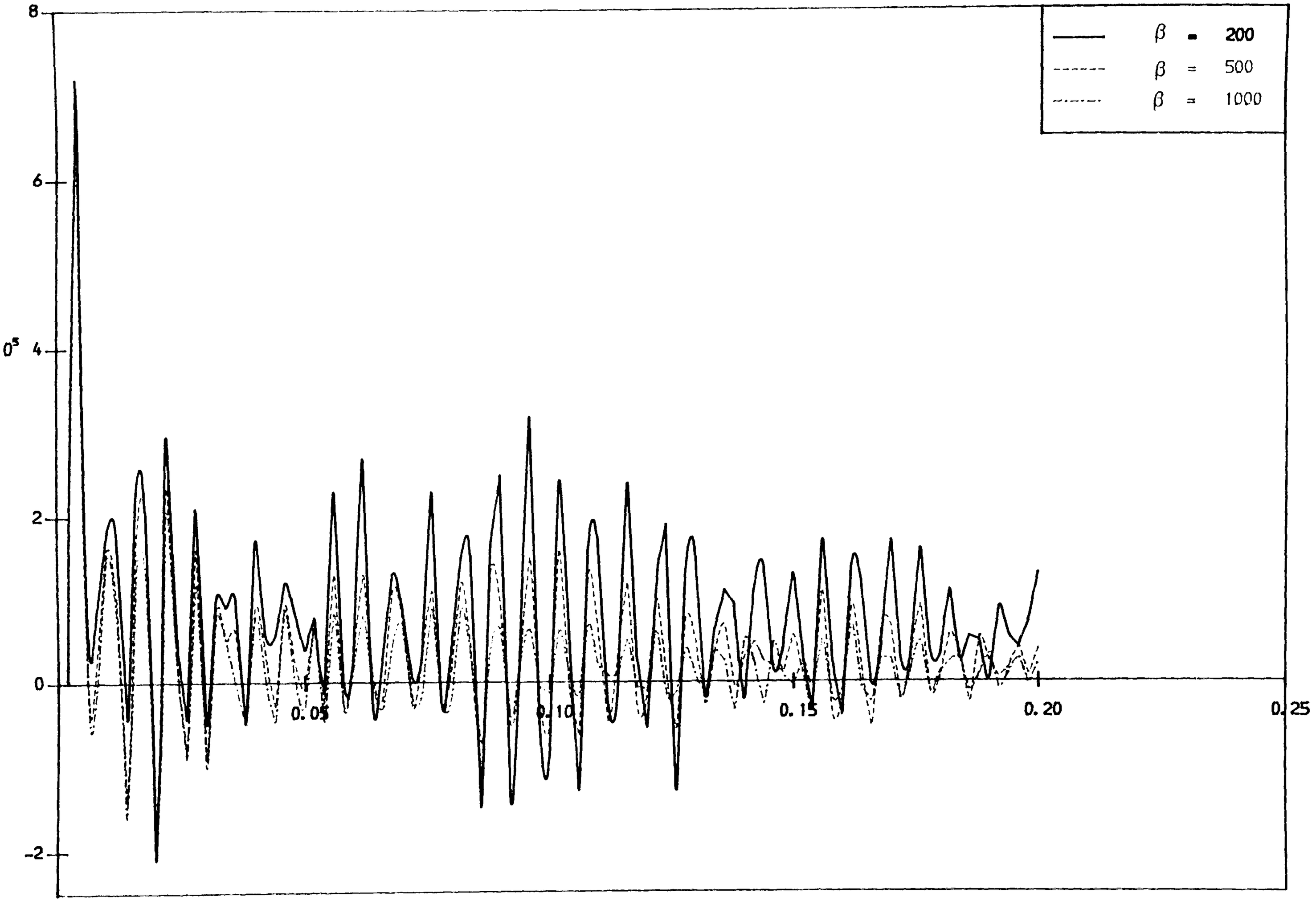

FIG. (5.18) MEAN STRESS IN SOIL UNDERNEATH PILE TIP_TIME RELATIONSHIP
(E = 10E6 N/SQ.M , α = 0.5 , P = 23E6 N/SQ.M)

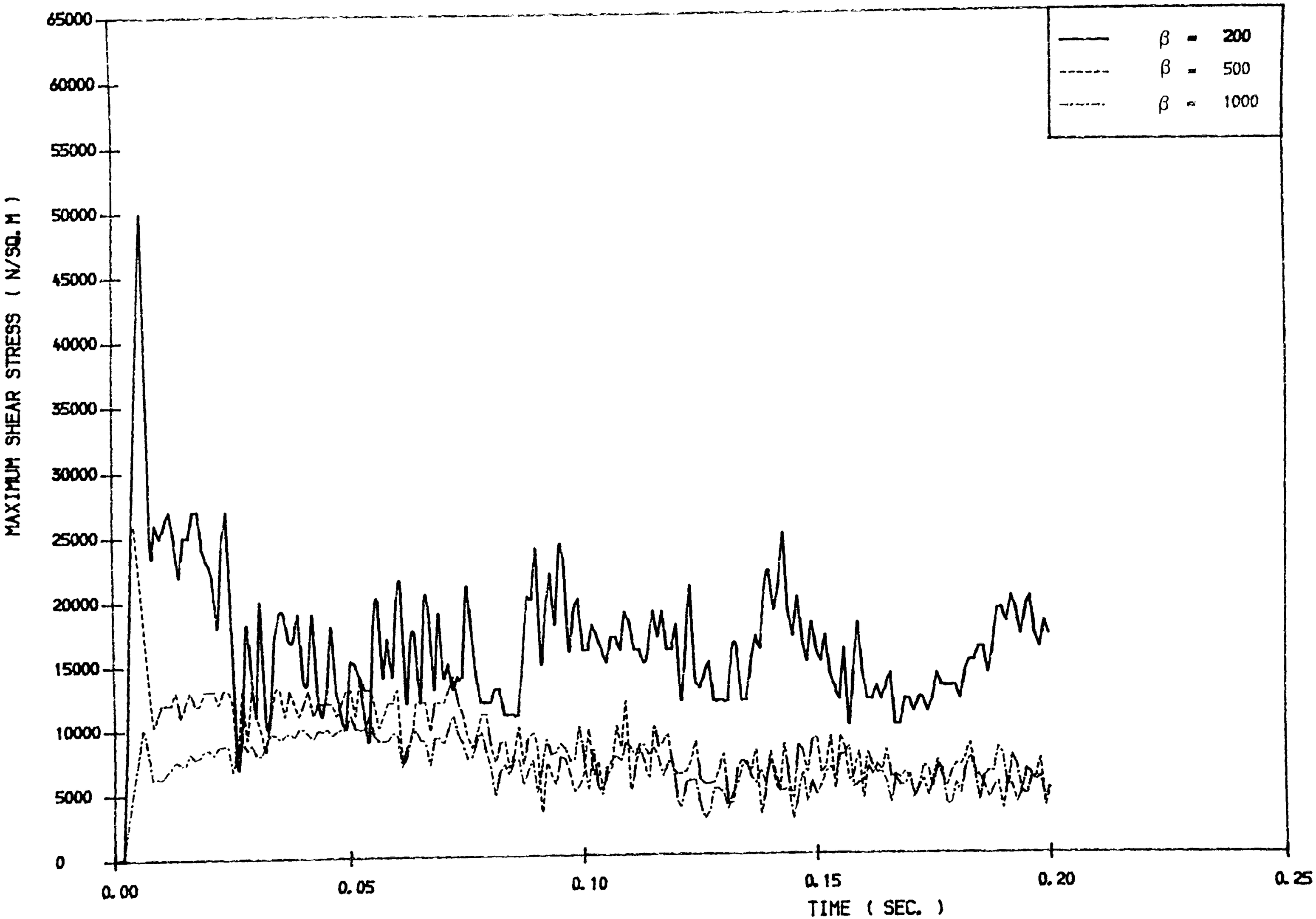

FIG. (5.19) MAXIMUM SHEAR STRESS IN SOIL UNDERNEATH PILE TIP_TIME RELATIONSHIP
(E = 10E6 N/SQ.M , α = 0.5 , P = 23E6 N/SQ.M)

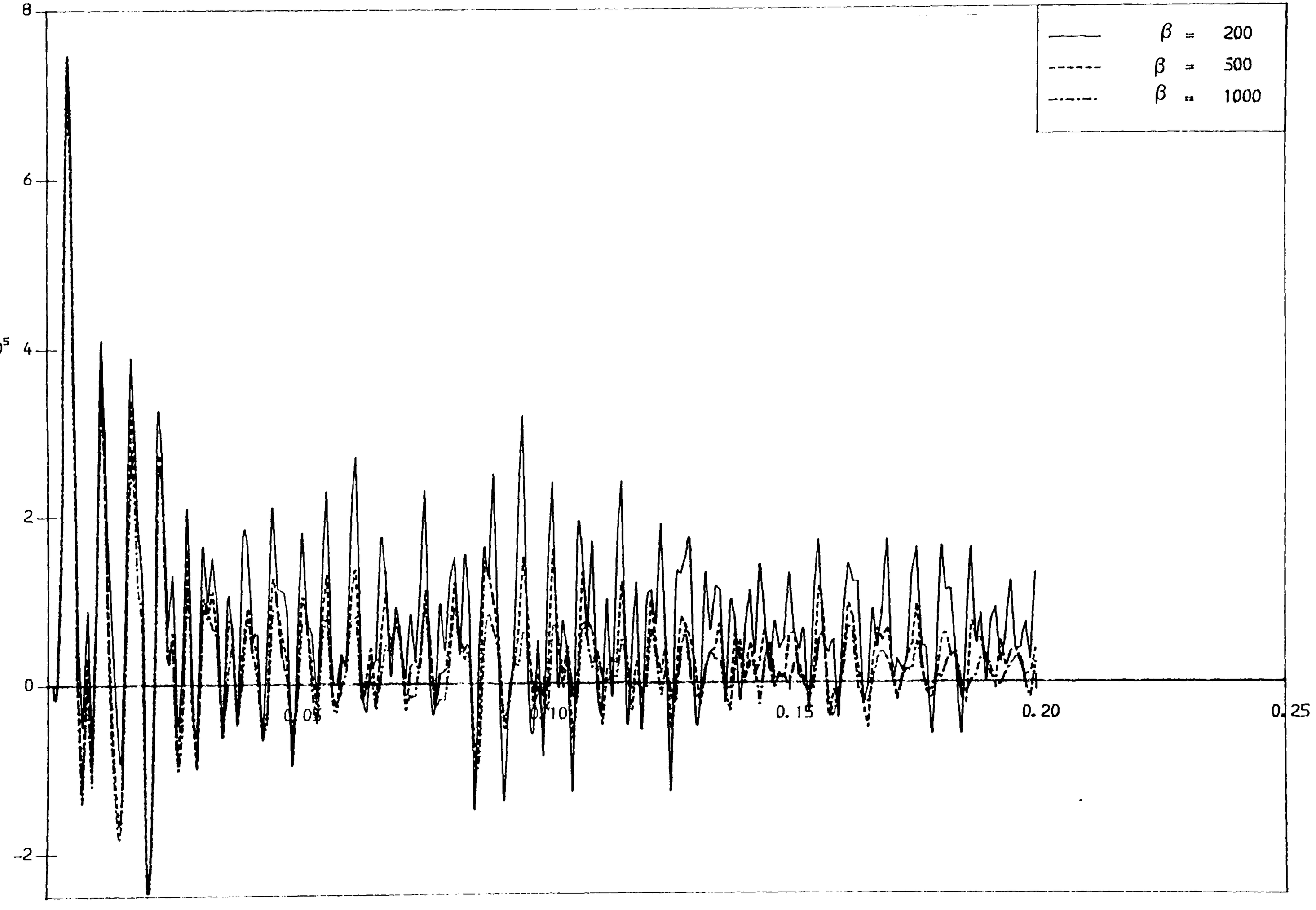

FIG. (5.20) MEAN STRESS IN SOIL UNDERNEATH PILE TIP_TIME RELATIONSHIP
(E = 10E6 N/SQ.M , α = 0.5 , P = 23E6 N/SQ.M)

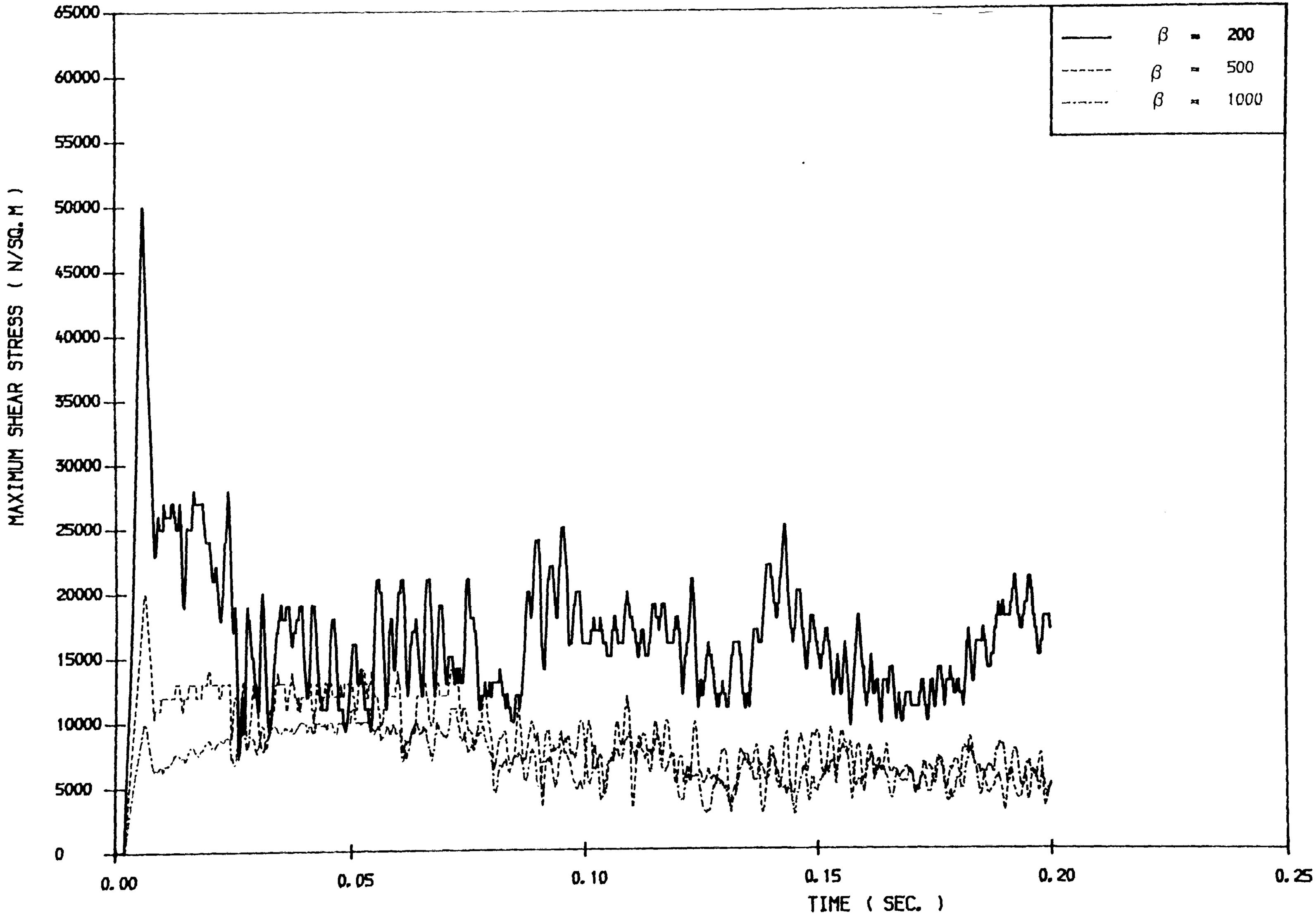

FIG. (5.21) MAXIMUM SHEAR STRESS IN SOIL UNDERNEATH PILE TIP_TIME RELATIONSHIP
(E = 10E6 N/SQ.M , α = 0.5 , P = 23E6 N/SQ.M)

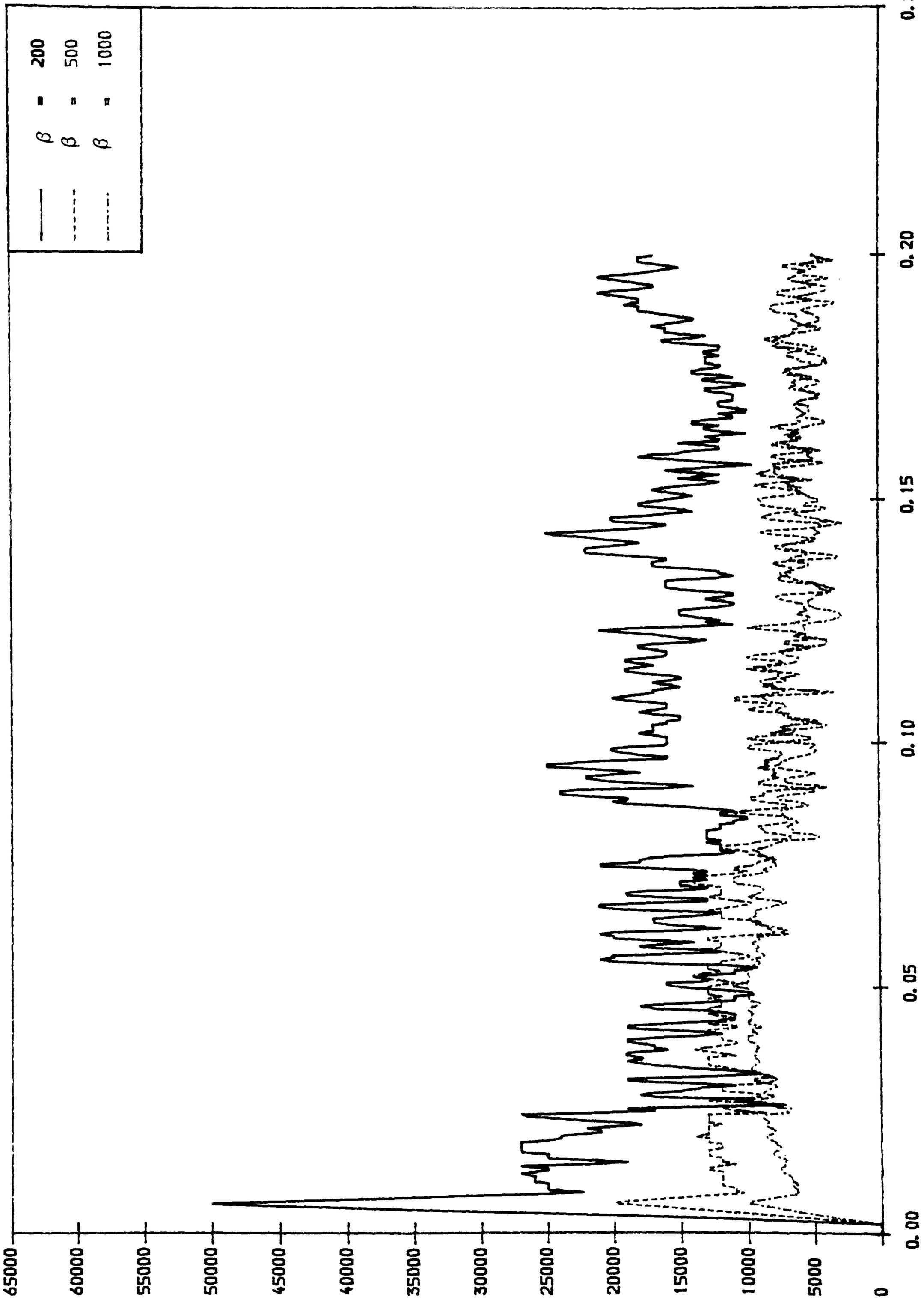

FIG. (5.22) MAXIMUM SHEAR STRESS IN SOIL UNDERNEATH PILE TIP_TIME RELATIONSHIP
(E = 10E6 N/SQ.M , α = 0.5 , P = 23E6 N/SQ.M)

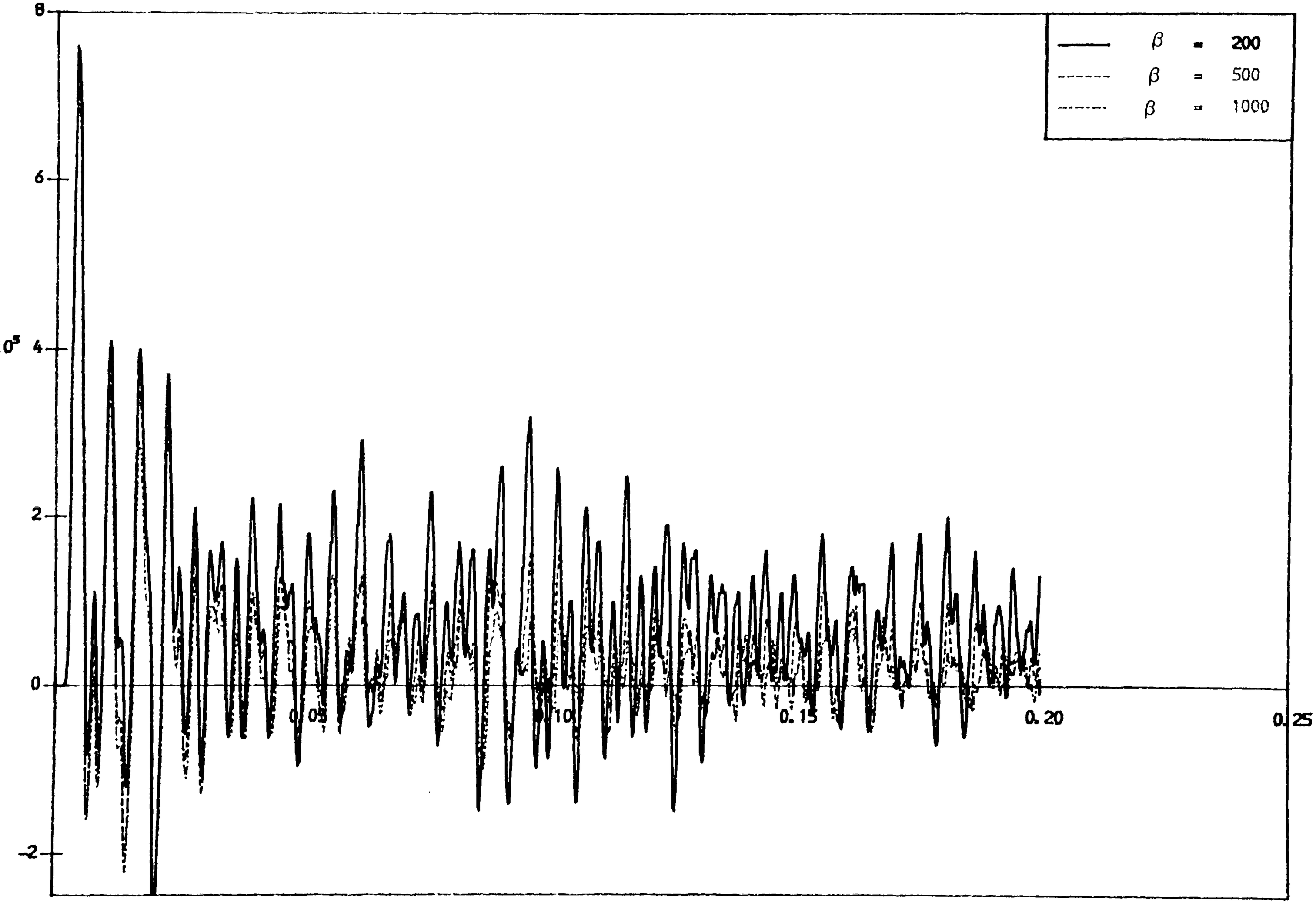

FIG. (5.23) MEAN STRESS IN SOIL UNDERNEATH PILE TIP_TIME RELATIONSHIP
(E = 10E6 N/SQ.M , α = 0.5 , P = 23E6 N/SQ.M)

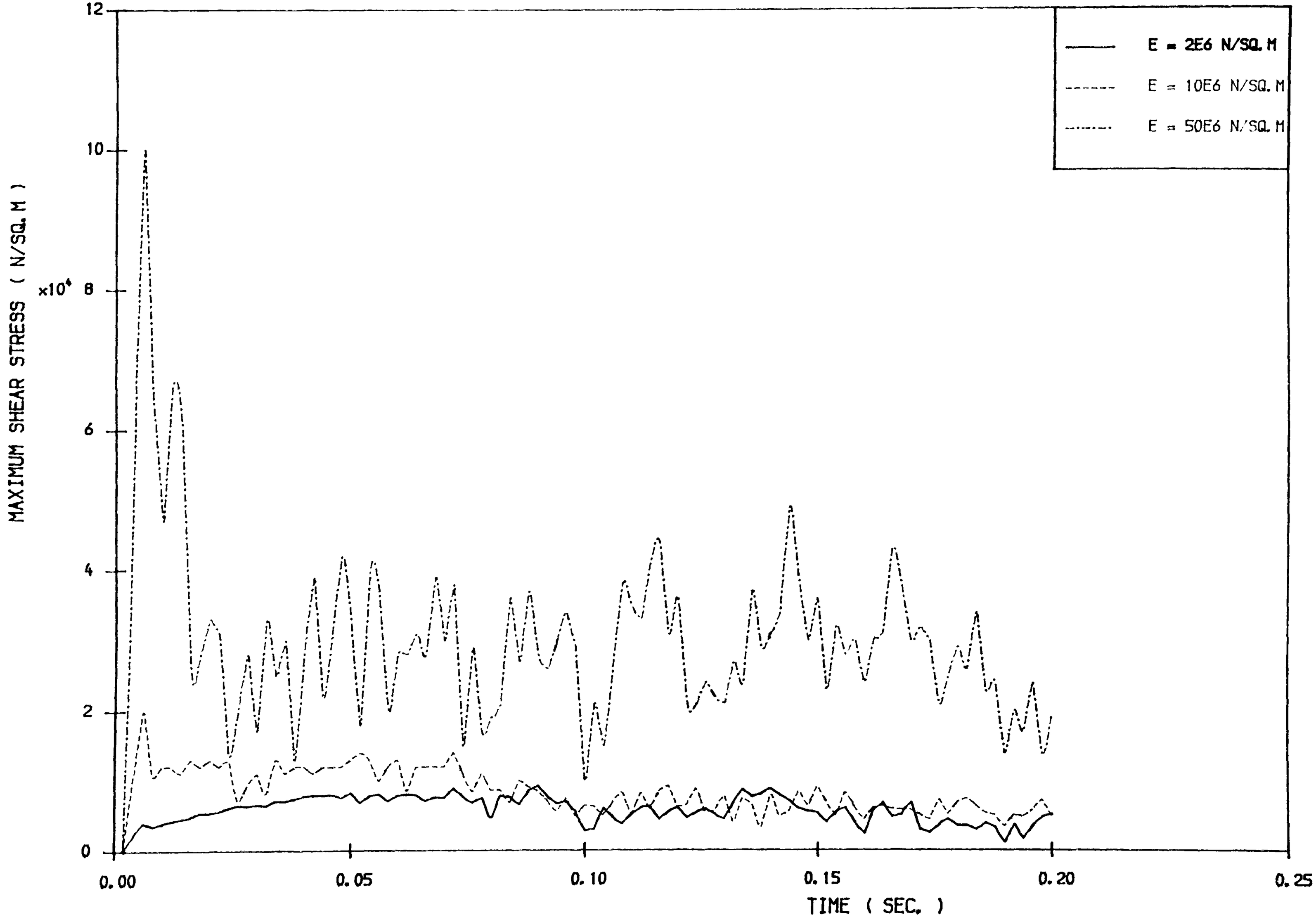

FIG. (5.24) MAXIMUM SHEAR STRESS IN SOIL UNDERNEATH PILE TIP_TIME RELATIONSHIP
(α = 0.5 , β = 500 , P = 23E6 N/SQ. M)

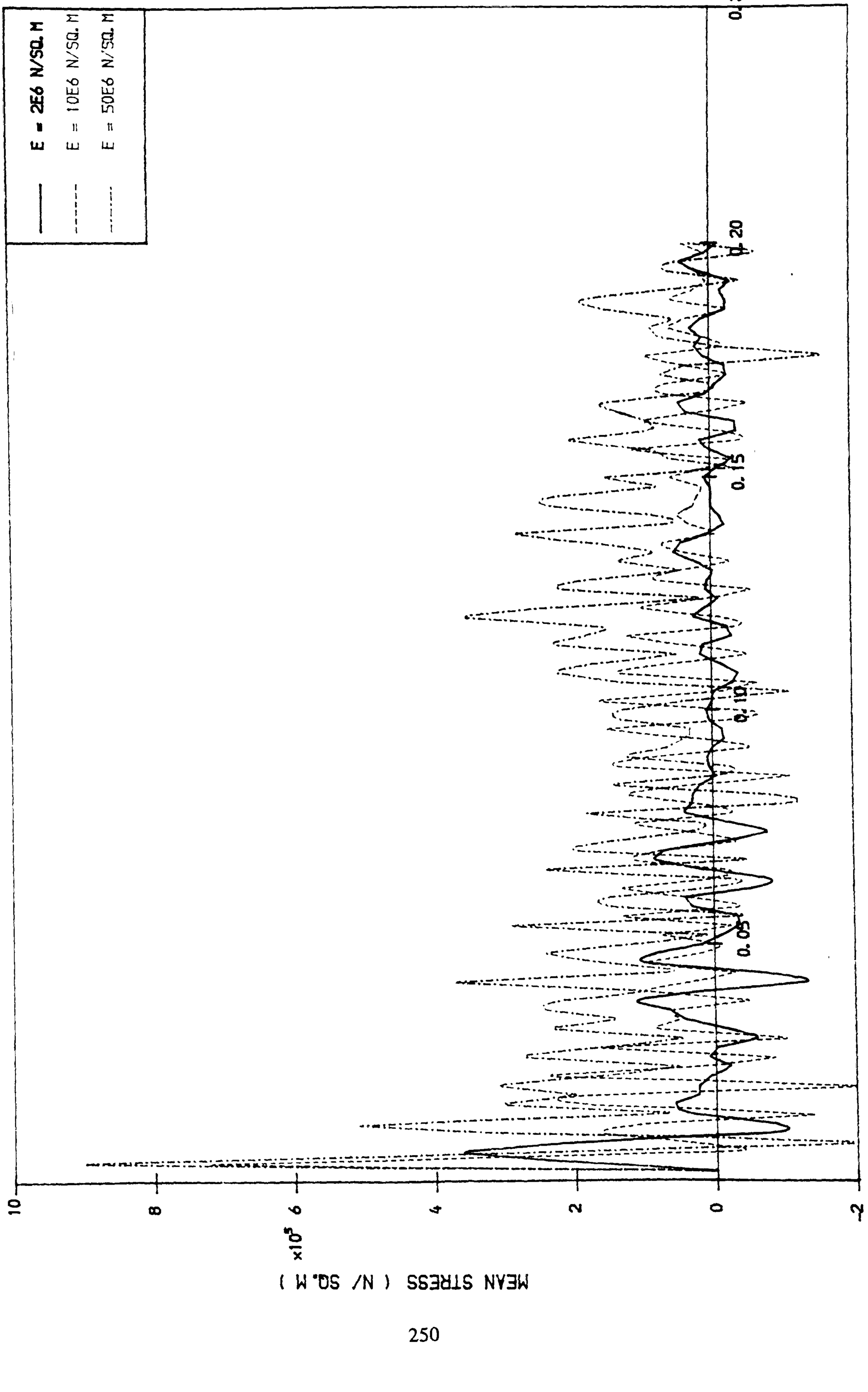

FIG. (5.25) MEAN STRESS IN SOIL UNDERNEATH PILE TIP_TIME RELATIONSHIP
(α = 0.5 , β = 500 , P = 23E6 N/SQ.M)

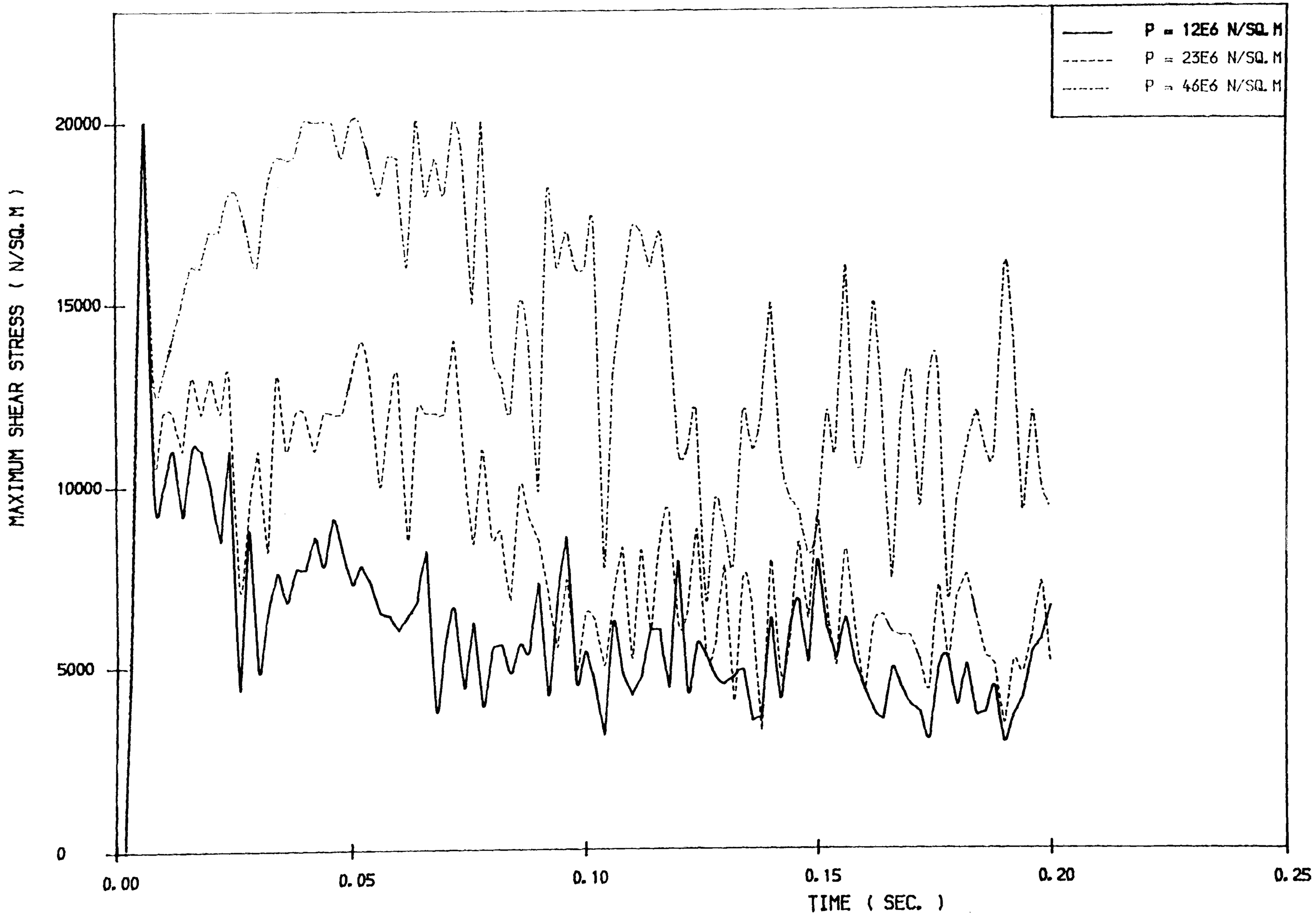

FIG. (5.26) MAXIMUM SHEAR IN SOIL UNDERNEATH PILE TIP_TIME RELATIONSHIP
(α = 0.5 , β = 500 , E = 10E6 N/SQ.M)

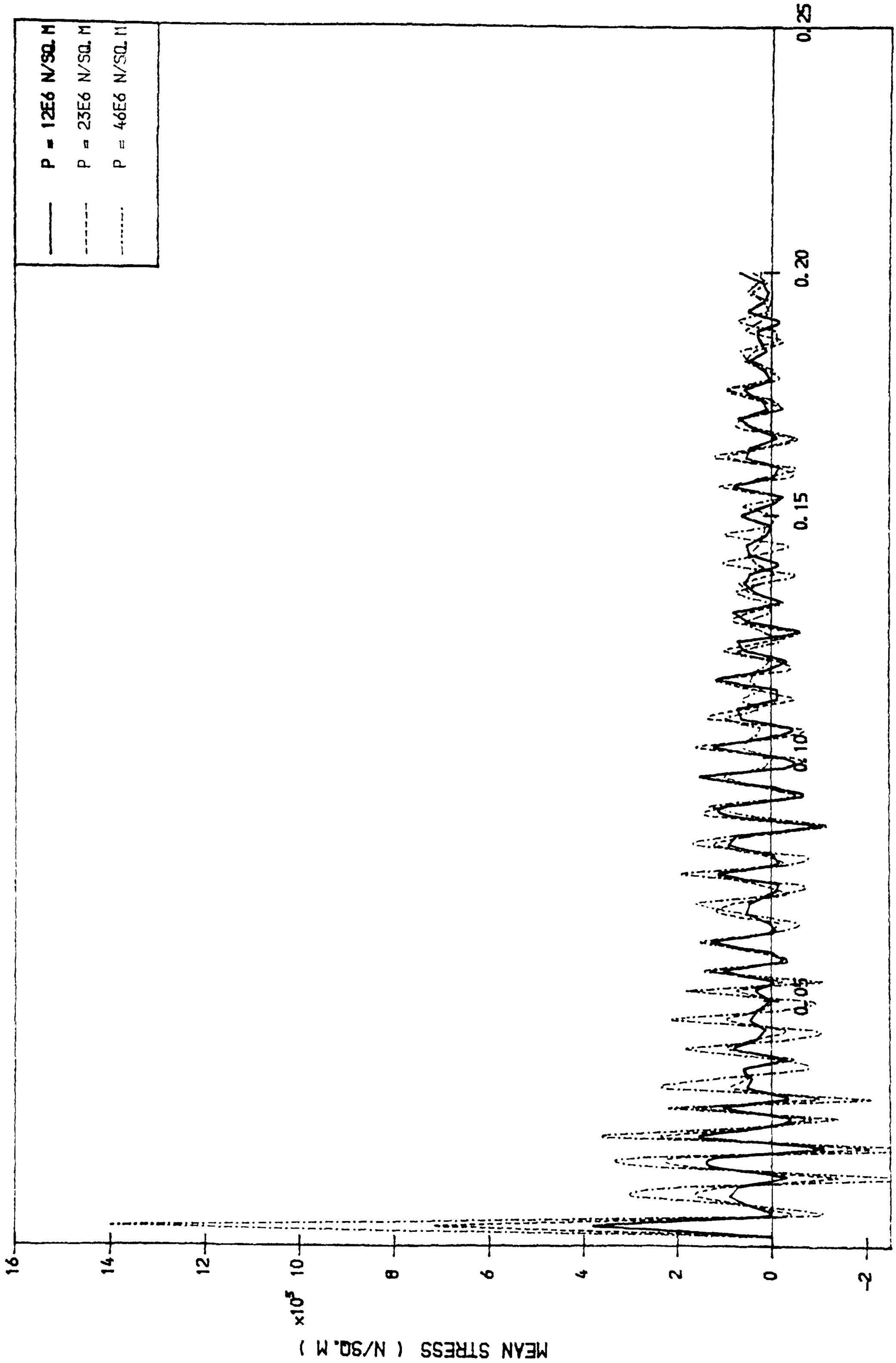
P = 12E6 N/SQ.M
P = 23E6 N/SQ.M
P = 46E6 N/SQ.M
0.25
0.20
0.15
TIME (SEC.)
UNDERNEATH PILE TIP_TIME RELATIONSHIP
(β = 500 , E = 10 N/SQ.M)
(5.27) MEAN STRESS IN SOIL U
(α = 0.5
FIG. (
16
14
12
10
8
6
4
2
0
-2
×10⁵
MEAN STRESS (N/SQ.M)

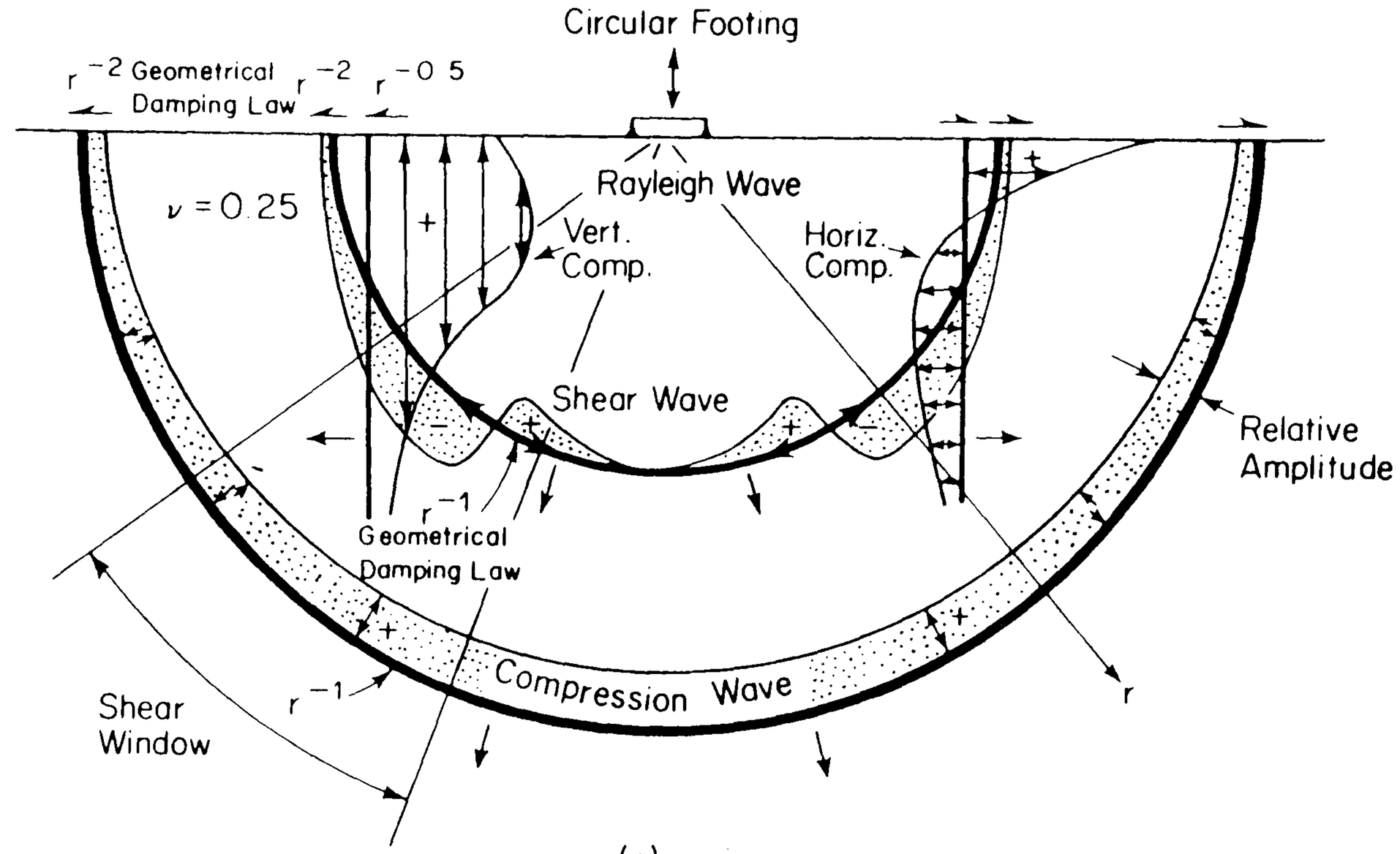

(a)

Wave Type	Per Cent of Total Energy
Rayleigh	67
Shear	26
Compression	7

(b)

FIGURE (5.28) DISTRIBUTION OF DISPLACEMENT WAVES FROM A CIRCULAR FOOTING ON A HOMOGENEOUS, ISOTROPIC, ELASTIC HALF_SPACE (AFTER WOODS, 1968)

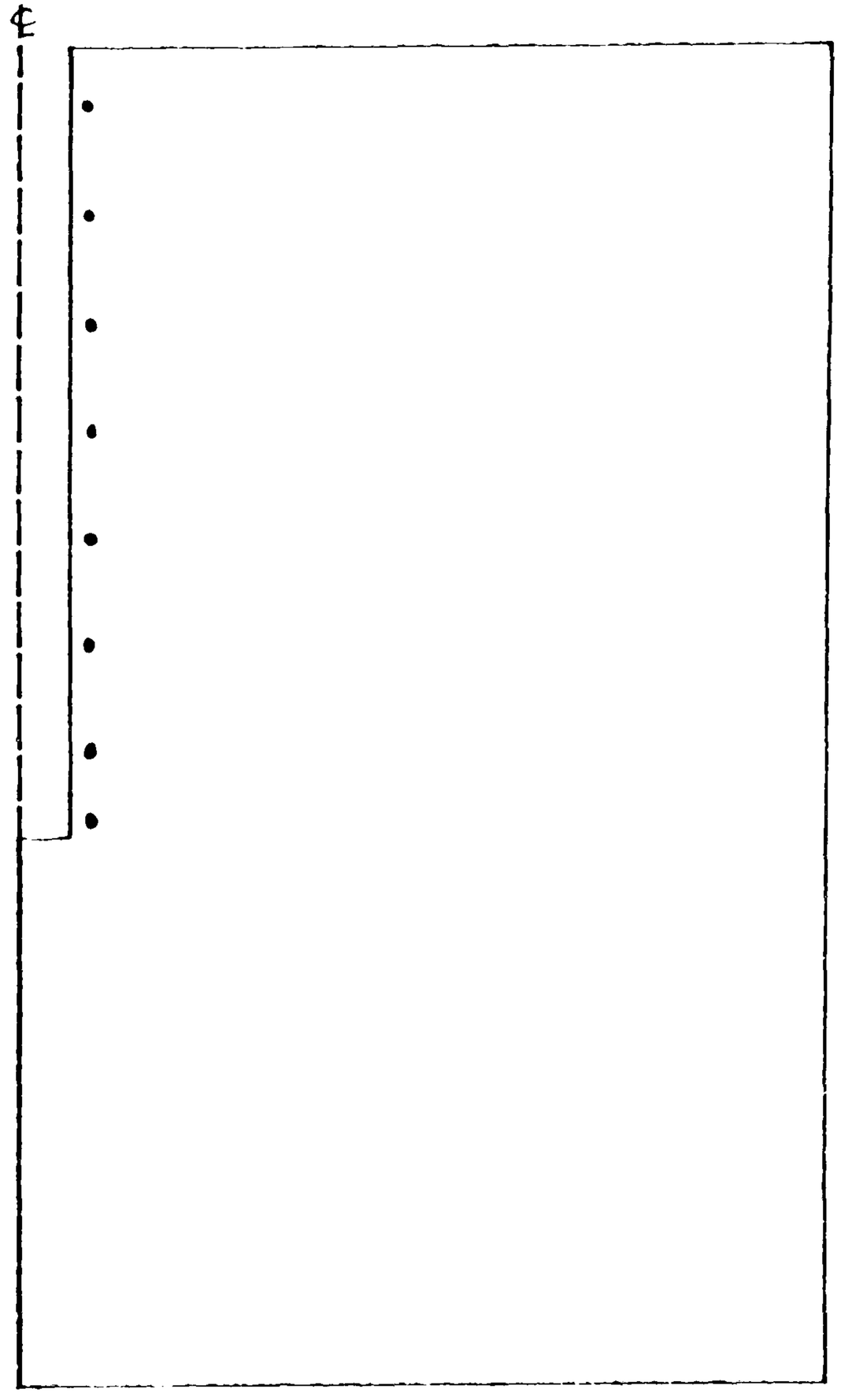

FIGURE (5.29) EVOLUTION OF FAILURE IN SOIL WITH TIME
(AT 2 MSEC.)

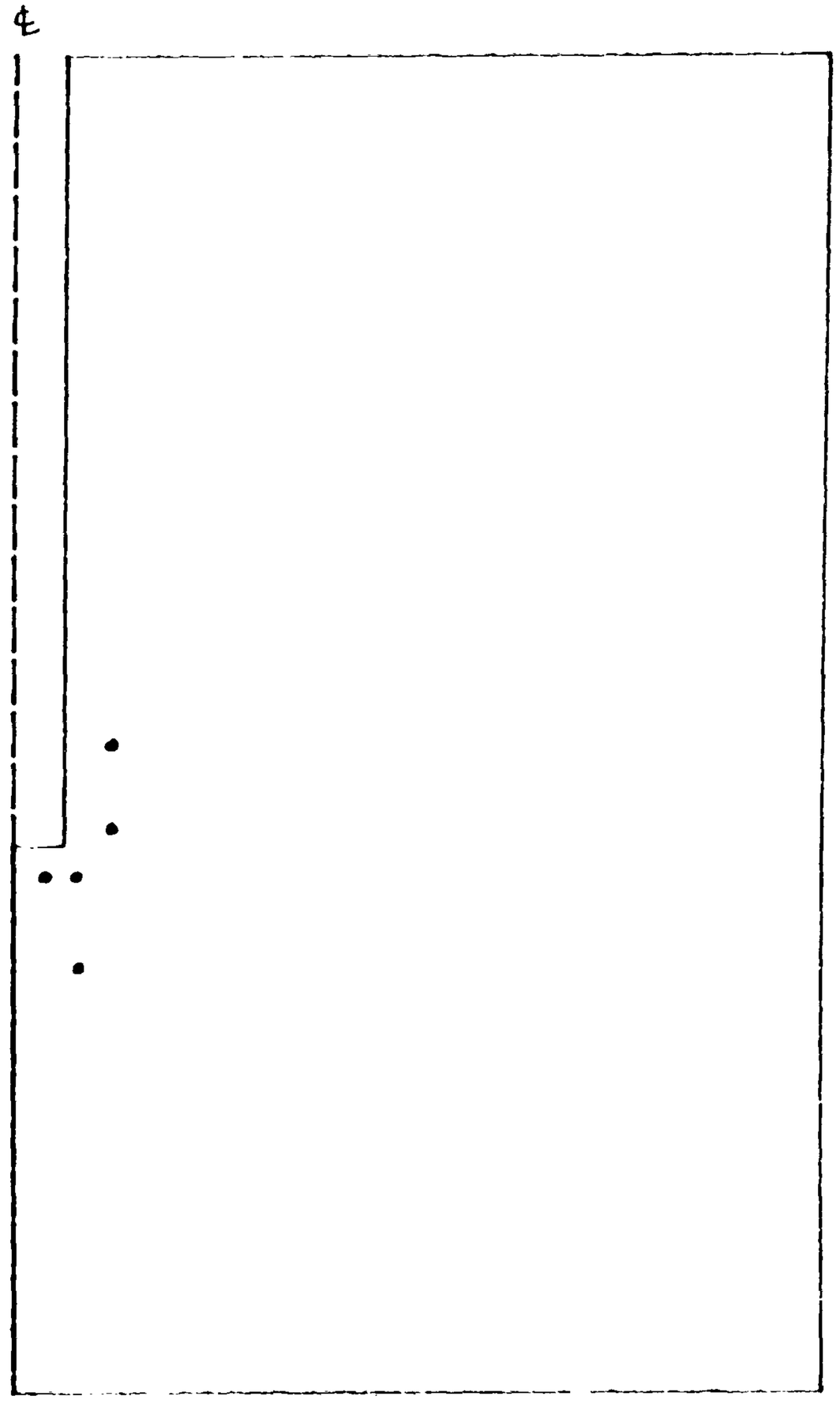

FIGURE (5.30) EVOLUTION OF FAILURE IN SOIL WITH TIME
(AT 4 MSEC.)

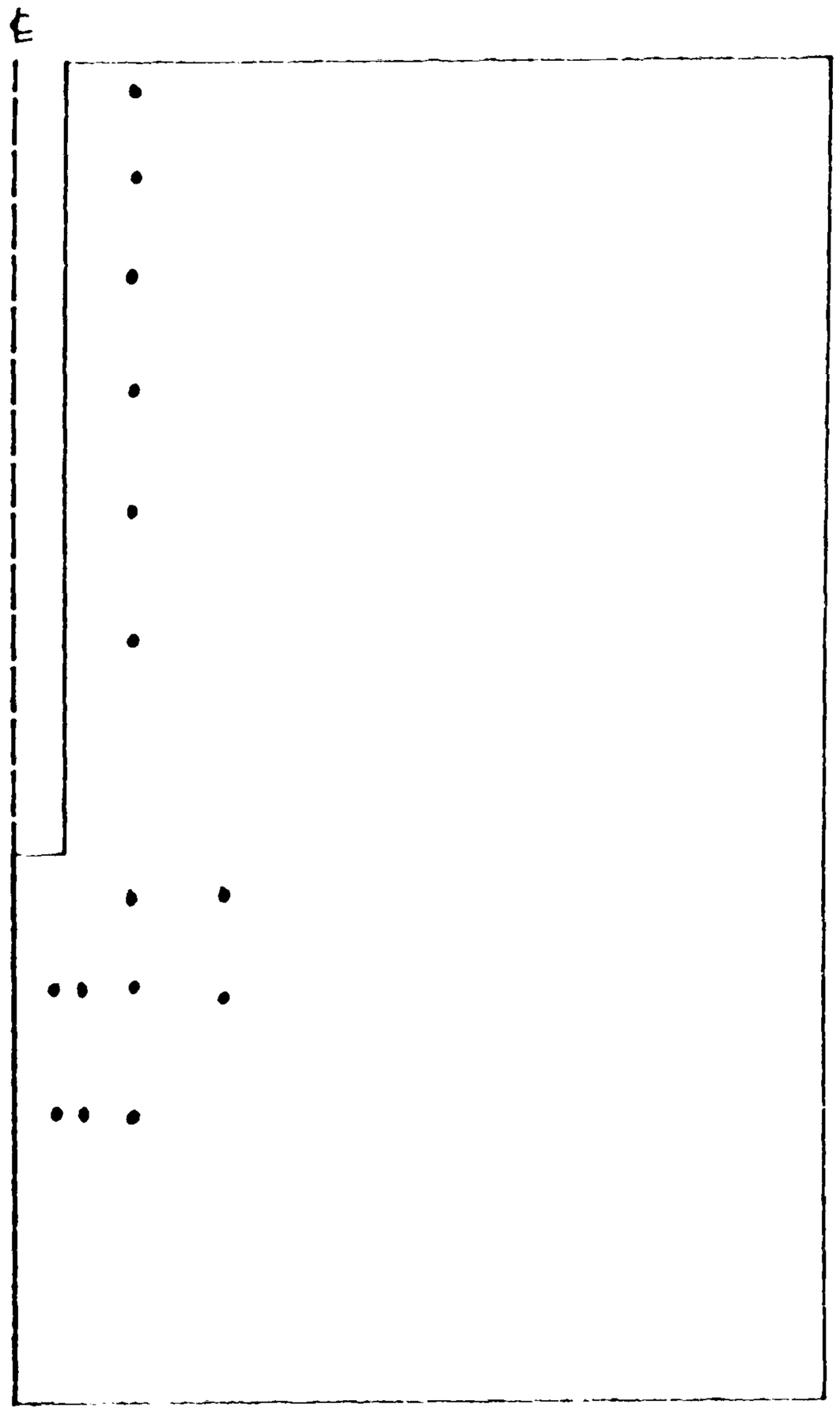

FIGURE (5.31) EVOLUTION OF FAILURE IN SOIL WITH TIME
(AT 8 MSEC.)

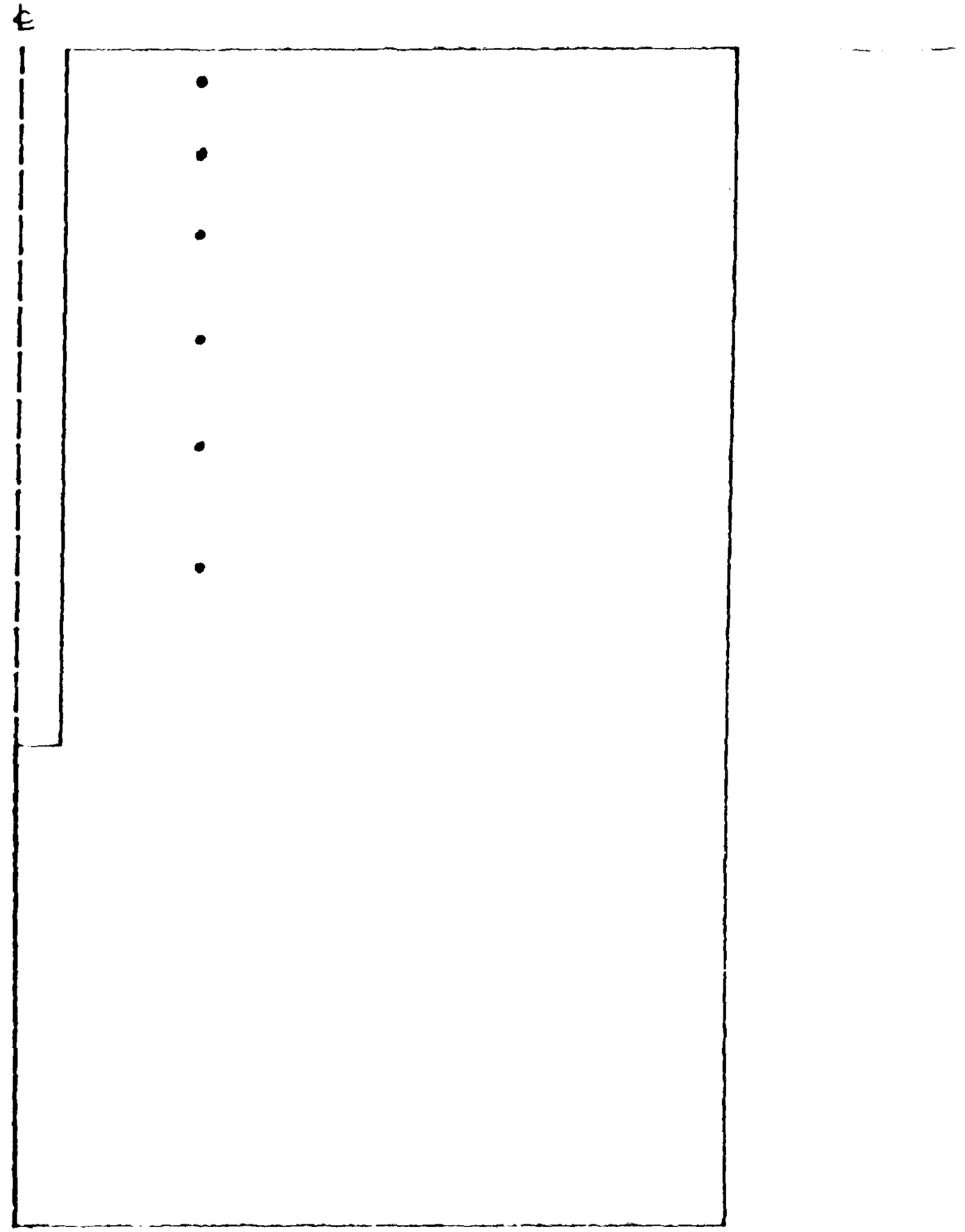

FIGURE (5.32) EVOLUTION OF FAILURE IN SOIL WITH TIME
(AT 32 MSEC.)

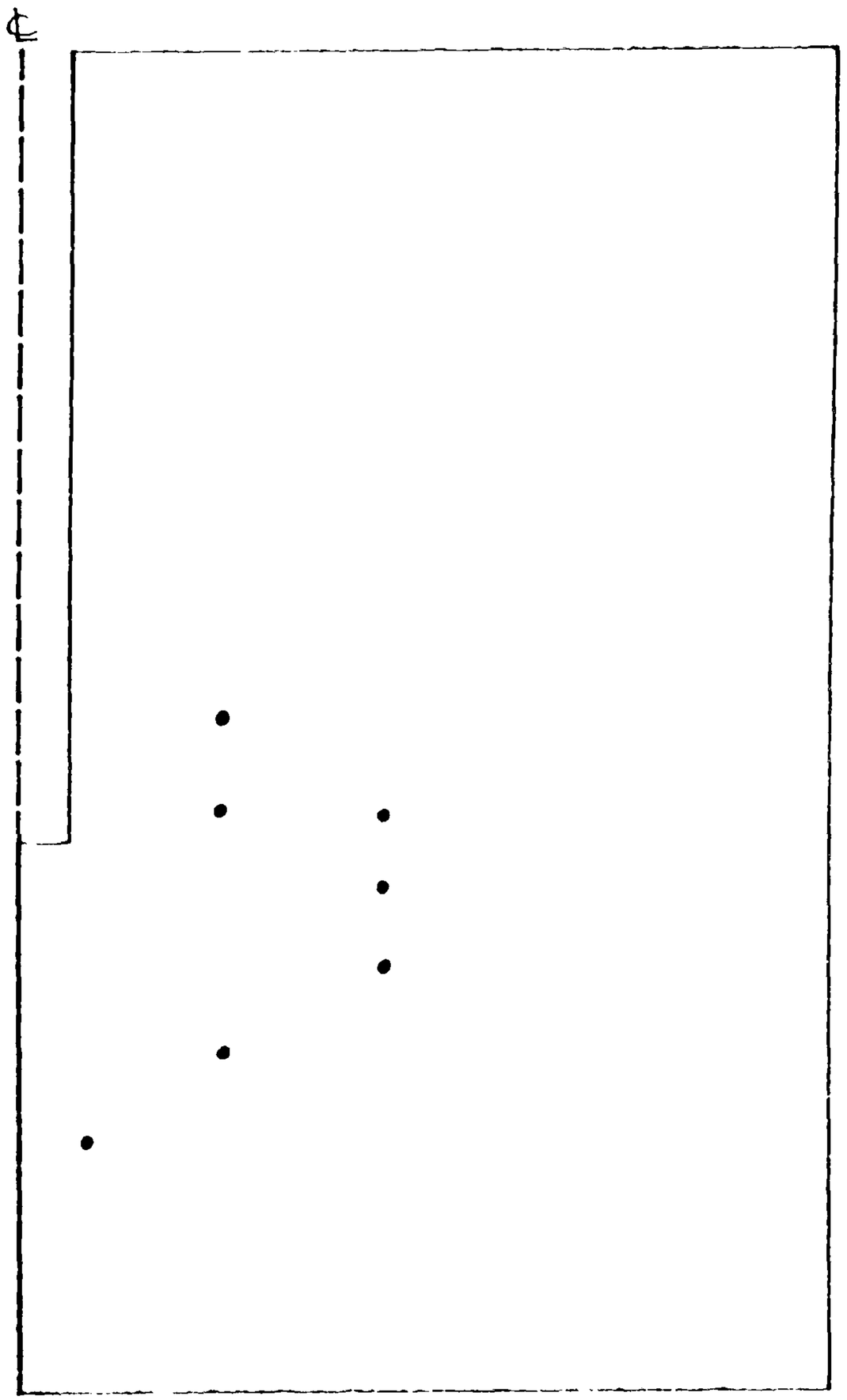

FIGURE (5.33) EVOLUTION OF FAILURE IN SOIL WITH TIME
(AT 64 MSEC.)

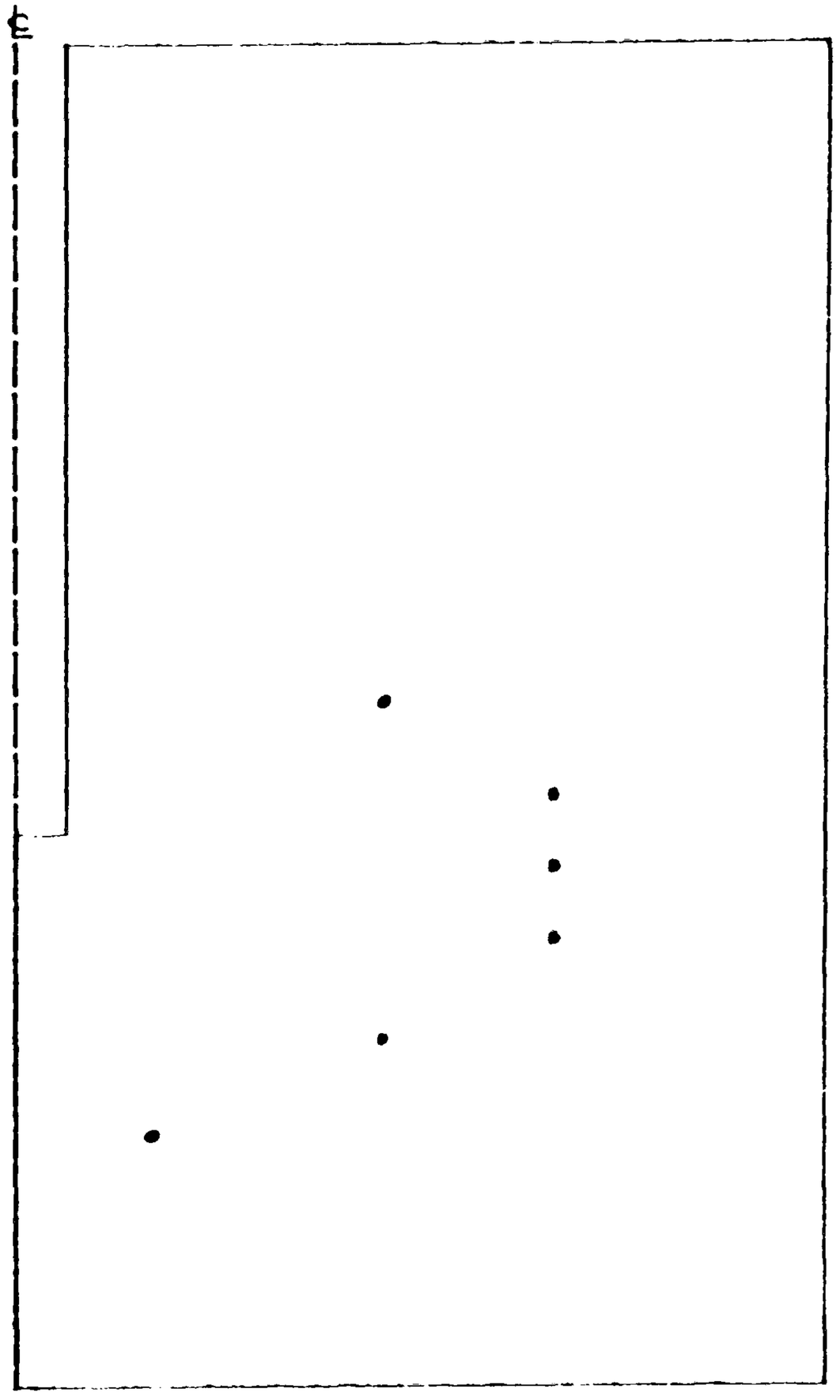

FIGURE (5.34) EVOLUTION OF FAILURE IN SOIL WITH TIME
(AT 128 MSEC.)

CHAPTER 6

CONCLUSIONS AND RECOMMENDATIONS FOR FUTURE STUDIES

6.1 CONCLUSIONS

6.2 RECOMMENDATIONS FOR FUTURE STUDIES

CHAPTER 6

CONCLUSIONS AND RECOMMENDATIONS FOR FUTURE STUDIES

6.1 CONCLUSIONS

The major thrust of this Thesis has been to compare alternative approaches to the dynamic analyses of pile driving. The methods considered include the pile driving formulae, single degree of freedom models, the wave equation method due to Smith (1960) and the finite element method of analysis. The single degree of freedom analysis (SDOF) involves the idealisation of the pile as a rigid mass while the soil is modelled as a slider–spring–dashpot mechanism. The SDOF model is probably comparable in accuracy to the well–known pile driving formulae, but it is not adequate from the practical point of view except perhaps for piling in very soft soils.

A computer program was developed based on the numerical solution of the wave equation described by Smith (1960) and a parametric study of the major hammer, cushion, pile and soil characteristics was undertaken. The results were compared with those obtained from the SDOF models and showed that pile compressibility was an important factor in pile driving performance. Basically rigid piles (SDOF) can be driven further into the ground than compressible piles.

From the results of the parametric study a new "pile driving formula", was developed which appears to give useful results. However, it is doubtful whether any simple analytical formula can provide results of wide generality.

Modelling of soil behaviour during pile driving should include the effect of remoulding and pore water pressure generation but these cannot be readily incorporated into numerical calculations. Thus the analyses in this Thesis are based on a total stress approach using the elastic–perfectly plastic Von Mises model as a description of the behaviour of saturated clay soils.

The dynamic finite element analyses of pile driving allows the soil to be explicitly included in the analysis using meaningful soil parameters and provides a more rigorous solution than either the elementary models or Smith's (1960) wave equation method. An implicit temporal integration is used since the relatively large time step sizes results in substantial cost savings by comparison with explicit schemes. However, computational costs are two or three orders of magnitude higher than those incurred in carrying out wave equation analyses.

The finite element analysis showed the evolution of the yielding zone around and beneath the pile propagating outwards from the pile directly after impact in the form of bands to some considerable distance.

6.2 RECOMMENDATIONS FOR FUTURE STUDIES

The Von Mises model has been used to simplify matters in this Thesis but the use of more sophisticated soil models (such as the Critical State Model) would give further insights into the behaviour of soils around driven piles during the driving process. This would allow some progress to be made into the problem of predicting pile "set–up" due to the reconsolidation of soils subsequent to pile driving.

There is also an urgent need to reduce computational costs and to that end utilisation of parallel processor technology may be useful although in the short term a more effective solution may be to develop boundary element solution algorithms. Possibly a hybrid FEM/BEM approach in which the far–field is represented by the boundary elements would be most effective strategy.

REFERENCES

AGERSCHOU, H.A. (1962) "Analysis of the Engineering News pile formula," Journal of the Soil Mechanics and Foundation Division, Proceedings of The American Society of Civil Engineers, vol. 88, No. SM5, pp. 1–11.

AKIYOSHI, T. (1978) "Compatible viscous boundary models," Journal of the Engineering Mechanics Division, Proceedings of The American Society of Civil Engineers, vol. 104, No. EM5, pp. 1253–1266.

ANGELIDES, D.C. and ROESSET, J.M. (1980) "Non–linear dynamic stiffness of piles," Research Report R80–13, Civil Engineering Department Massachusetts Institute of Technology, USA.

ATKINSON, J.H. and BRANSBY, P.L. (1978) "The Mechanics of Soils" an Introduction to Critical State Soil Mechanics," McGraw Hill Book Co., London.

AUTHIER, J. and FELLENIUS, B.H. (1980) "Quake values determined from dynamic measurements," International Seminar on The Application of Stress Wave Theory on Piles/ Stockholm / 4–5 June, pp. 197–216.

BATHE, K–J. and WILSON, E.L. (1976) "Numerical Methods in Finite Element Analysis," Prentice–Hall Inc., Englewood Cliffs, New Jersey, USA.

BETTESS, P. and ZIENKIEWICZ, O.C. (1977) "Diffraction and refraction of surface waves using finite and infinite elements," International Journal for Numerical Methods in Engineering, vol. 11, pp. 53–64.

BORJA, R.I. (1988) "Dynamics of pile driving by the finite element method," Computers and Geotechnics, vol. 5, pp. 39–49.

BRITTO, A.M. and GUNN, M.J. (1987) "Critical State Soil Mechanics via Finite Elements," Ellis Horwood Ltd., Chichester, West Sussex, England, U.K.

BURLAND, J.B. (1965) "The yielding and dilation of clay, correspondence,"

Geotechnique, vol. 15, pp.211–214.

CASAGRANDE, A. and SHANNON, W.L. (1948) "Stress deformation and strength of soils under dynamic loads," Proceedings of 2nd International Conference on Soil Mechanics and Foundation Engineering, ICSMFE, vol. V, pp. 29–34.

CELEP, Z. and BAZANT, Z.P. (1983) "Spurious reflection of elastic waves due to gradually changing finite element size," International Journal for Numerical Methods in Engineering, vol. 19, pp. 631–646.

CHELLIS, R.D. (1961) "Pile Foundations," Ch. 7 in Foundation Engineering, ed. by G.A. Leonards, McGraw–Hill, New York, USA.

CHOW, Y.K. (1981) "Dynamic behaviour of piles," Ph.D. Thesis, Manchester University, England, U.K.

CHOW, Y.K. and SMITH, I.M. (1981) "Static and periodic solid infinite elements," International Journal for Numerical Methods in Engineering, vol. 17, pp. 503–526.

CHOW, Y.K. and SMITH, I.M. (1984) "A numerical model for analysis of pile driveability," Proceedings of 2nd International Conference on The Application of Stress Wave Theory on Piles/ Stockholm / 27–30 May, pp. 319–325.

CORTE, J.–F. and LEPERT, P. (1986) "Lateral resistance during driving and dynamic pile testing," Proceedings of 3rd International Conference on Numerical Methods in Offshore Piling / Nantes–France / 21–22 May, pp.19–33.

COSTANTINO, C.J. (1967) "Finite element approach to stress wave problems," Journal of the Engineering Mechanics Division, Proceedings of The American Society of Civil Engineers, vol. 93, pp. 153–176.

COYLE, H.M. and REESE, L.C. (1966) "Load transfer for axially loaded piles in clay," Journal of the Soil Mechanics and Foundation Division, Proceedings of The American Society of Civil Engineers, vol. 92, No. SM2, pp. 1–26.

COYLE, H.M. and GIBSON, G.G. (1970) "Empirical damping constants for sand and clays," Journal of the Soil Mechanics and Foundation Division, Proceedings of the American Society of Civil Engineers, vol. 96, No. SM3, pp. 942–965.

COYLE, H.M., LOWERY,Jr., L.L. and HIRSCH, T.J. (1977) "Wave equation analysis of piling behaviour," Ch.8 in Numerical Methods in Geotechnical Engineering, ed. by DESAI, C.S. and CHRISTIAN, J.T., McGraw Hill Book Co., New York, USA.

CUNDALL, P.A., KUNAR, R.R., CARPENTER, P.C. and MARTI, J. (1978) " Solution of infinite dynamic problems by finite modelling in the time domain," Conference on Applied Numerical Modelling, Madrid, Sept.

CUMMINGS, A.E. (1940) "Dynamic pile driving formulas," Journal of Boston Society of Civil Engineers, vol. 27, pp. 6–27.

DAVIES, T.G. (1979) "Linear and non–linear analysis of pile groups," Ph.D. Thesis, University College Cardiff, Wales, U.K.

DAVIES, T.G. and BANERJEE, P.K. (1980) "Constitutive relationships for ocean sediments subjected to stress and tempereature gradients," Report No. AERE–R 9775 for U.K. Atomic Energy Authority, HARWELL, Oxfordshire.

DESAI, C.S. and CHRISTIAN, J.T. (1977) "Numerical Methods in Geotechnical Engineering," McGraw Hill Book Co., New York, USA.

DESAI, C.S. and GALLAGHER, R.H. (1983) editors of Proceedings, International Conference on Constitutive Laws for Engineering Materials–Theory and Application, 10–14 Jan. Arizona.

DESAI, C.S. and SAXENA, S.K. (1981) editors of Proceedings, Symposium on Implementation of Computer Procedures and Stress–Strain Laws in Geotechnical Engineering, Chicago, 3–6 August.

DESAI, C.S. and SIRIWARDANE, H.J. (1984) "Constitutive Laws for Engineering Materials, with Emphasis on Geologic Materials," Prentice–Hall, Inc., Englewood Cliffs, New Jersey, USA.

DESAI, C.S., ZAMAN, M.M., LIGHTNER, J.G. and SIRIWARDANE, H.J. (1984) "Thin layer element for interfaces and joints," International Journal for Numerical and Analytical Methods in Geomechanics, vol. 8, pp. 19–43.

ERINGEN, A.C. and SUHUBI, E.S. (1974) "Elasto Dynamics," Vol. I & Vol. II, Academic Press, New York, USA.

EBECKEN, N.F.E., LIMA, E.C.P., LANDAU, L. and COUTINHO, A.L.G.A. (1984) "Numerical simulation of pile driving by finite elements; some applications on the Brazilian coast," Proceedings 2nd International Conference on The Application os Stress Wave Theory on Piles/ Stockholm/ 27–30 May, pp.350–359.

FLAATE, K. (1964) "An investigation of the validity of three pile driving formulae in cohesionless materials," Norwegian Geotechnical Institute, Publications No. 56, pp. 11–22.

FOREHAND, P.W. and REESE,Jr., J.L. (1964) "Prediction of pile capacity by the wave equation," Journal of the Soil Mechanics and Foundation Division, Proceedings of The American Society of Civil Engineers, vol. 90, No. SM2, pp. 1–25.

FOX, E.N. (1932) "Stress phenomena occuring in pile driving," Engineering, vol. 134, 2nd Sept., pp. 263–265.

GHABOUSSI, J., WILSON, E.L. and ISENBERG, J. (1973) "Finite element for rock joints and interfaces," Journal of the Soil Mechanics and Foundation Division, Proceedings of The American Society of Civil Engineers, vol. 99, No. SM10, pp. 833–848.

GOBLE, G.G. and RAUSCHE, F. (1976) "WEAP – wave equation analysis of pile driving," Vol. I–III, Report No. FHWA IP–76–14, Federation Highway Administration, July.

GOBLE, G.G., RAUSCHE, F. and LINKINS,Jr., G.E. (1980) "The analysis of pile driving, a state–of–the–art," International Seminar on The Application of Stress Wave Theory on Piles / Stockholm / 4–5 June, pp. 131–161.

GOODMAN, R.E., TAYLOR, R.L. and BREKKE, T.L. (1968) "A model for the mechanics of jointed rock," Journal of the Soil Mechanics and Foundation Division, Proceedings of The American Society of Civil Engineers, vol. 94, No. SM3, pp. 637–659.

GRAFF, K.F. (1975) "Wave Motion in Elastic Solids," Ohio State University Press, USA.

GRIFFITHS, D.V. (1985) "Numerical modelling of interfaces using conventional finite elements," Proceedings of 5th International Conference on Numerical Methods in Geomechanics / Nagoya–Japan / 1–5 April, pp. 837–844.

HANNIGAN, P.I. (1984) "Large quake development during driving of low displacement piles," Proceedings of 2nd International Conference on Application of Stress Wave Theory on Piles / Stockholm / 27–30 May, pp. 118–125.

HANSEN, L.A. and SCHROEDER, W.L. (1977) "Penetration resistance for driven piling," Journal of the Construction Division, Proceedings of The American Society of Civil Engineers, vol. 103, No. CO3, pp. 513–528.

HEUZE, F.E. and BARBOUR, T.G. (1982) "New models for rock joints and interfaces," Journal of the Geotechnical Engineering Division, Proceedings of The American Society of Civil Engineers, vol. 108, No. GT5, pp. 757–776.

HILBER, H.M., HUGHES, T.J.R. and TAYLOR, R.L. (1977) "Improved numerical dissipation for time integration algorithms in structural dynamics," Earthequake Engineering and Structural Dynamics, vol. 5, No. 3, pp. 283–292.

HILEY, A. (1930) "Pile driving calculations with notes on driving forces and ground resistance," The Structural Engineer, vol. 8, July–August.

HILL, R. (1950) "The Mathematical Theory of Plasticity," Pergamon Press, U.K.

HINTON, E. and OWEN, D.R.J. (1977) "Finite Element Programming," Academic Press, London.

HIRSCH, T.J., LOWERY, L.L., COYLE, H.M. and SAMSON, C.H. (1970) "Pile

driving analysis by one dimensional wave theory : A state of the art," Highway Research Record, No. 333, pp. 33–54.

HOLMES, N. and BELYTSCHKO, T. (1976) "Postprocessing of finite element transient response calculations by digital filters," Computers and Structures, vol. 6, pp. 211–216.

HOUSEL, W.S. (1966) "Pile load capacity estimates and test results," Journal of the Soil Mechanics and Foundation Division, Proceedings of the American Society of Civil Engineers, vol. 92, No. SM4, pp. 1–29.

HUGHES, T.J.R. and LIU, W.K. (1978a) "Implicit–Explicit finite elements in transient analysis : stability theory," Journal of Applied Mechanics, Transactions of the American Society of Mechanical Engineers, vol. 45, pp. 371–374.

HUGHES, T.J.R. and LIU, W.K. (1978b) "Implicit–Explicit finite elements in transient analysis : Implementation and numerical examples," Journal of Applied Mechanics, Transactions of The American Society of Mechanical Engineers, vol. 45, pp. 375–378.

ISAACS, D.V. (1931) "Reinforced concrete pile formulas," Transactions of The Institute of Engineers, Australia, vol. 12, pp. 313–323.

ISENBERG, J. and VAUGHAN, D.K. (1981) "Non–linear effects in soil structure interaction," Proceedings Symposium on Implementation of Computer Procedures and Stress–Strain Laws in Geotechnique Engineering / Chicago–Illinois / ed. by DESAI and SAXENA, vol. 1, pp. 29–45.

KATO, S., SOHRI, T. and GOULD, P.L. (1986) "A modified thin–layered far field soil element for soil structure interaction of axisymmetric structures," Computer and Geotechnics, vol. 2, pp 167–184.

KAUSEL, E. (1974) "Forced vibrations of circular foundations in layered media," MIT Research Report RT74–11, Soil Publication No. 336, Structures Publication No.384, Massachusetts Institute of Technology, Cambridge, Mass., USA.

KATONA, M.G. (1983) "A simple contact friction interface element with application to buried culvert," International Journal for Numerical and Analytical Methods in Geomechanics, vol. 7, pp. 371–384.

KEZDI, A. (1957) "Bearing capacity of piles and pile groups," Proceedings 4th International Conference Soil Mechanics and Foundations Engineering, vol.2, ICE, London, pp.46–51.

KEZDI, A. (1975) "Pile foundations," Ch. 19 in Foundation Engineering Handbook, ed. by H.F. Winterkorn and H–Y Fang; Published by Van Nostrand Reinhold Co., N.W.

KUHLEMEYER, R.L. (1979) "Vertical vibration of piles," Journal of Geotechnical Engineering Division, Proceedings of The American Society of Civil Engineers, vol. 105, No. GT2, pp. 273–287.

LEE, S.L., CHOW, Y.K., KARUNARATNE, G.P. and WONG, K.Y. (1988) "Rational wave equation model for pile driving analysis," Journal of the Geotechnical Engineering Division, Proceedings of The American Society of Civil Engineers, vol. 114, No. GE3, pp. 306–325.

LITKOUHI, S. and POSKITT, T.J. (1980) "Damping constants for pile driveability calculations," Geotechnique, vol. 30, No. 1, pp. 77–86.

LYSMER, J. and KUHLEMEYER, R.L. (1969) "Finite dynamic model for infinite media," Journal of the Engineering Mechanics Division, Proceedings of The American Society of Civil Engineers, vol. 95, No. EM4, pp. 859–877.

LYSMER, J., UDAKA, T., TSAI, C.F. and SEED, H.B. (1975) "FLUSH computer program for approximate 3–D analysis of soil structure interaction problems," Report No. EERC 65–30, University of California, Berkely, USA.

LYSMER, J. and WAAS, G. (1972) "Shear waves in plane infinite structure," Journal of the Engineering Mechanics Division, Proceedings of The American Society of Civil Engineers, vol. 98, No. EM1, pp. 85–105.

MURAYAMO, S. and SCHOFIELD A.N. (1977) " Constitutive equations of soils,"

Special session 9, Proceedings, 9th ICSMFE, vol. 3, pp. 537–546, Tokyo.

NAYLOR, D.J. and PANDE, G.N. (1981) "Finite Elements in Geotechnical Engineering," Pineridge Press, Swansea, Wales, U.K.

NEWMARK, N.M. (1959) "A method of computation for structural dynamics," Journal of the Engineering Mechanics Division, Proceedings of the American Society of Civil Engineers, vol.85, No.EM3, pp.67–94.

NOGAMI, T. and KONAGAI, K. (1987) "Dynamic response of vertically loaded non–linear pile foundation," Journal of the Geotechnical Engineering Division, Proceedings of the American Society of Civil Engineers, vol. 113, No. GT2, pp. 147–160.

NOVAK, M. (1977) "Vertical vibration of floating piles," Journal of the Engineering Mechanics Division, Proceedings of The American Society of Civil Engineers, No. EM 103, pp. 153–168.

NOVAK, M. (1985) "Analysis of hammer foundations," Proceeding of 2nd International Conference for Dynamics and Earthquake Engineering, June–July a board QE 2, NY to Southampton, CML Publications, pp.4.60–4.70.

OLSEN, R.E. and FLAATE, K.S. (1967) "Pile driving formulas for friction piles in sand," Journal of the Soil Mechanics and Foundation Division, Proceedings of The American Society of Civil Engineers, vol. 93, No. SM5, pp. 59–73.

OWEN, D.R.J. and HINTON, E. (1980) "Finite Element in Plasticity, Theory and Practice," Pineridge Press, Swansea, Wales, U.K.

PALMER, A.C. (1973) editor of Proceedings, Symposium on Role of Plasticity in Soil Mechanics, Cambridge, 13–15 Sept.

PANDE, G.N. and SHARMA, K.J. (1979) "On joint/interface elements and associated problems of numerical ill–conditioning," International Journal of Numerical Methods in Geomechanics, vol. 14, pp. 293–300.

PARRY, R.G.H. (1972) editor of Proceedings, Roscoe Memorial Symposium:

Stress–Strain Behaviour of Soils, Henley–on–Thames, Foulis, USA.

POULOS, H.G. and DAVIS, E.H. (1980) "Load Capacity by Dynamic Methods," Ch.4 in Pile Foundation Analysis and Design, John Wiley and Sons., New York, USA.

RANDOLPH, M.F., CARTER, J.P. and WROTH, C.P. (1979) "Driven piles in clay – the effect of installation and subsequent consolidation," Geotechnique, vol. 29, No. 4, pp. 361–393.

RANDOLPH, M.F. and SIMONS, H.A. (1986) "An improved soil model for one dimensional pile driving analysis," Proceedings of 3rd International Conference on Numerical Methods in Offshore Piling/ Nantes–France / 21–22 May, pp.3–17.

RAUSCHE, F., MOSES, F. and GOBLE, G.G. (1972) "Soil resistance predictions from pile dynamics," Journal of the Soil Mechanics and Foundation Division, Proceedings of The American Society of Civil Engineers, vol. 89, No. SM9, pp. 917–937.

RAUSCHE, F., GOBLE, G.G. and LINKINS, G.E. (1985) "Dynamic determination of pile capacity," Journal of Geotechnical Engineering Division, Proceedings of The American Society of Civil Engineers, vol.111, No.GT3, pp.367–383.

RAO, S.S. (1982) "The Finite Element Method in Engineering," Pergamon Press, Oxford.

RICHART,Jr., F.E. (1962) "Foundation Vibrations," Transactions of The American Society of Civil Engineers, vol. 127, part 1, pp. 863–898.

RICHART,Jr., F.E. and WHITMAN, R.V. (1967) "Comparison of footing vibration tests with theory," Journal of the Soil Mechanics and Foundation Division, Proceedings of The American Society of Civil Engineers, vol. 93, No. SM6, pp. 143–168.

RIGDEN, W.J., PETTIT, J.J., St.JOHN, H.D. and POSKITT, T.J. (1979) "Developments in piling for Offshore structures," BOSS'79, Proceedings of 2nd

International Conference on Behaviour of Offshore Structures, Imperial College, London, 28–31 Aug., pp. 279–296.

ROSCOE, K.H., SCHOFIELD, A.N. and WROTH, C.P. (1958) "On the yielding of soils," Geotechnique, vol. 8, pp. 22–53.

SAMSON, C.H., HIRSCH, T.J. and LOWERY, L.L. (1963) "Computer study of dynamic behaviour of piling," Journal of the Structural Division, Proceedings of The American Society of Civil Engineers, vol. 89, No. ST4, pp. 413–449.

SCHOFIELD, A.N. and WROTH, C.P. (1968) "Critical State Soil Mechanics," McGraw Hill Book Co., London.

SEED, H.B. and IDRISS, I.M. (1970) "Soil moduli and damping factors for dynamic response analysis," Report No. EERC 70–10, University of California, Berkeley, USA.

SEED, H.B. and LUNDGREN, R. (1954) "Investigation of the effect of transient loading on the strength and deformation characterstics of saturated sands," Proceedings of the American Society for Testing and Materials, ASTM, vol. 54, pp. 1288–1306.

SHANTARAM, D., OWEN, D.R.J. and ZIENKIEWICZ, O.C. (1976) "Dynamic transient behaviour of two– and three–dimensional structures including plasticity, large deformation effects and fluid interaction," International Journal of Earthquake Engineering and Structural Dynamics, vol. 4, pp. 561–578.

SHIBATA, T., SEKIGUCHI, H., MATSUMOTO, T., KITA, K. and MOTOYAMA, S. (1989) "Pile driveability assessment by wave form analysis," Proceedings of 12th International Conference on Soil Mechanics and Foundation Engineering, ICSMFE, Rio de Janeiro–Brazil, pp. 1–14/4–14.

SHIPLEY, S.A., LEISTNER, H.G. and JONES, R.E. (1968) "Elastic wave propagation – a comparison between finite element predictions and exact solutions," Proceedings International Symposium on Wave Propagation and Dynamic Properties of Earth Materials, 23–25 Aug., University of New Mexico Press, pp. 509–519.

SIMONS, H.A. (1985) "A theoretical study of pile driving," Ph.D. Thesis, University of Cambridge, England, U.K.

SIMONS, H.A., and RANDOLPH, M.F. (1986) "Comparison of transmitting boundaries in dynamic finite element analyses using explicit time integration," International Journal for Numerical and Analytical Methods in Geomechanics, vol. 10, pp. 329–342.

SMITH, E.A.L. (1955) "Impact and longitudinal wave transmission," Transactions of The American Society of Mechanical Engineers, Aug., pp. 963–973.

SMITH, E.A.L. (1960) "Pile driving analysis by the wave equation," Journal of the Soil Mechanics and Foundation Division, Proceedings of The American Society of Civil Engineers, vol. 86, No. SM4, pp. 35–61.

SMITH, I.M. (1976) "Finite element analysis of axially loaded pile capacity and driveability," Report to Fugro–Cesco B.V., March.

SMITH, I.M. (1978) "Transient phenomena of Offshore foundations," Ch.15 in Numerical Methods in Offshore Engineering, ed. by O.C. ZIENKIEWICZ, R.W. LEWIS and K.G. STAGG, Pub. by John Wiley and Sons., London.

SMITH, I.M. (1981) "Some time dependent soil–structure interaction problems," Ch.8 in Finite Element in Geomechanics, ed. by G. GUDEHUS, pp. 251–291.

SMITH, I.M. (1982) "Programming The Finite Element Method with Application to Geomechanics," John Wiley and Sons., Chichester, U.K.

SMITH, I.M. and CHOW, Y.K. (1982) "Three–dimensional analysis of pile driveability," Proceedings 2nd International Conference on Numerical Methods in Offshore Piling, Austin, Texas, USA, pp. 1–19.

SMITH, W.D. (1974) "A non–reflecting plane boundary for wave propagation problems," Journal of Computational Physics, vol. 15, pp. 492–503.

TAYLOR, D.W. (1948) "Action of piles, pile foundations," Ch. 20 in Fundamentals of Soil Mechanics, John Wiley and Sons., New York, USA.

TO, W.T.P. (1985) "Dynamic response of footings and piles," Ph.D. Thesis, Manchester University, England, U.K.

TO, W.T.P. and SMITH, I.M. (1988) "A note on finite element simulation of pile driving," International Journal for Numerical and Analytical Methods in Geomechanics, vol. 12, No. 2, pp. 213–219.

VALLIAPPAN, S. and ANG, K.K. (1985) "Dynamic analysis applied to rock mechanics problems," Proceedings of 5th International Conference on Numerical Methods in Geomechanics / Nagoya–Japan / 1–5 April, vol. 1, pp. 119–132.

WAAS, G. (1972) "Linear two dimensional analysis of soil dynamics in semi–infinite layered media," Ph.D. Thesis, University of Calif. at Berkely, USA.

WERKLE, H. (1986) "Dynamic finite element analysis of three dimensional soil models with a transmitting element," Journal of Earthquake Engineering and Structural Dynamics, vol. 14, pp. 41–60.

WERKLE, H. (1987) "A transmitting boundary for the dynamic finite element analysis of cross–anisotropic soils," Journal of Earthquake Engineering and Structural Dynamics, vol. 15, pp. 831–838.

WHITAKER, T. (1970) "The Design of Piled Foundations," Pergamon, Oxford, UK.

WHITE, W., VALLIAPPAN, S. and LEE, I.K. (1977) "Unified boundary for finite dynamic models," Journal of the Engineering Mechanics Division, Proceedings of The American Society of Civil Engineers, vol. 13, No. EM5, pp. 949–964.

WHITMAN, R.V. and RICHART,Jr., F.E. (1967) "Design procedures for dynamically loaded foundations," Journal of the Soil mechanics and Foundation Division, Proceedings of The American Society of Civil Engineers, vol. 93, No. SM6, pp. 169–193.

WILLSON, S.M. (1985) "Finite element of piles and pentrometers," Ph.D. Thesis, Manchester University, England, U.K.

WILSON, E.L. (1981) "Finite elements for foundations, joints and fluids," Ch. 10 in Finite Elements in Geomechanics, ed. by G. GUDEHUS, pp. 319–350.

WOOD, D.M. (1984) "On stress parameters," Geotechnique, vol. 34, No. 2, pp. 282–287.

WOODS, R.D. (1968) "Screening of surface waves in soils," Journal of the Soil Mechanics and Foundation Division, Proceedings of The American Society of Civil Engineers, vol. 94, pp. 951–979.

WU, K.H., KUHLEMEYER, R.L. and TO, C.W.S. (1986) "Pile shaft soil model for wave equation analysis: verification by dynamic finite element approach," Proceeding of 3rd Canadian Conference on Marine Geotechnical Engineering, 11–13 June.

YIP, K.L. and POSKITT, T.J (1986) "Monitoring pile–soil interaction during driving," Computer Applications in Geotechnical Engineering, Proceeding of Midland Geotechnical Society, 16–17 April, pp. 127–136.

YONG, R.K. and KO, H.Y. (1981) "Proceedings, Workshop on Limit Equlibrium, Plasticity and Generalised Stress–Strain in Geotechnical Engineering," McGill University, 28–30 May, ASCE.

ZAMAN, M.M. (1985) "Evaluation of thin–layer element and modelling of interface behaviour in soil structure interaction," Proceeding of 5th International Conference on Numerical Methods in Geomechanics,/ Nagoya–Japan / 1–5 April, pp. 1797–1803.

ZIENKIEWICZ, O.C. (1971) "The Finite Element Method in Engineering Science," McGraw Hill Book Co., Maidenhead, U.K.

ZIENKIEWICZ, O.C. (1977) "The Finite Element Method," McGraw Hill Book Co., London.

ZIENKIEWICZ, O.C., BEST, B., DULLAGE, C. and STAGG, K.C. (1970) "Analysis of non–linear problems in rock mechanics with particular reference to jointed rock systems," Proc. of 2nd Int. Soc. of Rock Conf./ Belgrad/ pp. 8–14.

APPENDIX A

COMPUTER PROGRAM

A.1 INTRODUCTION

A.2 PROGRAM DESCRIPTION

A.3 INPUT PARAMETERS

A.4 RUN TIMES

APPENDIX A

COMPUTER PROGRAM

A.1 INTRODUCTION

The MIXDYN program used in this study is based on a program developed by Owen and Hinton (1980) but which has been enhanced to deal with infinite boundaries by implementing the viscous boundary of Lysmer and Kuhlemeyer (1969). This Appendix does not fully document the program MIXDYN since further information is readily available in the book by Owen and Hinton (1980).

A.2 PROGRAM DESCRIPTION

The finite element computer program MIXDYN, based on the Implicit–Explicit integration scheme, Hughes and Liu (1978*a*), can be used to solve two–dimensional plane strain (stress) and axisymmetric non–linear dynamic (harmonic or transient) problems. It accommodates geometric and material (elasto–plastic) non–linearity by adopting a total Lagrangian formulation. The interpolation functions (in space) are based on four, eight or nine noded quadrilateral isoparametric finite elements. Four yield criteria (Tresca, Von Mises, Drucker–Prager and Mohr–Coulomb) are currently coded into the program although alternatives may be easily incorporated if desired.

The program structure is depicted in Fig. A.1. Basically, the program consists of nine modules (composed of one or more subroutines) each with a distinct operational function. The master routine, MIXDYN, organises the calling of the main routines as depicted in Fig. A.1. In the subroutine CONTOL, control parameters are read to check the maximum problem dimensions. The following subroutines namely, INPUTD, INTIME and PREVOS read the mesh data, the

time data and the data for the current state of the structure, respectively. Subroutine LINKIN, links the rest of the program with the profile equation solver. Subroutine LUMASS and LOADPL generate the lumped mass and applied force vectors, respectively. This process is then followed by the calculation and assembly of the global stiffness matrix, in the subroutine GSTIFF. In the time step loop, subroutine IMPEXP performs the direct time integration using either implicit, explicit or implicit–explicit schemes. This is followed by the subroutine RESEPL which calculates the equivalent nodal forces.

A more detailed diagram of the program with the description of each subroutine and their functions is given in Fig. A.2. The main disadvantage of the MIXDYN program is apparent when dealing with the damping matrix C which is computed as follows:

$$C = \alpha M + B K \qquad (A.1)$$

where,

M,K are the mass and stiffness matrices, respectively, and,

α,β are viscous damping coefficients.

One value of α and β is specified for all elements in the mesh and from these data, the element damping matrices and the global damping matrix are evaluated in the IMPEXP subroutine. Greater latitude in the specification of damping coefficients is desirable.

Truncated boundaries also create difficulties as noted in the main text. The simple expedient of including damping in the material (soil) is not adequate because of excessive cost quite apart from the modelling errors. Fig. A.3 shows the full evaluation of the global damping matrix, in consistent form, for three axisymmetric 4 noded elements in the original version of this program. The program was enhanced by adding subroutines to model the viscous boundaries without affecting its general structure. Fig. A.4 shows the profile structure of the new global damping matrix. Subroutine SDAMP was developed to introduce separate element damping matrices for those elements adjacent to the boundary; a complete listing of this subroutine is given in Appendix B. Its function may

briefly be summarised as follows; it initiates the element damping matrices and calculates some of the constants needed in the evaluation of these matrices. The element mass matrices are then evaluated in LUMASS and the global damping matrix is then formed, (as depicted in Fig. A.4).

The performance of the enhanced version of the MIXDYN program was tested by analysing the response of an elastic solid steel column subjected to a Heaviside forcing function at one end and supported by a viscous dashpot on the other end. An explicit central difference scheme was employed in the solution. Column properties were as follows:

$L = 5$ m

$\nu = 0.3$

$E = 2 \times 10^{11}$ N/m^2

$d = 0.5$ m

$F = 20$ kN for 5 ms

The displacement–time relationship for the column is shown in Fig. A.5 and demonstrates the effect of viscous damping boundary on the overall response of the column.

Some other minor modifications to the program were made in order to facilitate the post processing of the output data for plotting purposes.

A.3 INPUT PARAMETERS

The input data consists of the mesh geometry, the boundary conditions, the loading conditions and the material properties. The data are read in a free format.

A.4 RUN TIMES

Finite element run times are much higher, of course, than corresponding wave equation analysis. Explicit integration schemes are more economical than implicit schemes per time step but, in practice, the conditional stability of the former method generally nullifies this advantage. The finite element analyses carried out during this study were normally performed on the powerful IBM 3090 computer at Glasgow University. Run times for typical pile driving analyses using the implicit integration scheme were four to five minutes. By contrast, run times on the alternative machine at Glasgow University (ICL 3890) were approximately two hours. Consequently, even on the IBM machine, the number of runs which could be obtained were limited.

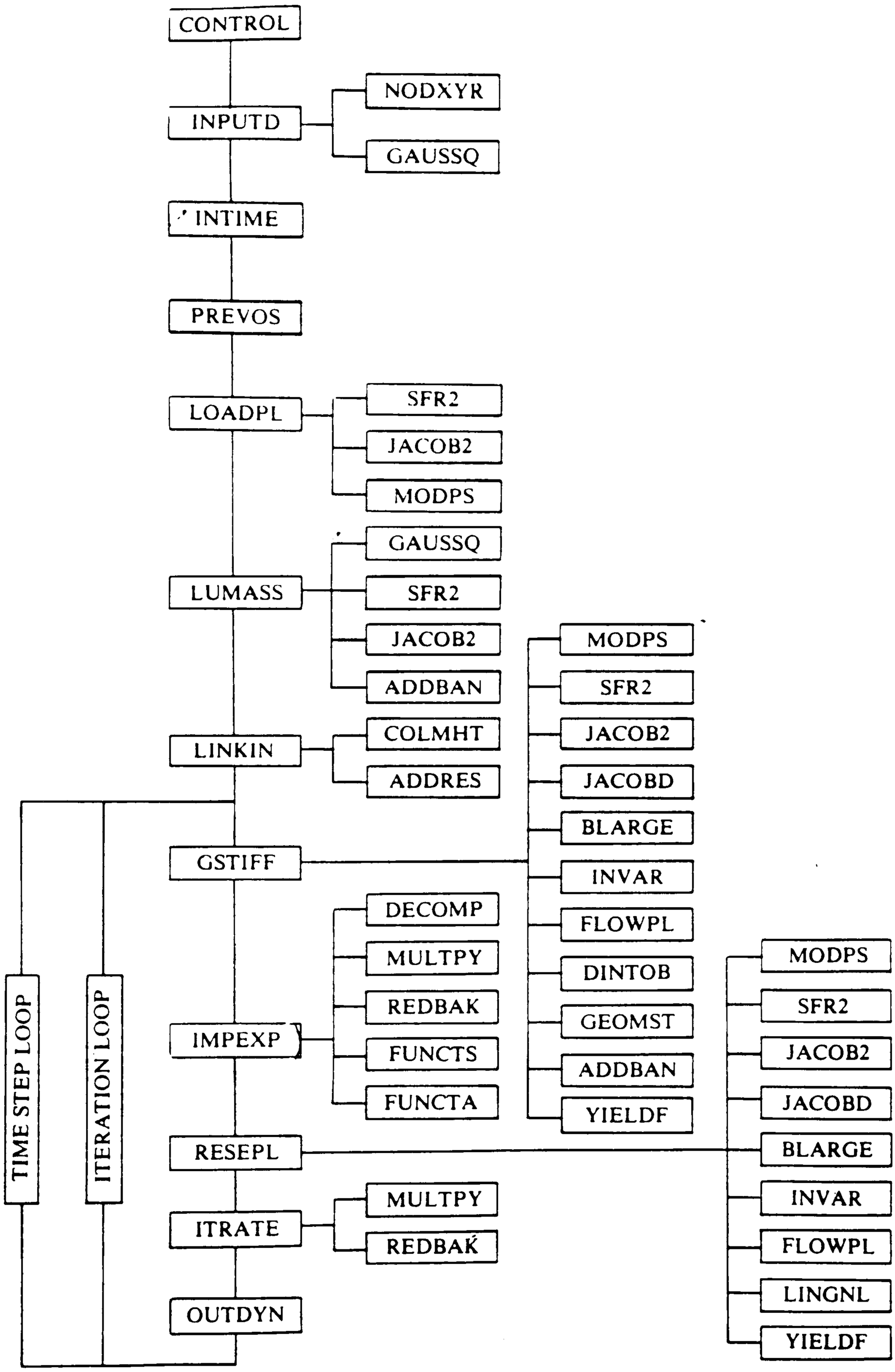

FIGURE (A.1) OVERALL STRUCTURE OF THE MIXDYN PROGRAM
(AFTER OWEN & HINTON, 1980)

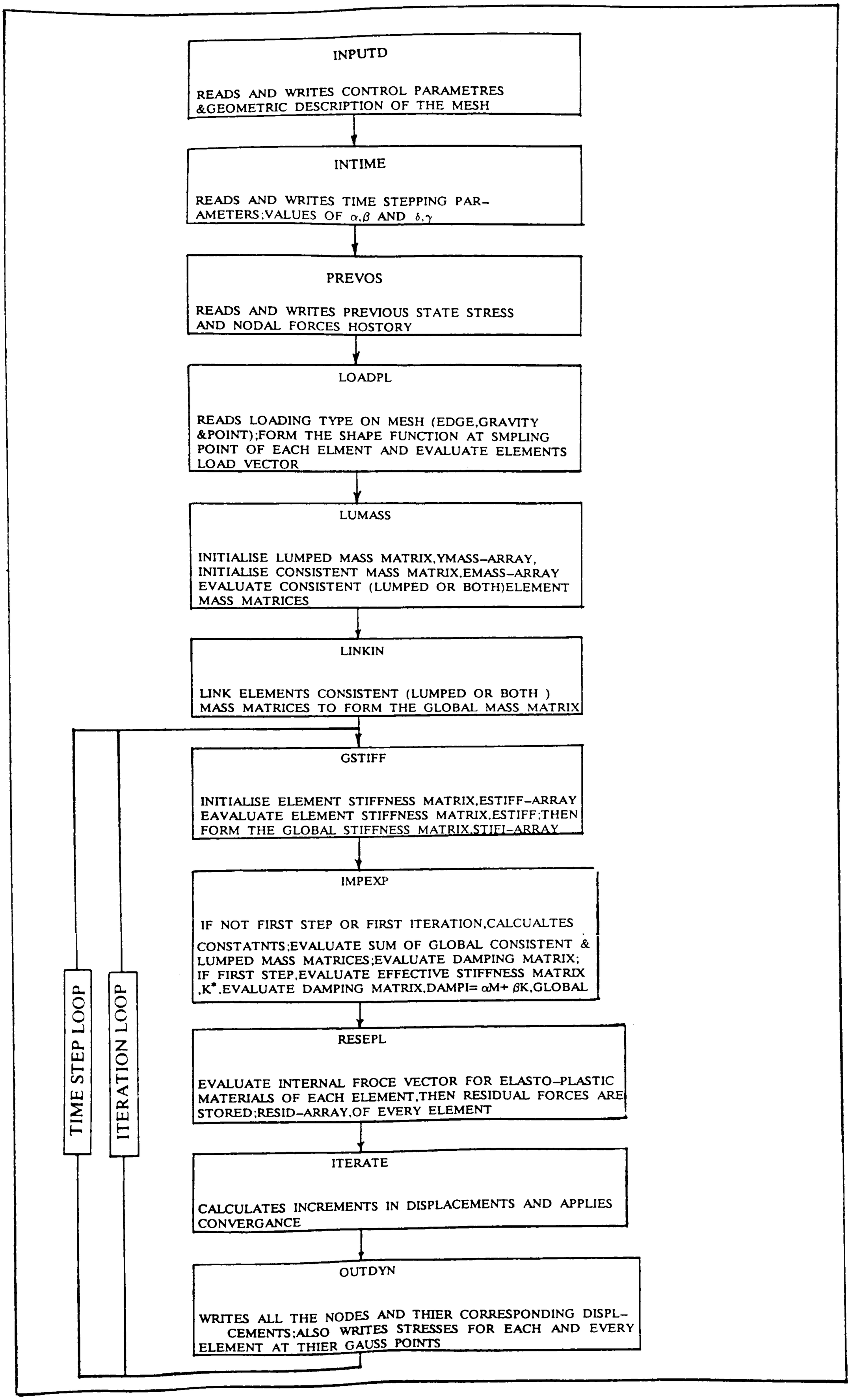

FIGURE (A.2) OVERALL DESCRIPTION OF THE MIXDYN PROGRAM
(AFTER OWEN & HINTON, 1980)

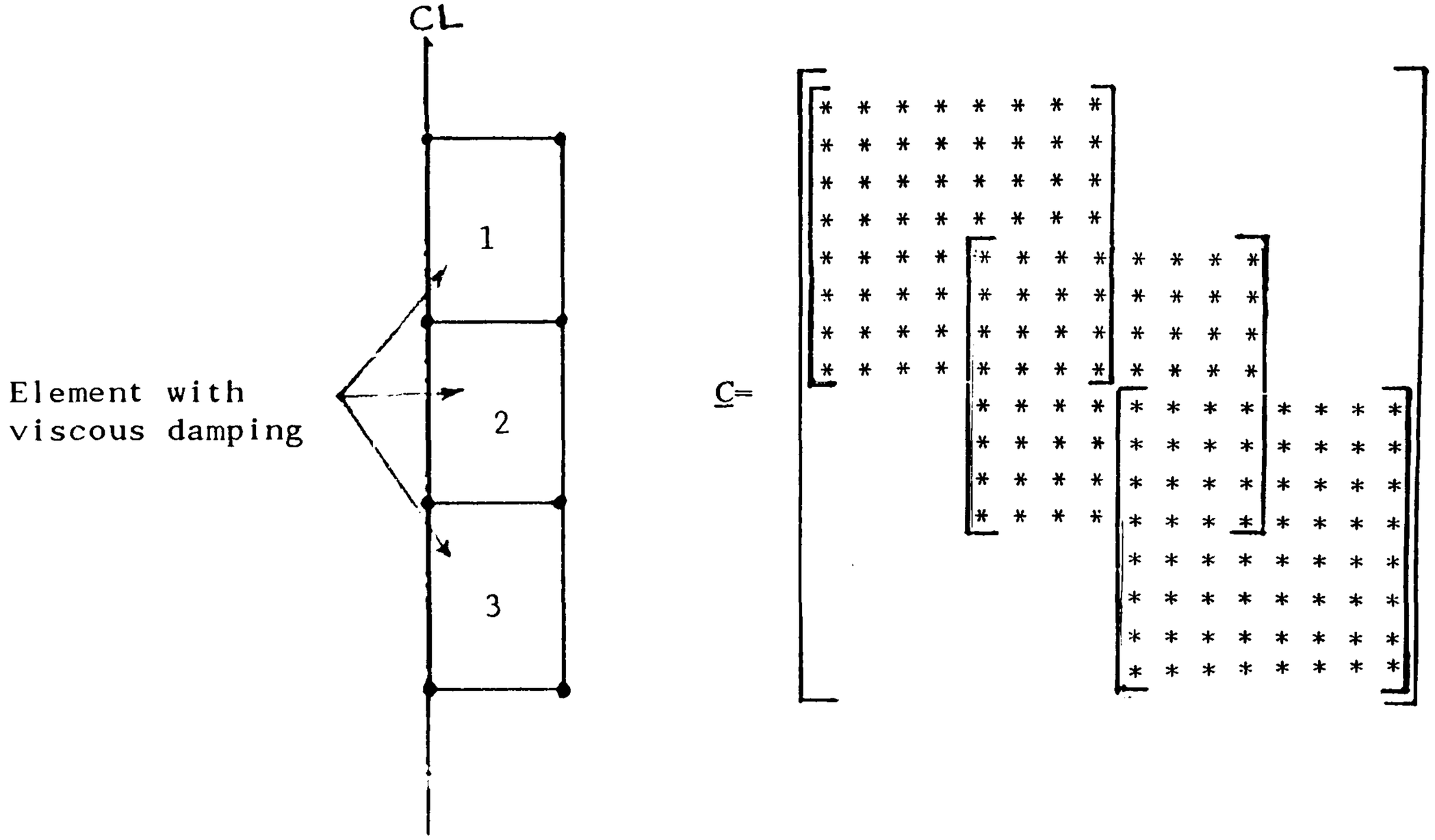

FIGURE (A.3) PROFILE STRUCTURE OF GLOBAL DAMPING MATRIX EVALUATED FROM STANDARD MIXDYN PROGRAM (AFTER OWEN & HENTON, 1980)

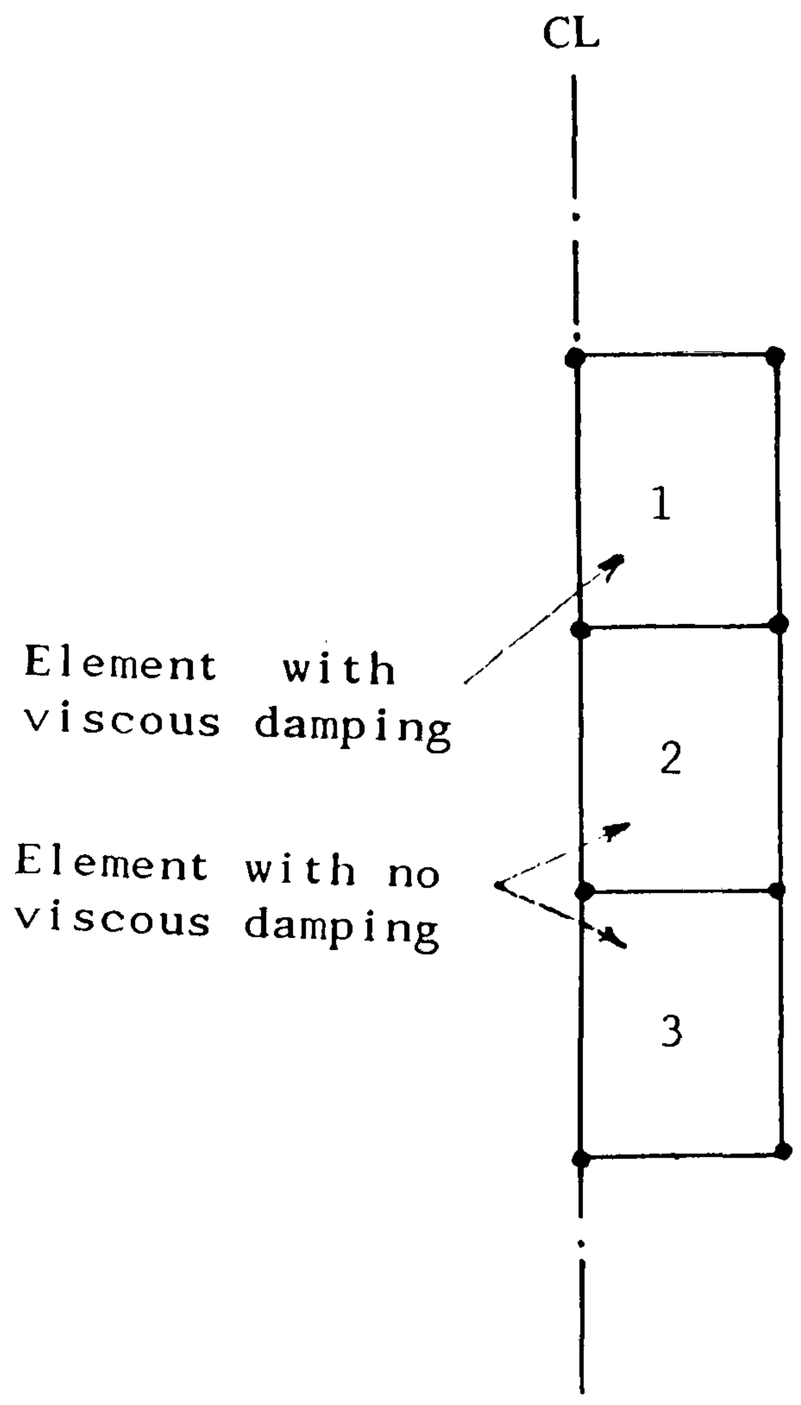

Two Dimensional F.E. mesh

$\underline{C}=$

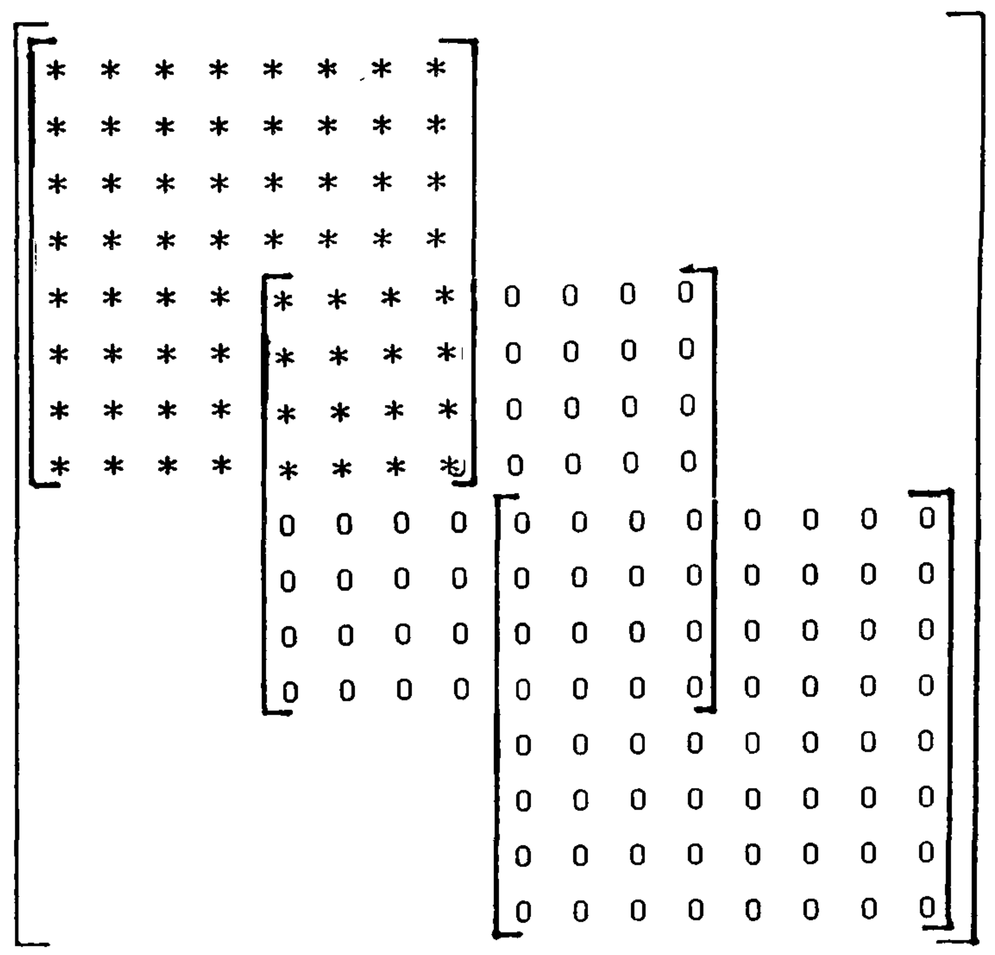

FIGURE (A.4) *PROFILE STRUCTURE OF GLOBAL DAMPING MATRIX EVALUATED FROM THE MODIFIED MIXDYN PROGRAM*

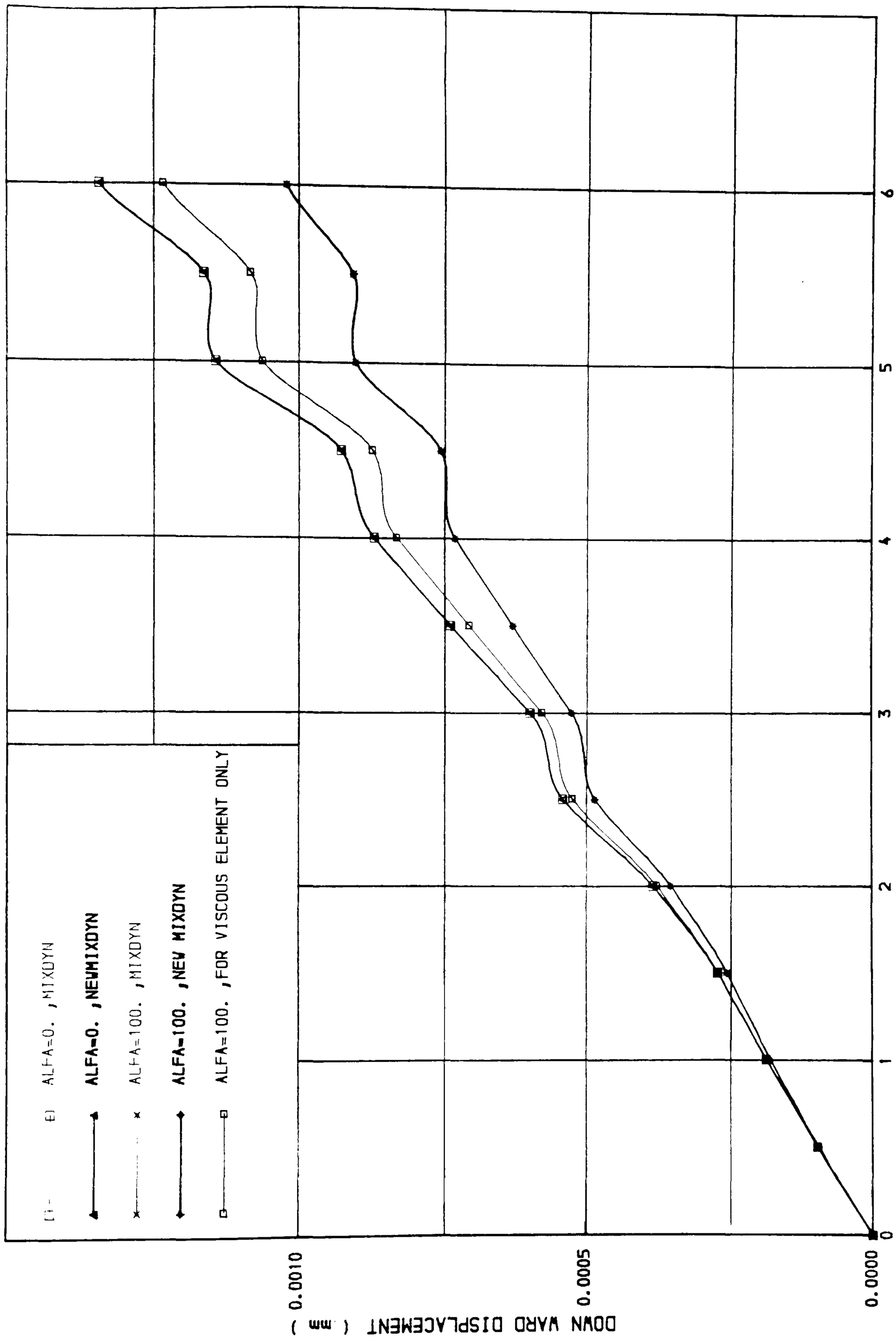

FIGURE (A.5) DISPLACEMENT TIME RELATION

APPENDIX B

SUBROUTINE SDAMP

```
      SUBROUTINE SDAMP(MATNO ,NDOFN ,NELEM ,NMATS ,NPOIN ,
     .PROPS ,LEQNS ,MAXAI ,MAXAJ ,GAAMA ,DTIME ,NWKTL)

C*****************************************************************
C***** THIS SUBROUTINE EVALUATES DAMPING MATRICES OF EACH
C***** ELEMENT THEN EVALUATES THE GLOBAL DAMPING MATRIX
C*****************************************************************
C
      COMMON/ZDAMP/QDAMP(28800),PDAMP(28800),NDAMP
      DIMENSION MAXAI(1),MAXAJ(1),LEQNS(18,240),EMASS(171),
     .          EDAMP(171),EDAMPI(171),MATNO(1),PROPS(10,13)
      REWIND 3
      NEVAB=NNODE*NDOFN
      DO 95 IWKTL=1,NWKTL
      QDAMP(IWKTL)=0.
      PDAMP(IWKTL)=0.

 95   CONTINUE
C
      DO 100 IELEM=1,NELEM
      DO 5 IEVAB=1,171
      EDAMP(IEVAB)=0.0
      EDAMPI(IEVAB)=0.0
 5    CONTINUE
C
      LPROP=MATNO(IELEM)
      NDAMP=PROPS(LPROP,12)
      IF(LPROP.EQ.1.AND.NDAMP.NE.1)AALFA=40.0
      IF(LPROP.EQ.1.AND.NDAMP.EQ.1)AALFA=0.0
      IF(LPROP.GT.1)AALFA=0.0
      WRITE(6,*) IELEM,NDAMP,LPROP,AALFA
      CONSH=GAAMA*AALFA*DTIME
      CONSE=1.+CONSH
C
      READ(3)EMASS
      IEVAB=1
```

```
      KOUNT=NEVAB
      DO 30 INODE=1,NNODE
      DO 60 JNODE=INODE,NNODE
      EDAMP(IEVAB)=EDAMP(IEVAB)+AALFA*EMASS(IEVAB)
      EDAMPI(IEVAB)=EDAMPI(IEVAB)+CONSE*EMASS(IEVAB)
      JEVAB=IEVAB+KOUNT
      EDAMP(JEVAB)=EDAMP(JEVAB)+AALFA*EMASS(JEVAB)
      EDAMPI(JEVAB)=EDAMPI(JEVAB)+CONSE*EMASS(JEVAB)
60    IEVAB=IEVAB+2
      KOUNT=KOUNT-2
      IEVAB=JEVAB+1
30    CONTINUE
C     WRITE(6,90)(EDAMP(I),I=1,171)
C     WRITE(6,91)(EDAMPI(J),J=1,171)
90    FORMAT(2X,  9E10.2)
91    FORMAT(2X,  9E12.3)
      CALL ADDBAN(QDAMP,MAXAI,EDAMP,LEQNS(1,IELEM),NEVAB)
      CALL ADDBAN(PDAMP,MAXAI,EDAMPI,LEQNS(1,IELEM),NEVAB)
100   CONTINUE
C
      RETURN
      END
```

APPENDIX C

COMPUTER PROGRAM WAVE

```
      PROGRAM WAV2
      COMMON/A/AM,AKS,AKP,Q,AJ,DLT
      DIMENSION XDPT(50),VELT(50),XDPW(50),VELW(50)
C
      READ(5,*)AKS,Q,AJ
      READ(5,*)RWP,ALEN,EP,AREA,NELEM
      READ(5,*)V0
      READ(5,*)DLT
      READ(5,*)N,IWR
      WRITE(6,890)
      WRITE(6,900)AKS,Q,AJ
      WRITE(6,910)RWP,ALEN,EP,AREA
      WRITE(6,915)NELEM
      WRITE(6,920)V0
      WRITE(6,930)DLT
      H=ALEN/FLOAT(NELEM)
      AM=H*AREA*RWP
      AKP=EP*AREA/H
      WRITE(6,940)H
      WRITE(6,950)AM
      WRITE(6,960)AKP
C
      T=0.0
      DO 20 I=1,NELEM
      XDPT(I)=0.0
      VELT(I)=0.0
 20   CONTINUE
      VELT(1)=V0
      IW=0
      DO 100 I=1,N
      IW=IW+1
      IWRITE=0
      IF(IW.EQ.IWR)IWRITE=1
      IF(IW.EQ.IWR)IW=0
C
      TZ=T+DLT
```

```
      DO 50 J=1,NELEM
      JR=J
      CALL NEWTON(XDPT,VELT,XDPW,VELW,NELEM,JR)
50    CONTINUE
      IF(IWRITE.EQ.0)GO TO 60
      WRITE(6,970)
      WRITE(6,980)I,TZ
      WRITE(6,990)(XDPW(K),K=1,NELEM)
      WRITE(6,995)(VELW(K),K=1,NELEM)
60    CONTINUE
      DO 70 J=1,NELEM
      XDPT(J)=XDPW(J)
      VELT(J)=VELW(J)
70    CONTINUE
      T=TZ
100   CONTINUE
890   FORMAT(1H ,'ONE DIMENSIONAL WAVE EQUATION"MULTIPLE MASSES"',//)

C
900   FORMAT(1H ,'KS  Q  J',1P3E10.2)
910   FORMAT(1H ,'ROP  LP  E  A',1P4E10.2)
915   FORMAT(1H ,'NELEM',I5)
920   FORMAT(1H ,'V0',1PE10.2)
930   FORMAT(1H ,'DLT',1PE10.2)
940   FORMAT(1H ,'H',1PE10.2)
950   FORMAT(1H ,'M',1PE10.2)
960   FORMAT(1H ,'KP',1PE10.2)
970   FORMAT(1H ,'   I       T     ',/)
980   FORMAT(1H ,I6,1PE10.2)
990   FORMAT(1H ,20X,'D=',3X,1P10E11.2)
995   FORMAT(1H ,20X,'V=',3X,1P10E11.2)
      STOP
      END
C
      SUBROUTINE NEWTON(XDPT,VELT,XDPW,VELW,M,JR)
      COMMON/A/AM,AKS,AKP,Q,AJ,DLT
      DIMENSION XDPT(M),VELT(M),XDPW(M),VELW(M)
```

```
X=XDPT(JR)
V=VELT(JR)
XM1=X
XP1=X
IF(JR.GT.1)XM1=XDPW(JR-1)
IF(JR.GT.M)XP1=XDPW(JR+1)
PM1=AKP*(X-XM1)
PP1=AKP*(XP1-X)
P=-PM1+PP1
XW=X+V*DLT
XBAR=0.5*(X+XW)
IF(XBAR.GT.Q)XBAR=Q
IF(XBAR.LT.-Q)XBAR=-Q
S=1.0+AJ*V
R=-XBAR*AKS*S
VW=V+(R+P)*DLT/AM
XDPW(JR)=XW
VELW(JR)=VW
RETURN
END
```